TECHNISCHE UNIVERSITÄT
BERGAKADEMIE FREIBERG
Die Ressourcenuniversität. Seit 1765.

Institut für Bohrtechnik
und Fluidbergbau

Well Testing in Gas Hydrate Reservoirs

To the Faculty of Geosciences, Geoengineering and Mining

of the Technical University Bergakademie Freiberg

approved

THESIS

to attain the academic degree of

Doktor-Ingenieur

(Dr. -Ing.)

submitted by

Dipl.- Ing. **Melvin Njumbe Kome**

born on 21st May 1985 in Tignere, Cameroon

Reviewers: Prof. Dr.-Ing. Moh'd M. Amro, TU Freiberg, Germany

Prof. Dr. Wilhelm Dominik, TU Berlin, Germany

Freiberg, 16.01.2015

Versicherung

Hiermit versichere ich, dass ich die vorliegende Arbeit ohne unzulässige Hilfe Dritter und ohne Benutzung anderer als der angegebenen Hilfsmittel angefertigt habe; die aus fremden Quellen direkt oder indirekt übernommenen Gedanken sind als solche kenntlich gemacht.

Bei der Auswahl und Auswertung des Materials sowie bei der Herstellung des Manuskripts habe ich Unterstützungsleistungen von folgenden Personen erhalten:

- Prof. Dr.-Ing. Mohd Amro, TU Bergakademie Freiberg, Betreuer
- Cara Faller und Anne Schulz, TU Bergakademie Freiberg: Unterstützung bei Fragen zu Layout.
- Kome Aileen, Universität von Padua '10, Italien und Akwo Fawah, Massachusetts Institute of Technology '08, USA: Unterstützung bei Fragen zu Grammatik und Rechtschreibung.
- Prof. Dr. rer. nat. habil. Steffen Wagner, TU Freiberg und Dipl.-Ing. Titus Douka, RWE Dea: Unterstützung bei Fragen zu Inhalt und Layout.

Weitere Personen waren an der Abfassung der vorliegenden Arbeit nicht beteiligt. Die Hilfe eines Promotionsberaters habe ich nicht in Anspruch genommen. Weitere Personen haben von mir keine geldwerten Leistungen für Arbeiten erhalten, die nicht als solche kenntlich gemacht worden sind.

Die Arbeit wurde bisher weder im Inland noch im Ausland in gleicher oder ähnlicher Form einer anderen Prüfungsbehörde vorgelegt.

Declaration

I hereby declare that I completed this work without any improper help from a third party and without using any aid other than those cited. All ideas derived directly or indirectly from other sources are identified as such.

In the selection, use of materials and in the writing of the manuscript, I received support from the following persons:

- Prof. Dr.-Ing. Mohd Amro, TU Bergakademie Freiberg: Supervisor
- Cara Faller and Anne Schulz, TU Bergakademie Freiberg: Assistance with layout problems
- Kome Aileen, University of Padova '10, Italy and Akwo Fawah, Massachusetts Institute of Technology '08, USA: Assistance with grammatical and orthographical problems.
- Prof. Dr. rer. nat. habil. Steffen Wagner, TU Freiberg and Dipl.-Ing. Titus Douka, RWE Dea: Assistance with layout problems as well as technical / scientific savvy.

Persons other than those above did not contribute to the writing of this thesis. I did not seek the help of a professional doctorate-consultant. Only those persons identified as having done so received any financial payment from me for any work done for me. This thesis has not previously been published in the same or a similar form in Germany or abroad.

Abstract

Melvin Njumbe Kome

Well Testing in Gas Hydrate Reservoirs

Thesis 2014; 235 Pages; 9 Tables; 72 Figures; 18 Appendices

TU Bergakademie Freiberg, Faculty of Geosciences, Geoengineering and Mining

Keywords: Gas Hydrate; Well Testing, Rate Transient, Pressure Transient, Hydrate Dissociation, Heat Influx, Multiphase Flow, Pseudo-Pressure, Crossflow, Moving Boundary, Mass Balance Model

Reservoir testing and analysis are fundamental tools in understanding reservoir fluid hydraulics and hence forecasting reservoir responses. The quality of the analysis is very dependent on the conceptual model used in investigating the responses under different flowing conditions.

The use of reservoir testing in the characterization and derivation of reservoir parameters is widely established, especially in conventional oil and gas reservoirs. However, with depleting conventional reserves, the quest for unconventional reservoirs to secure the increasing demand for energy is increasing; has triggered intensive research in the fields of reservoir characterization. Gas hydrate reservoirs, being one of the unconventional gas reservoirs with huge energy potential, is still in the juvenile stage with reservoir testing as compared to the other unconventional reservoirs. The endothermic dissociation of hydrates to gas and water requires addressing multiphase flow and heat energy balance, which has made efforts to develop reservoir testing models in this field difficult.

During depressurization, the heat energy stored in the reservoir is used up and due to the endothermic nature of the dissociation; heat flux begins from the confining layers. For Class 3 gas hydrates, just heat conduction would be responsible for the heat influx and further hydrate dissociation; yet, the moving boundary problem could also be an issue to address in this reservoir, depending on the equilibrium pressure. To address heat flux problem, a proper definition of the inner boundary condition for temperature propagation using a Clausius-Clapeyron type hydrate equilibrium model is required.

In Class 1 and 2, crossflow problems would occur and depending on the layer of production, convective heat influx from the free fluid layer and heat conduction from the cap rock of the hydrate layer would be further issues to address. All these phenomena make the derivation of a suitable reservoir testing model very complex. Nevertheless, with a strong combination of heat energy and mass balance techniques, a representative diffusivity equation can be derived.

Reservoir testing models have been developed and responses investigated for different boundary conditions in normally pressured Class 3 gas hydrates, over-pressured Class 3 gas hydrates (moving boundary problem) and Class 1 and 2 gas hydrates (crossflow problem). The effects of heat flux on the reservoir responses have been addressed in detail.

Acknowledgements

First and Foremost, I would like to express my deepest gratitude to my supervisor, Prof. Dr.-Ing. Mohd Amro, for his relentless efforts and remarkable guidance. Many thanks also go to Prof. Dr. Wilhelm Dominik for his acceptance to co-supervise this thesis.

I would like to thank the Federal Ministry for Economic Affairs and Energy (BMWI) for financing the project and hence making it possible for me to work on this thesis.

Many thanks go to Dipl.-Ing. Titus Douka, Prof. Dr. Steffen Wagner and Prof. Dr.-Ing. Frieder Häfner for the numerous constructive dialogues, which helped shape this thesis.

I would like to thank my beloved sister Kome Aileen and my bosom friend Akwo Fawah for their time and efforts with the orthographical improvements of the thesis.

I would like to thank my colleagues at the Institute of Drilling Engineering and Fluid Mining, especially Anne Schulz, for the wonderful working climate.

I would like to thank my fiancée, Cara Faller and the rest of my family for boosting up my moral and standing by me through good and bad times.

Lastly, I thank all my friends, most especially the African community in Freiberg, for their support and encouragement throughout this research.

Dedication

This thesis is dedicated to my father, late Dr.(med) Kome Nzume Leslie, my mother Mrs. Kome Edna Nzong, my fiancée Ms. Cara Faller and my son Jamarion Enrico Nzume Kome.

Table of Content

Nomenclature

Symbols

Symbol	Meaning	Unit
a(p)	pressure dependent pressure conductivity	[1/s]
B	formation volume factor	[-]
b_D	dimensionless interlayer heat flux coefficient	[-]
c_p	specific heat capacity	[J/kgK]
c	dimensionless heat function	[-]
c_T	total compressibility	[1/Pa]
$c_{T,w}$	total compressibility of water phase	[1/Pa]
$c_{T,g}$	total compressibility of gas phase	[1/Pa]
c_F	compressibility of pore space	[1/Pa]
c_g	gas compressibility	[1/Pa]
$c_{D,H}$	dimensionless hydrate decomposition compressibility	[-]
D(p)	pressure dependent diffusion coefficient	[kg/m³Pas]
E_g	hydrate-gas volume factor	[-]
E_w	hydrate-water volume factor	[-]
e_D	dimensionless conductive heat flux coefficient	[-]
f_m	MBM fractional mass flow rate	[-]
$f_D(p,t)$	dimensionless compressibility mobility term	[-]
$f_t(p)$	pseudo-pressure integral function	[kg/m³Pas]
F_{CD}	dimensionless temperature conductivity	[-]
f_D	dimensionless interlayer crossflow compressibility (NFB+CTOB)	[-]
g_D	dimensionless interlayer crossflow compressibility (CPOB+CTOB)	[-]
hd	hydrate dissociation energy per unit mass	[J/kg]
h, z	reservoir thickness	[m]
I_0, I_1	modified Bessel´s functions of the first kind	[-]
j_D	dimensionless interlayer mass flux coefficient (CPOB+CTOB)	[-]
k	absolute permeability	[m²]
k_{eff}	effective permeability	[m²]
k_r	relative permeability	[-]
k_g	gas effective permeability	[m²]
k_{rg}	gas relative permeability	[-]
k_{rg}^*	modified gas relative permeability	[-]
k_w	water effective permeability	[m²]
k_{rw}	water relative permeability	[-]
k_{rw}^*	modified water relative permeability	[-]
$k_g(p),_{avg}^*$	apparent effective gas permeability	[m²]
K_0, K_1	modified Bessel´s functions of the second kind	[-]

l_D	dimensionless distance to boundary	[-]
$\dot{m}$	mass flow rate	[kg/s]
$\dot{m}_{tD}$	dimensionless total mass flow rate	[-]
n_w	water relative permeability exponent	[-]
n_g	gas relative permeability exponent	[-]
N	hydrate permeability reduction exponent	[-]
p	reservoir pressure	[Pa]
p	Laplace complex variable	[-]
Q_{st}	flow rate at standard conditions	[m³/s]
R	universal gas constant	[J/molK]
$r_s(t)$, r_s	radius of dissociation	[m]
r_w	wellbore radius	[m]
r_D	dimensionless radius	[-]
r_{eD}	dimensionless drainage radius	[-]
r_{sD}	dimensionless radius of dissociation	[-]
S	saturation	[-]
S	storativity	[kg/m³Pa]
S_{girr}	connate gas saturation	[-]
S_{wirr}	connate water saturation	[-]
$S_{g,H}$	gas saturation from hydrate dissociation	[-]
$S_{w,H}$	water saturation from hydrate dissociation	[-]
S_D	modified dimensionless decomposition compressibility	[-]
S_{Dk}	modified dimensionless compressibility	[-]
s_s	skin effect due to hydrate dissociation	[-]
T	temperature	[°K]
t	time	[s]
t_D	dimensionless time	[-]
t_{Dw}, t_{DwD}	dimensionless time with respect to wellbore	[-]
t_f^*	semi-log time for boundary dominated flow with single barrier	[s]
t_{tf}^*	derivative time for boundary dominated flow with single barrier	[s]
w	Darcy velocity	[m/s]
V	volume	[m³]
dT_{eq}/dp	temperature gradient for hydrate dissociation	[°C/Pa]
Y_D	dimensionless interlayer mass flux coefficient (NFB+CTOB)	[-]
z_g	gas compressibility factor	[-]

Greek Symbols

Symbol	Meaning	Unit
φ	pseudo-pressure	[kg/sm³]
φ_D	dimensionless pseudo pressure,	[-]
φ_{sD}	dimensionless dissociation pseudo pressure	[-]
φRPI	pseudo pressure normalized rate	[1/m³]
φPI	normalized rate pseudo pressure	[m³]
ΔH	hydrate dissociation heat enthalpy	[J/mol]
ϖ	geothermal gradient	[°C /m]
ρ	density	[kg/m³]
ϕ	porosity	[-]
η	viscosity	[Pas]
μ_D	dimensionless interlayer compressibility	[-]
γ_D	dimensionless dissociation rate	[-]
γ_{De}	dimensionless dissociation rate for equilibrium model	[-]
γ_{Dk}	dimensionless dissociation rate for kinetic model	[-]
β(pi)	compressibility density product at initial reservoir pressure	[kg/m³Pa]
δ_D	interporosity flow coefficient	[-]
θ_D	dimensionless convective heat flux dissociation Coefficient	[-]
ω	storativity ratio	[-]
ε_D	dimensionless early time interlayer mass flux coefficient	[-]

Subscripts

Symbol	Meaning
g	gas
w	water
h, H	hydrate
st	standard condition
t	total
fl	fluid
p	pores
f	formation
avg	average
i, id	initial
wf	wellbore flowing
c	critical
s	skin
MP	match point
eq	equilibrium

Abbreviations

Symbol	Meaning
MBM	Mass Balance Model
VMBM	Volumetric Material Balance Model
CPOB	Constant Pressure Outer Boundary
NFB	No Flow Boundary
CTOB	Constant Temperature Outer Boundary
p-NFTB	Pseudo No Flow Temperature Boundary
IAR	Infinite Acting Reservoir
IACL	Infinite Acting Conducting Layer
IARF	Infinite Acting Radial Flow
IAHI	Infinite Acting Heat Influx
CPIB	Constant Pressure Inner Boundary
CRIB	Constant Rate Inner Boundary
CTHI	Constant Temperature Heat Influx
PSSHI	Pseudo Steady State Heat Influx
FFL	Free Fluid Layer
HL	Hydrate Layer
TL	Top Layer
CL	Confining Layer
EOS	Equation of State
RTA	Rate Transient Analysis
PTA	Pressure Transient Analysis
LHS	Left Hand Side
RHS	Right Hand Side

List of Tables

List of Figures

1 Introduction

In the last decade, a huge quest for unconventional reservoirs was perceived in the oil and gas industry, which can be related to the unremittingly increasing energy demand coupled with the depleting conventional reservoirs. As a result, unconventional reservoirs have become very attractive in meeting up with this energy demand.

The classification of gas reservoirs as unconventional is mainly based on their low formation permeability, to which gas hydrate reservoirs can also be related to. Though the absolute permeability of the hydrate formation might be high due to the porous and/or unconsolidated nature, the effective permeability of the hydrate layer can be very low as a result of hydrates occupying the pore space of the formation, making fluid flow through the pores difficult [1]. Regardless of the low effective permeabilities, the hydrate reserves have been widely classified as extremely enormous compared to other hydrocarbon reserves as depicted in Figure 1 and Figure 2, which makes them very attractive for the energy market as they are found around almost all continental shelves (see Figure 3).

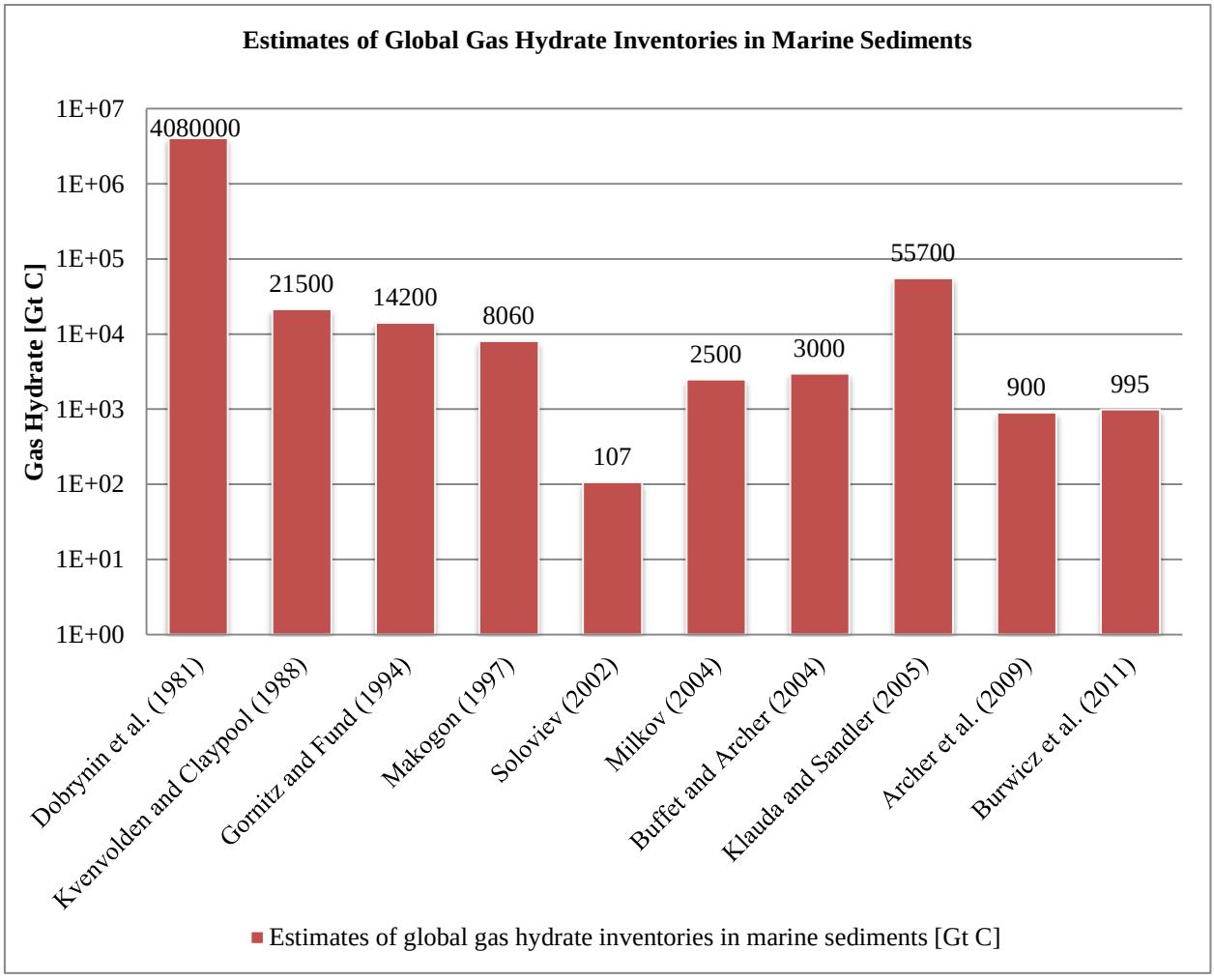

Figure 1: Global Gas Hydrate Inventory [2]

As depicted in Figure 1, the gas hydrate inventory varies enormously with some authors; nonetheless, the amount is still very large. Usually a consensus value of 10000 Gt C is taken and is the most widely

quoted [3]. To have a much better view on the amount of energy available or exploitable from the hydrates, a comparison of the hydrate inventory with the fossil energy sources is given in Figure 2. It is undisputable that the amount of fossil energy stored in gas hydrates surpasses all other fossil energy sources.

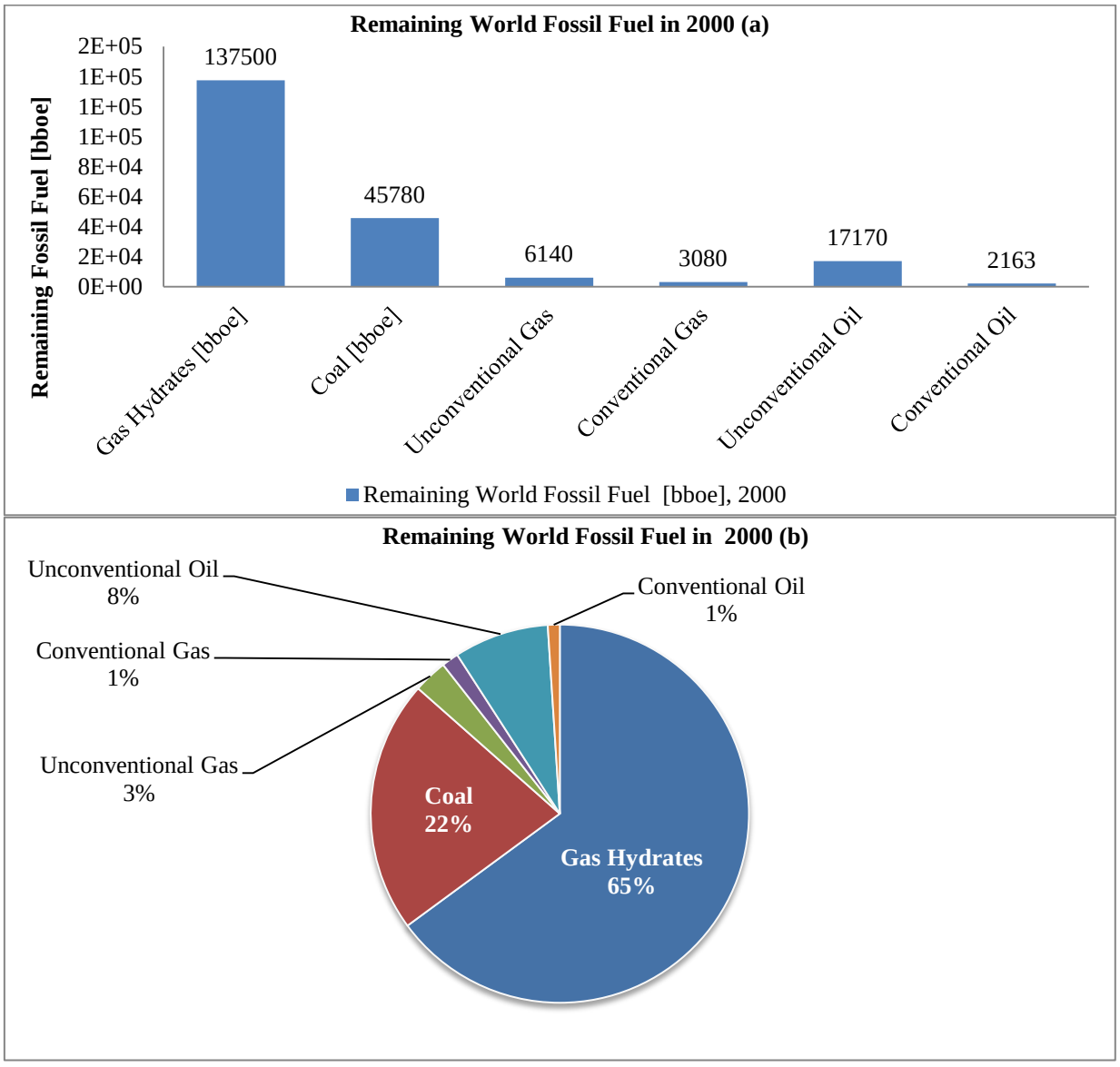

Figure 2: Comparison of Gas Hydrate to other Fossil Resources (a, b) [after [4]]

Regardless of the huge reserves, profuse uncertainties still persists regarding the behavior of gas hydrate reservoirs during production and as such, much effort has been invested in recent years to characterize the reservoir responses. Owing to the heterogenic nature of the hydrate behavior, much effort has however been dedicated in the numerical modeling to investigate the hydrate reservoir responses.

From well test/production data, we are faced with an inverse problem where the reservoir interpretation and characterization has to be performed from these data. Reducing the scope of the interpretation process to just numerical models requires numerous input parameters for a good history

match. It should still be emphasized that inaccurate input parameters for any gas hydrate numerical simulator can generate misleading predictions that would significantly affect further decisions in relevant projects. The inaccuracy in input parameters associated with a numerical simulator can be reduced with the use of reservoir testing characterization methods in conjunction with numerical simulators for gas hydrates [1], which is as of now a field of great interest in the oil and gas industry. However, for this process, a good understanding of the behavior of the hydrates and representative conceptual models are required for the reservoir response. Next, we identify a few aspects regarding gas hydrate and reservoir testing after which conceptual models will be developed to investigate the responses expected from the hydrates during various production scenarios.

1.1 Gas Hydrates: Occurrence, Properties and Production

Gas hydrates are classified under the group of clathrates which is used to denote a molecule of a substance enclosed in a structure built from molecules of other substances [5]. Hydrates in particular are hence crystalline solid compounds with small molecules enclosed in water [5]. Since their discovery in the early 19th century, gas hydrates only became of great interest in the oil and gas industry with the inception of plugging of gas pipelines and other downstream equipment in the 1930´s. Gas hydrates were then a big foe for the upstream sector and measures were taken to mitigate the occurrence of any hydrates.

1.1.1 Occurrence

With the discovery of natural gas hydrate occurrence in marine and permafrost regions in the mid 1960´s [6], more curiosity grew in the worldwide existence / distribution, which was then investigated by many researchers and characterized. Figure 3 depicts the global distribution of gas hydrates.

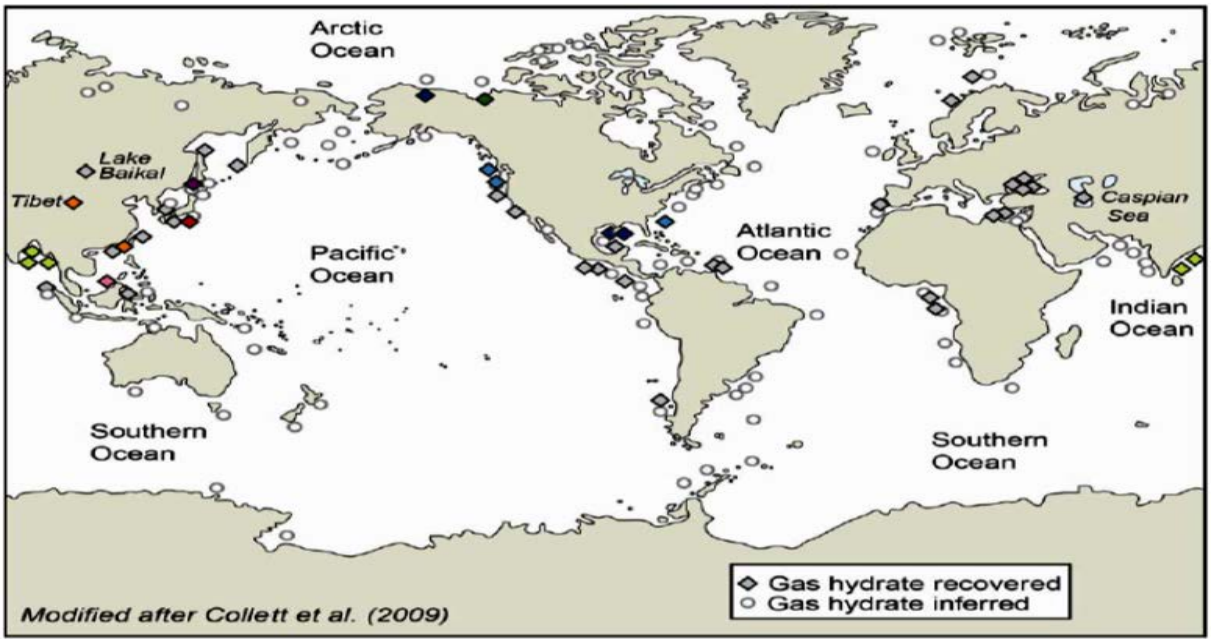

Figure 3: Global map of recovered and inferred gas hydrates [7]

From the global inventory, the next point of interest would be the amount of gas stored in the gas hydrates which has been investigated and quantified by various authors [[5], [8], [9], [10]]. Nonetheless, for 1m³ methane hydrate we get approximately 164-180 Sm³ methane and about 0,8 Sm³ water [[5], [10], [11]]. The model required to estimate this conversion is developed using a mass balance approach in Appendix 2.

Although huge amounts of gas hydrates are found all over the globe, producing them safely from the formation is challenging due to stability of the layer, all depending on the hydrate distribution in the formation as depicted in Figure 4. Preferably, hydrates occupying the pore space of the formation will be better candidates for much safer production as they have a relatively less significant contribution to the stability of the hydrate layer compared to the other microstructural models in Figure 4. Hereafter, the conceptual models developed in this work address the reservoir response of porous hydrate formations.

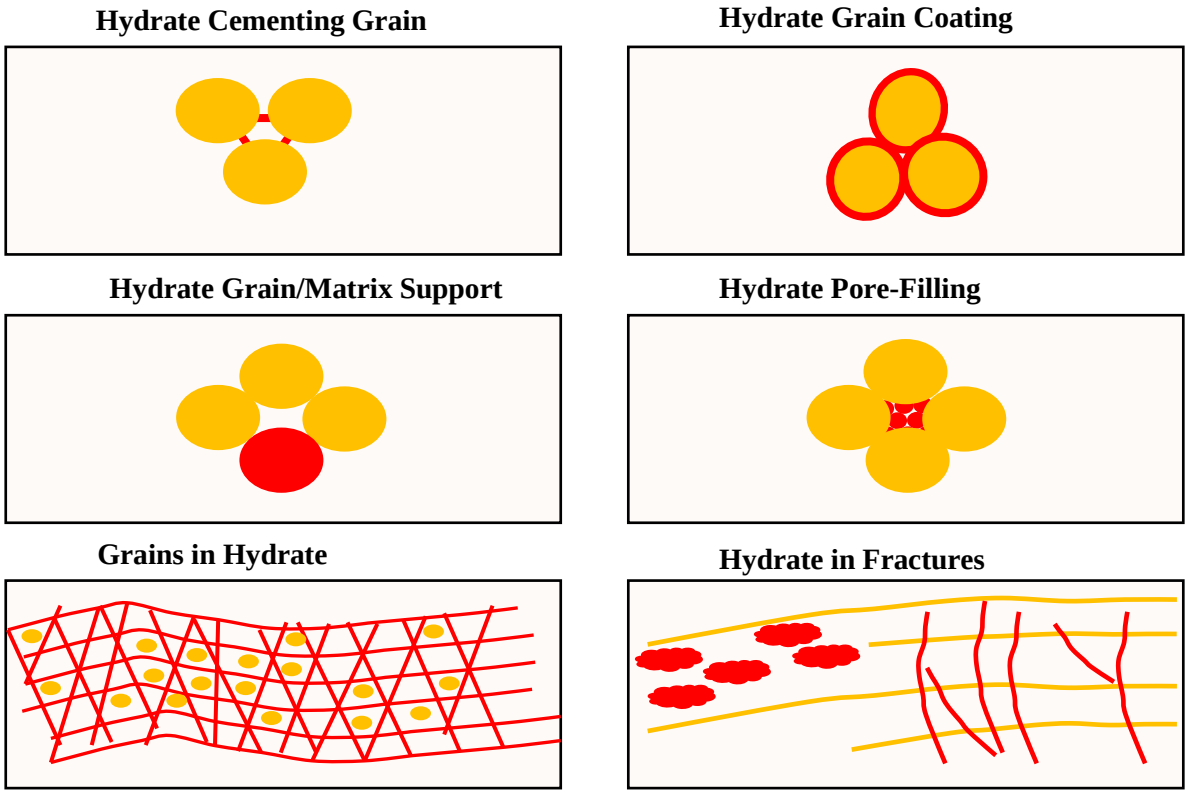

Figure 4: Microstructural Models for Hydrate Bearing Sediments [after [12]]

The occurrence of gas hydrates in sediments is determined by high pressure-low temperature (HP/LT) conditions and adequate supply of natural gas in the hydrate stable layers. Due to the favorable pressure-temperature conditions for hydrate formation in permafrost and marine sediments, gas hydrates are predominantly found in these regions, where they occur in a relatively narrow zone called the hydrate stability zone [9]. In oceanic areas, the hydrate stability zone typically begins below 300-600 m of water depth with a general temperature range from 2 to 20°C; which is still limited to the availability of methane [3]. In permafrost regions the hydrate stability zone characteristically occurs

around 100-300 m depth and the general temperature range is from −10 to 20°C [3]. Figure 5 and Figure 6 depict stability zones in permafrost and marine areas respectively.

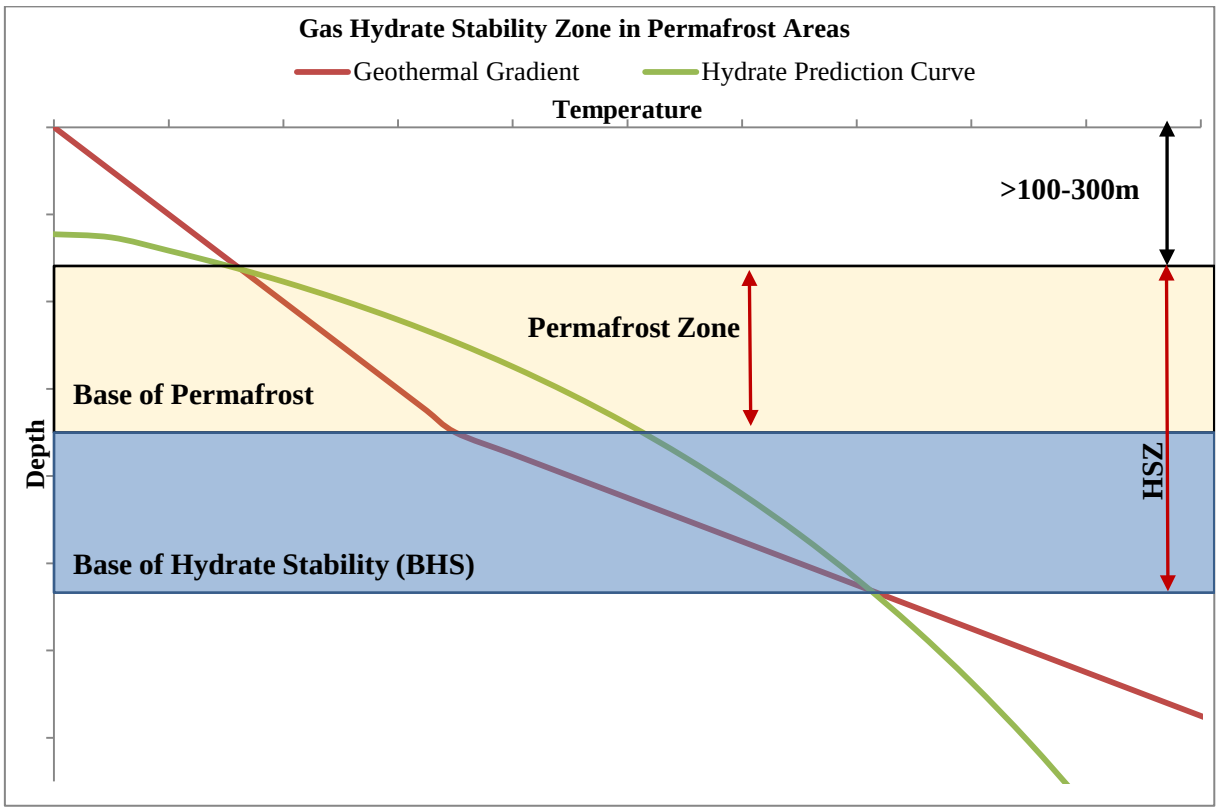

Figure 5: Gas Hydrate Stability Zone in Permafrost Areas [modified after [3]]

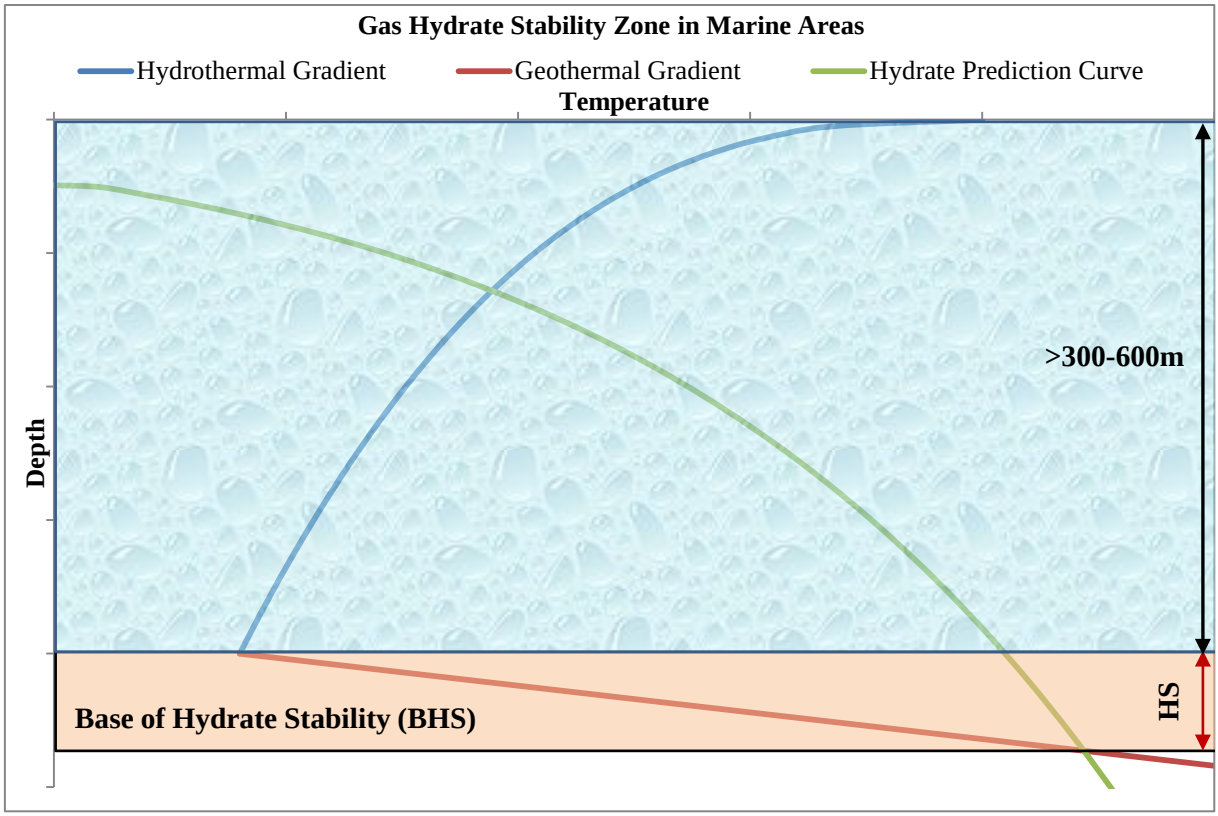

Figure 6: Gas Hydrate Stability Zone in Marine Areas [modified after [3]]

1.1.2 Properties

As mentioned earlier**,** gas hydrates are crystalline solid compounds with small molecules enclosed in water, meaning a variety of small molecules are capable of being trapped in the crystalline solids which is also given in Table 1.

Table 1: Potential Gas Hydrate Formers and Hydrate Types [5], [13]

	Hydrate Type		
	Type I (X)	Type II (X)	Type H (Y)
Potential Gas Hydrate Formers	• Methane • Ethane • Hydrogen Sulfide • Carbon dioxide • Oxygen • Sulfur dioxide • Chlorine	• Nitrogen • Propane • iso-Butane • Ethylene • Propylene • Benzene	• 2-methylbutane • 2,2-dimethylbutane • 2,3-dimethylbutane • 2,2,3-trimethylbutane • 2,2-dimethylpentane • 3,3-dimethylpentane • methylcyclopentane • ethylcyclopentane • methylcyclohexane • cycloheptane • cyclooctane
Theoretical Formula (All Cages Filled)	X. $5^{3/4}H_2O$	X. $5^{2/3}H_2O$	5X. Y. 34 H_2O

Regardless of the great number of substances capable of forming gas hydrates, of great interest to the energy market are the hydrocarbon gas hydrates, most of which is methane hydrate as reported in most literature [8] where very high concentrations of methane in the hydrates are perceptible.

Gas hydrates and ice look physically the same but exhibit different properties which was a field of research for many years after its discovery and an extensive coverage of these properties is given today in many literatures such as [6], [13], [5], [14].

Figure 7: Gas Hydrates; "Burning Ice Effect" [after Gary Klinkhammer [15]]

Apart from the inflammable property of gas hydrate which is not seen with ice, many more differences/similarities exist between the two substances, which are summarized in Table 2.

Table 2: Some peculiarities of ice and gas hydrates [5], [14]

Properties	**Hydrocarbon Hydrates**	**Ice**
Thermal Conductivity	0.50-0.01 W/m·K	2.2 W/m·K
Phase Changes	Solid ↔ Fluid	Solid ↔ Fluid
Dissociation	Endothermic	Endothermic
Heat of Dissociation/Melting	500-600 kJ/kg	335 kJ/kg
Volume Expansion When Formed	26-32%	9%
Density	913-934 kg/m³	917 kg/m³

For reservoir engineering purposes and for developing conceptual well testing models for the hydrate reservoir, indispensable knowledge on endothermic dissociation process, i.e. heat of dissociation and the hydrate equilibrium curve, is required. This is explicitly handled in Appendix 2 and Appendix 3.

1.1.3 Production Methods

Due to the dependence of hydrate stability on pressure and temperature conditions in the reservoir, production methods from these reservoirs basically involve maneuvering the p-T conditions in the reservoir such that the hydrates are no longer stable. Hence, the main production methods will either be to increase the temperature in the hydrate layer (thermal stimulation) or decrease the pressure (depressurization) or a combined effect of both. It should be mentioned that thermodynamic inhibitors and some gases are known to have an effect on the hydrate stability as depicted in Figure 8, which has made them potential candidates for production. With this said, the production methods in hydrate reservoirs could be summarized under the following groups [6]:

- Depressurization
- Thermal Stimulation (e.g. Supercritical CO_2)
- Inhibitor Injection (e.g. Methanol)
- Injection of Special Fluids (e.g. N_2)

It is worth mentioning that the applicability of any on the following methods is reservoir and cost dependent. Hence a thorough scrutiny of the applicability of any of the above methods has to be performed for the reservoir in question.

Figure 8 depicts the influence of inhibitors and special fluids on the hydrate stability curve. Here, we clearly observe the reduction in pressure depressions and thermal energy required when these fluids are used. This implies that for a speedy recovery of gas from the hydrates, a combination of the methods would be most favorable; yet the cost intensive nature of combining the methods, especially for long term purposes, makes it very challenging.

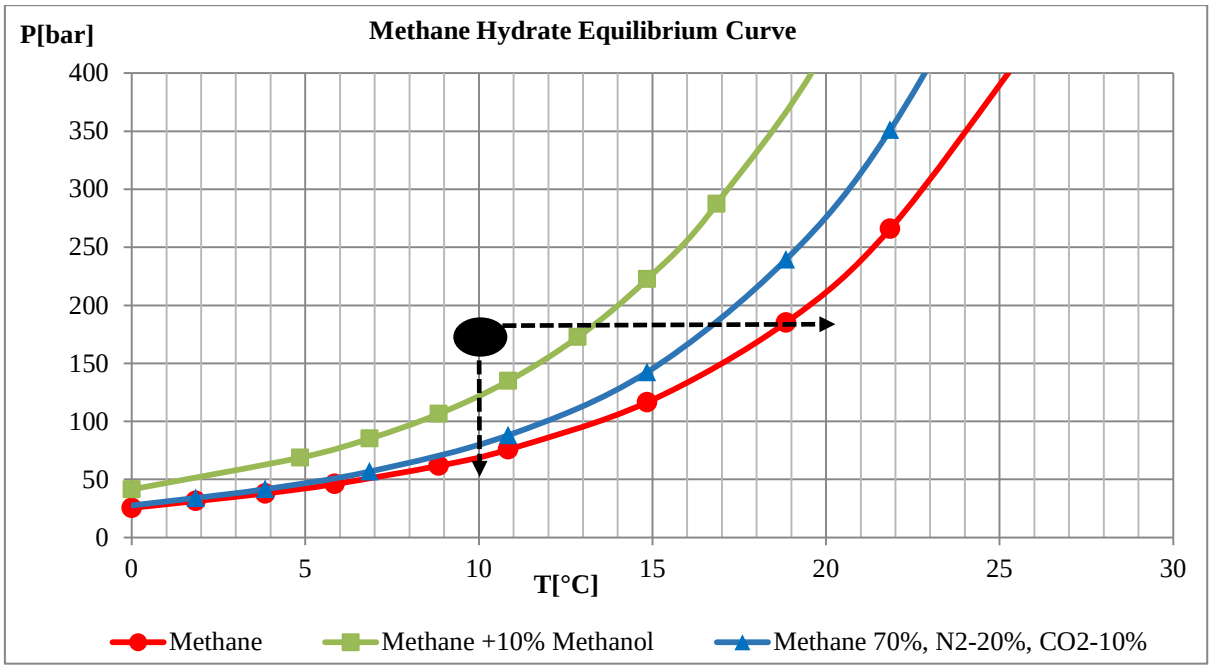

Figure 8: Ideology of Gas Hydrate Production Techniques

Of the production methods mentioned earlier, the depressurization technique is the most widely used as in the Messoyakha Gas Field and Japan Nankai Trough. As seen with the Messoyakha Gas Field, depressurization is the only method applied to produce a hydrate field for long lasting production periods [6] where about 36% of the gas produced was from the hydrate layer [11]. Although the Messoyakha Gas Field is a Class 1G hydrate reservoir, .i.e. predominantly free gas below the hydrate layer, also called a hydrate-capped gas reservoir [10], which are susceptible to crossflow problems, the effects of hydrate dissociation were only significant years after the commencement of production from the free gas layer. This implies the conceptual models for such reservoirs have to depict the early and late time response such that the effects of hydrate dissociation can be characterized.

1.2 Reservoir Testing

Understanding reservoir responses under different flowing conditions is very vital in forecasting reservoir performance and technical decisions in the life of the well/reservoir. The information derived from the test is very indispensable in reservoir engineering and reservoir management as it reflects the in-situ reservoir dynamic properties under realistic production situations [16]. Dynamic reservoir properties define the prerequisites to denoting the reservoir as economically viable as it must exhibit the capacity for storage and fluid transmissibility [17]. Estimating the fluid transmissibility of the reservoir has always been one of the main objectives in reservoir testing. Although numerous objectives of reservoir testing exist, they can be grouped into four classes [17]:

- Permeability and Formation Damage
- Characterization of Formation Fluid Samples
- Measurement of Formation Pressure

- Reservoir Characterization

The most common well testing methods include [17]:

- Open and cased hole wells with no completion string: DST
- Wireline Formation Testing: WFT
- Production /Injection Tests with Completion String

The deployment of any of the well test method is dependent on the objective of the well test and highly determined by environment, safety, time and cost [18]. The volume of producible fluid from the test method is very important as this defines the depth or radius of investigation of the reservoir. This makes WFT restricted compared to DST and Production tests, as just the near wellbore vicinity can be investigated with this method. A summary of DST and WFT types with pros and cons are meticulously addressed in the literature [17], [19], [16], [18], [20].

1.2.1 Methodology of Reservoir Test Analysis

The methodology of reservoir test analysis is classified under two groups, all based on what information is known about the reservoir. These include: the inverse and the direct problem.

Inverse (reverse) Problem

The inverse problem is characterized as the method of performing well test data analysis for reservoirs with unknown behavior and has therefore a huge role in the characterization of the reservoir. Here, the objective is to derive the interpretation model from the responses of the reservoir in question by constantly verifying conceptual models which exhibit the same qualitative characteristics as the system response [21]. Any false interpretation of the response at this stage will lead to wrong forecasting and poor reservoir management. The more complex the reservoir, the more difficult it is to identify the right model for the system, as ambiguity and non-uniqueness of the solution usually arises, also intensified by the interpretation method implemented. However, conceptual models have to be developed in order to properly identify the right reservoir model. Moreover, since diagnostic or derivative plots [22] gained wide use in model identification, and more recently the application of Deconvolution techniques [23], the identification process is becoming relatively less cumbersome. Nonetheless, for this work, we will limit to simpler techniques as the complex reservoir behavior of hydrates needs to be addressed first before more rigorous methods like the Convolution, Deconvolution and Non-linear parameter estimation techniques [16] and their applicability are later investigated.

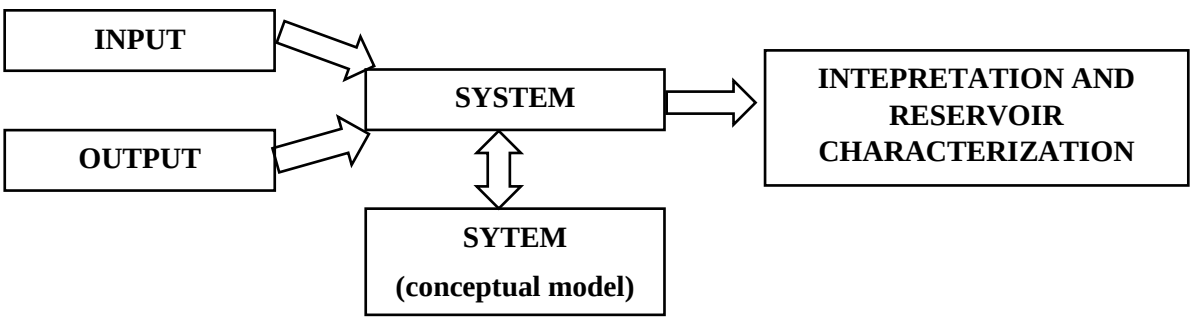

Here the reservoir (system) characterization is derived from the measured reservoir response (output) as a result of producing the well (input).

Direct (forward) Problem

In the direct problem, the reservoir model is known and hence analytical methods can be used to easily solve the problem. Here, if any of the well test interpretation techniques are properly applied for the known reservoir, the same results for the parameters will be achieved [21]. It should be noted that at this level and due to the absence of field data in this work, just the direct problem can be addressed. However, if the conceptual models are properly developed to represent the hydrate reservoir behavior, well test analysis with the indirect method becomes easier.

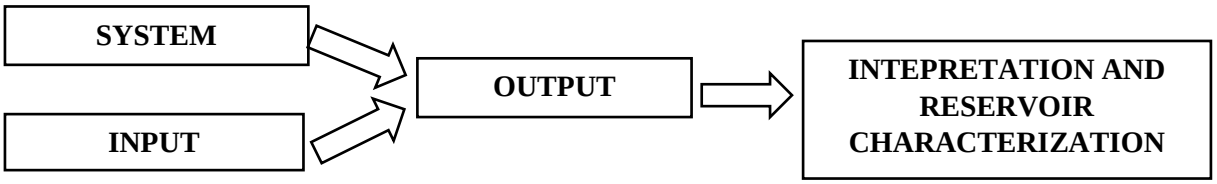

The workflow for the application of these methods is summarized once more below:

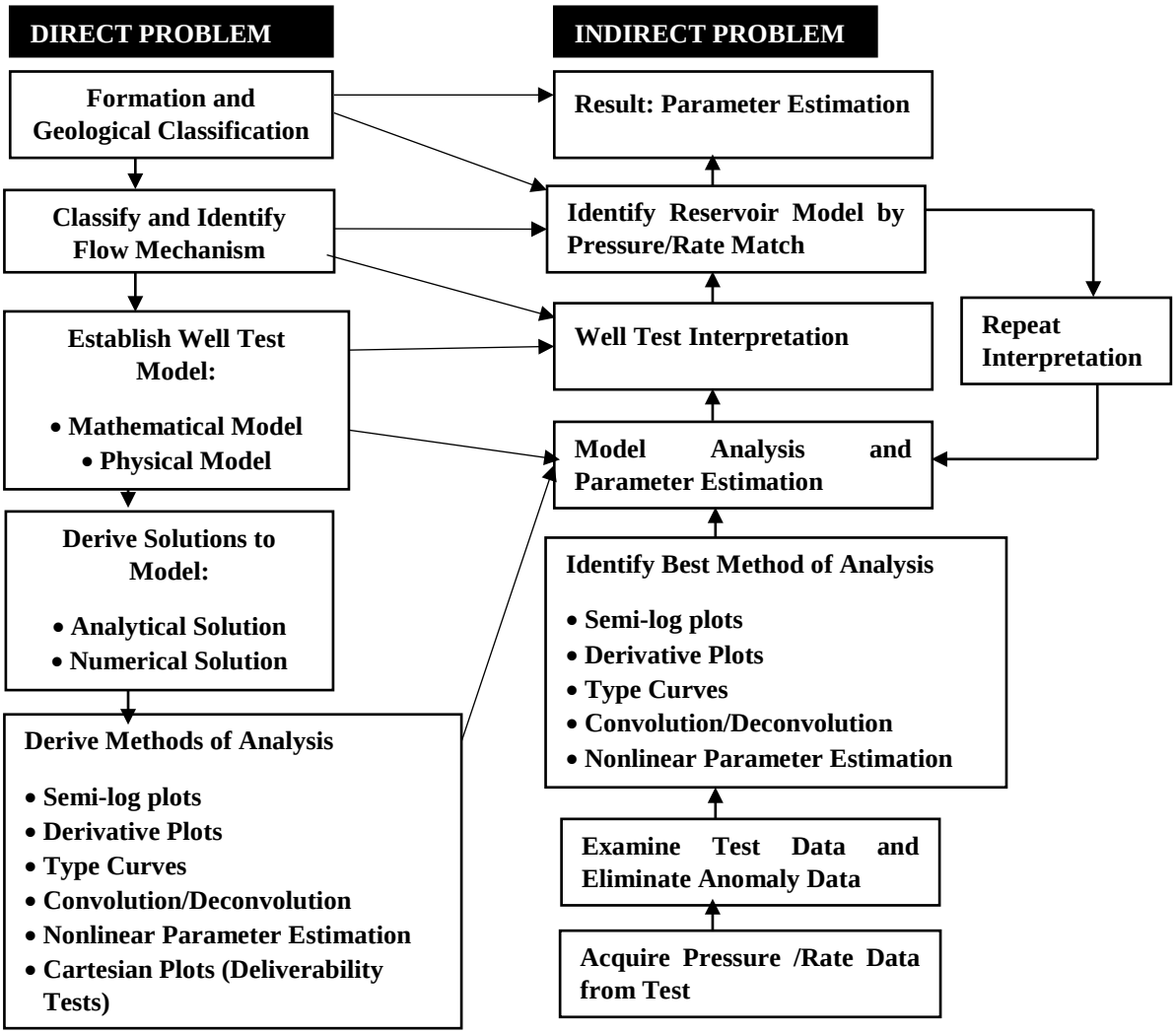

Figure 9: Methodology of Reservoir Test Analysis [modified after [24]]

The input which refers to the method of triggering reservoir response could either be a production or injection process, all depending on the purpose of the test. Be it injection or production methods, the controllable input parameters for the test are either the pressure or the flow rate. It should be emphasized that gas hydrate reservoirs are prone to two phase flow during the testing phase, hence assuring constant sandface rates might not be practically feasible. On the other hand, the dissociation of the hydrates is pressure dependent and hence regulating the downhole pressure for example with a downhole pump would be more effective for the dissociation process. Nonetheless, the conceptual models developed later will address both methods.

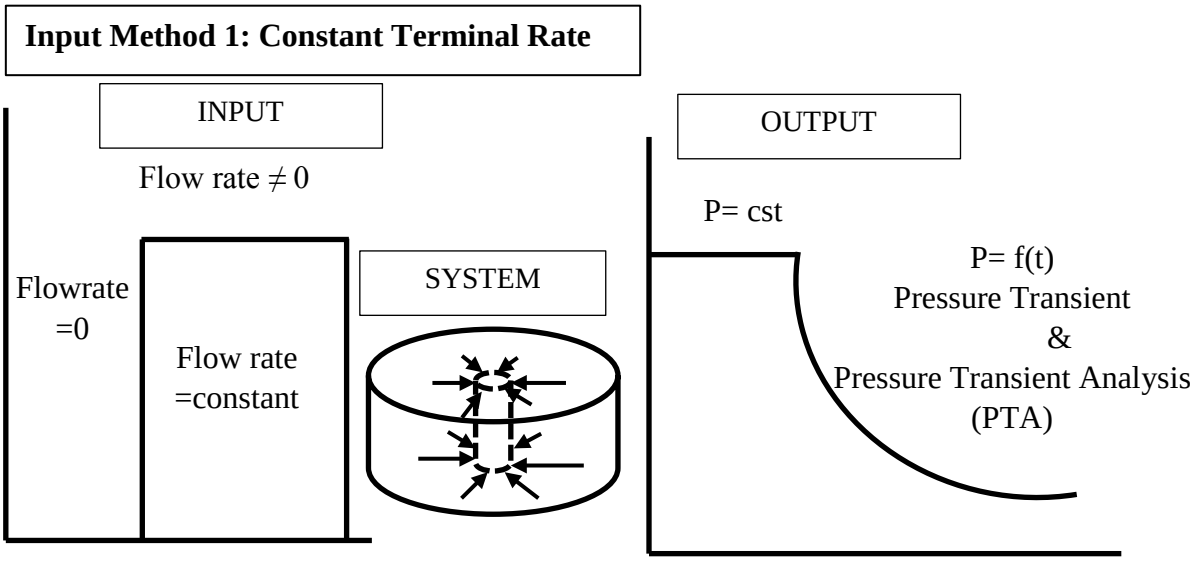

Figure 10: I-S-O for Constant Terminal Rate

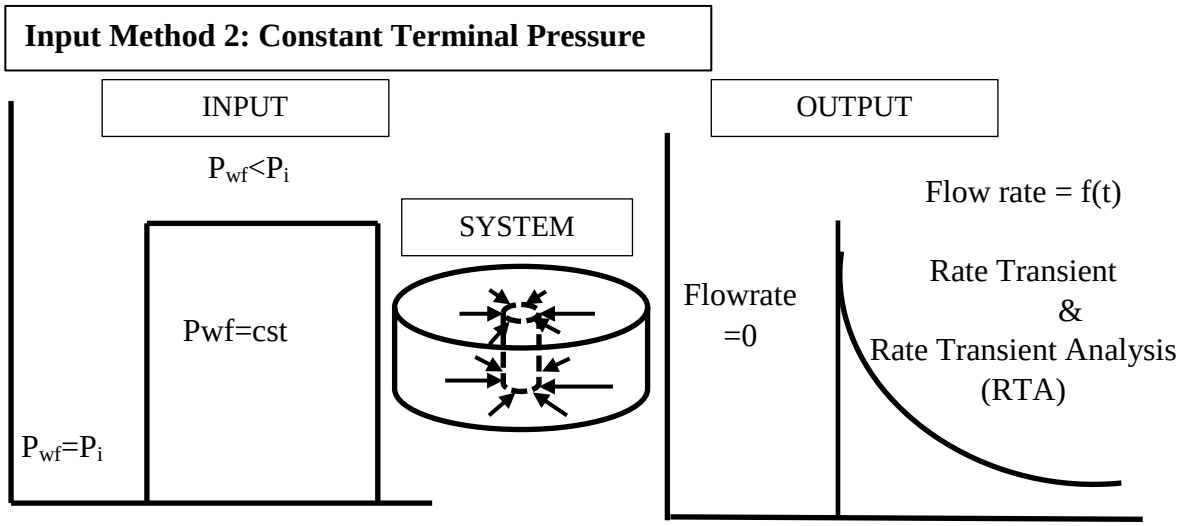

Figure 11: I-S-O for Constant Terminal Pressure

1.2.2 Methods of Analyzing Well Test Data: State of the Art

Reservoir testing and analysis are fundamental tools in understanding reservoir fluid dynamics. Nonetheless, the characterization and derivation of reservoir parameters requires a representative conceptual model for the reservoir hydraulics during different flowing conditions. From the

conceptual models the choice of the method of analysis is built to qualitatively investigate the behavior of the reservoir.

Methods of analysis can be classified under the following groups:

- Straight Lines or Semi-log Plots
- Type Curves
- Derivative Plots
- Deconvolution/Convolution
- Non-linear Parameter Estimation

Each of the above methods can be classified according to the accuracy of the analysis of well test data and hence quality interpretation and characterization of the reservoir. Table 3 depicts the different methods of analysis and strength in identifying reservoir parameters.

Table 3: Ranking of Well Test Interpretation Methods, after [21]

Date	**Analysis Method**	**Identification**
50s	Straight lines	Poor
70s	Pressure Type Curves	Fair
80s	Pressure Derivative	Very Good
Early 00s	Deconvolution	Much Better

Before the derivative or diagnostic plot became an indispensable and powerful tool in the analysis of well test data, other methods of analysis such as semi-log straight line and type curves existed. The evolution of new methods of analysis was backed by the growing complexity of the reservoir responses, whereby straight line plots were difficult to obtain, heterogeneity and reservoir boundaries were cumbersome to identify.

As will be shown later the following methods will be addressed for the characterization of gas hydrate reservoirs:

- Solutions in Real Time Domain (Approximate Solutions to the Conceptual Models)
    - semi-log
    - type curves
    - derivative
- Solutions in Laplace Domain (Exact Solutions to the Conceptual Models)
    - Laplace Domain Well Test Model Recognition Type Curves
    - Laplace Domain Well Test Model Recognition Derivatives

Although conventional methods such as the semi-log analysis and type curves in real time domain have been addressed in this work, their limitations could be very significant due to the complex

behavior of the hydrate formations. However, the robust Laplace Domain Well Test Model Recognition method proposed by [25] has proven to be a very effective tool in characterizing and identifying different reservoir responses. Moreover, the application of derivatives in Laplace Domain gives a much clearer representation of the different flow regimes during the hydrate dissociation process.

The absence of field data makes the application of Deconvolution techniques or nonlinear parameter estimation not practically feasible at this level. Although this method is becoming very useful and robust in the interpretation process, it is still very rigorous at this level and also involves computer aided analysis. Nevertheless, the methodology and development of algorithms are explicitly addressed in several literatures including [23], [26], [27], [16], [28].

Note that the ranking in Table 3 is based on analysis of pressure transient data and shows that very much has been done with regard to pressure transient analysis (PTA), which is not the case in rate transient analysis (RTA), as PTA has been implemented over decades in the oil and gas industry while RTA is still in its juvenile phase. Nonetheless, huge efforts are being made to qualitatively improve on the methods of RTA, especially during infinite acting radial flow (IARF).

As will be shown later, rate transient models have been developed to investigate the response of the hydrate reservoirs when subjected to constant wellbore pressure. This is very vital in gas hydrates as a controllable dissociation of the hydrates is comparatively guaranteed using this method.

1.3 Reservoir Testing Challenges in Gas Hydrate Reservoirs

The complexity of reservoir response when producing from gas hydrate reservoirs is a known phenomenon. This is reflected in the endothermic dissociation of the hydrates, gas and water generation from the dissociation process and the two phase flow in the reservoirs. Moreover, the hydrate layers are known to be unconsolidated which makes the choice of the wellbore flowing pressure for dissociation very crucial to mitigate sand production. The choice and design of a well test in such a reservoir should hence be carried out with great precaution.

Well test designs are carried out for each reservoir type in question, which means a characteristic behavior of the reservoir needs to be known for a proper design process.

Though the dissociation of gas hydrates is conventionally handled similarly to the classical Stefan problem of melting ice, several other problems may be encountered depending on the reservoir type in question. It is still important to depict the main groups under which gas hydrate reservoirs are classified.

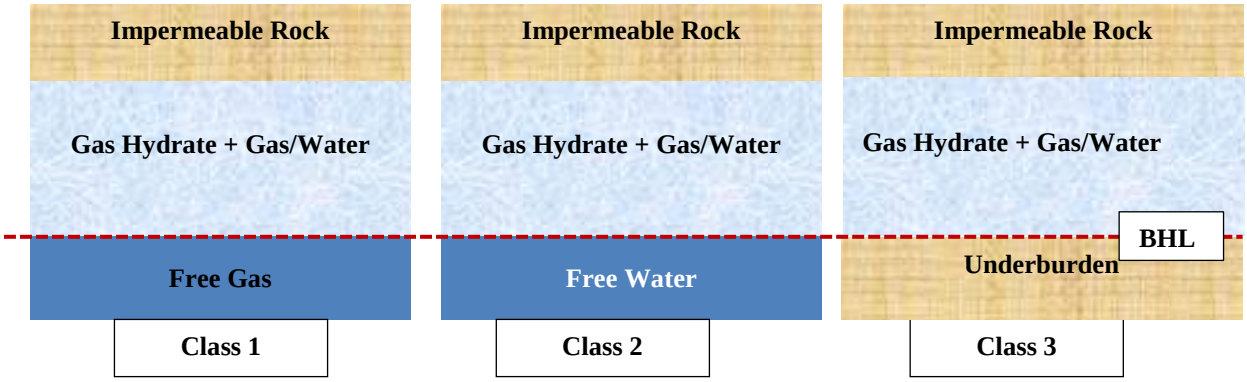

Figure 12: Gas Hydrate Reservoir Classification [after [29]]

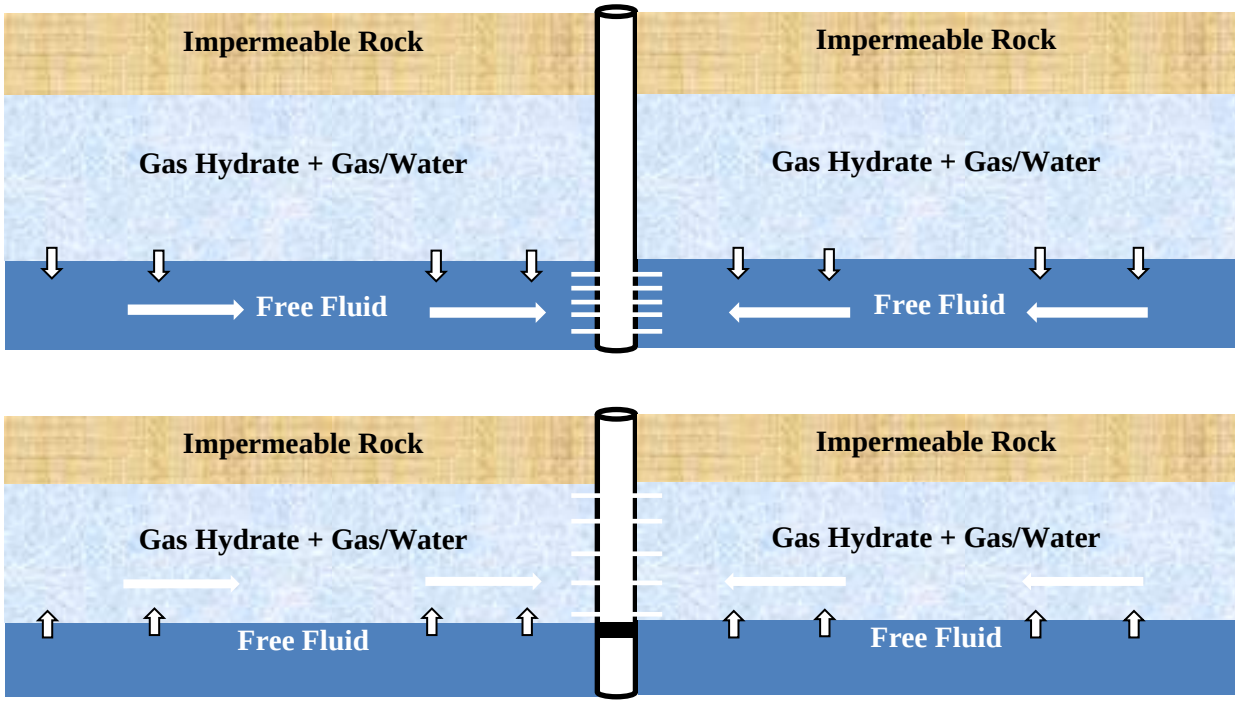

Figure 13: Crossflow Problems in Class 1 and 2 Gas Hydrates

Figure 13 depicts crossflow problems which might be encountered when producing from Class 1 and 2 gas hydrate reservoirs. Producing from the free fluid layer below the hydrate layer will cause pressure depressions in both layers and hence instigate hydrate dissociation. If the permeability of the free fluid layer is much higher than the hydrate layer, production will preferably be done from this layer as pressure propagation in the reservoir would be much faster compared to if production was carried out in the hydrate layer. The free fluid layer would act like conventional reservoirs and the crossflow problem could be better characterized. Conventionally, type curves are used for analysis of such reservoirs. Nonetheless using type curves for such reservoirs requires detailed characterization for the reservoir response, especially for the hydrate zone. On the other hand, production from the hydrate layer for such a reservoir type has two main problems to deal with. The first problem would be the gas and water masses released from the hydrate dissociation process, which could increase the pressure in

the reservoir as this would act like a source term in the hydrate layer, all depending on the hydrate dissociation rate. Furthermore, if crossflow problems embark, further distortion of production data could occur, where fluid influx is expected from the free fluid layer and increased hydrate dissociation due to the warmer fluid from the free fluid layer. Though both hydrate dissociation and crossflow problems could be quantified in a diffusivity problem and a well test model developed, the analysis of such reservoir responses to get reservoir parameters is cumbersome as will be seen later.

The hydrate dissociation is known to be dependent on the hydrate equilibrium pressure, which is a function of the reservoir temperature. For Class 1 and 2 gas hydrates, the presence of fluid below the hydrate layer marks the point of hydrate stability and hence the equilibrium pressure for hydrate dissociation. In such reservoirs and for developing reservoir testing models, the equilibrium pressure can be attributed as being approximately equal to the reservoir pressure at the crossflow point. For convenience, these reservoirs will be called normally pressured gas hydrate reservoirs. In Class 3 gas hydrates, the same assumption cannot be made due to the absence of free fluid beneath the hydrate layer. In this case, the equilibrium pressure for hydrate dissociation becomes very sensitive to the geothermal gradient. Figure 14 depicts such a behavior.

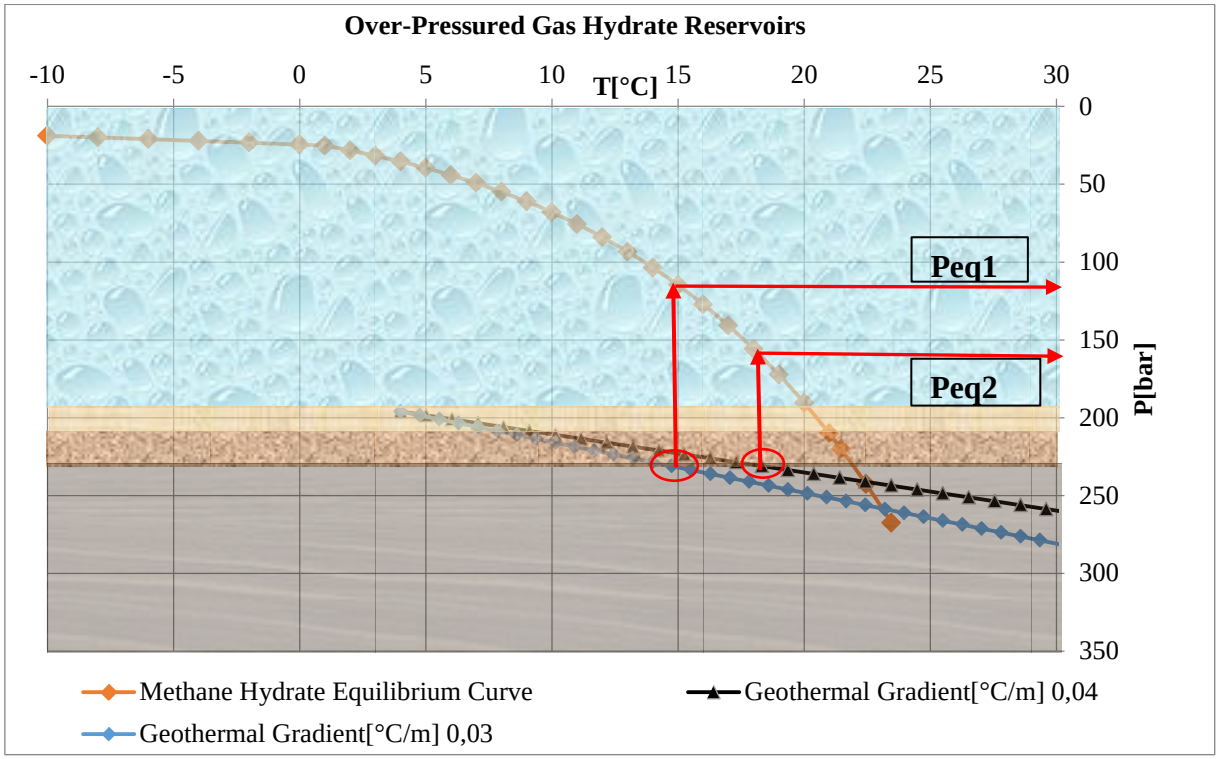

Figure 14: Sensitivity of Equilibrium Pressure with Geothermal Gradient [30]

Gas hydrate reservoirs with reservoir pressures above the equilibrium pressures will be called over-pressured gas hydrate reservoirs. The behavior and development of well test models for such reservoirs must be done with precaution. Conceptual models for such reservoir responses will be depicted later.

To conclude, Class 1 and 2 gas hydrates could be further classified as normally pressured hydrate reservoirs and crossflow is possible in these reservoirs. Class 3 gas hydrates could be normally pressured or over-pressured, depending on the geothermal gradient. Crossflow problems here are excluded. Due to the different responses expected from each reservoir type, well test design and analysis have to be carried out depending on the reservoir type in question. The different well test models for the different reservoir types will be handled in detail later.

1.3.1 Sand Production

Hydrate reservoirs are usually classified as unconsolidated formations, which means the formation stability is low and the formation is prone to sand production if measures are not taken to mitigate this. On the other hand, the dissociation of hydrates to produce gas and water is highly pressure and temperature dependent. The higher the pressure depression, the more hydrates will dissociate to the byproducts gas and water. Very high pressure depressions could be very detrimental in the stability of the formation, which implies, sand production cases should be considered in the design process of the well test.

1.3.2 Secondary Hydrate Formation in Tubing

High pressures and low temperatures in the tubing would provide favorable conditions for hydrates to form during production of the two phase fluid system. Although depressurization at the sandface will cause unfavorable conditions for hydrate formation, the decrease in temperature from the endothermic dissociation could influence the formation of the hydrates. Moreover, if pumps are used for depressurization and to lift the fluids to the surface, the increase in pressure at the pump outlet coupled with the low temperature of the produced fluids (if the heat generated by the pump has little significance) could highly influence the formation of secondary hydrates in the production string.

The formation of hydrates in the production string could highly affect the quality of the well test data and furthermore, workover interventions might be needed to remove the hydrate plug in the production string.

1.3.3 Hydrate Dissociation Model

Hydrates will dissociate to water and gas, meaning the hydrate dissociation process is basically a source of water and gas in the porous medium. Describing the diffusivity equation therefore requires a good description of the source term (hydrate dissociation); such that reservoir responses during pressure depletion could be characterized and as such well test models derived for estimating reservoir parameters. As of now, two main models exist in characterizing the hydrate dissociation rate.

Kinetic Model

The Kinetic Model for hydrate dissociation was developed by [31] based on laboratory experiments. The model depicts the relationship between hydrate dissociation rates and pressure depressions. The model proposed is given thus (see Appendix 1 for details):

$$\frac{dn_h}{dt} = K_d A_H (p_{eq} - p) \quad 1.1$$

With: K_d [kmol/m²Pas], A_H [m²], p [Pa], n [kmol]

The kinetic model is readily modified to:

$$\frac{dm_H}{dt} = K_d M_H A_H (p_{eq} - p) = K_o e^{\left(\frac{-E}{RT}\right)} M_H A_H (p_{eq} - p) \quad 1.2$$

As also depicted in Appendix 4, the kinetic model reflects the dissociation of hydrates considering a continuous constant source of heat energy, which limits the different sources of heat energy supplied by the reservoir for hydrate dissociation as seen with the equilibrium model described in Appendix 1. Hence the kinetic model encompasses all heat flux parameters and hence no further heat flux terms are required when using the kinetic model. However, the wrong choice of the dissociation rate might either overestimate or underestimate the rate of hydrate dissociation as defined by the equilibrium model. Hence precaution should be taken when using the model in numerical simulators. For this reason dimensionless parameters will be used to the conceptual models such that the reservoir behavior under different dissociation conditions is characterized.

Equilibrium Model

The equilibrium model is an energy balance model which quantifies the heat energy available in the reservoir and the quantity used up for every pressure depression. The model relates the dependence of changes in reservoir heat energy with pressure and the energy required in dissociating the hydrates. The application of the model at reservoir scale is much easier as the reservoir parameters can easily be quantified; however, the reservoir testing model developed with the equilibrium model is more complex as will be seen later. For numerical modeling purposes, where heat flux is better quantified, the equilibrium model could be very useful as this better quantifies the heat energy in the reservoir and the difficulty in quantifying the activation energy (E) and intrinsic rate constant (K_o) in the kinetic model from laboratory scale to reservoir scale is avoided. Details on the equilibrium model are given in Appendix 1-Appendix 4 for different production scenarios

1.4 Objectives and Structure of Thesis

Objectives of Thesis

From the various aspects and challenges addressed with regard to the hydrate behavior and problems involving well testing in these reservoirs, the following are main objectives of this thesis:

- Develop conceptual models for gas hydrate reservoir testing which should aid in the interpretation and characterization of gas hydrate reservoirs.
- Quantify different parameters which will affect the hydrate reservoir response during production.
- Understand reservoir responses during production from different hydrate reservoir types.

- Investigate the behavior of the hydrate reservoirs with different productions scenarios based on dimensionless parameters.
- Investigate the influential parameters during hydrate dissociation and identify the possible influence on reservoir response.
- Identify non-linear reservoir parameters which might be very determining in applying future more rigorous methods of analysis such as Deconvolution or nonlinear parameter estimation methods.
- Assist numerical simulators in narrowing down uncertainties of reservoir parameters and behavior from production data and hence reducing the non-uniqueness of the indirect reservoir test analysis.

Structure of Thesis

Chapter 2 summaries the challenges and methodology involved in developing conceptual models in these reservoir, which are also addressed in detail in the appendices.

Chapter 3 gives an overview of the approximate solutions to normally pressured class 3 gas hydrate reservoirs with conventional methods of analysis applicable to specific reservoir responses.

Chapter 4 depicts the behavior over-pressured class 3 gas hydrate reservoir using similarity solutions (approximate solutions).

Chapter 5 addresses crossflow problems in class 1 and 2 gas hydrate reservoirs considering the possibility of producing from either the free fluid layer or the hydrate layer. Approximate solutions in real time domain and conventional methods of analysis are addressed here.

Chapter 6 summarizes and concludes this thesis.

Appendices give a detailed derivation of the conceptual models for gas hydrate reservoirs. Bourgeois and Horne Laplace domain well test model recognition method is addressed in detail for each reservoir type, which gives a distinctive picture of the complexity of the reservoir behavior for each reservoir type and a much better approach for reservoir characterization.

2 Well Testing Models in Gas Hydrate Reservoirs: Challenges and Methodology

As described briefly in Chapter 1, production from hydrate reservoirs and the derivation of well test models requires great precaution. The challenges faced with the derivation of conceptual models for these reservoirs are summarized below:

- From the mass conservation principle used in deriving well test models, the hydrate dissociation would be the source term in the diffusivity equation which is also endothermic. Note that in conventional oil and gas reservoirs, source/sink terms are not commonly addressed in reservoir testing models; moreover, the effect of endothermic process means the temperature during depletion is not constant like in conventional reservoirs.
- Due to the hydrate dissociation byproducts, i.e. gas and water, we have two phase flow at almost all times, provided the prevailing pressure is below the hydrate equilibrium pressure. This implies multiphase flow has to be considered in all the models developed.
- The presence of gas in the system implies the consideration of the compressibility effects with changes in pressure and temperature.
- The endothermic process during dissociation requires the consideration of heat flux in deriving the well test model, which implies an energy balance approach to quantify the rate of heat consumption for hydrate dissociation has to be applied. Note that isothermal conditions are usually considered in conventional gas reservoirs, which cannot be applied here.

The dependence of most compressible and slightly compressible fluids with pressure in oil and gas reservoirs triggers non-linear reservoir response, as pressure transient also affects reservoir fluid properties. This problem was an issue of focus for many decades in the oil and gas industry till Al-Hussainy [32] introduced the use of the Kirchhoff transformation in linearizing the diffusivity equation in gas reservoirs. A further method of addressing the non-linearity of the diffusivity equation with the Kirchhoff transformation was given by Agarwal [33] to address the problem of the changes in the storativity term with time and pressure. In most of these methods, the permeability or effective permeability of the fluids was considered constant and pressure independent. In recent years, with the outburst of unconventional reservoirs or even conventional gas condensate reservoirs, the dependence of the effective permeability of the phases became crucial and needed to be addressed. Multiphase pseudo-pressures were then developed which addressed these effects (see Chapter 2.2 for details).

The problem of the dependence of the absolute permeability or effective permeability with pressure is similar to concentration dependent diffusion coefficient problems addressed by many authors including [34], [35], [36], [37], [38] . The authors proposed complex analytical solutions to the non-linear diffusivity equation, most of which were solved by applying the Boltzmann transformation. It should be emphasized that most of these mathematical methods considered single fluid phase

diffusivity problems which has however become obsolete in most diffusivity problems existing today, whereby multiphase fluid flow has become a standard process.

In gas hydrate reservoirs, the problem of gas and water flow has to be addressed at almost all production stages, as the hydrates will dissociate to gas and water; moreover, the hydrate layer could be partly filled with water and gas. This gives the first source of the non-linear behavior. Secondly, the endothermic dissociation of the hydrates causes temperature drop, increase in fluid saturation and effective permeability. This implies, for a proper linearization of the diffusivity equation for gas hydrate reservoirs, these processes need to be identified and quantified in the diffusivity equation.

Depending on the type of gas hydrate reservoir, different responses could be monitored during production. In Class 1 and 2 gas hydrates, crossflow behavior is very possible and hence crossflow problems would be addressed later. In Class 3 gas hydrate reservoirs, depending on the well test method or the equilibrium pressure of the hydrate layer, different characteristic behaviors will be observed such as the moving boundary problem which will be addressed in detail later.

Deriving the solution to non-linear diffusivity equations is gaining great interest in the oil and gas industry due to the complex responses observed with unconventional oil and gas reservoirs.

For gas hydrate reservoirs, the following approaches will be made in deriving the solution to the complex behavior:

Linearization

- Kirchhoff Transformation for the Multiphase Pseudo-pressure

The pressure dependent parameters in the diffusivity equation will be linearized using the Kirchhoff transformation, analog [32] for gas pseudo-pressure and for two phase pseudo pressure in gas condensate reservoirs [39], [40]. This is further addressed in Chapter 2.2. Note that although the pressure dependent diffusion coefficient, reflected later in the mass balance model (MBM) or volumetric material balance model (VMBM), is linearized using the Kirchhoff transformation, the conceptual model for the gas hydrate has to address the changes in the multiphase pseudo-pressure as a result of the dissociation effects as will be seen later.

Solutions

- Boltzmann Transformation (Similarity Solution)
- Laplace Transformations

The solutions for the diffusivity equation will be derived in dimensionless parameters using both the Boltzmann Transformation and the Laplace Transformation for the following boundary conditions:

Inner Boundary Conditions

- Constant Rate Inner Boundary (CRIB) or Constant Terminal Rate (constant mass rate).

Unlike in conventional oil and gas well test models, the solutions presented here will be given in pseudo-pressure and constant mass rate. The definition of the pseudo-pressure will be given later.

- Constant Pressure Inner Boundary (CPIB) or Constant Terminal Pressure (constant multiphase pseudo-pressure)

To develop the rate transient solutions using the CPIB, constant multiphase pseudo pressure conditions are imposed on the wellbore, which is a preliminary to applying further well testing methods like Deconvolution for changing inner boundary situations.

Outer Boundary Conditions

In deriving the solutions to the diffusivity equation, the following reservoir outer boundary conditions are considered

- Infinite Acting Reservoir (IAR): $r \to \infty$; $z \to \infty$
- Constant Pressure Outer Boundary (CPOB): $\left(\frac{dp}{dr}\right)_{r_e} > 0; (dp)_{r_e} = 0$
- No-Flow Outer Boundary (NFB): $\left(\frac{dp}{dr}\right)_{r_e} = 0$
- Constant Temperature Outer Boundary (CTOB): $\left(\frac{dT}{dz}\right)_{z_e} > 0; (dT)_{z_e} = 0$
- Pseudo No-Flow Temperature Boundary: $\left(\frac{dT}{dz}\right)_{z_e} = 0$

To investigate the effects of the reservoir boundaries on the wellbore response, the image well theory is usually applied to the infinite acting solutions of the diffusivity problem. Note that the image well theory proposed by [41] is one of the most widely used methods of investigating the wellbore response of a reservoir with different kinds of boundaries as seen in the works of [41], [42], [43], [44]; however, it is gradually being replaced by the use of Green´s functions. Although solutions for just single boundaries are addressed in this work, it is important to develop a general solution for which the image well theory could be investigated in future works. The image well theory is briefly discussed in Appendix 8 for both similarity and Laplace domain solutions.

On the other hand, most of the solutions presented in this work for bounded reservoir using the Bessel´s functions address reservoirs completely bounded by either a recharge or no-flow boundary but not both, for which the well is located at the center. For this reason, the reservoir responses are quite different from those derived with a single boundary using the image well theory.

2.1 Kirchhoff Transformation

In reservoir engineering, the Kirchhoff transformation is as of date, one of the most widely applied methods of linearization of non-linear diffusivity equations. Its application is very much seen in describing well test models in gas, gas condensate and Coalbed methane (CBM) reservoirs where the

fluid properties and flow are strongly pressure dependent. The diffusivity equation below depicts the application of the transformation.

$$\frac{1}{\mathrm{r}}\frac{\partial\left(\mathrm{r}*\mathrm{D(p)}\frac{\partial \mathrm{p}}{\partial \mathrm{r}}\right)}{\partial \mathrm{r}} = \frac{\mathrm{S}}{k}\frac{\partial \mathrm{p}}{\partial \mathrm{t}} \qquad 2.1$$

From the above equation, the diffusion coefficient is pressure dependent. Instead of incorporating the pressure dependent function of the diffusion coefficient, the Kirchhoff transformation is used. Although the use of the Kirchhoff transformation is a well-established method of solving many mathematical problems such as the pressure dependent diffusion coefficient problems [38], it only gained huge significance through the works of [32] and [45]. Unlike other models such as the solutions of [35] and [46] where the diffusion coefficient is assumed to behave in a particular manner and the diffusivity equation solved, the Kirchhoff transformation offers the use of arbitrary functions of the pressure dependent diffusion coefficient. The transformation is given below.

$$\varphi = \int \mathrm{D(p)dp} \qquad 2.2$$

The Kirchhoff transformed diffusivity equation is hence:

$$\frac{1}{\mathrm{r}}\frac{\partial\left(\mathrm{r}\frac{\partial \varphi}{\partial \mathrm{r}}\right)}{\partial \mathrm{r}} = \frac{\mathrm{S}}{\mathrm{kD(p)}}\frac{\partial \varphi}{\partial \mathrm{t}} \qquad 2.3$$

$$\frac{1}{\mathrm{r_D}}\frac{\partial\left(\mathrm{r_D}\frac{\partial \varphi}{\partial \mathrm{r_D}}\right)}{\partial \mathrm{r_D}} = \frac{\mathrm{S}}{\mathrm{kD(p)}}\mathrm{r_w^2}\frac{\partial \varphi}{\partial \mathrm{t}} \qquad 2.4$$

$$\frac{1}{\mathrm{r_D}}\frac{\partial\left(\mathrm{r_D}\frac{\partial \varphi}{\partial \mathrm{r_D}}\right)}{\partial \mathrm{r_D}} = \frac{1}{\mathrm{a(p)}}\frac{\partial \varphi}{\partial \mathrm{t}} \qquad 2.5$$

$$\frac{1}{\mathrm{r_D}}\frac{\partial\left(\mathrm{r_D}\frac{\partial \varphi}{\partial \mathrm{r_D}}\right)}{\partial \mathrm{r_D}} = \frac{1}{\mathrm{a(p_i)}}\frac{\mathrm{a(p_i)}}{\mathrm{a(p)}}\frac{\partial \varphi}{\partial \mathrm{t}} \qquad 2.6$$

Although the pressure and the diffusion coefficients have been linearized, the diffusivity coefficient can still be pressure dependent. Since the pressure in the reservoir is a function of time and radius, [33] proposed the use of the pseudo-time integral by similarly applying the Kirchhoff transformation to the time function. Nonetheless, the Agarwal pseudo-time considered just the dependence of the Storativity, S; with pressure since gas reservoirs were considered. For incompressible fluids, the storativity, S, is approximately constant or pressure independent, but this is not the case for compressible fluids such as gas. For this reason, the pseudo-time is usually written thus:

$$\mathrm{t_a} = \int \frac{\mathrm{a(p)}}{\mathrm{a(p_i)}}\mathrm{dt} \qquad 2.7$$

The precondition in applying these transformations is the functions in the integrals could be derived for a given pressure. Recent innovations in the computation of pseudo-time for single phase gas reservoirs are given in [47].

With the transformation of time and pressure using the Kirchhoff transformation, the equation is easily simplified to the linearized form thus:

$$\frac{1}{r_D}\frac{\partial\left(r_D\frac{\partial\varphi}{\partial r_D}\right)}{\partial r_D}=\frac{1}{a(p_i)}\frac{\partial\varphi}{\partial t_a} \qquad 2.8$$

$$\frac{\partial^2\varphi}{\partial r_D^2}+\frac{1}{r_D}\frac{\partial\varphi}{\partial r_D}=\frac{1}{a(p_i)}\frac{\partial\varphi}{\partial t_a} \qquad 2.9$$

Linearization of the models is possible using the above methods of pseudo-pressure and pseudo-time, however, analysis of real time and pressure data need a retransformation of the pseudo-parameters into real time and pressure models such that reservoir parameters can be obtained.

Instead of using the Agarwal pseudo-time, other transformations can be made for the diffusivity coefficient (with assumptions) such that the effects of hydrate dissociation on the reservoir response can be investigated, especially when developing type curves. This will be shown in detail later.

2.2 Multiphase Diffusivity Equations for Well Testing

As mentioned earlier, dissociation of hydrates will result to gas and water production; hence, multiphase flow is present in the reservoir at almost all times. For well test analysis, many multiphase models have been developed with time; yet with limitations depending on the validity of mass conservation which is a very useful principle used in many domains of fluid dynamics. The main assumptions common in most multiphase well testing models used are negligible capillary pressure and gravitation effects. With these assumptions, analytical models were proposed to describe multiphase flow in reservoirs. It should be emphasized that existing models have considered several other assumptions to simplify the diffusivity equation as much as possible which has also made their applicability in some cases very limited. The three mainly used models for two-phase flow in the reservoir are given below with validity of mass conservation [48].

2.2.1 Mass Balance Model (MBM)-State of the Art

The MBM, which can also be referred to as the composition model or EOS model type [49], is robust and is derived directly from mass conservation principle and no major simplification of fluid properties or further assumptions apart from the two stated above are made and is as of now the state of the art in addressing multiphase flow in reservoirs. The mass balance model in radial coordinates is given thus:

$$\frac{1}{r}\frac{\partial\left(r*\left(\rho_1\frac{k_1}{\eta_1}+\rho_2\frac{k_2}{\eta_2}\right)\frac{\partial p}{\partial r}\right)}{\partial r}=\emptyset\left(\rho_1 c_{T,1}+\rho_2 c_{T,2}\right)\frac{\partial p}{\partial t} \qquad 2.10$$

The diffusivity equation above is developed from mass conservation principle and since no simplification of the model has been done, mass conservation will always hold for the model.

Using the Kirchhoff transformation, pseudo-pressure models can be developed as also seen in CBM and gas condensate reservoirs. The pseudo-pressure for this model is given thus:

$$\varphi = \int \left(\rho_1 \frac{k_1}{\eta_1} + \rho_2 \frac{k_2}{\eta_2}\right) dp \qquad 2.11$$

The above model is a simplification of the reservoir integral as given by Jones and Raghavan [50] and is the state of the art with regard to pseudo-pressure for multiphase systems also seen in other literature such as [51], [52].

The general methodology of deriving the MBM pseudo-pressure is given in Table 4 for both rate transient and pressure transient. Note that the pseudo-pressure is valid only if the parameters in the pseudo-pressure integral are all pressure dependent.

Table 4: General Methodology of Deriving the MBM Pseudo-Pressure

RTA	PTA
$\dot{m}_t = \dot{m}_g + \dot{m}_w$	$\dot{m}_t = \dot{m}_g + \dot{m}_w$
$\downarrow$	$\downarrow$
$\dot{m}_t = 2\pi rhk\rho_g \frac{k^*_{rg}}{\eta_g}\frac{\partial p}{\partial r} + 2\pi rhk\rho_w \frac{k^*_{rw}}{\eta_w} k \frac{\partial p}{\partial r}$	$\dot{m}_t = 2\pi rhk\rho_g \frac{k^*_{rg}}{\eta_g}\frac{\partial p}{\partial r} + 2\pi rhk\rho_w \frac{k^*_{rw}}{\eta_w} k \frac{\partial p}{\partial r}$
$\downarrow$	$\downarrow$
$\frac{\dot{m}_t(t)}{2\pi hk}\frac{\partial r}{r} = \left(\rho_g \frac{k^*_{rg}}{\eta_g} + \rho_w \frac{k^*_{rw}}{\eta_w}\right)\partial p$	$\frac{\dot{m}_t}{2\pi hk}\frac{\partial r}{r} = \left(\rho_g \frac{k^*_{rg}}{\eta_g} + \rho_w \frac{k^*_{rw}}{\eta_w}\right)\partial p$
$\downarrow$	$\downarrow$
$\frac{\dot{m}_t(t)}{2\pi hk(\varphi_i - \varphi_{wf})}\frac{\partial r}{r} = \frac{\left(\rho_g \frac{k^*_{rg}}{\eta_g} + \rho_w \frac{k^*_{rw}}{\eta_w}\right)\partial p}{(\varphi_i - \varphi_{wf})}$	$\frac{\partial r}{r} = \frac{2\pi hk}{\dot{m}_t}\left(\rho_g \frac{k^*_{rg}}{\eta_g} + \rho_w \frac{k^*_{rw}}{\eta_w}\right)\partial p$
$\downarrow$	$\downarrow$
$\dot{m}_{tD}\frac{\partial r_D}{r_D} = \frac{\partial \varphi}{(\varphi_i - \varphi_{wf})}$	$\frac{\partial r}{r} = \frac{2\pi hk}{\dot{m}_t}\partial\varphi$
$\downarrow$	$\downarrow$
$\left(r_D \frac{\partial \varphi_D}{\partial r_D}\right)\frac{\partial r_D}{r_D} = \frac{\partial \varphi}{(\varphi_i - \varphi_{wf})}$	$\frac{\partial r_D}{r_D} = \frac{2\pi hk}{\dot{m}_t}\partial\varphi = \partial\varphi_D$
$\downarrow$	$\downarrow$
$\varphi_D = \frac{(\varphi_i - \varphi)}{(\varphi_i - \varphi_{wf})}$	$\ln r_D = \frac{2\pi hk}{\dot{m}_t}(\varphi_i - \varphi) = \varphi_D$

The workflow in Figure 15 depicts the methodology of applying the pseudo-pressure in combination with the energy balance model derived in Appendix 1.

2.2.2 Volumetric Material Balance Model (VMBM)

The VMBM which can also be referred to as the black oil model type [[49], [39]] can be considered as a simplification of the MBM with the assumption the fluids have approximately equal densities at standard or norm conditions and the model is given below:

$$\frac{1}{r}\frac{\partial\left(r*\left(\frac{k_1}{B_1\eta_1}+\frac{k_2}{B_2\eta_2}\right)\frac{\partial p}{\partial r}\right)}{\partial r} = \emptyset\left(\frac{c_{T,1}}{B_1} + \frac{c_{T,2}}{B_2}\right)\frac{\partial p}{\partial t} \qquad 2.12$$

Since the densities of gas and water vary vastly from another at standard conditions, the model is not appropriate for gas hydrate reservoirs. If undersaturated oil reservoirs are considered, with oil and water flow, the errors however diminish [48]. The pseudo-pressure for this model is given thus:

$$\varphi = \int \left(\frac{k_1}{B_1 \eta_1} + \frac{k_2}{B_2 \eta_2}\right) dp \qquad 2.13$$

The above model is the obsolete version of the pseudo-pressure used previously to model gas condensate and seen in several publications such as Boe [53].

2.2.3 Perrine Type VMBM

Another type of multiphase pseudo-pressure used for well testing is the Perrine Type VMBM, which is an obsolete multiphase well testing model and a simplification of the MBM with the assumption that the densities of the fluids are approximately equal and pressure independent.

Once more, the pressure of gas is pressure dependent and very different from that of water; this model cannot be used for gas hydrate reservoirs. Nevertheless, with a look at undersaturated oil reservoirs with basically oil and water as multiphase systems, the model can be applied to an extent. If the Perrine [54] mobility is used, the pseudo-pressure for this model is given thus:

$$\varphi = \int \left(\frac{k_1}{\eta_1} + \frac{k_2}{\eta_2}\right) dp \qquad 2.14$$

The pseudo-pressure clearly indicates that the Perrine´s model is a modification of single phase flow model [51] with the assumption of incompressible fluids.

All three models will yield the same results only for a single phase incompressible system. Note that other rigorous multiphase diffusivity equations exist to address capillary pressure effects but still difficult to implement for well test analysis purposes. A scrutiny of various multiphase diffusivity equations is given in [55].

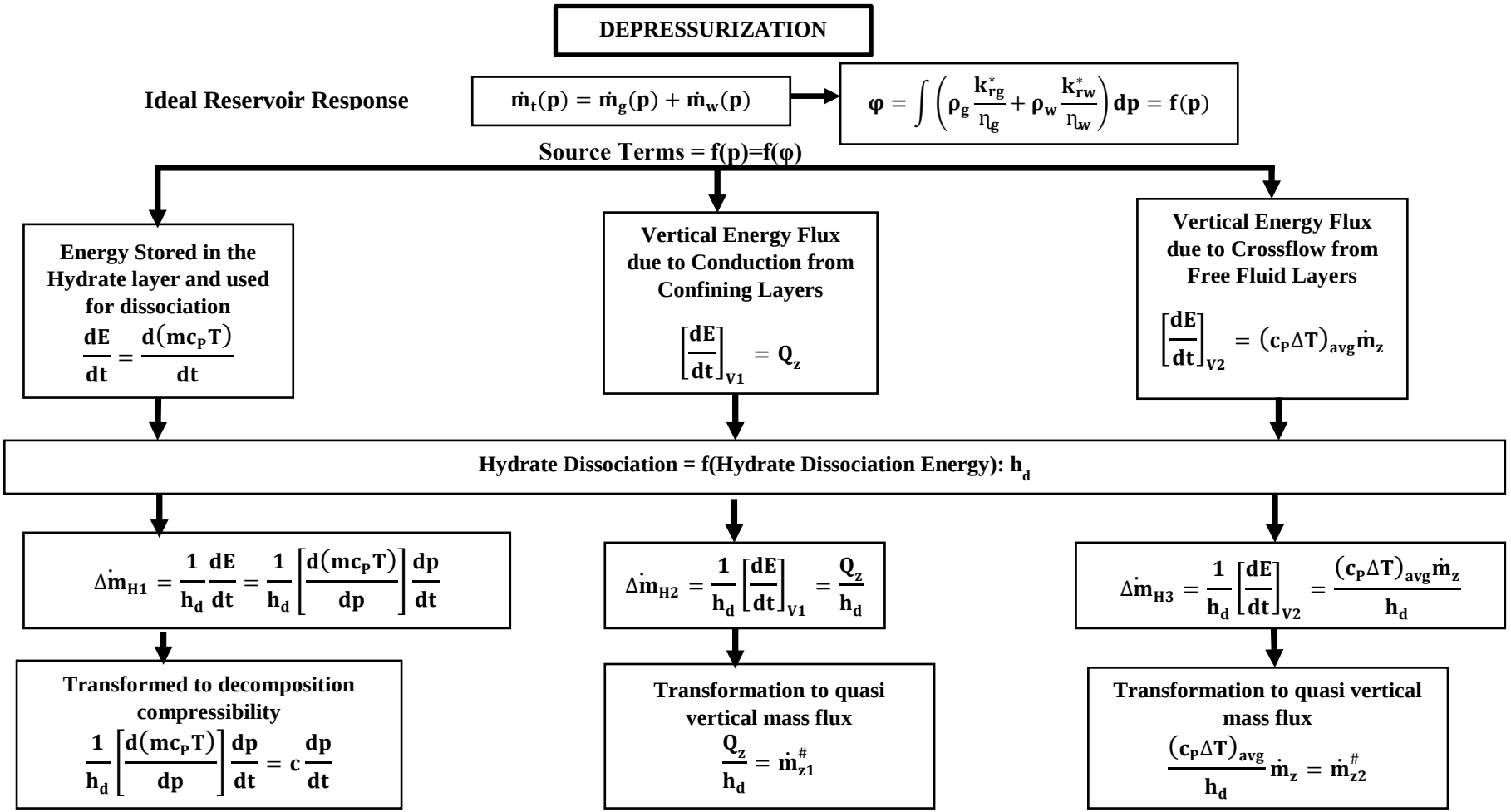

Figure 15: Workflow to Methodology of Applying the MMB Pseudo-pressure and the Energy Balance (Equilibrium) Model

2.3 Heat Conduction and Hydrate Dissociation in Class 3 Hydrates

In Appendix 1, an energy balance model has been used to fully address the heat energy terms responsible for hydrate dissociation. Note that the models are developed based on the assumption that the inner boundary conditions for heat flux can be defined by a Clausius-Clapeyron Type Equilibrium Model, which gives the dependence of pressure depressions to temperature depressions. This implies the temperature profile in the hydrate layer is solely pressure dependent as long as hydrates are present, as dissociation is endothermic and triggered by pressure depressions and also validates the use of a pseudo-pressure model. Figure 16 also gives a comparison of the measured wellbore temperatures from the Mallik gas hydrate production test of 2008 [56] with a Clausius Clapeyron type temperature depression model and we notice a very small deviation between measured data and predicted data (initial pressure of 110.05 bar and initial temperature 11.378°C; hence P_{eq} and $(dT/dp)_{eq}$ can be estimated according to Appendix 3). This further implies the model can be used as a relatively good estimation without huge falsification of the prediction models.

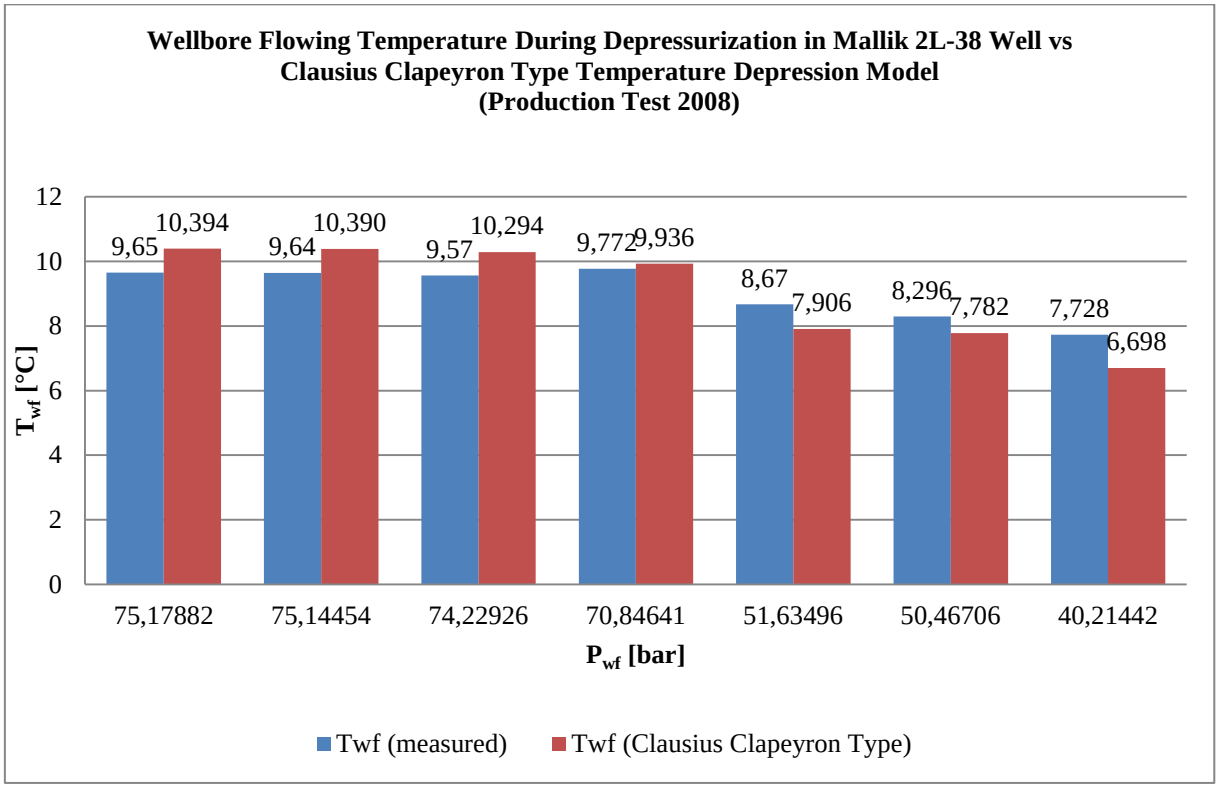

Figure 16: Comparison of the measured wellbore temperatures from the Mallik gas hydrate production test of 2008 (Uddin, et al., 2012 [56]) with a Clausius Clapeyron type temperature depression model

The workflow below depicts the methodology of the application for the Clausius Clapeyron type temperature depression model used in this work.

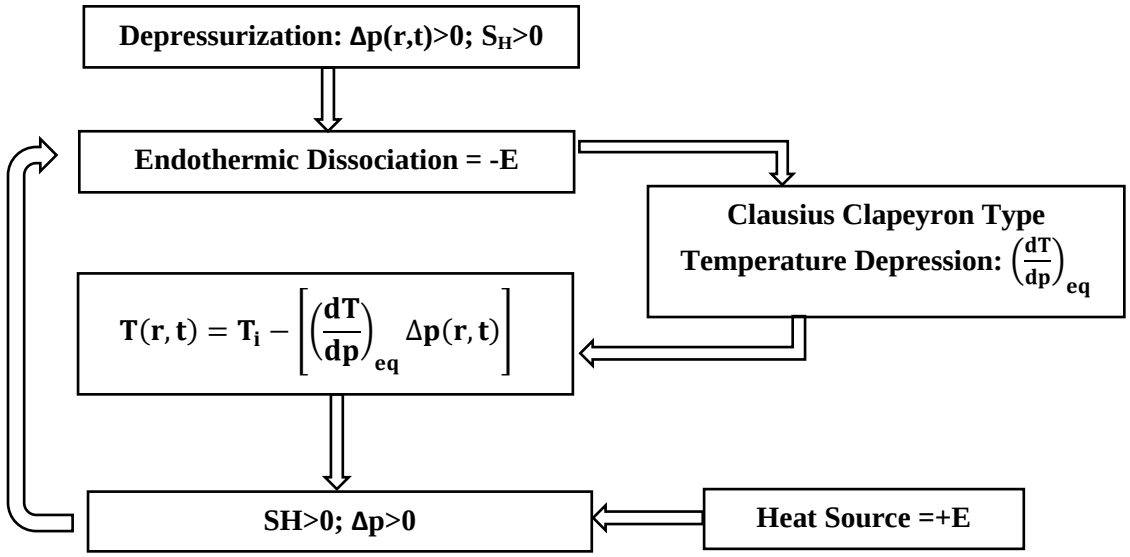

Figure 17: Methodology of the Clausius Clapeyron Type Temperature Depression Model

Using the hydrate prediction model given by [5], the Clausius Clapeyron Type Temperature Depression for Methane hydrate can be deduced as given in Figure 18.

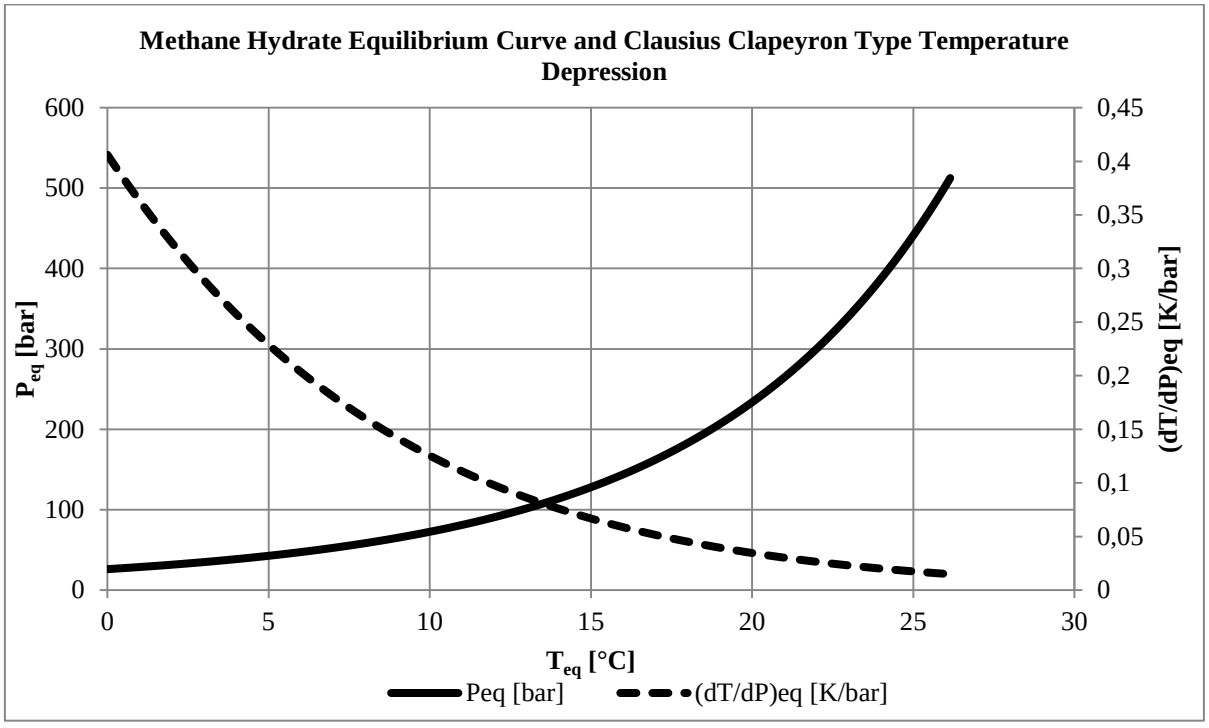

Figure 18: Methane Hydrate Equilibrium Curve and the Clausius Clapeyron Type Temperature Depression Model

From Figure 19 we can deduce that the heat of dissociation lies in the range 500-600 kJ/kg for most offshore gas hydrate reservoirs, i.e. 2-20°C [3]. This also endorses the values given in Table 2 by the different authors.

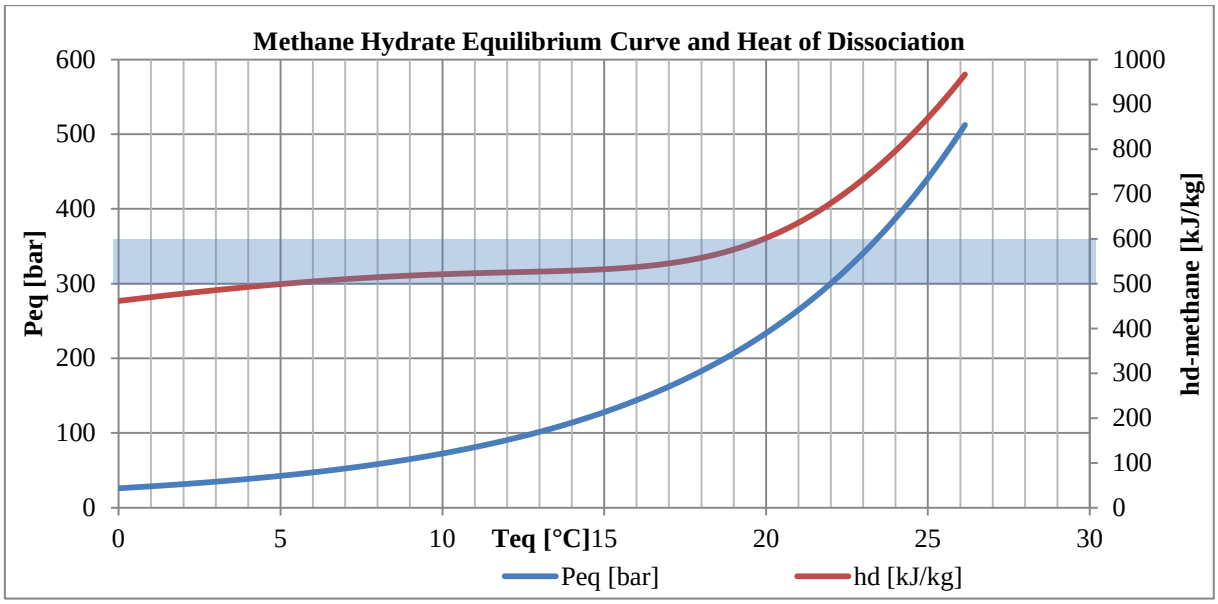

Figure 19: Methane Hydrate Equilibrium Curve and Methane Hydrate Heat of Dissociation

The equilibrium model addresses the heat energy sources responsible for hydrate dissociation, one of which is heat energy through conduction. Depending on the imposed boundary condition in the confining layer, as also given in Appendix 1, heat conduction could be transient, depleting or constant at some stage during production.

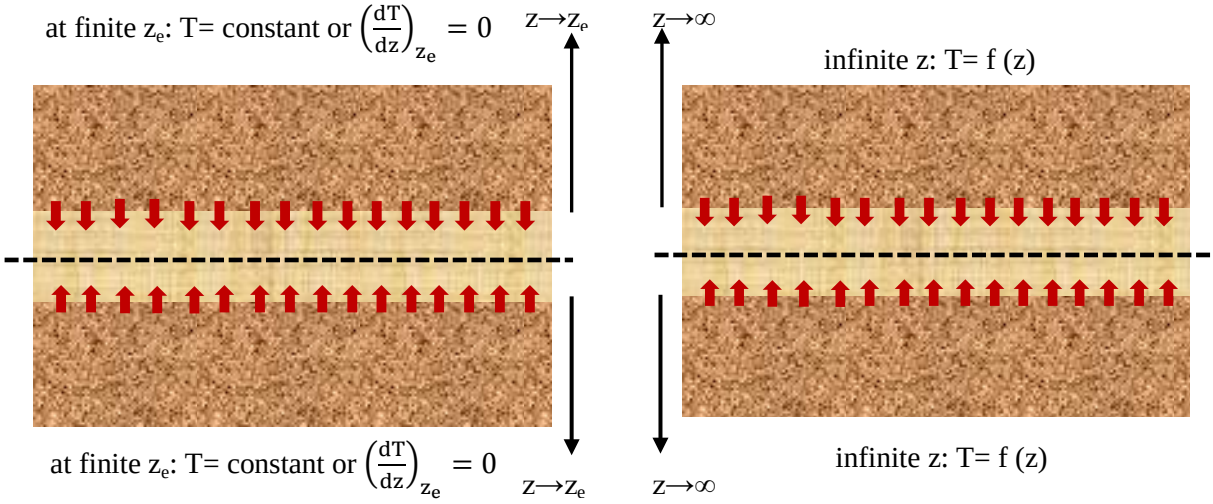

Figure 20: Boundary Conditions for Heat Influx through Conduction (No Fluid Crossflow)

Imposing one of the outer boundary conditions mentioned earlier to derive the rate of heat influx will have a tremendous effect on the rate of hydrate dissociation. Imposing constant temperature outer boundary (CTOB) conditions will imply constant continuous dimensionless heat supply from the top and bottom confining layers for hydrate dissociation at some time during production. Depending on the pressure depression in the hydrate layer and the hydrate saturation, the hydrate dissociation rate could increase significantly. Constant temperature outer boundary conditions will however give very optimistic predictions as this is seldom the case in the reservoir without any heat source to replenish the loss of heat energy at the boundary.

Due to the transient behavior of heat influx, the Laplace transformation would be a very useful tool in developing the solutions to such a problem. It should be noted that the kinetic model assumes constant heat source at all times during hydrate dissociation and is hence equivalent to the CTOB solution at late production times. It is once more worth emphasizing that the heat flux in the infinite acting vertical plane requires successive superposition of the solutions for each layer interval with a given temperature as described by the geothermal gradient. The derivation of the solution to such a problem could be very cumbersome, all depending on the thickness of the confining layer in question.

In general, at a given depth and production time, the temperature at the wellbore equals the temperature of the infinite acting overburden as a result of the geothermal profile. The confining layer then depicts a pseudo-NFB for heat influx although the system is infinite. This implies, in reality, the heat support from the top layer would stop after a given production time and at a given depth as a result of the decrease in the temperature of the reservoir with decreasing depth. For this reason, a pseudo-NFTB model can be imposed on the reservoir response for the top layer. It is worth mentioning that the pseudo-NFTB for heat influx is dependent on the degree of temperature depression in the reservoir and the depth at which the reservoir temperature equals the temperature of the confining layer. However, for the bottom layer, this would not be the case as temperature increases with depth and hence heat influx from the bottom confining layer would be continuous and mask the effect of the pseudo-NFB in the top confining layer.

To facilitate the computation of the heat influx and hence the hydrate dissociation rate, the temperature in the confining layers will be assumed constant. As such, IAR, CTOB and p-NFTB conditions will be imposed at the outer boundary to investigate the effects of heat influx on hydrate dissociation. This is fully addressed in Appendix 12.

2.4 Heat Conduction, Convection and Hydrate Dissociation in Class 1 and 2 Hydrates

In Class 1 and 2 hydrates, the energy influx responsible for hydrate dissociation after pressure and temperature drop in the hydrate layer is strongly dependent on the method of production. If the reservoir is produced or tested from the free fluid layer, just heat conduction would be the additional source of energy needed to be considered for hydrate dissociation as the cap rock above the hydrate layer is considered impermeable. On the other hand, if the well is tested from the hydrate layer, heat conduction from the top layer and convective heat transfer from the free fluid layer would have to be considered as well.

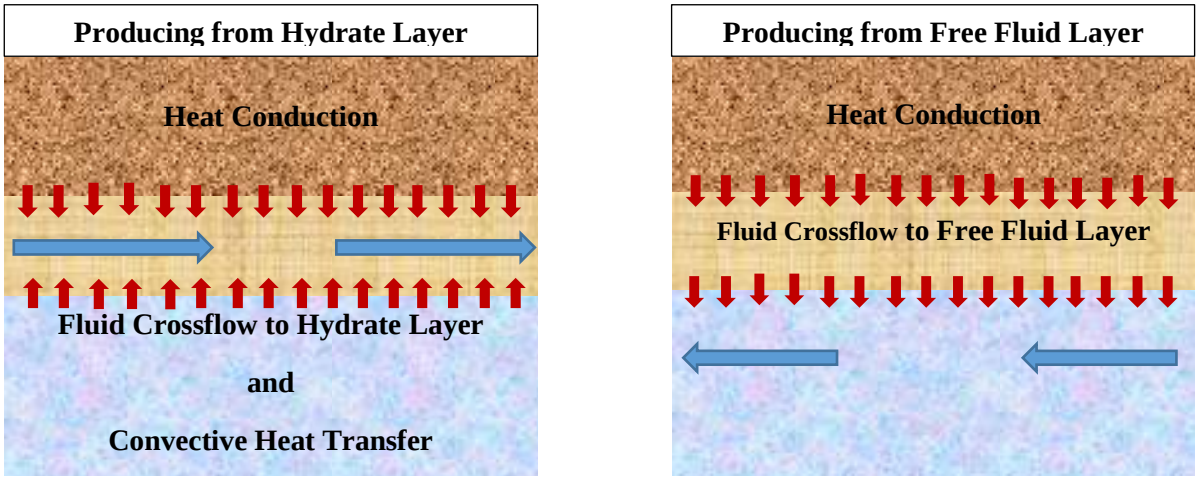

Figure 21: Heat Influx Problems in Class 1 and 2 Gas Hydrate Reservoirs

Though no-flow at the outer boundary of the hydrate layer has been considered, the effects of hydrate dissociation at the outer boundary of the hydrate layer could have significant influence on the reservoir response. Producing from the free fluid layer induces pressure propagation in the hydrate layer which is most often assumed to be dominantly vertical. When pressure depression reaches the upper boundary of the hydrate layer, temperature depressions are also experienced due to the endothermic hydrate dissociation. For this reason, heat flux from conduction will occur basically at the boundary and is controlled by the temperature depression at the boundary. When the hydrates dissociate at the boundary, the pressure at the dissociation front increases which implies, depending on the rate of hydrate dissociation, the pressure depression at the reservoir boundary could be supported by hydrate dissociation due to heat influx, which is a similar phenomenon seen in the production history of the Messoyakha Gas Field (Class 1G Gas Hydrate) . The effect of pressure support at the boundary is a known phenomenon and usually described as the constant pressure outer boundary condition where pressure depression at the boundary is zero due to fluid influx. The solution to such a complex problem could be derived with assumptions but however incorporating the solution in the crossflow model is very cumbersome. This problem is rigorously addressed in Appendix 14. To reduce the complexity of addressing such a system, we can assume the hydrate dissociation at the boundary due to heat influx is high enough to cause zero pressure depressions at the hydrate upper boundary; hence constant pressure outer boundary is imposed. If the hydrate dissociation due to heat influx is insignificant, just the hydrate dissociation due to pressure effects will be considered and true no-flow boundary imposed at the boundary. With this assumption, no-flow and constant pressure outer boundaries can be imposed at the outer boundaries of the hydrate layer.

2.5 Absolute, Effective and Relative Permeabilities in Hydrate Formations

The ability of porous media to allow fluid flow in the interconnected pores is characterized as the permeability. The permeability is further classified into subgroups depending on fluid phases present. The absolute permeability, k, of the porous media reflects the flow ability of pores fully saturated

(100%) with a single fluid phase [57]. In the presence of more than one phase in the pores, the term effective permeability is introduced. The effective permeability and absolute permeability are related by the following function:

$$k_{eff} = k_r k \qquad 2.15$$

The term k_r, denotes the relative permeability and it reflects the flow ability of a fluid relative to the other fluid components present. Hence the effective permeability simply denotes the ability of the porous media to allow flow of a given phase in the presence of another phase in the interconnected pores.

In conventional gas reservoirs, two main fluid phases are common, which are gas and water. In hydrate reservoirs, the presence of hydrates in the pores of the formation requires a further classification of the permeability concepts. Masuda [58] carried out rigorous experimental studies on hydrate dissociation and permeability changes and came up with the following correlation which is as of now the most widely used in most numerical simulators:

$$k_H = k_{rH} k = (1 - S_H)^N k \qquad 2.16$$

For convenience, the effective permeability of the gas and water phases will be represented thus:

$$k_g = k_{rg} k_H = \left(k_{rg} * k_{rH}\right) * k = k^*_{rg} * k \qquad 2.17$$

$$k_w = k_{rw} k_H = (k_{rw} * k_{rH}) * k = k^*_{rw} * k \qquad 2.18$$

Conventionally, fluid saturation, most especially gas, will decrease with pressure depletion. However; in gas hydrates, this will not be the case as hydrates will dissociate to gas and water hence replenishing the amount of gas withdrawn through production. The reservoir behavior in this case becomes a little complex. The presence of gas, water and hydrate in the system and their changes with depletion became an issue of concern as three phase relative permeability models had to be developed to address such a response. As of now the most widely used three phase relative permeability model to address hydrate behavior is the Stone [59] three phase model, modified by Aziz [55]. The effective and relative permeabilities of the gas and water phases using this model are [10], [60]:

$$k_g = k^*_{rg} * k = \left(\frac{S_g - S_{girr}}{1 - S_{girr}}\right)^{n_g} k \qquad 2.19$$

$$k_w = k^*_{rw} * k = \left(\frac{S_w - S_{wirr}}{1 - S_{wirr}}\right)^{n_w} k \qquad 2.20$$

Note that the pseudo-pressures developed earlier relate the dependence of relative permeability with pressure. To account for the changes in relative permeability with pressure the material balance saturation models in Appendix 4 can be used.

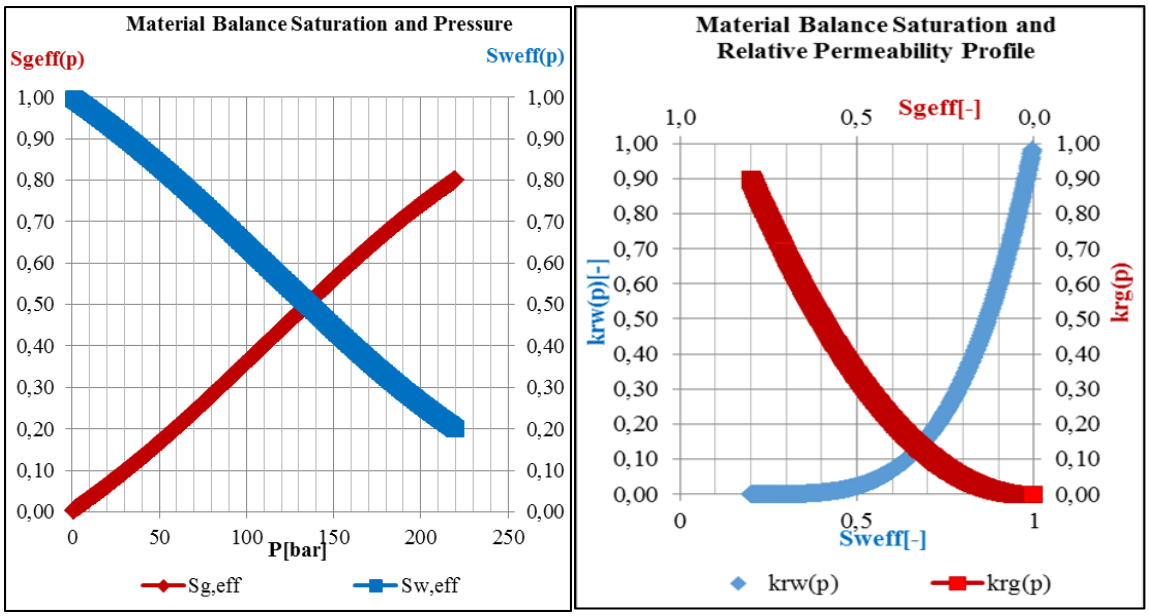

Figure 22: Material Balance Saturation and Relative Permeability with Pressure (S_{gi} =0.8, S_{wi}=0.2, n_g=2, n_w=4, S_{girr}=0.02, S_{wirr}=0.18)

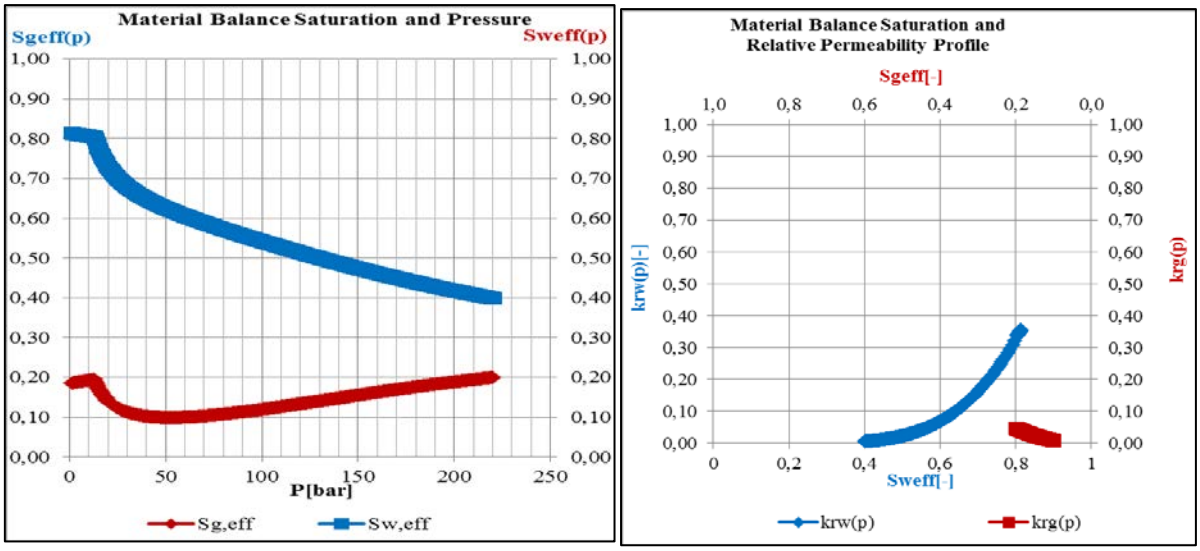

Figure 23: Material Balance Saturation and Relative Permeability with Pressure (Class 3 Hydrates, neglecting heat conduction, S_{gi} =0.2, S_{wi}=0.4, S_{Hi}=0.4, n_g=2, n_w=4, S_{girr}=0.02, S_{wirr}=0.18)

2.6 Boltzmann-Transformation (Similarity Variable Method)

The Boltzmann transformation is a very effective tool in transforming partial differential equations into ordinary differential equations. The method simply involves the use a similarity variable, which is a function of time and place, such that the derivatives of the variable can easily be incorporated into the diffusivity equation, hence transforming it into an ordinary differential equation for which a similarity solution can be obtained. In radial coordinates, the conventional Boltzmann similarity variable with dimensionless time and radius is given thus:

$$v_D^2 = \frac{r_D^2}{4t_{Dw}} \qquad 2.\,21$$

With the use of the above transformation complex methods of solving diffusivity equations could be avoided. On the other hand, the transformation is not applicable in all radial flow problems for well testing. The application of the Boltzmann transformation is given in Appendix 8.

The use of the Boltzmann transformation in solving the diffusivity equation analytically cannot be used for all diffusivity problems, hence the use of more rigorous analytical methods such as Laplace transforms are used. Nonetheless, most of the solutions of the diffusivity equations developed here will be presented using both the Boltzmann and Laplace transforms.

2.7 Laplace-Transformation

The Laplace transformation is one of the most widely used methods of solving partial differential equations in oil and gas reservoir engineering problems since its introduction by Van Everdingen and Hurst [61]. It involves the transformation of the diffusivity equation in a Laplace domain form. The Laplace transformation is given below:

$$L\{f(t)\} = \int_0^\infty e^{-pt} f(t)dt = \hat{f}(p) \qquad 2.22$$

Applying the Laplace transform in the dimensionless diffusivity equation takes the form:

$$\frac{\partial^2 L(\varphi_D)}{\partial r_D^2} + \frac{1}{r_D}\frac{\partial L(\varphi_D)}{\partial r_D} = \int_0^\infty e^{-pt_{Dw}} \frac{\partial \varphi_D}{\partial t_{Dw}} dt_{Dw} \qquad 2.23$$

$$\frac{\partial^2 \widehat{\varphi_D}}{\partial r_D^2} + \frac{1}{r_D}\frac{\partial \widehat{\varphi_D}}{\partial r_D} = \int_0^\infty e^{-pt_{Dw}} \partial\varphi_D \qquad 2.24$$

$$\frac{\partial^2 \widehat{\varphi_D}}{\partial r_D^2} + \frac{1}{r_D}\frac{\partial \widehat{\varphi_D}}{\partial r_D} = [-\varphi_D(r_D, t_{Dw} = 0) + p\widehat{\varphi_D}] \qquad 2.25$$

3 Conceptual Models for Well Testing in Normally Pressured Class 3 Gas Hydrates

The conceptual well testing models developed for the Class 3 gas hydrate reservoirs are developed based on the mass conservation principle as done in conventional oil and gas reservoirs, while considering the hydrate dissociation rate as the source term in the diffusivity equation.

As given in Appendix 5, the general mass conservation equation in radial coordinates is given thus:

$$2\pi h\Delta(r * \rho_g * w_g) + 2\pi h\Delta(r * \rho_w * w_w) = 2\pi rh\Delta r\frac{\Delta(S_g\emptyset\rho_g)}{\Delta t} + 2\pi rh\Delta r\frac{\Delta(S_w\emptyset\rho_w)}{\Delta t} + \dot{m}_H \quad 3.1$$

Based on the model used in addressing the hydrate dissociation rate, two different models can be generated for the response, namely:

Equilibrium Model

$$\frac{\partial^2\varphi_D}{\partial r_D{}^2} + \frac{1}{r_D}\frac{\partial\varphi_D}{\partial r_D} - \left[\frac{\partial T_{pD}}{\partial z_D}\right]_{Caprock,z_D=1} - \left[\frac{\partial T_{pD}}{\partial z_D}\right]_{Underburden,z_D=1} = S_D\frac{\partial\varphi_D}{\partial t_{Dw}} \quad 3.2$$

The above model takes the following form in Laplace domain by applying the temperature inner boundary conditions addressed in Appendix 6:

$$\frac{\partial^2\hat{\varphi}_D}{\partial r_D{}^2} + \frac{1}{r_D}\frac{\partial\hat{\varphi}_D}{\partial r_D} - \left[S_Dp + \left(e_D\widehat{\dot{Q}_{pD}}\right)_{caprock} + \left(e_D\widehat{\dot{Q}_{pD}}\right)_{Underburden}\right]\hat{\varphi}_D = 0 \quad 3.3$$

The above equation can simply be represented in the following form as also given in Appendix 7 and Appendix 12:

$$\frac{\partial^2\hat{\varphi}_D}{\partial r_D{}^2} + \frac{1}{r_D}\frac{\partial\hat{\varphi}_D}{\partial r_D} - (S_Dp + \gamma_{De})\hat{\varphi}_D = 0 \quad 3.4$$

Kinetic Model

In the kinetic model, the hydrate dissociation rate is considered constant and hence the diffusivity equation using this approach is written in time domain thus:

$$\frac{\partial^2\varphi_D}{\partial r_D{}^2} + \frac{1}{r_D}\frac{\partial\varphi_D}{\partial r_D} - \gamma_{Dk}\varphi_D = S_{Dk}\frac{\partial\varphi_D}{\partial t_{Dw}} \quad 3.5$$

The kinetic model in Laplace domain simply takes the form:

$$\frac{\partial^2\hat{\varphi}_D}{\partial r_D{}^2} + \frac{1}{r_D}\frac{\partial\hat{\varphi}_D}{\partial r_D} - (S_Dp + \gamma_{Dk})\hat{\varphi}_D = 0 \quad 3.6$$

The derivation of diffusivity equations of the normally pressured gas hydrate reservoir using the kinetic and the equilibrium model are given in detail in Appendix 5.

The solutions to the above equation with constant pressure inner boundary (CPIB) and constant rate inner boundary (CRIB) conditions using the Boltzmann and Laplace transforms are given in Appendix 12. The dimensionless pseudo-pressure and rate profiles are now depicted for the similarity solutions. A meticulous overview of different and more complex reservoir responses are given in Appendix 12 with the Laplace domain well test model recognition method.

3.1 Part 1: Constant Wellbore Pressure Cases

Part 1-Case 1: γ_D<<1

- Using the equilibrium model: $\gamma_D = \gamma_{De}$ denotes the dimensionless heat leakage rate due to heat conduction from the confining layers.
- Using the kinetic model: $\gamma_D = \gamma_{Dk}$ denotes the dimensionless hydrate dissociation rate.

Using the kinetic model, γ_D<<1 will mean negligible hydrate dissociation whereas the equilibrium model still considers hydrate dissociation due to pressure drop and neglects just the heat conduction term. Hence the two effects could be handled separately. For cases where heat conduction effects are negligible, the similarity solutions can be used.

Part 1-Case 1a: IAR Response

Using the equilibrium model and assuming negligible hydrate dissociation due to heat conduction, the effects of hydrate dissociation on the reservoir response considering the heat energy used up in the hydrate layer can be predicted using the following models (see Appendix 12 for details):

Pseudo-Pressure

$$\varphi_D(r_D, t_{Dw}) = \frac{\varphi(r,t)-\varphi_i}{\varphi_{wf}-\varphi_i} = \frac{\left[E_1\left(S_D\frac{r_D^2}{4t_{Dw}}\right)\right]}{\left[E_1\left(\frac{S_D}{4t_{Dw}}\right)\right]} \qquad 3.7$$

Transient Rate

$$\dot{m}_{tD} = \frac{\dot{m}_t(t)}{2\pi hk(\varphi_i-\varphi_{wf})} = \frac{2e^{-v_D^2}}{\left[E_1\left(\frac{S_D}{4t_{Dw}}\right)\right]} \qquad 3.8$$

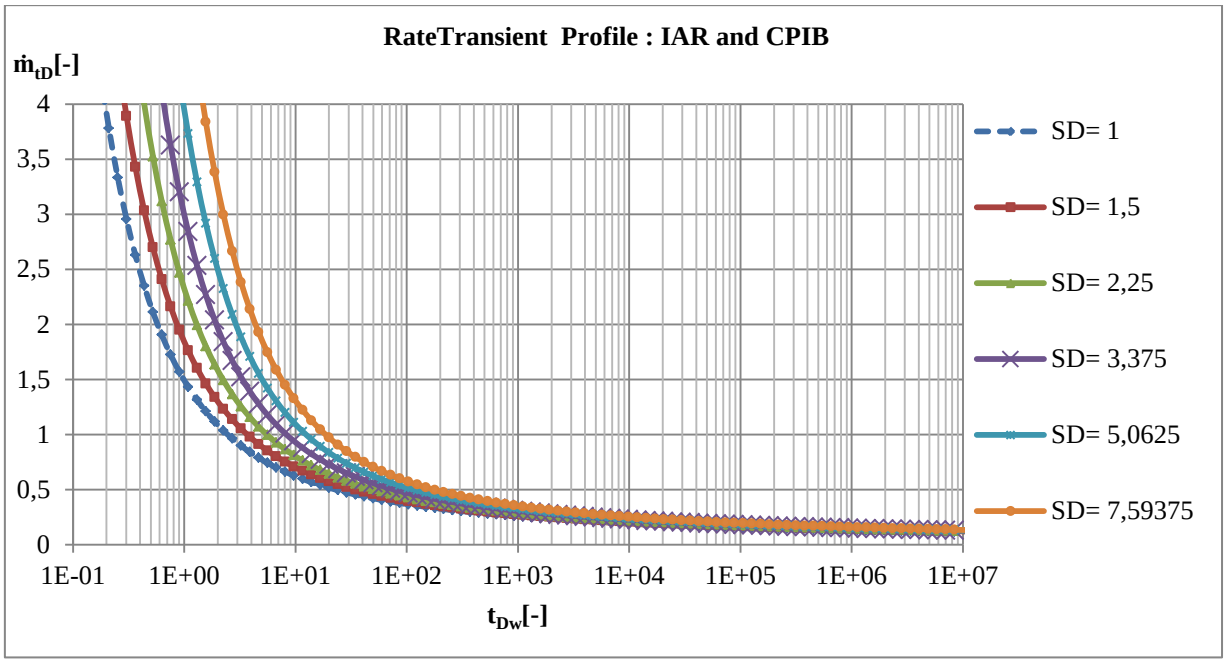

Figure 24: Transient Rate Profile with Effects of Heat Energy Consumed in Hydrate Layer

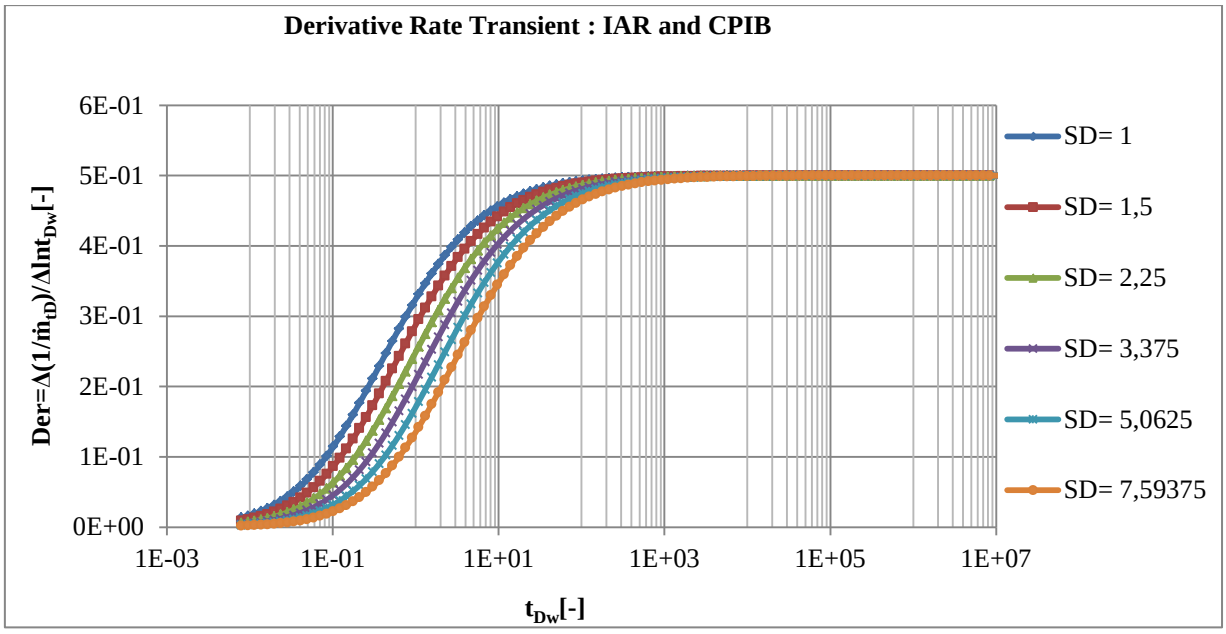

Figure 25: Derivative Plot for Rate Transient with Effects of Heat Energy Consumed in Hydrate Layer

To eliminate the influence of the modified dimensionless decomposition compressibility, S_D, from the reservoir response, the type curve is introduced with a modified time, whereby the modified time is given by t_{Dw}/S_D. The transient rate profile with the modified time is given in Figure 26.

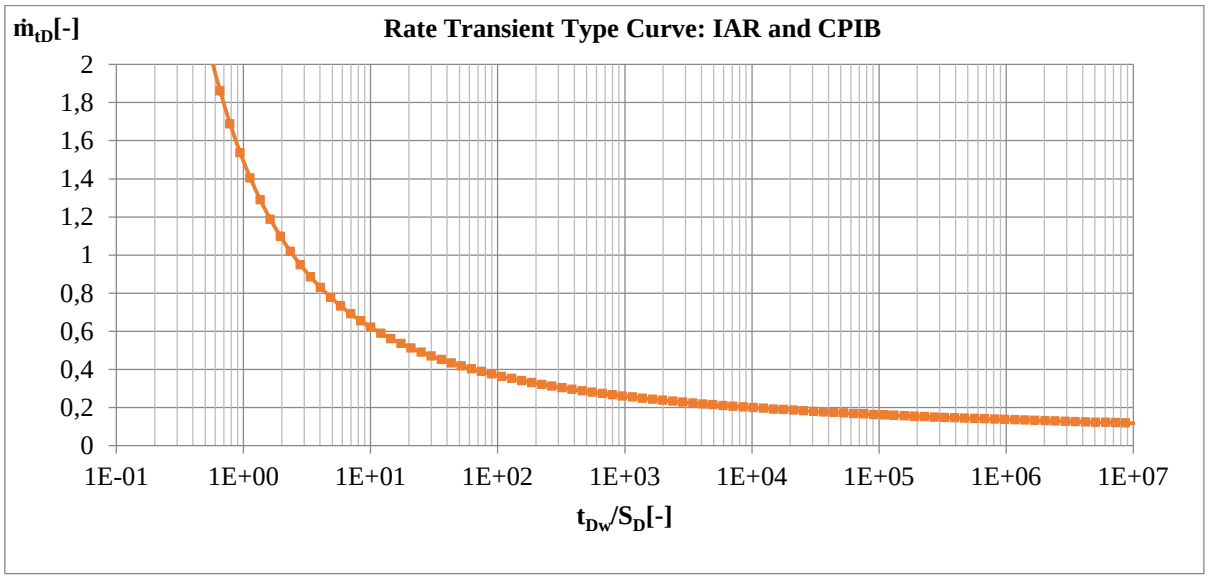

Figure 26: Type-Curve Transient Rate Profile for Infinite Acting Reservoir-Constant Pressure at Wellbore

As expected, the dimensionless rate transient here has the same profile as in conventional gas reservoirs due to the use of dimensionless parameters and the absence of γ_D. Maximum flow rates will be achieved during early time production before pressure depression propagates deep into the reservoir. Rate transient analysis for such reservoir types could be performed for the middle time region when the infinite acting radial flow begins. The methods of analysis will be described later.

Using the analytical models developed in Appendix 12, the pressure propagation for the infinite acting reservoir is depicted in Figure 27.

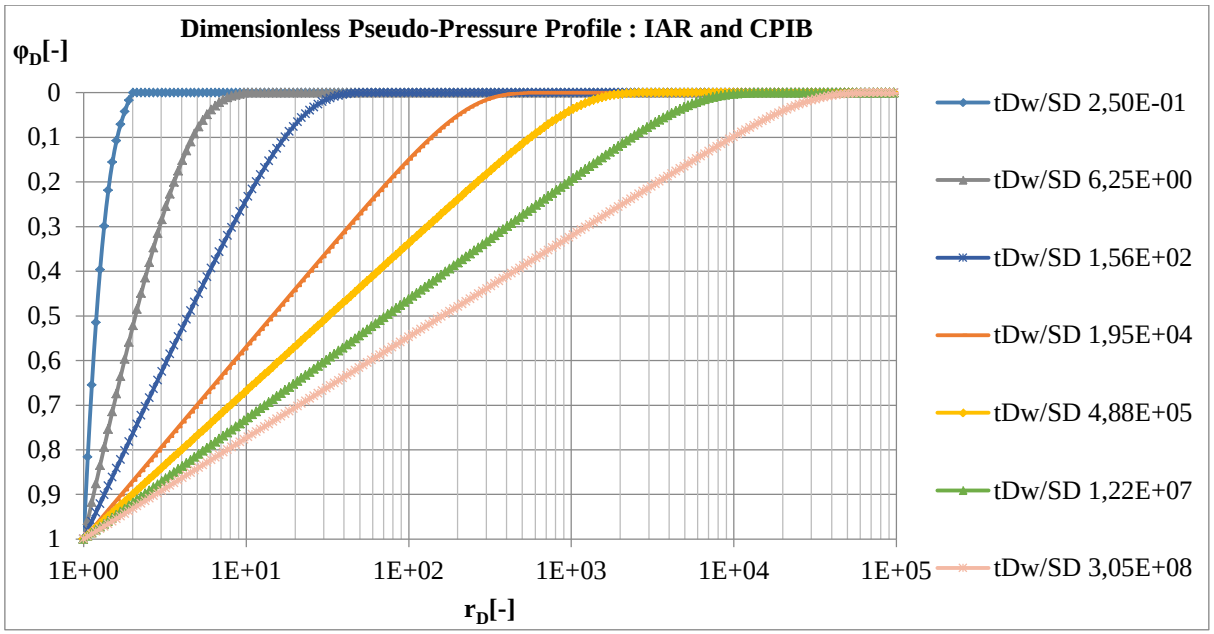

Figure 27: Dimensionless Pseudo-Profile for Infinite Acting Reservoir-Constant Pressure at Wellbore

Part 1-Case 1b: Recharge Boundary Response (Constant Pressure Outer Boundary)

In bounded or finite reservoirs, the rate transient responses are a little different. During recharge boundary dominated flow, no rate decline is noticed as pressure support (fluid influx) from the outer boundary prevents any pressure depletion in the reservoir. Dimensionless pseudo-pressure and rate profiles given in Figure 28 and Figure 29 depict this behavior.

The following models could be used to predict the reservoir response (see Appendix 12 for details):

Pseudo-Pressure

$$\varphi_D(r_D, t_{Dw}) = \frac{\varphi(r,t)-\varphi_i}{\varphi_{wf}-\varphi_i} = \frac{\left[E_1\left(S_D\frac{r_D^2}{4t_{Dw}}\right)\right]-\left[E_1\left(S_D\frac{(2l_D-r_D)^2}{4t_{Dw}}\right)\right]}{\left[E_1\left(\frac{S_D}{4t_{Dw}}\right)\right]-\left[E_1\left(S_D\frac{(2l_D-1)^2}{4t_{Dw}}\right)\right]} \quad 3.9$$

Transient Rate

$$\dot{m}_{tD}(r_D=1, t_{Dw}) = \frac{\dot{m}_t(t)}{2\pi hk(\varphi_i-\varphi_{wf})} = 2\frac{\left[e^{-\left(\frac{S_D}{4t_{Dw}}\right)}+(2l_D-1)^{-1}e^{-\frac{(2l_D-1)^2}{4t_{Dw}}S_D}\right]}{E_1\left(\frac{S_D}{4t_{Dw}}\right)-E_1\left(S_D\frac{(2l_D-1)^2}{4t_{Dw}}\right)} \quad 3.10$$

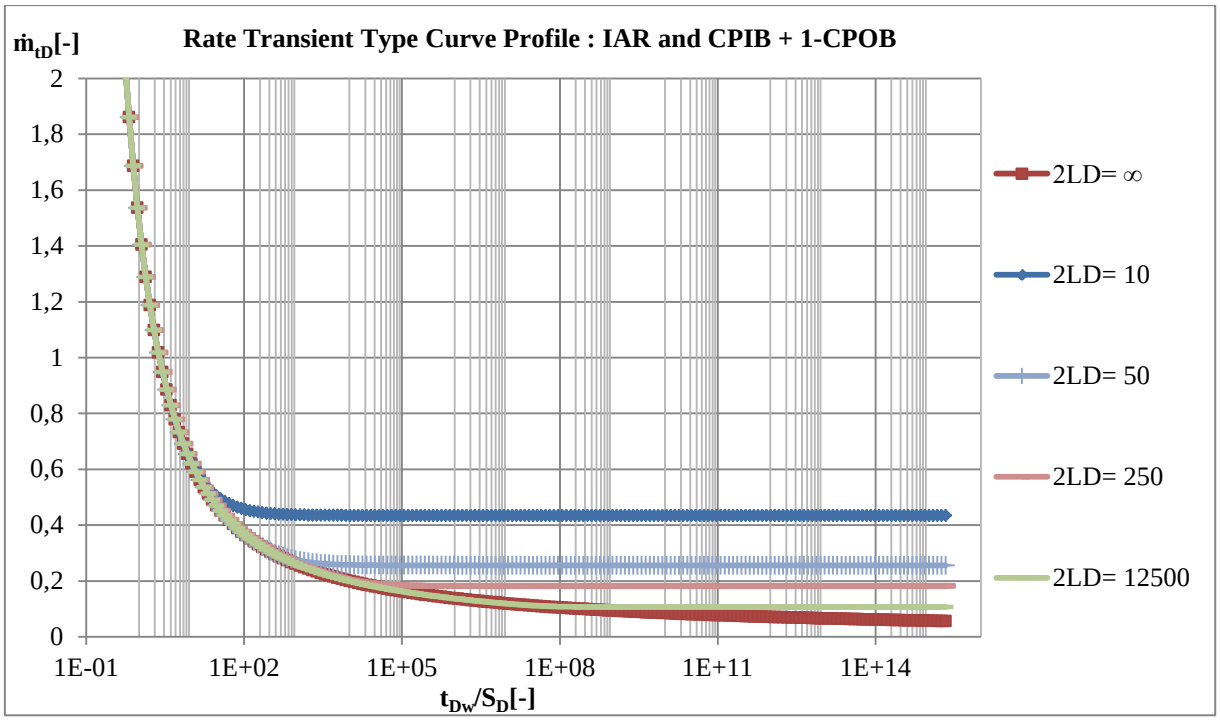

Figure 28: Type Curve Transient Rate Profile for Constant Pressure Bounded Reservoir-Constant Pressure at Wellbore

From Figure 28 it is clear that the smaller the drainage radius, the faster boundary dominated flow embarks. The dimensionless pseudo-pressure profile for reservoir with a recharge boundary at a distance $2l_D$=3500 from the wellbore is given in Figure 29 and clearly shows that no pressure depletion is experienced for $t_{Dw}/S_D>10^6$.

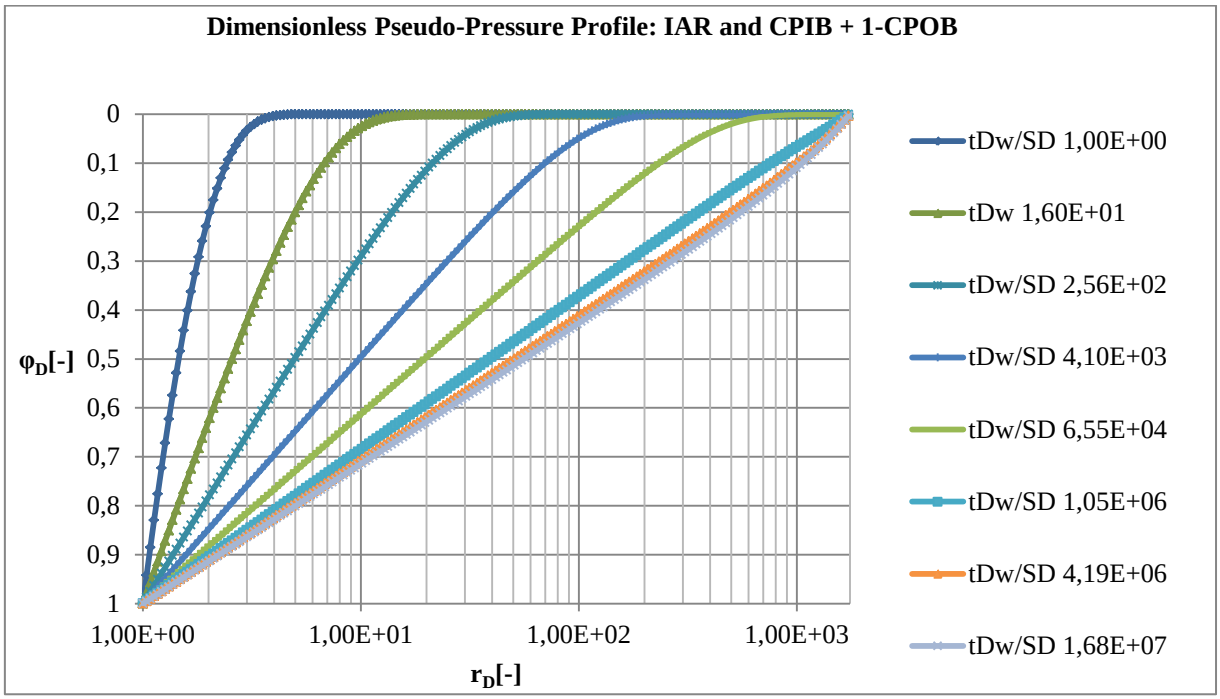

Figure 29: Dimensionless Pseudo-Profile for Constant Pressure Bounded Reservoir-Constant Pressure at Wellbore ($2l_D$=3500)

Part 1-Case 1c: Impermeable Boundary Response (No-Flow Outer Boundary)

Constant pressure outer boundary conditions are usually modeled to reflect the influence of pressure support from a strong aquifer or from an injection well. However, in most bounded reservoirs, this is not the case as sealed fault zones are usually present, limiting the influx of fluid at the reservoir boundary. To investigate such a problem, no-flow boundary models were developed as also given below (see Appendix 12 for details):

Pseudo-Pressure

$$\varphi_D(r_D, t_{Dw}) = \frac{\varphi(r,t)-\varphi_i}{\varphi_{wf}-\varphi_i} = \frac{\left[E_1\left(S_D\frac{r_D^2}{4t_{Dw}}\right)\right]+\left[E_1\left(S_D\frac{(2l_D-r_D)^2}{4t_{Dw}}\right)\right]}{\left[E_1\left(\frac{S_D}{4t_{Dw}}\right)\right]+\left[E_1\left(S_D\frac{(2l_D-1)^2}{4t_{Dw}}\right)\right]} \quad 3.11$$

Transient Rate

$$\dot{m}_{tD}(r_D=1, t_{Dw}) = \frac{\dot{m}_t(t)}{2\pi hk(\varphi_i-\varphi_{wf})} = 2\frac{\left[e^{-\left(\frac{S_D}{4t_{Dw}}\right)}-(2l_D-1)^{-1}e^{-\frac{(2l_D-1)^2}{4t_{Dw}}S_D}\right]}{E_1\left(\frac{S_D}{4t_{Dw}}\right)+E_1\left(S_D\frac{(2l_D-1)^2}{4t_{Dw}}\right)} \quad 3.12$$

Figure 30 and Figure 31 depict the rate transient and the pseudo-pressure profile in the reservoir for the no-flow boundary condition.

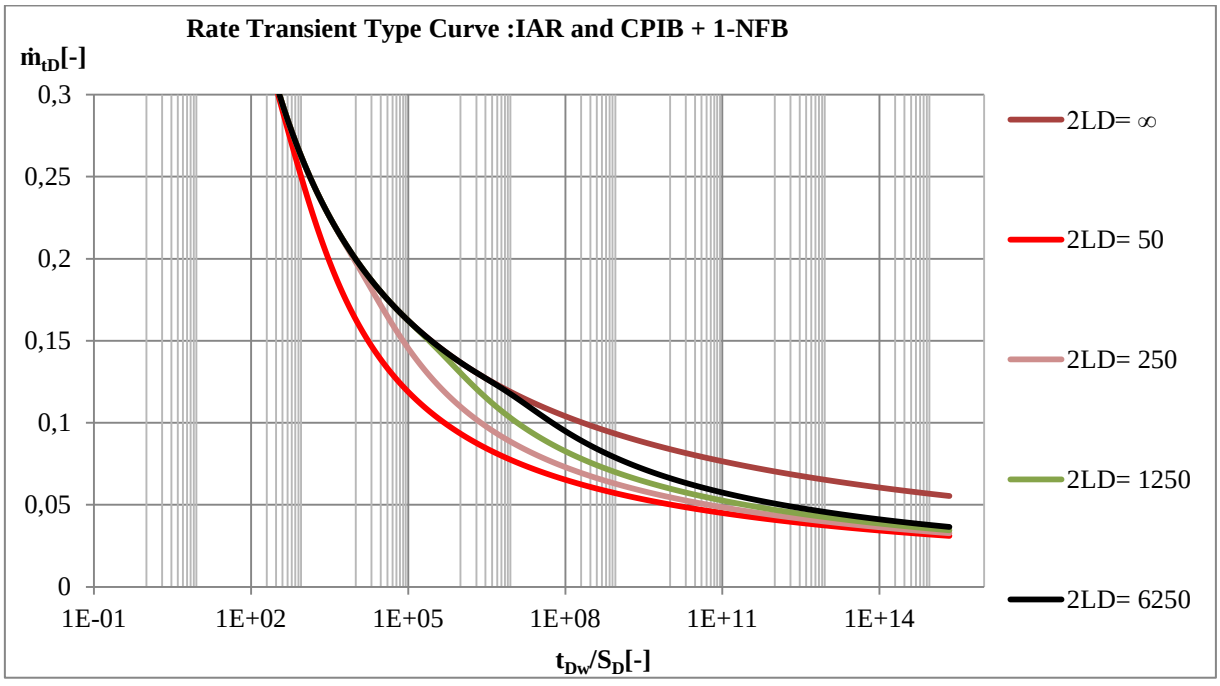

Figure 30: Type Curve Transient Rate Profile for No-Flow Bounded Reservoir-Constant Pressure at Wellbore

As depicted in Figure 31 the pressure at the boundary does not remain constant during boundary dominated flow as no pressure support is addressed in this model.

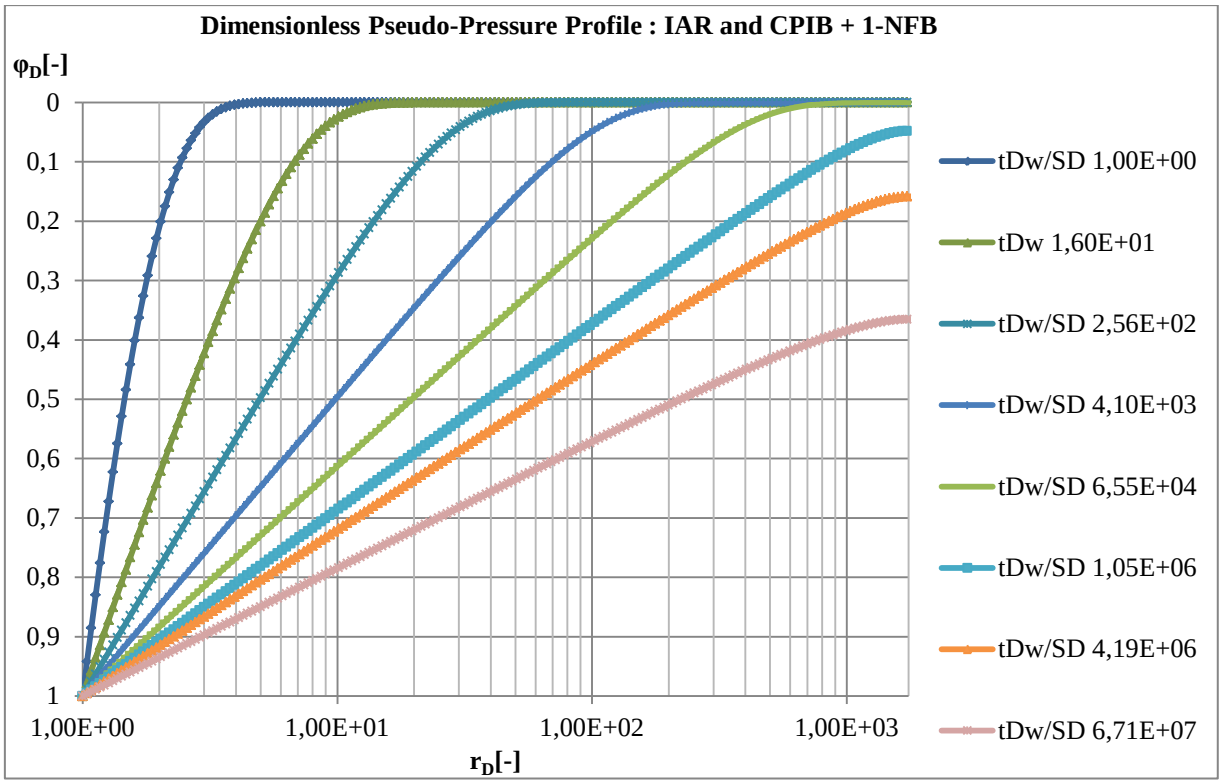

Figure 31: Dimensionless Pseudo-Profile for No-Flow Bounded Reservoir-Constant Pressure at Wellbore ($2l_D$=3500)

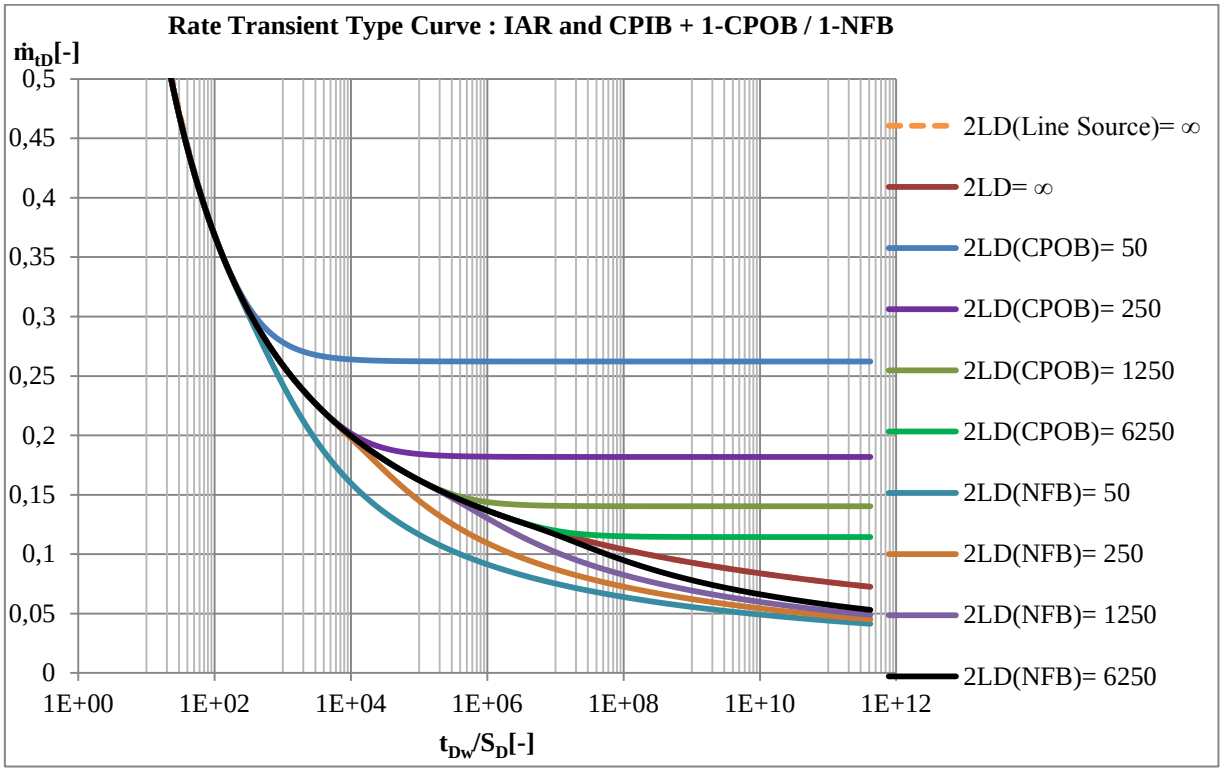

Figure 32: Type Curve Rate Transient Response for Infinite Acting and Bounded Reservoirs

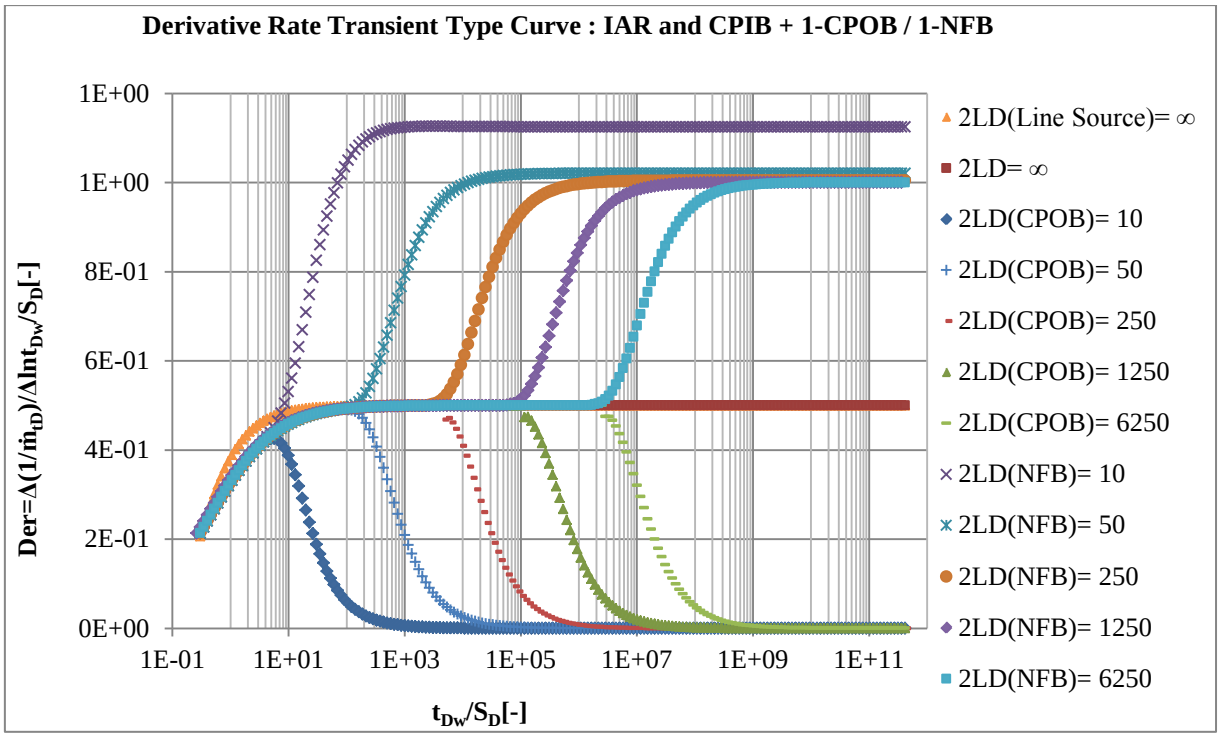

Figure 33: Derivative Plot of Rate Transient Response for Infinite Acting and Bounded Reservoirs

Part 1-Case 2: $0<\gamma_D<1$

In Case 1, the dimensionless hydrate dissociation term or the dimensionless heat leakage term was neglected, which is now considered here and the influence of hydrate dissociation or heat conduction on the transient rate profile investigated. As given in Appendix 12, heat influx effects were considered by applying the Laplace transforms for which approximate solutions can be derived in real time domain for specific time intervals.

Part 1-Case 2a: Infinite Acting Reservoir

The effect of heat conduction on the reservoir response can be investigated with the following models (see Appendix 12 and Appendix 18 for details):

Pseudo-Pressure

$$\varphi_D = \frac{\varphi(r,t)-\varphi_i}{\varphi_{wf}-\varphi_i} = Z\left(\frac{t_{Dw}}{S_D\mu_D}, r_D, \sqrt{b_D}\right) \qquad 3.\ 13$$

For $\frac{t_{Dw}}{S_D\mu_D}\sqrt{b_D} > 1$

$$\varphi_D = \frac{\varphi(r,t)-\varphi_i}{\varphi_{wf}-\varphi_i} = \frac{W\left(\frac{r_D^2}{4t_{Dw}}S_D\mu_D, r_D\sqrt{b_D}\right)}{W\left(\frac{S_D\mu_D}{4t_{Dw}}, \sqrt{b_D}\right)} \qquad 3.\ 14$$

Transient Rate at Wellbore

$$\dot{m}_{tD} = \frac{\dot{m}_t(t)}{2\pi hk(\varphi_i-\varphi_{wf})} = G\left(\frac{t_{Dw}}{S_D\mu_D}, \sqrt{b_D}\right) \qquad 3.\ 15$$

Where,

$$\mu_D = \left(1 + \frac{F_{CD} e_D (\Delta z_D - 1)}{3 S_D}\right) = \left\{1 + \frac{[F_{CD} e_D (\Delta z_D - 1)]_{TL} + [F_{CD} e_D (\Delta z_D - 1)]_{BL}}{3 S_D}\right\} \quad 3.16$$

$$b_D = \frac{e_D}{(\Delta z_D - 1)} = \left[\frac{e_D}{(\Delta z_D - 1)}\right]_{TL} + \left[\frac{e_D}{(\Delta z_D - 1)}\right]_{BL} \quad 3.17$$

The model hence quantifies the heat sources from both the top and bottom layers (TL & BL) of the hydrate. In a similar manner, solutions can also be derived using the kinetic model.

The Kinetic Model

Pseudo-Pressure

$$\varphi_D = \frac{\varphi(r,t) - \varphi_i}{\varphi_{wf} - \varphi_i} = Z\left(\frac{t_{Dw}}{S_{Dk}}, r_D, \sqrt{\gamma_{Dk}}\right) \quad 3.18$$

For $\frac{t_{Dw}}{S_{Dk}}\sqrt{\gamma_{Dk}} > 1$

$$\varphi_D = \frac{\varphi(r,t) - \varphi_i}{\varphi_{wf} - \varphi_i} = \frac{W\left(\frac{r_D^2}{4t_{Dw}} S_{Dk}, r_D\sqrt{\gamma_{Dk}}\right)}{W\left(\frac{1}{4t_{Dw}} S_{Dk}, \sqrt{\gamma_{Dk}}\right)} \quad 3.19$$

Transient Rate at Wellbore

$$\dot{m}_{tD} = \frac{\dot{m}_t(t)}{2\pi hk(\varphi_i - \varphi_{wf})} = G\left(\frac{t_{Dw}}{S_{Dk}}, \sqrt{\gamma_{Dk}}\right) \quad 3.20$$

The Hantush functions Z(μ,β,τ), W(μ,β), G(μ,β,) are given in Appendix 18.

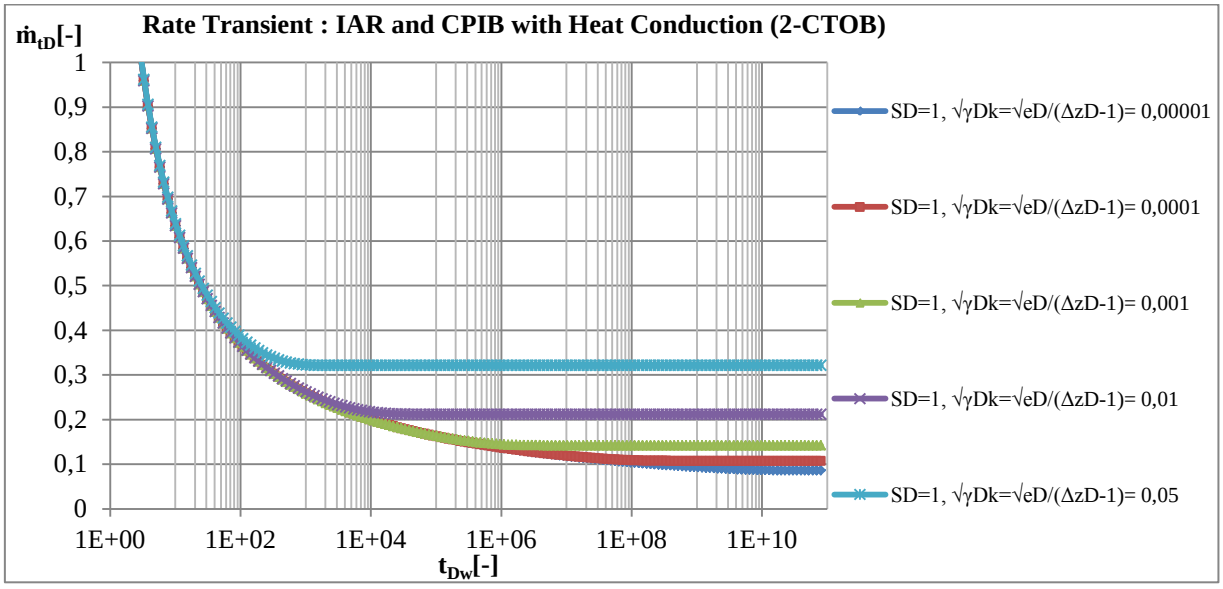

Figure 34: Transient Rate Profile in Gas Hydrates with Sensitivity on Gas hydrate Dissociation Rate (μ_D=1)

As seen in Figure 34, the effect of hydrate dissociation from heat conduction could have a noticeable effect on the rate transient profile. With very high and constant heat influx rates, rate decline stops and the wellbore rate transient remains constant. The reservoir hence behaves similar to constant outer boundary pressure reservoirs although this is not the case. Figure 36 shows the true behavior of the

constant pressure outer boundary case. Here it is noticeable that the boundary dominated effects commingle with hydrate dissociation effects as a distinction between the effects of high dissociation rates and boundary dominated flow are difficult to differentiate. However, the models depicted in the diagrams are reservoir responses based on the conceptual model and do not show the decrease in hydrate saturation due to dissociation. Hence in real data analysis, provided the hydrate saturation is very significant compared to the fluid phases and the dissociation rate is slow, boundary dominated flow can be identified. The type curve is once more used and the rate transient takes the form:

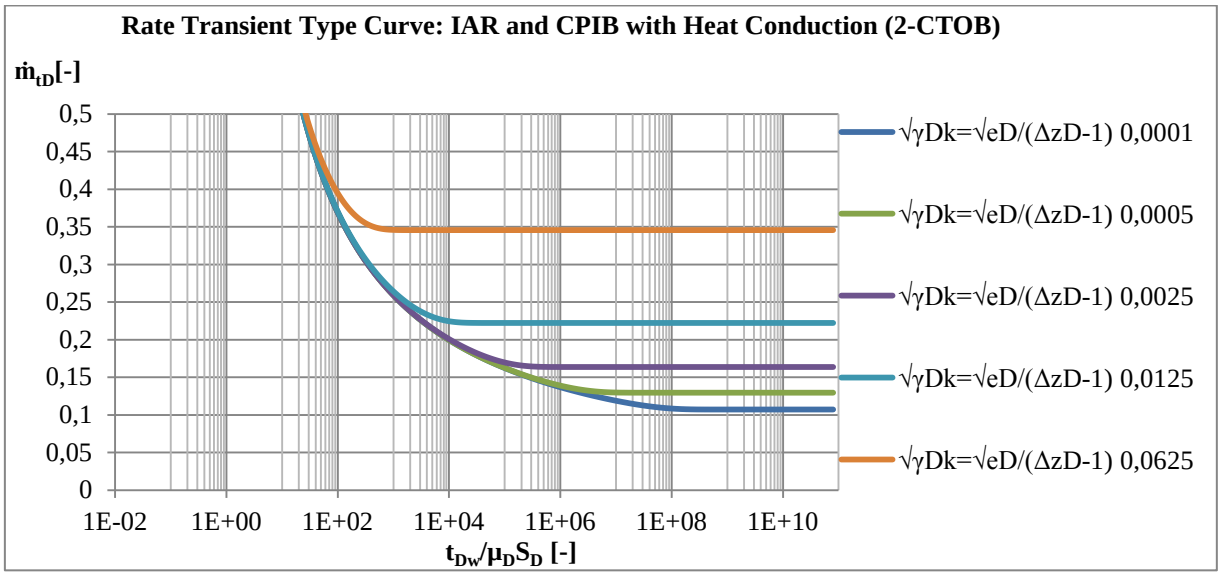

Figure 35: Type Curve Transient Rate Profile in Bounded Reservoirs with Constant Outer Pressure

Part 1-Case 2b: Constant Pressure Outer Boundary Reservoirs

Rate Transient Approximate Solution

$$\dot{m}_{tD} = \frac{\dot{m}_t(t)}{2\pi hk\left(\varphi_i - \varphi_{wf}\right)} \approx \frac{2}{W\left(\frac{S_D\mu_D}{4t_{Dw}}, \sqrt{b_D}\right) - W\left(\frac{S_D\mu_D(2l_D-1)^2}{4t_{Dw}}, (2l_D-1)\sqrt{b_D}\right)} \qquad 3.\ 21$$

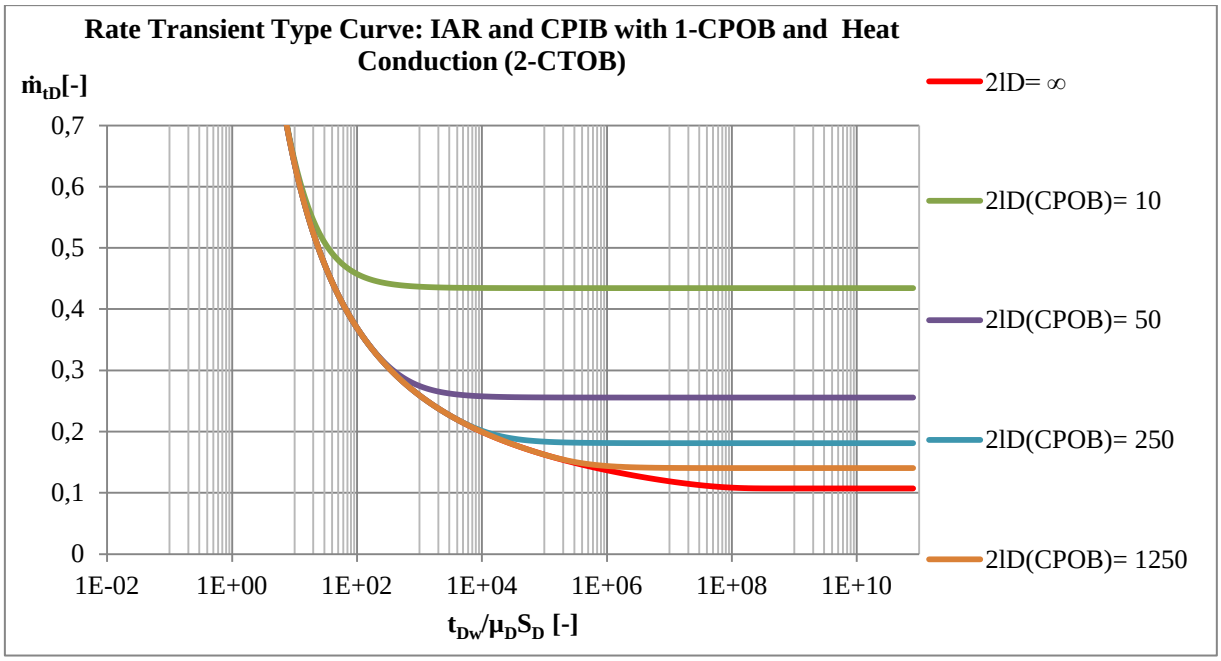

Figure 36: Type Curve Transient Rate Profile in IAR with two CTOB ($\sqrt{\gamma_{Dk}}$ or $\sqrt{e_D/(\Delta z_D}$-1) =0.0001)

The reservoir response of bounded reservoir using a single value of the dimensionless heat conduction term might seem easy to analyze; however, combining the influence of constant pressure bounded reservoirs and heat conduction does not depict any particular difference in the responses.

Hence, if the hydrate reservoir is characterized by a high dissociation rate and a recharge boundary, the effect of one of the factors cannot be entirely distinguished from the other with simple analysis of well test data, as both factors are pressure support (fluid influx or source) terms. If the hydrate dissociation rate is very high, the pressure transient does not travel to the boundary and would make the characterization of exploration wells difficult.

Part 1-Case 2c: No-Flow Outer Boundary

Rate Transient Approximate Solution

$$\dot{m}_{tD} \approx \frac{2}{W\left(\frac{S_D \mu_D}{4t_{Dw}}, \sqrt{b_D}\right) + W\left(\frac{S_D \mu_D (2l_D-1)^2}{4t_{Dw}}, (2l_D-1)\sqrt{b_D}\right)} \qquad 3.\ 22$$

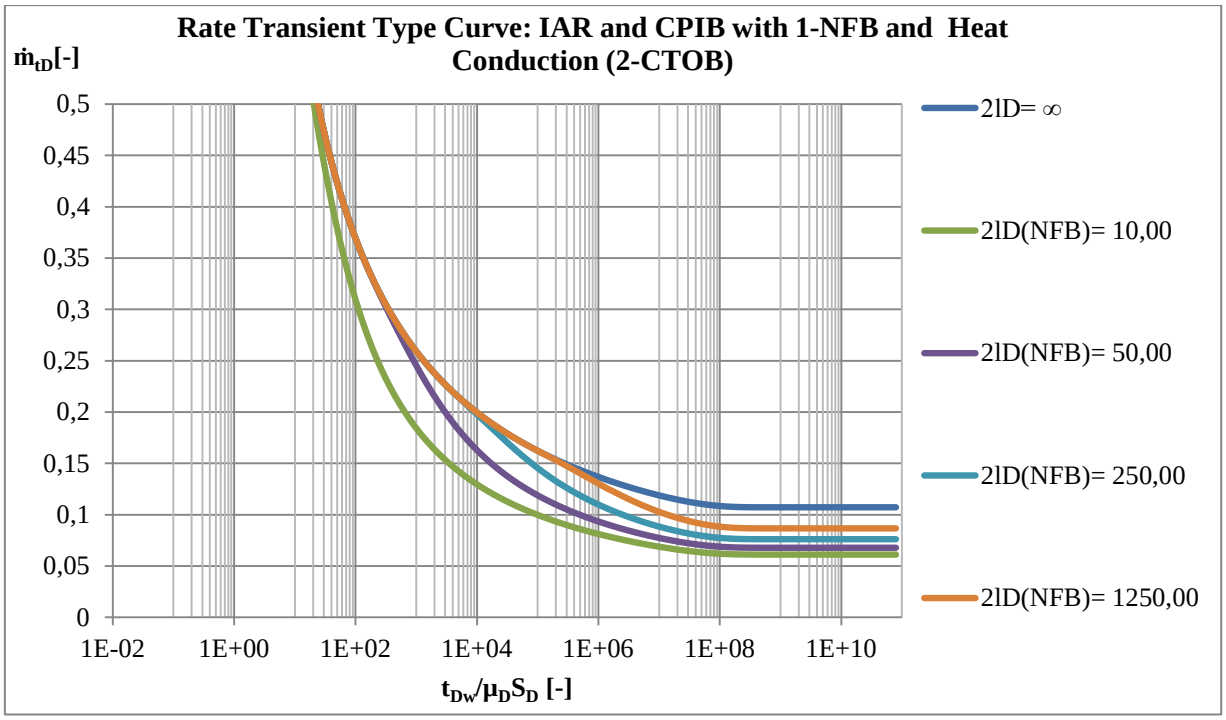

Figure 37: Type Curve Transient Rate Profile in Bounded Reservoirs with No-Flow at Outer Boundary ($\sqrt{\gamma_{Dk}}$ or $\sqrt{e_D/(\Delta z_D\text{-}1)}$ =0.0001)

Provided the heat influx rate is small as given in Figure 37, the reservoir response is characterized by an infinite acting period, after which boundary dominated flow embarks. With reduction in reservoir pressure during depletion, heat influx also increases and prohibits a further decline of mass rate.

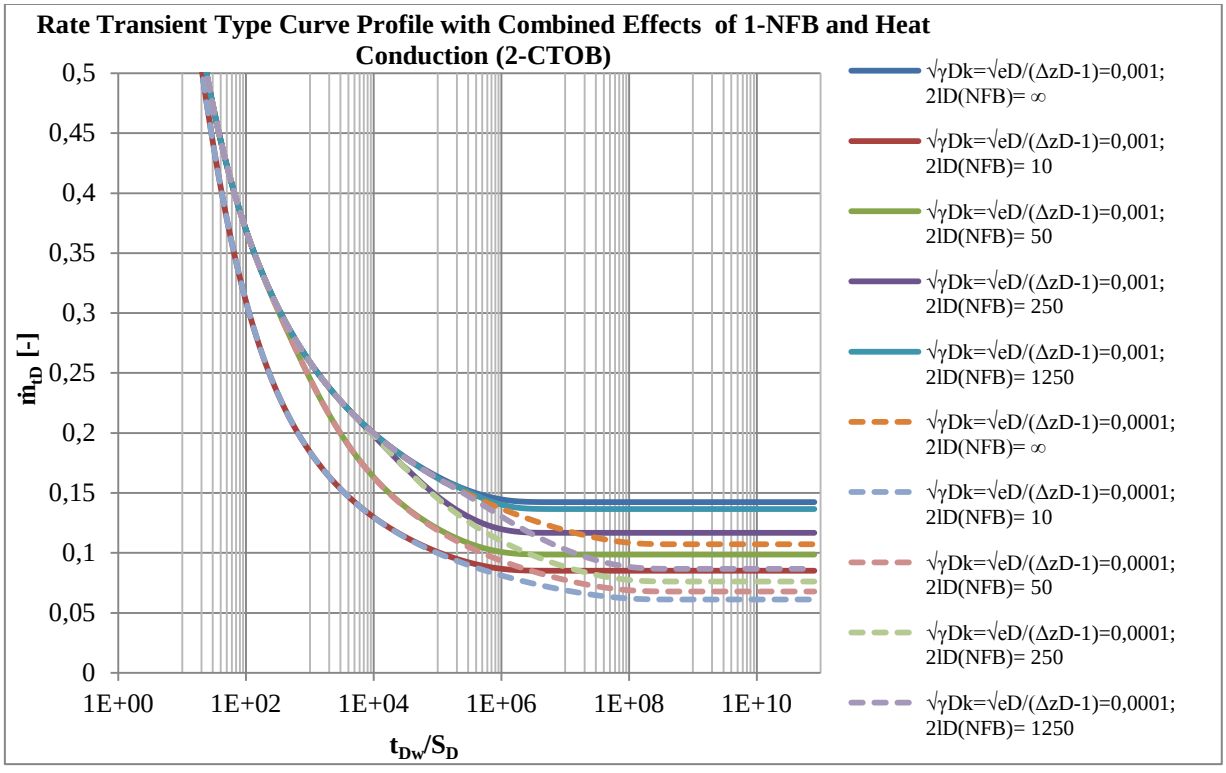

Figure 38: Transient Rate Profile in Bounded Reservoir with Influence of NFB and Heat Flux

Unlike the CPOB cases, the reservoir response with no flow boundaries differs significantly from reservoirs with the influence of heat conduction. Hence, performing a derivative plot will depict the no-flow boundary effects and if the heat influx rate or the hydrate dissociation rate becomes significant, constant outer boundary type responses will be noticed. The rate transient derivative is given below to depict this characteristic behavior.

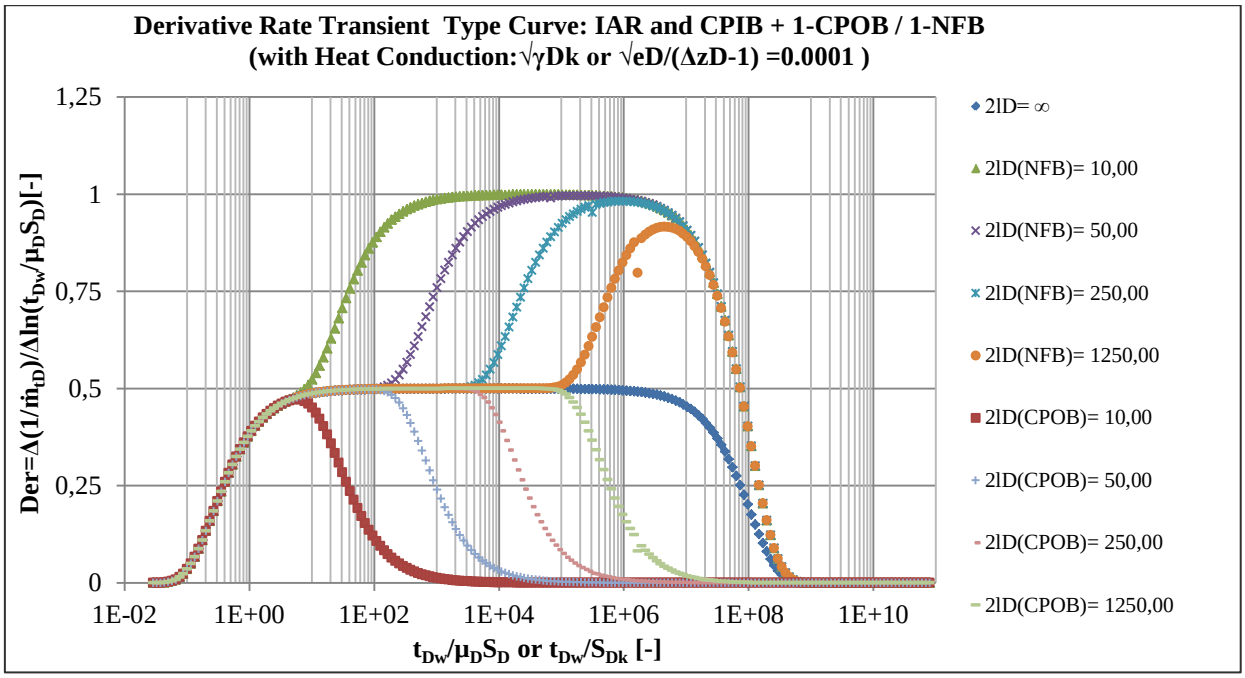

Figure 39: Transient Rate Profile in Bounded Reservoirs with No-Flow at Outer Boundary ($\sqrt{\gamma_{Dk}}$ or $\sqrt{e_D/(\Delta z_D\text{-}1)}$ =0.0001)

It is worth mentioning that the reservoir responses depicted here in real time domain, considering the effects of heat flux, are based on approximations using the line source solutions and image well theory for the single bounded reservoir. However, for more explicit study of the complex reservoir responses, the Laplace domain solutions with the application of the image theory as given in Appendix 8 can be used in conjunction with the Laplace domain well test model recognition methods.

3.2 Part 2: Constant Sandface Rate Cases

Although maintaining constant rates during well tests in reservoirs with multiphase flow is known to be difficult to achieve, the effects of conducting a hypothetical constant rate test in the hydrate reservoir are depicted below.

Part 2-Case 1: γ_D<<1

Part 2-Case 1a: Infinite Acting Reservoir

Finite Wellbore Solution

$$\varphi_D(r_D, t_{Dw}) = \frac{2\pi hk}{\dot{m}_t}\left[\varphi_i - \varphi(r,t)\right] = \frac{1}{2}e^{\frac{1}{4t_{Dw}}}E_1\left(S_D\frac{r_D^2}{4t_{Dw}}\right) \qquad 3.23$$

Line Source Solution

$$\varphi_D(r_D, t_{Dw}) = \frac{2\pi hk}{\dot{m}_t}\left[\varphi_i - \varphi(r,t)\right] = \frac{1}{2}E_1\left(S_D\frac{r_D^2}{4t_{Dw}}\right) \qquad 3.24$$

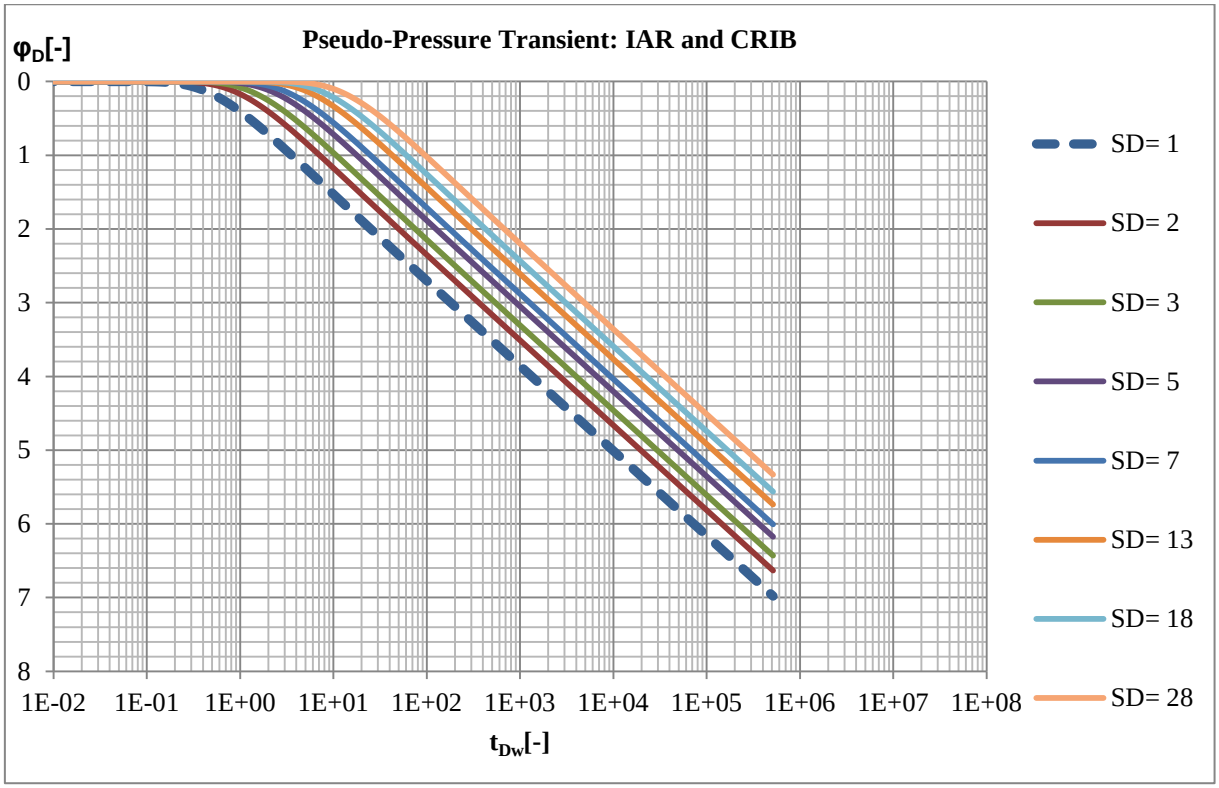

Figure 40: Pseudo-Pressure Transient in Infinite Reservoir

Note that the transient profiles in Figure 40 assume constant values of S_D for which the pressure transient is performed; however S_D could be changing with time from real reservoir responses, which could be identified by computing the average apparent permeability described in Appendix 10. Unlike the rate transient model, the pressure transient model does not converge for different values of S_D during late-time production.

The derivative plot given in Figure 41 however shows that the infinite acting radial flow (IARF) could be noticeable in the middle time region for all the values of S_D, although the IARF is masked for increasing values of S_D. Hence by neglecting heat conduction, the reservoir response could be analyzed much easier with the help of type curves and derivative plots.

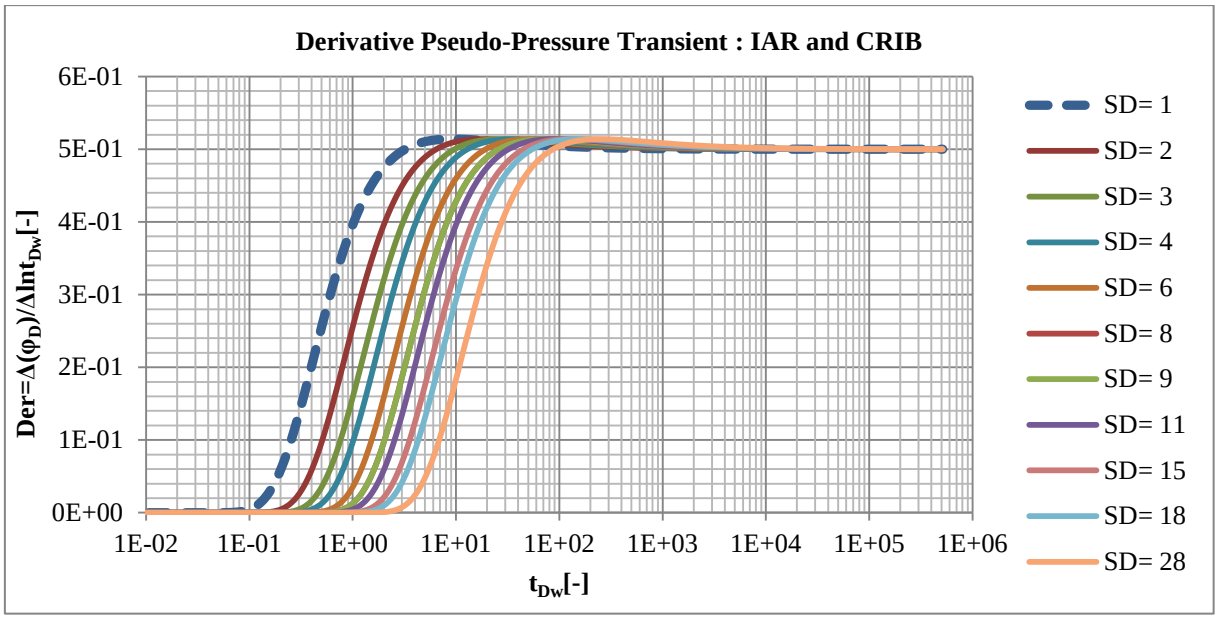

Figure 41: Derivative of Pseudo-Pressure Profile in Infinite Reservoir

To reduce the number of variables in the reservoir responses, type curves are once more used. The general reservoir derivative responses using the line source and finite well bore solutions are given in Figure 42 for the infinite acting reservoir.

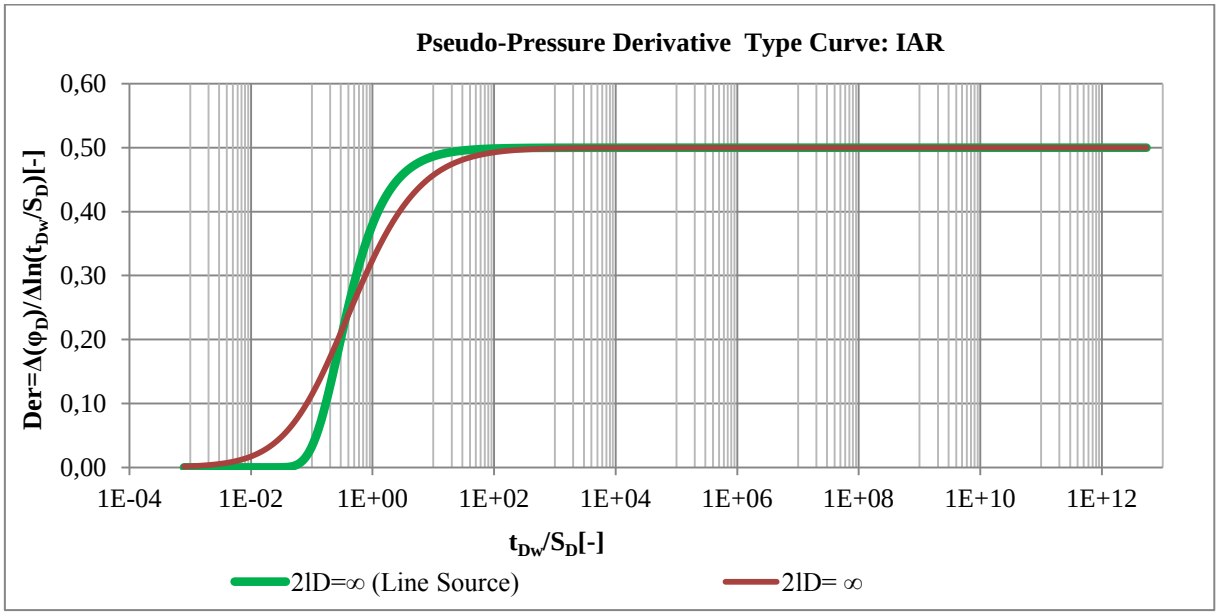

Figure 42: Generalized Transient Pseudo-Pressure Profile in Infinite Reservoir with Comparison of Finite Wellbore Solution and Line Source Solution

Note that the line source solution and finite wellbore solution are equivalent approximately for $t_{Dw}/S_D>100$ or for conventional reservoirs $t_{Dw}>100$.

The effects of recharge (constant pressure outer boundary) and no-flow at the reservoir boundary are depicted in Figure 43.

Part 2-Case 1b: Constant Pressure Outer Boundary Reservoir

$$\varphi_D(r_D,t_{Dw})=\frac{2\pi hk}{\dot{m}_t}[\varphi_i-\varphi(r,t)]=0.5\frac{\left[E_1\left(S_D\frac{r_D^2}{4t_{Dw}}\right)-E_1\left(S_D\frac{(2l_D-r_D)^2}{4t_{Dw}}\right)\right]}{\left[e^{-\left(\frac{S_D}{4t_{Dw}}\right)}+(2l_D-1)^{-1}e^{-S_D\frac{(2l_D-1)^2}{4t_{Dw}}}\right]} \quad 3.25$$

Part 2-Case 1c: No-Flow Outer Boundary Reservoir

$$\varphi_D(r_D,t_{Dw})=\frac{2\pi hk}{\dot{m}_t}[\varphi_i-\varphi(r,t)]=0.5\frac{\left[E_1\left(S_D\frac{r_D^2}{4t_{Dw}}\right)+E_1\left(S_D\frac{(2l_D-r_D)^2}{4t_{Dw}}\right)\right]}{\left[e^{-\left(\frac{S_D}{4t_{Dw}}\right)}-(2l_D-1)^{-1}e^{-S_D\frac{(2l_D-1)^2}{4t_{Dw}}}\right]} \quad 3.26$$

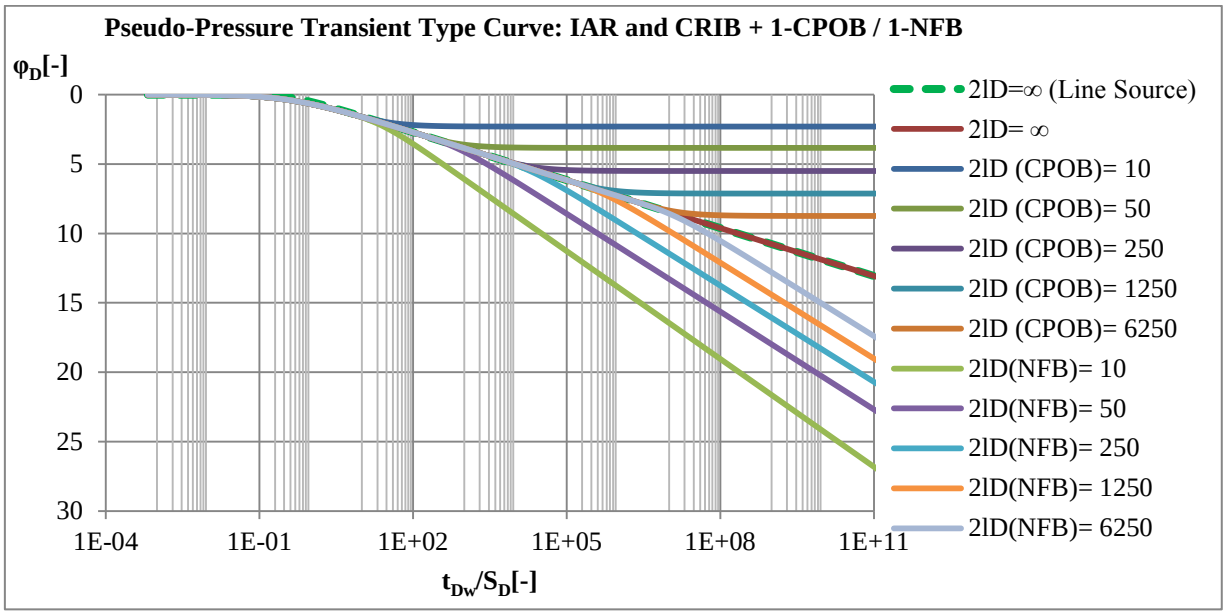

Figure 43: Transient Pseudo-Pressure Profile in Infinite Reservoir with One Recharge or One No-Flow Boundary at Distance l_D from Producing Well

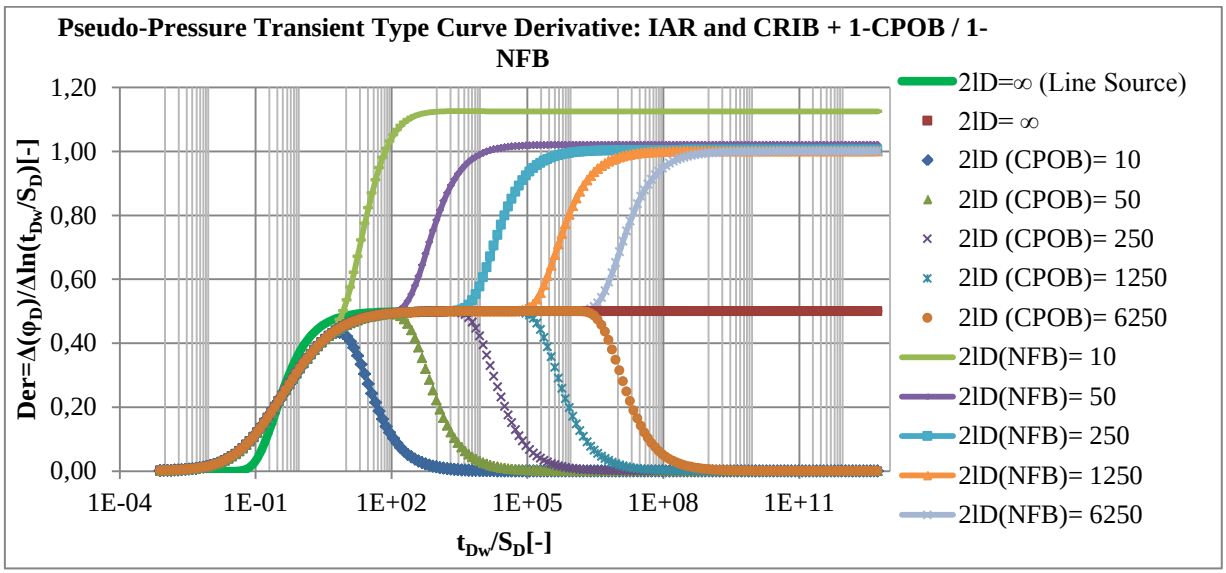

Figure 44: Derivative Pseudo-Pressure Profile in Infinite Reservoir with One Recharge or One No-Flow Boundary at Distance l_D from Producing Well

Part 2-Case 2: 0<γD<1

Part 2-Case 2a: Infinite Acting Reservoir

The transient pseudo-pressure response considering heat conduction can be estimated with the following models:

Early-Time Response

$$\varphi_D = \frac{2\pi hk}{\dot{m}_t}[\varphi_i - \varphi(r,t)] = H\left(\frac{S_D r_D^2}{4t_{Dw}}, \frac{r_D}{4}\frac{e_D\sqrt{F_{CD}}}{\sqrt{S_D}}\right) \quad 3.27$$

Late Time Response

$$\varphi_D = \frac{2\pi hk}{\dot{m}_t}[\varphi_i - \varphi(r,t)] = \frac{1}{2}W\left[\frac{r_D^2 S_D \mu_D}{4t_{Dw}}, r_D\sqrt{b_D}\right] \quad 3.28$$

The early and late time responses are very dependent on the thickness of the confining layers. As also given in Appendix 12 using the Laplace domain well test model recognition, late time solution can be conveniently used to describe the reservoir response at any production time provided the confining layers are thin.

Kinetic Model

With the Kinetic model, no early time and late time approximations are required; yet, the line source solution is still used. The solution to the kinetic model takes the form:

$$\varphi_D = \frac{2\pi hk}{\dot{m}_t}[\varphi_i - \varphi(r,t)] = \frac{1}{2}W\left(\frac{r_D^2}{4t_{Dw}}S_{Dk}, r_D\sqrt{\gamma_{Dk}}\right) \quad 3.29$$

Figure 45 depicts the dimensionless pseudo-pressure drawdown profile in a normally pressured gas hydrate reservoir with constant sandface rates. In the beginning, the hydrate dissociation is mainly influenced by the heat energy stored in the reservoir and when pressure drawdown is significant at later production times, the hydrate dissociation increases accordingly due to heat flux from conduction. If the heat flux is constant and the saturation of hydrate is extremely large, the hydrate dissociation would act as a strong pressure support and the reservoir responses will be similar to constant pressure outer boundary responses as seen in Figure 43.

From well test analysis, the first slope of the semi-log plot will depict the average reservoir permeability without the influence of heat conduction from the confining layers.

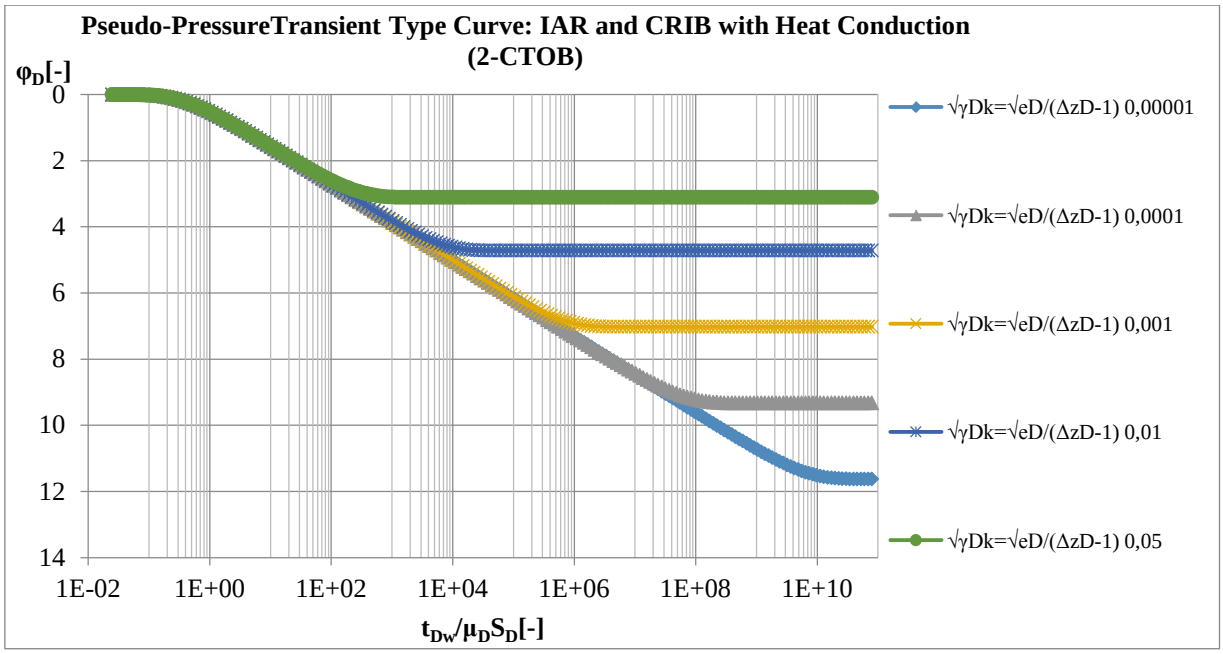

Figure 45: Transient Pseudo-Pressure Profile in Infinite Reservoir with Constant Sandface Rate

It should be emphasized that the analytical model does not address the secondary hydrate formation. As depicted in Figure 45, high dissociation rates would increase the wellbore flowing pressure. An increase in the wellbore flowing pressure will also mean a decrease in hydrate dissociation. Successive increase and decrease in hydrate dissociation can possibly occur during pressure drawdown hence distorting pressure transient responses significantly. Hence the constant rate method is not advisable for well test purposes in gas hydrate reservoirs as such responses would distort well test data and make analysis very cumbersome.

Part 2-Case 2b: Bounded Reservoirs

The effects of recharge and no-flow boundaries coupled with heat flux can be predicted using the image well theory analogue [44].

Approximate Line Source Solutions for Recharge Boundary

$$\varphi_D = \frac{2\pi hk}{\dot{m}_t}[\varphi_i - \varphi(r,t)] = \frac{1}{2}W\left[\frac{r_D^2 S_D \mu_D}{4t_{Dw}}, r_D\sqrt{b_D}\right] - \frac{1}{2}W\left[\frac{(2l_D - r_D)^2 S_D \mu_D}{4t_{Dw}}, \frac{(2l_D - r_D)}{2}\sqrt{b_D}\right] \quad 3.30$$

Using the kinetic model we get:

$$\varphi_D = \frac{2\pi hk}{\dot{m}_t}[\varphi_i - \varphi(r,t)] = \frac{1}{2}W\left(\frac{r_D^2}{4t_{Dw}} S_{Dk}, r_D\sqrt{\gamma_{Dk}}\right) - \frac{1}{2}W\left(\frac{(2l_D - r_D)^2}{4t_{Dw}} S_{Dk}, \frac{(2l_D - r_D)}{2}\sqrt{\gamma_{Dk}}\right) \quad 3.31$$

Approximate Line Source Solutions for No-flow Boundary

$$\varphi_D = \frac{2\pi hk}{\dot{m}_t}[\varphi_i - \varphi(r,t)] = \frac{1}{2}W\left[\frac{r_D^2 S_D \mu_D}{4t_{Dw}}, r_D\sqrt{b_D}\right] + \frac{1}{2}W\left[\frac{(2l_D - r_D)^2 S_D \mu_D}{4t_{Dw}}, \frac{(2l_D - r_D)}{2}\sqrt{b_D}\right] \quad 3.32$$

Using the kinetic model we get:

$$\varphi_D = \frac{2\pi hk}{\dot{m}_t}[\varphi_i - \varphi(r,t)] = \frac{1}{2}W\left(\frac{r_D^2}{4t_{Dw}} S_{Dk}, r_D\sqrt{\gamma_{Dk}}\right) + \frac{1}{2}W\left(\frac{(2l_D - r_D)^2}{4t_{Dw}} S_{Dk}, \frac{(2l_D - r_D)}{2}\sqrt{\gamma_{Dk}}\right) \quad 3.33$$

Figure 46 and Figure 47 depict the reservoir responses when producing in finite reservoirs. Profiles of dimensionless pseudo-pressure drawdowns and derivatives for constant pressure outer boundary and no-flow outer boundary are depicted.

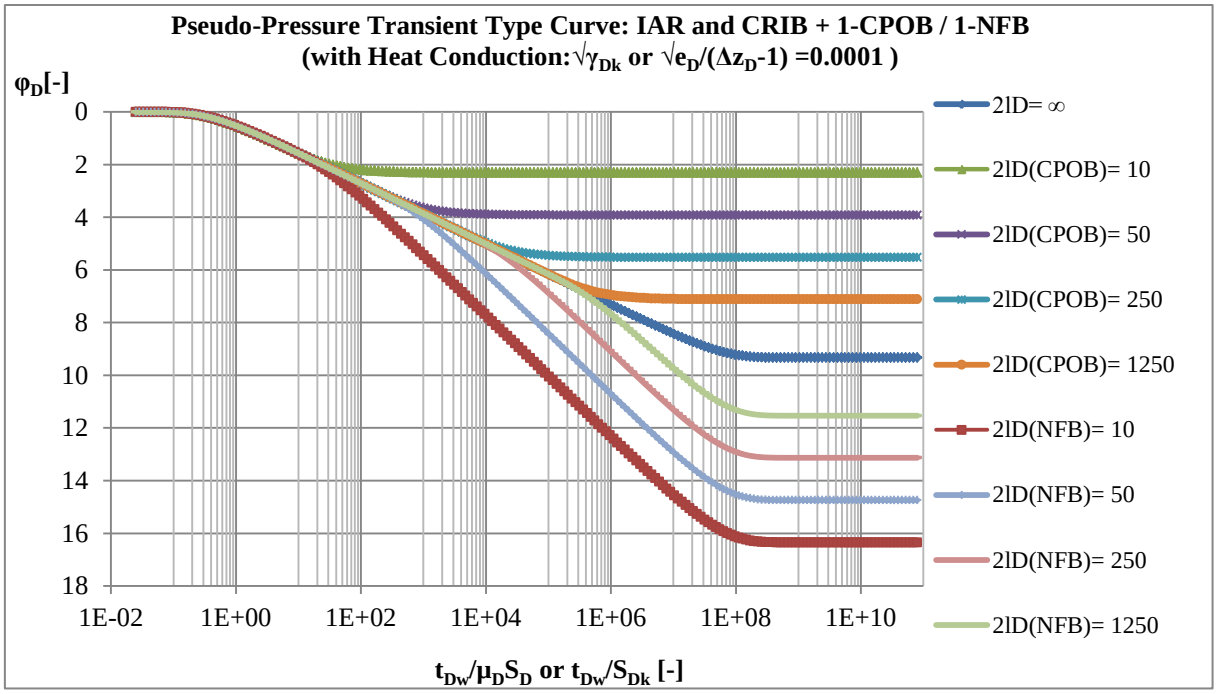

Figure 46: Transient Pseudo-Pressure Profile in Constant Pressure Bounded Reservoir with Constant Sandface Rate ($\sqrt{\gamma_{Dk}}=\sqrt{e_D/(\Delta z_D-1)}=0.0001$)

From Figure 46, it is noticeable that the influence of heat conduction could have a significant effect on the reservoir responses in bounded reservoirs, especially in reservoirs with no-flow barriers and significant amount of hydrates. In no-flow barriers, the no-flow boundary response could be masked by the hydrate dissociation rate during late time response. Conversely, if the heat dissociation rate is small, its influence will be noticeably predominantly in the late time period of flow.

As expected, hydrate dissociation would act as pressure support to the reservoir when producing with constant sandface rates. Hence identifying reservoir boundaries becomes cumbersome. Performing a derivative plot in such a reservoir will show both constant pressure outer boundary profiles and no-flow outer boundary profiles; provided the reservoir is produced for a long period of time and the dissociation rate is slow. In such reservoirs, it is therefore important to perform well test with small drawdowns such that significant hydrate dissociation effects do not distort well test data analysis for identifying the reservoir boundaries.

For both infinite, no-flow and constant pressure outer boundary conditions, both semi-log and derivative plots will exhibit constant pressure outer boundary responses at late time regions.

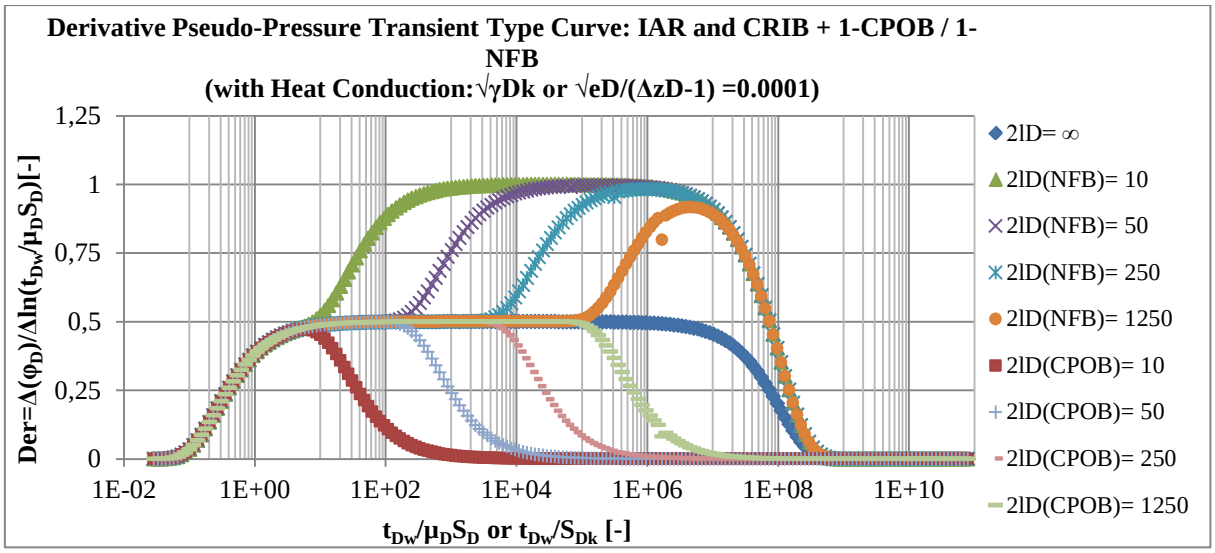

Figure 47: Transient Pseudo-Pressure Profile in Bounded Reservoir with Constant Sandface Rate ($\sqrt{\gamma_{Dk}}=\sqrt{e_D/(\Delta z_D-1)}=0.0001$)

3.3 Reservoir Parameters

In the models developed in the appendices and shown earlier, some dimensionless parameters responsible for dissociation were assumed constant such that type curves could be generated for the reservoir responses. However, it is important to investigate the significance of changes in the dimensionless parameters during depletion or for different reservoir types.

Modified Dimensionless Decomposition Compressibility

The modified decomposition compressibility reflects the total energy change in the hydrate layer during dissociation.

$$S_D = \frac{\left[\rho_t k\left(\frac{k_r}{\eta}\right)_t\right]_{id}}{\left[\rho_t k\left(\frac{k_r}{\eta}\right)_t\right]}\left(\frac{(\rho c_T)_{eff}}{(\rho c_T)_{eff,id}} + \frac{c}{h_d(\rho c_T)_{eff,id}}\right) \qquad 3.\,34$$

$$c = \left[c_{p,g}S_g\rho_g\left(\frac{T(c_g+c_F)}{\left[\frac{dT_{eq}}{dp}\right]}+1\right) + c_{p,w}S_w\rho_w\left(\frac{T(c_w+c_F)}{\left[\frac{dT_{eq}}{dp}\right]}+1\right) + c_{p,H}S_H\rho_H\left(\frac{T(c_F)}{\left[\frac{dT_{eq}}{dp}\right]}+1\right) + c_{p,m}\frac{(1-\emptyset)}{\emptyset}\rho_m\left(\frac{T(c_m)}{\left[\frac{dT_{eq}}{dp}\right]}+1\right) + S_H\rho_H\frac{dh_d}{dT_{eq}}\right]\left[\frac{dT_{eq}}{dp}\right] \qquad 3.\,35$$

The presence of water in the hydrate layer is very influential for hydrate dissociation due to its high specific heat capacity. Also notice that if the effective compressibility of the free fluid in the reservoir is high, coupled with high dissociation energy for the hydrate in question, the hydrate decomposition becomes insignificant as the modified dimensionless decomposition compressibility tends to 1, which reflects the ideal reservoir response. To summarize, if the free fluid saturation is relatively significant compared to the hydrate saturation, the hydrate dissociation effect on the reservoir response will not be noticeable.

Dimensionless Conductive Heat Flux Coefficient

$$e_D = \left\{\lambda\frac{1}{h_d k\left[\rho_t\left(\frac{k_r}{\eta}\right)_t\right]}\left[\frac{dT_{eq}}{dp}\right]\frac{r_w^2}{\pi h^2}\right\} \qquad 3.\,36$$

The amount of heat flux into the hydrate layer for dissociation is highly dependent on the interlayer heat flux coefficient given above. Recognizing the very little changes in the heat conductivity of formation rocks, we can conclude that the influence of heat conduction diminishes with increasing mobility of the free fluid layer and increasing thickness of the hydrate layer.

Dimensionless Interlayer Heat Flux Coefficient

$$b_D = \frac{e_D}{(\Delta z_D - 1)} \tag{3. 37}$$

$$\Delta z_D = \frac{\Delta z}{\left(\frac{h}{2}\right)} = \frac{\left[\left(\frac{h}{2}\right) + h_{\text{confining layer}}\right]}{\left(\frac{h}{2}\right)} \tag{3. 38}$$

From the definition of the dimensionless interlayer heat influx coefficient, the smaller the thickness of the confining layer coupled with the constant outer temperature imposed on this layer, the higher the heat influx rate. This implies even with a small value of the dimensionless heat flux coefficient, the value of the dimensionless interlayer coefficient could increase significantly for thin confining layers.

Dimensionless Interlayer Heat Flux Compressibility

$$S_D\mu_D = \left(S_D + \frac{F_{CD} e_D (\Delta z_D - 1)}{3}\right) \tag{3. 39}$$

$$F_{CD} = \frac{h^2}{4}\frac{(\rho c_p)_{eff}}{\lambda}\left[\frac{r_w^2[(\rho_w \emptyset c_{T,w}) + (\rho_g \emptyset c_{T,g})]}{k\left[\rho_t\left(\frac{k_r}{\eta}\right)_t\right]}\right]_i \tag{3. 40}$$

$$e_D = \left\{\lambda \frac{1}{h_d k\left[\rho_t\left(\frac{k_r}{\eta}\right)_t\right]}\left[\frac{dT_{eq}}{dp}\right]\frac{r_w^2}{\pi h^2}\right\} \tag{3. 41}$$

$$S_D\mu_D = S_D + \left(\frac{(\Delta z_D - 1)}{3}\left[\frac{dT_{eq}}{dp}\right]\frac{(\rho c_p)_{eff}}{4h_d k\left[\rho_t\left(\frac{k_r}{\eta}\right)_t\right]\pi}\left[\frac{r_w^4 \emptyset[(\rho_w c_{T,w}) + (\rho_g c_{T,g})]}{k\left[\rho_t\left(\frac{k_r}{\eta}\right)_t\right]}\right]_i\right) \tag{3. 42}$$

Similarly, hydrate reservoirs with high permeabilities and high dissociation energies will have negligible influence from heat conduction as the second term on the right hand side of the equation above becomes insignificant especially in the early time period of production.

3.4 Rate Transient Analysis in Normally Pressured Gas Hydrate Reservoirs

Pressure and rate transient data provide a good source of understanding reservoir behavior under different production scenarios. From test data we strive at obtaining vital reservoir parameters such as the permeability. However, the multiphase well test model developed earlier uses total mass rates of the whole system. Moreover, the multiphase pseudo-pressure used for linearization should be retransformed for well test analysis purposes. Other approaches still exist in analyzing two phase well test data such as [53], [62].

Rate Transient Analysis

The rate transient models developed in this work assumed constant multiphase pseudo pressure as a prerequisite for applying future superposition techniques. Hence, the methods of analysis developed hereafter address the constant multiphase pseudo-pressure. The next challenge lays in the derivation of the rate transient parameters of the different phases in the system. We first address the mass balance model as follows:

Multiphase

The dimensionless flow rate:

$$\dot{m}_{tD} = \frac{\rho_{t,st} Q_{t,st}(t)}{2\pi hk \int \rho_t \left(\frac{k_r}{\eta}\right)_t dp} = \frac{\dot{m}_t}{2\pi hk \int \rho_t \left(\frac{k_r}{\eta}\right)_t dp} \quad 3.43$$

$$\dot{m}_t = \dot{m}_{tD}\left[2\pi hk \int \rho_t \left(\frac{k_r}{\eta}\right)_t dp\right] = \dot{m}_{tD}[2\pi hk \int f_t(p)dp] \quad 3.44$$

The fractional mass flow:

$$\dot{m}_t = \dot{m}_{g,t} + \dot{m}_{w,t} \quad 3.45$$

$$\frac{\dot{m}_t}{\dot{m}_t} = \frac{\dot{m}_{g,t}}{\dot{m}_t} + \frac{\dot{m}_{w,t}}{\dot{m}_t} = f_{m,g} + f_{m,w} = f_{m,t} \quad 3.46$$

Gas Phase

$$\frac{\dot{m}_{g,t}}{\dot{m}_t} = \frac{\int \left(\rho_g \frac{k^*_{rg}}{\eta_g}\right) dp}{\int \rho_t \left(\frac{k_r}{\eta}\right)_t dp} = \frac{\int f_g(p)dp}{\int f_t(p)dp} = f_{m,g} \quad 3.47$$

$$k \int f_g(p)dp = \frac{\dot{m}_{g,t}}{\dot{m}_t} k \int f_t(p)dp = f_{m,g} k \int f_t(p)dp \quad 3.48$$

With the introduction of the pressure dependent pseudo-relative permeability [krg*(p)] given in Appendix 10, the equation above takes the form:

$$kk^*_{rg}(p) \int \frac{\rho_g}{\eta_g} dp = \frac{Q_{g,st}\rho_{g,st}}{\dot{m}_t} k \int f_t(p)dp \quad 3.49$$

$$kk^*_{rg}(p) = \frac{[\varphi PI(t)]_g}{\dot{m}_t}[k \int f_t(p)dp] \quad 3.50$$

Where,

$$[\varphi PI(t)]_g = \frac{Q_{g,st}\rho_{g,st}}{\int \frac{\rho_g}{\eta_g} dp} = \frac{Q_{g,st}}{\int \frac{1}{B_g \eta_g} dp}$$

The pseudo-pressure normalized rate (pseudo productivity index) representation above gives a relationship between the transient flow rate and the pseudo-pressure which is constant in this case for constant wellbore pressure tests.

Water Phase

Similarly, the effective permeability of the water phase could be given thus:

$$kk^{*}_{rw}(p) = \frac{[\varphi PI(t)]_w}{\dot{m}_t}[k\int f_t(p)dp] \quad 3.\ 51$$

Rate transient analyses should therefore be performed for the total system response, which is the linearized form of the reservoir response. From the derived parameters, the effective permeability of the different phases can be derived from the solutions derived for the dimensionless multiphase transient mass rate in Appendix 12.

3.4.1 Semi-log Analysis

To derive the reservoir parameters, it is essential to define a range for which IARF is easily noticeable such that semi-log analysis can be performed. From the models depicted earlier for the reservoir responses, the following range can be used:

Range: $10^2<t_{Dw}/\mu_D S_D<10^4$ and $\sqrt{\frac{e_D}{(\Delta z_D-1)}} < 0.01$

The numerical approximation given by [63] for rate transient solution in Appendix 12 can be simplified to:

$$\dot{m}_{tD} = \frac{1}{0.48465\ln\left(\frac{t_{Dw}}{S_D\mu_D}\right)+0.64757} \quad 3.\ 52$$

$$\frac{1}{\dot{m}_t} = \frac{1}{2\pi h[k\int f_t(p)dp]}\left[0.48465\ln\left(\frac{t_{Dw}}{S_D\mu_D}\right)+0.64757\right] \quad 3.\ 53$$

By expanding the dimensionless time, relating the gas density with the formation volume factor and considering the dimensionless compressibility-mobility, the above equation can be written in terms of real time:

$$\frac{1}{\dot{m}_t} = \frac{1.1161}{2\pi h[k\int f_t(p)dp]}\left[\log t + \log\left(\frac{k}{\emptyset r_w^2}\frac{f_t(p_i)}{\beta(p_i)}\right) - \log\left(S_D\mu_D\right) + 0.58018\right] \quad 3.\ 54$$

Where,

$$\frac{f_t(p_i)}{\beta(p_i)} = \frac{\rho_{t,i}\left(\frac{k_r}{\eta}\right)_{t,i}}{[(\rho_{w,i}c_{T,w,i})+(\rho_{g,i}c_{T,g,i})]} \quad 3.\ 55$$

Semi-log Plot

$$\frac{1}{\dot{m}_t}\ Versus\ t$$

A semi-log plot of the reciprocal total mass rate versus the time should give a straight line during infinite acting flow, provided the changes in the dimensionless dissociation terms ($S_D\mu_D$) with pressure are negligible. The gradient of the line can hence be used to estimate the effective permeability of the flowing phases.

The gradient of the semi-log plot:

$$m_{log} = \frac{1.1161}{2\pi h[k\int f_t(p)dp]} \quad 3.56$$

$$\left[k\int f_t(p)dp\right] = \frac{1.1161}{2\pi h m_{log}}$$

Effective gas permeability at IARF

$$kk^*_{rg}(p) = k^*_g(p) = \frac{[\varphi PI(t)]_g}{\dot{m}_t}[k\int f_t(p)dp] = \frac{[\varphi PI(t)]_g}{\dot{m}_t}\frac{1.1161}{2\pi h m_{log}} \quad 3.57$$

Dimensionless Dissociation Terms (IARF)

Applying the damage skin approach for well test analysis we get an approximation of the dissociation terms for the hydrate layer.

$$(S_D\mu_D)_{avg} = \left(S_D + \frac{F_{CD}e_D(\Delta z_D - 1)}{3}\right)_{avg} \approx \exp\left\{-0.434\left[\frac{\left[\frac{1}{\dot{m}_t}\right]_{t=1s}}{m_{log}} - \log\left(\frac{k}{\emptyset r_w^2}\frac{f_t(p_i)}{\beta(p_i)} * 10^{0.58018}\right)\right]\right\} \quad 3.58$$

It is worth mentioning that the above method of analysis just approximately quantifies the degree of hydrate dissociation.

Note that if heat conduction influence is negligible, the following are valid:

$10^2 < t_{Dw}/S_D$ and $\sqrt{\frac{e_D}{(\Delta z_D - 1)}} \ll 1$

$$(S_D\mu_D)_{avg} \approx S_{D,avg} \approx \exp\left\{-0.434\left[\frac{\left[\frac{1}{\dot{m}_t}\right]_{t=1s}}{m_{log}} - \log\left(\frac{k}{\emptyset r_w^2}\frac{f_t(p_i)}{\beta(p_i)} * 10^{0.58018}\right)\right]\right\} \quad 3.59$$

The rate transient solution can be simplified to:

$$\dot{m}_{tD} = \frac{1}{0.48465\ln\left(\frac{t_{Dw}}{S_D}\right) + 0.64757} \quad 3.60$$

The same procedures applied earlier are also applicable. It should be highlighted that some constant pressure tests are conducted by adjusting the surface pressure to constant values for example at separator point. From pressure profile calculations in wellbores, a constant wellhead pressure and changing flow rates will imply the flowing downhole pressure will constantly be changing. With this regard, it is vital to modify the rate transient equation for such a system and this could be done by applying the superposition principle for multi-pressure solutions [64]. This is though cumbersome for multiphase systems and will not be addressed in this work. To avoid complicated analyses, pump installations for depressurizing the hydrate layer should be as close to the reservoir producing layer as possible.

3.4.2 Rate Derivative Analysis

The derivative plot is principally used for diagnosis of the reservoir behavior and for a better view of the different flow regimes and boundary responses. However, the works of Tiab [[57], [65], [66]] have shown that the derivative analysis can be used in deriving reservoir parameter. Nonetheless, this will not be addressed in this work and just derivative responses are highlighted.

The derivative for RTA is given by:

$$\frac{d\left(\frac{1}{\dot{m}_t}\right)}{dlnt} = \frac{0.5}{2\pi h[k\int f_t(p)dp]} = Der \qquad 3.\ 61$$

The log-log derivative plot is given by:

$$\frac{d\left(\frac{1}{\dot{m}_t}\right)}{dlnt} = \frac{d\left(\frac{1}{\dot{m}_t}\right)}{dt}t = \frac{0.5}{2\pi h[k\int f_t(p)dp])} = Der \qquad 3.\ 62$$

$$\log\left[\frac{d\left(\frac{1}{\dot{m}_t}\right)}{dt}t\right] = \log\left[\frac{0.5}{2\pi h[k\int f_t(p)dp])}\right] \qquad 3.\ 63$$

Plot

$$\log\left[\frac{d\left(\frac{1}{\dot{m}_t}\right)}{dt}t\right] \text{ vs } \log t \qquad 3.\ 64$$

If the derivative is time independent, the log-log plot will remain constant during IARF.

$$k^*_{g,avg}(p) = \frac{[\varphi PI(t)]_g}{\dot{m}_t}[k\int f_t(p)dp] = \frac{[\varphi PI(t)]_g}{\dot{m}_t}\frac{0.5}{2\pi hDer} \qquad 3.\ 65$$

Characteristics of Type Curve Derivatives

Early Time Region

No skin response from model.

IARF

$$\frac{d\left[\frac{1}{\dot{m}_{tD}}\right]}{d\left[\ln\left(\frac{t_{Dw}}{\mu_D s_D}\right)\right]} = 0.5 \qquad 3.\ 66$$

Boundary dominated Flow with 1-NFB and negligible heat influx

$$\frac{d\left[\frac{1}{\dot{m}_{tD}}\right]}{d\left[\ln\left(\frac{t_{Dw}}{\mu_D s_D}\right)\right]} = 1 \qquad 3.\ 67$$

Boundary dominated Flow with 1-CPOB

$$\frac{d\left[\frac{1}{\dot{m}_{tD}}\right]}{d\left[\ln\left(\frac{t_{Dw}}{\mu_D s_D}\right)\right]} = 0 \qquad 3.\ 68$$

Boundary dominated Flow with 1-NFB or 1-CPOB and high heat influx

$$\frac{d\left[\frac{1}{\dot{m}_{tD}}\right]}{d\left[\ln\left(\frac{t_{Dw}}{\mu_D S_D}\right)\right]} = 0 \qquad 3.\ 69$$

3.4.3 Identifying Reservoir Boundaries (Heat conduction effects are negligible)

$$\dot{m}_{tD}(r_D = 1, t_{Dw}) = \frac{\dot{m}_t(t)}{2\pi hk\left(\varphi_i - \varphi_{wf}\right)} = 2\frac{\left[e^{-\left(\frac{S_D}{4t_{Dw}}\right)} \pm (2l_D - 1)^{-1} e^{-\frac{(2l_D-1)^2}{4t_{Dw}} S_D}\right]}{E_1\left(\frac{S_D}{4t_{Dw}}\right) \mp E_1\left(S_D \frac{(2l_D-1)^2}{4t_{Dw}}\right)} \qquad 3.\ 70$$

$$\dot{m}_{tD}(r_D = 1, t_{Dw}) = \frac{\dot{m}_t(t)}{2\pi hk\left(\varphi_i - \varphi_{wf}\right)} = 2\frac{\left[e^{-(x_1)} \pm \frac{e^{-x_2}}{(2l_D-1)}\right]}{E_1(x_1) \mp E_1(x_2)} \qquad 3.\ 71$$

Boundary dominated flow is perceived when the Ei-function containing the boundary term becomes noticeable. This is achieved approximately for values $x_2 \leq 701.828$ (where $E_1(x_2)$=2.2548E-308) or for more practical purposes (which could also be noticed from a derivative plot) at x_2=4 (where $E_1(x_2)$=3.78E-03). The second value of x_2 will be considered which actually denotes the transition point, much noticeable from a derivative plot; nevertheless, when using the semi-log plots, lower values can be used such as 1.785 [67], which has been described by the authors as the point whereby the IARF gradient intersects the boundary dominated flow gradient. With this said, the value of the distance to the boundary can be estimated thus:

$$S_D \frac{(2l_D-1)^2}{4t_{Dw,t}} = 4 \qquad 3.\ 72$$

$$l_D = \frac{l}{r_w} = \left[2 * \sqrt{\frac{t_{Dw,tf}}{S_D}}\right] + 0.5 \qquad 3.\ 73$$

$$l = \left[2 * \sqrt{\left[\frac{k}{\emptyset}\frac{f_t(p_i)}{\beta(p_i)} t_{tf}^*\right]\frac{1}{S_D}}\right] + 0.5 r_w \approx 2\left[* \sqrt{\left[\frac{k}{\emptyset}\frac{f_t(p_i)}{\beta(p_i)} t_{tf}^*\right]\frac{1}{S_D}}\right] \qquad 3.\ 74$$

The time t_{tf}^* reflects the time at which the deviation from IARF to boundary dominated flow immediately embarks and is best derived from the derivative plot.

Using the model given by [67] we get:

$$l = 0.75\left[\sqrt{\left[\frac{k}{\emptyset}\frac{f_t(p_i)}{\beta(p_i)} t_f^*\right]\frac{1}{S_D}}\right] \qquad 3.\ 75$$

$$l = 0.75 r_w \left[\sqrt{\frac{t_{Dw,f}}{S_D}}\right] \qquad 3.\ 76$$

The time t_f^* reflects the time whereby the IARF gradient intersects the boundary dominated flow gradient and is best derived from a semi-log plot. It should be noted that the intersection time is greater than the transition time; as such, the two models should give the same value if the flowing times are correctly deduced.

For more methods of determining the reservoir boundary, other works such as that of Robert Chapius [[42], [68]] can be investigated.

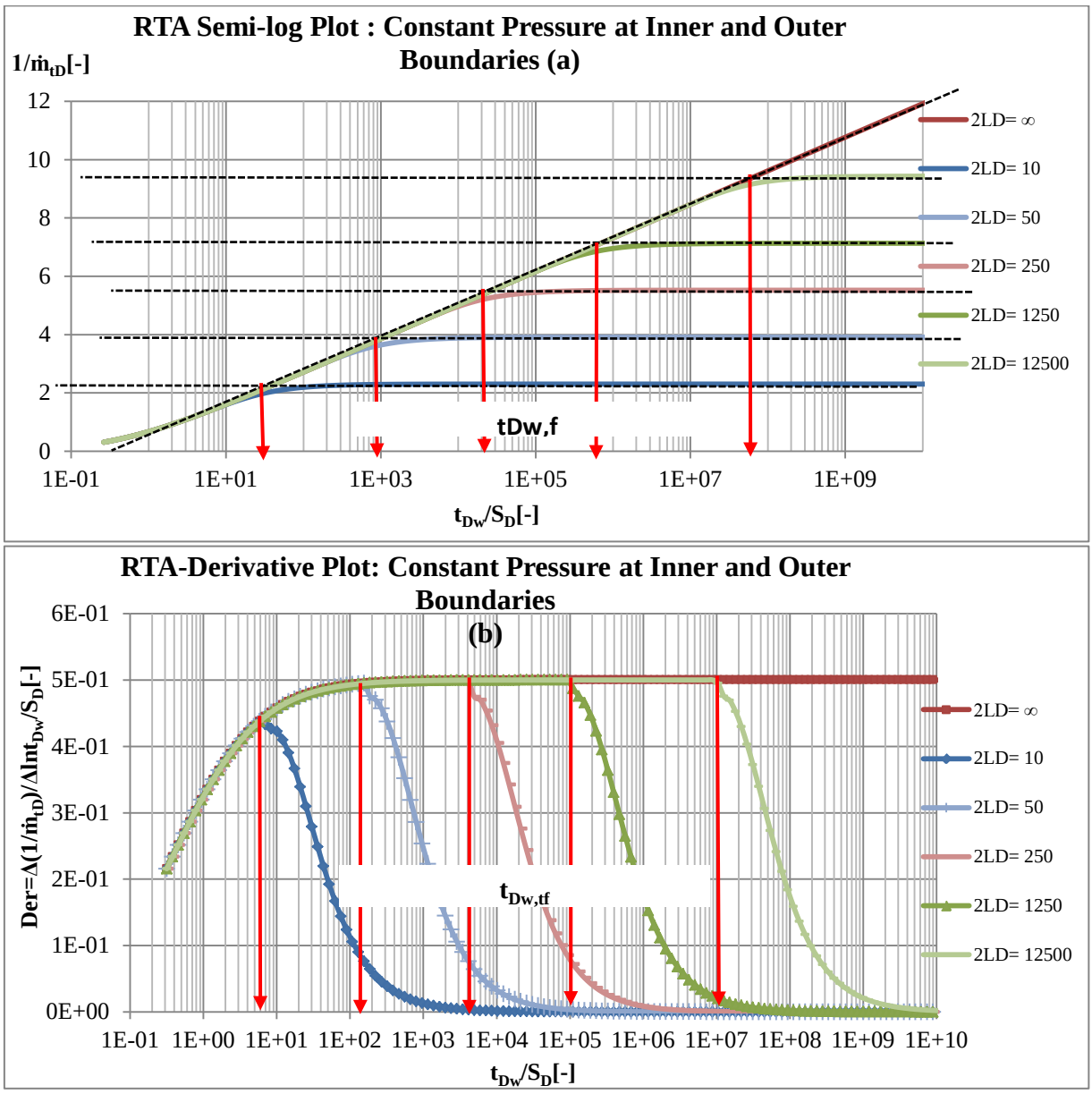

Figure 48: Boundary Identification: (a) with semi-log plot; (b) with derivative plot

3.4.4 Type Curve Matching (Heat Conduction Considered)

As was shown in Chapter 3.1, recharge boundary dominated flow and the influence of heat conduction will have the same reservoir response in the late time region as they are all pressure supporting parameters. However, it should be emphasized that the heat influx model is a transient model and if the dissociation process is quite significant and there is no rate decline, the pressure propagation in the reservoir stops and won´t reach the boundary. This implies the reservoir boundaries cannot be detected for such cases. From well test data, it is difficult to distinguish which of the parameters is the more influential or the determining parameter for such behavior.

For reservoirs with impermeable boundaries (NFB) the no flow boundary behavior might occur before the influence of heat conduction has a significant pressure support behavior on the reservoir response as seen in Figure 39. In such cases, it is possible to derive both the distance to boundary and make an estimate of the heat influx terms.

For the type curve matching method addressed here, we will ignore the effects of boundary and propose the type curve match required to estimate the reservoir parameters during transient flow regimes.

The type curve has an advantage over the semi-log plot in that the reservoir parameters are estimated at each time step whereas we obtain average values using the semi-log plot. As seen with the semi-log plots, the reciprocal of the rate transient is a much better method of characterizing the reservoir from a log scale. Hence, the type-curve matching done on a semi-log scale should be performed using the reciprocal of the rate transient.

Required Plots

- $\frac{1}{\dot{m}_{tD}}$ Versus t_{Dw}
- $\frac{1}{\dot{m}_{t}}$ Versus t
- $\varphi PI(t)$ Versus t

Time Match

The time match points along the vertical are:

$$\left[\frac{t_{Dw}}{S_D \mu_D}\right]_{MP};\ t_{MP};\left[\sqrt{b_D}\right]_{MP} \qquad 3.\ 77$$

Where,

$$t_{Dw} = t\frac{k}{\emptyset r_w^2}\frac{f_t(p_i)}{\beta(p_i)}$$

From the match points, the dimensionless interlayer heat flux compressibility is derived thus:

$$[S_D \mu_D]_{MP} = \frac{t_{Dw}}{\left[\frac{t_{Dw}}{S_D \mu_D}\right]_{MP}} = \frac{k}{\emptyset r_w^2}\frac{f_t(p_i)}{\beta(p_i)}\frac{t_{MP}}{\left[\frac{t_{Dw}}{S_D \mu_D}\right]_{MP}} \qquad 3.\ 78$$

Rate Match

The match along the horizontal is given by:

$$\left[\frac{1}{\dot{m}_{tD}}\right]_{MP};\left[\frac{1}{\dot{m}_{t}}\right]_{MP};[\varphi PI(t)]_{g,MP}$$

From the match points, the effective permeabilities of the different phases are derived thus:

$$[k\int f_t(p)dp]_{MP} = \frac{\left[\frac{1}{\dot{m}_{tD}}\right]_{MP}}{2\pi h\left[\frac{1}{\dot{m}_t}\right]_{MP}} \quad 3.\ 79$$

Conventionally, the match point of the multiphase pseudo-pressure at the wellbore would be a constant value from the imposed inner boundary condition used in deriving the models for this work. If this is not the case, the use of the type curve matching techniques will depict changing values and can still be used to derive the effective permeability of the flowing phases.

$$kk_{rg}^{*}(p) = [\varphi PI(t)]_{g,MP}\left[\frac{1}{\dot{m}_t}\right]_{MP}[k\int f_t(p)dp]_{MP} \quad 3.\ 80$$

Where,

$$[\varphi PI(t)]_g = \frac{Q_{g,st}\rho_{g,st}}{\int\frac{\rho_g}{\eta_g}dp} = \frac{Q_{g,st}}{\int\frac{1}{B_g\eta_g}dp}$$

Water Phase

Similarly, the effective permeability of the water phase could be given thus:

$$kk_{rw}^{*}(p) = \frac{[\varphi PI(t)]_w}{\dot{m}_t}[k\int f_t(p)dp] \quad 3.\ 81$$

For mass conservation to be valid and to improve on the accuracy of the match points, the following mass conservation equation must be valid:

$$\frac{\dot{m}_g(t)+\dot{m}_w(t)}{\dot{m}_t} = \frac{2\pi h\left\{\left[[kk_{rg}^{*}(p)]_{MP}\left(\int_{p_{wf}}^{p_i}\frac{1}{B_g\eta_g}dp\right)\right]+\left[[kk_{rw}^{*}(p)]_{MP}\left(\int_{p_{wf}}^{p_i}\frac{1}{B_w\eta_w}dp\right)\right]\right\}[\dot{m}_{tD}]_{MP}}{\dot{m}_t} = 1 \quad 3.\ 82$$

3.5 Pressure Transient Analysis in Normally Pressured Gas Hydrate Reservoirs

As mentioned earlier, pressure transient analysis in normally pressured gas hydrates could be handled likewise conventional gas reservoirs, however considering multiphase aspects. It is still worth mentioning that the assumptions of constant sandface rate or even surface rates are hardly achieved during well test analysis, especially with multiphase systems.

As was seen with the rate transient solution, the models have to be represented such that the measured data during the test (here the pressure) can be analyzed. With RTA, the linearized models were represented in terms of the transient total mass rate which is measurable from well test data, whereas in PTA the linearized models were represented in terms of the transient total pseudo-pressure which is not directly measured. This implies for a proper analysis of the pressure transient data, the computation of the pseudo-pressure of the reservoir system should be performed, which is

unfortunately not possible for newly tested reservoirs. As a result, the models will further be simplified such that effective permeabilities of the different phases can be estimated.

Multiphase

$$\varphi_D = 2\pi hk\frac{\int \rho_t\left(\frac{k_r}{\eta}\right)_t dp}{\dot{m}_t} = 2\pi hk\frac{\int f_t(p)dp}{\dot{m}_t} \quad 3.\,83$$

Gas Phase

$$Q_{g,st} = \frac{1}{\varphi_D}\frac{[2\pi hk\int f_t(p)dp]}{\rho_{g,st}} f_{m,g} \quad 3.\,84$$

$$Q_{g,st} = \frac{1}{\varphi_D}\frac{[2\pi hk\int f_g(p)dp]}{\rho_{g,st}} \quad 3.\,85$$

Water Phase

$$Q_{w,st} = \frac{1}{\varphi_D}\frac{[2\pi hk\int f_t(p)dp]}{\rho_{w,st}} f_{m,w} \quad 3.\,86$$

$$Q_{w,st} = \frac{1}{\varphi_D}\frac{[2\pi hk\int f_w(p)dp]}{\rho_{w,st}} \quad 3.\,87$$

Due to the constantly changing flow rate of the different phases during the pressure transient test for the multiphase system, the pseudo-pressure normalized rate method is best used to analyze the data as will be shown later.

Pressure Transient Analysis (PTA)

Depending on the rate of change of relative permeability of the fluid in question, the flow rate could be very time dependent, which makes the analysis of pressure transient responses difficult. For this reason, the pseudo reciprocal productivity index (rate normalized pseudo-pressure) is once more a good tool for analysis. However, Convolution/Deconvolution techniques could be most suitable for analysis of such reservoir responses.

$$\frac{\int \frac{\rho_g}{\eta_g}dp}{Q_{g,st}(t)\rho_{g,st}} = \frac{\int \frac{1}{B_g\eta_g}dp}{Q_{g,st}(t)} = [\varphi RPI(t)]_g = \frac{1}{2\pi hkk^*_{rg}(p)}\varphi_D$$

The rate normalized pseudo-pressure (pseudo reciprocal productivity index) representation above gives a relationship between the transient flow rate and the pseudo-pressure which is transient in this case for constant total sandface rate tests.

The PTA MBM during IARF is simplified for semi-log analysis thus:

Range: $10^2 < t_{Dw}/\mu_D S_D < 10^4$ and $\sqrt{\frac{e_D}{(\Delta z_D - 1)}} < 0.01$

$$[\varphi RPI(t)]_g = \frac{1.1515}{2\pi hkk^*_{rg}(p)}\left[\log t + \log\left(\frac{k}{\emptyset r_w^2}\frac{f_t(p_i)}{\beta(p_i)}\right) - \log(\mu_D S_D) + 0.3513\right] \quad 3.\,88$$

The same methods applied for RTA are applicable here with the above representation of the gas rate normalized pseudo-pressure. The characteristics of the rate normalized pseudo-pressure in this case are as follows:

- The pressure transient in the rate normalized pseudo-pressure reflects the reservoir behavior and hydrate dissociation effects
- The rate transient in the model reflects the changes in the effective permeability of the phase in question. Hence if the flow rate of a phase remains constant during production, a semi-log plot of the analysis could be made for the IARF model given above. However, for changing flow rates, the use of semi-log plots becomes impracticable; nonetheless, the semi-log analysis will still be addressed.

3.5.1 Semi-log Analysis

$[\varphi \mathrm{RPI(t)}]_g$ Versus t

The gradient of the semi-log plot:

$$m_{log} = \frac{1.1515}{2\pi h k k_{rg}^*(p)} \qquad 3.89$$

Effective gas permeability at IARF

$$k k_{rg}^*(p) = k_g^*(p) = \frac{1.1515}{2\pi h m_{log}} \qquad 3.90$$

Dimensionless Dissociation Terms (IARF)

Applying the damage skin approach for well test analysis we get an approximation of the dissociation terms for the hydrate layer.

$$(S_D \mu_D)_{avg} = \left(S_D + \frac{F_{CD} e_D (\Delta z_D - 1)}{3}\right)_{avg} \approx \exp\left\{-0.434\left[\frac{[[\varphi \mathrm{RPI(t)}]_g]_{t=1s}}{m_{log}} - \log\left(\frac{k}{\emptyset r_w^2}\frac{f_t(p_i)}{\beta(p_i)} * 10^{0.3513}\right)\right]\right\} \qquad 3.91$$

3.5.2 Pressure Derivative Analysis

Analogue derivative plots seen in RTA, the rate normalized pseudo-pressure can be applied for pressure transient analysis.

$$\frac{d\left([\varphi \mathrm{RPI(t)}]_g\right)}{d\ln t} = \frac{0.5}{2\pi h k k_{rg}^*(p)} = \mathrm{Der}$$

$$\log\left[\frac{d[\varphi \mathrm{RPI(t)}]_g}{dt} t\right] \text{ vs } \log t \qquad 3.92$$

If the derivative is time independent, the log-log plot will remain constant during IARF. The apparent effective gas permeability is given by (see Appendix 10 for details):

$$k_{g,avg}^*(p) = \frac{0.5}{2\pi h \mathrm{Der}} \qquad 3.93$$

3.5.3 Type Curve Matching (Heat Conduction Considered)

Required Plots

- φ_D Versus t_{Dw}
- $[\varphi_i - \varphi_{wf}(t)]$ Versus t
- $\varphi RPI(t)$ Versus t

Time Match

The time match points along the vertical are:

$$\left[\frac{t_{Dw}}{S_D\mu_D}\right]_{MP};\ t_{MP};\left[\sqrt{b_D}\right]_{MP} \qquad 3.\ 94$$

Where,

$$t_{Dw} = t\frac{k}{\emptyset r_w^2}\frac{f_t(p_i)}{\beta(p_i)}$$

From the match points, the dimensionless interlayer heat flux compressibility is derived thus:

$$[S_D\mu_D]_{MP} = \frac{t_{Dw}}{\left[\frac{t_{Dw}}{S_D\mu_D}\right]_{MP}} = \frac{k}{\emptyset r_w^2}\frac{f_t(p_i)}{\beta(p_i)}\frac{t_{MP}}{\left[\frac{t_{Dw}}{S_D\mu_D}\right]_{MP}} \qquad 3.\ 95$$

Pressure Match

The match along the horizontal is given by:

$$[\varphi_D]_{MP};[\varphi RPI(t)]_{g,MP};[\varphi_i - \varphi_{wf}]_{MP}$$

To perform the pressure matches above requires the use of the pseudo-pressure of the total system which is usually an unknown parameter for a newly tested reservoir and cannot be derived directly from the well test data as in the case of RTA. Hence, the pressure matching techniques to derive the effective permeability for different time could be very cumbersome.

4 Conceptual Models for Well Testing in Over-pressured Class 3 Gas Hydrates: The Composite Reservoir Moving Boundary Problem

As of now, most analytical models addressing over-pressured gas hydrate reservoirs apply the Stefan´s Problem. Authors such as Yuri F. Makogon [13] and Goodarz Ahmadi et al. [69], [70] have addressed this issue. Limitations of the models developed so far:

- The models were not developed for multiphase behavior
- The models did not consider the dependence of reservoir fluid properties to pressure and the solutions were presented in a linearized pressure form.
- The solutions for the dissociated zone considered the initial reservoir pressure as the equilibrium pressure. This further implies no fluid production would be expected for bottom-hole flowing pressures above the equilibrium pressure. Implying, the solutions cannot be used for reservoirs with free fluid in the hydrate layer, as fluid will be produced even at pressures above the equilibrium pressures.
- Constant terminal rate solutions were proposed although no free fluid was considered in the reservoir prior to dissociation. Constant terminal rate solutions are practically applicable only when free fluid is present, as this is the driving mechanism for pressure propagation.

The challenge with developing solutions to the moving boundary problem is deriving the radius of dissociation. In deriving the transient radius of dissociation, the model proposed by Verigin et al. [71] is till date most widely used. However, the model basically describes mass conservation at the dissociation front. In a similar manner, as also given in Appendix 13, the models derived here with different boundary conditions are developed such that mass conservation at the dissociation front and the equilibrium pressure are always valid. This boundary condition is analogous to composite reservoir systems but the main difference in the unknown radius of dissociation or front.

The diagrams below depict the behavior of the gas hydrates during dissociation under different pressure conditions.

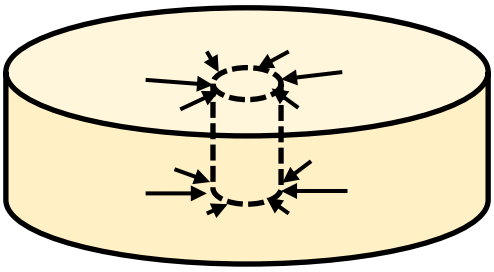

$P_{eq} < P_{wf} < P_i$

- Entire reservoir is un-dissociated
- Fluid production is possible if mobile fluid is present

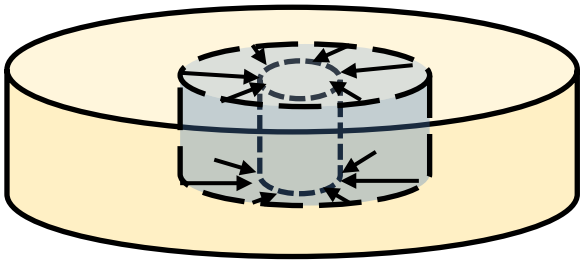

$P_{wf} < P_{eq}$
Composite Reservoir Model

- Dissociated Zone: $r_s(t)$ (Dynamic skin zone

4.1 Constant Pressure Solutions and RTA in Over-pressured Class 3 Gas Hydrates

The solutions presented for such reservoir responses with different boundary conditions have been developed analog to the Stefan Problem of melting ice in conjunction with the composite reservoir model. The solutions to the problem with different boundary conditions are given in Appendix 13.

MBM for the Multiphase Diffusivity Equation for Dissociated Zone

$$\frac{\partial^2 \hat{\varphi}_D}{\partial {r_D}^2} + \frac{1}{r_D}\frac{\partial \hat{\varphi}_D}{\partial r_D} - \left[S_D p + \left(e_D \widehat{\dot{Q}_{pD}}\right)_{caprock} + \left(e_D \widehat{\dot{Q}_{pD}}\right)_{Underburden}\right]\hat{\varphi}_D = 0 \qquad 4.1$$

MBM for the Multiphase Diffusivity Equation for Undissociated Zone

$$\frac{\partial^2 \hat{\varphi}_D}{\partial {r_D}^2} + \frac{1}{r_D}\frac{\partial \hat{\varphi}_D}{\partial r_D} - [S_{Dk} p]\hat{\varphi}_D = 0 \qquad 4.2$$

The linearization of the above diffusivity equation is done by applying the Kirchhoff transformation as was also done with the normally pressured gas hydrate reservoirs.

With proper definition of the boundary conditions, constant pressure solutions for infinite, constant outer boundary and no-flow boundary reservoirs are derived. The solutions to the problem are fully addressed in Appendix 13.

4.1.1 Infinite Acting Reservoirs

As given in Appendix 13, the boundary conditions at the dissociation front are defined such that mass conservation is satisfied and the pressure here equals the equilibrium pressure. With this definition, the pressure profile is derived for an infinite acting system. Due to the complexity of the system response, heat conduction effects from the confining layers were neglected in deriving similarity solutions. However, the solutions to the problem with heat conduction are given in Laplace domain. The Laplace domain well test model recognition method has also been applied to the solutions to depict the reservoir response and gives the exact solution to the problem. The models derived using the similarity variable, as also given in Appendix 13, are basically approximate solutions to the problem and are summarized below. For a detailed scrutiny of the reservoir response, the Laplace domain well test model recognition method should be used as also given in Appendix 13.

Dissociated Zone

$\boldsymbol{P_{wf} < P_{eq}}$

$$\varphi_D = (1-\varphi_{sD})\frac{E_1\left(S_D \frac{{r_D}^2}{4t_{Dw}}\right)}{\left[E_1\left(S_D \frac{1}{4t_{Dw}}\right) - E_1\left(S_D \frac{{r_{sD}}^2}{4t_{Dw}}\right)\right]} + \frac{\varphi_{sD} E_1\left(S_D \frac{1}{4t_{Dw}}\right) - E_1\left(S_D \frac{{r_{sD}}^2}{4t_{Dw}}\right)}{\left[E_1\left(S_D \frac{1}{4t_{Dw}}\right) - E_1\left(S_D \frac{{r_{sD}}^2}{4t_{Dw}}\right)\right]} \qquad 4.3$$

or

$$\varphi_D = \varphi_{sD}\frac{\left[E_1\left(S_D\frac{1}{4t_{Dw}}\right)-E_1\left(S_D\frac{{r_D}^2}{4t_{Dw}}\right)\right]}{\left[E_1\left(S_D\frac{1}{4t_{Dw}}\right)-E_1\left(S_D\frac{{r_{sD}}^2}{4t_{Dw}}\right)\right]}+\frac{\left[E_1\left(S_D\frac{{r_D}^2}{4t_{Dw}}\right)-E_1\left(S_D\frac{{r_{sD}}^2}{4t_{Dw}}\right)\right]}{\left[E_1\left(S_D\frac{1}{4t_{Dw}}\right)-E_1\left(S_D\frac{{r_{sD}}^2}{4t_{Dw}}\right)\right]} \quad 4.4$$

The model above gives a slight modification of the moving boundary model developed by [70] and [72] , as also given in Appendix 13, with the consideration of the possible mobile fluids in the hydrate zone and annulling the assumption of the reservoir pressure in the dissociated zone being equal to the equilibrium pressure. The dimensionless rate transient is given thus:

$$\dot{m}_{tD} = \frac{2(\varphi_{sD}-1)}{\left\{E_1\left(S_D\frac{{r_{sD}}^2}{4t_{Dw}}\right)-\left[E_1\left(\frac{S_D}{4t_{Dw}}\right)\right]\right\}}e^{-\left(S_D\frac{r_D^2}{4t_{Dw}}\right)} \quad 4.5$$

$P_{wf} \geq P_{eq}$

If the reservoir is produced above the equilibrium pressure, the dimensionless equilibrium pressure, φ_{sD}, equals zero and r_{sD} is infinite and models can be simplified to:

$$\varphi_D = \frac{E_1\left(S_{Dk}\frac{{r_D}^2}{4t_{Dw}}\right)}{E_1\left(\frac{S_{Dk}}{4t_{Dw}}\right)} \quad 4.6$$

$$\dot{m}_{tD} = \frac{2}{\left[E_1\left(\frac{S_{Dk}}{4t_{Dw}}\right)\right]}e^{-\left(S_{Dk}\frac{r_D^2}{4t_{Dw}}\right)} \quad 4.7$$

<u>Undissociated Zone</u> ***($P_{eq} \leq P_{wf} \leq P_i$)***

$$\varphi_D = \varphi_{sD}\frac{\left[E_1\left(\frac{{r_D}^2}{4t_{Dw}}S_{Dk}\right)\right]}{\left[E_1\left(\frac{{r_{sD}}^2}{4t_{Dw}}S_{Dk}\right)\right]} \quad 4.8$$

$$\dot{m}_{tD} = \frac{2\varphi_{sD}}{\left[E_1\left(\frac{{r_{sD}}^2}{4t_{Dw}}S_{Dk}\right)\right]}e^{-\left(\frac{r_D^2}{4t_{Dw}}S_{Dk}\right)} \quad 4.9$$

<u>Criterion for Valid Radius of Dissociation</u>

$$\frac{\left[E_1\left(\frac{{r_{sD}}^2}{4t_{Dw}}S_{Dk}\right)\right]e^{(S_{Dk}-S_D)\frac{r_{sD}^2}{4t_{Dw}}}}{\left\{E_1\left(S_D\frac{{r_{sD}}^2}{4t_{Dw}}\right)-\left[E_1\left(\frac{S_D}{4t_{Dw}}\right)\right]\right\}} = \frac{\varphi_{sD}}{(\varphi_{sD}-1)} \quad 4.10$$

From the dimensionless pseudo-pressure profile in Figure 49, we notice a higher pressure depression in the dissociated zone compared to the un-dissociated zone as dissociation increases the permeability of the dissociated zone and hence imposing constant pressure at the wellbore will cause much higher pressure depletion in the dissociation zone. However, notice that the effect becomes insignificant as pressure depletion propagates deeper into the reservoir which is also seen in the rate transient response.

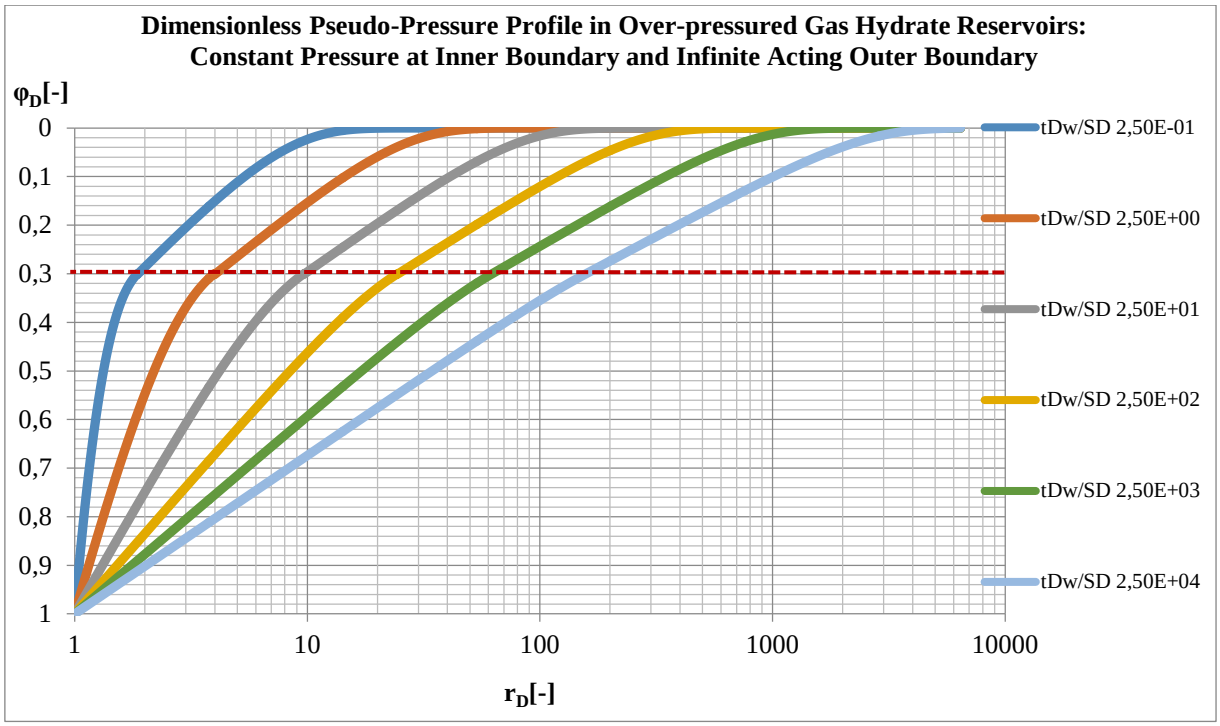

Figure 49: Pseudo-Pressure Profile in Infinite Reservoir with Constant Wellbore Pressure (Moving Boundary Problem), φ_{sD}=0.3, S_{Dk}/S_D (≤1)=0.01

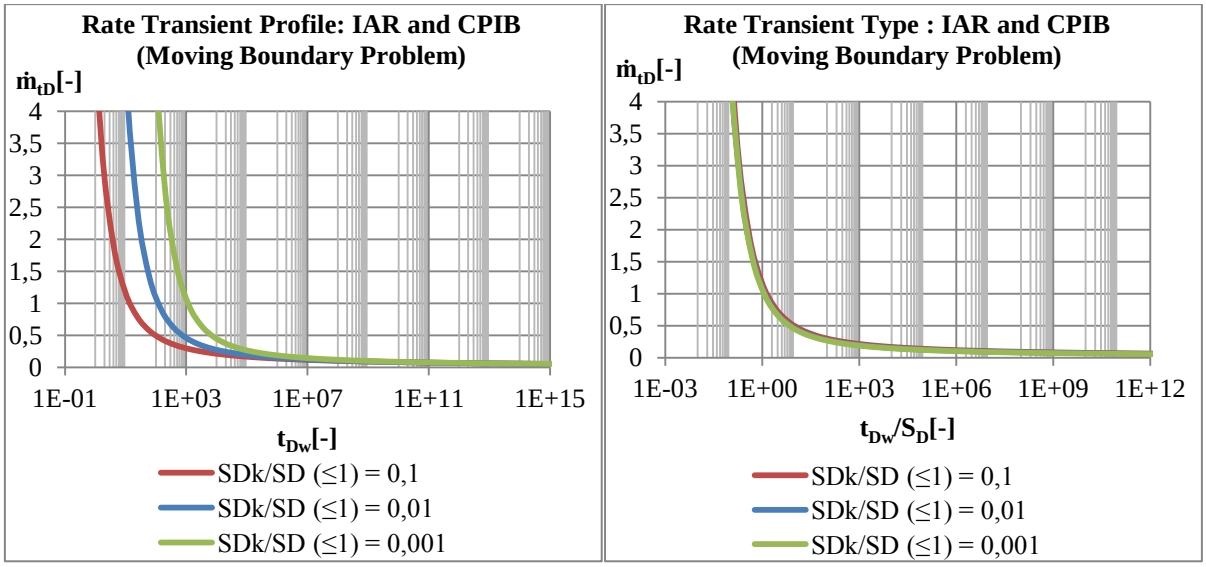

Figure 50: Rate Transient Profile in Infinite Reservoir with Constant Wellbore Pressure (Moving Boundary Problem), φ_{sD}=0.3

With a look at Figure 50, one would get the impression the reservoir response is similar to the normally pressured gas hydrate reservoir; however, the effect of skin or dissociated radius can be better seen with the use of type curve derivative plots as depicted in Figure 51.

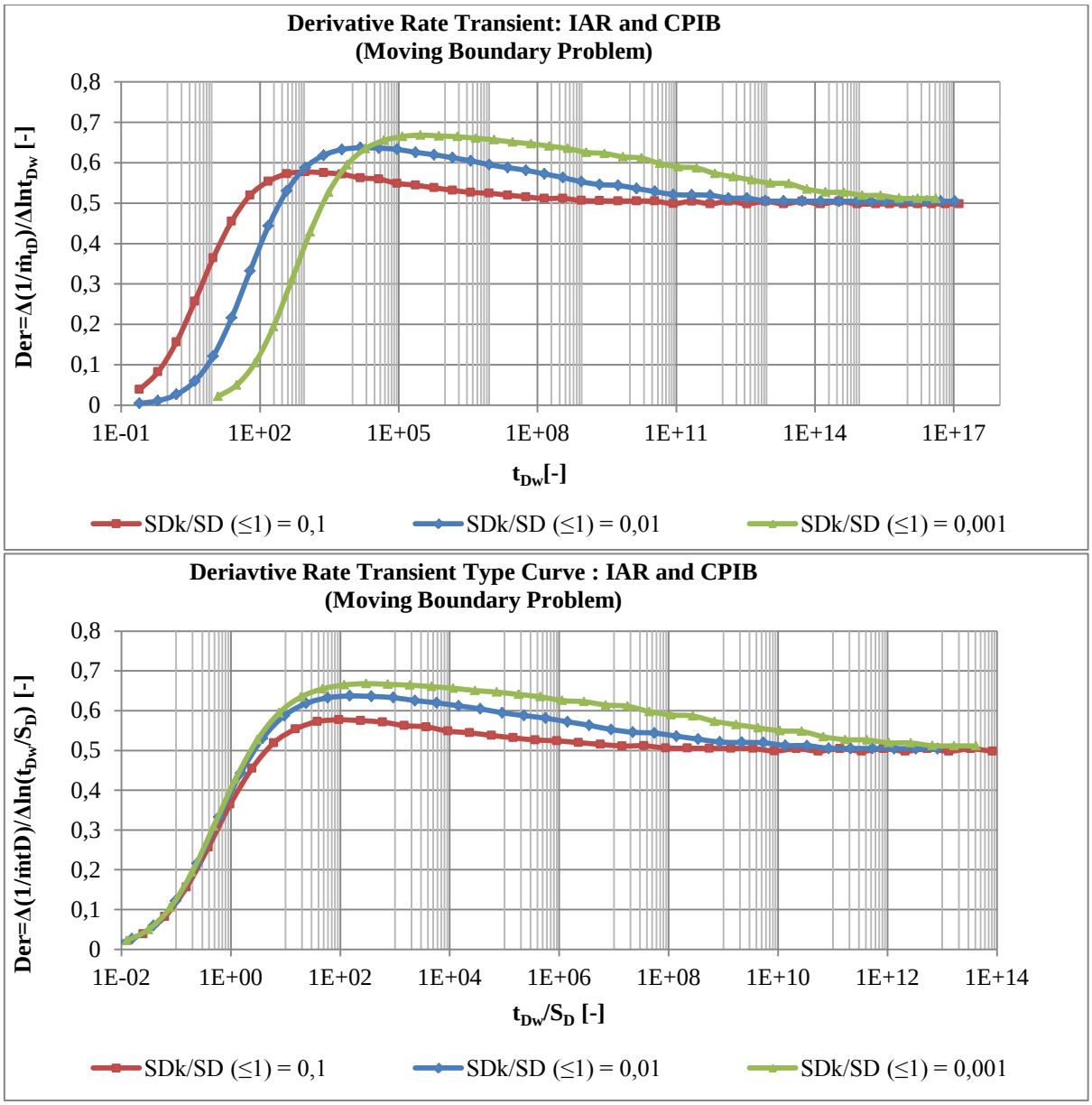

Figure 51: Derivative Plot in Infinite Reservoir with Constant Wellbore Pressure, φ_{sD}=0.3

This implies, using the derivative plot, the effect of increasing radius of dissociation can be observed and hence normally and over-pressured gas hydrate reservoirs identified. However, it should be noted that over-pressured gas hydrate reservoirs with high dissociation rates would require very long production times for IARF to be achieved. This implies, if a 0.5 slope is not observed during transient flow, the near wellbore area is highly dissociated compared to the rest of the reservoir.

4.1.2 Constant Pressure Outer Boundary Reservoirs

The moving boundary behavior of a reservoir with a recharge at the exterior boundary of the un-dissociated zone is given Appendix 13.

The models could be summarized below:

Dissociated Zone

$P_{wf} < P_{eq}$

$$\varphi_D = \varphi_{sD}\frac{\left[E_1\left(S_D\frac{1}{4t_{Dw}}\right)-E_1\left(S_D\frac{{r_D}^2}{4t_{Dw}}\right)\right]}{\left[E_1\left(S_D\frac{1}{4t_{Dw}}\right)-E_1\left(S_D\frac{{r_{sD}}^2}{4t_{Dw}}\right)\right]}+\frac{\left[E_1\left(S_D\frac{{r_D}^2}{4t_{Dw}}\right)-E_1\left(S_D\frac{{r_{sD}}^2}{4t_{Dw}}\right)\right]}{\left[E_1\left(S_D\frac{1}{4t_{Dw}}\right)-E_1\left(S_D\frac{{r_{sD}}^2}{4t_{Dw}}\right)\right]} \quad 4.\ 11$$

$$\dot{m}_{tD} = \frac{2\left(\varphi_{sD}-1\right)}{\left\{E_1\left(S_D\frac{{r_{sD}}^2}{4t_{Dw}}\right)-\left[E_1\left(S_D\frac{1}{4t_{Dw}}\right)\right]\right\}}e^{-\left(S_D\frac{{r_D}^2}{4t_{Dw}}\right)} \quad 4.\ 12$$

$P_{wf} \geq P_{eq}$

$$\varphi_D = \frac{\left[E_1\left(\frac{{r_D}^2}{4t_{Dw}}S_{Dk}\right)\right]-\left[E_1\left(\frac{\left(2l_D-r_D\right)^2}{4t_{Dw}}S_{Dk}\right)\right]}{\left[E_1\left(\frac{1}{4t_{Dw}}S_{Dk}\right)\right]-\left[E_1\left(\frac{\left(2l_D-1\right)^2}{4t_{Dw}}S_{Dk}\right)\right]} \quad 4.\ 13$$

$$\dot{m}_{tD} = \frac{2}{\left[E_1\left(\frac{S_{Dk}}{4t_{Dw}}\right)\right]-\left[E_1\left(\frac{\left(2l_D-1\right)^2}{4t_{Dw}}S_{Dk}\right)\right]}\left[e^{-\left(\frac{{r_D}^2}{4t_{Dw}}S_{Dk}\right)}+\left(2l_D-r_D\right)^{-1}r_D e^{-\frac{\left(2l_D-r_D\right)^2}{4t_{Dw}}S_{Dk}}\right] \quad 4.\ 14$$

Undissociated Zone

$$\varphi_D = \varphi_{sD}\frac{\left[E_1\left(\frac{{r_D}^2}{4t_{Dw}}S_{Dk}\right)\right]-\left[E_1\left(\frac{\left(2l_D-r_D\right)^2}{4t_{Dw}}S_{Dk}\right)\right]}{\left[E_1\left(\frac{{r_{sD}}^2}{4t_{Dw}}S_{Dk}\right)\right]-\left[E_1\left(\frac{\left(2l_D-r_{sD}\right)^2}{4t_{Dw}}S_{Dk}\right)\right]} \quad 4.\ 15$$

$$\dot{m}_{tD} = \frac{2\varphi_{sD}}{\left[E_1\left(\frac{{r_{sD}}^2}{4t_{Dw}}S_{Dk}\right)\right]-\left[E_1\left(\frac{\left(2l_D-r_{sD}\right)^2}{4t_{Dw}}S_{Dk}\right)\right]}\left[e^{-\left(\frac{{r_D}^2}{4t_{Dw}}S_{Dk}\right)}+\left(2l_D-r_D\right)^{-1}r_D e^{-\frac{\left(2l_D-r_D\right)^2}{4t_{Dw}}S_{Dk}}\right] \quad 4.\ 16$$

Criterion for Valid Radius of Dissociation ***($P_{avg} \geq P_{eq}$)***

$$\frac{e^{-S_D\frac{r_{sD}^2}{4t_{Dw}}}}{\left[e^{-\left(\frac{{r_{sD}}^2}{4t_{Dw}}S_{Dk}\right)}+\left(2l_D-r_{sD}\right)^{-1}r_{sD}e^{-\frac{\left(2l_D-r_{sD}\right)^2}{4t_{Dw}}S_{Dk}}\right]}\frac{\left[E_1\left(\frac{{r_{sD}}^2}{4t_{Dw}}S_{Dk}\right)-E_1\left(\frac{\left(2l_D-r_{sD}\right)^2}{4t_{Dw}}S_{Dk}\right)\right]}{\left\{E_1\left(\frac{{r_{sD}}^2}{4t_{Dw}}S_D\right)-\left[E_1\left(\frac{S_D}{4t_{Dw}}\right)\right]\right\}}=\frac{\varphi_{sD}}{\left(\varphi_{sD}-1\right)} \quad 4.\ 17$$

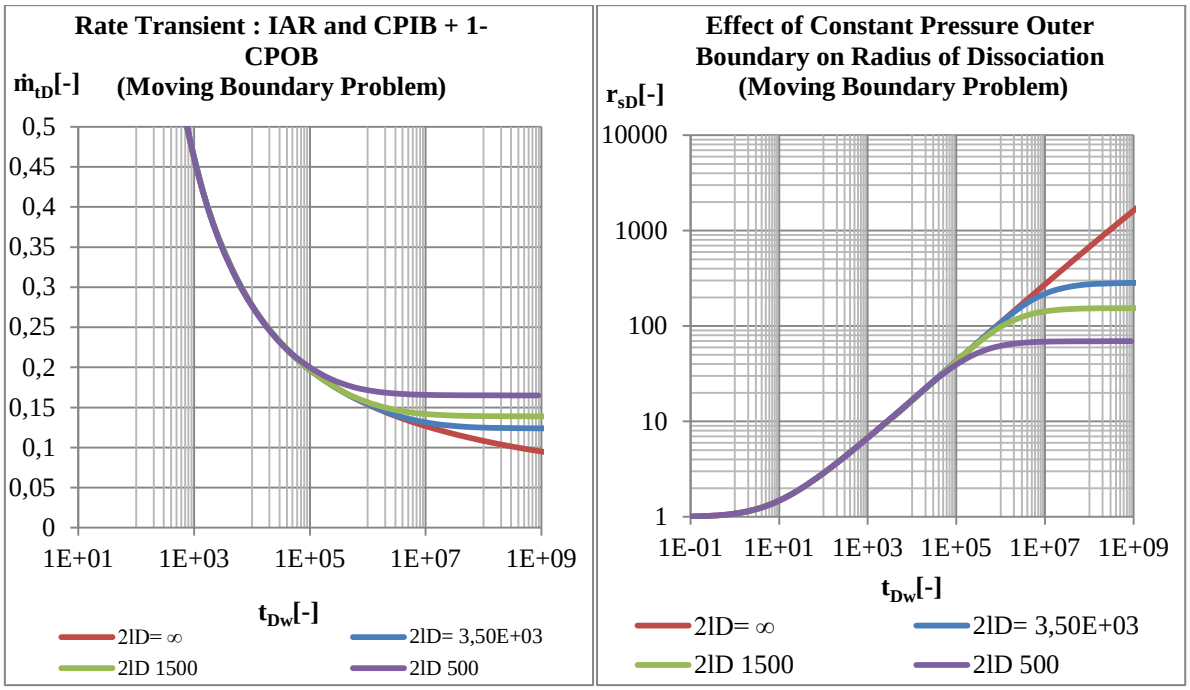

Figure 52: Rate Transient Profile in Constant Pressure Outer Boundary Reservoir with Constant Wellbore Pressure (Moving Boundary Problem), φ_{sD}=0.3, S_{Dk}/S_D (≤1)=0.01

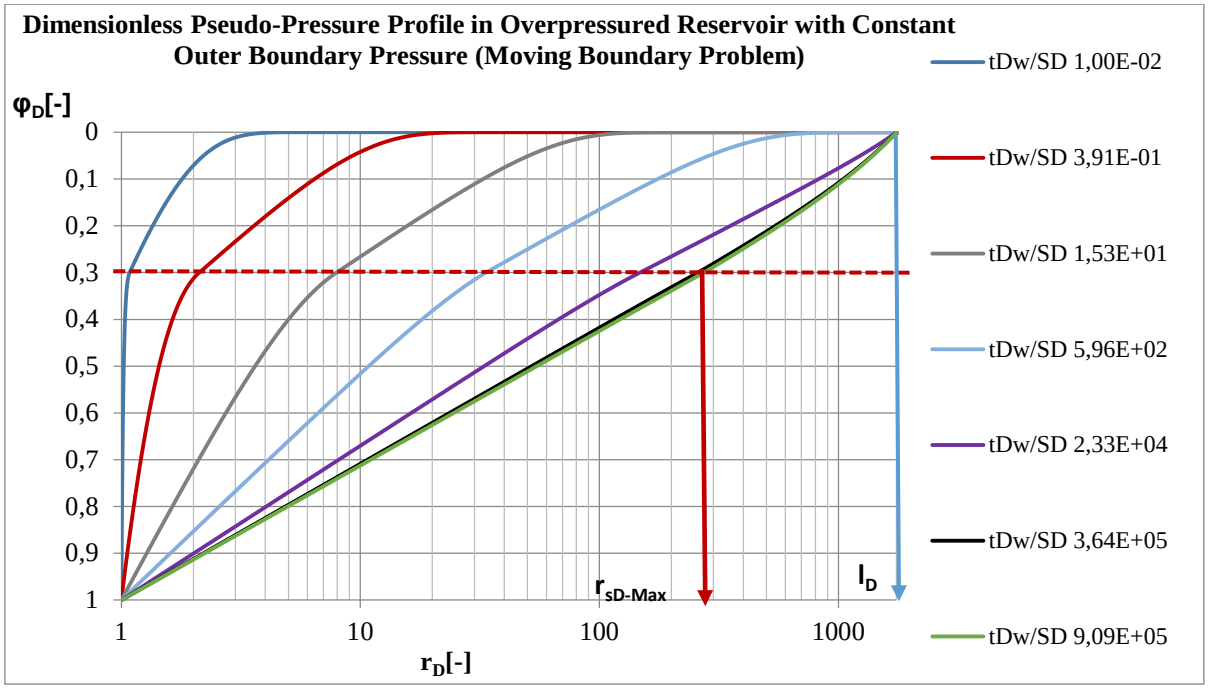

Figure 53: Pseudo-Pressure Profile in Constant Pressure Outer Boundary Reservoir with Constant Wellbore Pressure (Moving Boundary Problem), φ_{sD}=0.3, $2l_D$=3500, S_{Dk}/S_D (≤1)=0.01

Notice that for a well with recharge at the boundary, dissociation of the reservoir will stop as boundary conditions become significant, as no pressure depletion is expected at the boundary; hence no further pressure propagation.

4.1.3 No-Flow Outer Boundary Reservoirs

The moving boundary rate transient behavior of a reservoir with barrier boundary is given in Appendix 13. The no-flow boundary condition is very complex as the dissociated zone first experiences boundary effects before the radius of dissociation reaches the boundary. The model responses are summarized thus:

Dissociated zone

$P_{wf} \leq P_{eq}$

$$\varphi_D = \varphi_{sD}\frac{\left[E_1\left(S_D\frac{1}{4t_{Dw}}\right)-E_1\left(S_D\frac{{r_D}^2}{4t_{Dw}}\right)\right]}{\left[E_1\left(S_D\frac{1}{4t_{Dw}}\right)-E_1\left(S_D\frac{{r_{sD}}^2}{4t_{Dw}}\right)\right]}+\frac{\left[E_1\left(S_D\frac{{r_D}^2}{4t_{Dw}}\right)-E_1\left(S_D\frac{{r_{sD}}^2}{4t_{Dw}}\right)\right]}{\left[E_1\left(S_D\frac{1}{4t_{Dw}}\right)-E_1\left(S_D\frac{{r_{sD}}^2}{4t_{Dw}}\right)\right]} \quad 4.\ 18$$

$$\dot{m}_{tD} = \frac{2(\varphi_{sD}-1)}{\left\{E_1\left(S_D\frac{{r_{sD}}^2}{4t_{Dw}}\right)-\left[E_1\left(\frac{S_D}{4t_{Dw}}\right)\right]\right\}}e^{-\left(S_D\frac{{r_D}^2}{4t_{Dw}}\right)} \quad 4.\ 19$$

$P_{wf} \geq P_{eq}$

$$\varphi_D(r_D,t_{Dw}) = \frac{\left[E_1(\frac{r_D^2}{4t_{Dw}}S_{Dk})\right]+\left[E_1\left(\frac{(2l_D-r_D)^2}{4t_{Dw}}S_{Dk}\right)\right]}{\left[E_1(\frac{S_{Dk}}{4t_{Dw}})\right]+\left[E_1\left(\frac{(2l_D-1)^2}{4t_{Dw}}S_{Dk}\right)\right]} \quad 4.\ 20$$

$$\dot{m}_{tD}(r_D,t_{Dw}) = 2\frac{\left[e^{-\left(\frac{S_{Dk}}{4t_{Dw}}r_D\right)}-(2l_D-r_D)^{-1}r_De^{-\frac{(2l_D-r_D)^2}{4t_{Dw}}S_{Dk}}\right]}{E_1\left(\frac{S_{Dk}}{4t_{Dw}}\right)+E_1\left(S_{Dk}\frac{(2l_D-1)^2}{4t_{Dw}}\right)} \quad 4.\ 21$$

1. **$P_{avg} \leq P_{eq}$ (during production)**

$$\varphi_D = \frac{\left[E_1\left(\frac{{r_D}^2}{4t_{Dw}}S_D\right)\right]+\left[E_1\left(\frac{(2l_D-r_D)^2}{4t_{Dw}}S_D\right)\right]}{\left[E_1\left(\frac{1}{4t_{Dw}}S_D\right)\right]+\left[E_1\left(\frac{(2l_D-1)^2}{4t_{Dw}}S_D\right)\right]} \quad 4.\ 22$$

$$\dot{m}_{tD}(r_D,t_{Dw}) = 2\frac{\left[e^{-\left(\frac{S_D}{4t_{Dw}}r_D\right)}-(2l_D-r_D)^{-1}r_De^{-\frac{(2l_D-r_D)^2}{4t_{Dw}}S_D}\right]}{E_1\left(\frac{S_D}{4t_{Dw}}\right)+E_1\left(S_D\frac{(2l_D-1)^2}{4t_{Dw}}\right)} \quad 4.\ 23$$

Such that the solutions to the dissociated zone before and after the reservoir pressure depletes below the equilibrium pressure are equal, the dimensionless equilibrium pseudo-pressure during boundary dominated flow of the dissociated zone has to be defined thus:

$$\varphi_{sD} = 2\frac{\left[E_1\left(\frac{{l_D}^2}{4t_{Dw}}S_D\right)\right]}{\left[E_1\left(\frac{1}{4t_{Dw}}S_D\right)\right]+\left[E_1\left(\frac{(2l_D-1)^2}{4t_{Dw}}S_D\right)\right]} \quad 4.\ 24$$

It should be once more emphasized that the model above is only valid when the reservoir pressure depletes below the equilibrium pressure and the dissociated radius has reached the NFB.

Undissociated Zone

$$\varphi_D = \varphi_{sD}\frac{\left[E_1\left(\frac{r_D^2}{4t_{Dw}}S_{Dk}\right)+E_1\left(\frac{(2l_D-r_D)^2}{4t_{Dw}}S_{Dk}\right)\right]}{\left\{E_1\left(S_{Dk}\frac{r_{sD}{}^2}{4t_{Dw}}\right)+E_1\left(\frac{(2l_D-r_{sD})^2}{4t_{Dw}}S_{Dk}\right)\right\}} \qquad 4.\ 25$$

$$\dot{m}_{tD} = \frac{2\varphi_{sD}}{\left\{E_1\left(S_{Dk}\frac{r_{sD}{}^2}{4t_{Dw}}\right)+E_1\left(\frac{(2l_D-r_{sD})^2}{4t_{Dw}}S_{Dk}\right)\right\}}\left[e^{-\left(\frac{S_{Dk}}{4t_{Dw}}r_D\right)}-(2l_D-r_D)^{-1}r_D e^{-\frac{(2l_D-r_D)^2}{4t_{Dw}}S_{Dk}}\right] \qquad 4.\ 26$$

Criterion for Valid Radius of Dissociation

$$\frac{\left[E_1\left(\frac{r_{sD}^2}{4t_{Dw}}S_{Dk}\right)+E_1\left(\frac{(2l_D-r_{sD})^2}{4t_{Dw}}S_{Dk}\right)\right]}{\left\{E_1\left(S_D\frac{r_{sD}{}^2}{4t_{Dw}}\right)-\left[E_1\left(\frac{S_D}{4t_{Dw}}\right)\right]\right\}}\frac{e^{-\left(S_D\frac{r_{sD}{}^2}{4t_{Dw}}\right)}}{\left[e^{-\left(\frac{S_{Dk}}{4t_{Dw}}r_{sD}\right)}-(2l_D-r_{sD})^{-1}r_{sD}e^{-\frac{(2l_D-r_{sD})^2}{4t_{Dw}}S_{Dk}}\right]}=\frac{\varphi_{sD}}{(\varphi_{sD}-1)} \qquad 4.\ 27$$

The middle and late time response for different boundary distances are depicted below.

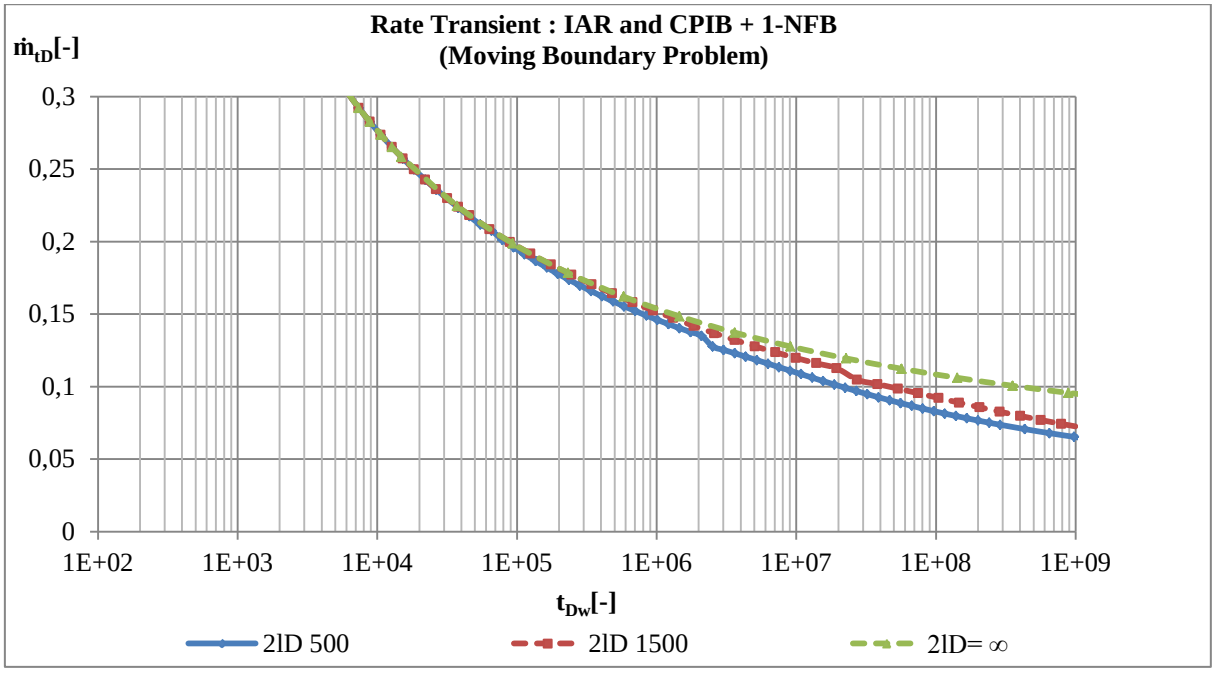

Figure 54: Rate Transient Profile in No-Flow Outer Boundary Reservoir with Constant Wellbore Pressure (Moving Boundary Problem), φ_{sD}=0.3, S_{Dk}/S_D (≤1)=0.01

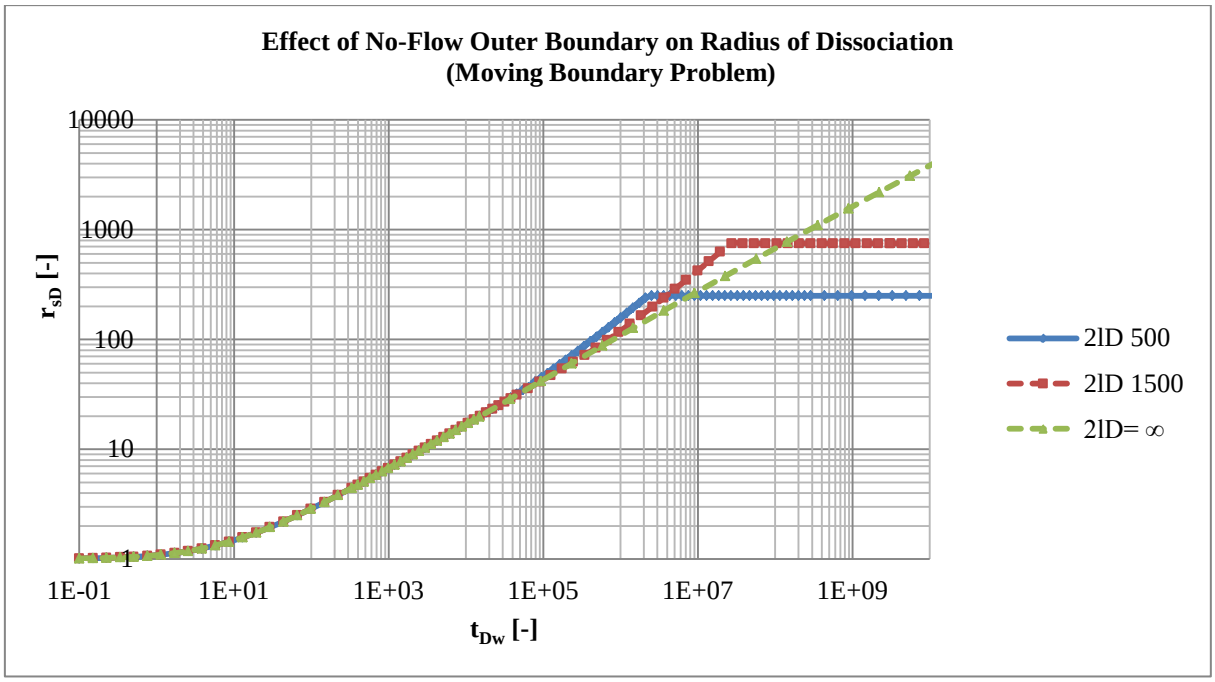

Figure 55: Rate radius Profile in No-Flow Outer Boundary Reservoir with Constant Wellbore Pressure, φ_{sD}=0.3, S_{Dk}/S_D (≤1)=0.01

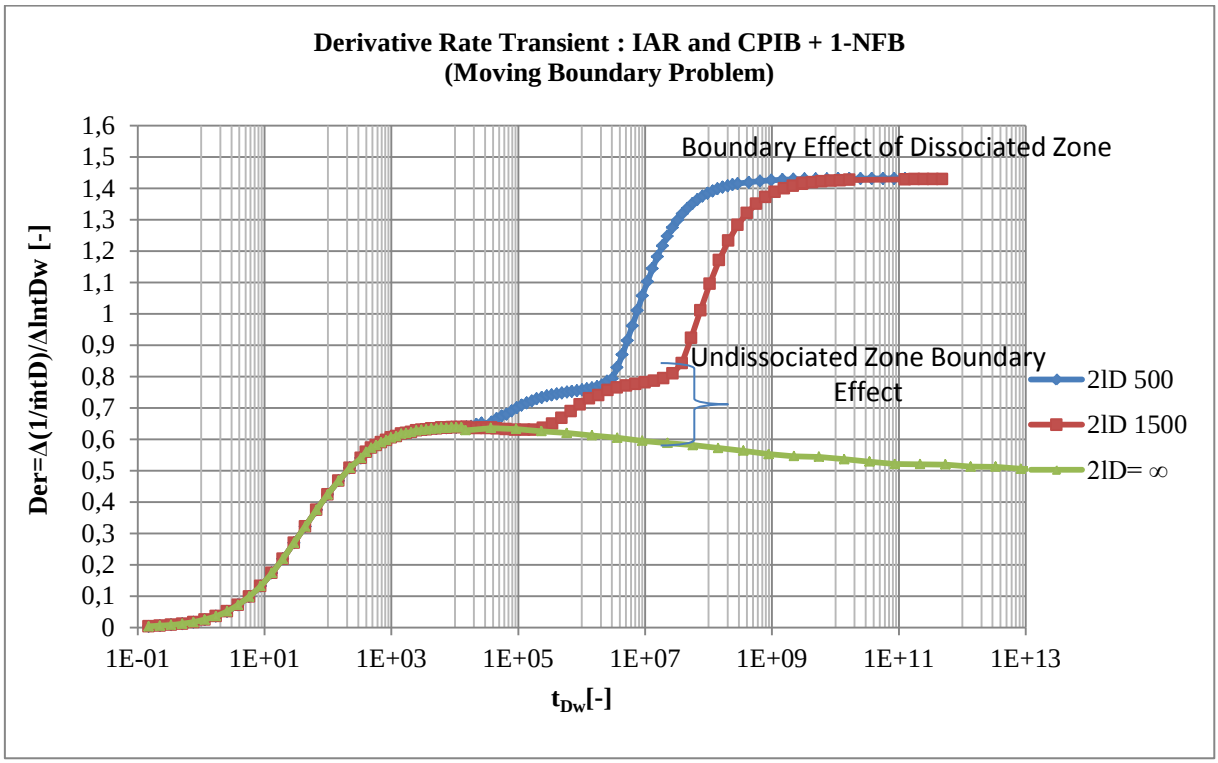

Figure 56: Derivative Plot in Reservoir with No-flow Boundary, φ_{sD}=0.3, S_{Dk}/S_D (≤1)=0.01

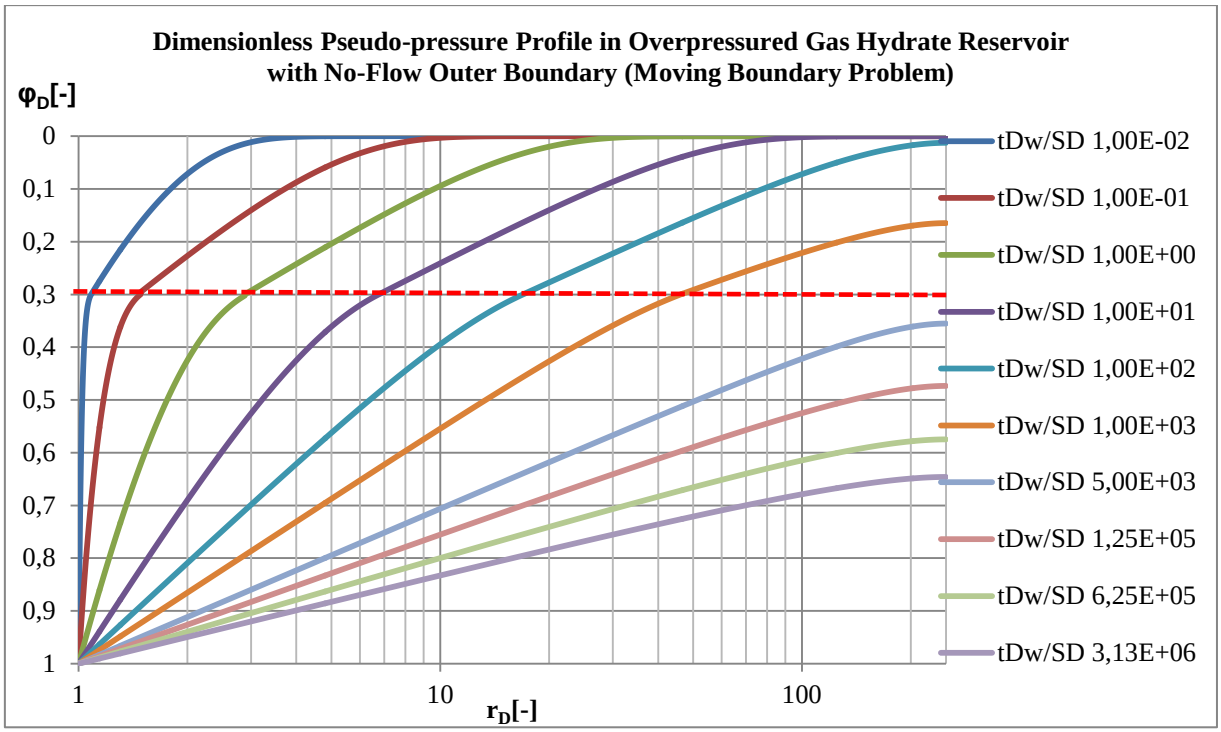

Figure 57: Pseudo-Pressure Profile in No-Flow Boundary Reservoir with Constant Wellbore Pressure, φ_{sD}=0.3, 2lD=500, S_{Dk}/S_D (≤1)=0.01

4.2 Rate Transient Analysis for the Dissociated Zone

The models addressed in Appendix 13 give the exact response to the reservoir behavior whereas the similarity solutions basically reflect approximate solutions to the model. Hereafter, the RTA performed in this work for the over-pressured gas hydrate reservoirs are based the approximate similarity solutions which do not consider heat influx effects. From Appendix 13, the rate transient model at the wellbore in the dissociated zone is given by:

$$\dot{m}_{tD} = \frac{2(1-\varphi_{sD})}{\left\{\left[E_1\left(\frac{S_D}{4t_{Dw}}\right)\right]-E_1\left(S_D\frac{r_{sD}{}^2}{4t_{Dw}}\right)\right\}} e^{-\left(S_D\frac{1}{4t_{Dw}}\right)} \qquad 4.\ 28$$

In the early time period, i.e. for short production periods, the radius of dissociation is very small and hence the arguments in the Ei-function are both large. Approximations of the Ei-function for early time response are difficult to analyze, hence late time approximations are made. In the late time period, as also given in the Figure 52, the dimensionless time is much higher than the radius of dissociation; hence we can assume that the arguments in the Ei-function are small such that the late time approximation of the Ei-function can be used and semi-log analysis performed.

4.2.1 Semi-log Analysis

Unlike the method of approach used in Chapter 3 for boundary dominated flow, here, the only period where boundary dominated flow is negligible would be at the very beginning of production. Since the radius of dissociation increases with depletion time, we have a multiple boundary problem which is time dependent. For this reason, the following approach is made.

$$\frac{1}{\dot{m}_{tD}} = \frac{0{,}5}{(1-\varphi_{sD})} e^{\left(S_D \frac{1}{4t_{Dw}}\right)} \{[E_1(x_1)] - E_1(x_2)\} \quad 4.\ 29$$

We know that the radius of dissociation is a time function and hence the quotient of the radius of dissociation to the dimensionless time is also a function less than 1 for most cases as also shown earlier, meaning, with increasing time, the E_1-function can be represented for both cases as a log function as given below:

x<0.01

$$\frac{1}{\dot{m}_{tD}} \approx \frac{0{,}5}{(1-\varphi_{sD})} \{-[\ln(1{,}781x_1)] + \ln(1{,}781x_2)\} \quad 4.\ 30$$

Since the relationship between the dimensionless time and the radius of dissociation has not been defined, we make the following approach.

Semi-log Plot and Radius of Dissociation

$$\frac{1}{\dot{m}_{tD}} = \frac{0{,}5}{(1-\varphi_{sD})} [\log t_{Dw} + \log(x_2) - \log(0.25 S_D)] \quad 4.\ 31$$

$$\frac{1}{\dot{m}_{tD}} = \frac{0{,}5}{(1-\varphi_{sD})} \left[\log t_{Dw} + \log\left(4 \frac{x_2}{S_D}\right)\right] \quad 4.\ 32$$

$$\frac{1}{\dot{m}_{tD}} = \frac{2\pi h k \int \rho_t \left(\frac{k_r}{\eta}\right)_t dp}{\dot{m}_t} = \frac{1{,}1515}{(1-\varphi_{sD})} \left[\log t + \log\left(\frac{k}{\emptyset r_w^2} \frac{f_t(p_i)}{\beta(p_i)}\right) + s_s\right] \quad 4.\ 33$$

$$\frac{1}{\dot{m}_t} = \frac{1{,}1515}{2\pi h \left[k \int \rho_t \left(\frac{k_r}{\eta}\right)_t dp\right] (1-\varphi_{sD})} \left[\log t + \log\left(\frac{k}{\emptyset r_w^2} \frac{f_t(p_i)}{\beta(p_i)}\right) + s_s\right] \quad 4.\ 34$$

If the hydrate layer is not severely depressurized, the value of S_{Dk}/S_D won´t deviate very much from 1 and hence the skin value s_s would be small or approximately constant at some point, with IARF noticeable in the middle time region as given in Figure 51 and Figure 58. Hence, for practical reasons, it would be advisable to produce the well with stepwise small depressions below the equilibrium pressure such that reservoir parameters can be derived. Though the flow rates might be small with this approach, a better reservoir characterization could be achieved.

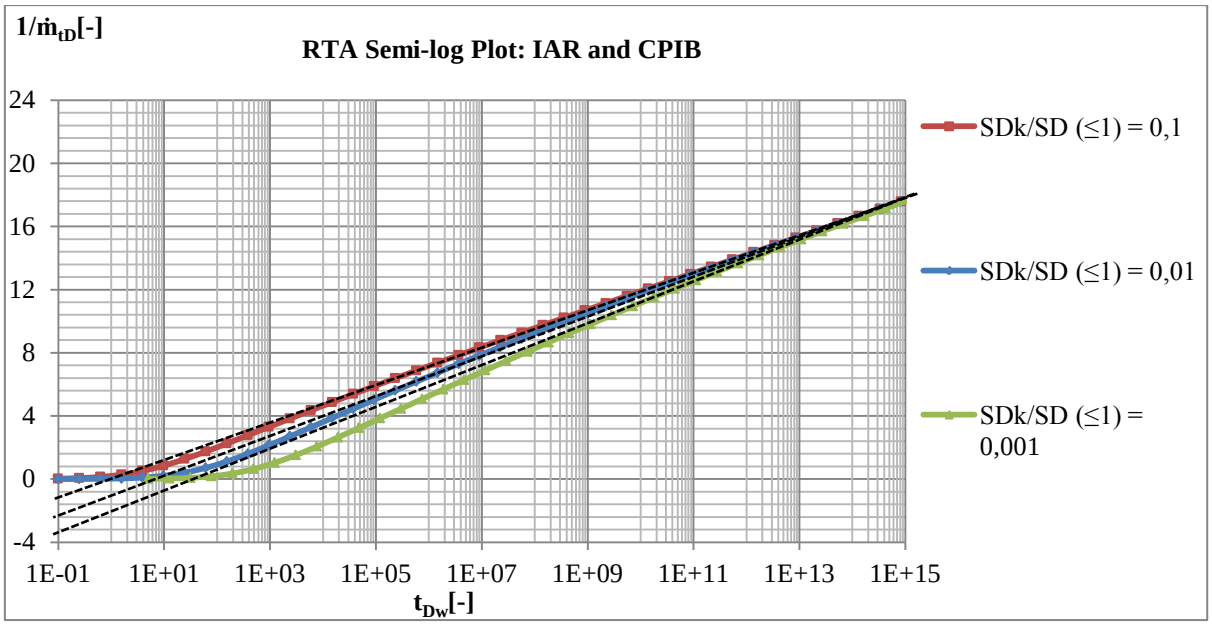

Figure 58: Rate Transient Analysis in Over-pressured Gas Hydrates

The observed gradient from the semi-log plot is given by:

$$m_{log} = \frac{1.1515}{2\pi h(1-\varphi_{sD})\left[k\int \rho_t\left(\frac{k_r}{\eta}\right)_t dp\right]} \quad 4.\ 35$$

$$(1-\varphi_{sD})\left[k\int \rho_t\left(\frac{k_r}{\eta}\right)_t dp\right] = \frac{1.1515}{2\pi h m_{log}} \quad 4.\ 36$$

Skin

$$s_{s,avg} \approx \frac{\left[\frac{1}{\dot{m}_t}\right]_{t=1s}}{m_{log}} - \log\left(\frac{k}{\emptyset r_w^2}\frac{f_t(p_i)}{\beta(p_i)}\right) \quad 4.\ 37$$

As seen with the normally pressured gas hydrate reservoirs, the effective gas permeability can be estimated from the mass balance approach thus:

$$kk_{rg}^* = k_g^* = \frac{[\varphi PI(t)]_g}{\dot{m}_t}[k\int f_t(p)dp] = \frac{1}{(1-\varphi_{sD})}\frac{[\varphi PI(t)]_g}{\dot{m}_t}\frac{1,1515}{2\pi h m_{log}} \quad 4.\ 38$$

Radius of Dissociation during Production

Deriving a clear gradient on the semi-log plot could be cumbersome; hence we use the average value of skin as given above. This implies the use of this model only gives an approximation of the radius of dissociation for any given time during IARF. From the total production time, the radius of dissociation during IARF is given by:

$$s_{s,avg} = \log\left(\frac{{r_{sD}}^2}{t_{Dw}}\right) \quad 4.\ 39$$

$$r_{s,avg} \approx \sqrt{{r_w}^2[t_{Dw}]\exp(2,303s_s)} = \sqrt{\left[\frac{k}{\emptyset}\frac{f_t(p_i)}{\beta(p_i)}t_f\right]\exp(2,303s_{s,avg})} \quad 4.\ 40$$

$$r_{s,avg} \approx r_w e^{(1.1515s_s)}\sqrt{t_{Dw}} \quad 4.\ 41$$

For infinite acting systems, t_f denotes the production time; however, the radius of dissociation would have maximum values for bounded systems.

Validity of Method

- x<0.01
- m_{log} can be obtained from semi-log plot
- The reservoir skin, $s_{s,avg}$, can be derived

4.2.2 Identifying Reservoir Boundaries

Due to the complexity of the reservoir behavior, it would be practically more effective to produce the overpressures reservoir above the equilibrium pressure such that conventional RTA techniques can be applied to derive the true reservoir boundary. However, producing the reservoir above equilibrium pressure can only be possible if a reasonable amount of free fluid is present in the hydrate layer. If this is not the case, the following approach can still be made:

CPOB Over-pressured hydrate layer

Here, we noticed that the radius of dissociation becomes a constant value when boundary dominated flow starts in the un-dissociated zone. At this point, both the dissociated zone and the undissociated zone portray constant pressure outer boundary behavior. With this phenomenon, we can easily derive the maximum possible radius of dissociation for that reservoir.

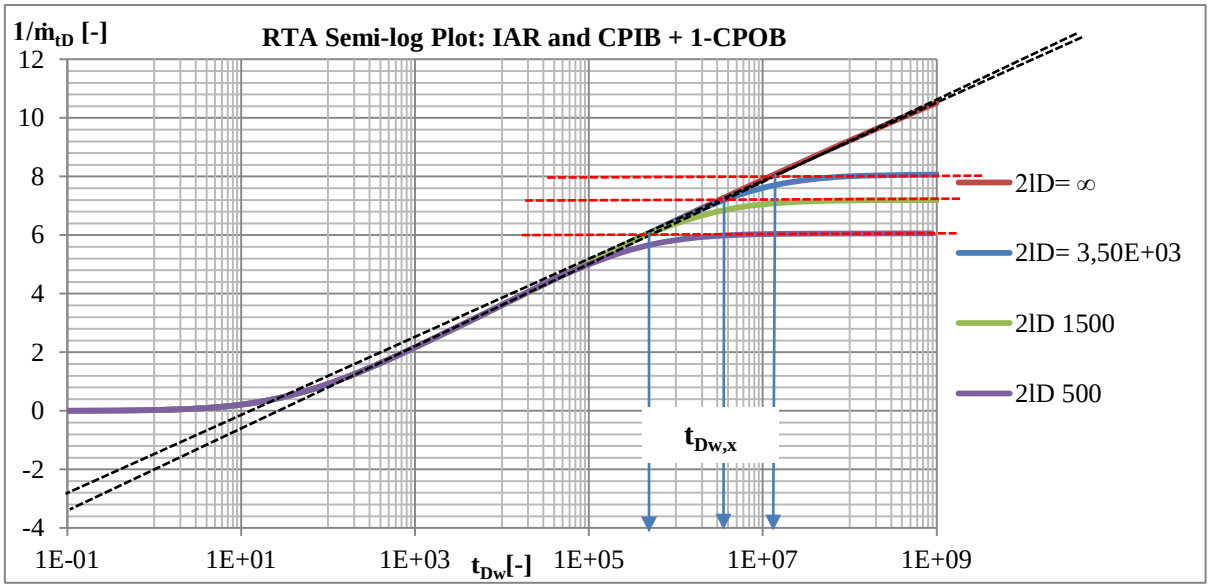

Figure 59: Identification of Maximum Radius of Dissociation s in Over-pressured Gas Hydrates (CPOB) (S_D/S_{Dk}=0.001)

$$r_{s,avg-max} \approx \sqrt{r_w^2[t_{Dw,x}]\exp(2{,}303 s_{s,avg})} = e^{(1.1515 s_s)}\sqrt{\left[\frac{k}{\emptyset}\frac{f_t(p_i)}{\beta(p_i)}t_f^*\right]} \quad 4.42$$

$$r_{s,avg-max} \approx r_w e^{(1.1515 s_{s,avg})}\sqrt{t_{Dw,x}} \quad 4.43$$

NFB Over-pressured hydrate layer

The NFB problem in over-pressured gas hydrates is much more complex compared to the CPOB case. As seen in Figure 56 and Appendix 13, the RTA of the model will depict two boundary dominated flow periods. Coupled with the effect of dissociation and the moving boundary problem, serious challenges can be encountered with the analysis. For this reason it is advisable at this level to apply computer aided methods of analysis for such problems as the use of semi-log plots to estimate reservoir parameters will not yield satisfactory results. Nonetheless, performing derivative plots for reservoir diagnostics would be very beneficial in identifying the complex behavior of NFB over-pressured gas hydrates as seen in Figure 56.

4.2.3 Type Curve Analysis

The conceptual models developed here for the over-pressured gas hydrates using the similarity solutions ignored the effect of heat conduction such that the complexity of the model can be reduced. With this assumption, solutions to the model were derived and hence a type curve method of analysis can be proposed. It should be noted that as long as well test data depict skin response for a long period of time, the reservoir could be considered as an over-pressured gas hydrate, which could also be verified from temperature depressions (i.e. if the reservoir experiences no temperature depressions when produced above the estimated equilibrium pressure). If this is the case, the over-pressured type curve can be used for the matching process.

Required Plots

- $\frac{(1-\varphi_{sD})}{\dot{m}_{tD}}$ Versus $\frac{t_{Dw}}{r_{sD}}$
- $\frac{1}{\dot{m}_t}$ Versus t
- $\varphi PI(t)$ Versus t

Time Match

The time match points along the vertical are:

$$\left[\frac{t_{Dw}}{r_{sD}}\right]_{MP};\ t_{MP};\left[\frac{S_D}{S_{Dk}}\right]_{MP} \qquad 4.\ 44$$

Where,

$$t_{Dw} = t\frac{k}{\emptyset r_w^2}\frac{f_t(p_i)}{\beta(p_i)}$$

From the match points, the dimensionless interlayer heat flux compressibility is derived thus:

$$[r_{sD}]_{MP} = \frac{t_{Dw}}{\left[\frac{t_{Dw}}{r_{sD}}\right]_{MP}} = \frac{k}{\emptyset r_w^2}\frac{f_t(p_i)}{\beta(p_i)}\frac{t_{MP}}{\left[\frac{t_{Dw}}{r_{sD}}\right]_{MP}} \qquad 4.\ 45$$

$$[r_s]_{MP} = \frac{k}{\emptyset r_w}\frac{f_t(p_i)}{\beta(p_i)}\frac{t_{MP}}{\left[\frac{t_{Dw}}{r_{sD}}\right]_{MP}} \quad 4.46$$

Rate Match

The match along the horizontal is given by:

$$\left[\frac{(1-\varphi_{sD})}{\dot{m}_{tD}}\right]_{MP}; \left[\frac{1}{\dot{m}_t}\right]_{MP}; [\varphi PI(t)]_{g,MP}$$

Where,

$$\frac{\dot{m}_{tD}}{(1-\varphi_{sD})} = \frac{\dot{m}_t}{2\pi h\left[(1-\varphi_{sD})k\int \rho_t\left(\frac{k_r}{\eta}\right)_t dp\right]} \quad 4.47$$

$$\left[(1-\varphi_{sD})k\int \rho_t\left(\frac{k_r}{\eta}\right)_t dp\right]_{MP} = \frac{\left[\frac{(1-\varphi_{sD})}{\dot{m}_{tD}}\right]_{MP}}{2\pi h\left[\frac{1}{\dot{m}_t}\right]_{MP}} \quad 4.48$$

$$kk^*_{rg}(p) = [\varphi PI(t)]_{g,MP}\left[\frac{1}{\dot{m}_t}\right]_{MP}\left[(1-\varphi_{sD})k\int \rho_t\left(\frac{k_r}{\eta}\right)_t dp\right]_{MP} \quad 4.49$$

4.2.4 Rate Derivative Analysis

The derivative plot is basically used for diagnosis of the reservoir behavior and for a better view of the different flow regimes and boundary responses.

Early Time Region

Unlike the normally pressured gas hydrates, the over-pressured gas hydrates show a characteristic skin response due to dissociation and the increasing radius of dissociation.

IARF

As seen in Figure 51, IARF could be difficult to achieve if the hydrate dissociation is very significant; however, the characteristic behavior during IARF is given by:

$$\frac{d\left[\frac{1}{\dot{m}_{tD}}\right]}{d\left[\ln\left(\frac{t_{Dw}}{S_D}\right)\right]} = f\left(\frac{S_D}{S_{Dk}}, \varphi_{sD}\right) \quad 4.50$$

Late Time IARF

$$\frac{d\left[\frac{1}{\dot{m}_{tD}}\right]}{d\left[\ln\left(\frac{t_{Dw}}{S_D}\right)\right]} = 0.5 \quad 4.51$$

Boundary dominated Flow with 1-NFB (negligible heat conduction)

$$\frac{d\left[\frac{1}{\dot{m}_{tD}}\right]}{d\left[\ln\left(\frac{t_{Dw}}{S_D}\right)\right]} = f\left(\frac{S_D}{S_{Dk}}, \varphi_{sD}\right) \quad 4.52$$

Reservoirs with NFB will depict the following responses:

- *Double NFB Response*: This would occur if the reservoir is produced long enough for the reservoir pressure to drop below the equilibrium pressure for the given constant wellbore pressure.
- *Single NFB Response*: This would occur if the reservoir is produced long enough till the NFB is reached but the reservoir pressure is still above the equilibrium pressure.

Boundary dominated Flow with 1-CPOB (negligible heat conduction)

$$\frac{d\left[\frac{1}{\dot{m}_{tD}}\right]}{d\left[\ln\left(\frac{t_{Dw}}{s_D}\right)\right]} = 0 \qquad 4.53$$

The rate derivative shows a zero slope during boundary dominated flow.

5 Conceptual Models for Well Testing in Class1 & 2 Gas Hydrates: The Crossflow Problem

Gas hydrate reservoirs with free fluid beneath the hydrate reservoir are susceptible to crossflow behavior with the presence of a pervious layer separating the hydrate layer and free fluid layer. Free fluid beneath the hydrate layer could be water, as in Class 2 hydrates, or gas as in Class 1 hydrates. Understanding and describing the reservoir response for such systems is necessary for all production forecasting and designing the production economics of the reservoir. In deriving the reservoir parameters of the reservoir system, a representative model for the reservoir fluid flow is required. Crossflow models in gas hydrate reservoir require a good representation of the dissociation products of the hydrates during pressure depressions. As mentioned in Chapter 1, quantifying the dissociation products for Class1 and 2 gas hydrate reservoirs depends very much on the layer of production due to heat influx.

5.1 Crossflow Behavior of Class 1 and 2 Gas Hydrate Reservoirs

The diagrams below show the crossflow effects in hydrate reservoirs Class 1 and 2 due to the pervious barrier between the hydrate layer and the underlying free fluid layer.

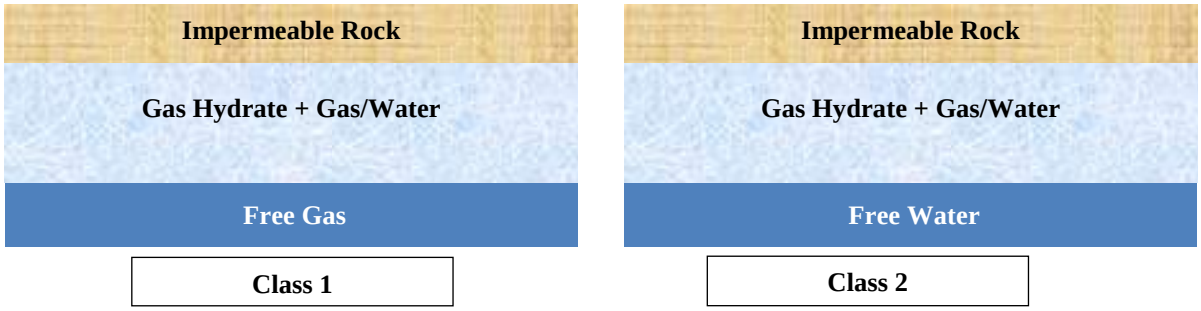

Case 1: Production from Free Fluid Zone

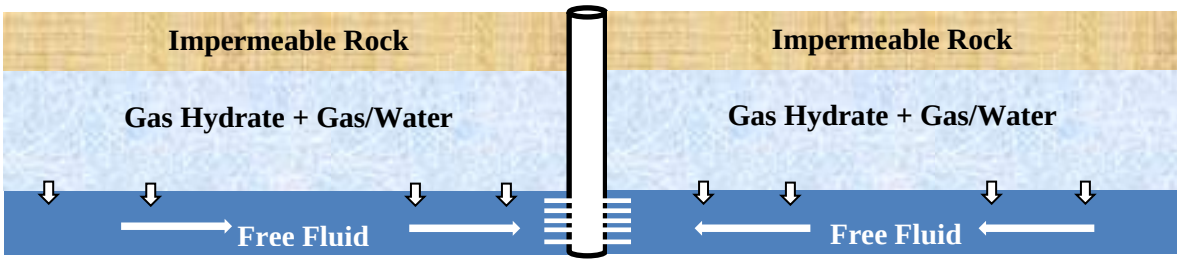

Case 2: Production from Hydrate Zone

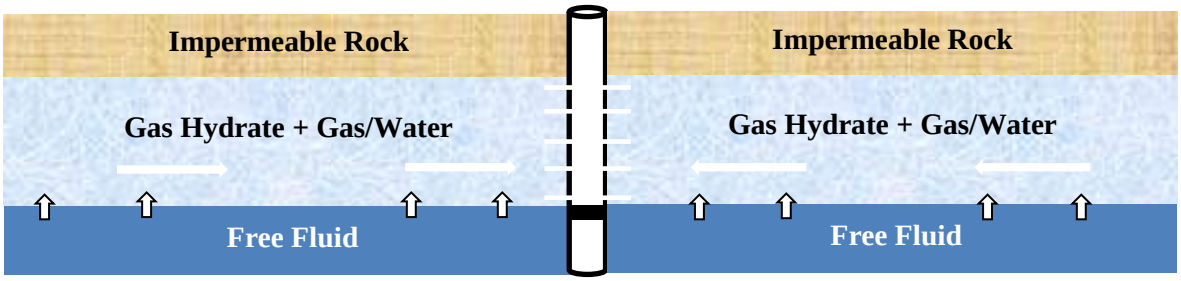

Figure 60: Production Scenarios from Class 1&2 Hydrate Reservoirs

Different production scenarios have been identified and depicted in the above diagrams. The choice of the production method will depend on various factors. One important aspect with the choice of production will be the more energy efficient method. With a look at the hydrate reservoirs Class 1 and 2, it can be noticed that the fluid layer beneath the hydrate zone is more likely to possess a higher permeability due to the absence of the hydrates in the pores. With such a case, it would be more preferable to produce from the layer beneath the hydrate zone, as depletion here is faster. If we have free water beneath the hydrate zone as in Class 2, production from the layer beneath the hydrate zone would be predominantly water as in Coal Bed Methane reservoirs and could be called the dewatering phase of the reservoir production, before the mobility of gas increases. For Class 1 with free gas beneath the hydrate zone, production with Case 1 method will be predominantly gas.

To develop a more general equation, applicable for both Class 1 and Class 2, which also makes the use of multiphase pseudo-pressure appropriate for crossflow problems, water and gas are assumed to be present in both the hydrate layer and the layer beneath. With this assumption, mass conservation and energy balance models could be used to describe flow in these reservoirs. Due to different outer boundary conditions in the crossflow layer, various crossflow models have been developed consequently. Most crossflow models are based on the extension of the non-leaky aquifer models. Hantush and Jacob [43] first addressed the problem of crossflow using the leaky aquifer type models. The influence of the fluid leakage from the confining layer (hydrate layer) to the producing layer (free fluid layer) is highly dependent on the permeability and thickness of the hydrate formation as will be shown later. The solutions presented by Hantush and Jacob [43] were derived for homogenous wells and just ground water flow was considered; hence, linearization of the partial differential equation was not necessary. However, dimensionless forms of the solutions have been presented by authors, which could be seen in the works of Haefner [73] for different inner boundary conditions. The main challenge with the crossflow problem in hydrate-capped reservoirs would be to linearize the equation and represent in dimensionless forms, such that the boundary conditions could be modified and the existing solutions in dimensionless form implemented. First, mass balance techniques are depicted for the crossflow models.

Description of Pore Contents in Layers

Hydrate Layer (HL)

Considering the gas hydrate zone, we assume the pores are filled with three phases, namely: hydrate, gas and water and the saturation is hence given by:

$$S_g + S_H + S_w = \frac{V_g}{V_P} + \frac{V_H}{V_P} + \frac{V_w}{V_P} = \frac{V_g + V_H + V_w}{V_p} = \frac{V_p}{V_p} = 1 \qquad 5.1$$

Considering the three phases in the reservoir, we could modify the storage term thus:

$$\frac{m_{t+\Delta t} - m_t}{\Delta t} = \frac{\Delta(\rho * V_p)}{\Delta t} = \frac{\Delta(\rho * \emptyset * V)}{\Delta t} = \frac{\Delta(\rho_g * \emptyset * V S_g)}{\Delta t} + \frac{\Delta(\rho_H * \emptyset * V S_H)}{\Delta t} + \frac{\Delta(\rho_w * \emptyset * V S_w)}{\Delta t} \qquad 5.2$$

This implies the rate of change of mass equation could be written in the form

$$\frac{m_{t+\Delta t}-m_t}{\Delta t} = \left(\frac{m_{t+\Delta t}-m_t}{\Delta t}\right)_g + \left(\frac{m_{t+\Delta t}-m_t}{\Delta t}\right)_H + \left(\frac{m_{t+\Delta t}-m_t}{\Delta t}\right)_w \quad 5.3$$

As demonstrated in Appendix 1, Appendix 2, Appendix 3, the hydrate mass rate change could be represented in terms of the dissociation components thus:

$$\left(\frac{m_{t+\Delta t}-m_t}{\Delta t}\right)_H = \frac{\Delta(\rho_H * \emptyset * VS_H)}{\Delta t} = \left(\frac{m_{t+\Delta t}-m_t}{\Delta t}\right)_{w,H} + \left(\frac{m_{t+\Delta t}-m_t}{\Delta t}\right)_{g,H} \quad 5.4$$

Free Fluid Layer (FFL)

Considering the free fluid zone, we assume the pores are filled with two phases, namely: gas and water and the saturations are hence given by:

$$S_g + S_w = \frac{V_g}{V_P} + \frac{V_w}{V_P} = \frac{V_g+V_w}{V_p} = \frac{V_p}{V_p} = 1 \quad 5.5$$

Considering the two phases in the free fluid layer, we could modify the storage term thus:

$$\frac{m_{t+\Delta t}-m_t}{\Delta t} = \frac{\Delta(\rho * V_p)}{\Delta t} = \frac{\Delta(\rho * \emptyset * V)}{\Delta t} = \frac{\Delta(\rho_g * \emptyset * VS_g)}{\Delta t} + \frac{\Delta(\rho_w * \emptyset * VS_w)}{\Delta t} \quad 5.6$$

This implies the rate of change of mass equation could be written in the form

$$\frac{m_{t+\Delta t}-m_t}{\Delta t} = \left(\frac{m_{t+\Delta t}-m_t}{\Delta t}\right)_g + \left(\frac{m_{t+\Delta t}-m_t}{\Delta t}\right)_w \quad 5.7$$

Diffusivity Equation in Producing Layer (Layer 1)

In developing the equation, the hydrate dissociation rate due to heat conduction and convection should be taking into consideration. Appendix 15 fully describes the derivation of the model.

Diffusivity Equation when producing from the Free Fluid Layer

$$\frac{\partial^2 \varphi_D}{\partial {r_D}^2} + \frac{1}{r_D}\frac{\partial \varphi_D}{\partial r_D} - \delta_D \left[\frac{\partial [\varphi_D]_{layer2}}{\partial z_D}\right]_{z_D=1} = \omega \frac{\partial \varphi_D}{\partial t_{DwD}} \quad 5.8$$

The equation above is represented in Laplace domain thus:

$$\frac{\partial^2 \hat{\varphi}_D}{\partial {r_D}^2} + \frac{1}{r_D}\frac{\partial \hat{\varphi}_D}{\partial r_D} - \delta_D \left[\frac{\partial [\hat{\varphi}_D]_{layer2}}{\partial z_D}\right]_{z_D=1} = \omega p \hat{\varphi}_D \quad 5.9$$

Diffusivity Equation when producing from the Hydrate Layer

$$\frac{\partial^2 \varphi_D}{\partial {r_D}^2} + \frac{1}{r_D}\frac{\partial \varphi_D}{\partial r_D} - \left[\frac{\partial T_{pD}}{\partial z_D}\right]_{Caprock, z_D=1} - \delta_D \left[\frac{\partial [\varphi_D]_{layer2}}{\partial z_D}\right]_{z_D=1} - \delta_D \theta_D \left[\frac{\partial [\varphi_D]_{layer2}}{\partial z_D}\right]_{z_D=1} = \omega \frac{\partial \varphi_D}{\partial t_{DwD}} \quad 5.10$$

The diffusivity equation when producing from the hydrate layer can be similarly transformed in Laplace domain as given below:

$$\frac{\partial^2 \hat{\varphi}_D}{\partial {r_D}^2} + \frac{1}{r_D}\frac{\partial \hat{\varphi}_D}{\partial r_D} - \left[\frac{\partial \hat{T}_{pD}}{\partial z_D}\right]_{Caprock, z_D=1} - \delta_D \left[\frac{\partial [\hat{\varphi}_D]_{layer2}}{\partial z_D}\right]_{z_D=1} - \delta_D \theta_D \left[\frac{\partial [\hat{\varphi}_D]_{layer2}}{\partial z_D}\right]_{z_D=1} = \omega p \hat{\varphi}_D \quad 5.11$$

Diffusivity Equation for the Crossflow Layer (Layer 2)

$$\left[\frac{\partial^2\hat{\varphi}_D}{\partial z_D^2}\right]_{layer2} = (1-\omega)p\left[\hat{\varphi}_D\right]_{layer\ 2} \quad 5.\ 12$$

Mass Influx from Hydrate Layer in Free Fluid Layer

Since the hydrate layer is considered to be bounded at the top with a caprock, NFB is imposed at the hydrate layer-caprock interface. Nonetheless, the endothermic dissociations favors heat inflow at this interface when pressure propagation reaches the boundary. This effect is considered in the following model:

NFB at top of Hydrate Layer

$$\left(\frac{\partial[\widehat{\varphi_D}]_{layer2}}{\partial z_D}\right)_{z_D=1} = \left[\sqrt{p[1-\omega]}\mathrm{Coth}\left[(1-\Delta z_D)\sqrt{p[1-\omega]}\right]\frac{\left\{\sqrt{p[1-\omega]}\tanh\left[(1-\Delta z_D)\sqrt{p[1-\omega]}\right]+\widehat{\dot{Q}_{pD}e_D}\right\}}{\left\{\sqrt{p[1-\omega]}\mathrm{Coth}\left[(1-\Delta z_D)\sqrt{p[1-\omega]}\right]+\widehat{\dot{Q}_{pD}e_D}\right\}}\right][\widehat{\varphi_D}]_{layer1} = M_i[\widehat{\varphi_D}]_{layer1} \quad 5.\ 13$$

Mass Influx from Free Fluid Layer in Hydrate Layer

The mass influx rate from the free fluid layer depends basically on the boundary condition imposed at the bottom of the free fluid layer. Two boundary conditions have been considered in this work, for which the mass influx rate is given by:

For CPOB at the bottom of the free fluid layer

$$\left(\frac{\partial[\widehat{\varphi_D}]_{layer2}}{\partial z_D}\right)_{z_D=1} = \left\{\sqrt{p[1-\omega]}\mathrm{Coth}\left[\sqrt{p[1-\omega]}(1-\Delta z_D)\right]\right\}[\widehat{\varphi_D}]_{layer1} = M_i\left[\widehat{\varphi_D}\right]_{layer1} \quad 5.\ 14$$

For NFB at the bottom of the free fluid layer

$$\left(\frac{\partial[\widehat{\varphi_D}]_{layer2}}{\partial z_D}\right)_{z_D=1} = \left\{\sqrt{p[1-\omega]}\tanh\left[\sqrt{p[1-\omega]}(1-\Delta z_D)\right]\right\}[\widehat{\varphi_D}]_{layer1} = M_i\left[\widehat{\varphi_D}\right]_{layer1} \quad 5.\ 15$$

We clearly see the difference in the NFB responses when producing from either one of the layers.

The final equations then take the form:

Final Model with Production from Hydrate Layer

$$\frac{\partial^2\hat{\varphi}_D}{\partial {r_D}^2} + \frac{1}{r_D}\frac{\partial\hat{\varphi}_D}{\partial r_D} - \left[\left(\widehat{\dot{Q}_{pD}e_D}\right)_{caprock} + \delta_D(1+\theta_D)M_i + \omega p\right]\widehat{\varphi_D} = 0 \quad 5.\ 16$$

Final Model with Production from Free Fluid Layer

$$\frac{\partial^2\hat{\varphi}_D}{\partial {r_D}^2} + \frac{1}{r_D}\frac{\partial\hat{\varphi}_D}{\partial r_D} - [\delta_D M_i + \omega p]\widehat{\varphi_D} = 0 \quad 5.\ 17$$

The models addressed here assume that flow in the producing layer is mainly horizontal and flow in the overlain layer is mainly vertical. In case the hydrate layer is much more permeable compared to the free fluid layer, production will be preferably done from the hydrate layer and the problem will be handled analog. Coupled with the heat flux from the free fluid zone, more hydrate will be dissociated.

5.2 Constant Rate Inner Boundary Solutions and Pressure Transient Analysis

From the models developed in Appendix 15 and the approximate solutions in real time domain, PTA can be performed from the reservoir responses.

5.2.1 Case 1: Pressure Transient Solutions when Producing from the Free Fluid Layer

The pseudo-pressure responses when producing from the hydrate layer are given below. Imposing two different boundary conditions at the top of the hydrate layer, .i.e. the NFB and CPOB has shown significant effects in the reservoir responses.

Early-Time Response for both No-Flow and Constant Pressure Outer Boundary in HL

$$\varphi_D = \frac{2\pi hk}{\dot{m}_t}[\varphi_i - \varphi(r,t)] = H\left(\frac{r_D^2}{4t_{DwD}}\omega, \frac{r_D\varepsilon_D}{4\sqrt{\omega}}\right) \quad 5.18$$

Where,

$$\varepsilon_D = \delta_D\sqrt{[1-\omega]} \quad 5.19$$

Late Time Response for No-Flow Outer Boundary in HL

$$\varphi_D = \frac{2\pi hk}{\dot{m}_t}[\varphi_i - \varphi(r,t)] = \frac{1}{2}E_1\left(\frac{r_D^2}{4t_{DwD}}\omega f_D\right) \quad 5.20$$

$$f_D = \left(1 + \frac{[1-\omega]}{\omega}\delta_D(\Delta z_D - 1)\right) \quad 5.21$$

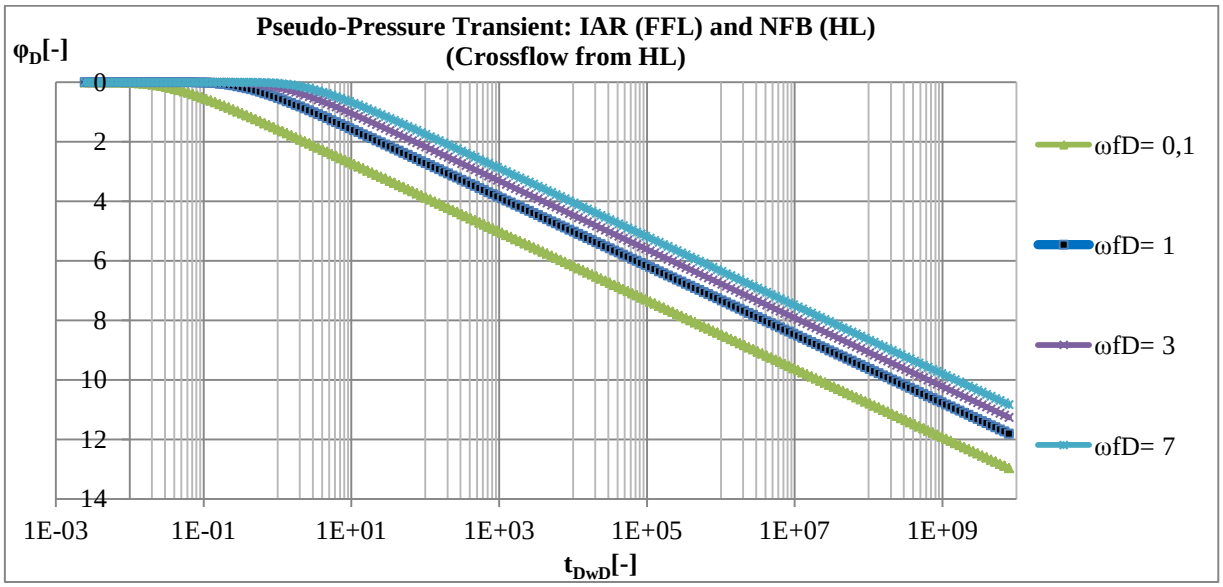

Figure 61: Reservoir Response in Infinite Acting Free Fluid Layer with NFB in HL (Crossflow from HL)

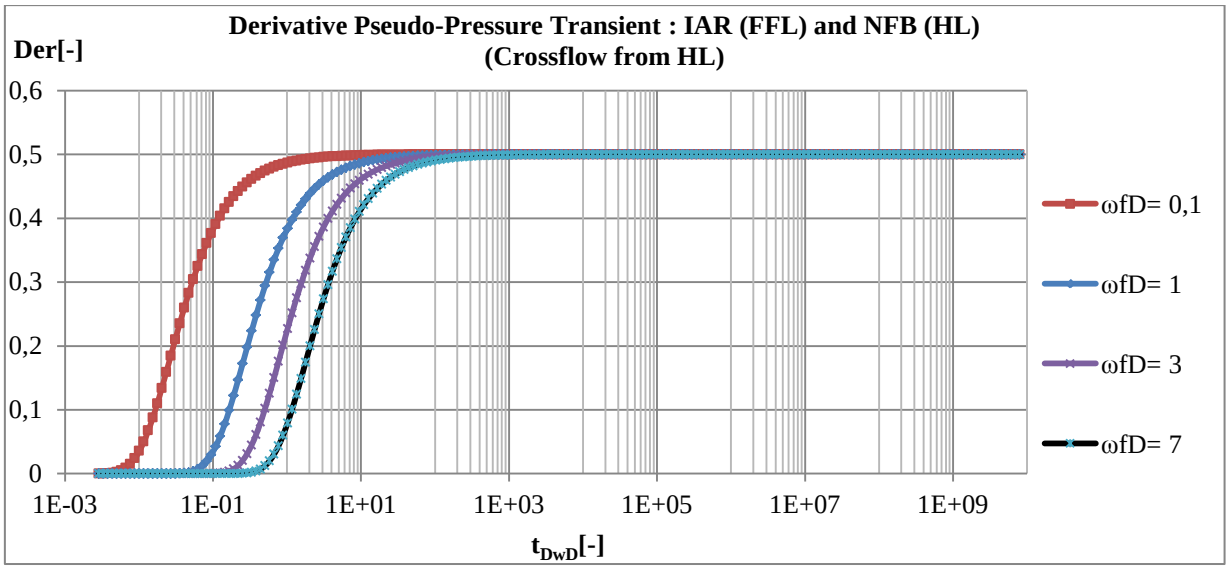

Figure 62: Pseudo-Pressure Transient Derivative Plot for Infinite Acting Free Fluid Layer with NFB in Hydrate Layer

The reservoir response here is similar to that of the normally pressured gas hydrate reservoir. The type curves for this reservoir are given in Figure 63.

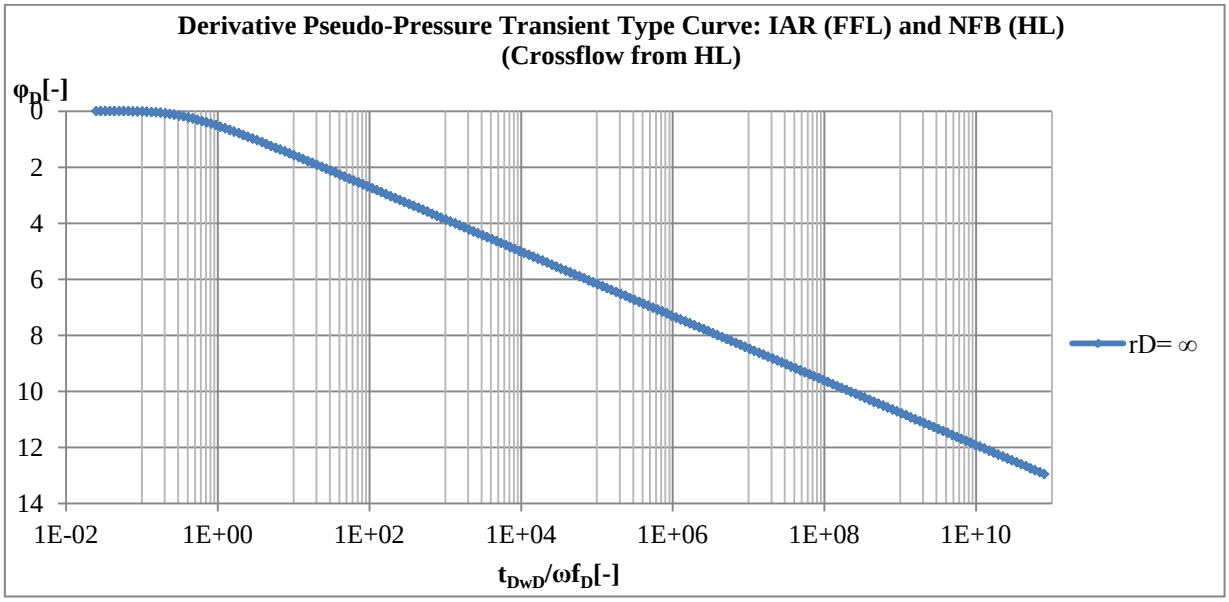

Figure 63: Type Curve Drawdown Plot for Infinite Acting Free Fluid Layer with NFB in Hydrate Layer (Crossflow from Hydrate Layer)

Late Time Response for Constant Pressure Outer Boundary in HL

$$\varphi_D = \frac{2\pi hk}{\dot{m}_t}[\varphi_i - \varphi(r,t)] = \frac{1}{2}W\left(\frac{r_D^2}{4t_{DwD}}\omega g_D, r_D\sqrt{j_D}\right) \qquad 5.\ 22$$

Where,

$$g_D = \left(1 + \frac{[1-\omega]}{3\omega}\delta_D(\Delta z_D - 1)\right) \qquad 5.\ 23$$

$$j_D = \frac{\delta_D}{(\Delta z_D - 1)} \qquad 5.\ 24$$

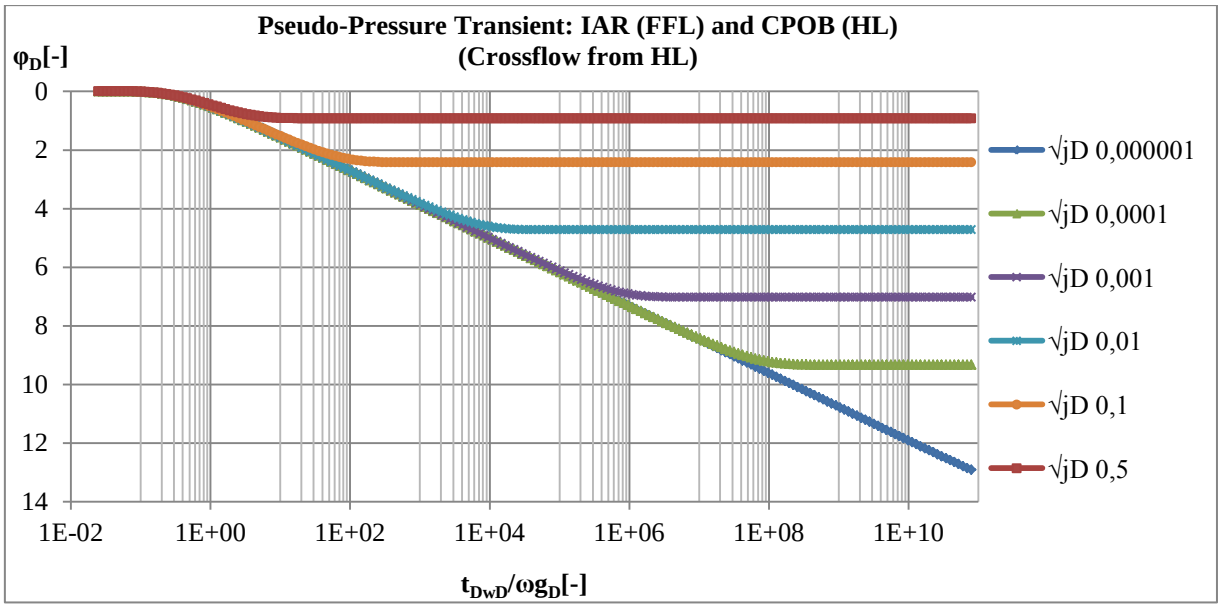

Figure 64: Pseudo-Pressure Transient Plot for Infinite Acting Free Fluid Layer with CPOB in Hydrate Layer (Crossflow from Hydrate Layer)

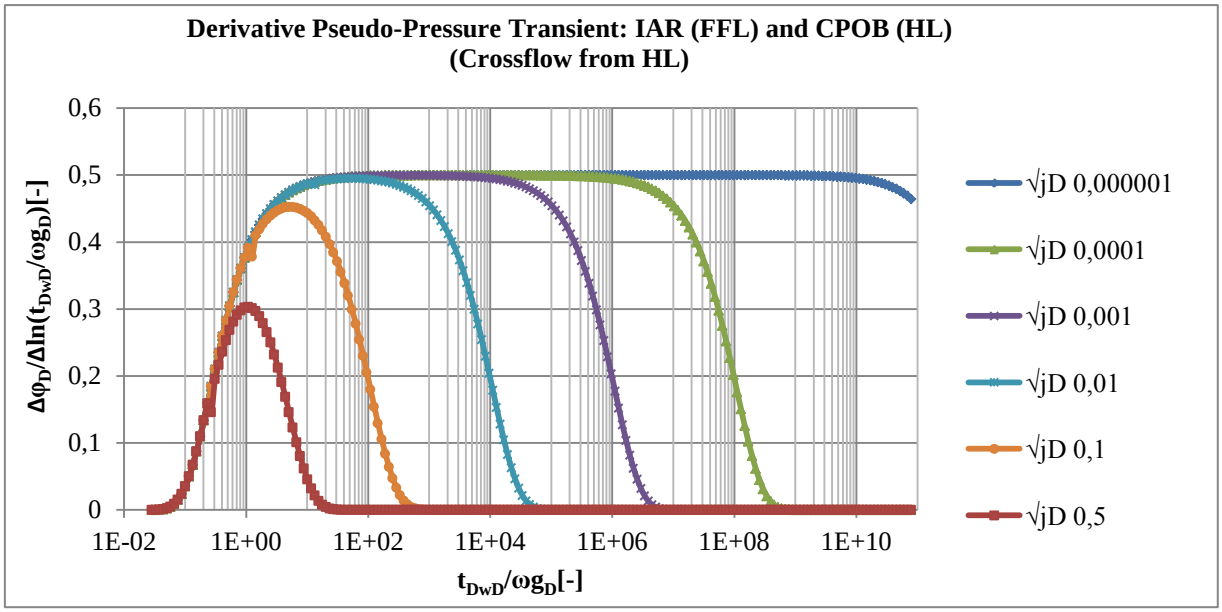

Figure 65: Derivative Plot for Infinite Acting Free Fluid Layer with CPOB in Hydrate Layer (Crossflow from Hydrate Layer)

5.2.2 Reservoir Parameters

For hydrate reservoirs with a no-flow outer boundary at the top, the influence of crossflow is predominant in the early time period of production, which is however very short. The significance of reservoir parameters in the dimensionless terms presented in the models earlier is now addressed.

Storativity Ratio

$$(1-\omega) = \frac{[a_v]_i}{a_v}\left[\left(\frac{a_h}{a_h + a_v}\right)\right]_i$$

$$\omega = \frac{[a_h]_i}{a_h}\left[\left(\frac{a_v}{a_h+a_v}\right)\right]_i \quad 5.25$$

$$\frac{a_h}{a_v} = \frac{(1-\omega)}{\omega} \quad 5.26$$

Interporosity Flow Coefficient

$$\delta_D = \frac{r_w^2}{\Delta z_2 \Delta z_1}\frac{k_{v2}}{k_{h1}} \quad 5.27$$

Dimensionless Early Time Interlayer Mass Flux Coefficient

$$\varepsilon_D = \delta_D\sqrt{[1-\omega]} \quad 5.28$$

Dimensionless Interlayer Crossflow Compressibility (NFB in HL)

$$f_D = \left(1 + \frac{[1-\omega]}{\omega}\delta_D(\Delta z_D - 1)\right) = \left(1 + \frac{a_h}{a_v}\frac{r_w^2}{\Delta z_2 \Delta z_1}\frac{k_{v2}}{k_{h1}}(\Delta z_D - 1)\right) \quad 5.29$$

With the above equation, we can conclude that the thicker the producing layer, the more insignificant the effects of crossflow. Moreover, if the reservoir permeability of the free fluid layer is much higher than the hydrate layer, which is also the precondition for producing from this layer and developing the model, the influence of the dimensionless interlayer crossflow compressibility diminishes.

Dimensionless Interlayer Crossflow Storativity Compressibility Product

$$\omega f_D = [\omega + (1-\omega)\delta_D(\Delta z_D - 1)] \quad 5.30$$

For hydrate reservoirs with much lower pressure conductivities with respect to the free fluid layer, the storativity ratio is very small. As such, the dimensionless interlayer crossflow storativity compressibility product could be less than 1, considering the interporosity flow coefficient is far less than 1. In this case, the hydrate layer acts similar to a no-flow boundary for the free fluid layer and hence the pressure depression in the free fluid layer is much higher as also seen in Figure 61. It should however be emphasized that the dissociation of the hydrate layer would lead to an increase in the pressure conductivity in the hydrate layer. With this increase, pressure depression in the hydrate layer increases more rapidly and hence boundary dominated flow in the hydrate layer is faster achieved.

Dimensionless Interlayer Crossflow Compressibility (CPOB in HL)

$$g_D = \left(1 + \frac{[1-\omega]}{3\omega}\delta_D(\Delta z_D - 1)\right) \quad 5.31$$

Dimensionless Interlayer Mass Flux Coefficient

$$j_D = \frac{\delta_D}{(\Delta z_D - 1)} \quad 5.32$$

Where,

$$\Delta z_D = \frac{\Delta z_2}{\left(\frac{h}{2}\right)} = \frac{\left[\left(\frac{h}{2}\right)+h_{\text{confining layer}}\right]}{\left(\frac{h}{2}\right)} \quad 5.33$$

$$\delta_D = \frac{r_w^2}{\Delta z_2 \Delta z_1}\frac{k_{v2}}{k_{h1}} \quad 5.34$$

As mentioned in the assumptions in deriving the model, NFB conditions at the top of the hydrate layer is a precondition for production as this has to serve as the cap rock of the reservoir, which should also guarantee safe production. However, if the hydrate dissociation is very high, the effects of pressure support in the hydrate layer could lead to a CPOB behavior of the reservoir response. Hence, if the hydrate dissociation rate is not that significant, NFB responses will be noticed and the CPOB responses will be noticed for high dissociation rates, especially at the top of the hydrate layer when heat conduction effects also become substantial.

PTA

Semi-log Analysis

Semi-log analysis as mentioned earlier is valid if and only if a gradient is deducible during IARF. However, the IARF period is valid only after a given duration of production.

NFB Model for the Hydrate Crossflow Layer

$$\varphi_D = \frac{2\pi hk}{\dot{m}_t}[\varphi_i - \varphi(r,t)] = \frac{1}{2}E_1\left(\frac{r_D^2}{4t_{DwD}}\omega f_D\right) \quad 5.35$$

Analogue methods of analysis proposed in Chapter 3 for infinite acting systems, we make the same approach here.

The pressure transient solution can be simplified to:

$$\varphi_D = 0.5\left[\ln\left(\frac{t_{DwD}}{\omega f_D}\right) + 0.80907\right]$$

With the introduction of the pressure dependent pseudo-relative permeability [krg*(p)] given in Appendix 10, pressure rate transient analysis could be carried out.

$$\frac{\int\frac{\rho_g}{\eta_g}dp}{Q_{g,st}(t)} = \frac{\rho_{g,st}}{4\pi hkk_{rg}^*(p)}\left[\ln\left(\frac{t_{DwD}}{\omega f_D}\right) + 0.80907\right] \quad 5.36$$

By expanding the dimensionless time, relating the gas density with the formation volume factor and considering the dimensionless compressibility-mobility, the above equation can be written in terms of real time.

$$\frac{\int\frac{1}{B_g\eta_g}dp}{Q_{g,st}(t)} = \varphi RPI(t) = \frac{1.1515}{2\pi hkk_{rg}^*(p)}\left[\log t - \log\left(\left[\left(\frac{a_h+a_v}{a_h a_v}\right)\right]_i\right) - \log(\omega f_D) + 0.3513\right] \quad 5.37$$

Where,

$$\frac{1}{a_h} = \frac{S_D}{a_{h,i}} = \frac{\rho_{t,i}\left(\frac{k_r}{\eta}\right)_t}{[(\rho_w c_{T,w})+(\rho_g c_{T,g})]} = \omega\left[\left(\frac{a_h+a_v}{a_h a_v}\right)\right]_i \quad 5.38$$

A semi-log plot of the gas rate normalized pseudo-pressure versus the time should give a straight line during infinite acting flow provided the relative permeability change with time or the changes in the dimensionless crossflow terms (ωf_D) with pressure is negligible. The gradient of the line can hence be used to estimate the effective permeability of the gas phase.

The gradient of the semi-log plot:

$$m_{log} = \frac{1.1515}{2\pi hkk^*_{rg}(p)\int\frac{1}{B_g\eta_g}dp} \quad 5.39$$

Effective gas permeability at IARF

$$kk^*_{rg}(p) = k^*_g(p) = \frac{1.1515}{2\pi h m_{log}\int\frac{1}{B_g\eta_g}dp} \quad 5.40$$

Skin= Dimensionless Dissociation Terms (IARF)

Applying the damage skin approach for well test analysis we get an approximation of the dissociation terms for the hydrate layer.

$$\omega f_D = [\omega + (1-\omega)\delta_D(\Delta z_D - 1)] \approx \exp\left\{-0.434\left[\frac{\left[\frac{\int\frac{1}{B_g\eta_g}dp}{Q_{g,st}(t)}\right]_{t=1s}}{m_{log}} + \log\left(\left[\left(\frac{a_h+a_v}{a_h a_v}\right)\right]_i 10^{-0.3513}\right)\right]\right\} \quad 5.41$$

<u>CPOB Model for the Hydrate Crossflow Layer</u>

$$\varphi_D = \frac{2\pi hk}{\dot{m}_t}[\varphi_i - \varphi(r,t)] = \frac{1}{2}W\left(\frac{r_D^2}{4t_{DwD}}\omega g_D, r_D\sqrt{j_D}\right) \quad 5.42$$

Although large values of the dimensionless interlayer mass flux coefficient have been used to develop the type curve, it is worth mentioning that its value is usually small for real reservoir engineering problems as the quotient of the wellbore radius to the layer thickness product is usually far less than 1 and so is the value of the ratio of the vertical permeability of the hydrate layer to the horizontal permeability of the free fluid layer, i.e.:

$$\frac{r_w^2}{\Delta z_2 \Delta z_1} \ll 1 \frac{k_{v2}}{k_{h1}} < 1 \qquad \delta_D = \frac{r_w^2}{\Delta z_2 \Delta z_1}\frac{k_{v2}}{k_{h1}} \ll 1 \qquad j_D = \frac{\delta_D}{(\Delta z_D - 1)} \ll 1$$

With this note, we can assume that the crossflow behavior is very significant only in the late time region of flow and hence the following approach can be made:

$$\sqrt{j_D}\frac{t_{DwD}}{\omega g_D} < 2$$

$$\varphi_D = \frac{2\pi hk}{\dot{m}_t}[\varphi_i - \varphi(r,t)] = \frac{1}{2}W\left(\frac{r_D^2}{4t_{DwD}}\omega g_D, r_D\sqrt{j_D}\right) \approx \frac{1}{2}E_1\left(\frac{r_D^2}{4t_{DwD}}\omega g_D\right) \quad 5.43$$

$\sqrt{j_D} \ll 1$ and $\sqrt{j_D}\frac{t_{DwD}}{\omega g_D} < 2$

$$\varphi_D = \frac{2\pi hk}{\dot{m}_t}[\varphi_i - \varphi(r,t)] = \frac{1}{2}W\left(\frac{r_D^2}{4t_{DwD}}\omega g_D, r_D\sqrt{j_D}\right) \approx \frac{1}{2}E_1\left(\frac{r_D^2}{4t_{DwD}}\omega\right) \quad 5.44$$

The above simplification indicates that semi-log plots applied be used to estimate reservoir parameters before crossflow behavior affects the reservoir response significantly in the late time region. Since the producing layer is the free fluid layer, changes in reservoir parameter will not be that significant compared to if the reservoir was produced from the hydrate layer; hence, reliable values from the semi-log plots can be derived. The semi-log analysis given for the NFB above is also applicable here.

Type Curve Matching

Note that type curve matching is usually used to identify the reservoir parameters from the Hantush leaky aquifer model.

Time Match for NFB Model for the Hydrate Crossflow Layer

$$\left[\frac{t_{DwD}}{\omega f_D}\right]_{MP};\ t_{MP} \quad 5.45$$

Where,

$$t_{DwD} = \frac{t}{\left[\left(\frac{a_h + a_v}{a_h a_v}\right)\right]_i}$$

From the match points, the dimensionless interlayer heat flux compressibility is derived thus:

$$[\omega f_D]_{MP} = \frac{t_{DwD}}{\left[\frac{t_{DwD}}{\omega f_D}\right]_{MP}} = \frac{1}{\left[\left(\frac{a_h+a_v}{a_h a_v}\right)\right]_i}\frac{t_{MP}}{\left[\frac{t_{DwD}}{\omega f_D}\right]_{MP}} \quad 5.46$$

Time Match for CPOB Model for the Hydrate Crossflow Layer

$$\left[\frac{t_{Dw}}{\omega g_D}\right]_{MP};\ t_{MP};\left[\sqrt{j_D}\right]_{MP} \quad 5.47$$

From the match points, the dimensionless interlayer heat flux compressibility is derived thus:

$$[\omega g_D]_{MP} = \frac{t_{DwD}}{\left[\frac{t_{DwD}}{\omega g_D}\right]_{MP}} = \frac{1}{\left[\left(\frac{a_h+a_v}{a_h a_v}\right)\right]_i}\frac{t_{MP}}{\left[\frac{t_{DwD}}{\omega g_D}\right]_{MP}} \quad 5.48$$

Pressure Match

For both the NFB and CPOB, the following match can be gotten. The match along the horizontal is given by:

$[\varphi_D]_{MP}$; $[\varphi \mathrm{RPI}(t)]_{MP}$

As mentioned in Chapter 3.5.3, the use of type curve matching for PTA in this case would be most feasibly if the rates of each phase remain constant during production.

Derivatives

The derivatives of the type curve will show the following characteristics for the infinite acting reservoir:

Early Time Region

No skin response

IARF (negligible crossflow)

$$\frac{d[\varphi_D]}{d\left[\ln\left(\frac{t_{DwD}}{\omega f_D}\right)\right]} = \frac{d[\varphi_D]}{d\left[\ln\left(\frac{t_{DwD}}{\omega g_D}\right)\right]} = 0.5 \qquad 5.\ 49$$

IARF and high crossflow

$$\frac{d[\varphi_D]}{d\left[\ln\left(\frac{t_{DwD}}{\omega f_D}\right)\right]} = \frac{d[\varphi_D]}{d\left[\ln\left(\frac{t_{DwD}}{\omega g_D}\right)\right]} = 0 \qquad 5.\ 50$$

5.2.3 Case 2: Pressure Transient Solutions and Analysis when Producing from the Hydrate Layer

From the models developed in Appendix 15, the pseudo-pressure responses when producing from the hydrate layer are given below. It should be noted that the combined effects of heat conduction from the top of the hydrate layer and mass flux from the free fluid layer are considered in the model.

Early-Time Response for both No-flow Boundary and Constant Pressure Outer Boundary (CPOB) in Crossflow

$$\varphi_D = \frac{2\pi hk}{\dot{m}_t}[\varphi_i - \varphi(r,t)] = H\left(\frac{\omega r_D^2}{4t_{DwD}}, \frac{r_D \varepsilon_{D,2}}{4\sqrt{\omega}}\right) \qquad 5.\ 51$$

Where,

$$\varepsilon_{D,2} = \left[e_D\sqrt{F_{CD}} + \delta_D(1+\theta_D)\sqrt{[1-\omega]}\right] \qquad 5.\ 52$$

Late Time Period for Constant Pressure Outer Boundary (CPOB) in Crossflow Layer+Constant Temperature Outer Boundary (CTOB) in Top Layer

$$\varphi_D = \frac{2\pi hk}{\dot{m}_t}[\varphi_i - \varphi(r,t)] = \frac{1}{2}W\left(\frac{r_D^2}{4t_{DwD}}\omega g_{D,2}, r_D\sqrt{j_{D,2}}\right) \qquad 5.\ 53$$

Where,

$$g_{D,2} = \left\{1 + \frac{1}{3\omega}\left[e_D F_{CD}\left(\Delta z_{D,TL} - 1\right) + \delta_D(1+\theta_D)[1-\omega]\left(\Delta z_{D,BL} - 1\right)\right]\right\} \qquad 5.\ 54$$

$$j_{D,2} = \left[\frac{\delta_D(1+\theta_D)}{(\Delta z_{D,BL}-1)} + \frac{e_D}{(\Delta z_{D,TL}-1)}\right] \qquad 5.\ 55$$

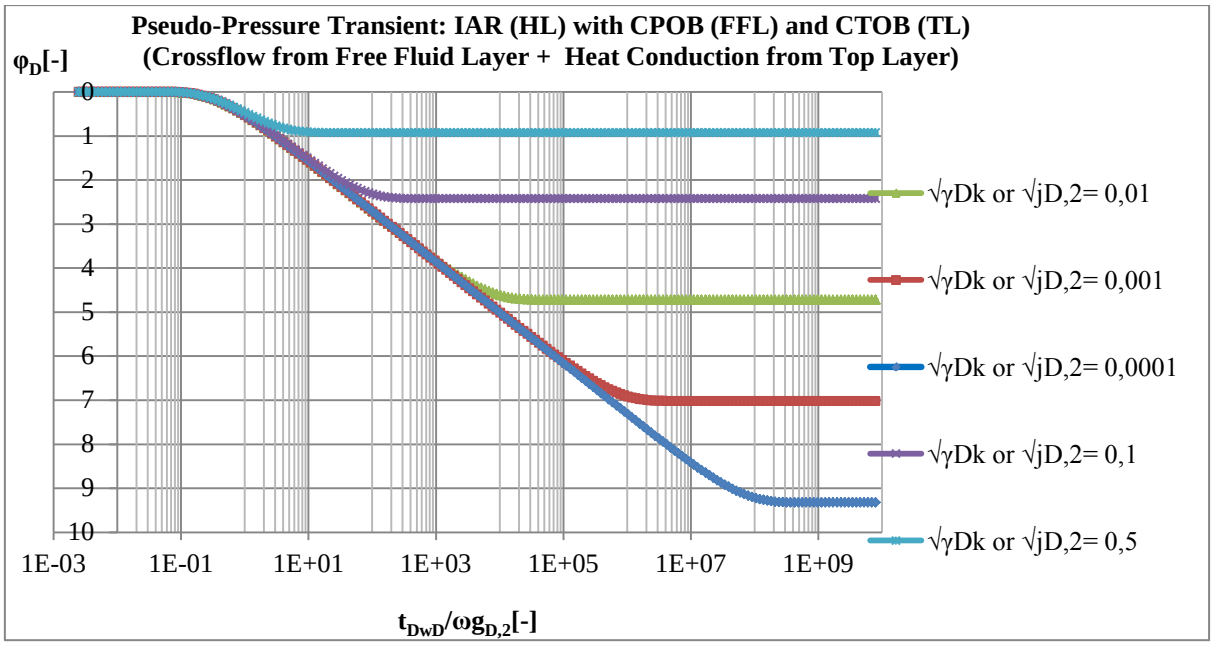

Figure 66: Drawdown Response in Infinite Acting Hydrate Layer with CPOB in Free Fluid Layer and CTOB in Top Layer (Crossflow from Free Fluid Layer + Heat Conduction from Top Layer)

Late Time Period for No-flow Boundary (NFB) in Crossflow Layer+Constant Temperature Outer Boundary (CTOB) in Top Layer (TL)

$$\varphi_D = \frac{2\pi hk}{\dot{m}_t}[\varphi_i - \varphi(r,t)] = \frac{1}{2}W\left(\frac{r_D^2}{4t_{DwD}}\omega f_{D,2}, r_D\sqrt{Y_D}\right) \quad 5.56$$

Where

$$f_{D,2} = \left[1 + \frac{1}{3\omega}\{(e_D F_{CD}(\Delta z_{D,TL} - 1) + 3[\delta_D(1+\theta_D)(1-\omega)(\Delta z_{D,BL} - 1)])\}\right] \quad 5.57$$

$$Y_D = \frac{e_D}{(\Delta z_{D,TL} - 1)} \quad 5.58$$

Here, although the free fluid layer consists of a NFB, the reservoir response is much different from when the reservoir is produced from the free fluid layer and the hydrate layer is a NFB layer. This is solely due to the influence of heat conduction from the top layer which shows a significant influence in the reservoir response during the late time period of production. We can hence conclude that when producing from the hydrate layer in Class 1&2 gas hydrate reservoirs, we expect a much higher gas recovery from the hydrate dissociation compared to Class 3 reservoirs, given the reservoirs have the same petro-physical properties and provided the heat influx from the caprock is strong enough to influence continuous hydrate dissociation. Note that the imposed CTOB at the caprock is an optimistic model analogous to the kinetic model.

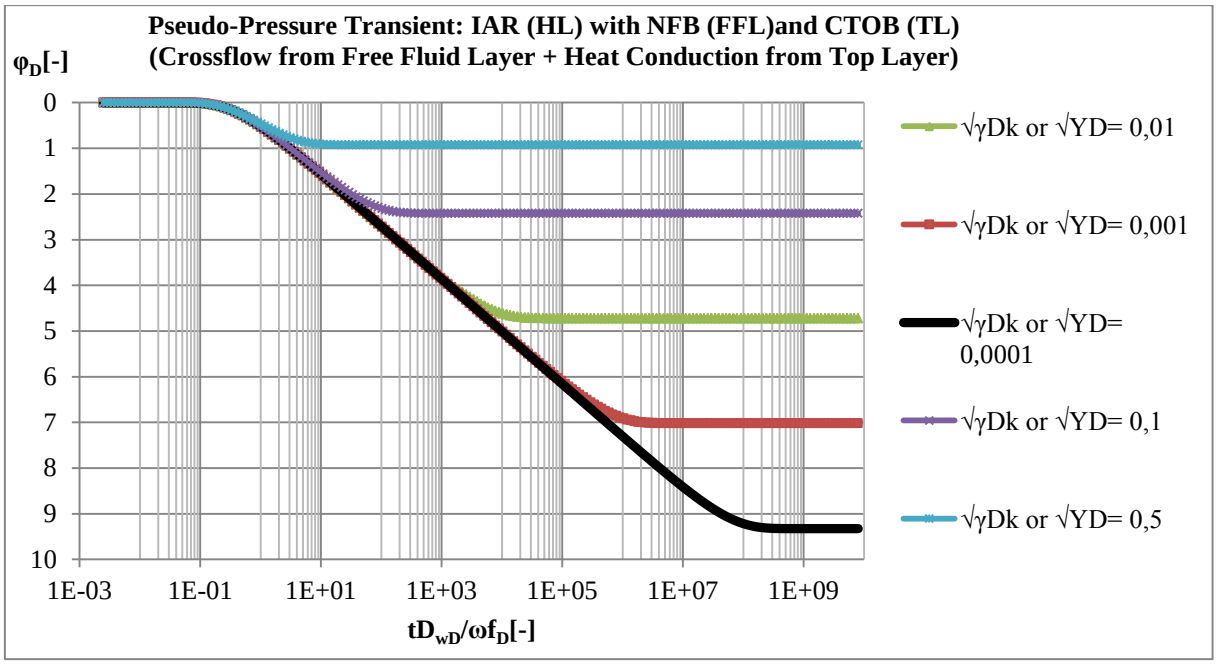

Figure 67: Drawdown Response in Infinite Acting Hydrate Layer with NFB in Free Fluid Layer and CTOB in Top Layer (Crossflow from Free Fluid Layer + Heat Conduction from Top Layer)

5.2.4 Reservoir Parameters

The effect of producing from the hydrate layer when crossflow from the free fluid layer is not negligible could have a tremendous effect on the reservoir response. This is due to the following:

- Heat used up in the hydrate layer dissociates the hydrates and would lead to pressure support.
- Convective heat flux from the fluids in the crossflow layer will lead to further hydrate dissociation and hence further pressure support.
- Mass flux due to fluids from the free fluid layer also serves as pressure support in the hydrate layer.

This implies, when producing from the hydrate layer at constant sandface rates, minimum pressure depletions could be experienced due to all these pressure support terms. For this reason, IARF would hardly be achieved for semi-log plots to be performed. Hence, the use of type curve matching would be very useful to estimate certain reservoir parameters.

Dimensionless Convective Heat Flux Dissociation Coefficient

$$\theta_D = \frac{[c_p \Delta T]_{avg}}{h_d} \qquad 5.59$$

Dimensionless Early Time Interlayer Mass Flux Coefficient

$$\varepsilon_{D,2} = \left[e_D \sqrt{F_{CD}} + \delta_D (1 + \theta_D) \sqrt{[1 - \omega]}\right] \qquad 5.60$$

Dimensionless Interlayer Crossflow Compressibility

$$g_{D,2} = \left\{1 + \frac{1}{3\omega}\left[e_D F_{CD}\left(\Delta z_{D,TL} - 1\right) + \delta_D(1 + \theta_D)[1 - \omega]\left(\Delta z_{D,BL} - 1\right)\right]\right\} \quad 5.61$$

Dimensionless Interlayer Mass Flux Coefficient

$$j_{D,2} = \left[\frac{\delta_D(1+\theta_D)}{(\Delta z_{D,BL}-1)} + \frac{e_D}{(\Delta z_{D,TL}-1)}\right] \quad 5.62$$

If the pressure depression in the hydrate layer and the interporosity flow coefficient are low, so will the mass influx from the free fluid layer. Hence the influence of convective heat influx is negligible. However, even with negligible mass flux from the free fluid layer during depressurization, we still have conductive heat flux from the upper layer which assists in the dissociation process. This implies the assumption of negligible dimensionless interlayer mass flux coefficient cannot be made with certainty in this case.

Notice that both the dimensionless mass flux coefficient and the dimensionless interlayer crossflow compressibility are functions of the storativity (energy used in the hydrate layer), the dimensionless heat conductive flux coefficient (heat energy used from conduction), dimensionless convective heat flux dissociation coefficient (energy used up from warmer fluids in the free fluid layer) and the interporosity flow coefficient.

When the interporosity flow coefficient is negligible, the effects of mass flux from the free fluid layer are also trivial and just heat conduction becomes very influential.

Dimensionless Interlayer Crossflow Compressibility

$$f_{D,2} = \left[1 + \frac{1}{3\omega}\left\{\left(e_D F_{CD}\left(\Delta z_{D,TL} - 1\right) + 3\left[\delta_D(1 + \theta_D)(1 - \omega)\left(\Delta z_{D,BL} - 1\right)\right]\right)\right\}\right] \quad 5.63$$

Dimensionless Interlayer Mass Flux Coefficient

$$Y_D = \frac{e_D}{(\Delta z_{D,TL}-1)} \quad 5.64$$

The dimensionless interlayer mass flux coefficient for the NFB case is solely dependent on the heat conduction term during late time production. However, if compared to producing from the free fluid layer, the influence of heat conduction is better quantified and its influence represented in the model.

PTA

CPOB in Crossflow Layer and CTOB in Top Layer

As was done for the case of producing from the free fluid layer, we make simplifications of the model for given ranges. With this note, we can assume that the crossflow behavior is not perceived in the early-time region of flow and hence the following approach can be made for the given intervals below:

$$\sqrt{j_{D,2}}\,\frac{t_{DwD}}{\omega g_{D,2}} < 2$$

$$\varphi_D = \frac{2\pi hk}{\dot{m}_t}[\varphi_i - \varphi(r,t)] = \frac{1}{2}W\left(\frac{r_D^2}{4t_{DwD}}\omega g_{D,2}, r_D\sqrt{j_{D,2}}\right) \approx \frac{1}{2}E_1\left(\frac{r_D^2}{4t_{DwD}}\omega g_{D,2}\right) \quad 5.65$$

$\sqrt{j_{D,2}} \ll 1$ and $\sqrt{j_{D,2}}\frac{t_{DwD}}{\omega g_{D,2}} < 2$

$$\varphi_D = \frac{2\pi hk}{\dot{m}_t}[\varphi_i - \varphi(r,t)] = \frac{1}{2}W\left(\frac{r_D^2}{4t_{DwD}}\omega g_{D,2}, r_D\sqrt{j_{D,2}}\right) \approx \frac{1}{2}E_1\left(\frac{r_D^2}{4t_{DwD}}\omega\right) \quad 5.66$$

With the representation of the models in Ei-functions, the methods of analysis in 5.2.1 are also applicable here.

NFB in Crossflow Layer and CTOB in Top Layer

$\sqrt{Y_D}\frac{t_{DwD}}{\omega f_{D,2}} < 2$

$$\varphi_D = \frac{2\pi hk}{\dot{m}_t}[\varphi_i - \varphi(r,t)] = \frac{1}{2}W\left(\frac{r_D^2}{4t_{DwD}}\omega f_{D,2}, r_D\sqrt{Y_D}\right) \approx \frac{1}{2}E_1\left(\frac{r_D^2}{4t_{DwD}}\omega f_{D,2}\right) \quad 5.67$$

$\sqrt{Y_D} \ll 1$ and $\sqrt{Y_D}\frac{t_{DwD}}{\omega g_{D,2}} < 2$

$$\varphi_D = \frac{2\pi hk}{\dot{m}_t}[\varphi_i - \varphi(r,t)] = \frac{1}{2}W\left(\frac{r_D^2}{4t_{DwD}}\omega f_{D,2}, r_D\sqrt{Y_D}\right) \approx \frac{1}{2}E_1\left(\frac{r_D^2}{4t_{DwD}}\omega\right) \quad 5.68$$

With the representation of the model in E_1-functions, the methods of analysis in Chapter 3 are also applicable here.

5.3 Constant Pressure Solutions and Rate Transient Analysis

Constant terminal solutions developed for the crossflow problem are now depicted with respect to the layer of production.

5.3.1 Case 1: Producing from the Free Fluid Layer

Late Time Response for No-flow in HL

Dimensionless Pseudo-Pressure

$$\varphi_D = A\left(\frac{t_{DwD}}{\omega f_D}, r_D\right) \quad 5.69$$

For $t_{DwD}/(\omega f_D r_D^2)>500$

$$\varphi_D = \frac{E_1\left(\frac{r_D^2\omega f_D}{4t_{DwD}}\right)}{E_1\left(\frac{\omega f_D}{4t_{DwD}}\right)} \quad 5.70$$

Dimensionless Flowrate at Wellbore

$$\dot{m}_{tD} = G\left(\frac{t_{DwD}}{\omega f_D}\right) \quad 5.71$$

For $t_{DwD}/(\omega f_D r_D^2)>500$

$$\dot{m}_{tD} = 2\frac{e^{-\left(\frac{\omega f_D}{4t_{DwD}}r_D^2\right)}}{E_1\left(\frac{\omega f_D}{4t_{DwD}}\right)} \qquad 5.\ 72$$

Where,

$$f_D = \left(1 + \frac{[1-\omega]}{\omega}\delta_D(\Delta z_D - 1)\right) \qquad 5.\ 73$$

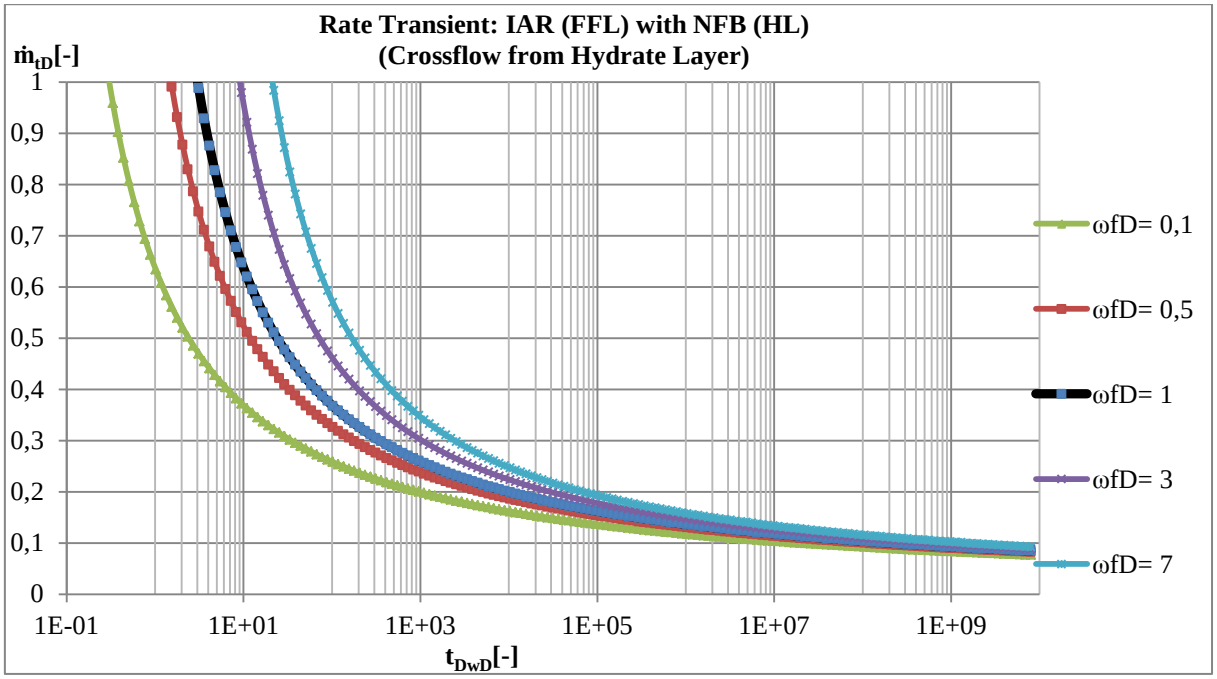

Figure 68: Rate Transient Response in Infinite Acting Free Fluid Layer and NFB in Hydrate Layer

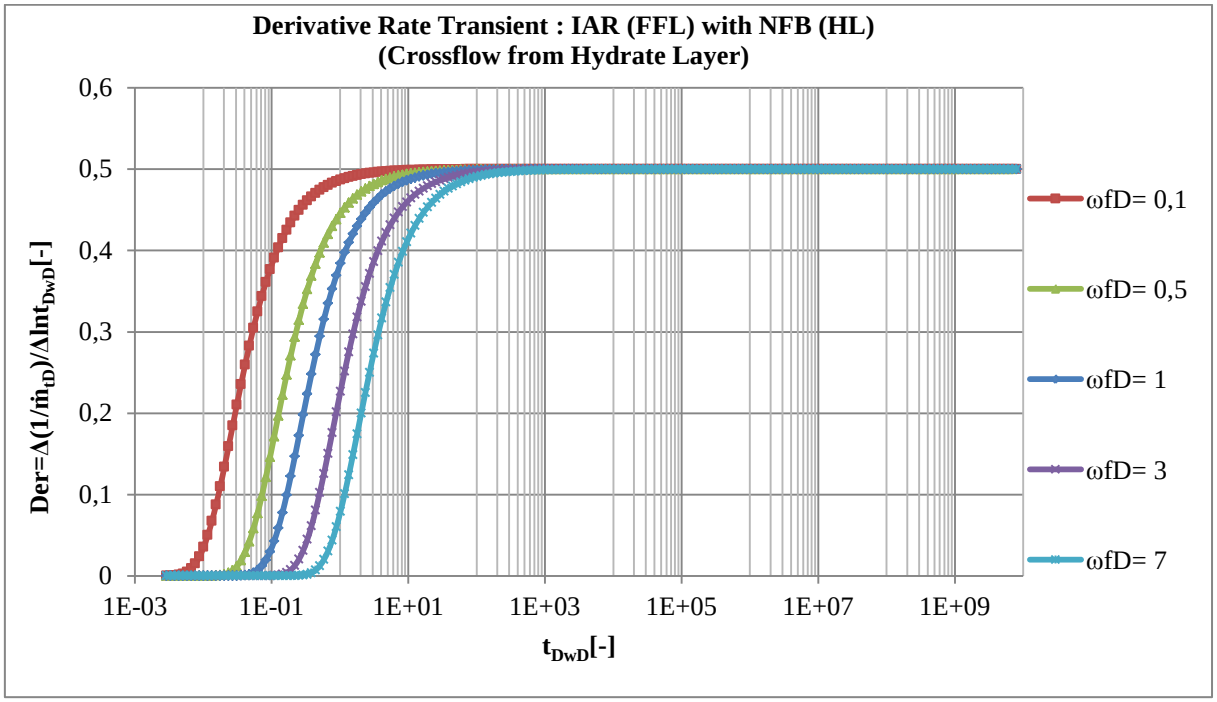

Figure 69: Rate Transient Derivative Plot in Infinite Acting Free Fluid Layer and NFB in Hydrate Layer

Due to NFB effects in the hydrate layer, crossflow will be trivial at the late time period of production where the free fluid layer start depleting based on its reservoir content since the rate transient responses converge as given in Figure 68. If the crossflow term for a given reservoir remains constant throughout production, semi-log plots can be performed.

Late Time Period for CPOB in HL

Dimensionless Pseudo-Pressure

$$\varphi_D = Z\left(\frac{t_{Dw}}{\omega g_D}, r_D, \sqrt{j_D}\right) \quad 5.74$$

For $\frac{t_{Dw}}{\omega g_D}\sqrt{j_D} > 1$

$$\varphi_D = \frac{W\left(\frac{r_D^2 \omega g_D}{4 t_{DwD}}, r_D\sqrt{j_D}\right)}{W\left(\frac{\omega g_D}{4 t_{DwD}}, \sqrt{j_D}\right)} \quad 5.75$$

Dimensionless Flowrate at Wellbore

$$\dot{m}_{tD} = G\left(\frac{t_{Dw}}{\omega g_D}, \sqrt{j_D}\right) \quad 5.76$$

For $\frac{t_{Dw}}{\omega g_D} j_D > 1$

$$\dot{m}_{tD} = \frac{2}{W\left(\frac{\omega g_D}{4 t_{DwD}}, \sqrt{j_D}\right)} \quad 5.77$$

Where,

$$g_D = \left(1 + \frac{[1-\omega]}{3\omega}\delta_D(\Delta z_D - 1)\right) \quad 5.78$$

$$j_D = \frac{\delta_D}{(\Delta z_D - 1)} \quad 5.79$$

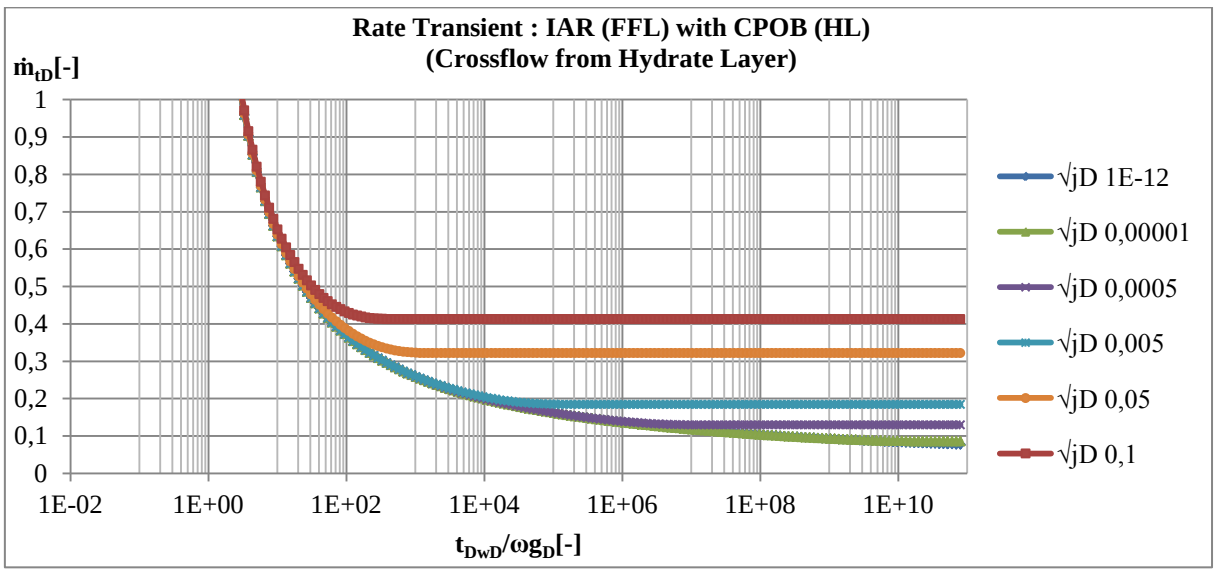

Figure 70: Rate Transient Response in Infinite Acting Free Fluid Layer and CPOB in Hydrate Layer

5.3.2 Rate Transient Analysis when Producing from Free Fluid Layer

5.3.2.1 Semi-log Analysis

NFB in Crossflow Layer

Dimensionless Flowrate at Wellbore

$$\dot{m}_{tD} = G\left(\frac{t_{Dw}}{\omega f_D}\right)$$

For $t_{DwD}/(\omega f_D)>500$

$$\dot{m}_{tD} = 2\frac{e^{-\left(\frac{\omega f_D}{4t_{DwD}}\right)}}{E_1\left(\frac{\omega f_D}{4t_{DwD}}\right)} \quad 5.80$$

$$\frac{1}{\dot{m}_t} = \frac{1}{2\pi h[k\int f_t(p)dp]}\left[0.48465\ln\left(\frac{t_{DwD}}{\omega f_D}\right) + 0.64757\right] \quad 5.81$$

$$\frac{1}{\dot{m}_t} = \frac{1.1161}{2\pi h[k\int f_t(p)dp]}\left[\log t - \log\left(\left[\left(\frac{a_h+a_v}{a_h a_v}\right)\right]_i\right) - \log(\omega f_D) + 0.58018\right] \quad 5.82$$

Where,

$$\frac{1}{a_h} = \frac{S_D}{a_{h,i}} = \frac{\rho_{t,i}\left(\frac{k_r}{\eta}\right)_t}{[(\rho_w c_{T,w})+(\rho_g c_{T,g})]} = \omega\left[\left(\frac{a_h+a_v}{a_h a_v}\right)\right]_i \quad 5.83$$

With the above representations, RTA addressed in Chapter 3.4 can be applied here.

CPOB in Crossflow Layer

Dimensionless Flowrate at Wellbore

$$\dot{m}_{tD} = G\left(\frac{t_{Dw}}{\omega g_D}, \sqrt{j_D}\right) \quad 5.84$$

For $\frac{t_{Dw}}{\omega g_D} j_D > 1$

$$\dot{m}_{tD} = \frac{2}{W\left(\frac{\omega g_D}{4t_{DwD}}, \sqrt{j_D}\right)} \quad 5.85$$

For $\frac{t_{Dw}}{\omega g_D}\sqrt{j_D} < 2$

$$\dot{m}_{tD} = \frac{2}{E_1\left(\frac{\omega g_D}{4t_{DwD}}\right)} \quad 5.86$$

$$\frac{1}{\dot{m}_t} = \frac{1}{2\pi h[k\int f_t(p)dp]}\left[0.4846\ln\left(\frac{t_{DwD}}{\omega g_D}\right) + 0.64757\right] \quad 5.87$$

With the above representation of the reservoir models, RTA methods in Chapter 3.4 can once more be applied here.

5.3.2.2 Type Curve Matching

Time Match for NFB Model for the Hydrate Crossflow Layer

$$\left[\frac{t_{DwD}}{\omega f_D}\right]_{MP};\ t_{MP} \qquad 5.\ 88$$

Where,

$$t_{DwD} = \frac{t}{\left[\left(\frac{a_h + a_v}{a_h a_v}\right)\right]_i}$$

From the match points, the dimensionless interlayer heat flux compressibility is derived thus:

$$[\omega f_D]_{MP} = \frac{t_{DwD}}{\left[\frac{t_{DwD}}{\omega f_D}\right]_{MP}} = \frac{1}{\left[\left(\frac{a_h+a_v}{a_h a_v}\right)\right]_i}\frac{t_{MP}}{\left[\frac{t_{DwD}}{\omega f_D}\right]_{MP}} \qquad 5.\ 89$$

Time Match for CPOB Model for the Hydrate Crossflow Layer

$$\left[\frac{t_{DwD}}{\omega g_D}\right]_{MP};\ t_{MP};\left[\sqrt{j_D}\right]_{MP} \qquad 5.\ 90$$

From the match points, the dimensionless interlayer heat flux compressibility is derived thus:

$$[\omega g_D]_{MP} = \frac{t_{DwD}}{\left[\frac{t_{DwD}}{\omega g_D}\right]_{MP}} = \frac{1}{\left[\left(\frac{a_h+a_v}{a_h a_v}\right)\right]_i}\frac{t_{MP}}{\left[\frac{t_{DwD}}{\omega g_D}\right]_{MP}} \qquad 5.\ 91$$

Rate Match

For both the NFB and CPOB, the following match can be gotten. The match along the horizontal is given by:

$$\left[\frac{1}{\dot{m}_{tD}}\right]_{MP};\left[\frac{1}{\dot{m}_t}\right]_{MP};[\varphi PI(t)]_{g,MP}$$

Similarly, the RTA methods in Chapter 3.4 can once more be applied here.

5.3.2.3 Derivatives

The derivatives of the type curves will show the following characteristics for the infinite acting reservoir:

Early Time Region

No skin response

IARF (negligible crossflow)

$$\frac{d\left[\frac{1}{\dot{m}_{tD}}\right]}{d\left[\ln\left(\frac{t_{DwD}}{\omega f_D}\right)\right]} = \frac{d\left[\frac{1}{\dot{m}_{tD}}\right]}{d\left[\ln\left(\frac{t_{DwD}}{\omega g_D}\right)\right]} = 0.5 \qquad 5.\ 92$$

IARF and high crossflow

$$\frac{d\left[\frac{1}{\dot{m}_{tD}}\right]}{d\left[\ln\left(\frac{t_{DwD}}{\omega f_D}\right)\right]} = \frac{d\left[\frac{1}{\dot{m}_{tD}}\right]}{d\left[\ln\left(\frac{t_{DwD}}{\omega g_D}\right)\right]} = 0 \quad 5.93$$

5.3.3 Case 2: Producing from the Hydrate Layer

Late Time Period for No-flow in Crossflow Layer + Constant Temperature Outer Boundary in Top Layer (TL)

$$\varphi_D = Z\left(\frac{t_{DwD}}{\omega f_{D,2}}, r_D, \sqrt{Y_D}\right) \quad 5.94$$

For $\frac{t_{Dw}}{\omega f_{D,2}}\sqrt{Y_D} > 1$

$$\varphi_D = \frac{W\left(\frac{r_D^2 \omega f_{D,2}}{4t_{DwD}}, r_D\sqrt{Y_D}\right)}{W\left(\frac{\omega f_{D,2}}{4t_{DwD}}, \sqrt{Y_D}\right)} \quad 5.95$$

Dimensionless Flowrate at Wellbore

$$\dot{m}_{tD} = G\left(\frac{t_{DwD}}{\omega f_{D,2}}, \sqrt{Y_D}\right) \quad 5.96$$

For $\frac{t_{Dw}}{\omega f_{D,2}} Y_D > 1$

$$\dot{m}_{tD} = \frac{2}{W\left(\frac{\omega f_{D,2}}{4t_{DwD}}, \sqrt{Y_D}\right)} \quad 5.97$$

For $\frac{t_{Dw}}{\omega f_{D,2}}\sqrt{Y_D} < 2$

$$\dot{m}_{tD} = \frac{2}{E_1\left(\frac{\omega f_{D,2}}{4t_{DwD}}\right)} \quad 5.98$$

$f_{D,2}$ and Y_D have been described earlier.

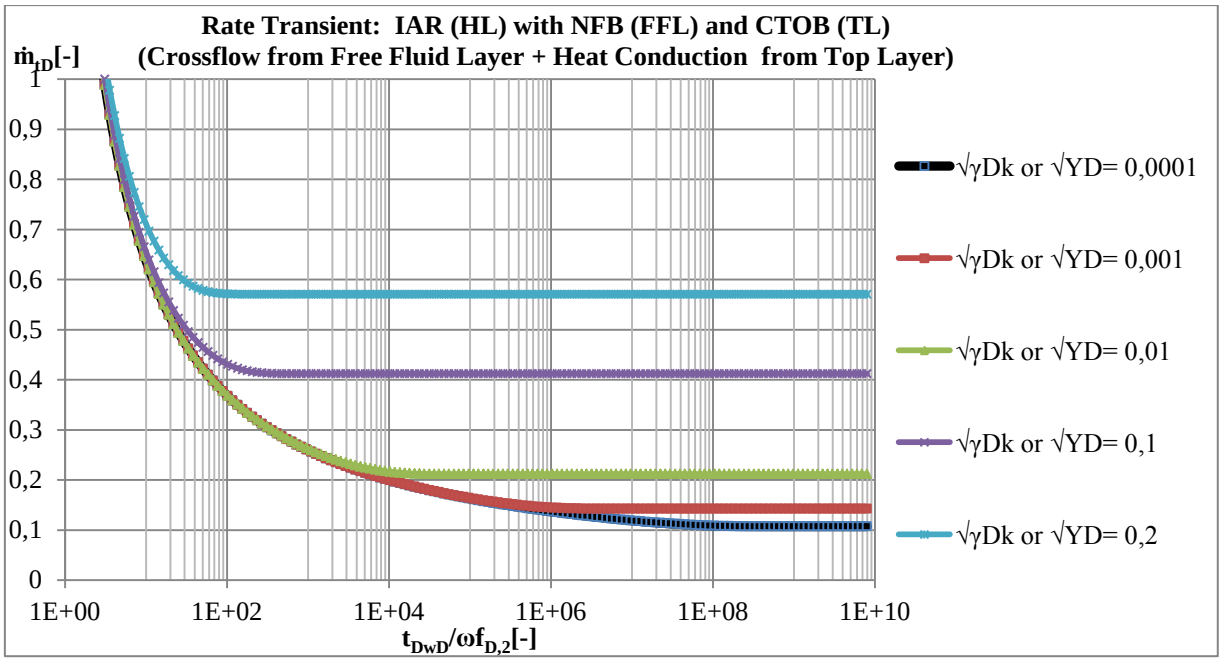

Figure 71: Rate Transient Response in Infinite Acting Hydrate Layer with NFB in Free Fluid Layer and CTOB in Top Confining Layer

Late Time Period for Constant Outer Pressure in Crossflow Layer+ Constant Temperature Outer Boundary in Top

Dimensionless Pseudo-Pressure

$$\varphi_D = Z\left(\frac{t_{DwD}}{\omega g_{D,2}}, r_D, \sqrt{j_{D,2}}\right) \qquad 5.\ 99$$

For $\frac{t_{Dw}}{\omega g_{D,2}}\sqrt{j_{D,2}} > 1$

$$\varphi_D = \frac{W\left(\frac{r_D^2 \omega g_{D,2}}{4t_{DwD}}, r_D\sqrt{j_{D,2}}\right)}{W\left(\frac{\omega g_{D,2}}{4t_{DwD}}, \sqrt{j_{D,2}}\right)} \qquad 5.\ 100$$

Dimensionless Flowrate at Wellbore

$$\dot{m}_{tD} = G\left(\frac{t_{Dw}}{\omega g_{D,2}}, \sqrt{j_{D,2}}\right) \qquad 5.\ 101$$

For $\frac{t_{Dw}}{\omega g_{D,2}} j_{D,2} > 1$

$$\dot{m}_{tD} = \frac{2}{W\left(\frac{\omega g_{D,2}}{4t_{DwD}}, \sqrt{j_{D,2}}\right)} \qquad 5.\ 102$$

For $\frac{t_{Dw}}{\omega f_{D,2}}\sqrt{j_{D,2}} < 2$

$$\dot{m}_{tD} = \frac{2}{E_1\left(\frac{\omega f_{D,2}}{4t_{DwD}}\right)} \qquad 5.\ 103$$

$g_{D,2}$ and $j_{D,2}$ have been described earlier.

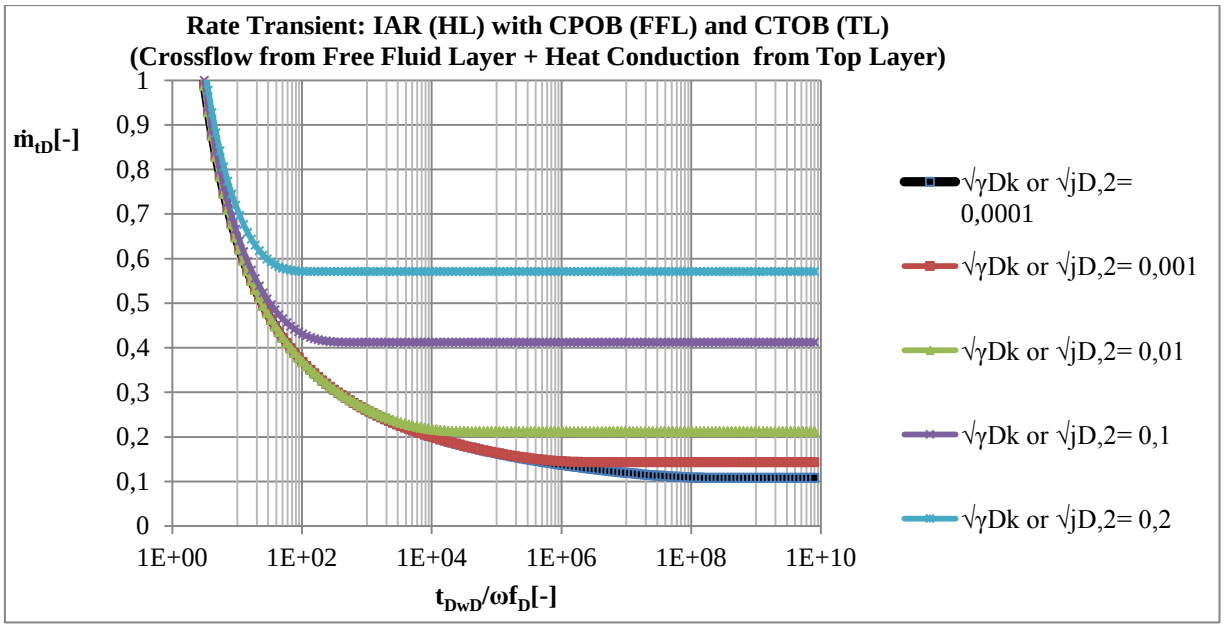

Figure 72: Rate Transient Response in Infinite Acting Hydrate Layer with CPOB in Free Fluid Layer and CTOB in Top Confining Layer

5.3.4 Rate Transient Analysis when Producing from Hydrate Layer

5.3.4.1 Semi-log Plot

The semi-log method of approach given in Chapter 5.3.2 is also applicable here for the following ranges

NFB in Crossflow Layer and CTOB in Top Layer

Dimensionless Flowrate at Wellbore

For $\frac{t_{Dw}}{\omega f_{D,2}}\sqrt{Y_D} < 2$

$$\dot{m}_{tD} = \frac{2}{E_1\left(\frac{\omega f_{D,2}}{4t_{DwD}}\right)} \qquad 5.\,104$$

CPOB in Crossflow Layer and CTOB in Top Layer

Dimensionless Flowrate at Wellbore

For $\frac{t_{Dw}}{\omega f_{D,2}}\sqrt{j_{D,2}} < 2$

$$\dot{m}_{tD} = \frac{2}{E_1\left(\frac{\omega f_{D,2}}{4t_{DwD}}\right)} \qquad 5.\,105$$

5.3.4.2 Type Curve Matching

Time Match for NFB in Crossflow Layer and CTOB in Top Layer

$$\left[\frac{t_{DwD}}{\omega f_{D,2}}\right]_{MP};\ t_{MP};\ \left[\sqrt{Y_D}\right]_{MP} \qquad 5.\,106$$

Where,

$$t_{DwD} = \frac{t}{\left[\left(\frac{a_h + a_v}{a_h a_v}\right)\right]_i}$$

From the match points, the dimensionless interlayer heat flux compressibility is derived thus:

$$\left[\omega f_{D,2}\right]_{MP} = \frac{t_{DwD}}{\left[\frac{t_{DwD}}{\omega f_{D,2}}\right]_{MP}} = \frac{1}{\left[\left(\frac{a_h+a_v}{a_h a_v}\right)\right]_i} \frac{t_{MP}}{\left[\frac{t_{DwD}}{\omega f_{D,2}}\right]_{MP}} \quad 5.107$$

Time Match for CPOB Model for the Hydrate Crossflow Layer

$$\left[\frac{t_{DwD}}{\omega g_{D,2}}\right]_{MP};\ t_{MP};\left[\sqrt{j_{D,2}}\right]_{MP} \quad 5.108$$

From the match points, the dimensionless interlayer heat flux compressibility is derived thus:

$$\left[\omega g_{D,2}\right]_{MP} = \frac{t_{DwD}}{\left[\frac{t_{DwD}}{\omega g_{D,2}}\right]_{MP}} = \frac{1}{\left[\left(\frac{a_h+a_v}{a_h a_v}\right)\right]_i} \frac{t_{MP}}{\left[\frac{t_{DwD}}{\omega g_{D,2}}\right]_{MP}} \quad 5.109$$

Rate Match

For both the NFB and CPOB, the following match can be gotten. The match along the horizontal is given by

$$\left[\frac{1}{\dot{m}_{tD}}\right]_{MP};\left[\frac{1}{\dot{m}_{t}}\right]_{MP};[\varphi PI(t)]_{g,MP}$$

The RTA methods in Chapter 3.4 can also be applied here.

5.3.4.3 Derivatives

The derivatives of the type curves will show the following characteristics for the infinite acting reservoir:

Early Time Region

No skin response

IARF (negligible crossflow)

$$\frac{d\left[\frac{1}{\dot{m}_{tD}}\right]}{d\left[\ln\left(\frac{t_{DwD}}{\omega f_{D,2}}\right)\right]} = \frac{d\left[\frac{1}{\dot{m}_{tD}}\right]}{d\left[\ln\left(\frac{t_{DwD}}{\omega g_{D,2}}\right)\right]} = 0.5 \quad 5.110$$

IARF and high crossflow

$$\frac{d\left[\frac{1}{\dot{m}_{tD}}\right]}{d\left[\ln\left(\frac{t_{DwD}}{\omega f_{D,2}}\right)\right]} = \frac{d\left[\frac{1}{\dot{m}_{tD}}\right]}{d\left[\ln\left(\frac{t_{DwD}}{\omega g_{D,2}}\right)\right]} = 0 \quad 5.111$$

6 Summary and Outlook

6.1 Summary

Conceptual models have been developed for Class 1, 2 and 3 gas hydrate reservoir and the reservoir responses under different flowing conditions illustrated. It has been clearly shown that crossflow and heat conduction effects in the hydrates can be taking into account in conceptual models as long as the MBM pseudo-pressure is used and the temperature dependence on pressure can be characterized using the Clausius-Clapeyron-Type hydrate equilibrium models. As depicted earlier, the characterization of the gas hydrate reservoir is very complex due to the numerous parameters required to be identified. However, the use of dimensionless parameters reduces the number of unknowns required for the reservoir characterization.

6.1.1 Class 3-Normally Pressured Gas Hydrates

The main advantage of producing from normally pressured gas hydrate reservoirs would be the reservoir pressure being considered to be approximately equal to the equilibrium pressure. In this case, every pressure depression below the reservoir pressure dissociates the hydrates; hence, a much higher recovery would be expected compared to the over-pressured gas hydrates. The absence of a pervious free fluid layer beneath the hydrates excludes mass crossflow from the bottom layer but however favors heat crossflow from both the top and bottom layers as a result of the endothermic hydrate dissociation. The influence of heat influx, though a slow process, could be very significant for long-term production scenarios as the negative rate declines could be noticed as the hydrate dissociation rate increases. The following important aspects can further summarize the Normally Pressured Class 3 gas hydrate reservoirs as addressed in this work:

- The energy components responsible for hydrate dissociation in this reservoir are the heat stored in the hydrate layer and the heat influx through conduction from the confining layers.
- Conceptual reservoir testing models have been developed for normally pressured Class 3 gas hydrate reservoirs by rigorously combining mass and energy balance techniques.
- The dimensionless temperature conductivity introduced in this work gives the relationship between the temperature and pressure conductivity in the confining and producing layers respectively. With this approach, the rate of heat influx with respect to producing layer is quantified. For reservoirs with high permeabilities, the pressure conductivity is much higher than the heat influx rate; hence hydrate dissociation is slower in this case.
- Due to decreasing temperature with decreasing depth, as given by the geothermal profile, pseudo-no-flow temperature boundaries would better describe the heat influx rate from the cap rock whereas constant temperature outer boundary conditions would be more suitable for the underlain layer due to increasing temperatures with increasing depths as also given by the geothermal profile. The solutions presented in Laplace domain coupled with the Laplace

domain well test model identification methods address the effects of the different boundary conditions. However, the solutions in real time domain adopted the constant temperature outer boundary as an optimistic approach similar to the kinetic model, which depicts continuous hydrate dissociation.

- Constant terminal rate and constant terminal pressure solutions and responses for the normally pressured Class 3 gas hydrates have been depicted using dimensionless parameters.
- The solutions to the diffusivity problem are represented in terms of dimensionless mass rate and dimensionless multiphase pseudo-pressures, developed using the mass balance model (MBM).
- The use of the dimensionless mass rates and dimensionless multiphase pseudo-pressures provides a huge advantage in the analysis, especially when performing RTA as mass conservation can be verified for type curve matching techniques.
- Semi-log plots of pseudo-pressure normalized rates versus time have been used in the estimation of the reservoir parameters in normally pressured Class 3 gas hydrates for specific reservoir responses. It should however be strongly emphasized that the use of semi-log plots is very limited due to the complex reservoir response, especially when hydrate dissociation is significant.
- Type curve matching techniques for the normally pressured gas hydrates have been developed for the derivation of the dimensionless parameters responsible for the hydrate dissociation in this gas hydrate reservoir type by applying the Hantush et al. [43] well functions.
- The Bourdet [51] diagnostic (derivative) plots have been performed for the reservoir responses to derive the theoretical characteristic behavior of the reservoir.
- The influence of heat conduction from the confining layers could have as significant effect of the rate or pressure transient due to the increase in hydrate dissociation hence supplementary pressure support.
- Boundary effects on the reservoir responses have been identified with semi-log and derivative methods of identifying and estimating the distance to the reservoir boundary for instances with reduced heat influx rates.
- The Bourgeois and Horne [25] Laplace domain well test model recognition method has been applied to the exact solution in Laplace domain, including diagnostic plots in the Appendices, which also gives a more explicit image of the complex reservoir behavior.

6.1.2 Class 3-Overpressured Gas Hydrates

Over-pressured gas hydrate reservoirs with reservoir pressures above the equilibrium pressures are much more complex in behavior, mainly due to the moving boundary problem which results in a skin response as seen on the derivative plots in this work. The reservoir model depicts two distinct zones,

analogous to composite reservoir models seen in conventional reservoir; however, the derivation of the dissociation radius is another hurdle to overcome. The analytical solutions developed here for the model using the similarity variable method neglect the effect of heat influx due to conduction such that the complexity of the problem is reduced. Nonetheless, the solutions to the problem considering the heat conduction have been developed in Laplace domain which still requires the use of numerical inverse transforms to develop the solutions in time domain but have not been further addressed in this work. However, Laplace domain well test model recognition methods have been fully addressed to depict the reservoir response and aid in the characterization of these reservoirs. Most importantly, for the development of the conceptual models for such a reservoir, mass conservation must be defined at the dissociation front. In addition, the pressure propagation model for both the dissociated and undissociated zone must be equal at the dissociation front. With these conditions, the radius of dissociation can be derived for which both conditions hold, as shown in the models developed here. For over-pressured gas hydrate reservoirs with a CPOB, just part of the reservoir can be dissociated as long as pressure propagation has reached the reservoir boundary and boundary dominated flow is felt. At this point, the wellbore, the dissociation front and the exterior boundary of the undissociated zone all experience constant pressure boundary conditions. Pressure propagation stops and so does the radius of dissociation. The total mass rate at both the wellbore and the dissociation front remain constant with time as a result of the replenishment or pressure support at the exterior CPOB. With a NFB at the exterior of the reservoir, quite a different phenomenon is seen. Here, the entire hydrate reservoir could be dissociated as no pressure support at the reservoir exterior boundary is characterized here. However, the undissociated zone first reaches the NFB and a reservoir pressure decline is experienced although the dissociated zone is still in the transient flow regime. Due to this effect the wellbore flow rate depicts a first boundary dominated decline while the dissociation radius further increases. When the dissociation front reaches the NFB, the entire dissociated zone exhibits a second boundary dominated responses as the average pressure drops below the equilibrium pressure. The reservoir then behaves similarly to the normally pressured gas hydrate reservoir. The characteristic behavior of these reservoirs is summarized in the type curve derivative or diagnostic responses in Table 5. The following important aspects can further summarize the Over-Pressured Class 3 gas hydrate reservoirs as depicted in this work:

- Like in normally-pressured Class 3 gas hydrates, the energy components responsible for hydrate dissociation in this reservoir are the heat stored in the hydrate layer and the heat influx through conduction from the confining layers.
- The moving boundary problem depicts a characteristic skin response from diagnostic plots, which is not seen in the normally pressured Class 3 gas hydrate reservoirs, which is due to the difference in the storativity of the dissociated and undissociated zones coupled with the transient radius of dissociation.

- Reservoir boundaries have a significant effect on the moving boundary problem especially with the presence no-flow boundaries.
- Constant pressure outer boundaries limit the extent to which the hydrates will dissociate; i.e. only partial hydrate dissociation is possible.
- In the presence of no-flow boundaries, the reservoir depicts a characteristic double no-flow boundary behavior due to the undissociated region reaching the no-flow boundary before the entire reservoir is dissociated and depict a second no-flow boundary response.
- The application of semilog plots for such a case is very limited; especially if the dissociation rate is high or the pressure depression at the wellbore is very significant.
- Derivative or diagnostic plots on the other hand are very vital in such cases as the skin effect and the double no-flow boundary response can been easily identified.
- Type curve matching methods have been developed to estimate reservoir parameters for the moving boundary problem.
- The Bourgeois and Horne [25] Laplace domain well test model recognition method have also been applied to the exact solution in Laplace domain, including diagnostic plots for a better view of the reservoir responses.

6.1.3 Class 1 and 2 Gas Hydrates

Class 1 and 2 gas hydrates reservoirs have been described as hydrate reservoirs demarcated from a free fluid beneath the hydrate layer owing to the geothermal gradient or hydrate equilibrium conditions. The crossflow problem in such a reservoir is the main issue to address here, coupled with the determining factors for hydrate dissociation. As has been addressed in this work, the heat sources responsible for hydrate dissociation when producing from the hydrate layer are heat stored in the reservoir, heat conduction from the hydrate top layer (cap rock) and heat influx from the warm fluid in the free fluid layer beneath the hydrates. All these factors accelerate the dissociation of the hydrates, provided the reservoir is produced from the hydrate layer and hence the gas recovery factor for such a production scenario could be much faster. The influence of heat conduction can be addressed similar to the Class 3 gas hydrates for this case.

If the hydrate reservoir is produced from the free fluid layer, just heat stored in the hydrate layer and heat influx due to heat conduction from the cap rock are responsible for the dissociation process. When producing from the free fluid layer, heat conduction only starts when pressure depression in the hydrate layer has reached the vertical outer boundary, i.e. the hydrate layer-cap rock interface. This implies this will occur in the late time period of production. When hydrates dissociate at the vertical outer boundary, this will depict a pressure support which if strong enough, will enable zero pressure depressions at the vertical outer boundary. With the identification of these phenomena, a constant pressure outer boundary can be imposed at the boundary and the influence of heat conduction addressed in the crossflow model. This implies if the reservoir is produced from the free fluid layer,

CPOB response will only be seen if hydrate dissociation at the vertical outer boundary becomes significant, provided the free fluid layer is not bounded in the horizontal by another CPOB. The bounded reservoir models for the crossflow behavior have also been developed in Laplace domain which can be transformed in real time domain using a suitable numerical inversion method but have not been addressed further in this work. The characteristic behavior of these reservoirs is summarized in the type curve derivative or diagnostic responses in Table 5.

The following important aspects can further summarize the Class 1 & 2 gas hydrate reservoirs as depicted in this work:

- Since the two layers (free fluid and hydrate layer) are separated at the equilibrium point, they can be considered as normally pressured, i.e. the reservoir pressure is approximately equal to the equilibrium pressure.
- Production from one of the layers can result to crossflow.

Production Scenario 1: Producing from Hydrate Layer

- When producing from the hydrate layer, the heat energy balance for the hydrate dissociation has to account for the heat conduction from the cap rock, the heat stored in the hydrate layer and the heat from the warmer fluids in the free fluid layer moving into the hydrate layer as a result of crossflow.
- The hydrate dissociation would be much faster when producing from the hydrate layer as compared to the normally pressured Class 3 due to the supplementary heat source from the crossflow fluids.
- Constant terminal rate methods can be very tedious for such a production scenario due to the constant increase in pressure from dissociation, which could further result to a zero depression at the sandface. This could make pressure transient analysis very cumbersome, especially with significant changes in fractional flow.
- Constant terminal pressure on the other hand could be more beneficial as the wellbore pressure would be maintained constant and the flow rates would increase significantly.
- Semi-log plots can be made only when the dissociation of crossflow effects are still at minimum.
- Diagnostic plots are still a powerful tool in identifying the flow regimes and reservoir characterization.
- Type curve matching techniques can be used to estimate reservoir parameters.
- The Bourgeois and Horne (1993) Laplace domain well test model recognition method have also been applied to the exact solution in Laplace domain.

Production Scenario 2: Producing from Free Fluid Layer

- When producing from the free fluid layer, the heat energy balance for the hydrate dissociation has to account for the heat conduction from the cap rock and the heat stored in the hydrate layer.
- The heat energy due to conduction from the top layer occurs only during late time production periods when pressure depression has reached the outer boundary of the hydrate layer and a temperature depression exists due to dissociation.
- The complexity of developing the model can be addressed by considering the dissociation of the hydrates at the outer boundary in the late time period as a pressure support , which if strong enough can lead to constant pressure at the outer boundary of the hydrate layer.
- Semi-log plots can also be made here if and only if the crossflow effects are still at minimum.
- Derivative plots can be used to better identify flow regimes and reservoir characterization.
- The Bourgeois and Horne [25] Laplace domain well test model recognition method have also been applied to the exact solution in Laplace domain.

To conclude, the hydrate dissociation is a pressure or mass source and hence tends to replenish pressure or rate declines during production. For this reason, most of the reservoir response models with significant hydrate dissociation depict a similar characteristic behavior. However, the parameters influencing such a behavior are different for each reservoir type as seen in this work using the equilibrium model. Hence, knowledge about the reservoir in question is essential for qualitative analysis of rate / pressure data. The well testing models developed here did not consider wellbore storage or mechanical skin damage effects on the reservoir behavior such that the true reservoir responses can be identified, after which other parameters can be addressed and incorporated in the model.

Table 5: Summary of Characteristic Behavior of Gas Hydrate Reservoirs from Type Curve Derivatives in Real Time Domain (Total System Response)

	Type Curve Derivative and Skin	Type Curve Derivative and IARF	Type Curve Derivative and 1-CPOB	Type Curve Derivative and 1-NFB
Class 3 Normally Pressured Gas Hydrates ($P_i=P_{eq}$) • Heat Stored in Reservoir Considered • Heat Conduction Considered	No Skin	**0.5 ($1xm_{log}$)** with negligible heat flux at middle time region **0** with high heat flux at middle time region	**0** with negligible heat flux at late time region **Not Applicable** with high heat flux, pressure transient does not reach boundary	**1 ($2xm_{log}$)** with negligible heat flux at late time region **Not Applicable** with high heat flux, pressure transient does not reach boundary
Class 3 Over- Pressured Gas Hydrates ($P_i>P_{eq}$) • Heat Stored in Reservoir Considered	Skin Present Skin = $f(S_D/S_{Dk}, P_{eq})$	**0.5 ($1xm_{log}$)** For low dissociation rates or at late times infinite acting systems	**0** Partial Reservoir dissociation due to double CPOB	**$f(S_D/S_{Dk}, \varphi_{sD})$** Double NFB response for extended flow and $P_{avg}<P_{eq}$ Single NFB for extended flow but $P_{avg}>P_{eq}$
Class 1 and 2 Gas Hydrates ($P_i=P_{eq}$) • Heat Stored in Reservoir Considered • Heat Conduction Considered • Mass Crossflow • Convective Heat Crossflow	No Skin	**0.5 ($1xm_{log}$)** For low crossflow rates at middle time region **0-Slope** with high crossflow rates at middle time region	Not Considered	Not Considered

Table 6: Summary of Reservoir Parameters obtained from RTA/PTA in Class 3 Gas Hydrate Reservoirs

	Modified Dimensionless Decomposition Compressibility	**Dimensionless Temperature Conductivity**	**Dimensionless Conductive Heat Flux Coefficient**	**Dimensionless Early Time Interlayer Mass Flux Coefficient**	**Dimensionless Interlayer Compressibility**	**Dimensionless Interlayer Heat Flux Coefficient**
Normally Pressured Class 3 and Over-pressured Class 3	$S_D = \frac{\left[\rho_t k\left(\frac{k_r}{\eta}\right)_t\right]_{id}}{\left[\rho_t k\left(\frac{k_r}{\eta}\right)_t\right]}\left(\frac{(\rho c_T)_{eff}}{(\rho c_T)_{eff,id}} + \frac{c}{h_d(\rho c_T)_{eff,id}}\right)$ When c=0 (no decomposition or undissociated zone) $S_D = \frac{\left[\rho_t k\left(\frac{k_r}{\eta}\right)_t\right]_{id}}{\left[\rho_t k\left(\frac{k_r}{\eta}\right)_t\right]}\left(\frac{(\rho c_T)_{eff}}{(\rho c_T)_{eff,id}}\right) = S_{Dk}$	$F_{CD} = \frac{h^2}{4}\frac{(\rho c_p)_{eff}}{\lambda}\frac{r_w^2(\rho c_T)_{eff,id}}{\left[\rho_t k\left(\frac{k_r}{\eta}\right)_t\right]_{id}}$	$e_D = \left\{\lambda\frac{1}{h_d k\left[\rho_t\left(\frac{k_r}{\eta}\right)_t\right]}\left[\frac{dT_{eq}}{dp}\right]\frac{r_w^2}{\pi h^2}\right\}$	$\varepsilon_D = e_D\sqrt{F_{CD}}$	$\mu_D = \left(1 + \frac{F_{CD}e_D(\Delta z_D - 1)}{3S_D}\right)$	$b_D = \frac{e_D}{(\Delta z_D - 1)}$ $\frac{e_D}{(\Delta z_D - 1)} = \left[\frac{e_D}{(\Delta z_D - 1)}\right]_{TL} + \left[\frac{e_D}{(\Delta z_D - 1)}\right]_{BL}$

Table 6 gives a summary of relevant reservoir parameters obtainable from Class 3 gas hydrate reservoir testing as shown on Chapters 3 and 4. Although the heat conduction parameters where not addressed in Chapter 4 for the over-pressured gas hydrates, they are still valid for the models addressed in Laplace domain given in Appendix 13.

Table 7: Summary of Reservoir Parameters obtained from RTA/PTA in Class 1&2 Gas Hydrate Reservoirs when producing from the Free Fluid Layer

		Storativity Ratio	**Interporosity Flow Coefficient**	**Dimensionless Early Time Interlayer Mass Flux Coefficient**	**Dimensionless Interlayer Crossflow Compressibility**	**Dimensionless Interlayer Crossflow Storativity Compressibility Product**	**Dimensionless Interlayer Mass Flux Coefficient**
Class 1&2 Producing from Free Fluid Layer	NFB in Hydrate Layer	$\omega = \frac{[a_h]_i}{a_h}\left[\left(\frac{a_v}{a_h + a_v}\right)\right]_i$	$\delta_D = \frac{r_w^2}{\Delta z_2 \Delta z_1}\frac{k_{v2}}{k_{h1}}$	$\varepsilon_D = \delta_D\sqrt{[1-\omega]}$	$f_D = \left(1 + \frac{[1-\omega]}{\omega}\delta_D(\Delta z_D - 1)\right)$	$\omega f_D = [\omega + (1-\omega)\delta_D(\Delta z_D - 1)]$	0
	CPOB in Hydrate Layer	$\omega = \frac{[a_h]_i}{a_h}\left[\left(\frac{a_v}{a_h + a_v}\right)\right]_i$	$\delta_D = \frac{r_w^2}{\Delta z_2 \Delta z_1}\frac{k_{v2}}{k_{h1}}$	$\varepsilon_D = \delta_D\sqrt{[1-\omega]}$	$g_D = \left(1 + \frac{[1-\omega]}{3\omega}\delta_D(\Delta z_D - 1)\right)$	$\omega g_D = \left(\omega + \frac{[1-\omega]}{3}\delta_D(\Delta z_D - 1)\right)$	$j_D = \frac{\delta_D}{(\Delta z_D - 1)}$

In addition to the storativity ratio and interporosity flow coefficient given in Table 7, the relevant reservoir parameters for Class 1&2 Hydrates when producing from the hydrate layer are summarized in Table 8.

Table 8: Summary of Reservoir Parameters obtained from RTA/PTA in Class 1&2 Gas Hydrate Reservoirs when producing from the Hydrate Layer

		Dimensionless Convective Heat Flux Dissociation Coefficient	**Dimensionless Early Time Interlayer Mass Flux Coefficient**	**Dimensionless Interlayer Crossflow Compressibility**	**Dimensionless Interlayer Mass Flux Coefficient**
Class 1&2 Producing from Hydrate Layer	NFB in Free Fluid Layer + CTOB in Cap rock	$\theta_D = \frac{[c_p \Delta T]_{avg}}{h_d}$	$\varepsilon_{D,2} = \left[e_D \sqrt{F_{CD}} + \delta_D (1+\theta_D)\sqrt{[1-\omega]}\right]$	$f_{D,2} = \left[1 + \frac{1}{3\omega}\{(e_D F_{CD}(\Delta z_{D,TL} - 1) + 3[\delta_D (1+\theta_D)(1-\omega)(\Delta z_{D,BL} - 1)])\}\right]$	$Y_D = \frac{e_D}{(\Delta z_{D,TL} - 1)}$
	CPOB in Free Fluid Layer + CTOB in Cap rock	$\theta_D = \frac{[c_p \Delta T]_{avg}}{h_d}$	$\varepsilon_{D,2} = \left[e_D \sqrt{F_{CD}} + \delta_D (1+\theta_D)\sqrt{[1-\omega]}\right]$	$g_{D,2} = \left\{1 + \frac{1}{3\omega}[e_D F_{CD}(\Delta z_{D,TL} - 1) + \delta_D (1+\theta_D)[1-\omega](\Delta z_{D,BL} - 1)]\right\}$	$j_{D,2} = \left[\frac{\delta_D (1+\theta_D)}{(\Delta z_{D,BL} - 1)} + \frac{e_D}{(\Delta z_{D,TL} - 1)}\right]$

6.2 Outlook

The constant sandface rate and constant wellbore pressure methods have been addressed in this work although maintaining constant sandface rates for multiphase systems is very difficult; moreover, the use of constant sandface rates has many disadvantages over the constant pressure method with regard to the effective production of gas hydrates and the ease of analyzing the well test data as briefly described in Table 9.

Table 9: Pros and Cons of Applying Different Well Test Techniques in Gas Hydrate Reservoirs

Constant Flowrate (sandface) Test (PTA)	Constant Wellbore Pressure Test (RTA)
Hydrate dissociation is pressure controlled; hence no systematic control of hydrate dissociation since pressure is transient.	Systematic control of hydrate dissociation with defined constant wellbore pressure
Hydrate reservoirs are usually unconsolidated; hence the critical flowing pressure for formation destabilization has to be known for well test design purposes to mitigate sand production. With transient pressure in the wellbore, the formation integrity cannot be guaranteed if this aspect is not thoroughly addressed in the well test design process.	With known critical flowing pressure for formation destabilization, the constant wellbore pressure test can be properly and easily designed, reducing the possibility of sand production, formation destabilization and subsidence of reservoirs.
Even if we assume constant sandface rates, the flow rates of the individual phases are usually not constant for multiphase systems. Hence we are faced with a rate and pressure transient case, for which analysis is cumbersome	As long as the pressure in the wellbore can be maintained constant, rate transient even with fractional flow of the multiphase system can still be performed.
With rate and pressure transient problems for multiphase systems, just convolution/ deconvolution techniques will be appropriate for analysis.	Unless pressure at the wellbore becomes transient, convolution/ deconvolution techniques are not required.

The following are vital aspects which could be considered in future works:

- Wellbore storage and mechanical skin effects were ignored in the conceptual models developed in this work, which could be addressed in future works.
- Just vertical wells were considered in this work; however, with the use of constant wellbore pressure tests, horizontal wells could accelerate the hydrate dissociation rate along the extensive horizontal length.

Due to the lack of field data, the true variation of the derived reservoir parameters in this work with time and pressure is not feasible; hence, the optimization of the proposed models at this level is impossible. The following could help improve on the well test interpretation:

- Validation and optimization of proposed models with available field data.
- Application of more rigorous methods of analysis such as Deconvolution (especially for PTA) or nonlinear parameter estimation.
- Computer assisted well testing techniques in the analysis.

7 References

[1] M. Kome, M. Amro and Y. Cinar, „SPE-165975-MS: Analytical Models for Well Test Analysis in Class 3 Gas Hydrate Reservoirs," Abu Dhabi, UAE, 2013.

[2] E. Pinero, M. Marquardt, C. Hensen, M. Haeckel and K. Wallmann, „Estimation of the global inventory of methane hydrates in marine sediments using transfer functions," *Biogeosciences 10, pg 959-975,* 2013.

[3] K. C. Hester and P. G. Brewer, „Clathrate Hydrates in Nature," *Annual Review of Marine Science, pg 303-307,* 2009.

[4] http://www.futurist.com, „http://www.futurist.com," 17 06 2014. [Online]. Available: http://www.futurist.com/articles-archive/energy-the-future-and-us/. [Accessed on17 06 2014].

[5] J. Carroll, Natural Gas Hydrates: A Guide for Engineers, USA: Elsevier, 2009.

[6] J. E. Dendy Sloan, Clathrate of Hydrates of Natural Gases, USA: Marcel Dekker Inc., 1990.

[7] C. Ruppel, „Methane Hydrates and the Future of Natural Gas," USGS, USA, 2011.

[8] K. A. Kvenvolden, „Gas Hydrates- Geological Perspectives and Global Change," *Reviews of Geophysics 31, pg. 173-187,* 1993.

[9] M. D. Max, Natural Gas Hydrates in Oceanic and Permafrost Environment, Netherlands: Kluwer Academeic Publisher, 2000.

[10] S. Germai and M. Pooladi-Darvish, „An Early Time Model for Drawdown Testing of a Hydrate-Capped Gas Reservoir," *SPE Reservoir Evaluationand Engieering, pg 595-609,* 2009.

[11] T. C. Collett and G. D. Ginsburg, „Gas Hydrates in the Messoyakha Gas Field of the West Siberian Basin: A Re-Examination of the Geologic Evidence," *International Journal of Offshore and Polar Engineering Vol.8, No.1, pg 22-29,* 1998.

[12] R. Birchwood, J. Dai, D. Shelander, R. Boswell, T. Collett, A. Cook, S. Dallimore, K. Fujii, Y. Imasato, M. Fukuhara, K. Kusaka, D. Murray and T. Saeki, „Developments in Gas Hydrates," *Oilfield Review 22, no. 1, pg 18-33,* 2010.

[13] Y. F. Makogon, Hydrates of Hydrocarbons, USA: PennWell Publishing Company, 1997.

[14] Y. Ye and C. Liu, Natural Gas Hydrates:Experimental Techniques and Their Applications, Germany : Springer , 2013.

[15] http://www.giss.nasa.gov, „http://www.giss.nasa.gov/research/features/200409_methane/," NASA, 19 06 2014. [Online]. Available: http://www.giss.nasa.gov/research/features/200409_methane/. [Accessed on19 06 2014].

[16] F. J. Kuckuck, M. Onur and F. Hollaender, Pressure Transient Formation and Well Testing, Great Britain: Elsevier, 2010.

[17] Schlumberger, Fundamentals of Formation Testing, Texas, USA: Schlumberger Marketing Communications, 2006.

[18] S. Cantini, D. Baldini, E. Beretta, D. Loi and S. Mazzoni, „SPE 164924: Reservoir Permeability

from Wireline Formation Testers," SPE, London, UK, 2013.

[19] L. Ostrowski, „SPE 100234: Revival of Openhole DST: Compromising Between Wireline-Formation Testing and Cased-Hole DST," SPE/EAGE, Vienna, Austria, 2006.

[20] S. Ramaswami, M. Hows, D. Frese and H. Elshahawi, „SPE 164733: Pressure Transient Data from Wireline Formation Testers: When and How to use it?," SPE, Cairo, Egypt, 2013.

[21] A. C. Gringarten, „From Straight Lines to Deconvolution: The Evolution of the State of the Art in Well Test Analysis," *SPE Reservoir Evaluation and Engineering, pg. 41-62*, pp. 41-62, February 2008.

[22] J. A. P. D. Bourdet, „Use of Pressure Derivative in Well-Test Interpretation," *SPE Formation Evaluation*, 1989.

[23] T. v. Schroeter, F. Hollaender and A. C. Gringarten, „SPE 71574:Deconvolution of Well Test Data as a Nonlinear Total Least Squares Problem," SPE, New Orleans, Louisiana, USA, 2001.

[24] H. Zhuang, Dynamic Well Testing in Petroleum Exploration and Development, USA: Elsevier, 2013.

[25] M. J. Bourgeois and R. N. Horne, „Well-Test-Model Recognition With Laplace Space," *SPE Formation Evaluation, pg. 17-25*, 1993.

[26] T. v. Schroeter, F. Hollaender and A. C. Gringarten, „SPE 77688: Analysis of Well Test Data From Permanent Downhole Gauges by Deconvolution," SPE, San Antonio, Texas, USA, 2002.

[27] M. M. Levitan, „Practical Application of Pressure-Rate Deconvolution to Analysis of Real Well Tests," *SPE Reservoir Evaluation & Engineering*, Bde. %1 von %2http://dx.doi.org/10.2118/84290-PA, 2005.

[28] A. Dastan, „PhD Thesis:"A New Look At Nonlinear Regression In Well Testing"," USA, 2010.

[29] G. Moridis and M. Kowalsky, „Depressurization-induced gas pdroduction from Class 1 and Class2 hydrate deposits," 2006.

[30] M. Kome and M. AMro, „Welltest-Konzepte für Gashydratlagerstätten (Poster and Manuscript)," DGMK/ÖGEW Frühjahrestagung, Fachbereich Aufsuchung und Gewinnung, Celle, Deutschland, 2014.

[31] H. Kim, P. Bishnoi, R. Heidemann and S. Rizvi, „Kinetics of Methane Hydrate Decomposition," *Chemical Engineering Science 42, pg 1645-1653*, 1987.

[32] R. Al-Hussainy, „Application of Real Gas Flow Theory to Well Testing and Deliverability Forecasting," *JPT, pg 637-642*, 1965.

[33] R. G. Agarwal, „SPE 8279: Real Gas Pseudo-Time," SPE, 1979.

[34] H. Fujita, „The Exact Pattern of a Concentration-Dependent Diffusion in a smei-infinite Mdeium, Part 2," *Textile Research Journal, pg 823-827*, 1952.

[35] H. Fujita, „The Exact Pattern of a Concentration-Dependent Diffusion in a smei-infinite Mdeium, Part 3," *Textile Research Journal, pg 234-240*, 1954.

[36] J. Philip, „General Method of Exact Solution of the Concentration-Dependent Equation," CSIRO,

1959.

[37] J. Knight and J. Philips, „Exact solutions in nonlinear diffusion," *Journal of Engineering Mathematics, pg 219-227,* 1974.

[38] J. Crank, The Mathematics of Diffusion, Great Britain: Oxford University Press, 1975.

[39] K. Singh and C. Whitson, „Gas-Condensate Pseudo-pressure in Layered Reservoirs," *SPE Reservoir Evaluation and Engineering, pg 203-213,* 2010.

[40] C. W. Ø. Fevang, „Modeling Gas-Condensate Well Deliverability," *SPE Reservoir Engineering, pg 221-230,* 1996.

[41] J. Ferris, D. Knowles, R.H.Brwon and R.W.Stallman, Theory of Aquifer Tests, USA: UNITED STATES GOVERNMENT PRINTING OFFICE, 1962.

[42] H. J. R. J. P. B. C. R. Al-Hussainy, „The Flow of Real Gases Through Porous Media," *JPT, pg 624-636,* 1966.

[43] H. Fujita, „The Exact Pattern of a Concentration-Dependent Diffusion in a smei-infinite Mdeium, Part 1," *Textile Research Journal, pg 757-760,* 1952.

[44] L.Matter and D. Anderson., „An improved Pseudo-Time for Gas Reservoirs with Significant Transient Flow," *JCPT, pg 49-54,* 2007.

[45] M. Kome and M. Amro, „SPE 167682-MS: The Impact of Multiphase Flow on Well Testing Models in Gas Hydrate Reservoirs without Crossflow," Vienna, Austria, 2014.

[46] O. Fevang and C. H. Whitson, „Modeling Gas-Condensate Well Deliverability," *SPE Reservoir Engineering 1996, pg 221-230,* 1996.

[47] J. Jones, D. Vo and R. Raghavan, „Interpretation of Pressure-Buiildup Responses in Gas-Condensate Wells," *SPE Formation Evaluation, pg 93-104,* 1989.

[48] D. Bourdet, Well Test Analysis: The Use of Advanced Interpretation Models, Elsevier, 2002.

[49] G. Stewart, Well Test Design and Analysis, USA: PennWell Corporation , 2011.

[50] A. Boe, S. M. Skjaeveland and C. Whitson, „Two-Phase Pressure Tests Analysis," *SPE Formation Evaluation, Vol. 4, pg. 604-610,* 1989.

[51] R. L. Perrine, „Analysis of Pressure-buildup Curves," *Drilling and Production Practice, API, pg. 482-509,* 1956.

[52] K. Aziz and A. Settari, „Petroleum Reservoir Simulation," Applied Science Publishers Ltd, England, 1979.

[53] M. Uddin, J. W. S. Dallimore and D. Coombe, „Gas hydrate production from the Mallik reservoir: numerical history matching and long-term production forecasting," Geological Survey of Canada, Bulletin 601, Canada, 2012.

[54] D. Tiab and E. C. Donaldson, Petrophysics: Theory and Practice of Measuring Reservoir Rock and Fluid Transport Properties, USA: Elsevier, 2004.

[55] Y. Masuda, Y. Konno, C. L. Sheu, H. Oyama, H. Ouchi and M. Kurihara, „Relative Permeability

Curves during Hydrate Dissociation in Depressurization," Proceedings of the 6th International Conference on Gas Hydrates (ICGH 2008),, Canada, 2008.

[56] H. L. Stone, „Probability Model for Estimating Three-Phase Relative Permeability," *JPT , pg 214-218,* 1970.

[57] G. Moridis and M. Kowalsky, „Comparison of kinetic and equilibrium reaction models in simulating gas hydrate behaivior in porous media," *Energy Conversion and Management 48, pg 1850-1863,* 2007.

[58] A. F. V. Everdingen and W. Hurst, „The Application of the Laplace Transformation to Flow Problems in Reservoirs," *Petroleum Transactions, AIME, pg 305-324,* 1949.

[59] A. Vandenberg, „Type Curves for Analysis of Pump Tests in Leaky Strip," *Journal of Hydrology 33, pg 15-26,* 1977.

[60] M. Kamal and Y. Pan, „SPE 141572: Pressure Transient Testing Under Multiphase Flow Conditions," SPE, 2011.

[61] M. J. Edwardson, H. M. Girner, H. R. Parkinson, C. D. Williams and C. S. Matthews, „Calculation of Formation Temperature Disturbances Caused by Mud Circulation," *SPE Journal of Petroleum Technology* , pp. 416-426, April 1962.

[62] B. F. Towler, Fundamental Principles of Reservoir Engineering, USA: SPE Inc., 2002.

[63] F. Haefner, H. Voigt, H. Bamberg and M. Lauterbach, Geohydrodynamische Erkundgung von Erdöl-, Erdgas- und Grundwasserlagerstätten, Berlin: Zentrales Geologisches Institut, 1985.

[64] R. P. Chapius, „Assessment of Methods and Conditions to Locate Boundaries:One or Two Straight Impervious Boundaries," *Groundwater, Volume 32, Issue 4, pg 576–582,* 1994.

[65] V. Batu, Aquifer Hydraulics : A comrehensive guide to hydrogeologic data analysis, Canada: John WIley and Sons Inc., 1998.

[66] G. Ahmadi, C. Ji and D. H. SMith, „Natural gas production from gas hydrate decomposition by depressurization," *Chemical Engineering Science 56, pg 5801-5814,* 2001.

[67] G. Ahmadi, C. Ji and D. H. Smith, „Natural gas production from hydrate dissociation: An axisymmetric model," *Journal of Petroleum Science Engineering, pg. 245-258,* 2007.

[68] N. N. Verigin, I. L. Khabibullin and G. A. Khalikov, „Linear Problem of the Dissociation of the Hydrates of Gas in a Porous Medium," Plenum Publishing Corporation, 1980.

[69] G. Ahmadi, C. Ji and D. H. Smith, „Production of Natural Gas from Methane Hydrate by Constant Downhole Pressure Well," *Elsevier: Energy Conversion and Mangement 48,* pp. 2053-2068, 2007.

[70] M. Hantush, B. Becken, F. Burt, S. H. Jr. and A. E. Scheidegger, Advances in Hydrosciences: Hydraulics of Wells, USA: Academic Press Inc, 1964.

[71] F. Haefner, D. Sames and H. Voigt, Wärme und Stofftransport, Springer, 1992.

[72] G. Moridis, M. B. Kowalsky and K. Pruess, TOUGH+HYDRATE v1.0 Manual, 2008.

[73] M. N. Özisik, Heat Conduction, USA: John wiley and Sons Inc, 1993.

[74] H. S. Carslaw and J. C. Jaeger, Conduction of Heat in Solids, UK: Oxford University Press, 1959.

[75] A. Tarek, Reservoir Engineering Handbook, USA: Gulf Professional Publishing, 2006.

[76] B. P. Ramagost and F. F. Farshad, „SPE-10125-MS: P/Z Abnormally Pressured Gas Reservoirs," SPE, Texas, USA, 1981.

[77] A. C. Gringarten and H. J. R. Jr., „The Use of Source and Green´s Functions in Solving Unsteady-Flow Problems in Reservoirs," *SPEJ Vol. 13 , pg 285 - 296,* 1973.

[78] M. Abramowitz and I. Stegun, Handbook of Mathematical Functions with Formulas, Graphs, and Mathematical Tables, USA: Dover Publications, 1964.

[79] M. Kuo, W. Wang, D. Lin and C. Chiang, „An Image-Well Method for Predicting Drawdown Distribution in Aquifers with Irregularly Shaped Boundaries," *Ground Water, Vol 32, No.5,* pp. pg 794-804, September 1994.

[80] P. Renard, „Approximate Discharge for Constant Head Test with Recharging Boundary," *Ground Water Vol 43,* pp. 439-442, June 2005.

[81] A. U. Chaudhry, Gas Well Testing Handbook, USA: Elsevier, 2003.

[82] T. Engler and D. Tiab, „Analysis of pressure and pressure derivative without type curve matching, 4 Naturally fractured reservoirs," *Elsevier:Journal of Petroleum Science and Engineering,* Nr. 15, pg 127-138, 1996.

[83] F.-. H. Escobar, J. A. Sánchez and J. H. Cantillo, „Rate Transient Analysis for Homogeneous and Hetergeneous Gas Reservoirs Using the TDS Technique," *CT&F - Ciencia, Tecnología y Futuro,* Bd. Vol 3, Nr. 4, pg 45-59, 2008.

[84] F.-H. Escobar and M. Montealegre-M., „Application of TDS Technique to Multiphase Flow," *CT&F - Ciencia, Tecnología y Futuro,* Bd. Vol 3, Nr. 4, pg 94-105, 2008.

[85] D. Tiab, „Analysis of pressure and pressure derivative without type-curve matching - Skin and Wellbore Storage," *Elsevier: Journal of Petroleum Science and Engineering,* Nr. 12, pg 171-181, 1995.

[86] D. Tiab, „Analysis of pressure and pressure derivative without type-curve matching : Vertically fractured wells in closed systems," *Elsevier: Journal of Petroleum Science and Engineering,* Nr. 11, pg 323-333, 1994.

[87] J. Warren and P. Root, „The Behavior of Naturally Fractured Reservoirs," *SPEJ, pg 245-255,* 1963.

[88] M. A. Chaudhry and S. Zubair, „Generalized Incomplete Gamma Function with Applications," *Journal of Computational and Applied Mathematics 55, pg 99-124,* 1994.

[89] J. B. R. Lee John, Pressure Transient Testing, USA: SPE Inc., 2003.

[90] J. Lee and R. A. Wattenberg, Gas Reservoir Engineering, USA: SPE Inc., 1996.

[91] C. A. Ehlig-Economides, „Dissertation: Well Test Analysis for Wells Produced at a Constant Pressure," California, USA, 1979.

[92] B. Buffet and D. Acher, „Global inventory of methane clathrate: sensitivity to changes in the deep ocean,“ *Elsevier: Earth and Planetary Science Letters 227, pg 185-199,* 2004.

8 Publications

1. Kome, M.; Amro, M,: “ Challenges in Gas Hydrate Reservoir Testing and Analysis“, SPE Reservoir Testing: Key Enabler for Accurate Reservoir Characterisation (Poster) Dubai, United Arab Emirates, 26–27 May 2014
2. Kome, M.; Amro, M,: “ Welltest-Konzepte für Gashydratlagerstätten“, DGMK/ÖGEW-Frühjahrestagung 2014 (Poster Präsentation and Manuscript), Fachbereich Aufsuchung und Gewinnung, Celle, 24./25.April 2014
3. Kome, M.; Amro, M: SPE 167682-MS “The Impact of Multiphase Flow on Well Testing Models in Gas Hydrate Reservoirs without Crossflow” , SPE, Wien, 2014
4. Kome, M.; Amro, M.; Cinar, Y.: SPE-165975-MS “Analytical Models for Well Test Analysis in Class 3 Gas Hydrate Reservoirs” , SPE ,Abu Dhabi, 2013
5. Kome, M.; Amro, M.; Rehmer, K.-P.: “Untersuchung und Berechnung zur Berücksichtigung von Buckling in Tubing und Komplettierung“, DGMK/ÖGEW-Frühjahrestagung 2013, Fachbereich Aufsuchung und Gewinnung, Celle, 18./19.April 2013.
6. Kome, M.; Amro,M.; Hossain, M. M.: A new practical approach to evaluate near wellbore formation damage parameters based on well test analysis for gas reservoir, SPE Paper 160867, presented at the 2012 SPE Saudi Arabia Section Technical Symposium and Exhibition held in AlKhobar, Saudi Arabia, 8–11 April 2012,
7. Kome, M.; Fang, Ch.; Amro; M.: Well testing in unconventional gas reservoirs, Presented in the Annual German Society for Petroleum Sciences and Coal Chemistry (DGMK), 19-20 April 2012, Celle (Germany).

Appendix 1: Introduction to the Thermodynamics of Hydrate Dissociation

As of now, the kinetic model and the equilibrium model are the most widely used models in quantifying the hydrate dissociation rate as a result of pressure depressurization. The kinetic model is based on experimental work carried out by Kim et al. [31] to determine the hydrate dissociation rate, as also given below. The model was developed based on laboratory experiments and limits a better quantification of the heat energy available for hydrate dissociation in the reservoir. The equilibrium model is based on the heat energy balance principle. It quantifies the rate of hydrate dissociation by addressing the heat used up in the reservoir and heat supplied from the confining layers. These heat source terms are related to the heat of hydrate dissociation as given by the Clausius Clapeyron-Type Equilibrium model, such that the mass of hydrate dissociated can be quantified. The two models are described below:

Kinetic Dissociation Model [31]

$$\frac{dn_h}{dt} = K_d A_H (p_{eq} - p_g) \quad \text{A1: 1}$$

with K_d [kmol/m²Pas], A_H [m²], p [Pa], n [kmol]

$$\frac{d}{dt}\left(\frac{m_H}{M_H}\right) = \left(\frac{1}{M_H}\right)\frac{dm_H}{dt} = K_d A_H (p_{eq} - p) \quad \text{A1: 2}$$

$$\frac{dm_H}{dt} = K_d M_H A_H (p_{eq} - p) \quad \text{A1: 3}$$

The quantification of the reaction area has been an issue of discussion for many years since the kinetic model was developed on laboratory scale and difficulties were being faced in describing this area at reservoir scale. Different definitions of the reaction area have been proposed by several authors, as also seen in [74]; however it should be noted that for a producing reservoir and for the purpose of developing well test models, the reaction area would be the depleted zone on a macroscopic scale and hence needs to be accounted for when developing a well test model. This is shown in Appendix 5. A comparison of the numerical results of the reservoir response by using either the kinetic or equilibrium model is given in [60].

CASE 1: Class 3 Hydrates and Energy Balance /Equilibrium Dissociation Model

As mentioned above, the equilibrium model is a heat energy balance model which addresses the different heat sources in the hydrate layer. Due to the absence on free fluid beneath the hydrate layer in Class 3 hydrate reservoirs, convective heat transfer from the underlain layer can be neglected. Hence the energy balance model here will consider just heat conduction form confining layers and the heat stored in the hydrate layer as the energy sources for hydrate dissociation.

Energy Balance Model

$$\left[\frac{dE}{dt}\right]_{total} = \left[\frac{dE}{dt}\right]_{Hydrate\ Layer} + \left[\frac{dE}{dt}\right]_{Heat\ Conduction\ (CL)} \quad \text{A1: 4}$$

Part 1: Stored Energy in the Hydrate Layer consumed during Dissociation

In addressing the rate of heat change stored in the reservoir, the total heat energy available in the hydrate reservoir needs to be quantified and is given by [73], [75] and [76]:

$$E_{\text{Hydrate Layer}} = mc_pT \qquad \text{A1: 5}$$

The rate of change of the energy with time can hence be quantified and related to the rate of consumed energy due to hydrate dissociation.

$$\left[\frac{dE}{dt}\right]_{\text{Hydrate Layer}} = \frac{d(m_H h_d)}{dt} = -\frac{d(mc_pT)}{dt} \qquad \text{A1: 6}$$

Differentiating the first term on the RHS of the above equation leads to:

$$\frac{d(mc_pT)}{dt} = \frac{d(mc_pT)}{dp}\frac{dp}{dt} = \left[c_pT\frac{d(m)}{dp} + m\frac{d(c_pT)}{dp}\right]\frac{dp}{dt} \qquad \text{A1: 7}$$

Note that for pure heat conduction problems in reservoirs, the warm fluid flux is zero as there is no mass change with pressure or time. As seen with diffusivity equations for well testing, the mass change with pressure basically reflects the storativity of the formation which can also be related to the pressure conductivity of the reservoir. With this said, we can conclude that the warm fluid flux and hydrate dissociation can be well represented in the diffusivity equation.

The next step involves handling the phases separately and combining since it involves an energy balanced system.

Gas Phase

$$\frac{d(m_g c_{p,g}T)}{dt} = \left[c_{p,g}T\frac{d(V\emptyset S_g\rho_g)}{dp} + (V\emptyset S_g\rho_g)\frac{d(c_{p,g}T)}{dp}\right]\frac{dp}{dt} \qquad \text{A1: 8}$$

By assuming negligible changes in the heat capacity with pressure, the differential of the above equation takes the form:

$$\frac{d(m_g c_{p,g}T)}{dt} = c_{p,g}V\emptyset S_g\rho_g\left[T(c_g + c_F) + \left[\frac{dT_{eq}}{dp}\right]\right]\frac{dp}{dt} \qquad \text{A1: 9}$$

Water Phase

$$\frac{d(m_w c_{p,w}T)}{dt} = c_{p,w}V\emptyset S_w\rho_w\left[T(c_w + c_F) + \left[\frac{dT_{eq}}{dp}\right]\right]\frac{dp}{dt} \qquad \text{A1: 10}$$

Hydrate Phase

$$\frac{d(m_H c_{p,H}T)}{dt} = c_{p,H}V\emptyset S_H\rho_H\left[T(c_F) + \left[\frac{dT_{eq}}{dp}\right]\right]\frac{dp}{dt} \qquad \text{A1: 11}$$

Formation (Matrix)

$$\frac{d(m_m c_{p,m}T)}{dt} = \left[c_{p,F}T\frac{d(V_m)}{dp} + (V_m)\frac{d(c_{p,m}T)}{dp}\right]\frac{dp}{dt} \qquad \text{A1: 12}$$

$$\frac{d(m_m c_{p,m} T)}{dt} = \rho_m V_m c_{p,F} \left[T c_m + \frac{dT_{eq}}{dp} \right] \frac{dp}{dt} \quad \text{A1: 13}$$

Part 2: Energy Supplied through Heat Conduction from Confining Layers

$$\left[\frac{dE}{dt}\right]_{\text{Heat Conduction}} = \text{Rate of Heat Influx from Confining Layers} \quad \text{A1: 14}$$

Incorporating the heat conduction term could be very cumbersome for the analytical well testing model due to its time dependence. As a result, Laplace transforms will be used to address this problem such that the effects of heat influx are also quantified.

From the definition of heat flux through conduction we get [76], [75]:

$$\left[\frac{dE}{dt}\right]_{\text{Heat Conduction}} = \dot{Q} = -\lambda A \frac{dT}{dz} \quad \text{A1: 15}$$

From the above equation, it is imperative to develop the heat conduction model such that the heat energy supplied can be quantified and hence the mass of hydrate dissociated with this energy.

Note that according to the geothermal gradient and depending on the degree of temperature depression in the hydrate layer, heat coming from both layers would be heat source terms as the system was initially in temperature equilibrium. Hence temperature depression would result to heat influx. The transient heat conduction model in the confining layer is given by:

$$\frac{\partial^2 T}{\partial z^2} = \frac{(\rho c_p)_{eff}}{\lambda} \frac{\partial T}{\partial t} \quad \text{A1: 16}$$

The following dimensionless terms are introduced:

$$z_D = \frac{z}{\left(\frac{h}{2}\right)} \quad \text{A1: 17}$$

$$t_{Dh} = \left(\frac{\lambda}{\rho c_p}\right)_{eff} \frac{t}{\left(\frac{h}{2}\right)^2} = \frac{4t}{h^2} \left(\frac{\lambda}{\rho c_p}\right)_{eff} \quad \text{A1: 18}$$

$$\frac{\partial^2 T}{\partial {z_D}^2} = \frac{\partial T}{\partial t_{Dh}} \quad \text{A1: 19}$$

The hydrate dissociation process is endothermic, which is triggered by pressure depressions during production; hence, the inner boundary condition for conduction or heat flux through conduction from the confining layers has to be related to the pressure depression in the producing layer.

The model assumes that, in the presence of hydrates in the formation and provided the reservoir is depressurized below the equilibrium pressure, a temperature depression can always be defined using the Clausius-Clapeyron-Type equilibrium model as the process is endothermic. This further implies, regardless of energy influx in the depressurized hydrate layer or dissociating region, the energy is all used up for hydrate dissociation and the temperature depression is pressure determined. This is also verifiable with the comparison made in Chapter 2.3.

Similarly, the dimensionless heat energy supplied through conduction can be defined thus:

$$\dot{Q}_D = \frac{h\dot{Q}}{2\lambda A(T_i - T_{wf})} = -\frac{dT_D}{dz_D} \quad \text{A1: 20}$$

Such that the same dimensionless time is used for both the hydrate layer and the confining layers and a more homogenous solution is derived, the above equation is modified using the dimensionless time for the hydrate layer as will be seen later. This is done thus:

$$dt_{Dw} = \left[\frac{k\left[\rho_t\left(\frac{k_r}{\eta}\right)_t\right]}{r_w^2[(\rho_w \emptyset c_{T,w}) + (\rho_g \emptyset c_{T,g})]}\right]_i dt \quad \text{A1: 21}$$

$$\frac{\partial^2 T_D}{\partial {z_D}^2} = \frac{h^2}{4}\frac{(\rho c_p)_{eff}}{\lambda}\left[\frac{r_w^2[(\rho_w \emptyset c_{T,w}) + (\rho_g \emptyset c_{T,g})]}{k\left[\rho_t\left(\frac{k_r}{\eta}\right)_t\right]}\right]_i \frac{\partial T_D}{\partial t_{Dw}} \quad \text{A1: 22}$$

$$\frac{\partial^2 T_D}{\partial {z_D}^2} = F_{CD}\frac{\partial T_D}{\partial t_{Dw}} \quad \text{A1: 23}$$

Where,

$$F_{CD} = \frac{h^2}{4}\frac{(\rho c_p)_{eff}}{\lambda}\left[\frac{r_w^2[(\rho_w \emptyset c_{T,w}) + (\rho_g \emptyset c_{T,g})]}{k\left[\rho_t\left(\frac{k_r}{\eta}\right)_t\right]}\right]_i \quad \text{A1: 24}$$

To solve the dimensionless heat conduction equation, the following similarity variable can be used:

$$u_D^2 = \frac{F_{CD}}{4t_{Dw}} {z_D}^2 \quad \text{A1: 25}$$

With the similarity variable above, the solutions to the above problem with different boundary conditions can be readily gotten, as seen in various literature including [38], [73], [75], [76]. The derivative of the solutions to the models gives the rate of heat flux in the hydrate layer.

The heat lost from the confining layer to the hydrate layer can be written thus:

$$\dot{Q} = -\frac{2\lambda}{h}\left[\frac{dT_{eq}}{dp}\right] A\dot{Q}_D dp = -\frac{2\lambda}{h}\left[\frac{dT_{eq}}{dp}\right] A\frac{dT_D}{dz_D} dp \quad \text{A1: 26}$$

We can now relate the heat supplied through conduction to the hydrate dissociation rate, but first, we differentiate the LHS of the energy balance equation also given below:

$$\frac{d(m_H h_d)}{dt} = m_H\frac{d(h_d)}{dt} + h_d\frac{d(m_H)}{dt} = m_H\frac{d(h_d)}{dp}\frac{dp}{dt} + h_d\frac{d(m_H)}{dt} \quad \text{A1: 27}$$

It should be noted that the hydrate heat of dissociation energy is pressure dependent, hence; the changes with pressure depression should be accounted for as this will also determine the amount of hydrates dissociated.

From the derived energy balance components, the energy balance model could hence be written thus:

$$\frac{dE}{dt} = m_H\frac{d(h_d)}{dp}\frac{dp}{dt} + h_d\frac{d(m_H)}{dt} = -\left[\frac{d(m_g c_{p,g} T)}{dt} + \frac{d(m_w c_{p,w} T)}{dt} + \frac{d(m_H c_{p,H} T)}{dt} + \frac{d(m_m c_{p,m} T)}{dt}\right] - \frac{2\lambda}{h}\dot{Q}_D\left[\frac{dT_{eq}}{dp}\right] Adp \quad \text{A1: 28}$$

$$h_d\frac{d(m_H)}{dt} = -\left[\frac{d(m_g c_{p,g} T)}{dt} + \frac{d(m_w c_{p,w} T)}{dt} + \frac{d(m_H c_{p,H} T)}{dt} + \frac{d(m_m c_{p,m} T)}{dt} + m_H\frac{d(h_d)}{dp}\frac{dp}{dt}\right] - \frac{2\lambda}{h}\dot{Q}_D\left[\frac{dT_{eq}}{dp}\right] Adp \quad \text{A1: 29}$$

$$h_d \frac{dm_H}{dt} = -\Delta V \emptyset \left\{ \left[c_{p,g} S_g \rho_g \left(\frac{T(c_g + c_F)}{\left[\frac{dT_{eq}}{dp}\right]} + 1 \right) + c_{p,w} S_w \rho_w \left(\frac{T(c_w + c_F)}{\left[\frac{dT_{eq}}{dp}\right]} + 1 \right) + c_{p,H} S_H \rho_H \left(\frac{T(c_F)}{\left[\frac{dT_{eq}}{dp}\right]} + 1 \right) + c_{p,m} \frac{(1-\emptyset)}{\emptyset} \rho_m \left(\frac{T(c_m)}{\left[\frac{dT_{eq}}{dp}\right]} + 1 \right) \right] \left[\frac{dT_{eq}}{dp}\right] \right\} \frac{dp}{dt} - m_H \frac{d(h_d)}{dp} \frac{dp}{dt} - \frac{2\lambda}{h} \dot{Q}_D \left[\frac{dT_{eq}}{dp}\right] Adp \quad \text{A1: 30}$$

Considering positive mass loss (mass injection rate to the system):

$$h_d \frac{dm_H}{dt} = \Delta V \emptyset \left\{ \left[c_{p,g} S_g \rho_g \left(\frac{T(c_g + c_F)}{\left[\frac{dT_{eq}}{dp}\right]} + 1 \right) + c_{p,w} S_w \rho_w \left(\frac{T(c_w + c_F)}{\left[\frac{dT_{eq}}{dp}\right]} + 1 \right) + c_{p,H} S_H \rho_H \left(\frac{T(c_F)}{\left[\frac{dT_{eq}}{dp}\right]} + 1 \right) + c_{p,m} \frac{(1-\emptyset)}{\emptyset} \rho_m \left(\frac{T(c_m)}{\left[\frac{dT_{eq}}{dp}\right]} + 1 \right) \right] \left[\frac{dT_{eq}}{dp}\right] \right\} \frac{dp}{dt} + m_H \frac{d(h_d)}{dp} \frac{dp}{dt} + \frac{2\lambda}{h} \dot{Q}_D \left[\frac{dT_{eq}}{dp}\right] Adp \quad \text{A1: 31}$$

$$h_d \frac{dm_H}{dt} = \Delta V \emptyset \left\{ \left[c_{p,g} S_g \rho_g \left(\frac{T(c_g + c_F)}{\left[\frac{dT_{eq}}{dp}\right]} + 1 \right) + c_{p,w} S_w \rho_w \left(\frac{T(c_w + c_F)}{\left[\frac{dT_{eq}}{dp}\right]} + 1 \right) + c_{p,H} S_H \rho_H \left(\frac{T(c_F)}{\left[\frac{dT_{eq}}{dp}\right]} + 1 \right) + c_{p,m} \frac{(1-\emptyset)}{\emptyset} \rho_m \left(\frac{T(c_m)}{\left[\frac{dT_{eq}}{dp}\right]} + 1 \right) \right] \left[\frac{dT_{eq}}{dp}\right] + S_H \rho_H \frac{dh_d}{dT_{eq}} \frac{dT_{eq}}{dp} \right\} \frac{dp}{dt} + \frac{2\lambda}{h} \dot{Q}_D \left[\frac{dT_{eq}}{dp}\right] Adp \quad \text{A1: 32}$$

$$h_d \frac{dm_H}{dt} = \Delta V \emptyset \left\{ \left[c_{p,g} S_g \rho_g \left(\frac{T(c_g + c_F)}{\left[\frac{dT_{eq}}{dp}\right]} + 1 \right) + c_{p,w} S_w \rho_w \left(\frac{T(c_w + c_F)}{\left[\frac{dT_{eq}}{dp}\right]} + 1 \right) + c_{p,H} S_H \rho_H \left(\frac{T(c_F)}{\left[\frac{dT_{eq}}{dp}\right]} + 1 \right) + c_{p,m} \frac{(1-\emptyset)}{\emptyset} \rho_m \left(\frac{T(c_m)}{\left[\frac{dT_{eq}}{dp}\right]} + 1 \right) + S_H \rho_H \frac{dh_d}{dT_{eq}} \right] \left[\frac{dT_{eq}}{dp}\right] \right\} \frac{dp}{dt} + \frac{2\lambda}{h} \dot{Q}_D \left[\frac{dT_{eq}}{dp}\right] Adp \quad \text{A1: 33}$$

The final equation for the hydrate dissociation rate is given thus:

$$\frac{dm_H}{dt} = \frac{\Delta V \emptyset}{h_d} \left\{ \left[c_{p,g} S_g \rho_g \left(\frac{T(c_g + c_F)}{\left[\frac{dT_{eq}}{dp}\right]} + 1 \right) + c_{p,w} S_w \rho_w \left(\frac{T(c_w + c_F)}{\left[\frac{dT_{eq}}{dp}\right]} + 1 \right) + c_{p,H} S_H \rho_H \left(\frac{T(c_F)}{\left[\frac{dT_{eq}}{dp}\right]} + 1 \right) + c_{p,m} \frac{(1-\emptyset)}{\emptyset} \rho_m \left(\frac{T(c_m)}{\left[\frac{dT_{eq}}{dp}\right]} + 1 \right) + S_H \rho_H \frac{dh_d}{dT_{eq}} \right] \left[\frac{dT_{eq}}{dp}\right] \right\} \frac{dp}{dt} + \frac{2\lambda}{h} \frac{\dot{Q}_D}{h_d} \left[\frac{dT_{eq}}{dp}\right] Adp \quad \text{A1: 34}$$

$$\frac{dm_H}{dt} = \frac{\Delta V \emptyset}{h_d} \left\{ \left[\left(c_{p,g} S_g \rho_g + c_{p,w} S_w \rho_w + c_{p,H} S_H \rho_H + c_{p,m} \frac{(1-\emptyset)}{\emptyset} \rho_m \right) + \frac{T}{\left[\frac{dT_{eq}}{dp}\right]} \left(c_{p,g} S_g \rho_g (c_g + c_F) + c_{p,H} S_H \rho_H (c_F) + c_{p,w} S_w \rho_w (c_w + c_F) + c_{p,m} \frac{(1-\emptyset)}{\emptyset} \rho_m (c_m) \right) + S_H \rho_H \frac{dh_d}{dT_{eq}} \right] \left[\frac{dT_{eq}}{dp}\right] \right\} \frac{dp}{dt} + \frac{2\lambda}{h} \frac{\dot{Q}_D}{h_d} \left[\frac{dT_{eq}}{dp}\right] Adp \quad \text{A1: 35}$$

$$\frac{dm_H}{dt} = \frac{\Delta V \emptyset}{h_d} c \frac{dp}{dt} + \frac{2\lambda}{h} \frac{\dot{Q}_D}{h_d} \left[\frac{dT_{eq}}{dp}\right] Adp \quad \text{A1: 36}$$

We now relate the kinetic model with the equilibrium model.

$$\frac{dm_H}{dt} = \frac{\Delta V \emptyset}{h_d} c \frac{dp}{dt} + \frac{2\lambda}{h} \frac{\dot{Q}_D}{h_d} \left[\frac{dT_{eq}}{dp}\right] A dp = K_d M_H A_H dp \qquad \text{A1: 37}$$

Knowing that the kinetic model was developed in the laboratory, considering continuous heat supply, the different sources of the heat energy responsible for hydrate dissociation cannot be clearly identified. Moreover, maintaining constant temperature in the laboratory for hydrate dissociation and quantifying the hydrate dissociation rate with this model might not be applicable in all cases in the reservoir. For this reason, the use of the kinetic model does not require incorporating any supplementary heat source terms as this is already reflected in the model.

CASE 2: Class 1&2 Hydrates and Energy Balance /Equilibrium Dissociation Model

Due to possible crossflow behavior in Class 1 and 2 reservoirs, supplementary heat source terms which could influence the hydrate dissociation rate have to be considered. The energy balance model is used analogue the previous case.

Energy Balance Model

$$\text{Total Heat Consumed through Dissociation} =$$
$$[\text{Heat From Hydrate Layer}] + [\text{Heat Influx from Confining Layers}] \qquad \text{A1: 38}$$

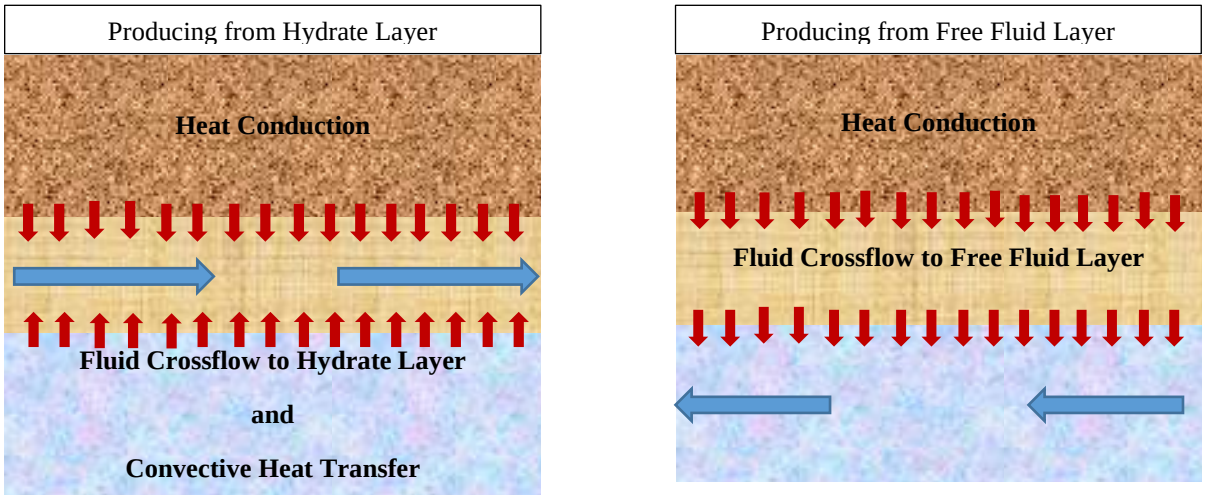

Figure A1- 1: Heat Flux from Confining Layers of Class 1&2 Gas Hydrates

$$[\text{Heat Influx from Confining Layers}] = \left[\frac{dE}{dt}\right]_{\text{Heat Conduction (TL)}} + \left[\frac{dE}{dt}\right]_{\text{Convective Heat Flux}} \qquad \text{A1: 39}$$

The heat components from the hydrate layer and through conduction have been handled in the previous section. Hence the flux through convective heat transfer from the free fluid zone to the hydrate layer is simply given by:

$$[E]_{\text{Warm Fluidflux}} = c_p T \dot{m} \qquad \text{A1: 40}$$

The representation assumes that the temperature in the free fluid zone is approximately constant throughout the depletion period and the rate of hydrate dissociation would be a function of the temperature difference between the hydrate layer after endothermic dissociation and the incoming fluid. Hence the hydrate dissociation rate from the energy supplied is given by:

$$\frac{dm_H}{dt} = \frac{c_p}{h_d}\dot{m}_z\Delta T = \frac{[c_p\Delta T]_{avg}}{h_d}\left[\Delta x * \Delta y * \Delta(\rho_g * w_g) + \Delta x * \Delta y * \Delta(\rho_w * w_w)\right] \quad \text{A1: 41}$$

Incorporating the above model in the diffusivity equation is addressed comprehensively in Appendix 14.

Conventionally, the mass rate of each phase would have to be addressed separately and the specific heat capacities as well. However, since the diffusivity equation developed here considers the total mass rate, an average specific heat capacity will be assumed and the total mass leakage rate for the crossflow layer derived.

The rate of hydrate dissociation can hence be defined thus:

$$\frac{dm_H}{dt} = \frac{[c_p\Delta T]_{avg}}{h_d}\dot{m}_z + \frac{\Delta V\emptyset}{h_d}c\frac{dp}{dt} + \frac{2\lambda}{h}\frac{\dot{Q}_D}{h_d}\left[\frac{dT_{eq}}{dp}\right]Adp \quad \text{A1: 42}$$

If energy and mass balance hold, the kinetic and equilibrium model should be equal; hence:

$$\frac{dm_H}{dt} = K_d M_H A_H dp = \frac{[c_p\Delta T]_{avg}}{h_d}\dot{m}_z + \frac{\Delta V\emptyset}{h_d}c\frac{dp}{dt} + \frac{2\lambda}{h}\frac{\dot{Q}_D}{h_d}\left[\frac{dT_{eq}}{dp}\right]Adp \quad \text{A1: 43}$$

$$\frac{dm_H}{dt} = K_d M_H A_H dp = \Delta\dot{m}_{H,2}(p,t) + \dot{m}_H(p) + \Delta\dot{m}_{H,1}(p,t) \quad \text{A1: 44}$$

This implies, instead of using the different heat energy sources, the kinetic model could be used to investigate the rate of hydrate dissociation and hence type curves generated. Nonetheless, the effects of the different heat source terms can be comprehensively investigated using the equilibrium model.

Appendix 2: Equation of State (EOS) for Hydrate Dissociation

In Appendix 1, the rate of hydrate dissociation was quantified using the equilibrium model; however, it is still essential in depicting the equivalent masses or volumes of the hydrate components generated from the dissociation process. The amount of gas generated from the gas hydrate at standard conditions could be estimated using the simple EOS as given below:

Methane Hydrate = CH_4*5.75 H_2O A2: 1

Note that water and gas in the hydrate have a non-stoichiometric bond and hence in the Methane Hydrate above, a total of 6.75 Moles is usually assumed, as given in [5]. Though this is the case for the hydrate, it is usually considered to be equal to a mole of hydrate [6] and the dissociation enthalpies are given for this unit mole of Hydrate.

From mass balance principle, the total mass of the hydrate is the sum of the masses in the hydrates:

$$m_{Hydrate} = m_{CH4} + m_{H2O} \quad \text{A2: 2}$$

This could be represented in form of the moles and molar masses thus:

$$M_{Hydrate}(n_{CH4} + n_{H2O}) = n_{CH4}M_{CH4} + n_{H2O}M_{H2O} \quad \text{A2: 3}$$

$$M_{Hydrate} = \frac{n_{CH4}}{(n_{CH4}+n_{H2O})}M_{CH4} + \frac{n_{H2O}}{(n_{CH4}+n_{H2O})}M_{H2O} \quad \text{A2: 4}$$

By assuming the number of moles in the hydrate to be equal 1, which is the case in some literature [6], the molar mass deduced equals:

$$M_{Hydrate} = n_{CH4}M_{CH4} + n_{H2O}M_{H2O} = 119{,}61\text{kg/kmol} \quad \text{A2: 5}$$

By assuming the total number of moles in the non-stoichiometric bond of hydrates to be equal to the sum of the number of moles present, which is also the case in some literature [5] we get the following:

$$M_{\text{Methane Hydrate}} = \frac{n_{CH4}}{(n_{CH4}+n_{H2O})}M_{CH4} + \frac{n_{H2O}}{(n_{CH4}+n_{H2O})}M_{H2O} = 17.72\ \text{kg/kmol} \quad \text{A2: 6}$$

This is very crucial in determining the heat of dissociation per unit mass of the hydrates as the dissociation enthalpies are given in joules per mole hydrate, i.e. $\Delta H = h_F[J/kg] * M_{Hyd}$ [kg/mol].

It should strongly be emphasized that the enthalpy of dissociation is derived for the total number of moles present in the gas hydrate as given by the Clausius Clapeyron models. Hence caution should be taken in deriving the heat of dissociation per unit mass hydrate which is required for the well testing model.

Equivalent Volumes of Byproducts

The aim of these calculations is to derive the equivalent volumes of water and gas producible from the hydrates at standard conditions after depressurization. Mass balance principle is applied for each of the phases as given below:

Gas Phase

From Mass Balance

$$m_{CH4} = \frac{P_{st}V_{CH4,st}}{RT_{st}} M_{CH4} \quad \text{A2: 7}$$

$$m_{CH4} = n_{CH4}M_{CH4} = \frac{n_{CH4}}{(n_{CH4}+n_{H2O})} * \frac{m_{hydrate}}{M_{hydrate}} M_{CH4} = \frac{n_{CH4}}{(n_{CH4}+n_{H2O})} * \frac{V_{hydrate}\rho_{hydrate}}{M_{hydrate}} M_{CH4} \quad \text{A2: 8}$$

Applying mass balance to the two equations above yields:

$$\frac{V_{CH4,st}}{V_{hydrate}} = E_g = \frac{n_{CH4}}{(n_{CH4}+n_{H2O})} * \frac{\rho_{hydrate}}{M_{hydrate}} \frac{RT_{st}}{P_{st}} = 0.14815 \frac{913}{17.72} \frac{8.314*288.15*1000}{101325} = 180.47 \quad \text{A2: 9}$$

From the formation volume factor concept we can get the equivalent volume at reservoir conditions thus:

$$\frac{V_{CH4}}{V_{hydrate}} = E_g B_g \quad \text{A2: 10}$$

Water Phase

As was done with the gas phase, the same mass balance approach is made here:

$$V_{w,st} = \frac{n_w M_w}{\rho_{w,st}} = \frac{n_{H2O}}{(n_{CH4}+n_{H2O})} * n_{hydrate} \frac{M_w}{\rho_{w,st}} = \frac{n_{H2O}}{(n_{CH4}+n_{H2O})} * \frac{\rho_{hydrate}V_{hydrate}}{M_{hydrate}} \frac{M_w}{\rho_{w,st}} \quad \text{A2: 11}$$

$$\frac{V_{w,st}}{V_{hydrate}} = E_w = \frac{n_{H2O}}{(n_{CH4}+n_{H2O})} * \frac{\rho_{hydrate}}{M_{hydrate}} \frac{M_w}{\rho_{w,st}} = 0.85185 \frac{913}{17.72} \frac{18.015}{1000} = 0.79 \quad \text{A2: 12}$$

$$\frac{V_w}{V_{hydrate}} = E_w B_w \quad \text{A2: 13}$$

Equivalent Masses of Byproducts

Total Gas Concentration and Gas Production Rate

$$\frac{m_{g,H}}{m_h} = \frac{\frac{n_g}{(n_g+n_w)} * \frac{V_H\rho_H}{M_H} M_g}{\rho_H V_H} = \frac{n_g}{(n_g+n_w)} * \frac{M_g}{M_H} \quad \text{A2: 14}$$

$$\dot{m}_{g,H} = \left[\frac{n_g}{(n_g+n_w)} * \frac{M_g}{M_H}\right] \dot{m}_H \quad \text{A2: 15}$$

Total Water Concentration and Water Production Rate

$$\frac{m_{w,H}}{m_h} = \frac{\frac{n_w}{(n_g+n_w)} * \frac{V_H\rho_H}{M_H} M_w}{\rho_H V_H} = \frac{n_w}{(n_g+n_w)} * \frac{M_w}{M_H} \quad \text{A2: 16}$$

$$\dot{m}_{w,H} = \left[\frac{n_w}{(n_g+n_w)} * \frac{M_w}{M_H}\right] \dot{m}_H \quad \text{A2: 17}$$

Hydrate Dissociation Rate with Fluid Components

$$\dot{m}_H = \dot{m}_{w,H} + \dot{m}_{g,H} = \frac{[n_w M_w + n_g M_g]}{(n_g+n_w)M_H} \dot{m}_H \quad \text{A2: 18}$$

Appendix 3: Clausius Clapeyron Type Equations and the Heat of Hydrate Dissociation

In Appendix 1 and Appendix 2, the mass dissociation rate is given as a function of the hydrate dissociation energy which must be derived from the Clausius-Clapeyron model represented thus [5]:

$$\frac{dT}{dP} = \frac{zRT^2}{p\Delta H} = \frac{zRT^2}{ph_F M_{Hyd}} \qquad \text{A3: 1}$$

ΔH [J/mol] represents the enthalpy of fusion, also denoted by $\Delta H = h_F$[J/kg]*M_{Hyd} [kg/mol]; P and T represent the reservoir pressure and temperature conditions at which the hydrate is stable.

Integrating the Clausius-Clapeyron equation results to:

$$\ln p = -\frac{\Delta H}{zRT} \qquad \text{A3: 2}$$

In order to derive the analytically the hydrate dissociation energy, a Clausius Clapeyron type phase equilibrium model is required. For this work, the Carroll and Duan [5] prediction model will be used. The model is given below:

$$\ln P = A + BT + \frac{C}{T} + D\ln T \qquad \text{A3: 3}$$

Where A, B, C, D are empirical constants, also given below for methane hydrates.

Differentiating Carroll´s equation with respect to temperature results to:

$$\frac{d\ln p}{dT} = B - \frac{C}{T^2} + \frac{D}{T} \qquad \text{A3: 4}$$

Or

$$\frac{dp}{dT} = \left(B - \frac{C}{T^2} + \frac{D}{T}\right) e^{A+BT+\frac{C}{T}+D\ln T} \qquad \text{A3: 5}$$

$$\frac{dT_{eq}}{dp} = \frac{1}{\left(\frac{dp}{dT}\right)} = \frac{1}{\left[\left(B-\frac{C}{T^2}+\frac{D}{T}\right)e^{A+BT+\frac{C}{T}+D\ln T}\right]} \qquad \text{A3: 6}$$

From the model above, the temperature depression due to hydrate dissociation can be estimated as given below.

<u>Temperature Change from Hydrate Dissociation</u>

$$T(p) = T_{eq} - \left(\frac{dT_{eq}}{dp}\right)(p_{eq} - p) \qquad \text{A3: 7}$$

The equation above suggests that depressurization is the activating mechanism for any heat influx in the hydrate layer which will further trigger hydrate dissociation. This further implies, as long as hydrates are depressurized, the temperature in the hydrate layer will be pressure controlled and any heat flux in the layer will be used up for dissociation and the endothermic process continues.

Heat of Fusion/Dissociation for Unit Mass Hydrate

Using the Clausius-Clapeyron model and Carroll´s equation, we could derive the heat of dissociation for a given hydrate at known reservoir p, T conditions thus:

$$\frac{d\,\ln p}{dT} = B - \frac{C}{T^2} + \frac{D}{T} = \frac{\Delta H}{zRT^2} = \frac{h_F M_{Hyd}}{zRT^2} \quad \text{A3: 8}$$

From Carroll´s Equation for methane hydrate:

A= -146.1094 [-]; B=0.3165 [1/K]; C=16556.78 [K]; D=0 [-]

Method 1

The enthalpy of dissociation is usually derived per unit mole thus:

$$M_{Hydrate} = n_{CH4} M_{CH4} + n_{H2O} M_{H2O} = 119{,}61 \text{kg/kmol}$$

$$\frac{d\,\ln p}{dT} = \frac{\Delta H}{zRT^2} = \frac{h_F M_{Hyd}}{zRT^2} \quad \text{A3: 9}$$

Hence the heat of dissociation could be derived thus:

$$h_F = \frac{\Delta H}{M_{Hyd}} = h_d \quad \text{A3: 10}$$

Method 2

By assuming the total number of moles in the non-stoichiometric bond of hydrates to be equal to the sum of the moles, we get:

$$M_{Hyd2} = \frac{n_{CH4}}{(n_{CH4}+n_{H2O})} M_{CH4} + \frac{n_{H2O}}{(n_{CH4}+n_{H2O})} M_{H2O} = 17.72 \text{ kg/kmol} \quad \text{A3: 11}$$

The heat of dissociation should be derived thus:

$$h_F = \frac{\Delta H}{(n_{CH4}+n_{H2O}) * M_{Hyd2}} = h_d \quad \text{A3: 12}$$

Change of Dissociation Enthalpy with Temperature / Pressure

As shown in Appendix 1, the changes in the hydrate dissociation energy with pressure needs to be derived in order to better quantify the hydrate dissociation rate. This is derived thus:

$$\Delta H = (BT^2 - C + DT)zR \quad \text{A3: 13}$$

$$\frac{d\Delta H}{dT} = (2BT + D)zR \quad \text{A3: 14}$$

Hence the heat of dissociation could be derived thus:

$$\frac{dh_F}{dp} = \frac{dh_F}{dT} * \frac{dT}{dp} = \frac{(2BT+D)zR}{M_{Hyd}} * \frac{1}{\left[\left(B - \frac{C}{T^2} + \frac{D}{T}\right) e^{A+BT+\frac{C}{T}+D\ln T}\right]} \quad \text{A3: 15}$$

Appendix 4: Permeability and Saturation for Hydrate Dissociation

In the previous appendices, efforts were made to quantify the mass of gas and water generated from the hydrate dissociation. In this section, the increase in gas and water saturation will be quantified such that this can be incorporated into the relative permeability terms and would give a stronger support for future reservoir simulation works and computer aided well testing approaches. This should further give a clearer image of the influence of the different heat source terms on the dissociation rate and the quantity of water and gas generated. Ignoring convective heat flux due to crossflow, the following approach can be made:

Gas Phase

$$\dot{m}_{g,H} = \left[\frac{n_g}{(n_g+n_w)} * \frac{M_g}{M_H}\right] \dot{m}_H \qquad \text{A4: 1}$$

$$m_{g,H} = \left[\frac{n_g}{(n_g+n_w)} * \frac{M_g}{M_H}\right] m_H = \left[\frac{n_g}{(n_g+n_w)} * \frac{M_g}{M_H}\right] \left[\frac{V\emptyset}{h_d}\{c\} + \frac{2\lambda}{h}\frac{\dot{Q}_D}{h_d}\left[\frac{dT_{eq}}{dp}\right] At\right] [p_{eq} - p] \qquad \text{A4: 2}$$

$$S_{g,H}(p,t) = \left(\frac{E_g B_g}{E_g B_g + E_w B_w}\right)\left[c + \frac{2\lambda}{hV\emptyset}\dot{Q}_D\left[\frac{dT_{eq}}{dp}\right] At\right]\frac{[p_{eq}-p]}{h_d \rho_H} S_H \qquad \text{A4: 3}$$

Where,

$$\left[\frac{n_g}{(n_g+n_w)} * \frac{M_g}{M_H} * \frac{\rho_H}{\rho_{g,eq}}\right] = \left(\frac{E_g B_g}{E_g B_g + E_w B_w}\right) \qquad \text{A4: 4}$$

Without Heat Conduction

$$S_{g,H}(p) = \left(\frac{E_g B_g}{E_g B_g + E_w B_w}\right)[c]\frac{[p_{eq}-p]}{h_d \rho_H} S_H \qquad \text{A4: 5}$$

Water Phase

$$\dot{m}_{w,H} = \left[\frac{n_w}{(n_g+n_w)} * \frac{M_w}{M_H}\right] \dot{m}_H \qquad \text{A4: 6}$$

$$S_{w,H}(p) = \left(\frac{E_w B_w}{E_g B_g + E_w B_w}\right)\left[c + \frac{2\lambda}{hV\emptyset}\dot{Q}_D\left[\frac{dT_{eq}}{dp}\right] At\right]\frac{[p_{eq}-p]}{h_d \rho_H} S_H \qquad \text{A4: 7}$$

Where,

$$\left[\frac{n_w}{(n_g+n_w)} * \frac{M_w}{M_H} * \frac{\rho_H}{\rho_{w,eq}}\right] = \left(\frac{E_g B_g}{E_g B_g + E_w B_w}\right) \qquad \text{A4: 8}$$

Without Heat Conduction

$$S_{w,H}(p) = \left(\frac{E_w B_w}{E_g B_g + E_w B_w}\right)[c]\frac{[p_{eq}-p]}{h_d \rho_H} S_H \qquad \text{A4: 9}$$

Let;

$$c^*(p,t) = \left[c + \frac{2\lambda}{hV\emptyset}\dot{Q}_D\left[\frac{dT_{eq}}{dp}\right] At\right] \qquad \text{A4: 10}$$

Hydrate Phase

$$S_H(p,t) = \left\{1 - [c^*]\frac{[p_{eq}-p]}{h_d\rho_H}\right\}S_H \quad \text{A4: 11}$$

$$S_H(p,t) = S_H - [c^*]\frac{[p_{eq}-p]}{h_d\rho_H}S_H = S_H - \Delta S_H \quad \text{A4: 12}$$

$$\Delta S_H = \left\{\left(\frac{E_w B_w}{E_g B_g + E_w B_w}\right)[c^*]\frac{[p_{eq}-p]}{h_d\rho_H}S_H\right\} + \left\{\left(\frac{E_g B_g}{E_g B_g + E_w B_w}\right)[c^*]\frac{[p_{eq}-p]}{h_d\rho_H}S_H\right\} = [c^*]\frac{[p_{eq}-p]}{h_d\rho_H}S_H \quad \text{A4: 13}$$

$$\Delta S_H = S_{w,H} + S_{g,H} \quad \text{A4: 14}$$

Effective and Relative Permeability of Gas hydrate

$$k_H = k(1 - S_H)^N = k * k_{rH} \quad \text{A4: 15}$$

$$k_g = k_{rg}k_H = (k_{rg} * k_{rH}) * k = k^*_{rg} * k = \left(\frac{S_{geff} - S_{girr}}{1 - S_{girr}}\right)^{n_g} k \quad \text{A4: 16}$$

$$k_w = k_{rw}k_H = (k_{rw} * k_{rH}) * k = k^*_{rw} * k = \left(\frac{S_{weff} - S_{wirr}}{1 - S_{wirr}}\right)^{n_w} k \quad \text{A4: 17}$$

Care should be taken when computing the relative permeabilities as hydrate dissociation causes an increase in saturation for both phases and hence conventional relative permeability curves will differ from this.

Gas is a very compressible medium and is hence very pressure sensitive. This implies the volume of gas or saturation is also very pressure sensitive. Pressure depletion decreases the saturation of free fluid available and simultaneously, fluid is produced through hydrate dissociation, which increases the saturation once more. The material balance in terms of saturation can be represented below:

$$S_{wi} = 1 - S_{gi} - S_{Hi} \quad \text{A4: 18}$$

$$S_w(p) + \Delta S_w(p) = 1 - \left[S_g(p) + \Delta S_g(p)\right] - \left[S_H(p) + \Delta S_H\right] \quad \text{A4: 19}$$

$$S_w(p) + \Delta S_w(p) = 1 - \left[S_g(p) + \Delta S_g(p)\right] - \left[S_H(p) + S_{w,H} + S_{g,H}\right] \quad \text{A4: 20}$$

The above equation could be rearranged such that we get the effective changes in saturation as a result of production of each phase. The resulting equation would be:

$$S_{w,eff} = 1 - S_{g,eff} - S_H(p) \quad \text{A4: 21}$$

Where,

$$S_{w,eff} = S_w(p) + S_{w,H} + \Delta S_g(p) \quad \text{A4: 22}$$

$$S_{g,eff} = S_g(p) + S_{g,H} + \Delta S_w(p) \quad \text{A4: 23}$$

The above equations for the effective saturations depict that a reduction in saturation of one phase increases the saturation of the other phase. Although the increase in gas and water saturations as a

result of hydrate dissociation have been addressed earlier, the dependence of fluid saturation on pressure has not been depicted.

Material Balance Approach for Fluid Saturation Dependence on Pressure

The dependence of the hydrate saturation on pressure has been fully discussed in the previous appendices. It is now imperative to investigate the changes in free fluid saturation on pressure, which is relevant for any simulation calculation and also in investigating the changes in relative permeability during depletion.

Fluid saturation in the pores of the formation could be represented thus:

$$S_{fl} = \frac{V_{fl}}{V_p} = \frac{V_{st}B}{V_p} = \frac{V_{st}}{V_p}\frac{\rho_{st}}{\rho_{fl}} = \frac{V_{st}}{\emptyset V}\frac{\rho_{st}}{\rho_{fl}} \quad \text{A4: 24}$$

In the above equation, the density of the reservoir fluids and the porosity are pressure dependent. Hence, the derivative of the above function with pressure is given by:

$$\frac{dS_{fl}}{dp} = \frac{V_{st}\rho_{st}}{V}\frac{d\left(\frac{1}{\emptyset\rho_{fl}}\right)}{dp} \quad \text{A4: 25}$$

From the above equation, it should be noted that for positive pressure depressions in the reservoir, the saturation change is negative. To eliminate this effect, a negative sign is introduced in front of the RHS of the above equation.

$$\frac{dS_{fl}}{dp} = -\frac{V_{st}\rho_{st}}{V}\frac{d\left(\frac{1}{\emptyset\rho_{fl}}\right)}{dp} \quad \text{A4: 26}$$

$$\frac{dS_{fl}}{dp} = \frac{V_{st}B}{V_p}\left[\frac{1}{\emptyset}\frac{d\emptyset}{dp} + \frac{1}{\rho_{fl}}\frac{d\rho_{fl}}{dp}\right] \quad \text{A4: 27}$$

$$\int \frac{1}{S_{fl}} dS_{fl} = \int \left[\frac{1}{\emptyset} d\emptyset + \frac{1}{\rho_{fl}} d\rho_{fl}\right] \quad \text{A4: 28}$$

$$S_{fl} = S_{fl,i}\left(\frac{\emptyset}{\emptyset_i} * \frac{\rho_{fl}}{\rho_{fl,i}}\right) \quad \text{A4: 29}$$

Since the porosity and density are pressure dependent parameters, the saturation will also show pressure dependent properties.

Gas Phase

$$S_g(p) = S_{g,i}\left(\frac{\emptyset}{\emptyset_i} * \frac{\rho_g}{\rho_{g,i}}\right) \quad \text{A4: 30}$$

$$\Delta S_g(p) = S_{g,i} - S_g(p) = S_{g,i}\left[1 - \left(\frac{\emptyset}{\emptyset_i} * \frac{\rho_g}{\rho_{g,i}}\right)\right] \quad \text{A4: 31}$$

Water Phase

$$S_w(p) = S_{w,i}\left(\frac{\emptyset}{\emptyset_i} * \frac{\rho_w}{\rho_{w,i}}\right) \quad \text{A4: 32}$$

$$\Delta S_w(p) = S_{w,i} - S_w(p) = S_{w,i}\left[1 - \left(\frac{\emptyset}{\emptyset_i} * \frac{\rho_w}{\rho_{w,i}}\right)\right] \quad \text{A4: 33}$$

It can be easily shown that the above models can be used to derive volumetric material balance method used in deriving the original gas in place from p/z-plots, which further validates the above model proposed for the dependence of fluid saturation on pressure.

Material Balance Approach for Fluid Saturation and P/Z-Plot for Gas Reservoirs

$$\frac{S_{fl,i}}{S_{fl,i}} - \frac{S_{fl(r,t)}}{S_{fl,i}} = G_p(t) = \left(\frac{\emptyset_i}{\emptyset_i} * \frac{\rho_{fl,i}}{\rho_{fl,i}}\right) - \left(\frac{\emptyset}{\emptyset_i} * \frac{\rho_{fl}}{\rho_{fl,i}}\right) \quad \text{A4: 34}$$

$$G_p(t) = \frac{\rho_{st}}{\rho_{fl,i}\emptyset_i}\left[\left(\emptyset_i \frac{p_i T_{st}}{p_{st} T_i z_i}\right) - \left(\emptyset \frac{p T_{st}}{p_{st} T z}\right)\right] \quad \text{A4: 35}$$

$$G_{p,st}(t) = \frac{G_p(t)}{B_{gi}} = \frac{T_{st}}{p_{st}}\left[\left(\frac{p_i}{T_i z_i}\right) - \left(\frac{\emptyset}{\emptyset_i}\frac{p}{Tz}\right)\right] \quad \text{A4: 36}$$

The porosity change with pressure is given by [77]:

$$\frac{\emptyset}{\emptyset_i} = e^{-c_{f,i}(p_i - p)} \quad \text{A4: 37}$$

We write the general material balance equation thus:

$$\left(\frac{p}{Tz} e^{-c_{f,i}(p_i - p)}\right) = \left[\left(\frac{p_i}{T_i z_i}\right) - \frac{p_{st}}{T_{st}} G_{p,st}(t)\right] \quad \text{A4: 38}$$

For conventional gas reservoirs where the temperature is assumed constant during depletion, the above equation is simplified thus:

$$\frac{p}{z}\left[1 - c_{f,i}(p_i - p)\right] = \frac{p_i}{z_i} - \frac{p_{st} T_i}{T_{st}} G_{p,st}(t) \quad \text{A4: 39}$$

$$\frac{p}{z}\left[1 - c_{f,i}(p_i - p)\right] = \frac{p_i}{z_i}\left(1 - \frac{p_{st} T_i z_i}{T_{st} p_i} G_{p,st}(t)\right) \quad \text{A4: 40}$$

$$\frac{p}{z}\left[1 - c_{f,i}(p_i - p)\right] = \frac{p_i}{z_i}\left(1 - \frac{G_{p,st}(t)}{G}\right) \quad \text{A4: 41}$$

The model has now been represented similar to the material balance model given by Ramagost and Farshad [78] with the modification of the apparent compressibility. It should be highlighted at this point that the effect of hydrate dissociation will lead to an increase in the amount of gas produced and hence a deviation to the right from the normal p/z-plot which is similar to aquifer-drive reservoirs.

If the porosity change is assumed to be trivial throughout depletion, then the above equation is further simplified to the conventional volumetric p/z-plot thus:

$$\frac{p}{z} = \frac{p_i}{z_i} - \frac{p_{st} T}{T_{st}} G_{p,st}(t) \quad \text{A4: 42}$$

Material Balance Approach for Gas Hydrate Reservoirs

If the same procedure is applied to the gas hydrate reservoir and considering the multiphase system, the following material balance model can be developed for gas hydrate reservoirs:

$$\frac{G_p}{B_{g,i}} + \frac{W_p}{B_{w,i}} = V\emptyset_i S_{g,i}\left\{\left[\left(\frac{1}{B_{g,i}}\right) - \left(\frac{\emptyset}{\emptyset_i} * \frac{1}{B_g}\right)\right] + \frac{1}{B_{g,i}}\frac{S_{g,H}}{S_{g,i}}\right\} + V\emptyset_i S_{w,i}\frac{B_{w,i}}{B_{g,i}}\left\{\left[\left(\frac{1}{B_{w,i}}\right) - \left(\frac{\emptyset}{\emptyset_i} * \frac{1}{B_w}\right)\right] + \frac{1}{B_{w,i}}\frac{S_{w,H}}{S_{w,i}}\right\} \quad \text{A4: 43}$$

Appendix 5: Basics of Diffusivity Equations in Gas Hydrate Reservoirs

The mass balance equation for the hydrate layer is given in cylindrical coordinates thus:

$$2\pi h\Delta(r * \rho_g * w_g) + 2\pi h\Delta(r * \rho_w * w_w) = 2\pi rh\Delta r\frac{\Delta(S_g\emptyset\rho_g)}{\Delta t} + 2\pi rh\Delta r\frac{\Delta(S_w\emptyset\rho_w)}{\Delta t} + \text{Source} \quad \text{A5: 1}$$

$$2\pi h\Delta(r * \rho_g * w_g) + 2\pi h\Delta(r * \rho_w * w_w) = 2\pi rh\Delta r\frac{\Delta(S_g\emptyset\rho_g)}{\Delta t} + 2\pi rh\Delta r\frac{\Delta(S_w\emptyset\rho_w)}{\Delta t} + \dot{m}_H \quad \text{A5: 2}$$

The source term in the above mass balance equation is due to hydrate dissociation into its byproducts and can be defined using the equilibrium model or the kinetic model as given below and also in Appendix 1.

Kinetic Model

The kinetic model as given by [31] considers the rate of hydrate dissociation considering the available area for reaction and the activation energy needed to initiate hydrate dissociation. It however does not quantify the heat energy available in the reservoir and does not define the source of heat responsible for hydrate dissociation. However, as shown in Appendix 1, the total heat supplied and the total hydrate dissociated could be assumed to be reflected in the kinetic model, and hence the hydrate dissociation rate can better be reflected in type curves. Incorporating the kinetic model proposed by Kim et al. [31] into the diffusivity equation, we get:

$$2\pi h\Delta(r * \rho_g * w_g) + 2\pi h\Delta(r * \rho_w * w_w) - K_d M_H A_H \Delta p = 2\pi rh\Delta r\frac{\Delta(S_g\emptyset\rho_g)}{\Delta t} + 2\pi rh\Delta r\frac{\Delta(S_w\emptyset\rho_w)}{\Delta t} \quad \text{A5: 3}$$

As mentioned in Appendix 1, the hydrate reaction area for a producing reservoir will be defined such that it reflects the depleting zone.

$$\frac{\Delta(r*\rho_g*w_g)}{r\Delta r} + \frac{\Delta(r*\rho_w*w_w)}{r\Delta r} - \frac{K_d M_H \pi r\Delta r}{2\pi h}\frac{\Delta p}{r\Delta r} = \frac{\Delta(S_g\emptyset\rho_g)}{\Delta t} + \frac{\Delta(S_w\emptyset\rho_w)}{\Delta t} \quad \text{A5: 4}$$

$$\frac{1}{r}\frac{\partial(r*\rho_g*w_g)}{\partial r} + \frac{1}{r}\frac{\partial(r*\rho_w*w_w)}{\partial r} - \frac{K_d M_H}{2h}(p_i - p) = (\rho c_T)_{eff}\frac{\partial p}{\partial t} \quad \text{A5: 5}$$

Where,

$$(\rho c_T)_{eff} = \left\{S_g\emptyset\rho_g[c_g + c_F] + S_w\emptyset\rho_w[c_w + c_F]\right\} \quad \text{A5: 6}$$

$$\frac{\partial(r*\rho_g*w_g)}{\partial r} + \frac{1}{r}\frac{\partial(r*\rho_w*w_w)}{\partial r} - \frac{K_d M_H}{2h}(p_i - p) = (\rho c_T)_{eff}\frac{\partial p}{\partial t} \quad \text{A5: 7}$$

Considering mass balance and neglecting capillary pressure effects, the above equation takes the form:

$$\frac{\partial\left[r*\left(\rho_g*k_h\frac{k_{rg}}{\eta_g}+\rho_w*k_h\frac{k_{rw}}{\eta_w}\right)\frac{\partial p}{\partial r}\right]}{\partial r} - \frac{K_d M_H}{2h}(p_i - p) = (\rho c_T)_{eff}\frac{\partial p}{\partial t} \quad \text{A5: 8}$$

By using the pseudo-pressure model, the diffusivity equation can be written in the form:

$$\frac{1}{r}\frac{\partial\left(r\frac{\partial\varphi}{\partial r}\right)}{\partial r} - \frac{K_d M_H}{2hk\left[\rho_t\left(\frac{k_r}{\eta}\right)_t\right]}(\varphi_i - \varphi) = (\rho c_T)_{eff}\frac{\partial p}{\partial t} \quad \text{A5: 9}$$

Such that the effects of changes in the effective compressibility are accounted for in the well test model, the following approach is made (It should be noted that other approaches such as the use of pseudo-time could be used):

$$\frac{1}{r}\frac{\partial\left(r\frac{\partial\varphi}{\partial r}\right)}{\partial r}-\frac{K_d M_H}{2hk\left[\rho_t\left(\frac{k_r}{\eta}\right)_t\right]}(\varphi_i-\varphi)=(\rho c_T)_{eff}\frac{(\rho c_T)_{eff,id}}{(\rho c_T)_{eff,id}}\frac{\partial p}{\partial t} \quad \text{A5: 10}$$

$$\frac{\partial^2\varphi_D}{\partial {r_D}^2}+\frac{1}{r_D}\frac{\partial\varphi_D}{\partial r_D}-\frac{K_d M_H {r_w}^2}{2hkf_t(p)}\varphi_D=\frac{(\rho c_T)_{eff}}{(\rho c_T)_{eff,id}}\frac{\left[\rho_t\left(\frac{k_r}{\eta}\right)_t\right]_{id}}{\left[\rho_t\left(\frac{k_r}{\eta}\right)_t\right]}\frac{\partial\varphi_D}{\partial t_{Dw}} \quad \text{A5: 11}$$

$$\frac{\partial^2\varphi_D}{\partial {r_D}^2}+\frac{1}{r_D}\frac{\partial\varphi_D}{\partial r_D}-\gamma_{Dk}\varphi_D=S_{Dk}\frac{\partial\varphi_D}{\partial t_{Dw}} \quad \text{A5: 12}$$

Where,

$$\gamma_{Dk}=\frac{K_d M_H {r_w}^2}{2hkf_t(p)}=\frac{K_o e^{\left(\frac{-E}{RT}\right)}M_H {r_w}^2}{2hk\left[\rho_t\left(\frac{k_r}{\eta}\right)_t\right]} \quad \text{A5: 13}$$

$$S_{Dk}=\frac{\left[\rho_t\left(\frac{k_r}{\eta}\right)_t\right]_{id}}{\left[\rho_t\left(\frac{k_r}{\eta}\right)_t\right]}\left(\frac{(\rho c_T)_{eff}}{(\rho c_T)_{eff,id}}\right) \quad \text{A5: 14}$$

$$t_{Dw}=\frac{k\left[\rho_t\left(\frac{k_r}{\eta}\right)_t\right]_{id}}{{r_w}^2(\rho c_T)_{eff,id}}t \quad \text{A5: 15}$$

Equilibrium Model

In the equilibrium model, the source term is quantified using an energy balance approach, such that the available energy in the reservoir and its changes are related to the energy required for hydrate dissociation. Using the equilibrium model we get:

$$2\pi hA(r*\rho_g*w_g)+2\pi hA(r*\rho_w*w_w)=2\pi rhAr\frac{A(S_g\emptyset\rho_g)}{At}+2\pi rhAr\frac{A(S_w\emptyset\rho_w)}{At}+\dot{m}_H \quad \text{A5: 16}$$

<u>Equilibrium Model for Class 3 Gas Hydrate Reservoir</u>

We first derive the diffusivity equation for Class 3 gas hydrates by incorporating the hydrate dissociation rate derived in Appendix 1 into the mass balance equation given above:

$$2\pi hA(r*\rho_g*w_g)+2\pi hA(r*\rho_w*w_w)-\frac{2\lambda}{h}\frac{\dot{Q}_D}{h_d}\left[\frac{dT_{eq}}{dp}\right]A(p_i-p)=2\pi rhAr\left[\frac{A(S_g\emptyset\rho_g)}{At}+\frac{A(S_w\emptyset\rho_w)}{At}+\frac{A(S_h\emptyset\rho_h)}{At}\right] \quad \text{A5: 17}$$

$$\frac{1}{r}\frac{\partial\left[r*\left(\rho_g*k\frac{k^*_{rg}}{\eta_g}+\rho_w*\frac{k^*_{rw}}{\eta_w}\right)\frac{\partial p}{\partial r}\right]}{\partial r}-\frac{\lambda}{h^2}\frac{\dot{Q}_D}{h_d}\left[\frac{dT_{eq}}{dp}\right](p_i-p)=\left[(\rho_w\emptyset c_{T,w})+(\rho_g\emptyset c_{T,g})\right]\frac{\partial p}{\partial t}+\frac{c}{h_d}\frac{\partial p}{\partial t} \quad \text{A5: 18}$$

$$\frac{1}{r_D}\frac{\partial\left(r_D\frac{\partial\varphi}{\partial r_D}\right)}{\partial r_D}-\frac{\lambda}{h^2}\frac{\dot{Q}_D {r_w}^2}{h_d k\left[\rho_t\left(\frac{k_r}{\eta}\right)_t\right]}\left[\frac{dT_{eq}}{dp}\right](\varphi_i-\varphi)=\frac{(\rho c_T)_{eff}{r_w}^2}{\left[\rho_t k\left(\frac{k_r}{\eta}\right)_t\right]}\frac{\partial\varphi}{\partial t}+\frac{c}{h_d}\frac{{r_w}^2}{\left[\rho_t k\left(\frac{k_r}{\eta}\right)_t\right]}\frac{(\rho c_T)_{eff,id}}{(\rho c_T)_{eff,id}}\frac{\partial\varphi}{\partial t} \quad \text{A5: 19}$$

$$\frac{1}{r_D}\frac{\partial\left(r_D\frac{\partial\varphi}{\partial r_D}\right)}{\partial r_D}-\frac{\lambda}{h^2}\frac{\dot{Q}_D {r_w}^2}{h_d k f_t(p)}\left[\frac{dT_{eq}}{dp}\right](\varphi_i-\varphi)=\frac{(\rho c_T)_{eff}{r_w}^2}{\left[\rho_t k\left(\frac{k_r}{\eta}\right)_t\right]}\frac{\partial\varphi}{\partial t}+\frac{c}{h_d}\frac{{r_w}^2}{\left[\rho_t k\left(\frac{k_r}{\eta}\right)_t\right]}\frac{(\rho c_T)_{eff,id}}{(\rho c_T)_{eff,id}}\frac{\partial\varphi}{\partial t} \quad \text{A5: 20}$$

$$\frac{1}{r_D}\frac{\partial\left(r_D\frac{\partial\varphi}{\partial r_D}\right)}{\partial r_D}-e_D\dot{Q}_D(\varphi_i-\varphi)=\frac{(\rho c_T)_{eff}{r_w}^2}{\left[\rho_t k\left(\frac{k_r}{\eta}\right)_t\right]}\frac{\partial\varphi}{\partial t}+\frac{c}{h_d}\frac{{r_w}^2}{\left[\rho_t k\left(\frac{k_r}{\eta}\right)_t\right]}\frac{(\rho c_T)_{eff,id}}{(\rho c_T)_{eff,id}}\frac{\partial\varphi}{\partial t} \quad \text{A5: 21}$$

$$\frac{1}{r_D}\frac{\partial\left(r_D\frac{\partial\varphi}{\partial r_D}\right)}{\partial r_D}-e_D\dot{Q}_D(\varphi_i-\varphi)=\frac{(\rho c_T)_{eff}}{(\rho c_T)_{eff,id}}\frac{\left[\rho_t k\left(\frac{k_r}{\eta}\right)_t\right]_{id}}{\left[\rho_t k\left(\frac{k_r}{\eta}\right)_t\right]}\frac{{r_w}^2(\rho c_T)_{eff,id}}{\left[\rho_t k\left(\frac{k_r}{\eta}\right)_t\right]_{id}}\frac{\partial\varphi}{\partial t}+\frac{c}{h_d(\rho c_T)_{eff,id}}\frac{\left[\rho_t k\left(\frac{k_r}{\eta}\right)_t\right]_{id}}{\left[\rho_t k\left(\frac{k_r}{\eta}\right)_t\right]}\frac{{r_w}^2(\rho c_T)_{eff,id}}{\left[\rho_t k\left(\frac{k_r}{\eta}\right)_t\right]_{id}}\frac{\partial\varphi}{\partial t} \quad \text{A5: 22}$$

$$\frac{\partial^2\varphi_D}{\partial {r_D}^2}+\frac{1}{r_D}\frac{\partial\varphi_D}{\partial r_D}-\gamma_{De}\varphi_D=\frac{\left[\rho_t k\left(\frac{k_r}{\eta}\right)_t\right]_{id}}{\left[\rho_t k\left(\frac{k_r}{\eta}\right)_t\right]}\left(\frac{(\rho c_T)_{eff}}{(\rho c_T)_{eff,id}}+\frac{c}{h_d(\rho c_T)_{eff,id}}\right)\frac{\partial\varphi_D}{\partial t_{Dw}} \quad \text{A5: 23}$$

$$\frac{\partial^2\varphi_D}{\partial {r_D}^2}+\frac{1}{r_D}\frac{\partial\varphi_D}{\partial r_D}-\gamma_{De}\varphi_D=S_D\frac{\partial\varphi_D}{\partial t_{Dw}} \quad \text{A5: 24}$$

Where,

$$(\rho c_T)_{eff}=(\rho_w\emptyset c_{T,w})+(\rho_g\emptyset c_{T,g})$$

$$c_{T,g}=S_g c_g+S_g c_F+S_H c_F\left(\frac{E_g B_g}{(B_g E_g+B_w E_w)}\right) \quad \text{A5: 25}$$

$$c_{T,w}=S_w c_w+S_w c_F+S_H c_F\left(\frac{E_w B_w}{(B_g E_g+B_w E_w)}\right) \quad \text{A5: 26}$$

$$c=\left[c_{p,g}S_g\rho_g\left(\frac{T(c_g+c_F)}{\left[\frac{dT_{eq}}{dp}\right]}+1\right)+c_{p,w}S_w\rho_w\left(\frac{T(c_w+c_F)}{\left[\frac{dT_{eq}}{dp}\right]}+1\right)+c_{p,H}S_H\rho_H\left(\frac{T(c_F)}{\left[\frac{dT_{eq}}{dp}\right]}+1\right)+c_{p,m}\frac{(1-\emptyset)}{\emptyset}\rho_m\left(\frac{T(c_m)}{\left[\frac{dT_{eq}}{dp}\right]}+1\right)+S_H\rho_H\frac{dh_d}{dT_{eq}}\right]\left[\frac{dT_{eq}}{dp}\right] \quad \text{A5: 27}$$

$$\gamma_{De}=\frac{\lambda}{h^2}\frac{\dot{Q}_D {r_w}^2}{h_d k\left[\rho_t\left(\frac{k_r}{\eta}\right)_t\right]}\left[\frac{dT_{eq}}{dp}\right]=\frac{\lambda}{h^2}\frac{\dot{Q}_D {r_w}^2}{h_d k}\left[\frac{dT_{eq}}{d\varphi}\right] \quad \text{A5: 28}$$

$$S_D=\frac{\left[\rho_t k\left(\frac{k_r}{\eta}\right)_t\right]_{id}}{\left[\rho_t k\left(\frac{k_r}{\eta}\right)_t\right]}\left(\frac{(\rho c_T)_{eff}}{(\rho c_T)_{eff,id}}+\frac{c}{h_d(\rho c_T)_{eff,id}}\right) \quad \text{A5: 29}$$

$$S_D=\left(\frac{(\rho c_T)_{eff}}{(\rho c_T)_{eff,id}}\frac{\left[\rho_t k\left(\frac{k_r}{\eta}\right)_t\right]_{id}}{\left[\rho_t k\left(\frac{k_r}{\eta}\right)_t\right]}+\frac{c}{h_d(\rho c_T)_{eff,id}}\frac{\left[\rho_t k\left(\frac{k_r}{\eta}\right)_t\right]_{id}}{\left[\rho_t k\left(\frac{k_r}{\eta}\right)_t\right]}\right)=S_{Dk}+c_{D,H} \quad \text{A5: 30}$$

The model required for deriving solutions in Laplace domain is given thus:

$$\frac{1}{r}\frac{\partial\left[r*\left(\rho_g*k\frac{k^*_{rg}}{\eta_g}+\rho_w*\frac{k^*_{rw}}{\eta_w}\right)\frac{\partial p}{\partial r}\right]}{\partial r}-\frac{1}{2h}\frac{1}{h_d}\left[\lambda\frac{\partial T}{\partial z}\right]_{Caprock}-\frac{1}{2h}\frac{1}{h_d}\left[\lambda\frac{\partial T}{\partial z}\right]_{Underlain}=\left[(\rho_w\emptyset c_{T,w})+(\rho_g\emptyset c_{T,g})+\frac{c}{h_d}\right]\frac{\partial p}{\partial t} \quad \text{A5: 31}$$

$$\frac{\partial^2\varphi_D}{\partial {r_D}^2}+\frac{1}{r_D}\frac{\partial\varphi_D}{\partial r_D}-\left[\frac{\partial T_{pD}}{\partial z_D}\right]_{Caprock,z_D=1}-\left[\frac{\partial T_{pD}}{\partial z_D}\right]_{Underburden,z_D=1}=S_D\frac{\partial\varphi_D}{\partial t_{Dw}} \quad \text{A5: 32}$$

Appendix 6: Inner Boundary Conditions for Diffusivity Equations in Gas Hydrates

The inner boundary conditions handled here do not consider any wellbore storage or mechanical skin effects.

Constant Pressure Inner Boundary (CPIB)

Pseudo-Pressure Transient

$$\varphi_D(r_D, t_{Dw}) = \frac{\varphi_i - \varphi(r,t)}{(\varphi_i - \varphi_{wf})} = \frac{\varphi(r,t) - \varphi_i}{\varphi_{wf} - \varphi_i} \quad \text{A6: 1}$$

$$\varphi_D(r_D = 1, t_{Dw}) = \frac{\varphi_i - \varphi_{wf}}{\varphi_i - \varphi_{wf}} = 1 \quad \text{A6: 2}$$

Rate Transient

$$\dot{m}_{tD}(r_D, t_{Dw}) = \frac{\dot{m}_t(t)}{2\pi hk(\varphi_i - \varphi_{wf})} = -r_D \frac{d\varphi_D(r_D, t_{Dw})}{dr_D} \quad \text{A6: 3}$$

Temperature Transient

$$T_{pD} = \left(\frac{\lambda}{kh_d}\frac{r_w^2}{h^2}\frac{1}{(\varphi_i - \varphi_{wf})}\right)(T_i - T) \quad \text{A6: 4}$$

$$T_{pD}(r_D, t_{Dw}, z_D = 1) = \left(\frac{\lambda}{kh_d}\frac{r_w^2}{h^2}\frac{1}{(\varphi_i - \varphi_{wf})}\right)\left[\frac{dT_{eq}}{dp}\right][P_i - P(r,t)] \quad \text{A6: 5}$$

$$T_{pD}(r_D, t_{Dw}, z_D = 1) = \left(\frac{\lambda}{kh_d}\frac{r_w^2}{h^2}\frac{1}{(\varphi_i - \varphi_{wf})}\right)\left[\frac{dT_{eq}}{dp}\right]\frac{[\varphi_i - \varphi(r,t)]}{\left[\rho_t\left(\frac{k_r}{\eta}\right)_t\right]} \quad \text{A6: 6}$$

$$T_{pD}(r_D, t_{Dw}, z_D = 1) = \left(\frac{\lambda}{kh_d}\frac{r_w^2}{h^2}\frac{1}{\left[\rho_t\left(\frac{k_r}{\eta}\right)_t\right]}\left[\frac{dT_{eq}}{dp}\right]\right)\varphi_D(r_D, t_{Dw}) \quad \text{A6: 7}$$

Constant Rate Inner Boundary (CRIB)

Pseudo-Pressure Transient

$$\varphi_D(r_D, t_{Dw}) = \frac{2\pi hk}{\dot{m}_t}[\varphi_i - \varphi(r,t)] \quad \text{A6: 8}$$

$$\dot{m}_{tD}(r_D = 1, t_{Dw}) = -\left[r_D \frac{d\varphi_D(r_D, t_{Dw})}{dr_D}\right]_{r_D = 1} = 1 \quad \text{A6: 9}$$

Temperature Transient

$$T_{pD}(r_D, t_{Dw}, z_D) = \left(\frac{\lambda}{kh_d}\frac{r_w^2}{h^2}\frac{2\pi hk}{\dot{m}_t}\right)(T_i - T) \quad \text{A6: 10}$$

$$T_{pD}(r_D, t_{Dw}, z_D = 1) = \left(\frac{\lambda}{kh_d}\frac{r_w^2}{h^2}\frac{2\pi hk}{\dot{m}_t}\right)\left[\frac{dT_{eq}}{dp}\right][P_i - P(r,t)] \quad \text{A6: 11}$$

$$T_{pD}(r_D, t_{Dw}, z_D = 1) = \left(\frac{\lambda}{kh_d}\frac{r_w^2}{h^2}\frac{2\pi hk}{\dot{m}_t}\right)\left[\frac{dT_{eq}}{dp}\right]\frac{[\varphi_i - \varphi(r,t)]}{\left[\rho_t\left(\frac{k_r}{\eta}\right)_t\right]} \quad \text{A6: 12}$$

$$T_{pD}(r_D, t_{Dw}, z_D = 1) = \left(\frac{\lambda}{kh_d}\frac{r_w^2}{h^2}\left[\frac{dT_{eq}}{dp}\right]\frac{1}{\left[\rho_t\left(\frac{k_r}{\eta}\right)_t\right]}\right)\varphi_D(r_D, t_{Dw}) \quad \text{A6: 13}$$

Appendix 7: Laplace Transformation of the Diffusivity Equation in Class 3 Gas Hydrates

In developing the diffusivity equation in the hydrate layer, the time dependent heat flux due to conduction should be taken into account.

Equilibrium Model

$$\frac{\partial^2 \varphi_D}{\partial {r_D}^2} + \frac{1}{r_D}\frac{\partial \varphi_D}{\partial r_D} - \frac{\partial T_{pD}}{\partial z_D} = S_D \frac{\partial \varphi_D}{\partial t_{Dw}} \quad \text{A7: 1}$$

The above inhomogeneous partial differential equation can be solved by applying different methods such as the Green function [77]; however, Laplace transforms are used in this work. The Laplace transformed equation takes the form:

$$\frac{\partial^2 \hat{\varphi}_D}{\partial {r_D}^2} + \frac{1}{r_D}\frac{\partial \hat{\varphi}_D}{\partial r_D} - \frac{\partial \widehat{T_{pD}}}{\partial z_D} = S_D p \hat{\varphi}_D \quad \text{A7: 2}$$

From the solutions to the heat leakage rate below, the diffusivity equation in Laplace domain with the heat conduction term is given by:

$$\frac{\partial^2 \hat{\varphi}_D}{\partial {r_D}^2} + \frac{1}{r_D}\frac{\partial \hat{\varphi}_D}{\partial r_D} - \gamma_{De}\hat{\varphi}_D = S_D p \hat{\varphi}_D \quad \text{A7: 3}$$

$$\frac{\partial^2 \hat{\varphi}_D}{\partial {r_D}^2} + \frac{1}{r_D}\frac{\partial \hat{\varphi}_D}{\partial r_D} - (S_D p + \gamma_{De})\hat{\varphi}_D = 0 \quad \text{A7: 4}$$

It should be noted that the heat flux rate is also in Laplace domain as will be shown later.

Kinetic Model

$$\frac{\partial^2 \varphi_D}{\partial {r_D}^2} + \frac{1}{r_D}\frac{\partial \varphi_D}{\partial r_D} - \gamma_{Dk}\varphi_D = S_{Dk} \frac{\partial \varphi_D}{\partial t_{Dw}} \quad \text{A7: 5}$$

$$\frac{\partial^2 \hat{\varphi}_D}{\partial {r_D}^2} + \frac{1}{r_D}\frac{\partial \hat{\varphi}_D}{\partial r_D} - (S_{DK} p + \gamma_{DK})\hat{\varphi}_D = 0 \quad \text{A7: 6}$$

Both the kinetic and equilibrium models can be transformed in the Bessel equation thus:

$${r_D}^2 \frac{\partial^2 \hat{\varphi}_D}{\partial {r_D}^2} + r_D \frac{\partial \hat{\varphi}_D}{\partial r_D} - {r_D}^2 s \hat{\varphi}_D = 0 \quad \text{A7: 7}$$

General Solution in Laplace Domain

$$\hat{\varphi}_D = c_1 I_o(\beta) + c_2 K_o(\beta) \quad \text{A7: 8}$$

Equilibrium Model

$$\beta = r_D \sqrt{S_D p + \gamma_{De}} = r_D \sqrt{s} \quad \text{A7: 9}$$

Kinetic Model

$$\beta = r_D \sqrt{S_{Dk} p + \gamma_{Dk}} = r_D \sqrt{s} \quad \text{A7: 10}$$

The behavior of the modified Bessel functions are given in Figure A7- 1.

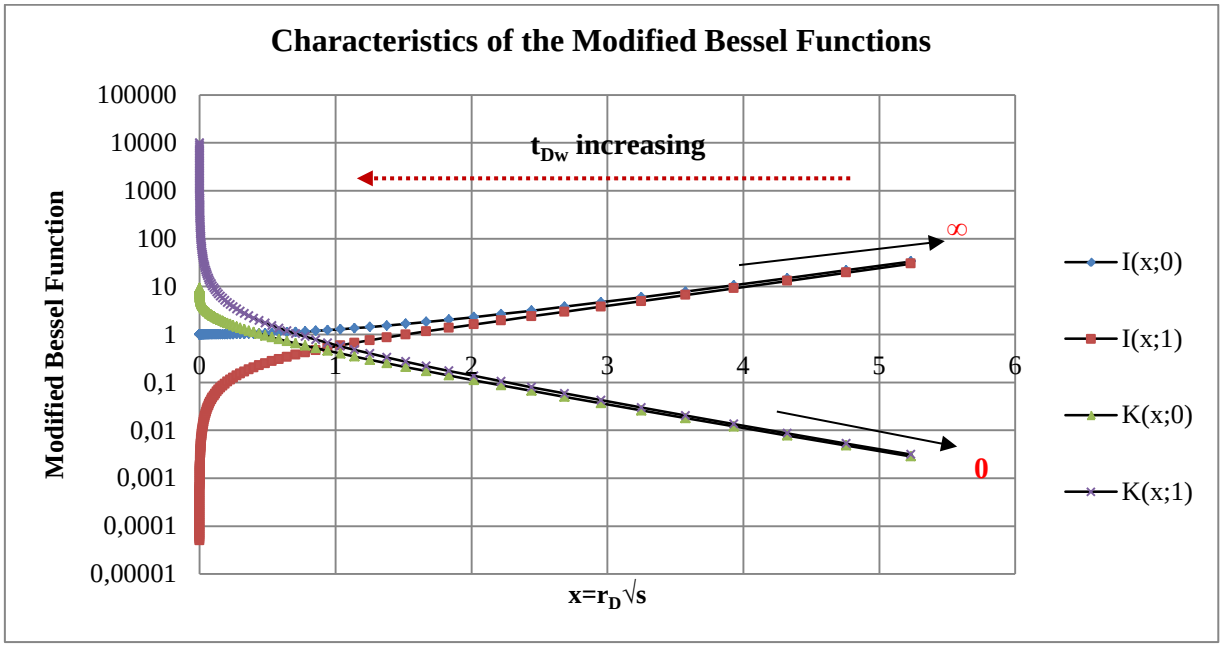

Figure A7- 1 : Characteristics of the Modified Bessel Functions

The characteristics of the modified Bessel functions are important in the computation and simplification of the Laplace domain well identification models, especially during the early time period where the modified Bessel functions of the first kind ($I(x;0)=I_0(x)$ and $I(x;1)=I_1(x)$) approach infinity and the modified Bessel functions of the second kind ($K(x;0)=K_0(x)$ and $K(x;1)=K_1(x)$) approach zero.

Heat Leakage Rate

The dimensionless heat leakage rate is a constant using the kinetic model and a time function using the equilibrium model. However, the dimensionless leakage rate would be constant for CTOB in the confining layers after a given period of production. Such that a general correlation is derived for the dimensionless heat leakage rate, we represent the solution to the problem in Appendix 1 in Laplace domain with a modification of the dimensionless temperature as given in the inner boundary conditions and the diffusivity equation.

$$\frac{\partial^2 T_{pD}}{\partial {z_D}^2} = F_{CD}\frac{\partial T_{pD}}{\partial t_{Dw}} \qquad \text{A7: 11}$$

The Laplace transformed heat conduction equation takes the form:

$$\left[\frac{\partial^2 \widehat{T_{pD}}}{\partial z_D^2}\right]_{layer2} = pF_{CD}[\widehat{T_{pD}}] \qquad \text{A7: 12}$$

General Solution for Finite Reservoirs with Linear Flow

$$\widehat{T_{pD}} = A\cosh\left(z_D\sqrt{pF_{CD}}\right) + B\sinh\left(z_D\sqrt{pF_{CD}}\right) \qquad \text{A7: 13}$$

The constant A and B can be derived by implementing the inner and outer boundary condition.

Constant Temperature Outer Boundary (CTOB)

Inner Boundary Condition

From the dimensionless Temperature given in Appendix 6, we get:

$$T_{pD}(r_D, t_{Dw}, z_D = 1) = \left(\frac{\lambda}{h_d}\frac{r_w^2}{h^2}\right)\left[\frac{dT_{eq}}{dp}\right]\frac{1}{k\left[\rho_t\left(\frac{k_r}{\eta}\right)_t\right]}\varphi_D \qquad \text{A7: 14}$$

The Laplace transform of the above model is hence:

$$\widehat{T_{pD}}(r_D, p, z_D = 1) = \left\{\left(\frac{\lambda}{h_d}\frac{r_w^2}{h^2}\right)\left[\frac{dT_{eq}}{dp}\right]\frac{1}{k\left[\rho_t\left(\frac{k_r}{\eta}\right)_t\right]}\right\}\hat{\varphi}_D = \left\{\left(\frac{\lambda}{h_d}\frac{r_w^2}{h^2}\right)\left[\frac{dT_{eq}}{dp}\right]\frac{1}{kf_t(p)}\right\}\hat{\varphi}_D = e_D\hat{\varphi}_D \qquad \text{A7: 15}$$

Outer Boundary Condition

$$T_i - T(r, t, z_D = \Delta z_D) = 0$$

Using the boundary conditions above, the general equation takes the form:

$$\widehat{T_{pD}} = \left\{\frac{\mathrm{Sinh}(z_D\sqrt{pF_{CD}})\mathrm{Cosh}(\Delta z_D\sqrt{pF_{CD}}) - \mathrm{Sinh}(\Delta z_D\sqrt{pF_{CD}})\mathrm{Cosh}(z_D\sqrt{pF_{CD}})}{[\mathrm{Sinh}(\sqrt{pF_{CD}})\mathrm{Cosh}(\Delta z_D\sqrt{pF_{CD}}) - \mathrm{Sinh}(\Delta z_D\sqrt{pF_{CD}})\mathrm{Cosh}(\sqrt{pF_{CD}})]}\right\}e_D\hat{\varphi}_D \qquad \text{A7: 16}$$

The above equation can further be simplified thus:

$$\widehat{T_{pD}} = \left\{\frac{\mathrm{Sinh}[\sqrt{pF_{CD}}(z_D - \Delta z_D)]}{\mathrm{Sinh}[\sqrt{pF_{CD}}(1 - \Delta z_D)]}\right\}e_D\hat{\varphi}_D = -\left\{\frac{\mathrm{Sinh}[\sqrt{pF_{CD}}(\Delta z_D - z_D)]}{\mathrm{Sinh}[\sqrt{pF_{CD}}(\Delta z_D - 1)]}\right\}e_D\hat{\varphi}_D \qquad \text{A7: 17}$$

The heat leakage rate to the hydrate layer in Laplace domain is given thus:

$$\widehat{\dot{Q}_D} = \frac{d\widehat{T_{pD}}}{dz_D} = \left\{\sqrt{pF_{CD}}\frac{\mathrm{Cosh}[\sqrt{pF_{CD}}(\Delta z_D - z_D)]}{\mathrm{Sinh}[\sqrt{pF_{CD}}(\Delta z_D - 1)]}\right\}e_D\hat{\varphi}_D \qquad \text{A7: 18}$$

At the crossflow point, the above differential is:

$$\frac{d\widehat{T_{pD}}}{dz_D} = \left\{\sqrt{pF_{CD}}\frac{\mathrm{Cosh}[\sqrt{pF_{CD}}(\Delta z_D - 1)]}{\mathrm{Sinh}[\sqrt{pF_{CD}}(\Delta z_D - 1)]}\right\}e_D\hat{\varphi}_D = \left\{\sqrt{pF_{CD}}\mathrm{Coth}\left[\sqrt{pF_{CD}}(\Delta z_D - 1)\right]\right\}e_D\hat{\varphi}_D \qquad \text{A7: 19}$$

$$\frac{d\widehat{T_{pD}}}{dz_D} = \left\{\sqrt{pF_{CD}}\mathrm{Coth}\left[\sqrt{pF_{CD}}(\Delta z_D - 1)\right]\right\}e_D\hat{\varphi}_D \qquad \text{A7: 20}$$

$$\frac{d\widehat{T_{pD}}}{dz_D} = \widehat{\dot{Q}_{pD}}e_D\hat{\varphi}_D \qquad \text{A7: 21}$$

Pseudo-No Flow Temperature Boundary (p-NFTB)

The p-NFTB basically considers the effect of temperature drop at the exterior boundary, especially in the top confining layer which is sensitive to the geothermal profile and decreases with decreasing depth.

$$\frac{d\widehat{T_D}}{dz_D} = \left\{\sqrt{pF_{CD}}\tanh\left[\sqrt{pF_{CD}}(\Delta z_D - 1)\right]\right\}e_D\hat{\varphi}_D \qquad \text{A7: 22}$$

$$\frac{d\widehat{T_D}}{dz_D} = \widehat{\dot{Q}_{pD}}e_D\hat{\varphi}_D \qquad \text{A7: 23}$$

General Solution for Infinite Outer Boundary

$$\widehat{T_D} = Ae^{-z_D\sqrt{pF_{CD}}} \qquad \text{A7: 24}$$

Using the inner boundary and considering the temperature dependence on the pressure in the hydrate layer, we get the following general equation:

$$\widehat{T_D} = \left\{\frac{e^{-z_D\sqrt{pF_{CD}}}}{e^{-\sqrt{pF_{CD}}}}\right\} e_D \widehat{\varphi}_D \qquad \text{A7: 25}$$

$$\frac{d\widehat{T_D}}{dz_D} = \left\{\sqrt{pF_{CD}}\frac{e^{-z_D\sqrt{pF_{CD}}}}{e^{-\sqrt{pF_{CD}}}}\right\} e_D \widehat{\varphi}_D \qquad \text{A7: 26}$$

At the crossflow point, the above differential is:

$$\frac{d\widehat{T_D}}{dz_D} = \left[\sqrt{pF_{CD}}\right] e_D \widehat{\varphi}_D \qquad \text{A7: 27}$$

$$\frac{d\widehat{T_D}}{dz_D} = \widehat{\dot{Q}_{pD}} e_D \widehat{\varphi}_D \qquad \text{A7: 28}$$

The general dimensionless heat leakage rate is given by:

$$\gamma_{De} = \left\{\lambda \frac{1}{h_d k\left[\rho_t\left(\frac{k_r}{\eta}\right)_t\right]}\left[\frac{dT_{eq}}{dp}\right]\frac{r_w^2}{h^2}\right\}\widehat{\dot{Q}_{pD}} = e_D\widehat{\dot{Q}_{pD}} \qquad \text{A7: 29}$$

This could be incorporated in the Laplace transformed diffusivity equation and the solution derived. This makes the use of the Laplace transformation for such problems very useful.

Hence,

$$\beta = r_D\sqrt{S_D p + e_D\widehat{\dot{Q}_{pD}}} \qquad \text{A7: 30}$$

Appendix 8: Boltzmann Transformation of Diffusivity Equation in Class 3 Gas Hydrates

$$\frac{\partial^2 \varphi_D}{\partial {r_D}^2} + \frac{1}{r_D}\frac{\partial \varphi_D}{\partial r_D} = S_D \frac{\partial \varphi_D}{\partial t_{Dw}} \quad \text{A8: 1}$$

The similarity variable for the Boltzmann transformation is given below:

$$v_D^2 = S_D \frac{r_D^2}{4t_{Dw}} \quad \text{A8: 2}$$

Inserting the above transformations into the diffusivity equation results to the following:

$$\frac{\partial^2 \varphi_D}{\partial {v_D}^2} + \left(\frac{1}{v_D} + 2v_D\right)\frac{\partial \varphi_D}{\partial v_D} = 0 \quad \text{A8: 3}$$

Note that other representations of the transformed diffusivity equation exist with the similarity variable defined earlier, however; the solutions to the diffusivity equation are the same.

By introducing the parameter below and separating variables, the general solution to the transient pseudo-pressure can be derived.

$$y = \frac{d\varphi_D}{dv_D} \quad \text{A8: 4}$$

The general solution is hence:

$$\varphi_D = B\int_{v_D}^{\infty} \frac{e^{-{v_D}^2}}{v_D} dv_D = \frac{B}{2}\int_u^{\infty} \frac{e^{-u}}{u} du + C = \frac{B}{2}[E_1({v_D}^2)] \quad \text{A8: 5}$$

The derivative of the E_1-function as given by Abramowitz and Stegun [80] is:

$$\frac{dE_1({v_D}^2)}{d{v_D}^2} = -\frac{e^{-{v_D}^2}}{{v_D}^2} \quad \text{A8: 6}$$

General Solution for negligible heat influx (Exponential Integral Function)

$$\varphi_D = \frac{B}{2}[E_1({v_D}^2)] \quad \text{A8: 7}$$

General Solution for Finite Reservoirs Using the Image Well Theory

The well image theory proposed by [41] is the most widely used method in reservoir engineering to investigate the influence of sealing faults and recharge at reservoir boundaries. The method simply involves the application of the superposition principle of the pressure drop from an image well opposite the production well where the boundary is located. With this method, multiple boundaries can be incorporated at different distances from the producing well and hence the reservoir response estimated. Using the line source image well theory with constant rate inner boundary, the general well response can be defined thus [41], [81]:

$$\varphi_D = \varphi_{D,pumped} \pm \sum_{i=1}^{n} \varphi_{Dimage,i} \quad \text{A8: 8}$$

$$\varphi_D = \frac{B}{2}\left[E_1({v_D}^2) \pm \sum_{i=1}^{n} E_1\left(\frac{S_D(2l_{D,i} - r_D)^2}{4t_{Dw}}\right)\right] \quad \text{A8: 9}$$

$2l_D$ denotes the dimensionless distance between the producing well and the image well for the boundary in question. For a recharging image well (constant pressure outer boundary), the negative sign is valid and for no-flow boundaries (sealing boundary), the plus sign is valid. Note that using the image well, theory, the inner boundary conditions in the producing well are still imposed. Methods of incorporating multiple boundaries have also been given by [41], [81] however; reservoir responses with just single boundaries at different distances from the producing well will be developed using the similarity solutions. Solutions for confined reservoirs will be given using the Laplace transform.

Finite Wellbore Image Well Theory for Single Boundary Reservoirs

The model presented by [41] describes the line source solution of the reservoir response which needs modifications when handling finite wellbore problems. In a similar manner, we develop the models for the finite wellbore case for both CPIB and CRIB. The general solution for this case is given thus:

$$\varphi_D = \left[AE_1({v_D}^2) + BE_1\left(\frac{S_D(2l_D - r_D)^2}{4t_{Dw}}\right)\right] \quad \text{A8: 10}$$

The image well theory can also be applied to the Laplace domain solutions to investigate the effects of a single boundary on the reservoir response, as also seen in the works of [82]. The general equation for the image well theory in Laplace domain is given thus:

$$\hat{\varphi}_D = AK_0\left(r_D\sqrt{s}\right) + BK_0\left((2l_D - r_D)\sqrt{s}\right) \quad \text{A8: 11}$$

Case 1: Constant Pressure Inner Boundary

Case 1a: CPIB and CPOB

CPIB

$$\varphi_D = 1 = AE_1\left(S_D\frac{1}{4t_{Dw}}\right) + BE_1\left(S_D\frac{(2l_D-1)^2}{4t_{Dw}}\right) \quad \text{A8: 12}$$

CPOB

$$\varphi_D = 0 = AE_1\left(S_D\frac{{l_D}^2}{4t_{Dw}}\right) + BE_1\left(S_D\frac{{l_D}^2}{4t_{Dw}}\right) \quad \text{A8: 13}$$

$$A = -B$$

$$\varphi_D = \left[\frac{E_1\left(S_D\frac{{r_D}^2}{4t_{Dw}}\right) - E_1\left(\frac{S_D(2l_D-r_D)^2}{4t_{Dw}}\right)}{E_1\left(S_D\frac{1}{4t_{Dw}}\right) - E_1\left(S_D\frac{(2l_D-1)^2}{4t_{Dw}}\right)}\right] \quad \text{A8: 14}$$

In Laplace Domain, this is given thus:

$$\hat{\varphi}_D = \frac{\sqrt{s}}{p}\left\{\frac{K_0\left(r_D\sqrt{s}\right) - K_0\left((2l_D - r_D)\sqrt{s}\right)}{K_0\left(\sqrt{s}\right) - K_0\left((2l_D-1)\sqrt{s}\right)}\right\} \quad \text{A8: 15}$$

Case 1b: CPIB and NFB

CPIB

$$\varphi_D = 1 = AE_1\left(S_D\frac{1}{4t_{Dw}}\right) + BE_1\left(S_D\frac{(2l_D-1)^2}{4t_{Dw}}\right) \quad \text{A8: 16}$$

NFB

$$\left(\frac{d\varphi_D}{dr_D}\right)_{r_D} = -A\left[\frac{2S_D r_D}{4t_{Dw}}\frac{e^{-\left(S_D\frac{r_D{}^2}{4t_{Dw}}\right)}}{\left(S_D\frac{r_D{}^2}{4t_{Dw}}\right)}\right] + B\left[\frac{2S_D(2l_D-r_D)}{4t_{Dw}}\frac{e^{-\left(\frac{S_D(2l_D-r_D)^2}{4t_{Dw}}\right)}}{\left(\frac{S_D(2l_D-r_D)^2}{4t_{Dw}}\right)}\right] \quad \text{A8: 17}$$

$$\left(\frac{d\varphi_D}{dr_D}\right)_{r_D=l_D} = 0 = -A\left[2\frac{e^{-\left(S_D\frac{l_D{}^2}{4t_{Dw}}\right)}}{l_D}\right] + B\left[2\frac{e^{-\left(S_D\frac{l_D{}^2}{4t_{Dw}}\right)}}{l_D}\right] \quad \text{A8: 18}$$

$A = B$

$$\varphi_D = \left[\frac{E_1\left(S_D\frac{r_D{}^2}{4t_{Dw}}\right)+E_1\left(\frac{S_D(2l_D-r_D)^2}{4t_{Dw}}\right)}{E_1\left(S_D\frac{1}{4t_{Dw}}\right)+E_1\left(S_D\frac{(2l_D-1)^2}{4t_{Dw}}\right)}\right] \quad \text{A8: 19}$$

In Laplace domain, this is given thus:

$$\widehat{\varphi}_D = \frac{\sqrt{s}}{p}\left\{\frac{K_0\left(r_D\sqrt{s}\right)+K_0\left((2l_D-r_D)\sqrt{s}\right)}{K_0\left(\sqrt{s}\right)+K_0\left((2l_D-1)\sqrt{s}\right)}\right\} \quad \text{A8: 20}$$

Case 2: Constant Rate Inner Boundary

Case 2a: CRIB and CPOB

CPOB

$$\varphi_D = 0 = AE_1\left(-S_D\frac{r_{eD}{}^2}{4t_{Dw}}\right) + BE_1\left(-S_D\frac{l_D{}^2}{4t_{Dw}}\right) \quad \text{A8: 21}$$

$A = -B$

$$-r_D\left(\frac{d\varphi_D}{dr_D}\right)_{r_D} = r_D A\left\{\left[2\frac{e^{-\left(S_D\frac{r_D{}^2}{4t_{Dw}}\right)}}{r_D}\right] + \left[2\frac{e^{-\left(\frac{S_D(2l_D-r_D)^2}{4t_{Dw}}\right)}}{(2l_D-r_D)}\right]\right\} \quad \text{A8: 22}$$

$$1 = -r_D\frac{d\varphi_D}{dr_D} = \dot{m}_{tD} = 2A\left\{e^{-\left(S_D\frac{1}{4t_{Dw}}\right)} + \left[\frac{e^{-\left(\frac{S_D(2l_D-1)^2}{4t_{Dw}}\right)}}{(2l_D-1)}\right]\right\} \quad \text{A8: 23}$$

$$A = \frac{1}{2}\frac{1}{\left\{e^{-\left(S_D\frac{1}{4t_{Dw}}\right)}+\left[\frac{e^{-\left(\frac{S_D(2l_D-1)^2}{4t_{Dw}}\right)}}{(2l_D-1)}\right]\right\}} \quad \text{A8: 24}$$

If the well is produced long enough and the distance to the boundary is relatively far from the wellbore, the above coefficient takes the line source approximation, i.e.:

$$A = \frac{1}{2}\frac{1}{\left\{e^{-\left(S_D\frac{1}{4t_{Dw}}\right)}+\left[\frac{e^{-\left(\frac{S_D(2l_D-1)^2}{4t_{Dw}}\right)}}{(2l_D-1)}\right]\right\}} \approx \frac{1}{2} \qquad \text{A8: 25}$$

$$\varphi_D = \frac{1}{2}\frac{1}{\left\{e^{-\left(S_D\frac{1}{4t_{Dw}}\right)}+\left[\frac{e^{-\left(\frac{S_D(2l_D-1)^2}{4t_{Dw}}\right)}}{(2l_D-1)}\right]\right\}}\left[E_1\left(S_D\frac{{r_D}^2}{4t_{Dw}}\right)-E_1\left(\frac{S_D(2l_D-r_D)^2}{4t_{Dw}}\right)\right] \qquad \text{A8: 26}$$

In Laplace domain, this is given thus:

$$\widehat{\varphi}_D = \frac{1}{p\sqrt{s}}\left\{\frac{K_0(r_D\sqrt{s})-K_0\left((2l_D-r_D)\sqrt{s}\right)}{K_1(\sqrt{s})+K_1\left((2l_D-1)\sqrt{s}\right)}\right\} \qquad \text{A8: 27}$$

Case 2b: CRIB and NFB

By applying the same methodology we get the following representation for the reservoir response:

$$\varphi_D = \frac{1}{2}\frac{1}{\left\{e^{-\left(S_D\frac{1}{4t_{Dw}}\right)}+\left[\frac{e^{-\left(\frac{S_D(2l_D-1)^2}{4t_{Dw}}\right)}}{(2l_D-1)}\right]\right\}}\left[E_1\left(S_D\frac{{r_D}^2}{4t_{Dw}}\right)+E_1\left(\frac{S_D(2l_D-r_D)^2}{4t_{Dw}}\right)\right] \qquad \text{A8: 28}$$

In Laplace domain, this is given thus:

$$\widehat{\varphi}_D = \frac{1}{p\sqrt{s}}\left\{\frac{K_0(r_D\sqrt{s})+K_0\left((2l_D-r_D)\sqrt{s}\right)}{K_1(\sqrt{s})-K_1\left((2l_D-1)\sqrt{s}\right)}\right\} \qquad \text{A8: 29}$$

Appendix 9: Definition of pseudo-gas relative permeability for rate and pressure transient analyses (MBM)

As defined earlier, the pseudo-pressure model is developed based on mass balance techniques, which could be split to different fluid components. In performing well test analysis for the multiphase system, such that effective permeability changes during production are quantified, it is important to break down the pseudo-pressure model for each phase such that the conventional pseudo-pressure model in gas reservoirs can be used. This is done thus:

$$\int_{p}^{p_i}\left(\mathrm{k}_{\mathrm{rg}}^{*}\right)\left(\frac{\rho_{\mathrm{g}}}{\eta_{\mathrm{g}}}\mathrm{dp}\right)=\int_{p}^{p_i}\mathrm{Udv} \qquad \text{A9: 1}$$

After integrating by parts we get:

$$\int_{p}^{p_i}\left(\mathrm{k}_{\mathrm{rg}}^{*}\right)\left(\frac{\rho_{\mathrm{g}}}{\eta_{\mathrm{g}}}\mathrm{dp}\right)=\mathrm{k}_{\mathrm{rg}}^{*}(\mathrm{p})\int_{p}^{p_i}\frac{\rho_{\mathrm{g}}}{\eta_{\mathrm{g}}}\mathrm{dp} \qquad \text{A9: 2}$$

Where,

$$\mathrm{k}_{\mathrm{rg}}^{*}(\mathrm{p})=\left\{\mathrm{k}_{\mathrm{rg}}^{*}\Big|_{p}^{p_i}-\frac{\int_{p}^{p_i}\left[\left(\int_{p}^{p_i}\frac{\rho_{\mathrm{g}}}{\eta_{\mathrm{g}}}\mathrm{dp}\right)\mathrm{d}\left(\mathrm{k}_{\mathrm{rg}}^{*}\right)\right]dp}{\int_{p}^{p_i}\frac{\rho_{\mathrm{g}}}{\eta_{\mathrm{g}}}\mathrm{dp}}\right\} \qquad \text{A9: 3}$$

The pseudo-pressure integral function for the gas phase reduces then to:

$$\int_{p}^{p_i}\left(\mathrm{k}_{\mathrm{rg}}^{*}\right)\left(\frac{\rho_{\mathrm{g}}}{\eta_{\mathrm{g}}}\mathrm{dp}\right)=\mathrm{k}_{\mathrm{rg}}^{*}(\mathrm{p})\int_{p}^{p_i}\frac{\rho_{\mathrm{g}}}{\eta_{\mathrm{g}}}\mathrm{dp}=\mathrm{k}_{\mathrm{rg}}^{*}(\mathrm{p})\rho_{\mathrm{g,st}}\int_{p}^{p_i}\frac{\mathrm{dp}}{B_{\mathrm{g}}\eta_{\mathrm{g}}} \qquad \text{A9: 4}$$

With the above approximate solution of the pseudo-pressure integral, rate transient analysis for the gas phase becomes easier as the approximate solution to the pseudo-pressure integral is very much easier to compute.

Note that for ideal reservoir response, the relative permeability term is pressure independent, i.e.:

$$\int_{p}^{p_i}\left(\mathrm{k}_{\mathrm{rg}}^{*}\right)\left(\frac{\rho_{\mathrm{g}}}{\eta_{\mathrm{g}}}\mathrm{dp}\right)=\left(\mathrm{k}_{\mathrm{rg}}^{*}\right)\int_{p}^{p_i}\frac{\rho_{\mathrm{g}}}{\eta_{\mathrm{g}}}\mathrm{dp} \qquad \text{A9: 5}$$

Appendix 10: Apparent Effective Gas Permeability for Multiphase Flow in Gas Hydrates and Derivatives

Kome et al [48] introduced the equivalent average effective permeability (or just apparent effective permeability) for heterogeneous reservoir behavior which is also applied here. The use of this model is applicable to gas class 3 gas hydrate reservoirs with negligible heat flux through conduction. The gas phase is analyzed. The methodology applied by [48] is based on the derivative analysis used for reservoir diagnosis. Before addressing the model of the equivalent average effective permeability, the methods used in derivative analysis are addressed first.

Rate and Pressure Transient Derivatives

It is simply the differential of the solutions presented for rate or pressure transient with respect to time and is usually computed using the finite difference quotient method as given by [22], [83] and can be computed for RTA and PTA thus:

$$\text{Der (RTA)} = t_{Dw}\frac{d\left(\frac{1}{\dot{m}_{tD}}\right)}{dt_{Dw}} = \frac{d\left(\frac{1}{\dot{m}_{tD}}\right)}{dlnt_{Dw}} \qquad \text{A10: 1}$$

$$\text{Der(PTA)} = t_{Dw}\frac{d(\varphi_D)}{dt_{Dw}} = \frac{d(\varphi_D)}{dlnt_{Dw}} \qquad \text{A10: 2}$$

Bourdet Differentiation Algorithm

$$\text{Der (PTA)} = \frac{\left\{\frac{\left[(\varphi_D)_{n+2}-(\varphi_D)_{n+1}\right]}{\left[(lnt_{Dw})_{n+2}-(lnt_{Dw})_{n+1}\right]}\left[(lnt_{Dw})_{n+1}-(lnt_{Dw})_n\right]\right\}+\left\{\frac{\left[(\varphi_D)_{n+1}-(\varphi_D)_n\right]}{\left[(lnt_{Dw})_{n+1}-(lnt_{Dw})_n\right]}\left[(lnt_{Dw})_{n+2}-(lnt_{Dw})_{n+1}\right]\right\}}{\left[(lnt_{Dw})_{n+2}-(lnt_{Dw})_{n+1}\right]+\left[(lnt_{Dw})_{n+1}-(lnt_{Dw})_n\right]} \qquad \text{A10: 3}$$

$$\text{Der (RTA)} = \frac{\left\{\frac{\left[\left(\frac{1}{\dot{m}_{tD}}\right)_{n+2}-\left(\frac{1}{\dot{m}_{tD}}\right)_{n+1}\right]}{\left[(lnt_{Dw})_{n+2}-(lnt_{Dw})_{n+1}\right]}\left[(lnt_{Dw})_{n+1}-(lnt_{Dw})_n\right]\right\}+\left\{\frac{\left[\left(\frac{1}{\dot{m}_{tD}}\right)_{n+1}-\left(\frac{1}{\dot{m}_{tD}}\right)_n\right]}{\left[(lnt_{Dw})_{n+1}-(lnt_{Dw})_n\right]}\left[(lnt_{Dw})_{n+2}-(lnt_{Dw})_{n+1}\right]\right\}}{\left[(lnt_{Dw})_{n+2}-(lnt_{Dw})_{n+1}\right]+\left[(lnt_{Dw})_{n+1}-(lnt_{Dw})_n\right]} \qquad \text{A10: 4}$$

The smoothness of the Bourdet derivative above is dependent on the consistency of the time spacing and would hence show a significant deviation from the exact derivative solutions.

Exact Derivative

The exact derivative of the pressure transient solutions can be represented in terms of the generalized incomplete gamma function given in Appendix 18 as will be seen later in the solutions to the diffusivity equation.

$$\frac{d\Gamma(a,\mu;\beta)}{dt_{Dw}} = \frac{d\Gamma(a,\mu;\beta)}{dx} * \frac{dx}{dt_{Dw}} = -\frac{1}{x^{1-a}}\exp\left(-x-\frac{\beta^2}{4x}\right) * \frac{dx}{dt_{Dw}} \qquad \text{A10: 5}$$

$$\text{Der (PTA)} = t_{Dw}\frac{d\Gamma(a,\mu;\beta)}{dt_{Dw}} = -\frac{t_{Dw}}{x^{1-a}}\exp\left(-x-\frac{\beta^2}{4x}\right) * \frac{dx}{dt_{Dw}} \qquad \text{A10: 6}$$

Conventionally, β represents the influx of mass or increase in saturation in the system. Hence, for all values of $\beta>0$, the system characterizes an increase in saturation which is also reflected in the effective permeability of the phases.

To address the changes in the effective permeability during production, the gas pseudo-pressure normalized rate representation is used and the derivative during infinite acting radial flow could be represented thus:

$$\Delta\left(\frac{\Delta\varphi}{Q_{g,st}}\right)=\frac{\Delta(\varphi RPI(t))}{\Delta lnt}=\frac{0.5p_{st}}{\pi hk^{*}_{g,avg}T_{st}}[\ln(t_2)-\ln(t_1)] \quad \text{A10: 7}$$

$$Der=\frac{\Delta\left(\frac{\Delta\varphi}{Q_{g,st}}\right)}{\Delta lnt}=\frac{0.5p_{st}}{\pi hk^{*}_{g,avg}T_{st}} \quad \text{A10: 8}$$

$$k^{*}_{g,avg}=\frac{0.5p_{st}}{\pi hDerT_{st}} \quad \text{A10: 9}$$

$$k^{*}_{g,avg}=\frac{k^{*}_{g2}k^{*}_{g1}[\ln(t_2)-\ln(t_1)]}{k^{*}_{g1}\left[\ln\left(\frac{\left[\rho_t\left(\frac{k_r}{\eta}\right)_t\right]_{id}\ t_2}{r_w{}^2(\rho c_T)_{eff,id}S_{D2}}\right)+0.80907\right]-k^{*}_{g2}\left[\ln\left(\frac{\left[\rho_t\left(\frac{k_r}{\eta}\right)_t\right]_{id}\ t_1}{r_w{}^2(\rho c_T)_{eff,id}S_{D1}}\right)+0.80907\right]} \quad \text{A10: 10}$$

The above equation could be simplified by introducing an apparent dimensionless pseudo-skin component thus:

$$k^{*}_{g,avg}=k^{*}_{g1}\frac{\ln\left(\frac{t_2}{t_1}\right)}{s_{Da}+\ln\left[\left(\frac{t_2}{S_{D2}}\right)^{\frac{k^{*}_{g1}}{k^{*}_{g2}}}*\frac{S_{D1}}{t_1}\right]} \quad \text{A10: 11}$$

Where,

$$s_{Da}=\left(\frac{k^{*}_{g1}}{k^{*}_{g2}}-1\right)\left[\ln\left(\frac{\left[\rho_t\left(\frac{k_r}{\eta}\right)_t\right]_{id}}{r_w{}^2(\rho c_T)_{eff,id}}\right)+0.80907\right] \quad \text{A10: 12}$$

Under ideal conditions, $k_{g1}{}^{*}=k_{g2}{}^{*}$ and $S_{D1}=S_{D2}$, hence:

$$k^{*}_{g,avg}=k^{*}_{g1}\frac{\ln\left(\frac{t_2}{t_1}\right)}{\ln\left(\frac{t_2}{t_1}\right)}=k^{*}_{g1} \quad \text{A10: 13}$$

The derivative is therefore a very powerful tool in addressing changes in reservoir behavior or permeability which has also been addressed in detail in the works of [84], [85], [86], [65], [66] , whereby derivative plots have been used to derive reservoir parameters with the application of the Tiabs Direct Synthesis (TDS) Technique.

Appendix 11: Multiphase Crossflow Storativity Transformations

To account for the storativity of the two layers involved in crossflow behavior, the storativity ratio as given by Warren and Root [87] is usually used. In a similar manner, the storativity ratio for the hydrate and free fluid layer are developed here.

$$\omega^* + (1-\omega^*) = \frac{a_v}{a_h+a_v} + \frac{a_h}{a_h+a_v} = 1 \qquad \text{A11: 1}$$

The storativity in the crossflow layer is given thus:

$$\frac{1}{a_v} = (1-\omega^*)\left(\frac{1}{a_h} + \frac{1}{a_v}\right) \qquad \text{A11: 2}$$

$$\frac{1}{a_v} = (1-\omega)\left[\left(\frac{a_h+a_v}{a_h a_v}\right)\right]_i \qquad \text{A11: 3}$$

Similarly, the same can be done for the producing layer thus:

$$\frac{1}{a_h} = \omega^*\left(\frac{1}{a_h} + \frac{1}{a_v}\right) \qquad \text{A11: 4}$$

$$\frac{1}{a_h} = \omega\left[\left(\frac{a_h+a_v}{a_h a_v}\right)\right]_i \qquad \text{A11: 5}$$

Where,

$$\omega^* = \frac{a_v}{a_h+a_v} \qquad \text{A11: 6}$$

$$(1-\omega^*) = \frac{a_h}{a_h+a_v} \qquad \text{A11: 7}$$

Storativity Ratio

$$(1-\omega) = (1-\omega^*)\frac{\left[\left(\frac{a_h+a_v}{a_h a_v}\right)\right]}{\left[\left(\frac{a_h+a_v}{a_h a_v}\right)\right]_i} = \frac{1}{a_v}\frac{1}{\left[\left(\frac{a_h+a_v}{a_h a_v}\right)\right]_i} = \frac{[a_v]_i}{a_v}\left[\left(\frac{a_h}{a_h+a_v}\right)\right]_i \qquad \text{A11: 8}$$

$$\omega = \omega^*\frac{\left[\left(\frac{a_h+a_v}{a_h a_v}\right)\right]}{\left[\left(\frac{a_h+a_v}{a_h a_v}\right)\right]_i} = \frac{1}{a_h}\frac{1}{\left[\left(\frac{a_h+a_v}{a_h a_v}\right)\right]_i} = \frac{[a_h]_i}{a_h}\left[\left(\frac{a_v}{a_h+a_v}\right)\right]_i \qquad \text{A11: 9}$$

$$\frac{a_h}{a_v} = \frac{(1-\omega)}{\omega} \qquad \text{A11: 10}$$

Interporosity Flow Coefficient

$$\delta_D = \frac{r_w^2}{\Delta z_2 \Delta z_1}\frac{k_{v2}}{k_{h1}} \qquad \text{A11: 11}$$

Appendix 12: Analytical Solutions to Diffusivity Problems in Normally Pressured Gas Hydrates

Diffusivity Equation with Negligible Heat Influx

$$\frac{\partial^2 \varphi_D}{\partial {r_D}^2} + \frac{1}{r_D}\frac{\partial \varphi_D}{\partial r_D} = S_D \frac{\partial \varphi_D}{\partial t_{Dw}} \quad \text{A12: 1}$$

The solutions to the above equation will be presented using the Boltzmann transformation (similarity solutions)

Diffusivity Equation with considerable Heat Influx

$$\frac{\partial^2 \varphi_D}{\partial {r_D}^2} + \frac{1}{r_D}\frac{\partial \varphi_D}{\partial r_D} - \gamma_{De}\varphi_D = S_D \frac{\partial \varphi_D}{\partial t_{Dw}} \quad \text{A12: 2}$$

Diffusivity Equation with Kinetic Model

$$\frac{\partial^2 \varphi_D}{\partial {r_D}^2} + \frac{1}{r_D}\frac{\partial \varphi_D}{\partial r_D} - \gamma_{Dk}\varphi_D = S_{Dk} \frac{\partial \varphi_D}{\partial t_{Dw}} \quad \text{A12: 3}$$

Case 1: Constant Pressure Inner Boundary Solutions

General Similarity Solution

$$\varphi_D = \frac{B}{2} E_1({v_D}^2) = \frac{B}{2} E_1\left(\frac{r_D^2}{4t_{Dw}} S_D\right) \quad \text{A12: 4}$$

Case 1a: Infinite Acting Reservoirs: Constant Pressure Inner Boundary Conditions

$\varphi_D(r_D, t_{Dw}) = 1$ at r_D=1 and t_{Dw}>0 $v_D^2 = \frac{S_D}{4t_{Dw}}$

For the above inner boundary condition, the constant B can be derived thus:

$$\frac{1}{E_1\left(\frac{1}{4t_{Dw}}\right)} = \frac{B}{2} \quad \text{A12: 5}$$

Dimensionless Pseudo-Pressure

$$\varphi_D(r_D, t_{Dw}) = \frac{\varphi(r,t) - \varphi_i}{\varphi_{wf} - \varphi_i} = \frac{\left[E_1\left(S_D \frac{r_D^2}{4t_{Dw}}\right)\right]}{\left[E_1\left(\frac{S_D}{4t_{Dw}}\right)\right]} \quad \text{A12: 6}$$

Transient Rate

$$\dot{m}_{tD} = -r_D \frac{d\varphi_D}{dr_D} = -2v_D^2 \frac{d\varphi_D}{dv_D^2} = -2v_D^2 \frac{1}{\left[E_1\left(\frac{S_D}{4t_{Dw}}\right)\right]} \frac{d\left[[E_1(v_D^2)]\right]}{dv_D^2} \quad \text{A12: 7}$$

Using the differential of the E_1-function as given by [80] we get:

$$\dot{m}_{tD} = \frac{2e^{-v_D^2}}{\left[E_1\left(\frac{S_D}{4t_{Dw}}\right)\right]} \quad \text{A12: 8}$$

Solutions in Laplace Domain

$$\hat{\varphi}_D = c_1 I_o(\beta) + c_2 K_o(\beta) \qquad \text{A12: 9}$$

For the infinite acting system, the constants are defined by the following boundary conditions:

$r_D \rightarrow \infty$ $\quad c_1 = 0$

$r_D = 1$ $\quad \hat{\varphi}_D = \frac{1}{p}$ $\quad c_2 = \frac{1}{pK_o(\sqrt{s})}$

The dimensionless pseudo-pressure and rates are hence given by:

Dimensionless Pseudo-Pressure

$$\hat{\varphi}_D = \frac{K_o(r_D\sqrt{s})}{pK_o(\sqrt{s})} \qquad \text{A12: 10}$$

Dimensionless Flow rate

$$\hat{m}_{tD} = -r_D \frac{d\hat{\varphi}_D}{dr_D} = -r_D \frac{d\left(\frac{K_o(r_D\sqrt{s})}{pK_o(\sqrt{s})}\right)}{dr_D} \qquad \text{A12: 11}$$

The solution to the above function is given thus:

$$\hat{m}_{tD} = \frac{r_D\sqrt{s}K_1(r_D\sqrt{s})}{pK_o(\sqrt{s})} \qquad \text{A12: 12}$$

Note that the Laplace transformed variable s contains the heat conduction term (using the equilibrium model) or the hydrate dissociation rate (using the kinetic model). Due to the time dependence of the heat conduction term as given in Appendix 1 and Appendix 7, approximate solutions are usually used for small and large time intervals. However, using the Bourgeois and Horne [25] methodology of well test model recognition with Laplace space, the reservoir response using any of the heat flux models can be thoroughly investigated.

Rate Transient Plots in Laplace Domain

$\widehat{pm}_{tD}$ Versus $\frac{1}{p}$

$\hat{\varphi}_D p = \frac{K_o(r_D\lambda_D)}{K_o(\lambda_D)}$ Versus r_D

$$\text{Der} = \frac{\Delta\left(\frac{1}{\widehat{pm}_{tD}}\right)}{\Delta\left(\frac{1}{p}\right)} \quad \text{Versus} \quad \frac{1}{p}$$

A comparison of the rate transient solution in Laplace space using the methodology of [25] and other solutions including the similarity solution and the numerical Laplace inverse of the rate solutions as given by [64], [63] and [43] is depicted in Figure A12- 1.

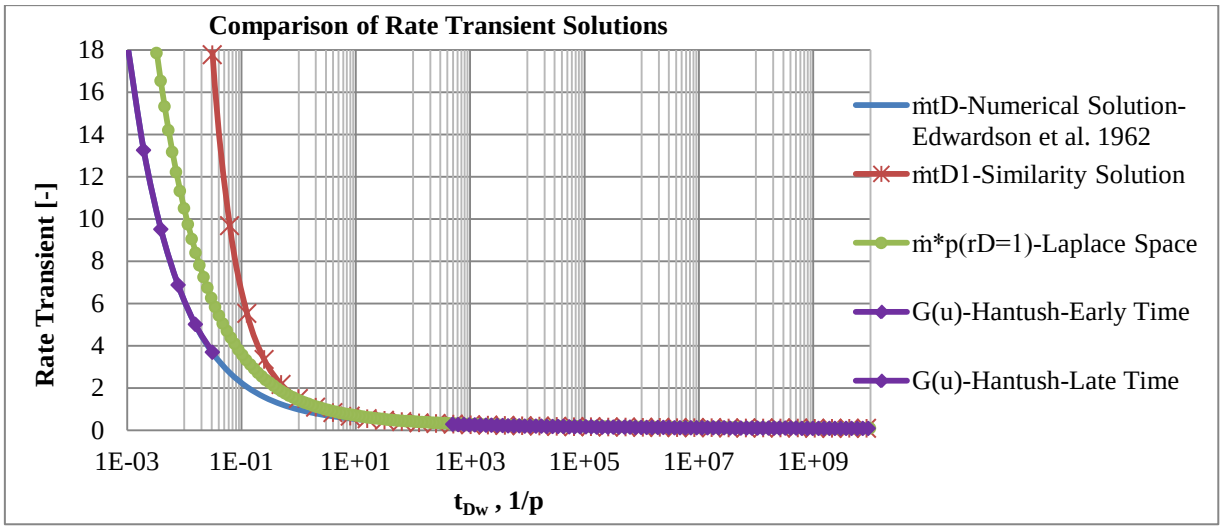

Figure A12- 1: Comparison of Rate Transient Solutions

From a look at the various representations, the Hantush [43] flowing well discharge function perfectly matches the numerical solutions given by Edwardson [63]. However, with a comparison of the late time approximations of both authors, a clear difference is seen.

The deviation in almost all models is seen in the early phase of production, which diminishes during late time periods. The derivative when using the similarity or the late time solutions of Hantush [43] perfectly match the derivative given by the Laplace domain method. However, for the purpose of well testing and for consistency, the approximate solutions presented by Edwardson [63] will be considered for analysis.

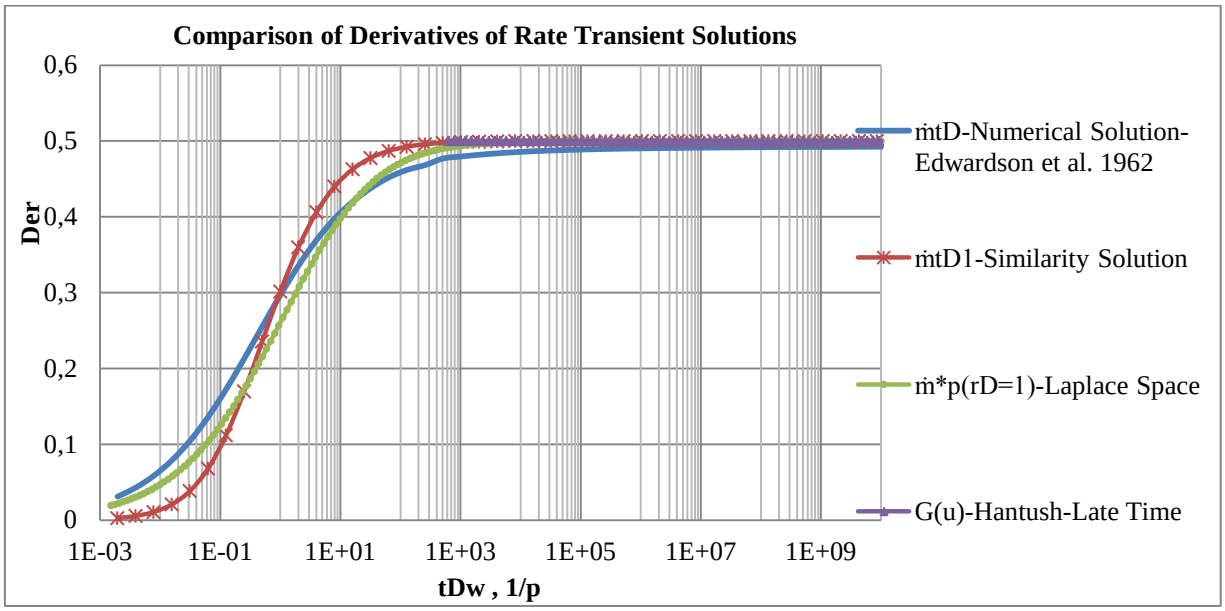

Figure A12- 2: Comparison of Derivatives of Rate Transient Solutions

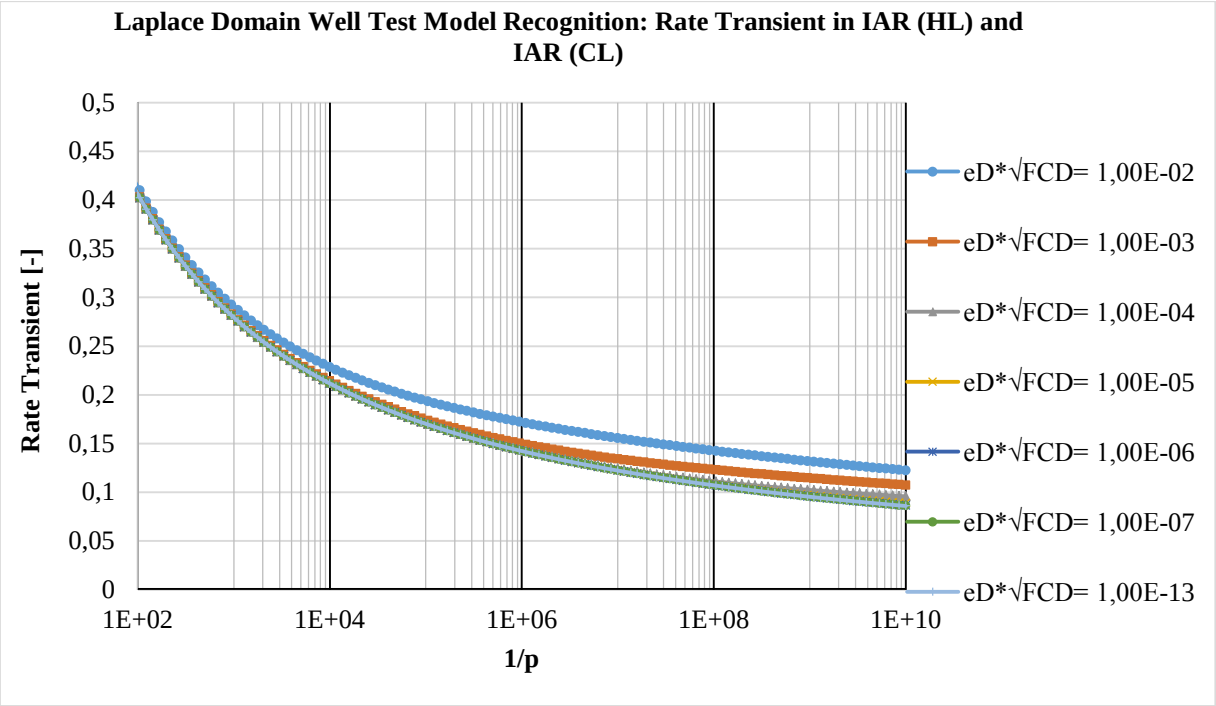

Figure A12- 3: Rate Transient in IAR (HL) and IAR (CL)

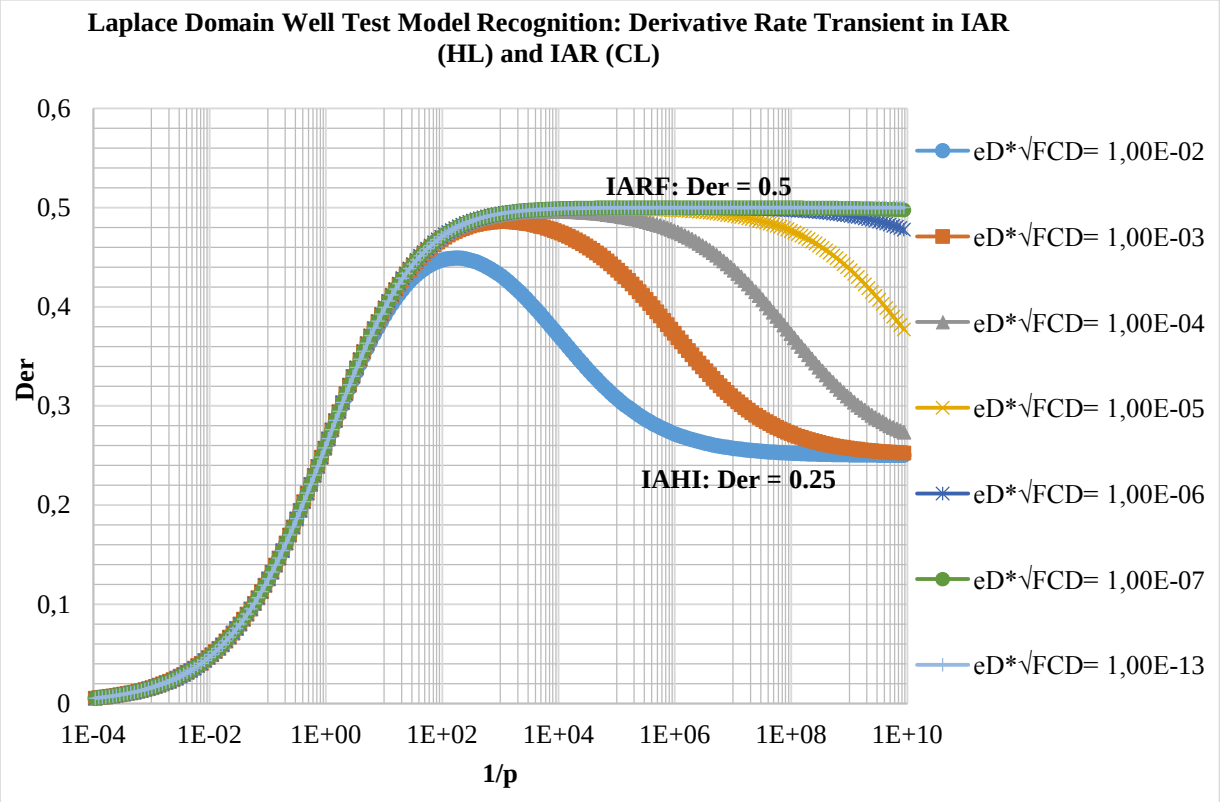

Figure A12- 4: Derivative Rate Transient in IAR (HL) and IAR (CL)

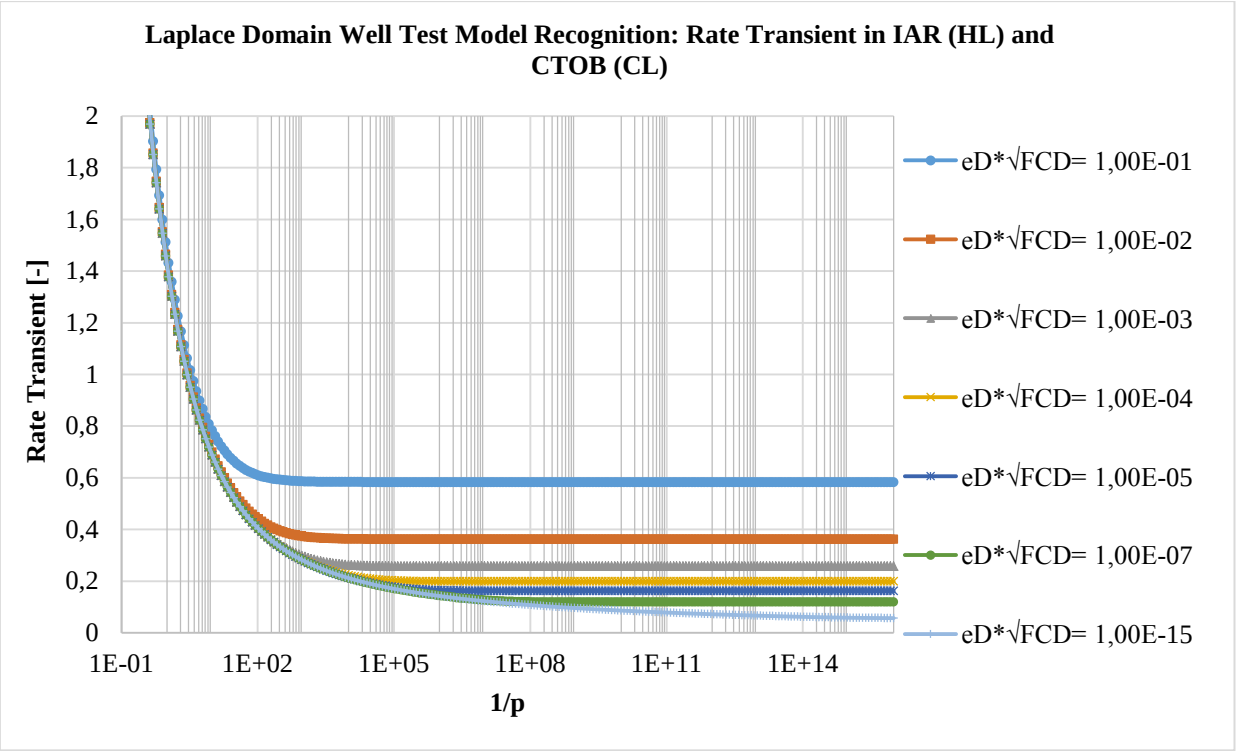

Figure A12- 5: Rate Transient in IAR (HL) and CTOB (CL)

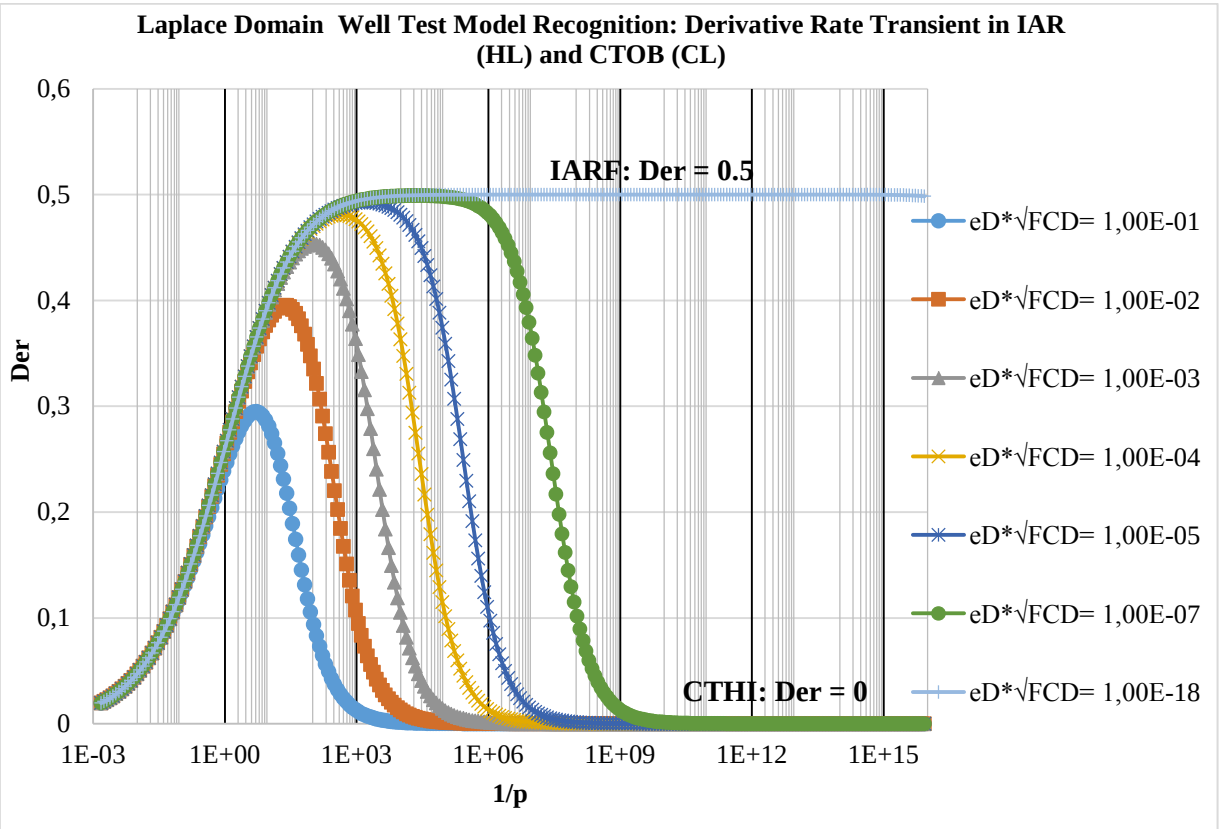

Figure A12- 6: Derivative Rate Transient in IAR (HL) and CTOB (CL)

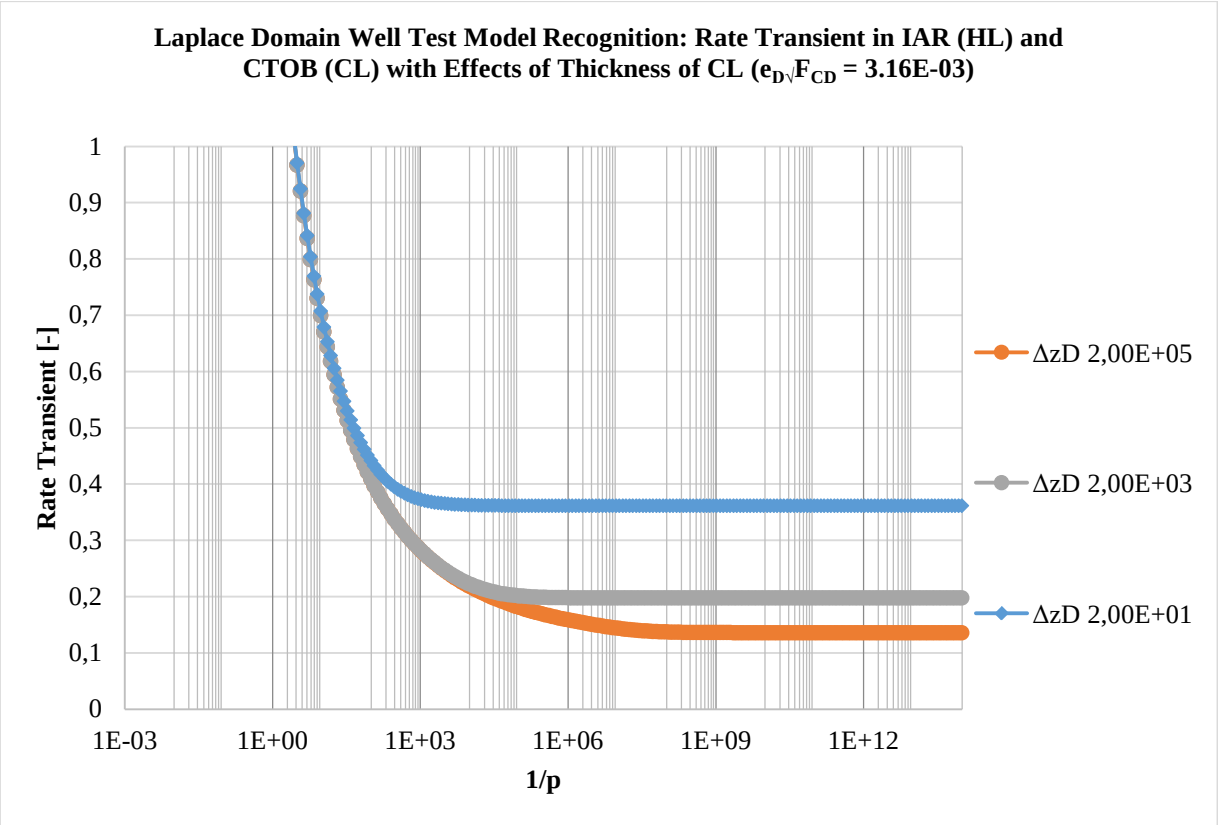

Figure A12- 7: Rate Transient in IAR (HL) and CTOB (CL) and Effects of Thickness of CL

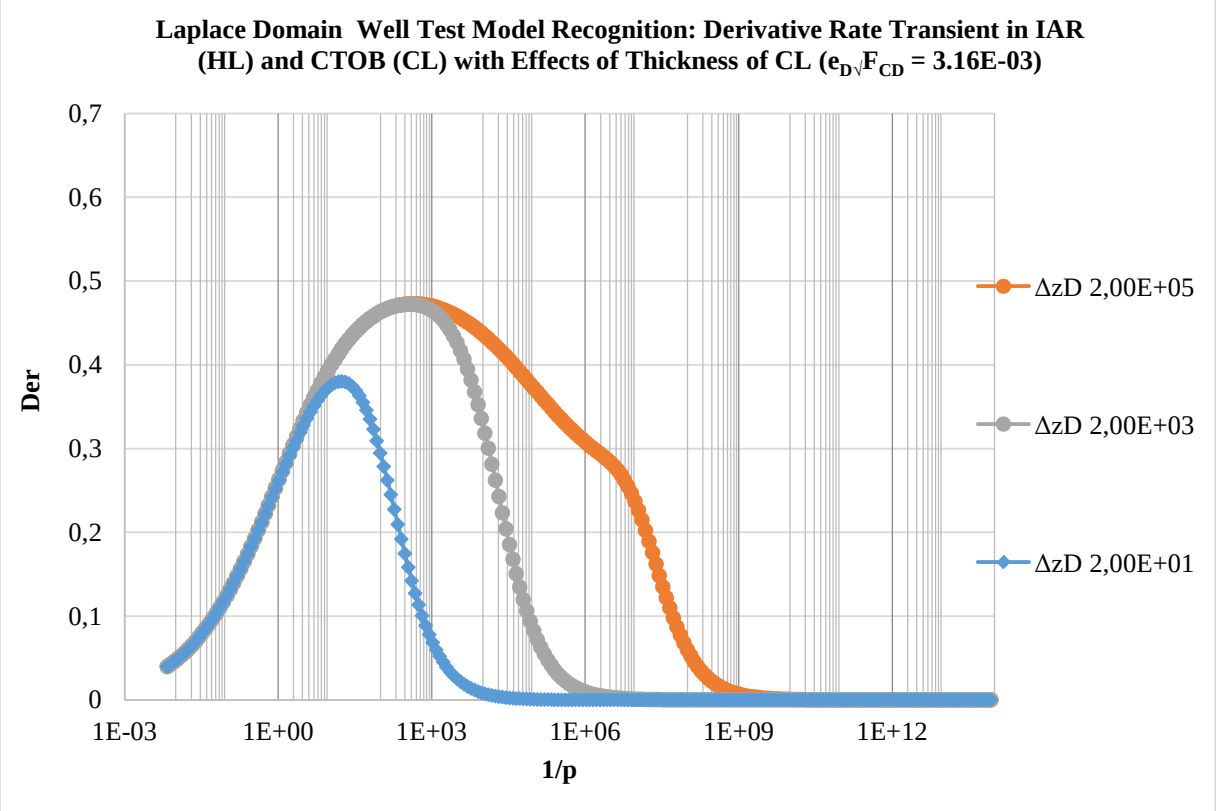

Figure A12- 8: Rate Transient Derivative in IAR (HL) and CTOB (CL) and Effects of Thickness of CL

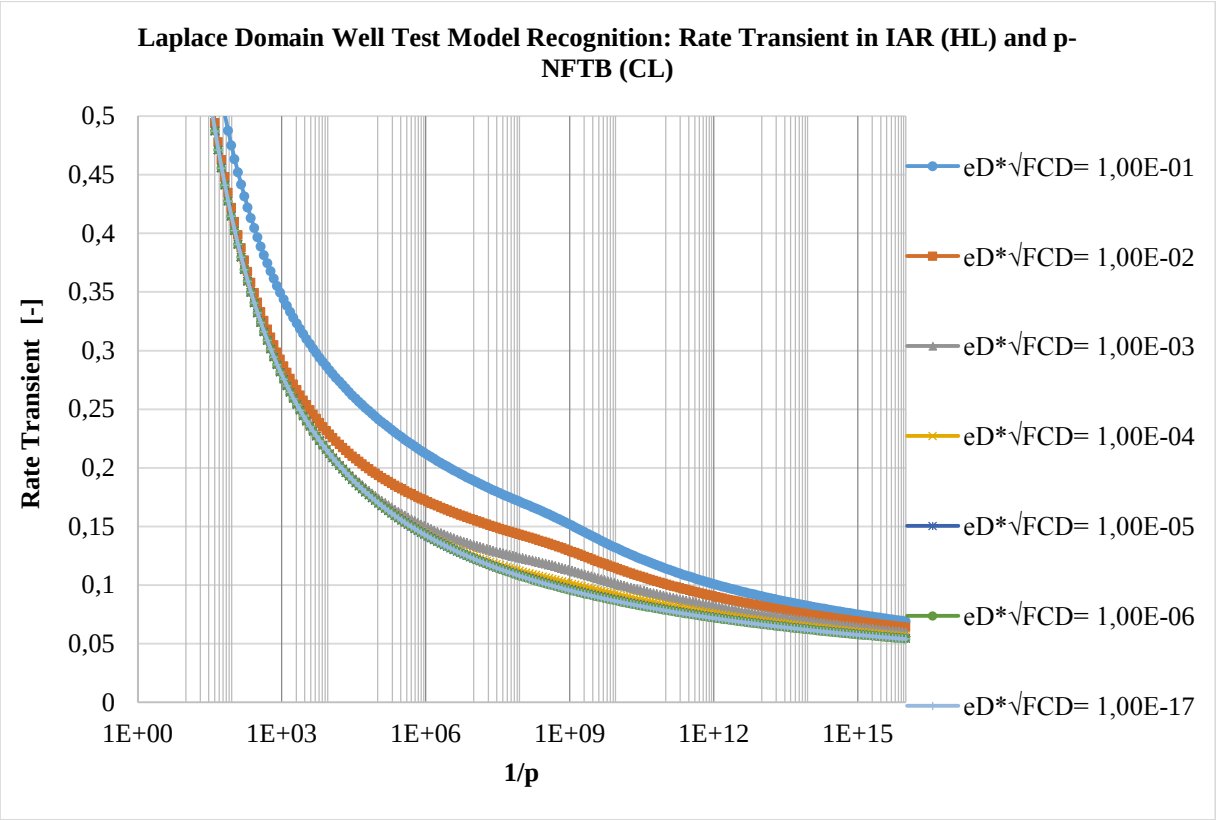

Figure A12- 9: Rate Transient in IAR (HL) and p-NFTB (CL)

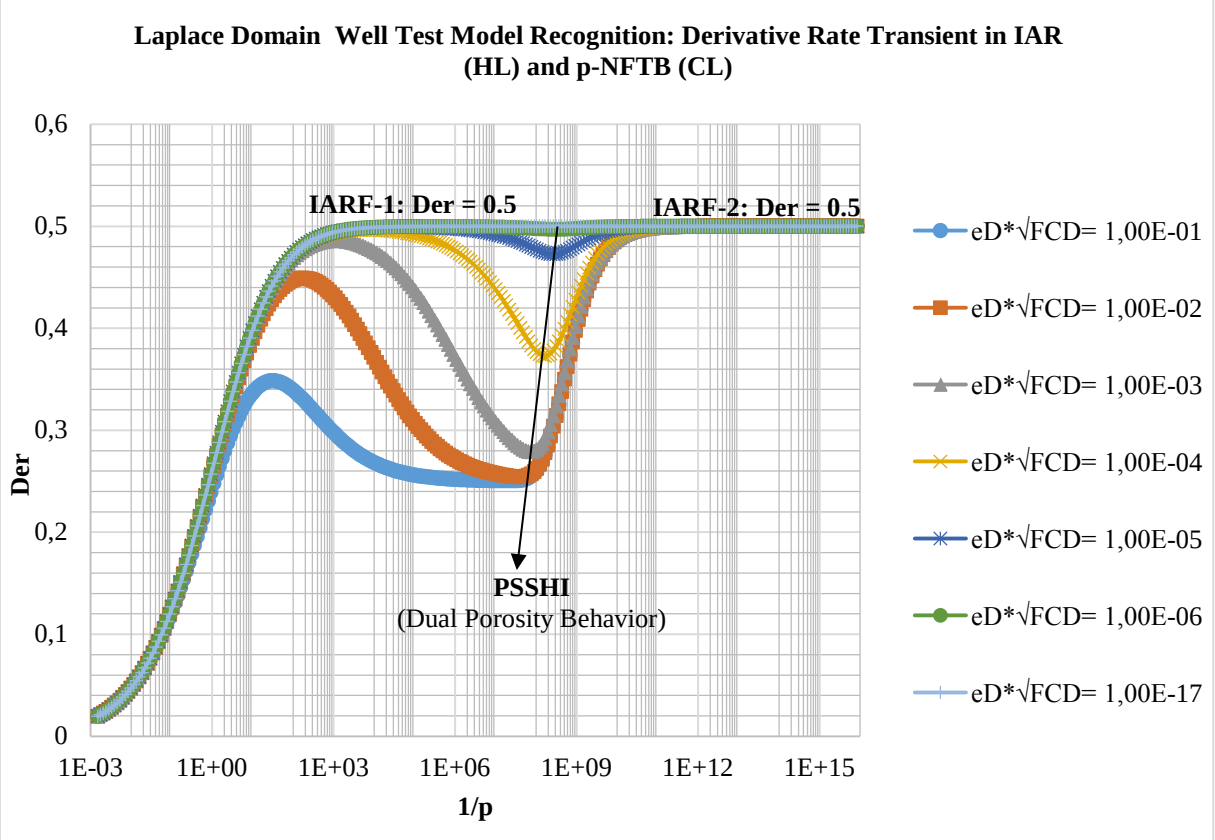

Figure A12- 10: Derivative Rate Transient in IAR (HL) and p-NFTB (CL)

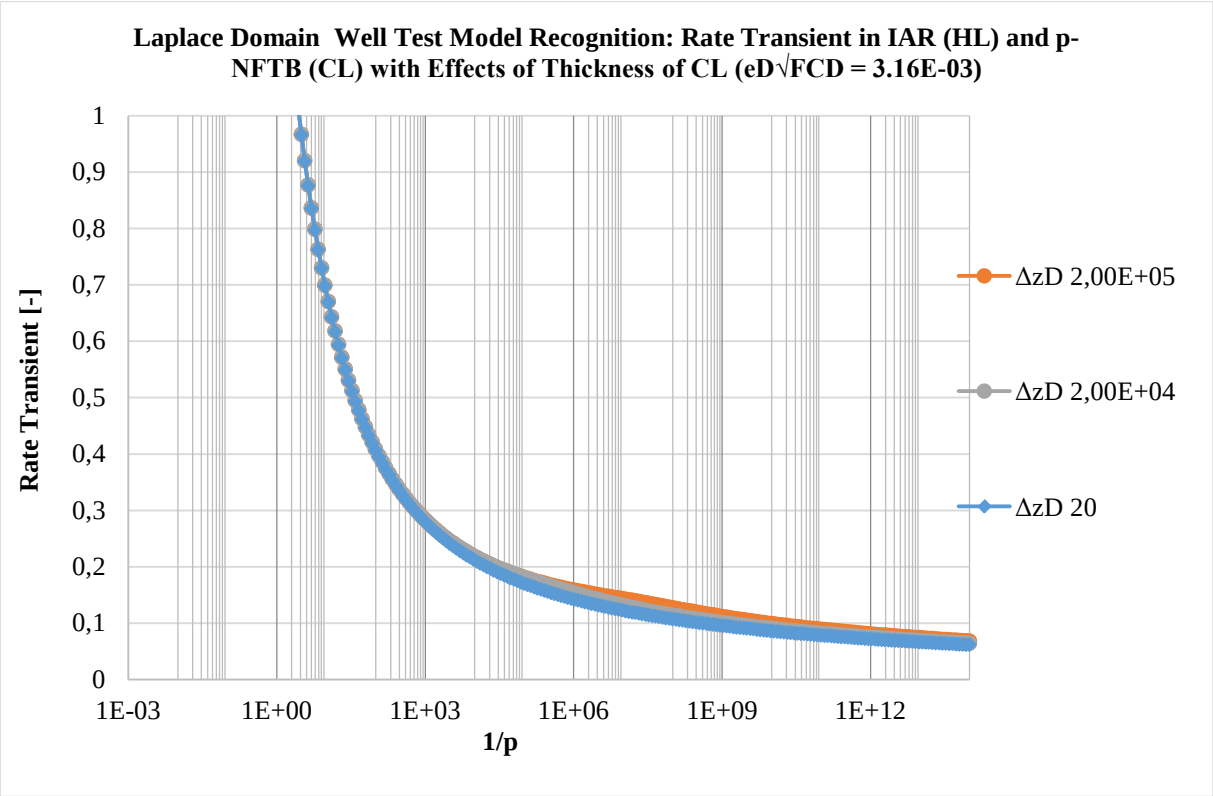

Figure A12- 11: Rate Transient in IAR (HL) and p-NFTB (CL) and Effects of Thickness of CL

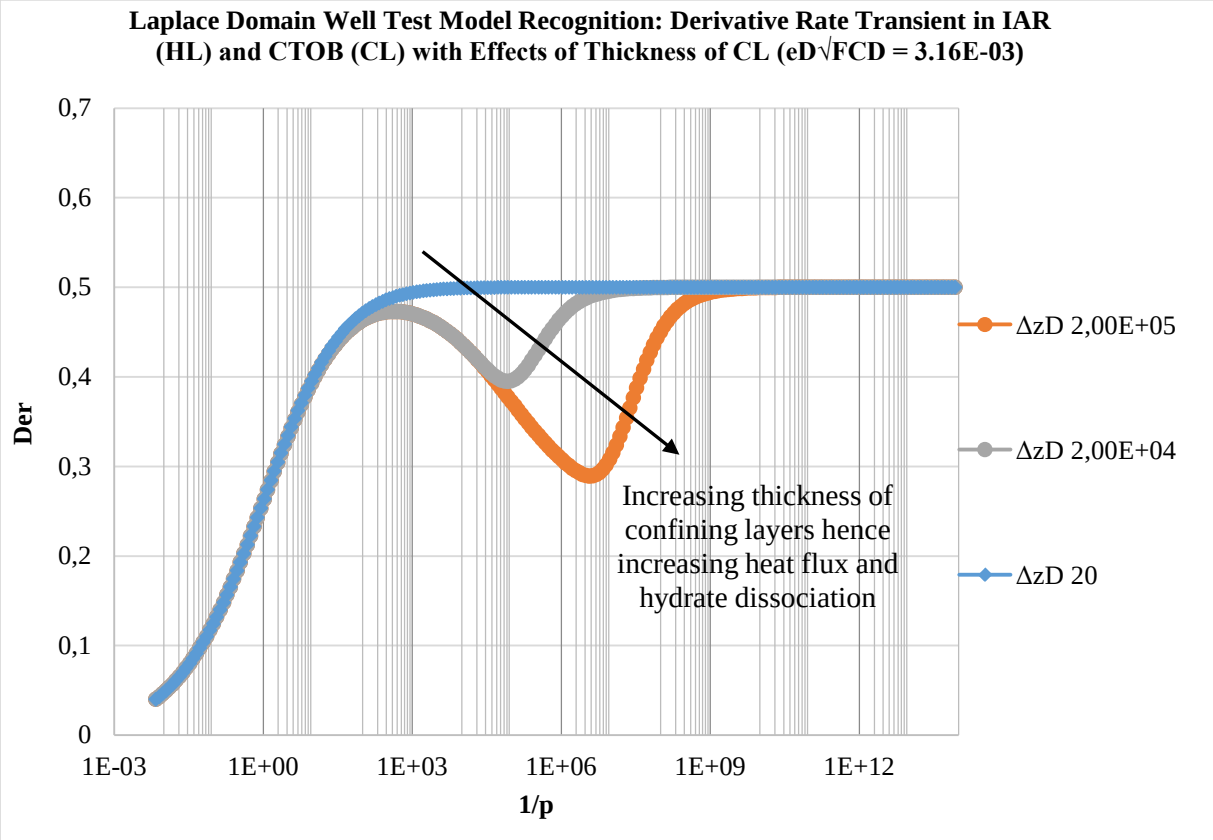

Figure A12- 12: Rate Transient Derivative in IAR (HL) and p-NFTB (CL) and Effects of Thickness of CL

As seen with the Laplace Domain Well Recognition models, a thorough investigation of the reservoir response can be made which can be very useful in the interpretation of well tests and hence reservoir characterization. The use of the p-NFTB is only useful for reservoirs with limited heat influx or reservoirs with low hydrate saturation since the heat influx rate has been related to the rate of hydrate dissociation, i.e. reservoirs with low hydrate saturation will dissociate much faster and the dual porosity behavior will be noticeable with diminishing hydrate saturation.

To generate more optimistic models for which type curves are more applicable in real time domain and which better fit the responses when using the kinetic model, the CTOB models for both confining layer are used.

The Laplace transformed variable s is defined below for the different outer boundary conditions imposed in deriving solutions to the heat conduction problem in the hydrate layer during depletion.

CTOB in Confining Layers

$$s = S_D p + \frac{e_D}{(\Delta z_D - 1)}\sqrt{pF_{CD}}(\Delta z_D - 1)\mathrm{Coth}\left[\sqrt{pF_{CD}}(\Delta z_D - 1)\right] \qquad \text{A12: 13}$$

Since the reservoir producing layer is confined by layers responsible for heat supply, the above model can be written thus:

$$\frac{e_D}{(\Delta z_D - 1)}\sqrt{pF_{CD}}(\Delta z_D - 1)\mathrm{Coth}\left[\sqrt{pF_{CD}}(\Delta z_D - 1)\right] =$$
$$\left\{e_D \frac{\sqrt{pF_{CD}}(\Delta z_D - 1)\mathrm{Coth}\left[\sqrt{pF_{CD}}(\Delta z_D - 1)\right]}{(\Delta z_D - 1)}\right\}_{TL} + \left\{e_D \frac{\sqrt{pF_{CD}}(\Delta z_D - 1)\mathrm{Coth}\left[\sqrt{pF_{CD}}(\Delta z_D - 1)\right]}{(\Delta z_D - 1)}\right\}_{BL} \qquad \text{A12: 14}$$

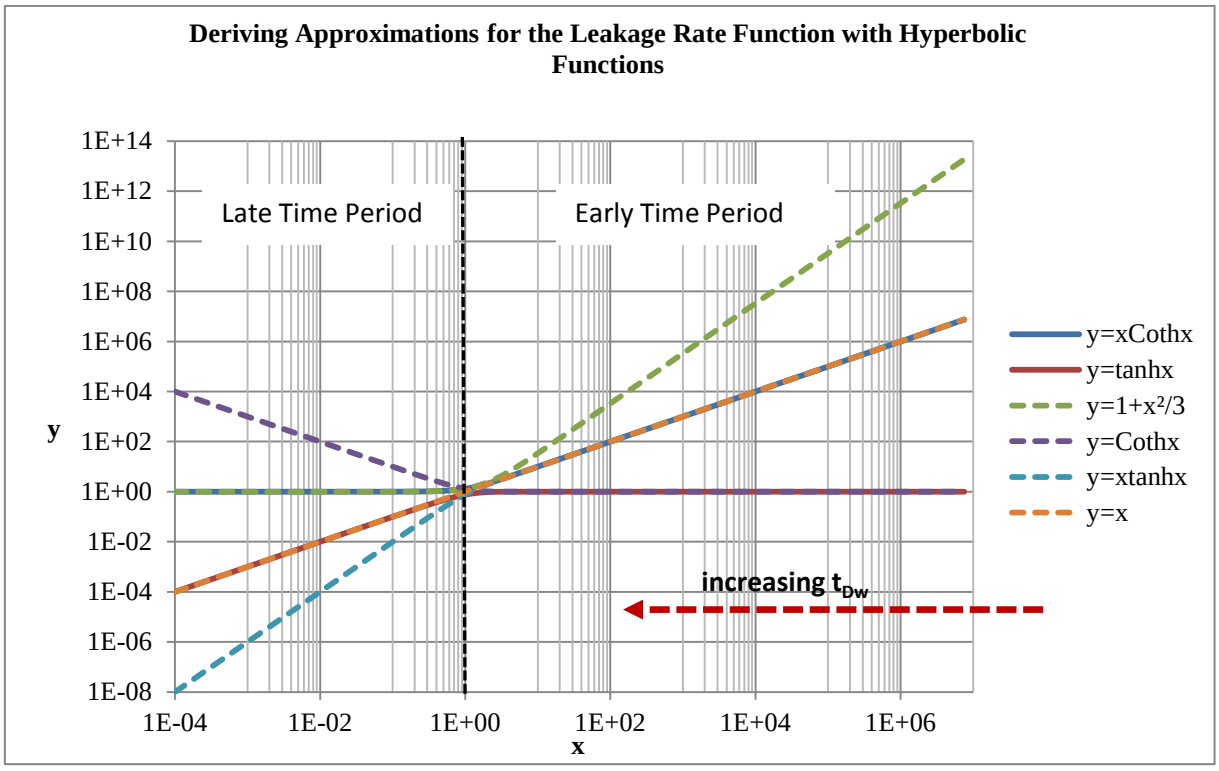

Figure A12- 13: Approximations for the Leakage Rate Function with Hyperbolic Functions

Early Time Production

For large values of Laplace variable (p) i.e. short production periods, the hyperbolic function has the following approximation, [68], [43], [73]:

$$\mathrm{Cothx} \approx 1 \qquad \text{A12: 15}$$

With the above approximation, the Laplace variable takes the form:

$$s = S_D p + e_D\sqrt{F_{CD}}\sqrt{p} \qquad \text{A12: 16}$$

Where,

$$e_D\sqrt{F_{CD}} = \left\{e_D\sqrt{F_{CD}}\right\}_{TL} + \left\{e_D\sqrt{F_{CD}}\right\}_{BL}$$

Late Time Production

For small values of Laplace time i.e. long production periods, the hyperbolic function has the following approximation [68], [43], [73]:

$$x\mathrm{Cothx} \approx 1 + \frac{x^2}{3} \qquad \text{A12: 17}$$

With the above representation, the Laplace variable takes the form:

$$s = S_D p + \frac{e_D}{(\Delta z_D - 1)}\left(1 + \frac{\left[\sqrt{pF_{CD}}(\Delta z_D - 1)\right]^2}{3}\right) \qquad \text{A12: 18}$$

$$s = p\left(S_D + \frac{F_{CD}}{3}e_D(\Delta z_D - 1)\right) + \frac{e_D}{(\Delta z_D - 1)} \qquad \text{A12: 19}$$

Where,

$$\frac{F_{CD}}{3}e_D(\Delta z_D - 1) = \left\{\frac{F_{CD}}{3}e_D(\Delta z_D - 1)\right\}_{TL} + \left\{\frac{F_{CD}}{3}e_D(\Delta z_D - 1)\right\}_{BL} \qquad \text{A12: 20}$$

$$\frac{e_D}{(\Delta z_D - 1)} = \left\{\frac{e_D}{(\Delta z_D - 1)}\right\}_{TL} + \left\{\frac{e_D}{(\Delta z_D - 1)}\right\}_{BL} \qquad \text{A12: 21}$$

Note that if the p-NFTB was imposed on the top confining layer, the above leakage during late time would be:

$$\frac{e_D}{(\Delta z_D - 1)} = \left\{\frac{e_D}{(\Delta z_D - 1)}\right\}_{BL} \qquad \text{A12: 22}$$

Nonetheless, the heat leakage from the bottom layer is still influential in the late time behavior. For this reason, we will simply impose CTOB on both layers for the solutions in real time domain, which gives an optimistic approach to the hydrate dissociation process as also reflected in the kinetic model.

Another approximation to the above function for the late time period would be:

$$x\mathrm{Cothx} \approx 1$$

With this representation, the Laplace variable takes the form:

$$s = \mu_D^2 = pS_D + \frac{e_D}{(\Delta z_D - 1)} \qquad \text{A12: 23}$$

With the approximations made for early and late time periods, solutions to the diffusivity equation can also be derived analogue Hantush (1964) and given in the literature [68], [43], [73].

Note that late time approximations could occur at different times in both layers, all depending on the petrophysical properties of each layer.

Approximate Solutions to the Heat Flux Problem in Time-Domain

Late Time Period for Constant Outer Temperature in Confining Layer

$$\lambda_D = \sqrt{pS_D\left(1 + \frac{F_{CD}}{3S_D} e_D(\Delta z_D - 1)\right) + \frac{e_D}{(\Delta z_D - 1)}} = \sqrt{pS_D\mu_D + b_D} \qquad \text{A12: 24}$$

Dimensionless Pseudo-Pressure

$$\varphi_D = L^{-1}(\hat{\varphi}_D) = L^{-1}\left\{\frac{K_o\left[r_D\sqrt{p(S_D\mu_D) + b_D}\right]}{pK_o\left[\sqrt{p(S_D\mu_D) + b_D}\right]}\right\} = Z\left(\frac{t_{Dw}}{S_D\mu_D}, r_D, \sqrt{b_D}\right)$$

$$\varphi_D = Z\left(\frac{t_{Dw}}{S_D\mu_D}, r_D, \sqrt{b_D}\right) = Z\left(\frac{t_{Dw}}{\left(1 + \frac{F_{CD}}{3S_D} e_D(\Delta z_D - 1)\right)}, r_D, \sqrt{\frac{e_D}{(\Delta z_D - 1)}}\right) \qquad \text{A12: 25}$$

By using the other approximation of the hyperbolic function during the late time period we get:

$$\varphi_D = Z\left(\frac{t_{Dw}}{S_D}, r_D, \sqrt{b_D}\right) = Z\left(\frac{t_{Dw}}{S_D}, r_D, \sqrt{\frac{e_D}{(\Delta z_D - 1)}}\right) \qquad \text{A12: 26}$$

The above flowing well function for leaky aquifers as given by [43] is expressed fully in Appendix 18.

Late Time Approximation for Hydrate Layer:

$$\varphi_D = \frac{W\left(\frac{r_D^2}{4t_{Dw}} S_D\mu_D, r_D\sqrt{b_D}\right)}{W\left(\frac{S_D\mu_D}{4t_{Dw}}, \sqrt{b_D}\right)} \qquad \text{A12: 27}$$

The above well function for leaky aquifers as given by [43] is expressed fully in Appendix 18.

Dimensionless Flowrate

$$\dot{m}_{tD} = L^{-1}(\hat{m}_{tD}) = L^{-1}\left\{r_D\sqrt{p(S_D\mu_D) + b_D}\,\frac{K_1\left[r_D\sqrt{p(S_D\mu_D) + b_D}\right]}{pK_o\left[\sqrt{p(S_D\mu_D) + b_D}\right]}\right\} = G\left(\frac{t_{Dw}}{S_D\mu_D r_D^2}, r_D\sqrt{\frac{e_D}{(\Delta z_D - 1)}}\right)$$

The above flowing well discharge function for leaky aquifers as given by [43] is expressed fully in Appendix 18.

Dimensionless Flowrate at Wellbore

$$\dot{m}_{tD} = G\left(\frac{t_{Dw}}{S_D \mu_D}, \sqrt{\frac{e_D}{(\Delta z_D - 1)}}\right) \quad \text{A12: 28}$$

By using the other approximation of the hyperbolic function during the late time period we get:

$$\dot{m}_{tD} = G\left(\frac{t_{Dw}}{S_D}, \sqrt{\frac{e_D}{(\Delta z_D - 1)}}\right) \quad \text{A12: 29}$$

In a similar manner, solutions can also be derived using the kinetic model.

The Kinetic Model

$$s = \mu_D^2 = pS_{Dk} + \gamma_{Dk} \quad \text{A12: 30}$$

$$\varphi_D = Z\left(\frac{t_{Dw}}{S_{Dk}}, r_D, \sqrt{\gamma_{Dk}}\right) \quad \text{A12: 31}$$

Late Time Approximation for Producing Layer:

$$\varphi_D = \frac{W\left(\frac{r_D^2}{4t_{Dw}} S_{Dk}, r_D\sqrt{\gamma_{Dk}}\right)}{W\left(\frac{1}{4t_{Dw}} S_{Dk}, \sqrt{\gamma_{Dk}}\right)} \quad \text{A12: 32}$$

$$\dot{m}_{tD} = G\left(\frac{t_{Dw}}{S_D}, \sqrt{\gamma_{Dk}}\right) \quad \text{A12: 33}$$

Case 1b: Finite Acting Reservoirs with Constant Pressure Outer Boundary

Constant Pressure Outer Boundary Condition

Similarity Solutions

Using the image well theory discussed in Appendix 8, solutions to the constant pressure outer boundary problem can be deduced. For a reservoir with one recharge boundary, the reservoir response can be estimated thus:

Dimensionless Pseudo-Pressure

$$\varphi_D(r_D, t_{Dw}) = \frac{\left[E_1(S_D\frac{r_D^2}{4t_{Dw}})\right] - \left[E_1\left(S_D\frac{(2l_D - r_D)^2}{4t_{Dw}}\right)\right]}{\left[E_1(\frac{S_D}{4t_{Dw}})\right] - \left[E_1\left(S_D\frac{(2l_D - 1)^2}{4t_{Dw}}\right)\right]} \quad \text{A12: 34}$$

Transient Rate

$$\dot{m}_{tD}(r_D, t_{Dw}) = 2\frac{e^{-\left(S_D\frac{r_D^2}{4t_{Dw}}\right)}}{E_1\left(\frac{S_D}{4t_{Dw}}\right) - E_1\left(S_D\frac{(2l_D-1)^2}{4t_{Dw}}\right)} + 2\frac{(2l_D - r_D)^{-1} r_D e^{-\frac{(2l_D - r_D)^2}{4t_{Dw}} S_D}}{E_1\left(\frac{S_D}{4t_{Dw}}\right) - E_1\left(S_D\frac{(2l_D-1)^2}{4t_{Dw}}\right)} \quad \text{A12: 35}$$

$$\dot{m}_{tD}(r_D = 1, t_{Dw}) = 2\frac{e^{-\left(\frac{S_D}{4t_{Dw}}\right)} + (2l_D - 1)^{-1} e^{-\frac{(2l_D-1)^2}{4t_{Dw}} S_D}}{E_1\left(\frac{S_D}{4t_{Dw}}\right) - E_1\left(S_D\frac{(2l_D-1)^2}{4t_{Dw}}\right)} \quad \text{A12: 36}$$

Solutions in Laplace Domain

$$\hat{\varphi}_D = c_1 I_o(r_D\sqrt{s}) + c_2 K_o(r_D\sqrt{s}) \qquad \text{A12: 37}$$

For finite acting reservoirs, the constants c1 is not zero. By imposing the inner and outer boundary conditions, the solution to the constant pressure outer boundary problem for the confined layer can be deduced.

r_{eD} $\quad \hat{\varphi}_D = 0$

r_D=1 $\quad \hat{\varphi}_D = \frac{1}{p}$

$$c_1 = -\frac{1}{p}\left[\frac{K_o(r_{eD}\sqrt{s})}{\left(K_o(\sqrt{s})I_o(r_{eD}\sqrt{s})\right) - I_o(\sqrt{s})K_o(r_{eD}\sqrt{s})}\right] \qquad \text{A12: 38}$$

$$c_2 = \frac{1}{p}\left[\frac{K_o(r_{eD}\sqrt{s})I_o(r_{eD}\sqrt{s})}{\left(K_o(\sqrt{s})I_o(r_{eD}\sqrt{s})\right) - I_o(\sqrt{s})K_o(r_{eD}\sqrt{s})}\right]\frac{1}{K_o(r_{eD}\sqrt{s})} \qquad \text{A12: 39}$$

Dimensionless Pseudo-Pressure

$$\hat{\varphi}_D = \frac{1}{p}\left[\frac{K_o(r_D\sqrt{s})I_o(r_{eD}\sqrt{s}) - K_o(r_{eD}\sqrt{s})I_o(r_D\sqrt{s})}{I_o(r_{eD}\sqrt{s})K_o(\sqrt{s}) - I_o(\sqrt{s})K_o(r_{eD}\sqrt{s})}\right]$$

Dimensionless Flow rate

$$\hat{m}_{tD} = \frac{r_D\sqrt{s}}{p}\left[\frac{\left[K_1(r_D\sqrt{s})I_o(r_{eD}\sqrt{s}) + K_o(r_{eD}\sqrt{s})I_1(r_D\sqrt{s})\right]}{I_o(r_{eD}\sqrt{s})K_o(\sqrt{s}) - I_o(\sqrt{s})K_o(r_{eD}\sqrt{s})}\right] \qquad \text{A12: 40}$$

$$\hat{m}_{tD}(r_D = 1, p) = \frac{\sqrt{s}}{p}\left[\frac{K_1(\sqrt{s})I_o(r_{eD}\sqrt{s}) + K_o(r_{eD}\sqrt{s})I_1(\sqrt{s})}{I_o(r_{eD}\sqrt{s})K_o(\sqrt{s}) - I_o(\sqrt{s})K_o(r_{eD}\sqrt{s})}\right] \qquad \text{A12: 41}$$

Rate Transient Plot in Laplace Domain

$\widehat{pm}_{tD}$ Versus $\frac{1}{p}$

$\hat{\varphi}_D p$ Versus r_D

$$\text{Der} = \frac{\Delta\left(\frac{1}{\widehat{pm}_{tD}}\right)}{\Delta\left(\frac{1}{p}\right)} \quad \text{Versus} \quad \frac{1}{p}$$

For large values of p i.e. early time production period where boundary dominated flow has not been reached, the reservoir is still acting infinite and from the characteristics of the modified Bessel´s functions given in Figure A7- 1, the solutions to the infinite acting reservoir are applicable. The image well theory can also be applied to the solutions in Laplace domain as given in Appendix 8.

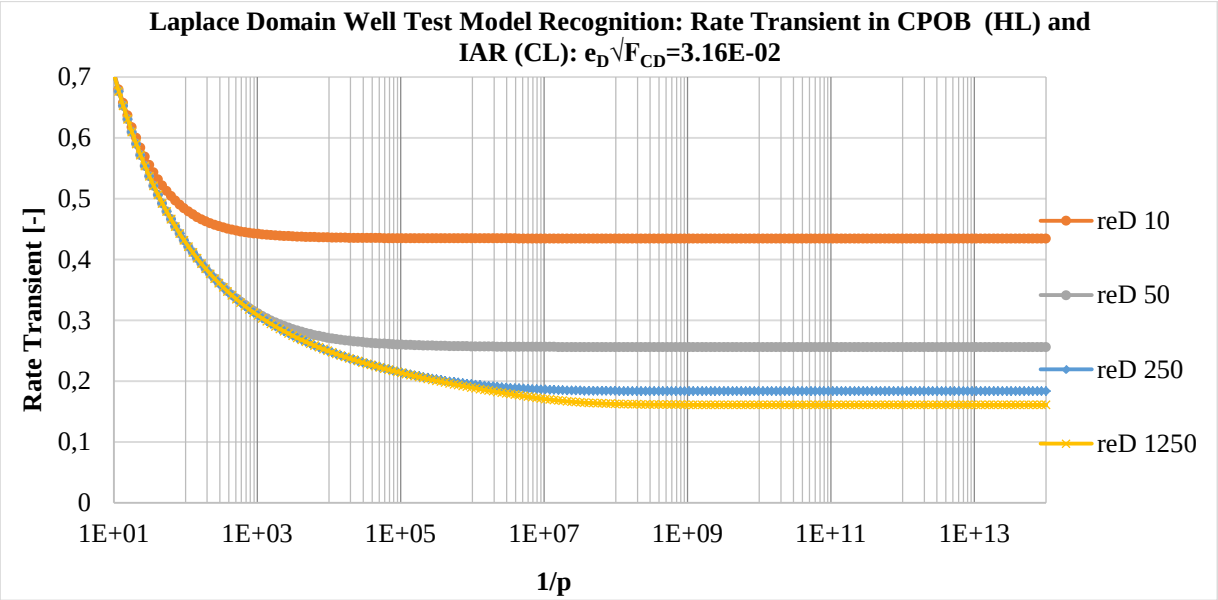

Figure A12- 14: Rate Transient in CPOB (HL) and IAR (CL)

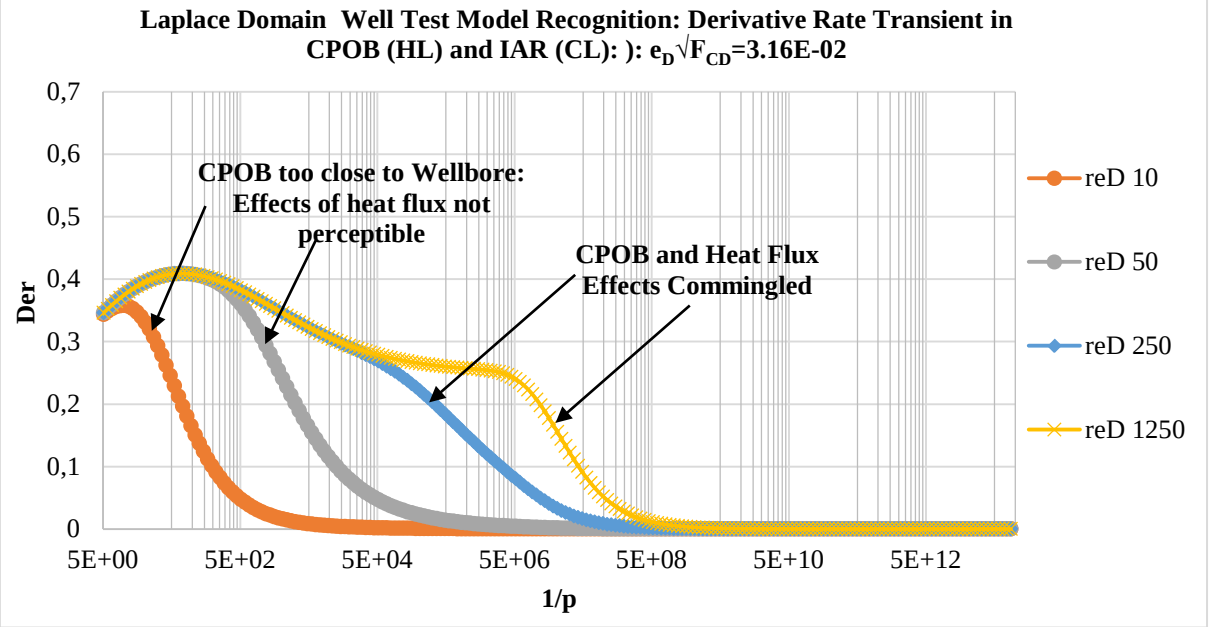

Figure A12- 15: Derivative Rate Transient in CPOB (HL) and IAR (CL)

Case 1c: Finite Acting Reservoirs: No Flow Outer Boundary

Similarity Solutions

Using the image well theory discussed in Appendix 8, the reservoir response with one no-flow boundary can be estimated thus:

Dimensionless Pseudo-Pressure

$$\varphi_D(r_D, t_{Dw}) = \frac{\left[E_1\left(S_D\frac{r_D^2}{4t_{Dw}}\right)\right]+\left[E_1\left(S_D\frac{(2l_D-r_D)^2}{4t_{Dw}}\right)\right]}{\left[E_1\left(\frac{S_D}{4t_{Dw}}\right)\right]+\left[E_1\left(S_D\frac{(2l_D-1)^2}{4t_{Dw}}\right)\right]} \qquad \text{A12: 42}$$

Dimensionless Transient Rate

$$\dot{m}_{tD}(r_D, t_{Dw}) = 2\frac{\left[e^{-\left(\frac{S_D}{4t_{Dw}}r_D\right)} - (2l_D - r_D)^{-1} r_D e^{-\frac{(2l_D - r_D)^2}{4t_{Dw}}S_D}\right]}{\left[E_1\left(\frac{S_D}{4t_{Dw}}\right)\right] + \left[E_1\left(S_D\frac{(2l_D-1)^2}{4t_{Dw}}\right)\right]} \quad \text{A12: 43}$$

$$\dot{m}_{tD}(r_D = 1, t_{Dw}) = 2\frac{\left[e^{-\left(\frac{S_D}{4t_{Dw}}\right)} - (2l_D - 1)^{-1} e^{-\frac{(2l_D-1)^2}{4t_{Dw}}S_D}\right]}{\left[E_1\left(\frac{S_D}{4t_{Dw}}\right)\right] + \left[E_1\left(S_D\frac{(2l_D-1)^2}{4t_{Dw}}\right)\right]} \quad \text{A12: 44}$$

Solutions in Laplace Domain

$$\hat{\varphi}_D = c_1 I_o(r_D\sqrt{s}) + c_2 K_o(r_D\sqrt{s})$$

For finite acting reservoirs, the constants c1 is not zero. For constant inner pressure and no-flow outer boundary conditions, the above equation is:

r_{eD} $\quad \left(\frac{d\hat{\varphi}_D}{dr_D}\right)_{r_{eD}} = 0 \quad \left(\frac{d\hat{\varphi}_D}{dr_D}\right)_{r_{eD}} = c_1\sqrt{s}I_1(r_{eD}\sqrt{s}) - c_2\sqrt{s}K_1(r_{eD}\sqrt{s}) = 0$

r_D=1 $\quad \hat{\varphi}_D = \frac{1}{p}$

With the above boundary conditions, the constants c_1 and c_2 are given thus:

$$c_1 = \frac{1}{p}\left[\frac{K_1(r_{eD}\sqrt{s})}{K_o(\sqrt{s})I_1(r_{eD}\sqrt{s}) + K_1(r_{eD}\sqrt{s})I_o(\sqrt{s})}\right] \quad \text{A12: 45}$$

$$c_2 = \frac{1}{p}\left[\frac{K_1(r_{eD}\sqrt{s})}{K_o(\sqrt{s})I_1(r_{eD}\sqrt{s}) + K_1(r_{eD}\sqrt{s})I_o(\sqrt{s})}\right]\frac{I_1(r_{eD}\sqrt{s})}{K_1(r_{eD}\sqrt{s})} \quad \text{A12: 46}$$

Dimensionless Pseudo-Pressure

$$\hat{\varphi}_D = \frac{1}{p}\left[\frac{K_1(r_{eD}\sqrt{s})I_o(r_D\sqrt{s}) + I_1(r_{eD}\sqrt{s})K_o(r_D\sqrt{s})}{K_o(\sqrt{s})I_1(r_{eD}\sqrt{s}) + K_1(r_{eD}\sqrt{s})I_o(\sqrt{s})}\right] \quad \text{A12: 47}$$

Dimensionless Flow rate

$$\hat{m}_{tD} = \frac{r_D\sqrt{s}}{p}\left[\frac{[I_1(r_{eD}\sqrt{s})K_1(r_D\sqrt{s}) - K_1(r_{eD}\sqrt{s})I_1(r_D\sqrt{s})]}{K_o(\sqrt{s})I_1(r_{eD}\sqrt{s}) + K_1(r_{eD}\sqrt{s})I_o(\sqrt{s})}\right] \quad \text{A12: 48}$$

$$\hat{m}_{tD}(r_D = 1, p) = \frac{\sqrt{s}}{p}\left[\frac{[I_1(r_{eD}\sqrt{s})K_1(\sqrt{s}) - K_1(r_{eD}\sqrt{s})I_1(\sqrt{s})]}{K_o(\sqrt{s})I_1(r_{eD}\sqrt{s}) + K_1(r_{eD}\sqrt{s})I_o(\sqrt{s})}\right] \quad \text{A12: 49}$$

Rate Transient Plot in Laplace Domain

$\widehat{p\dot{m}}_{tD}$ Versus $\frac{1}{p}$

$\hat{\varphi}_D p$ Versus r_D

$$\text{Der} = \frac{\Delta\left(\frac{1}{\widehat{\text{pm}}_{\text{tD}}}\right)}{\Delta\left(\frac{1}{\text{p}}\right)} \quad \text{Versus} \quad \frac{1}{\text{p}}$$

For large values of p i.e. early time production period where boundary dominated flow has not been reached, the reservoir is still acting infinite and from the characteristics of the modified Bessel´s functions given in Figure A7- 1, the solutions to the infinite acting reservoir are applicable.

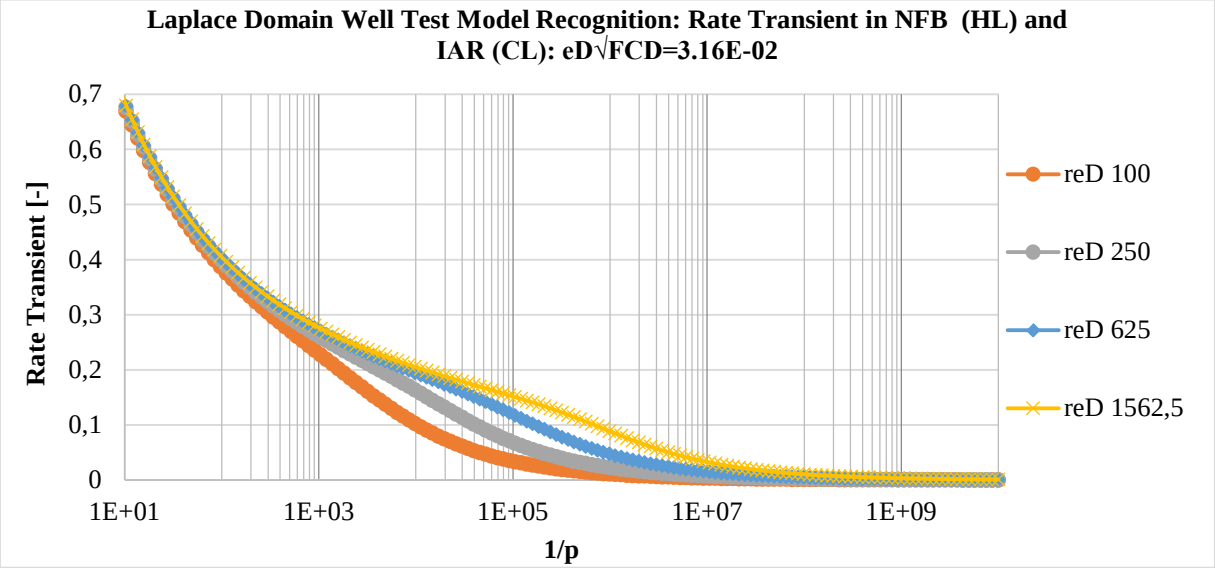

Figure A12- 16: Rate Transient in NFB (HL) and IAR (CL)

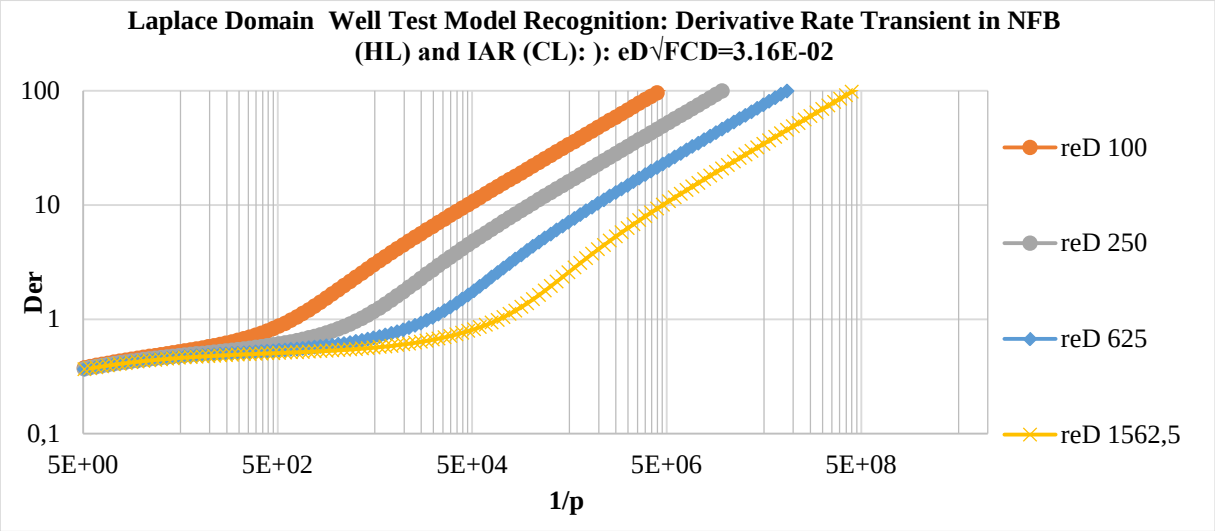

Figure A12- 17: Derivative Rate Transient in NFB (HL) and IAR (CL)

Case 2: Constant Rate Inner Boundary

In most well testing models, the line source solution is used whose inner boundary condition is valid for radius turning zero. Analytical solutions nowadays correct this assumption by using inner boundary conditions reservoirs with finite wellbore radius, which is also seen in the works of [61], [43]. However, due to the complexity of some solutions to the diffusivity equation line source

assumptions are imposed such that the inverse Laplace transform of the solution is deduced, as will be seen later.

Case 2a: Infinite Acting

Similarity Solution

$$\varphi_D = \frac{B}{2} E_1(v_D{}^2)$$

Inner Boundary Condition

$$r_D \frac{\partial \varphi_D}{\partial r_D} = -1 \qquad \text{at} \qquad r_D \to 1 \qquad v_D \to \frac{S_D}{4t_{Dw}}$$

From the inner boundary condition, the constant B is given thus:

$$B = e^{\frac{S_D}{4t_{Dw}}} \qquad \text{A12: 50}$$

$$\varphi_D(r_D, t_{Dw}) = \frac{1}{2} e^{\frac{1}{4t_{Dw}}} E_1\left(S_D \frac{r_D^2}{4t_{Dw}}\right) \qquad \text{A12: 51}$$

Notice the similarity between the CPIB solution and the CRIB which are simply related thus:

$$\varphi_D(r_D = 1, t_{Dw}) = \frac{1}{\dot{m}_{tD}(r_D=1, t_{Dw})} \qquad \text{A12: 52}$$

$$\varphi_{wf}(r_D, t_{Dw}) = \varphi_i - \frac{\dot{m}_t}{4\pi hk}\left[e^{\frac{S_D}{4t_{Dw}}} E_1(S_D \frac{r_D^2}{4t_{Dw}})\right] \qquad \text{A12: 53}$$

$$\varphi_{wf}(r_D = 1, t_{Dw}) = \varphi_i - \frac{\dot{m}_t}{4\pi hk}\left[e^{\frac{S_D}{4t_{Dw}}} E_1(\frac{S_D}{4t_{Dw}})\right] \qquad \text{A12: 54}$$

Solution in Laplace Domain

$$\hat{\varphi}_D = c_1 I_o(r_D\sqrt{s}) + c_2 K_o(r_D\sqrt{s})$$

By transforming the Neumann boundary conditions in Laplace domain, the solution to the Bessel equation results to:

$r_D \to \infty$ $\qquad c_1 = 0$

$r_D = 1$ $\qquad \hat{m}_{tD} = r_D \frac{d\hat{\varphi}_D}{dr_D} = -\frac{1}{p} \qquad c_2 = \frac{1}{p[\sqrt{s} K_1(\sqrt{s})]}$

The final equation is hence:

$$\hat{\varphi}_D = \frac{K_o(r_D\sqrt{s})}{p[\sqrt{s} K_1(\sqrt{s})]} \qquad \text{A12: 55}$$

Pseudo-Pressure Transient Plot in Laplace Domain

$$\hat{\varphi}_D p = \frac{K_o(r_D\sqrt{s})}{\sqrt{s} K_1(\sqrt{s})} = \frac{1}{p\hat{m}_{tD}}$$

$\widehat{\varphi}_D p$ Versus $\frac{1}{p}$

$\text{Der} = \frac{\Delta(\widehat{\varphi}_D p)}{\Delta\left(\frac{1}{p}\right)}$ Versus $\frac{1}{p}$

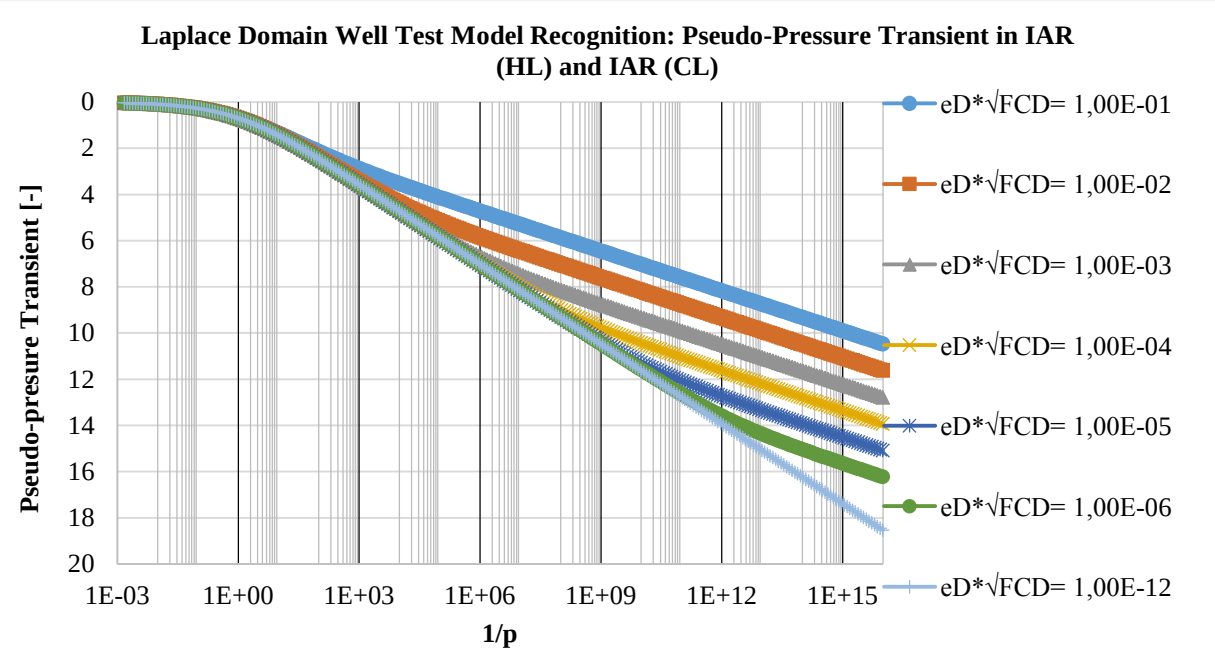

Figure A12- 18: Pseudo-Pressure Transient in IAR (HL) and IAR (CL)

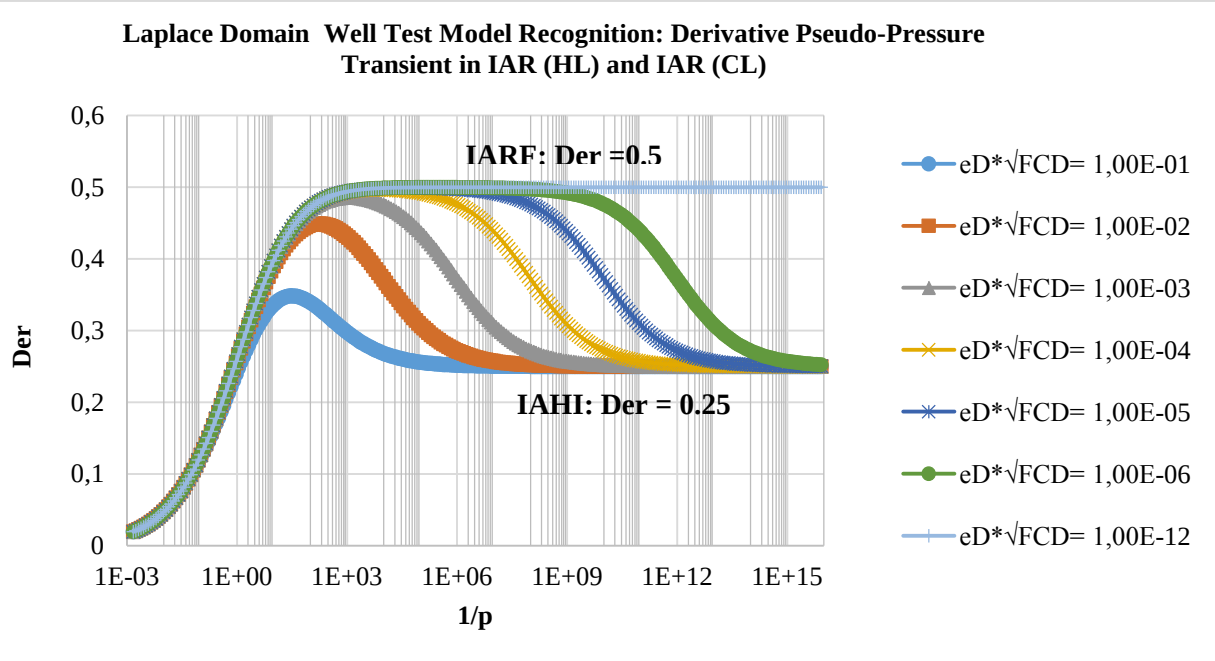

Figure A12- 19: Pseudo-Pressure Derivative in IAR (HL) and IAR (CL)

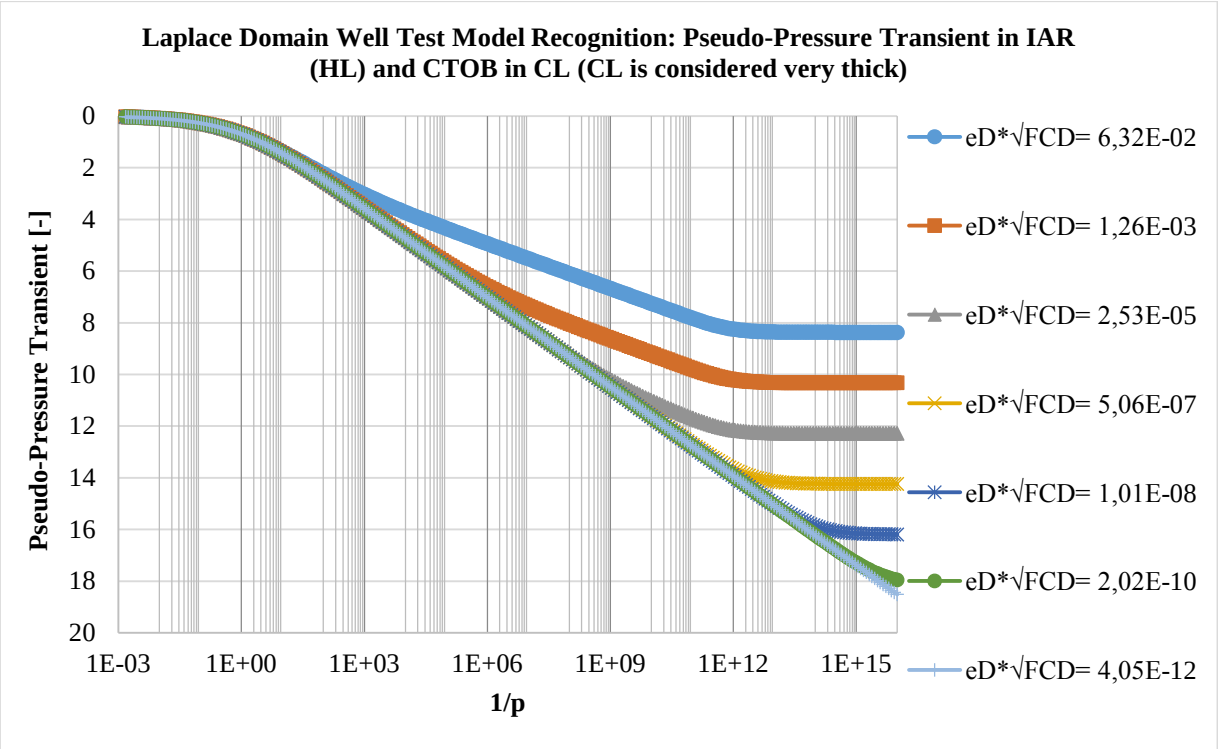

Figure A12- 20: Pseudo-Pressure in IAR (HL) and CTOB (CL is assumed very thick)

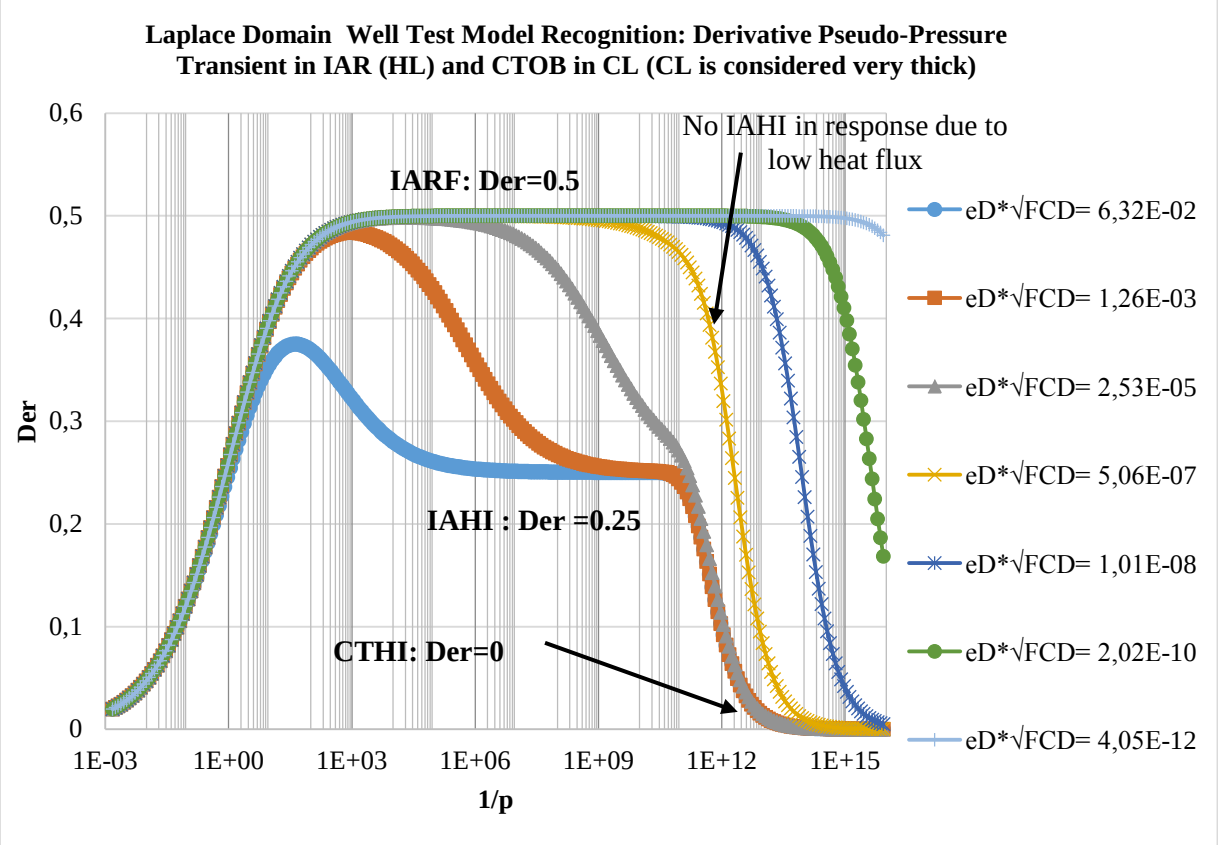

Figure A12- 21: Pseudo-Pressure Derivative in IAR (HL) and CTOB (CL is assumed very thick)

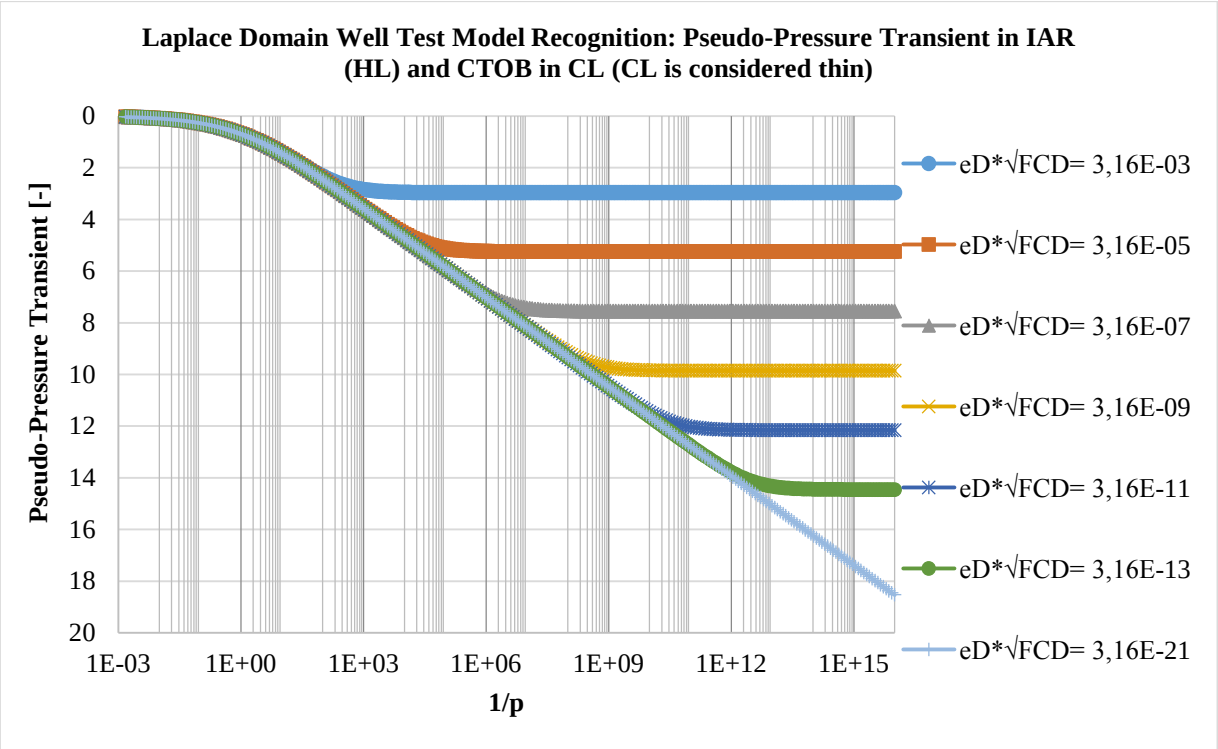

Figure A12- 22: Pseudo-Pressure in IAR (HL) and CTOB (CL is assumed thin)

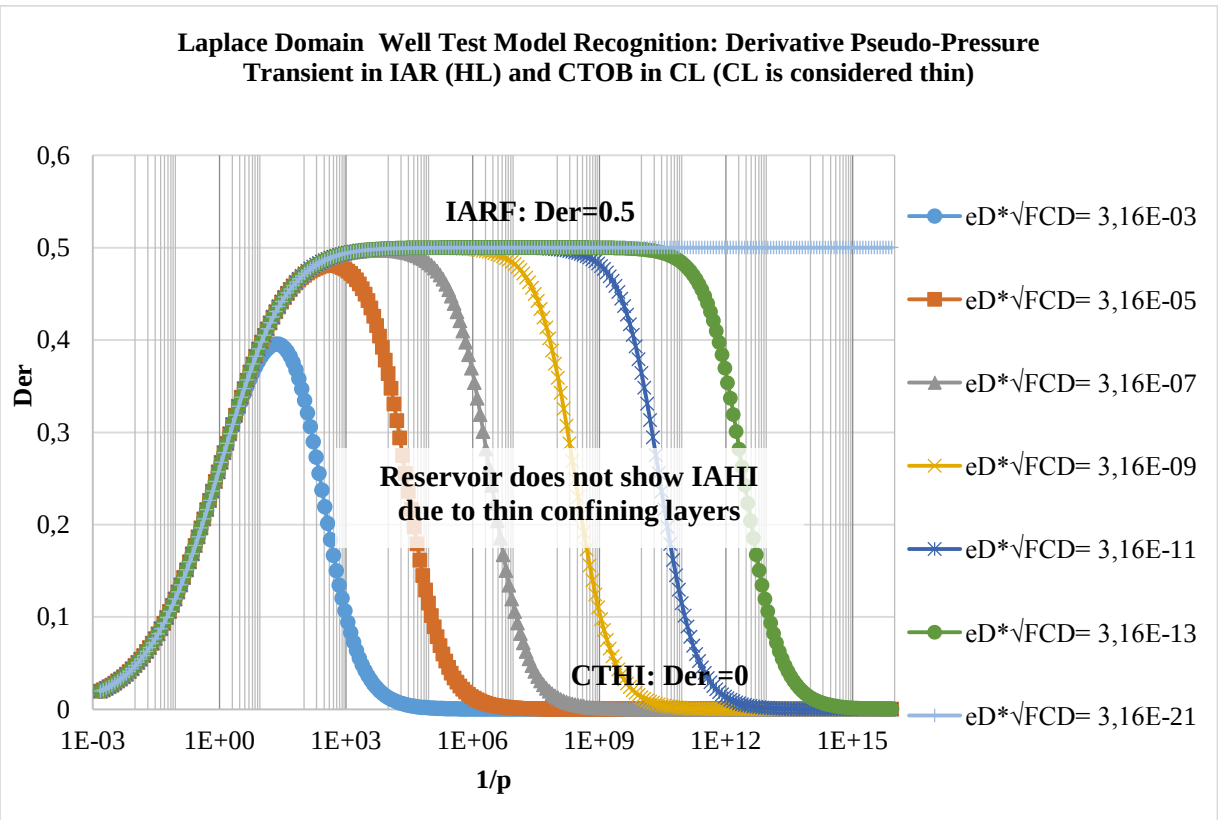

Figure A12- 23: Pseudo-Pressure Derivative in IAR (HL) and CTOB (CL is assumed thin)

By considering hydrate reservoirs with thin CTOB confining layers, the effects of heat influx could be very significant as seen above. IAHI is not perceived in the reservoir response during early time

production phase which makes late time approximate solutions given by Hantush [43] applicable for both the early and late time periods of production.

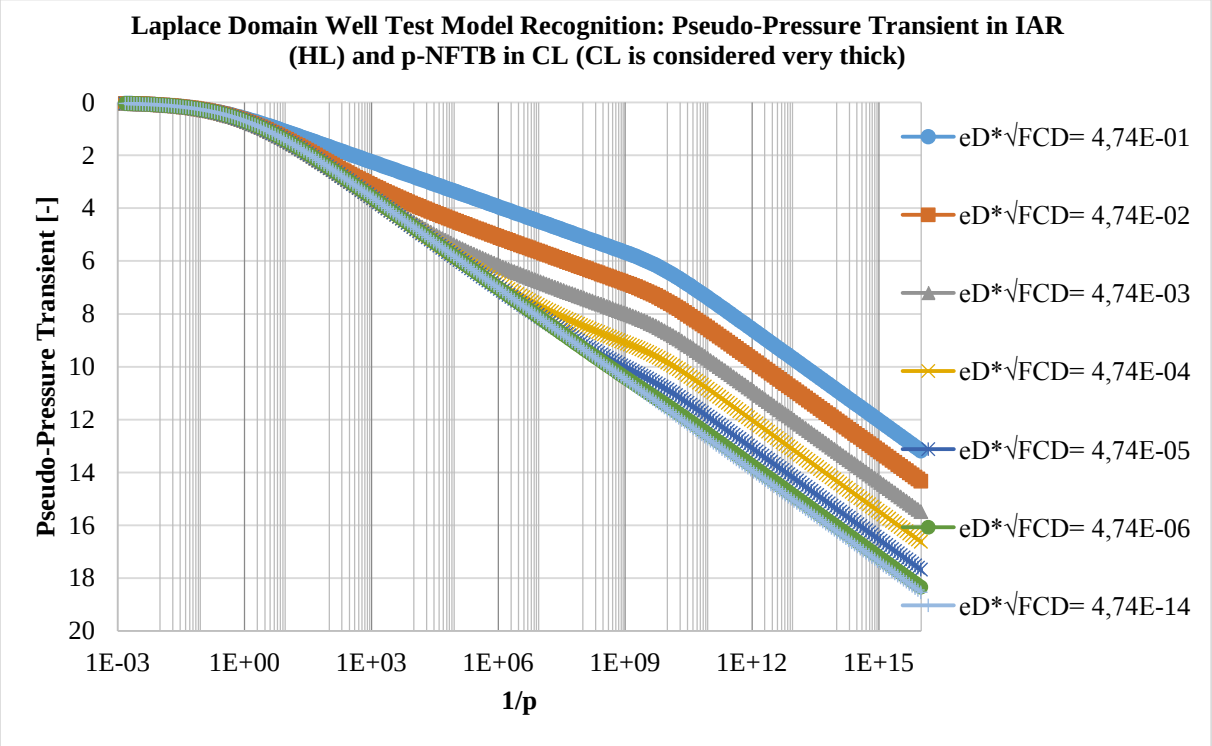

Figure A12- 24: Pseudo-Pressure in IAR (HL) and CTOB (CL is assumed thin)

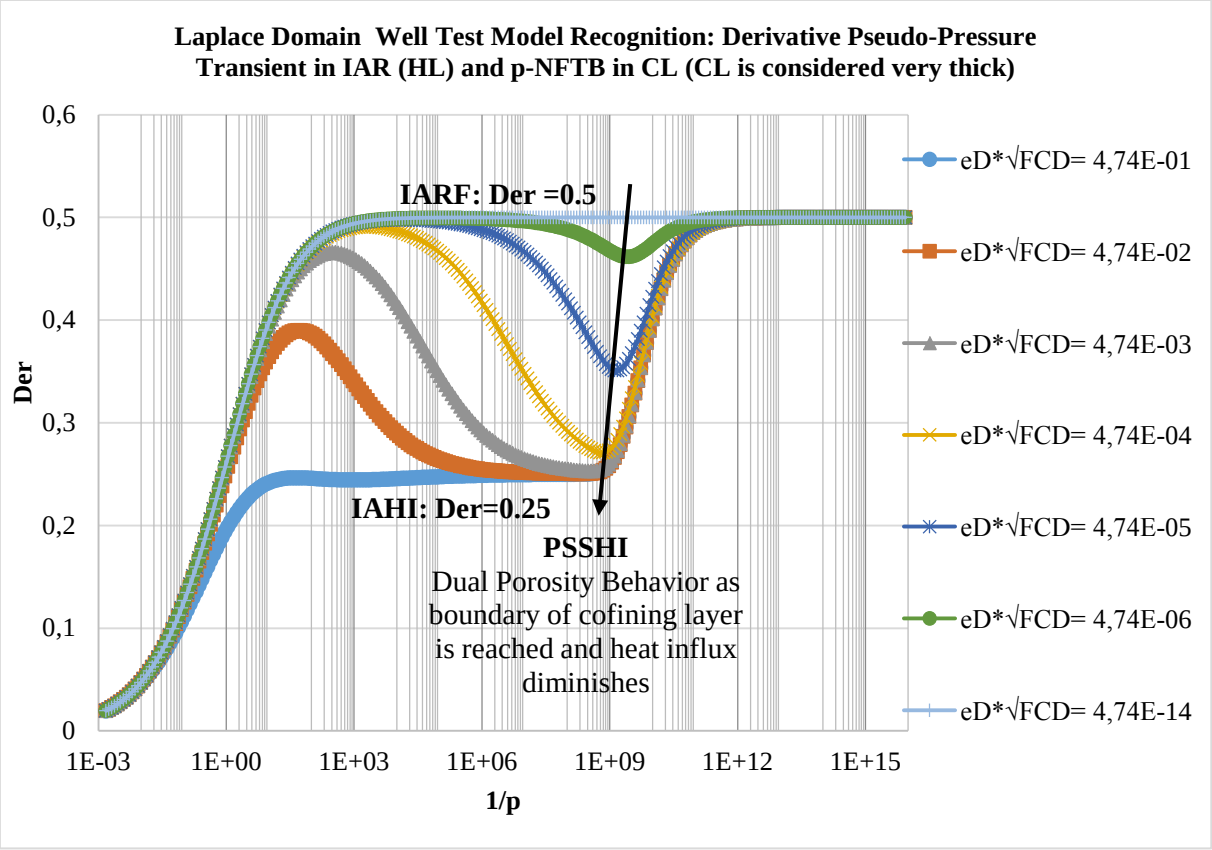

Figure A12- 25: Pseudo-Pressure Derivative in IAR (HL) and p-NFTB in CL (CL is assumed very thick)

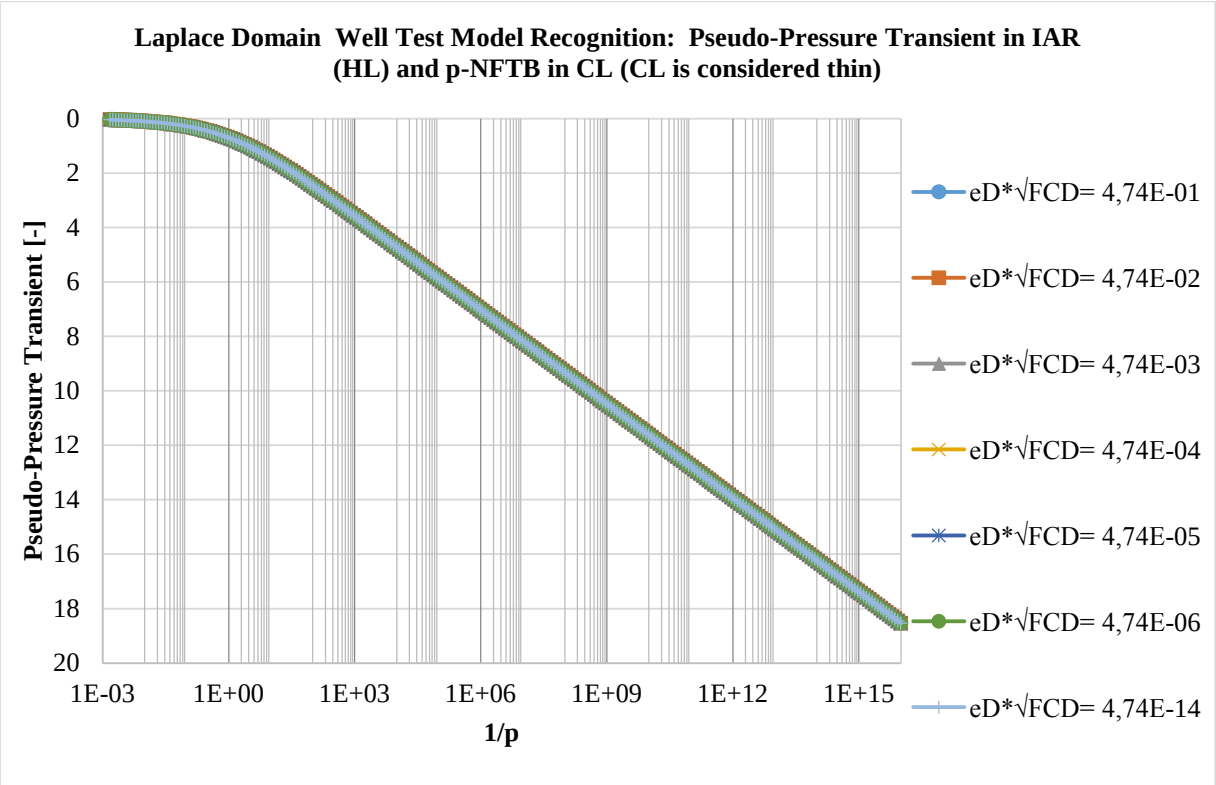

Figure A12- 26: Pseudo-Pressure in IAR (HL) and p-NFTB in CL (CL is assumed thin)

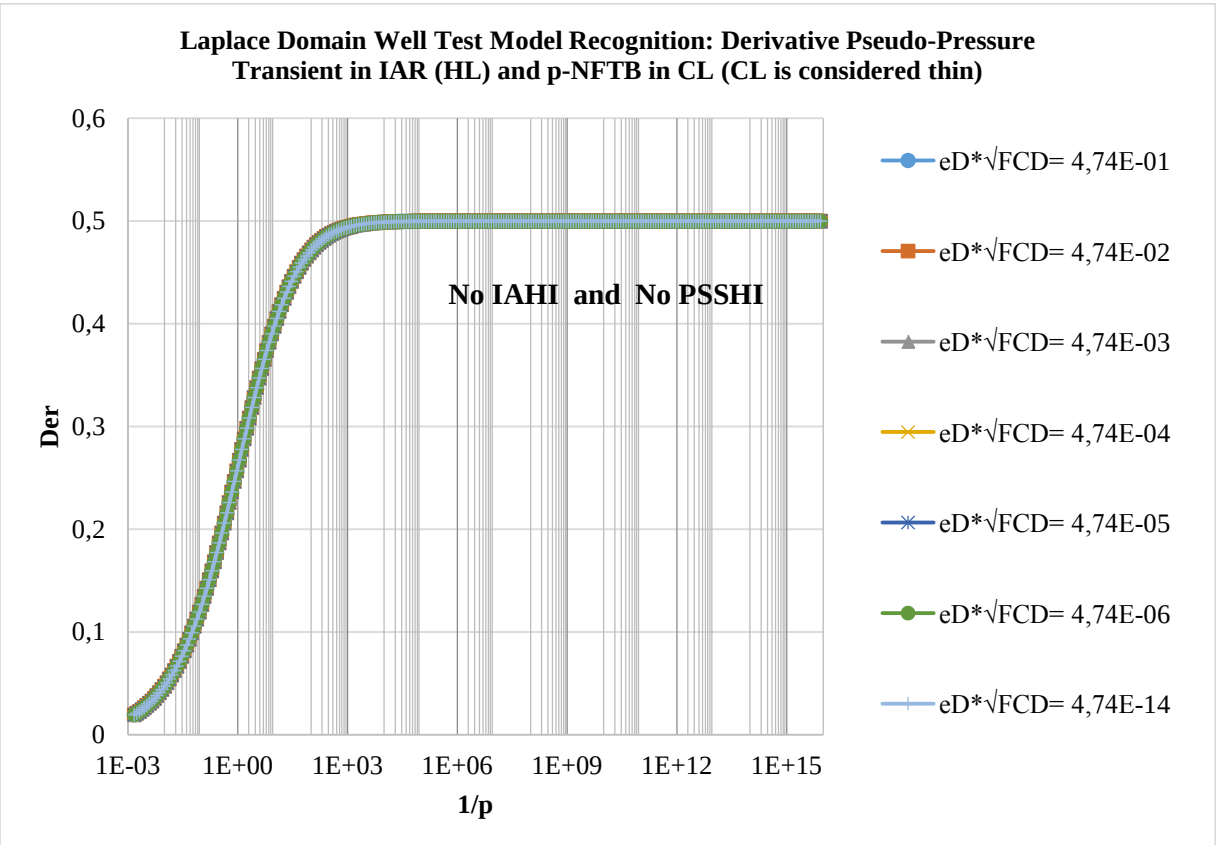

Figure A12- 27: Pseudo-Pressure in IAR (HL) and p-NFTB in CL (CL is assumed thin)

For hydrate reservoir with thin confining layers and p-NFTB, the effects of heat influx can be considered as negligible which will be seen in the approximate solutions derived later analogue Hantush [43].

To derive the solution to the diffusivity problem, Hantush [43] proposed the line source solution method, which facilitates the inverse Laplace transform of the solution. It should however be noted that the line source and finite wellbore radius solutions are equal at late time periods which is also a relevant period for most reservoir engineering calculations.

Line Source Condition

$$\lim_{r_{D\to 0}} p\left[\sqrt{s}K_1\left(\sqrt{s}\right)\right] = 1 \qquad \text{A12: 56}$$

The solution in Laplace domain takes the form:

$$\hat{\varphi}_D = K_o\left(r_D\sqrt{s}\right) \qquad \text{A12: 57}$$

Using the early and late time approximations of the heat conduction terms given earlier, solutions for the pressure response could be deduced.

Early-Time Response

$$\lambda_D = \sqrt{S_D p + \left(e_D\sqrt{F_{CD}}\right)\sqrt{p}} \qquad \text{A12: 58}$$

Analogue [43], the solution is given by:

$$\varphi_D = L^{-1}(\hat{\varphi}_D) = L^{-1}\left\{K_o\left[r_D\sqrt{S_D p + \left(e_D\sqrt{F_{CD}}\right)\sqrt{p}}\right]\right\} = H\left(\frac{S_D r_D^2}{4t_{Dw}}, \frac{r_D}{4}\frac{e_D\sqrt{F_{CD}}}{\sqrt{S_D}}\right)$$

$$\varphi_D = H\left(\frac{S_D r_D^2}{4t_{Dw}}, \frac{r_D}{4}\frac{e_D\sqrt{F_{CD}}}{\sqrt{S_D}}\right) \qquad \text{A12: 59}$$

Late Time Period for Constant Outer Pressure in Crossflow Layer

$$\varphi_D = L^{-1}(\hat{\varphi}_D) = L^{-1}\left\{K_o\left[r_D\sqrt{\left(S_D\mu_D\right)p + b_D}\right]\right\} = \frac{1}{2}W\left[\frac{r_D^2}{4t_{Dw}}S_D\mu_D, r_D\sqrt{b_D}\right] \qquad \text{A12: 60}$$

or

$$\varphi_D = \frac{1}{2}W\left(\frac{r_D^2}{4t_{Dw}}S_D, r_D\sqrt{\frac{e_D}{(\Delta z_D - 1)}}\right) \qquad \text{A12: 61}$$

Kinetic Model

With the Kinetic model, no early time and late time approximations are required however, the line source solution is still used. The solution to the kinetic model takes the form:

$$\varphi_D = \frac{1}{2}W\left(\frac{r_D^2}{4t_{Dw}}S_{Dk}, r_D\sqrt{\gamma_{Dk}}\right) \qquad \text{A12: 62}$$

Case 2b: Constant Pressure Outer Boundary

$$\varphi_D = \frac{B}{2}E_1(v_D{}^2) - \frac{B}{2}E_1\left(S_D\frac{(2l_D - r_D)^2}{4t_{Dw}}\right)$$

Inner Boundary Condition

$$r_D\frac{\partial\varphi_D}{\partial r_D} = -1 \qquad \text{at} \qquad r_D \to 1 \qquad v_D \to \frac{S_D}{4t_{Dw}}$$

From the inner boundary condition, the constant B is given thus:

$$B = \frac{1}{e^{-\left(\frac{1}{4t_{Dw}}\right)} + (2l_D-1)^{-1}e^{-\frac{(2l_D-1)^2}{4t_{Dw}}}} \qquad \text{A12: 63}$$

From the inner boundary condition,

$$\varphi_D(r_D, t_{Dw}) = 0.5\frac{1}{\left[e^{-\left(\frac{1}{4t_{Dw}}\right)} + (2l_D-1)^{-1}e^{-\frac{(2l_D-1)^2}{4t_{Dw}}}\right]}\left[E_1\left(S_D\frac{r_D^2}{4t_{Dw}}\right) - E_1\left(S_D\frac{(2l_D-r_D)^2}{4t_{Dw}}\right)\right] \qquad \text{A12: 64}$$

$$\varphi_D(r_D = 1, t_{Dw}) = 0.5\frac{1}{\left[e^{-\left(\frac{1}{4t_{Dw}}\right)} + (2l_D-1)^{-1}e^{-\frac{(2l_D-1)^2}{4t_{Dw}}}\right]}\left[E_1\left(S_D\frac{r_D^2}{4t_{Dw}}\right) - E_1\left(S_D\frac{(2l_D-r_D)^2}{4t_{Dw}}\right)\right] \qquad \text{A12: 65}$$

Late Time Approximation

$$\varphi_D(r_D = 1, t_{Dw}) \approx 0.5\left[E_1\left(S_D\frac{r_D^2}{4t_{Dw}}\right) - E_1\left(S_D\frac{(2l_D-r_D)^2}{4t_{Dw}}\right)\right] \qquad \text{A12: 66}$$

Solutions in Laplace Domain

$$\hat{\varphi}_D = c_1 I_o(r_D\sqrt{s}) + c_2 K_o(r_D\sqrt{s})$$

Boundary Conditions

r_{eD} $\qquad\qquad$ $\hat{\varphi}_D = 0$

r_D=1 $\qquad\qquad$ $r_D\frac{d\hat{\varphi}_D}{dr_D} = -\frac{1}{p}$

With the above boundary conditions, the constants c_1 and c_2 can be derived.

$$c_1 = -\frac{K_o(r_{eD}\sqrt{s})}{p\sqrt{s}[K_1(\sqrt{s})I_o(r_{eD}\sqrt{s}) + K_o(r_{eD}\sqrt{s})I_1(\sqrt{s})]} \qquad \text{A12: 67}$$

$$c_2 = \frac{I_o(r_{eD}\sqrt{s})}{p\sqrt{s}[K_1(\sqrt{s})I_o(r_{eD}\sqrt{s}) + K_o(r_{eD}\sqrt{s})I_1(\sqrt{s})]} \qquad \text{A12: 68}$$

Dimensionless Pseudo-Pressure

$$\hat{\varphi}_D = \left[\frac{K_o(r_D\sqrt{s})I_o(r_{eD}\sqrt{s}) - K_o(r_{eD}\sqrt{s})I_o(r_D\sqrt{s})}{p\sqrt{s}[K_1(\sqrt{s})I_o(r_{eD}\sqrt{s}) + K_o(r_{eD}\sqrt{s})I_1(\sqrt{s})]}\right] \qquad \text{A12: 69}$$

The rate transient model (CPIB) and pressure transient model (CRIB) are related thus:

$$p\hat{m}_{tD}(r_D = 1, p) = \sqrt{s}\left[\frac{K_1(\sqrt{s})I_o(r_{eD}\sqrt{s}) + K_o(r_{eD}\sqrt{s})I_1(\sqrt{s})}{I_o(r_{eD}\sqrt{s})K_o(\sqrt{s}) - I_o(\sqrt{s})K_o(r_{eD}\sqrt{s})}\right] = \frac{1}{p\hat{\varphi}_D}$$

Pseudo-Pressure Transient Plot in Laplace Domain

$\hat{\varphi}_D p$ Versus $\frac{1}{p}$

$\text{Der} = \frac{\Delta(\hat{\varphi}_D p)}{\Delta\left(\frac{1}{p}\right)}$ Versus $\frac{1}{p}$

For large values of p i.e. early time production period where boundary dominated flow has not been reached, the reservoir is still acting infinite and from the characteristics of the modified Bessel´s functions given in Figure A7- 1, the solutions to the infinite acting reservoir are applicable.

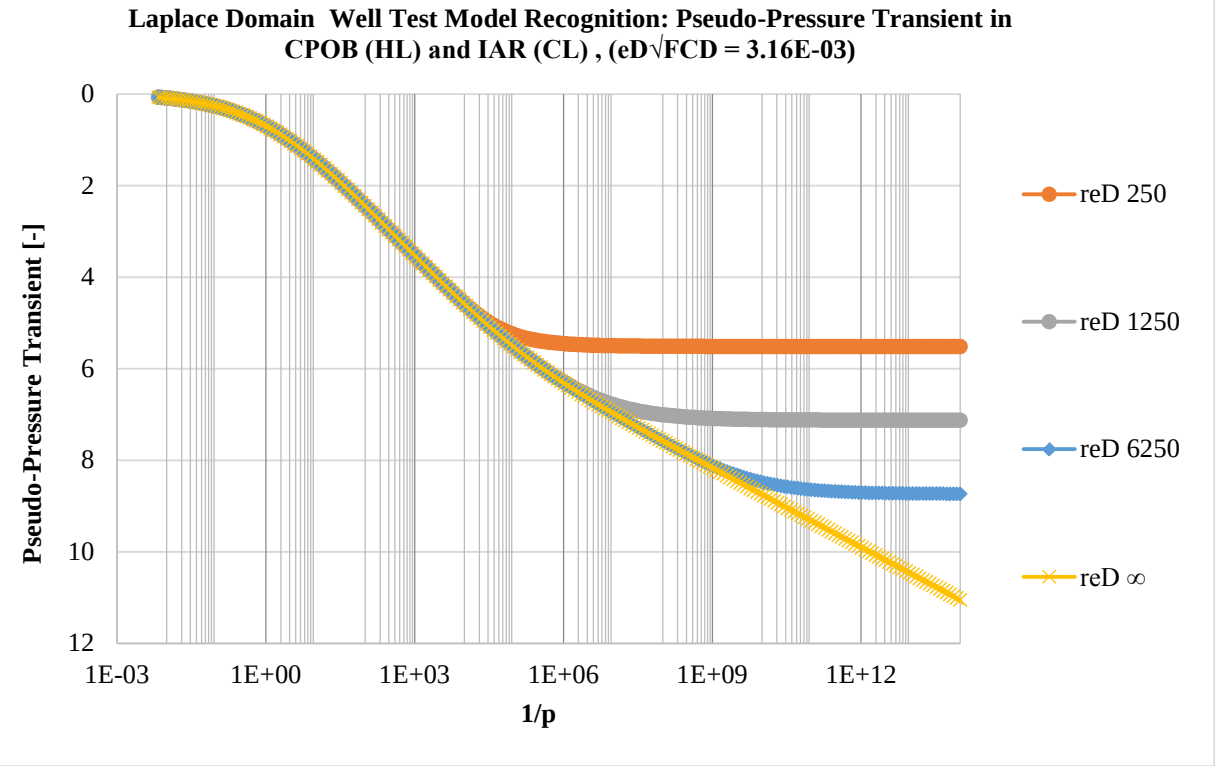

Figure A12- 28: Pseudo-Pressure in CPOB (HL) and IAR in CL

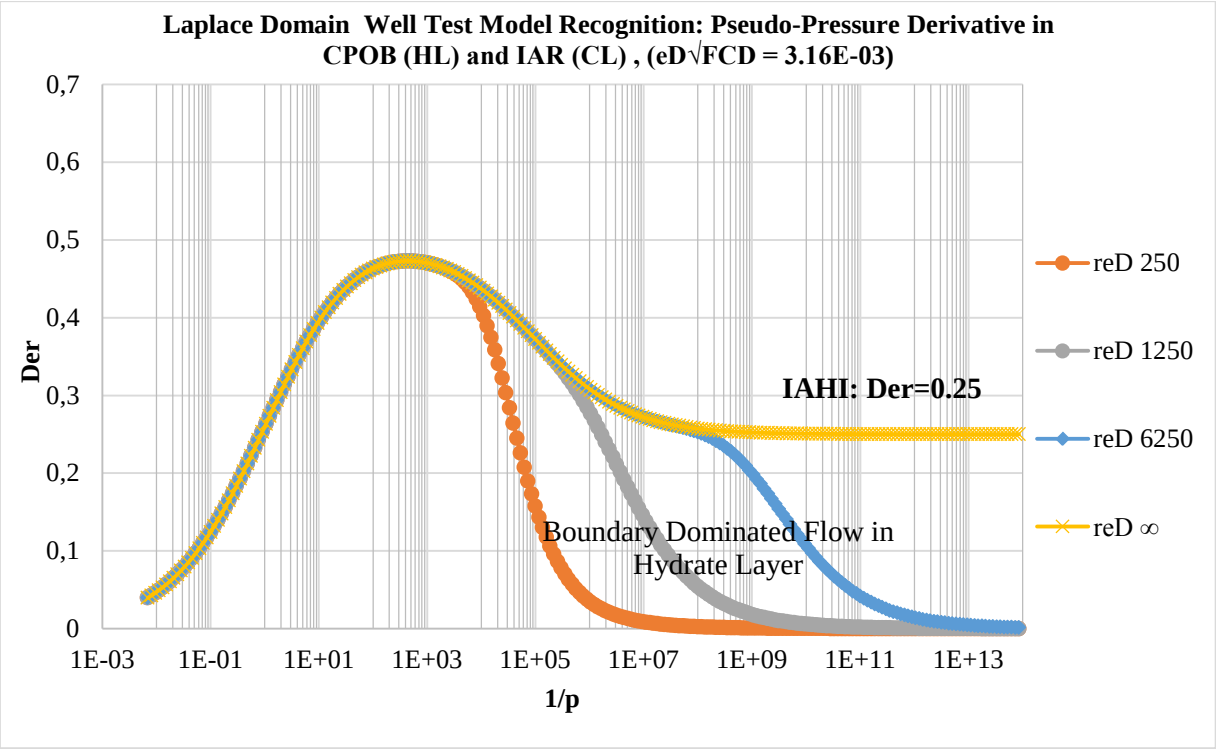

Figure A12- 29: Pseudo-Pressure Derivative in CPOB (HL) and IAR in CL

Approximate Line Source Solution Using the Image Well Theory analogue [44]

$$\varphi_D = \frac{1}{2}W\left(\frac{r_D^2}{4t_{Dw}}S_D\mu_D, r_D\sqrt{b_D}\right) - \frac{1}{2}W\left(\frac{(2l_D-r_D)^2}{4t_{Dw}}S_D\mu_D, (2l_D - r_D)\sqrt{b_D}\right) \quad \text{A12: 70}$$

Kinetic Model

$$\varphi_D = \frac{1}{2}W\left(\frac{r_D^2}{4t_{Dw}}S_{Dk}, r_D\sqrt{\gamma_{Dk}}\right) - \frac{1}{2}W\left(\frac{(2l_D-r_D)^2}{4t_{Dw}}S_{Dk}, (2l_D - r_D)\sqrt{\gamma_{Dk}}\right) \quad \text{A12: 71}$$

Case 2c: No-Flow Outer Boundary

From the image well theory and using the inner boundary condition to derive the constant B in the general solution, the dimensionless pseudo-pressure profile is given by:

$$\varphi_D(r_D, t_{Dw}) = 0.5\frac{1}{\left[e^{-\left(\frac{1}{4t_{Dw}}\right)} - (2l_D-1)^{-1}e^{-\frac{(2l_D-1)^2}{4t_{Dw}}}\right]}\left[E_1\left(\frac{r_D^2}{4t_{Dw}}S_D\right) + E_1\left(S_D\frac{(2l_D-r_D)^2}{4t_{Dw}}\right)\right] \quad \text{A12: 72}$$

$$\varphi_D(r_D = 1, t_{Dw}) = 0.5\frac{1}{\left[e^{-\left(\frac{1}{4t_{Dw}}\right)} - (2l_D-1)^{-1}e^{-\frac{(2l_D-1)^2}{4t_{Dw}}}\right]}\left[E_1\left(\frac{r_D^2}{4t_{Dw}}S_D\right) + E_1\left(S_D\frac{(2l_D-r_D)^2}{4t_{Dw}}\right)\right] \quad \text{A12: 73}$$

Late Time Approximation

$$\varphi_D(r_D = 1, t_{Dw}) \approx 0.5\left[E_1\left(\frac{r_D^2}{4t_{Dw}}S_D\right) + E_1\left(S_D\frac{(2l_D-r_D)^2}{4t_{Dw}}\right)\right] \quad \text{A12: 74}$$

Solutions in Laplace Domain

$$\hat{\varphi}_D = c_1 I_o(r_D\sqrt{s}) + c_2 K_o(r_D\sqrt{s})$$

Boundary Conditions

r_{eD} $\quad \left(\frac{d\hat{\varphi}_D}{dr_D}\right)_{r_{eD}} = 0 \quad \left(\frac{d\hat{\varphi}_D}{dr_D}\right)_{r_{eD}} = c_1\sqrt{s}I_1(r_{eD}\sqrt{s}) - c_2\sqrt{s}K_1(r_{eD}\sqrt{s}) = 0$

r_D=1 $\quad r_D\frac{d\hat{\varphi}_D}{dr_D} = -\frac{1}{p}$

From the boundary conditions, the constants c_1 and c_2 are given thus:

$$c_1 = \frac{K_1(r_{eD}\sqrt{s})}{p\{\sqrt{s}\{[K_1(\sqrt{s})I_1(r_{eD}\sqrt{s})]-[K_1(r_{eD}\sqrt{s})I_1(\sqrt{s})]\}\}} \qquad \text{A12: 75}$$

$$c_2 = \frac{I_1(r_{eD}\sqrt{s})}{p\{\sqrt{s}\{[K_1(\sqrt{s})I_1(r_{eD}\sqrt{s})]-[K_1(r_{eD}\sqrt{s})I_1(\sqrt{s})]\}\}} \qquad \text{A12: 76}$$

Dimensionless Pseudo-Pressure

$$\hat{\varphi}_D = \frac{[K_1(r_{eD}\sqrt{s})I_o(r_D\sqrt{s})]+[K_o(r_D\sqrt{s})I_1(r_{eD}\sqrt{s})]}{p\sqrt{s}\{[K_1(\sqrt{s})I_1(r_{eD}\sqrt{s})]-[K_1(r_{eD}\sqrt{s})I_1(\sqrt{s})]\}} \qquad \text{A12: 77}$$

Pseudo-Pressure Transient Plot in Laplace Domain

$\hat{\varphi}_D p$ Versus $\frac{1}{p}$

$\text{Der} = \frac{\Delta(\hat{\varphi}_D p)}{\Delta\left(\frac{1}{p}\right)}$ Versus $\frac{1}{p}$

For large values of p i.e. early time production period where boundary dominated flow has not been reached, the reservoir is still acting infinite and from the characteristics of the modified Bessel´s functions given in Figure A7- 1, the solutions to the infinite acting reservoir are applicable.

The rate transient model (CPIB) and pressure transient model (CRIB) are related thus:

$$p\hat{m}_{tD}(r_D = 1, p) = \sqrt{s}\left[\frac{[I_1(r_{eD}\sqrt{s})K_1(\sqrt{s})-K_1(r_{eD}\sqrt{s})I_1(\sqrt{s})]}{K_o(\sqrt{s})I_1(r_{eD}\sqrt{s})+K_1(r_{eD}\sqrt{s})I_o(\sqrt{s})}\right] = \frac{1}{p\hat{\varphi}_D} \qquad \text{A12: 78}$$

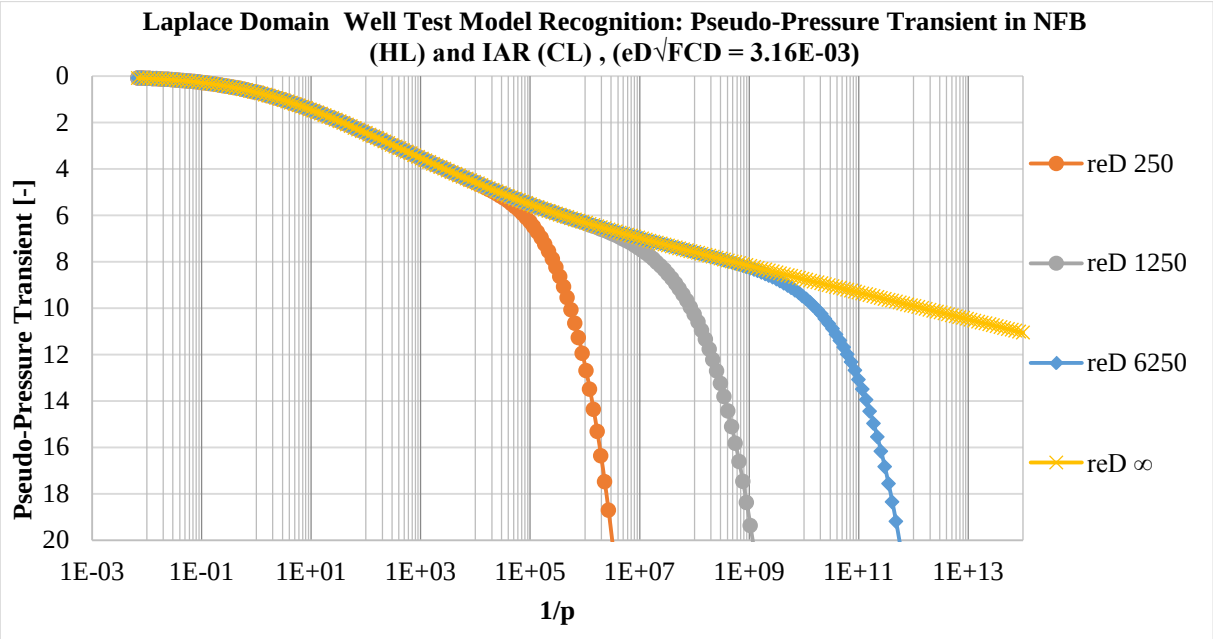

Figure A12- 30: Pseudo-Pressure in NFB (HL) and IAR in CL

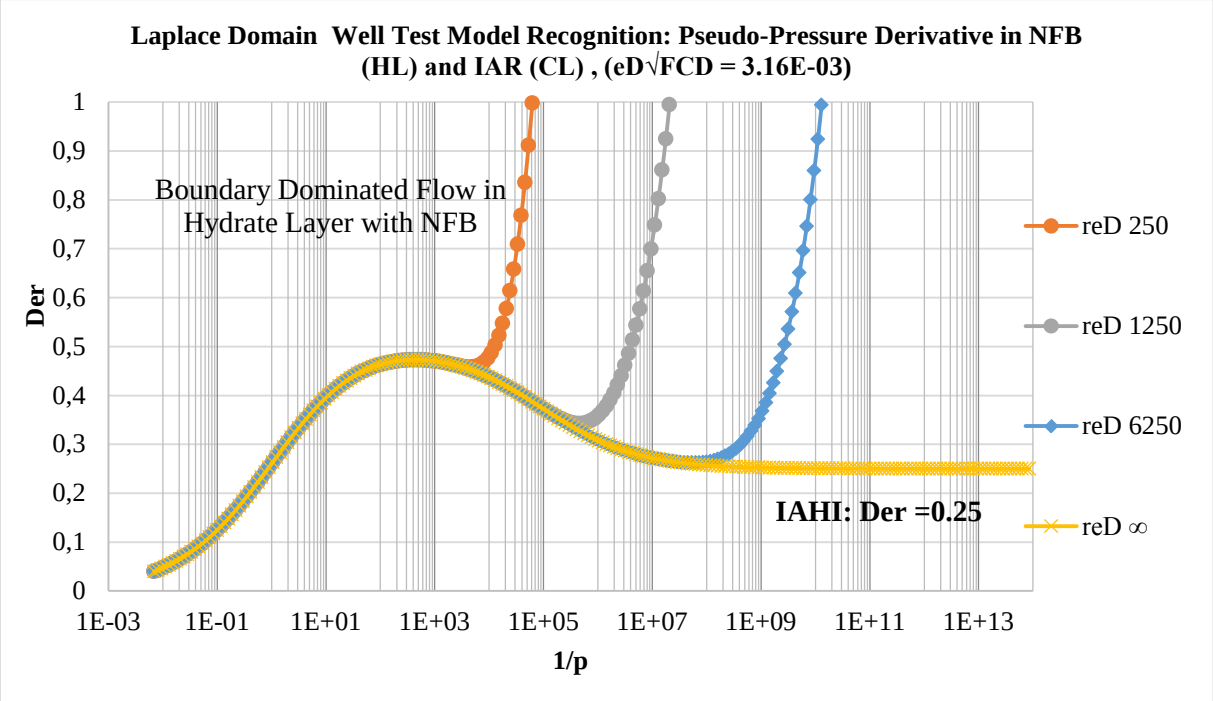

Figure A12- 31: Pseudo-Pressure in NFB (HL) and IAR in CL

Approximate Line Source Solution Using the Image Well Theory analogue [44]

$$\varphi_D = \frac{1}{2}W\left(\frac{r_D^2}{4t_{Dw}}S_D\mu_D, r_D\sqrt{b_D}\right) + \frac{1}{2}W\left(\frac{(2l_D-r_D)^2}{4t_{Dw}}S_D\mu_D, (2l_D - r_D)\sqrt{b_D}\right) \quad \text{A12: 79}$$

Kinetic Model

$$\varphi_D = \frac{1}{2}W\left(\frac{r_D^2}{4t_{Dw}}S_{Dk}, r_D\sqrt{\gamma_{Dk}}\right) + \frac{1}{2}W\left(\frac{(2l_D-r_D)^2}{4t_{Dw}}S_{Dk}, (2l_D - r_D)\sqrt{\gamma_{Dk}}\right) \quad \text{A12: 80}$$

Appendix 13: Analytical Solutions to Diffusivity Problems in Over-Pressured Gas Hydrates

We represent the diffusivity equations for both the dissociated and un-dissociated zones in dimensionless parameters thus:

Dissociated Zone	Undissociated Zone
$r_D = \frac{r}{r_w}$ $\quad r_w \le r \le r_s\ (t)$ $r_{sD} = \frac{r_s(t)}{r_w} \ge 1$ For the dissociation zone, we get $1 \le r_D \le r_{sD}$ **Constant Terminal Pressure** $\varphi_D = \frac{\varphi(r,t) - \varphi_i}{\varphi_{wf} - \varphi_i}$ **Dimensionless Form of the diffusivity Equation** $\frac{\partial^2 \hat{\varphi}_D}{\partial {r_D}^2} + \frac{1}{r_D}\frac{\partial \hat{\varphi}_D}{\partial r_D} - \left[S_D p + \left(e_D \widehat{Q_{pD}}\right)_{caprock} + \left(e_D \widehat{Q_{pD}}\right)_{Underburden}\right]\hat{\varphi}_D = 0$	$r_D = \frac{r}{r_w}$ $\quad r_s\ (t) \le r \le \infty$ $r_D \ge r_{sD}$ For an infinite acting reservoir, we get $r_{sD} \le r_D \le \infty$ **Constant Terminal Pressure** $\varphi_D = \frac{\varphi(r,t) - \varphi_i}{\varphi_{wf} - \varphi_i}$ **Dimensionless Form of the diffusivity Equation** $\frac{\partial^2 \hat{\varphi}_D}{\partial {r_D}^2} + \frac{1}{r_D}\frac{\partial \hat{\varphi}_D}{\partial r_D} - [S_{Dk} p]\hat{\varphi}_D = 0$

By transforming the diffusivity equation into dimensionless parameters and redefining the boundary conditions as shown earlier, the constant terminal pressure solutions could be derived.

Constant Terminal Pressure Models for Over-pressured Gas Hydrate Reservoir

Case 1: Infinite Acting Reservoir

The dimensionless pseudo-pressures for both the dissociated and un-dissociated zones have been similarly defined such that a dimensionless pseudo-pressure at the crossover or dissociation front can be characterized. This is defined thus:

Crossover Point

$$\varphi_{sD}(r_{sD}, t_{Dw}) = \frac{\varphi_{eq} - \varphi_i}{\varphi_{wf} - \varphi_i} \qquad \text{A13: 1}$$

Note that the dissociated zone will behave similar to constant pressure outer boundary problems; hence the solution to the constant pressure outer boundary problem can be applied for the dissociated zone. The similarity variable method can be used in addressing such a problem; however with many limitations as compared to the Laplace transforms. CPOB cases using the similarity variable are usually addressed by applying the image well theory which is in this case very complex as no fixed

boundary is actually present for an IAR. Only approximate solutions can be derived using the similarity variable method and for more accurate results, the Laplace domain solution should be used.

Solutions with Boltzmann Transformation

Dimensionless Pseudo-Pressure

Dissociated Zone

Although the dissociated zone would act like the constant outer pressure boundary problem, the pressure drop at the boundary is not zero. Hence the equilibrium pressure needs to be accounted for in the model.

Boundary Conditions

$\varphi_D(r_D, t_{Dw}) = 1$ at $r_D=1$ and $t_{Dw}>0$ $v_D^2 = \frac{S_D}{4t_{Dw}}$

$\varphi_D(r_D, t_{Dw}) = \varphi_{sD}$ at r_{sD} and $t_{Dw}>0$ $v_D^2 = \frac{{r_{sD}}^2}{4t_{Dw}}$

To solve the problem of the moving boundary, the following facts must be considered:

- The reservoir is infinite acting which implies the dissociated radius will act infinite at some point during production
- When the dissociated zone starts acting infinite, the pressure at the boundary is equal to the equilibrium pressure and not zero s seen with the normally pressured reservoir.

With the above facts, the general solution to the infinite acting system is given thus:

$$\varphi_D = AE_1\left(S_D\frac{{r_D}^2}{4t_{Dw}}\right) + BE_1\left(S_D\frac{{r_{sD}}^2}{4t_{Dw}}\right) \quad \text{A13: 2}$$

Using the boundary conditions, the coefficients A and B are derived and the pseudo-pressure solution is given thus:

$$\varphi_D = (1-\varphi_{sD})\frac{E_1\left(S_D\frac{{r_D}^2}{4t_{Dw}}\right)}{\left[E_1\left(S_D\frac{1}{4t_{Dw}}\right)-E_1\left(S_D\frac{{r_{sD}}^2}{4t_{Dw}}\right)\right]} + \frac{\varphi_{sD}E_1\left(S_D\frac{1}{4t_{Dw}}\right)-E_1\left(S_D\frac{{r_{sD}}^2}{4t_{Dw}}\right)}{\left[E_1\left(S_D\frac{1}{4t_{Dw}}\right)-E_1\left(S_D\frac{{r_{sD}}^2}{4t_{Dw}}\right)\right]} \quad \text{A13: 3}$$

or

$$\varphi_D = \varphi_{sD}\frac{\left[E_1\left(S_D\frac{1}{4t_{Dw}}\right)-E_1\left(S_D\frac{{r_D}^2}{4t_{Dw}}\right)\right]}{\left[E_1\left(S_D\frac{1}{4t_{Dw}}\right)-E_1\left(S_D\frac{{r_{sD}}^2}{4t_{Dw}}\right)\right]} + \frac{\left[E_1\left(S_D\frac{{r_D}^2}{4t_{Dw}}\right)-E_1\left(S_D\frac{{r_{sD}}^2}{4t_{Dw}}\right)\right]}{\left[E_1\left(S_D\frac{1}{4t_{Dw}}\right)-E_1\left(S_D\frac{{r_{sD}}^2}{4t_{Dw}}\right)\right]} \quad \text{A13: 4}$$

Note that if the well is produced at pressures above the equilibrium pressure, provided free fluid is present in the hydrate layer, no hydrates will dissociate and the reservoir would behave similar to conventional reservoirs.

The solution to the problem takes the form:

$\mathbf{P_{wf} \geq P_{eq}}$

$$\varphi_D = \frac{E_1\left(S_{Dk}\frac{r_D{}^2}{4t_{Dw}}\right)}{E_1\left(\frac{S_{Dk}}{4t_{Dw}}\right)} \quad \text{A13: 5}$$

The moving boundary model proposed by [70] and [72] considered the reservoir pressure in the dissociated zone to be equal to the equilibrium pressure, making the dimensionless equilibrium pressure equal zero at the dissociation front and their model can be represented in terms of pseudo-pressure thus [70], [72]:

$$\varphi_D = \frac{\varphi(r,t)-\varphi_{eq}}{\varphi_{wf}-\varphi_{eq}} = \frac{\left[E_1\left(S_D\frac{r_D{}^2}{4t_{Dw}}\right)-E_1\left(S_D\frac{r_{sD}{}^2}{4t_{Dw}}\right)\right]}{\left[E_1\left(S_D\frac{1}{4t_{Dw}}\right)-E_1\left(S_D\frac{r_{sD}{}^2}{4t_{Dw}}\right)\right]} \quad \text{A13: 6}$$

Radius of Dissociation

The definition of the radius of dissociation has been a challenge for many analytical models for the moving boundary problem. Most models used in deriving the transient radius of dissociation are based on the model proposed by [71], which simply addresses mass balance at the dissociation front.

In a similar manner, we address the following boundary conditions at the dissociation front:

$$[\varphi_D]_{\text{dissociation front}} = \varphi_{sD} \quad \text{A13: 7}$$

$$[\dot{m}_{tD}]_{\text{front(dissociated zone)}} = [\dot{m}_{tD}]_{\text{front(undissociated zone)}} \quad \text{A13: 8}$$

Efforts will now be made to derive the solutions for the rate transient at the fronts.

Rate Transient

Dissociated Zone

$$\dot{m}_{tD} = -r_D\frac{d\varphi_D}{\partial r_D}$$

From the deduced pressure profile in the dissociated zone, we get:

$$\dot{m}_{tD} = (1-\varphi_{sD})\frac{2e^{-\left(\frac{r_D{}^2}{4t_{Dw}}S_D\right)}}{\left[E_1\left(S_D\frac{1}{4t_{Dw}}\right)-E_1\left(S_D\frac{r_{sD}{}^2}{4t_{Dw}}\right)\right]} \quad \text{A13: 9}$$

$\mathbf{P_{wf} \geq P_{eq}}$

$$\dot{m}_{tD} = \frac{2}{\left[E_1\left(\frac{S_{Dk}}{4t_{Dw}}\right)\right]}e^{-\left(S_{Dk}\frac{r_D^2}{4t_{Dw}}\right)} \quad \text{A13: 10}$$

Undissociated Zone

$$\varphi_D = B\left[E_1\left(\frac{r_D{}^2}{4t_{Dw}}S_{Dk}\right)\right] \quad \text{A13: 11}$$

Unlike methods seen earlier in deducing the constant B in the above equation, here, the constant has to be derived based on the boundary conditions at the dissociation front and the outer boundary of the undissociated zone.

We now apply the first boundary condition at the crossover point such that the constant B is obtained.

$$\varphi_D = \varphi_{sD}\frac{\left[E_1\left(\frac{r_D{}^2}{4t_{Dw}}S_{Dk}\right)\right]}{\left[E_1\left(\frac{r_{sD}{}^2}{4t_{Dw}}S_{Dk}\right)\right]} \qquad \text{A13: 12}$$

The mass rate at the dissociation front obtained front the solution of the undissociated region is given by:

$$\dot{m}_{tD} = \frac{2\varphi_{sD}}{\left[E_1\left(\frac{r_{sD}{}^2}{4t_{Dw}}S_{Dk}\right)\right]}e^{-\left(\frac{r_D^2}{4t_{Dw}}S_{Dk}\right)} \qquad \text{A13: 13}$$

By equating the solutions for the dimensionless mass rates for each zone we get the following relationship which must always be satisfied.

$$\dot{m}_{tD} = \frac{2\varphi_{sD}}{\left[E_1\left(\frac{r_{sD}{}^2}{4t_{Dw}}S_{Dk}\right)\right]}e^{-\left(\frac{r_{sD}^2}{4t_{Dw}}S_{Dk}\right)} = (1-\varphi_{sD})\frac{2e^{-\left(\frac{r_{sD}{}^2}{4t_{Dw}}S_D\right)}}{\left[E_1\left(S_D\frac{1}{4t_{Dw}}\right)-E_1\left(S_D\frac{r_{sD}{}^2}{4t_{Dw}}\right)\right]} \qquad \text{A13: 14}$$

Criterion for Valid Radius of Dissociation

$$\frac{2\varphi_{sD}}{\left[E_1\left(\frac{r_{sD}{}^2}{4t_{Dw}}S_{Dk}\right)\right]}e^{-\left(\frac{r_{sD}^2}{4t_{Dw}}S_{Dk}\right)} = (1-\varphi_{sD})\frac{2e^{-\left(\frac{r_{sD}{}^2}{4t_{Dw}}S_D\right)}}{\left[E_1\left(S_D\frac{1}{4t_{Dw}}\right)-E_1\left(S_D\frac{r_{sD}{}^2}{4t_{Dw}}\right)\right]} \qquad \text{A13: 15}$$

For a given value of φ_{sD}, t_{Dw} and S_{Dk}/S_D, the above equation should be computed for arbitrary values of r_{sD} till the criterion is fulfilled. For all boundary conditions to be valid, the above criterion must be obeyed at all times. Note that if $\varphi_{sD}=0$, the transient rate solution for the dissociated zone reduces to the solution for the normally pressured gas hydrates as $r_{sD}\rightarrow\infty$.

Solution in Laplace Domain

The solutions in Laplace domain give the exact solution to the problem.

Dimensionless Pseudo-Pressure

Dissociated Zone

$$\hat{\varphi}_D = c_1 I_o\left(r_D\sqrt{s}\right) + c_2 K_o\left(r_D\sqrt{s}\right)$$

Boundary Conditions

r_{sD} $\qquad\qquad$ $\hat{\varphi}_D = \frac{\varphi_{sD}}{p}$

$r_D=1$ $\qquad\qquad$ $\hat{\varphi}_D = \frac{1}{p}$

With the defined boundary conditions, the coefficients are hence:

$$c_1 = \frac{K_o(r_{sD}\sqrt{s}) - \varphi_{sD}K_o(\sqrt{s})}{p[I_o(\sqrt{s})K_o(r_{sD}\sqrt{s}) - I_o(r_{sD}\sqrt{s})K_o(\sqrt{s})]} \quad \text{A13: 16}$$

$$c_2 = \frac{\varphi_{sD}I_o(\sqrt{s}) - I_o(r_{sD}\sqrt{s})}{p[I_o(\sqrt{s})K_o(r_{sD}\sqrt{s}) - I_o(r_{sD}\sqrt{s})K_o(\sqrt{s})]} \quad \text{A13: 17}$$

Inserting c_1 and c_2 in the general equation yields:

Solution in Laplace Domain

The solutions in Laplace domain give the exact solution to the problem.

Dimensionless Pseudo-Pressure

$$\hat{\varphi}_D = \frac{[K_o(r_D\sqrt{s})I_o(r_{sD}\sqrt{s}) - K_o(r_{sD}\sqrt{s})I_o(r_D\sqrt{s})] - \varphi_{sD}[K_o(r_D\sqrt{s})I_o(\sqrt{s}) - K_o(\sqrt{s})I_o(r_D\sqrt{s})]}{p[I_o(r_{sD}\sqrt{s})K_o(\sqrt{s}) - I_o(\sqrt{s})K_o(r_{sD}\sqrt{s})]} \quad \text{A13: 18}$$

Rate Transient

Dissociated Zone

$$\hat{m}_{tD} = -r_D\frac{d\hat{\varphi}_D}{dr_D}$$

$$\hat{m}_{tD} = r_D\frac{\sqrt{s}}{p}\left\{\frac{[K_1(r_D\sqrt{s})I_o(r_{sD}\sqrt{s}) + K_o(r_{sD}\sqrt{s})I_1(r_D\sqrt{s})] - \varphi_{sD}[K_1(r_D\sqrt{s})I_o(\sqrt{s}) + K_o(\sqrt{s})I_1(r_D\sqrt{s})]}{[I_o(r_{sD}\sqrt{s})K_o(\sqrt{s}) - I_o(\sqrt{s})K_o(r_{sD}\sqrt{s})]}\right\} \quad \text{A13: 19}$$

Undissociated Zone

$$\hat{\varphi}_D = c_1 I_o\left(r_D\sqrt{s_u}\right) + c_2 K_o\left(r_D\sqrt{s_u}\right)$$

Where,

$$s_u = S_{Dk}p$$

Boundary Condition

$r_D \to \infty$ $\qquad$ $c_1 = 0$

$$\hat{\varphi}_D = c_2 K_o\left(r_D\sqrt{s_u}\right)$$

As was done in deriving the solutions using the similarity variable, the same boundary conditions are imposed at the dissociation front such that the coefficient c_2 is derived.

$r_D = r_{sD}$ $\qquad$ $\hat{\varphi}_D = \frac{\varphi_{sD}}{p}$

$$\frac{\varphi_{sD}}{pK_o\left(r_{sD}\sqrt{s_u}\right)} = c_2$$

$$\hat{\varphi}_D = \varphi_{sD}\frac{K_o\left(r_D\sqrt{s_u}\right)}{pK_o\left(r_{sD}\sqrt{s_u}\right)}$$

$$\widehat{m}_{tD} = -r_D \frac{d\widehat{\varphi}_D}{dr_D} = r_D \varphi_{sD} \sqrt{s_u} \frac{K_1(r_D\sqrt{s_u})}{pK_o(r_{sD}\sqrt{s_u})} \quad \text{A13: 20}$$

For mass conservation to be obeyed at the dissociation front, the following must hold:

$$\widehat{m}_{tD} = r_{sD} \varphi_{sD} \sqrt{s_u} \frac{K_1(r_{sD}\sqrt{s_u})}{pK_o(r_{sD}\sqrt{s_u})} = \left\{ r_{sD} \frac{\sqrt{s}}{p} \frac{[K_1(r_{sD}\sqrt{s})I_o(r_{sD}\sqrt{s}) + K_o(r_{sD}\sqrt{s})I_1(r_{sD}\sqrt{s})] - \varphi_{sD}[K_1(r_{sD}\sqrt{s})I_o(\sqrt{s}) + K_o(\sqrt{s})I_1(r_{sD}\sqrt{s})]}{[I_o(r_{sD}\sqrt{s})K_o(\sqrt{s}) - I_o(\sqrt{s})K_o(r_{sD}\sqrt{s})]} \right\} \quad \text{A13: 21}$$

Criterion for Valid Radius of Dissociation

Such that all boundary conditions are met, the following criterion has to be obeyed at all times:

$$\varphi_{sD} = \left\{ \sqrt{\frac{s}{s_u}} \frac{[K_1(r_{sD}\sqrt{s})I_o(r_{sD}\sqrt{s}) + K_o(r_{sD}\sqrt{s})I_1(r_{sD}\sqrt{s})] - \varphi_{sD}[K_1(r_{sD}\sqrt{s})I_o(\sqrt{s}) + K_o(\sqrt{s})I_1(r_{sD}\sqrt{s})]}{[I_o(r_{sD}\sqrt{s})K_o(\sqrt{s}) - I_o(\sqrt{s})K_o(r_{sD}\sqrt{s})]} \right\} \frac{K_o(r_{sD}\sqrt{s_u})}{K_1(r_{sD}\sqrt{s_u})} \quad \text{A13: 22}$$

We notice that the use of the Laplace transform in solving the moving boundary problem becomes very cumbersome when heat conduction or the kinetic model is used as the inverse Laplace transformation is also required for the criterion of valid radius of dissociation. However, using the Laplace domain well recognition model, rate transient and derivative plots can be made as given below.

Rate Transient Plots in Laplace Domain for Infinite Acting Hydrate Layer with Moving Boundary

Rate Transient at Wellbore

$$\widehat{m}_{tD}p = \sqrt{s}\left\{ \frac{[K_1(\sqrt{s})I_o(r_{sD}\sqrt{s}) + K_o(r_{sD}\sqrt{s})I_1(\sqrt{s})] - \varphi_{sD}[K_1(\sqrt{s})I_o(\sqrt{s}) + K_o(\sqrt{s})I_1(\sqrt{s})]}{[I_o(r_{sD}\sqrt{s})K_o(\sqrt{s}) - I_o(\sqrt{s})K_o(r_{sD}\sqrt{s})]} \right\}$$

$$p\widehat{m}_{tD} \quad \text{Versus} \quad \frac{1}{p}$$

Pseudo-Pressure Profile for Reservoir

1. Dissociated Region

$$\widehat{\varphi}_D p = \frac{[K_o(r_D\sqrt{s})I_o(r_{sD}\sqrt{s}) - K_o(r_{sD}\sqrt{s})I_o(r_D\sqrt{s})] - \varphi_{sD}[K_o(r_D\sqrt{s})I_o(\sqrt{s}) - K_o(\sqrt{s})I_o(r_D\sqrt{s})]}{[I_o(r_{sD}\sqrt{s})K_o(\sqrt{s}) - I_o(\sqrt{s})K_o(r_{sD}\sqrt{s})]}$$

2.Undissociated Region

$$\widehat{\varphi}_D p = \varphi_{sD} \frac{K_o(r_D\sqrt{s_u})}{K_o(r_{sD}\sqrt{s_u})}$$

Criterion for Valid Radius of Dissociation

$$\varphi_{sD} = \left\{ \sqrt{\frac{s}{s_u}} \frac{[K_1(r_{sD}\sqrt{s})I_o(r_{sD}\sqrt{s}) + K_o(r_{sD}\sqrt{s})I_1(r_{sD}\sqrt{s})] - \varphi_{sD}[K_1(r_{sD}\sqrt{s})I_o(\sqrt{s}) + K_o(\sqrt{s})I_1(r_{sD}\sqrt{s})]}{[I_o(r_{sD}\sqrt{s})K_o(\sqrt{s}) - I_o(\sqrt{s})K_o(r_{sD}\sqrt{s})]} \right\} \frac{K_o(r_{sD}\sqrt{s_u})}{K_1(r_{sD}\sqrt{s_u})}$$

Rate Transient Diagnostic Plot in Laplace Domain: Rate Derivative

$$\text{Der} = \frac{\Delta\left(\frac{1}{p\widehat{m}_{tD}}\right)}{\Delta\left(ln\frac{1}{p}\right)} \quad \text{Versus} \quad \frac{1}{p}$$

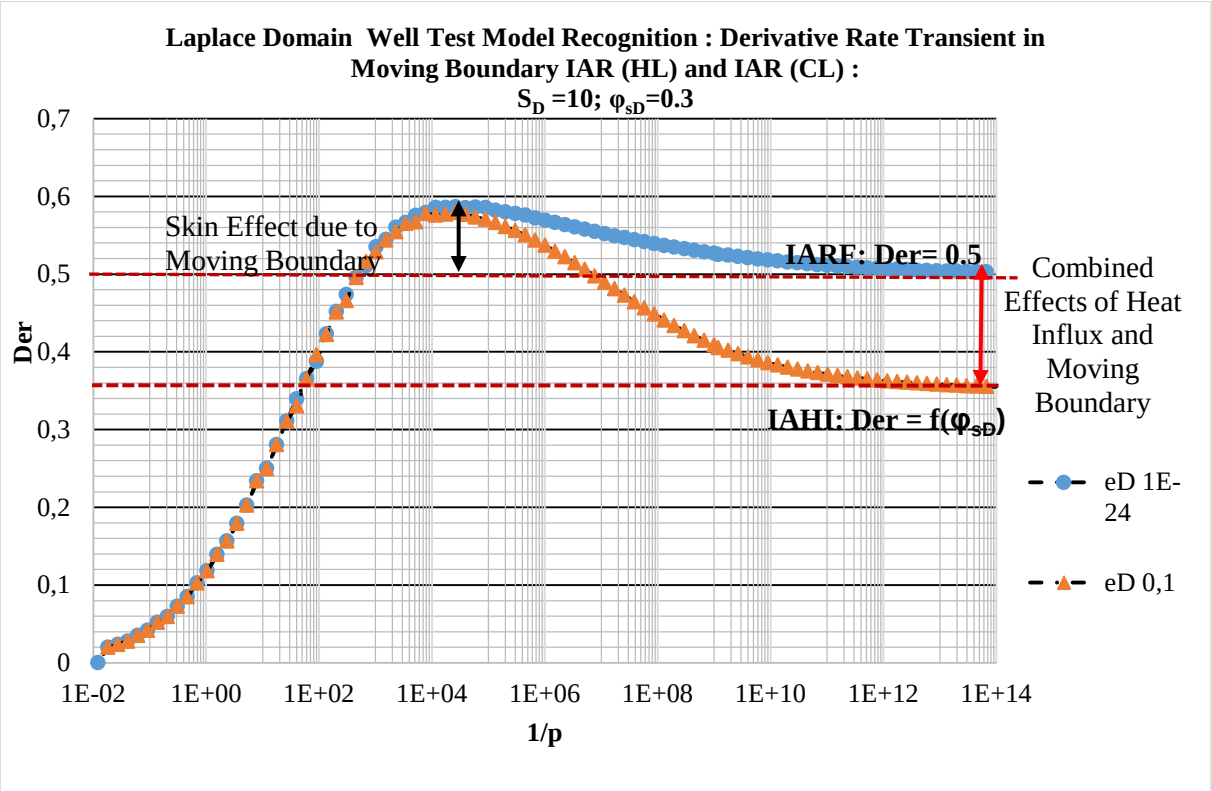

Figure A13- 1: Derivative Rate Transient in Moving Boundary IAR (HL) and IAR in CL

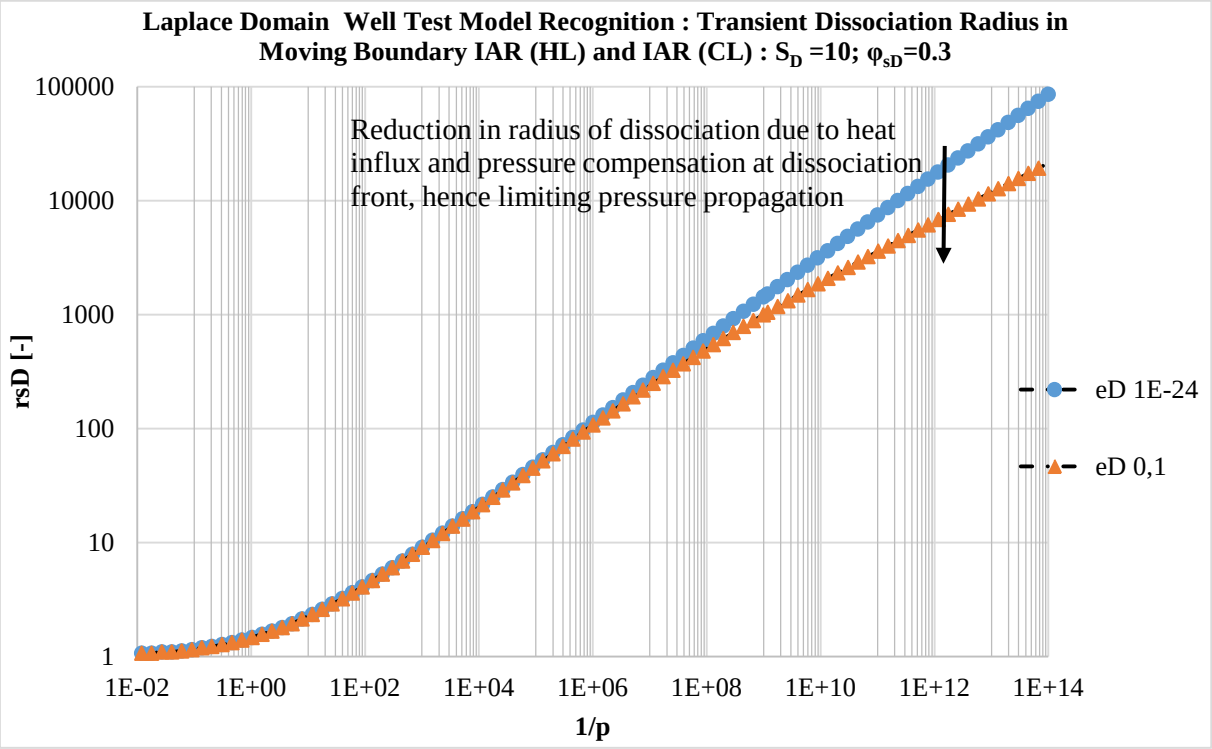

Figure A13- 2: Transient Dissociation Radius in Moving Boundary IAR (HL) and IAR (CL)

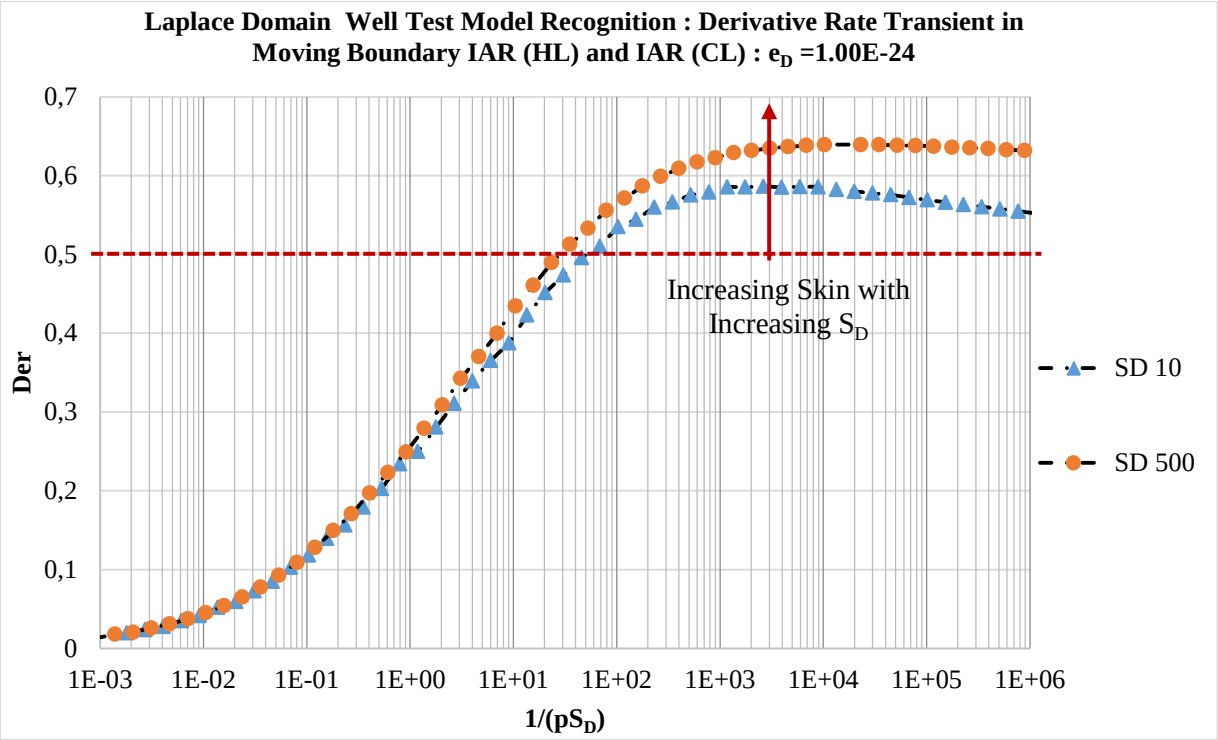

Figure A13- 3: Derivative Rate Transient in Moving Boundary IAR (HL) and IAR in CL with insignificant Heat flux

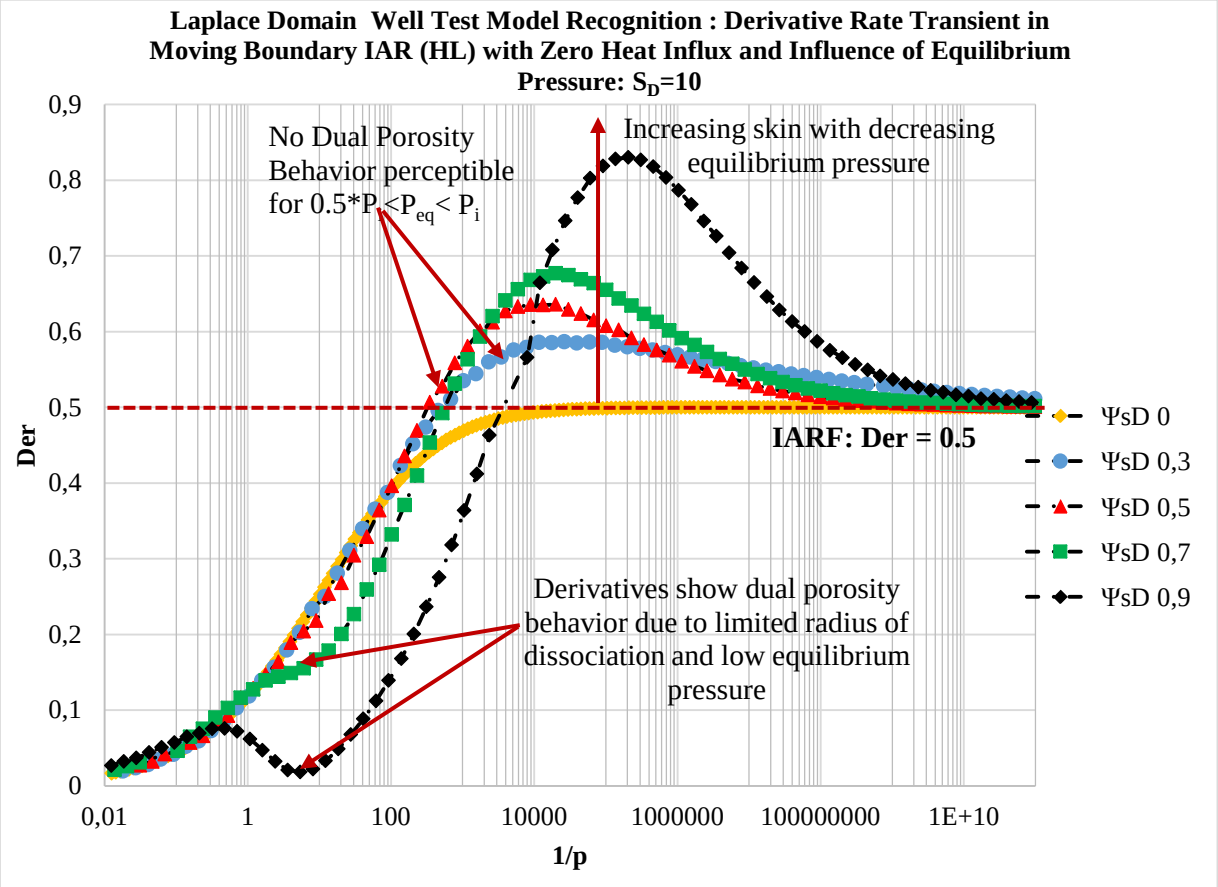

Figure A13- 4: Derivative Rate Transient in Moving Boundary IAR (HL) and IAR in CL with insignificant Heat flux

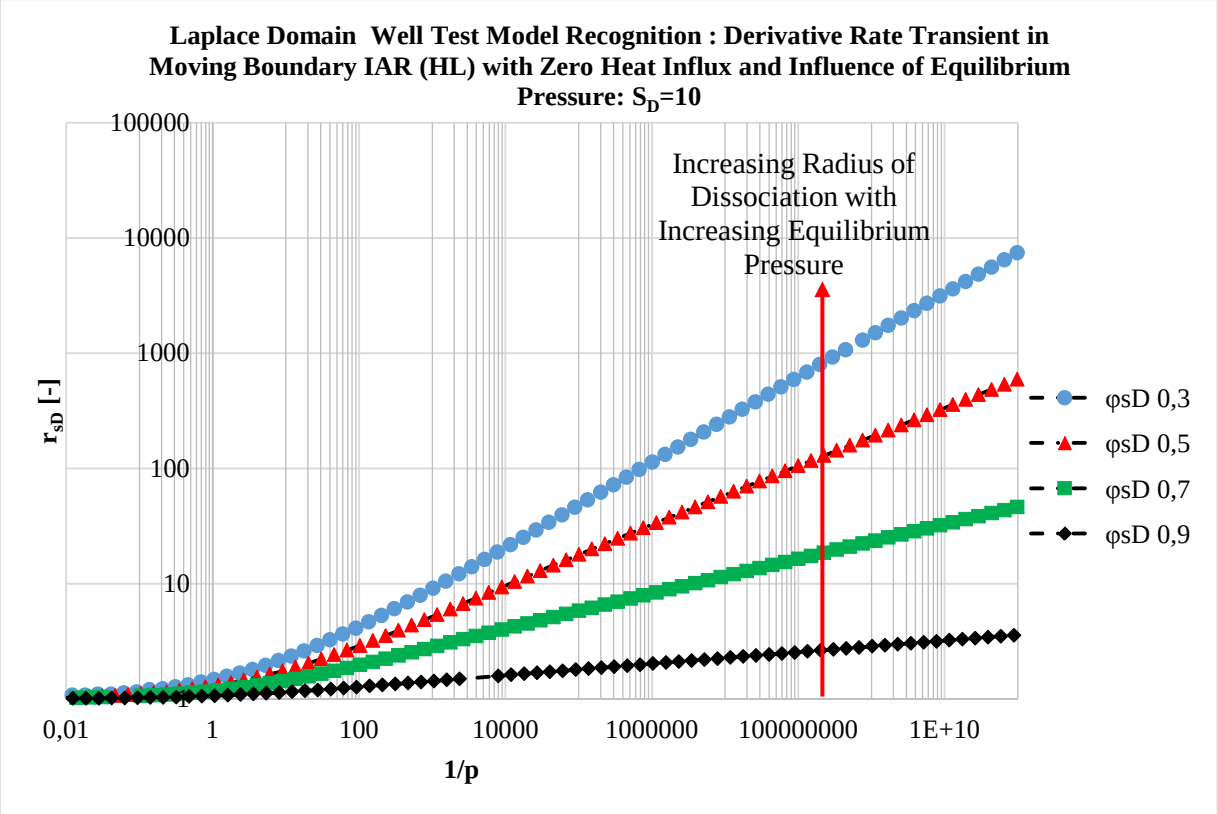

Figure A13- 5: Transient Dissociation Radius in Moving Boundary IAR (HL) and IAR (CL) with no Heat flux

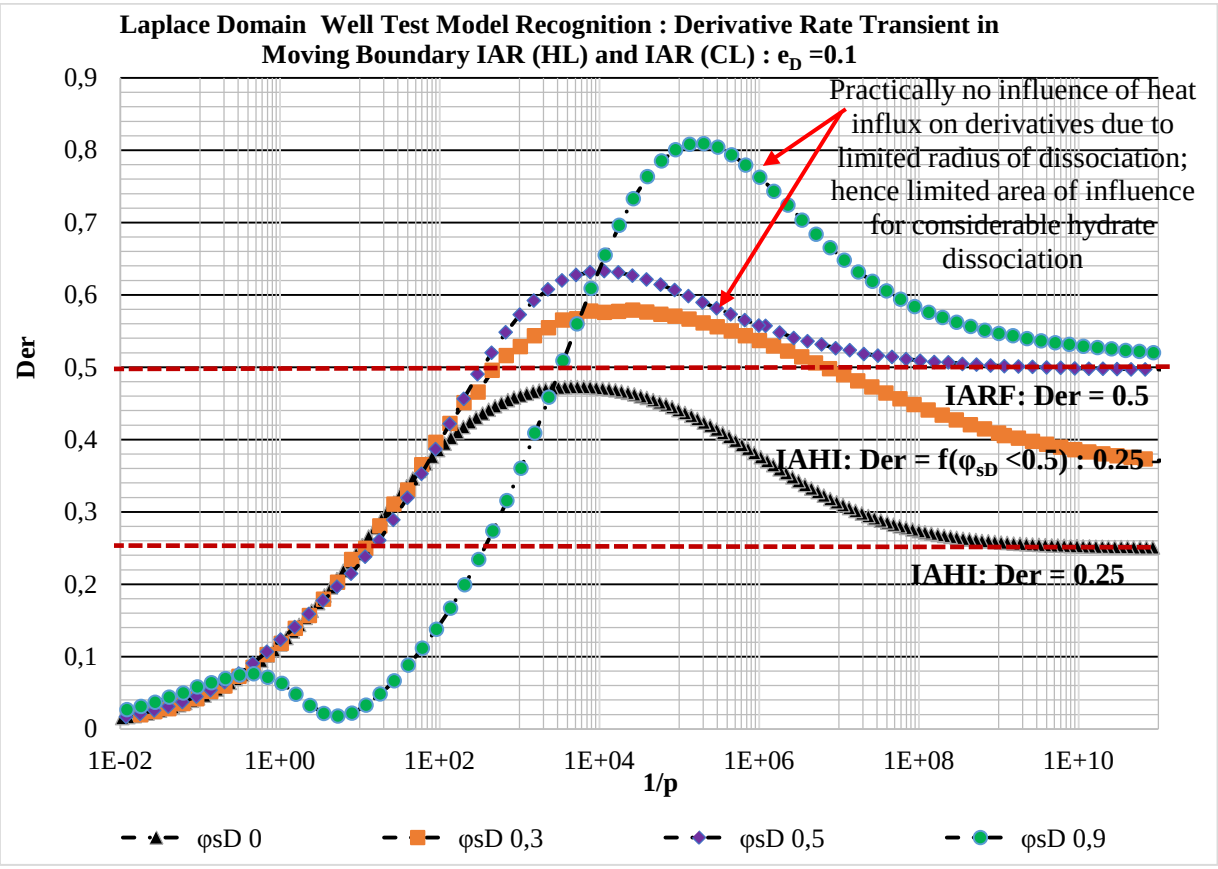

Figure A13- 6: Derivative Rate Transient in Moving Boundary IAR (HL) and IAR in CL with Heat flux

CTOB Responses

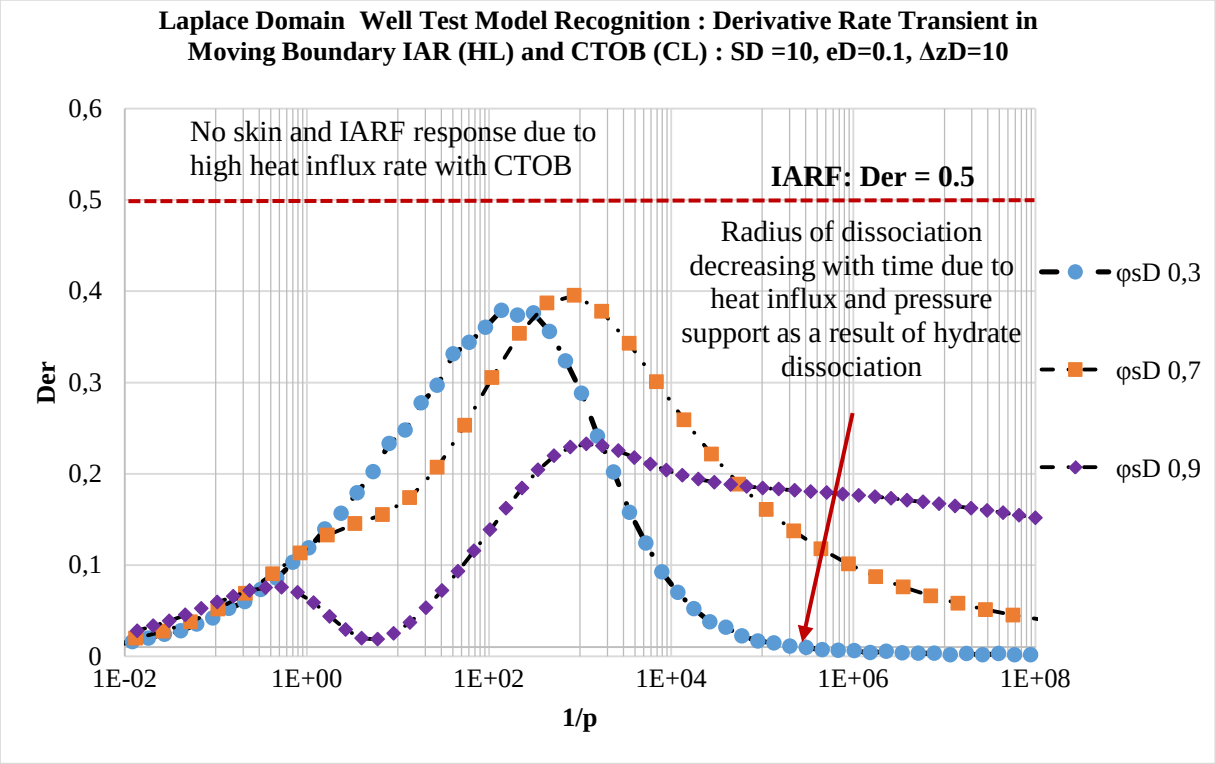

Figure A13- 7: Derivative Rate Transient in Moving Boundary IAR (HL) and CTOB in CL

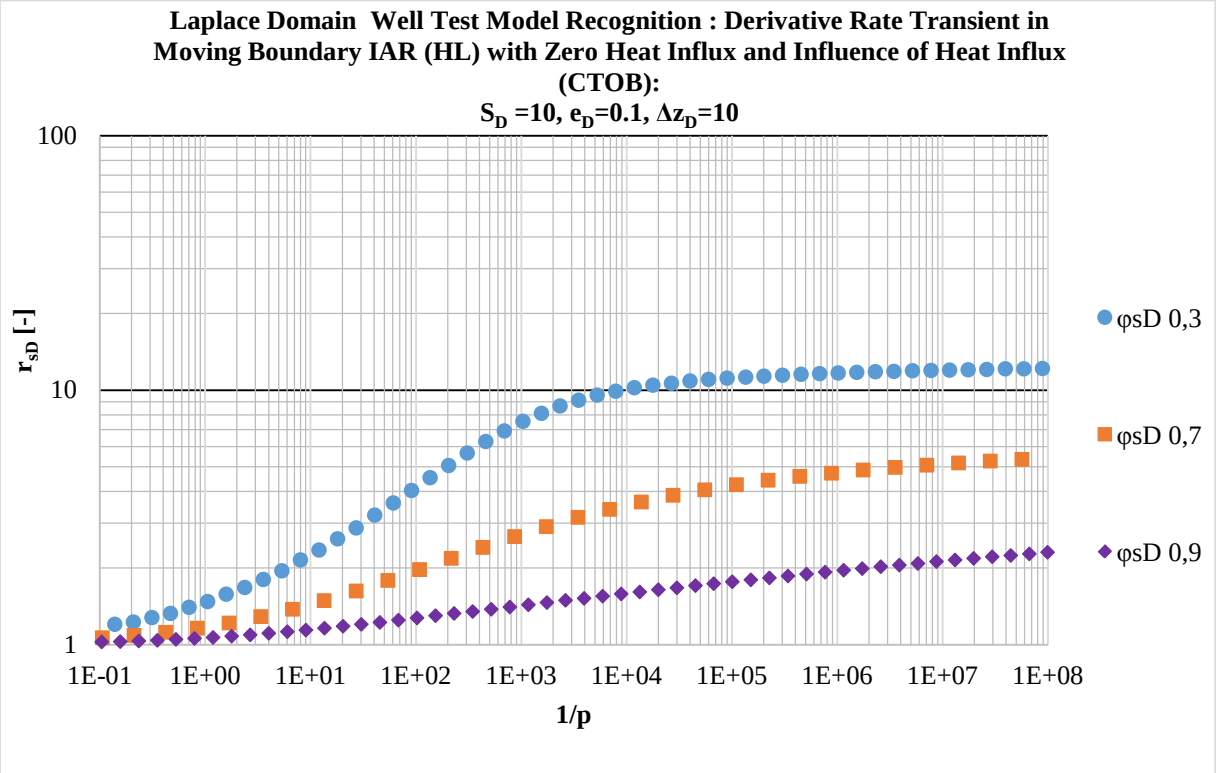

Figure A13- 8: Transient Dissociation Radius in Moving Boundary IAR (HL) and CTOB (CL)

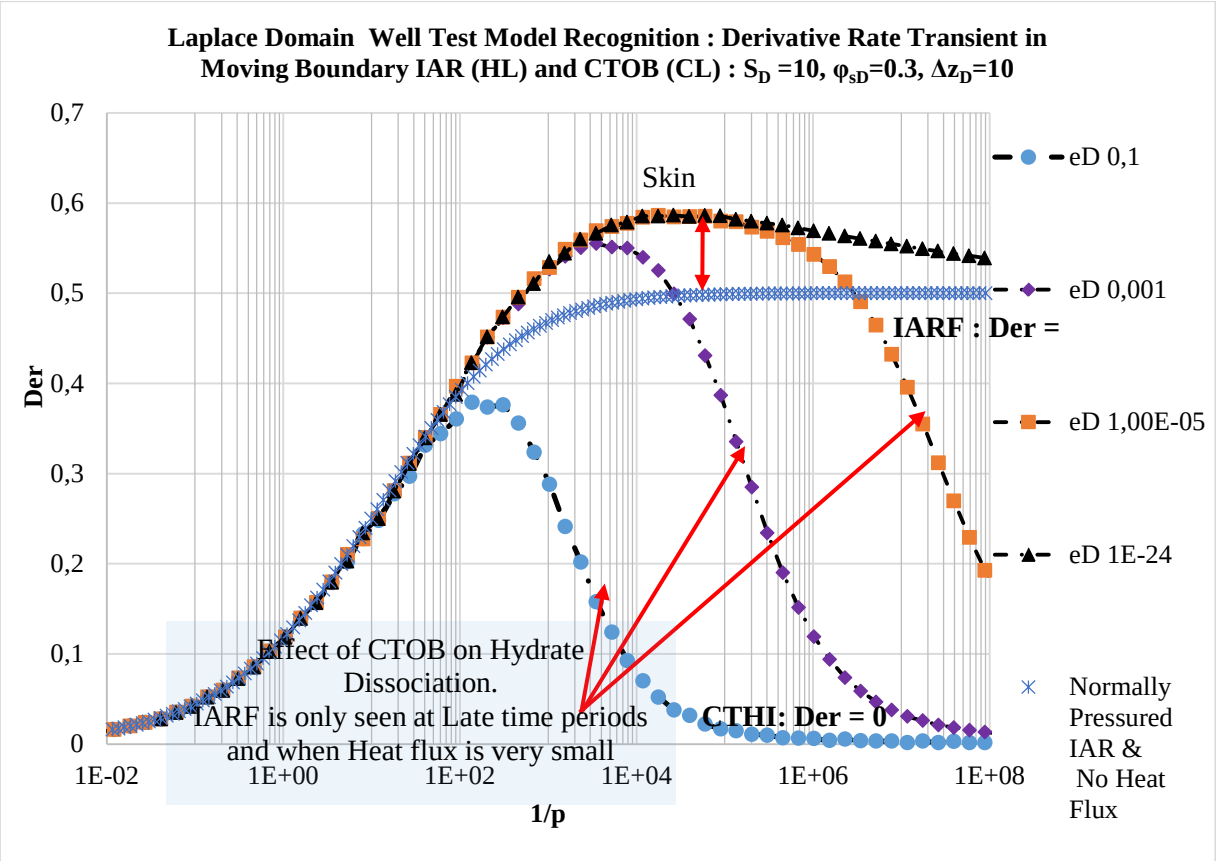

Figure A13- 9: Derivative Rate Transient in Moving Boundary IAR (HL) and CTOB in CL with Influence of Heat Flux

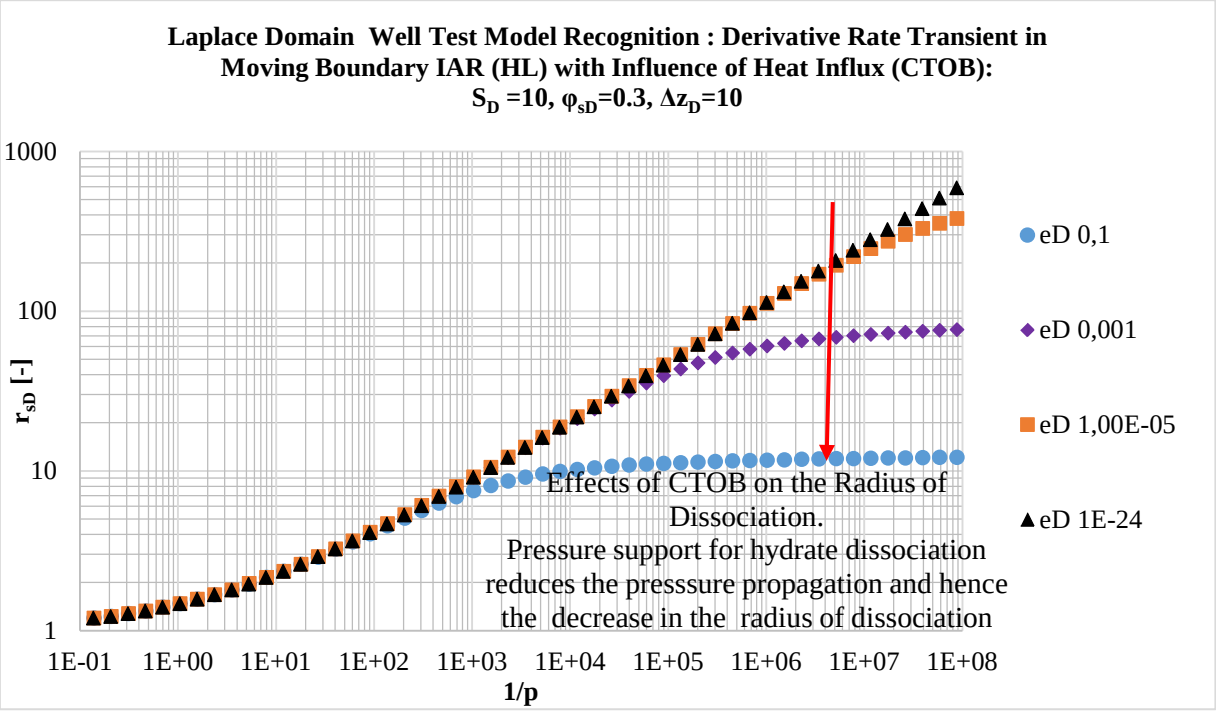

Figure A13- 10: Transient Dissociation Radius in Moving Boundary IAR (HL) and CTOB (CL) with Influence of Heat Flux

p-NFTB Responses

As shown in the normally pressured gas hydrate reservoir, the p-NFTB is not noticeable when the thickness of the confining layer is small. For this reason an extreme case can once more be considered and the effects on the rate transient derivative analyzed.

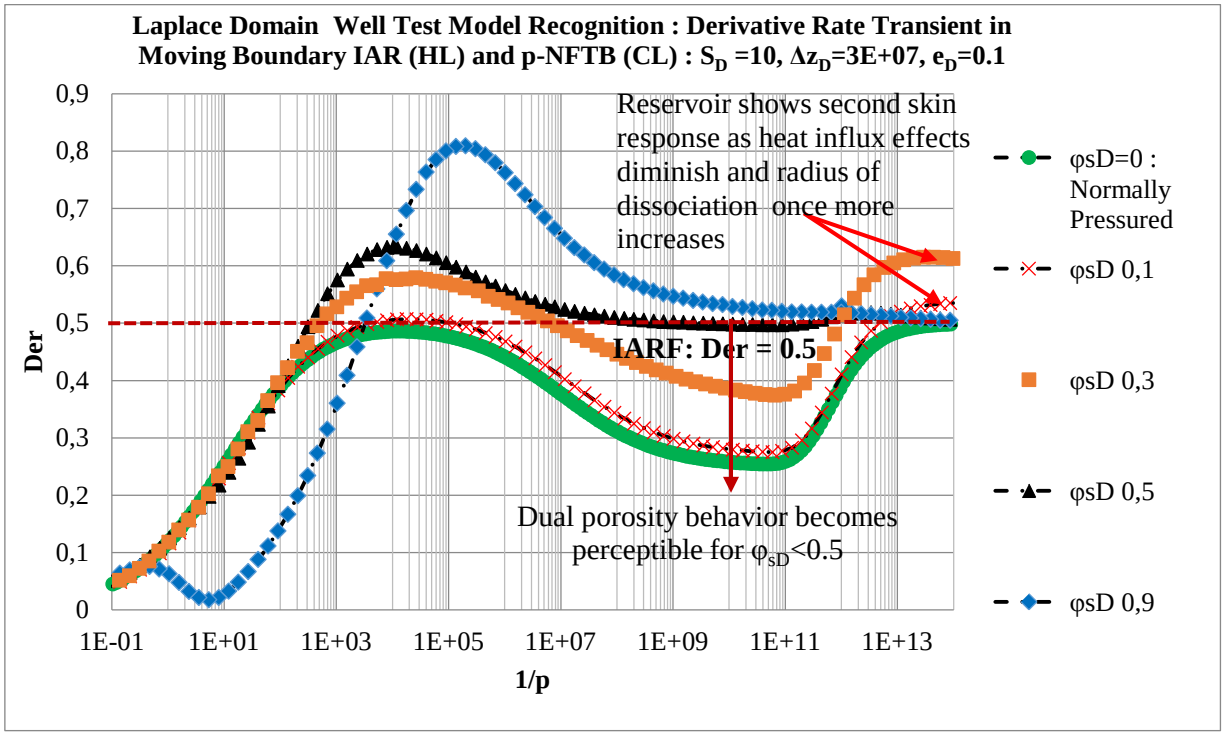

Figure A13- 11: Derivative Rate Transient in Moving Boundary IAR (HL) and p-NFTB in CL

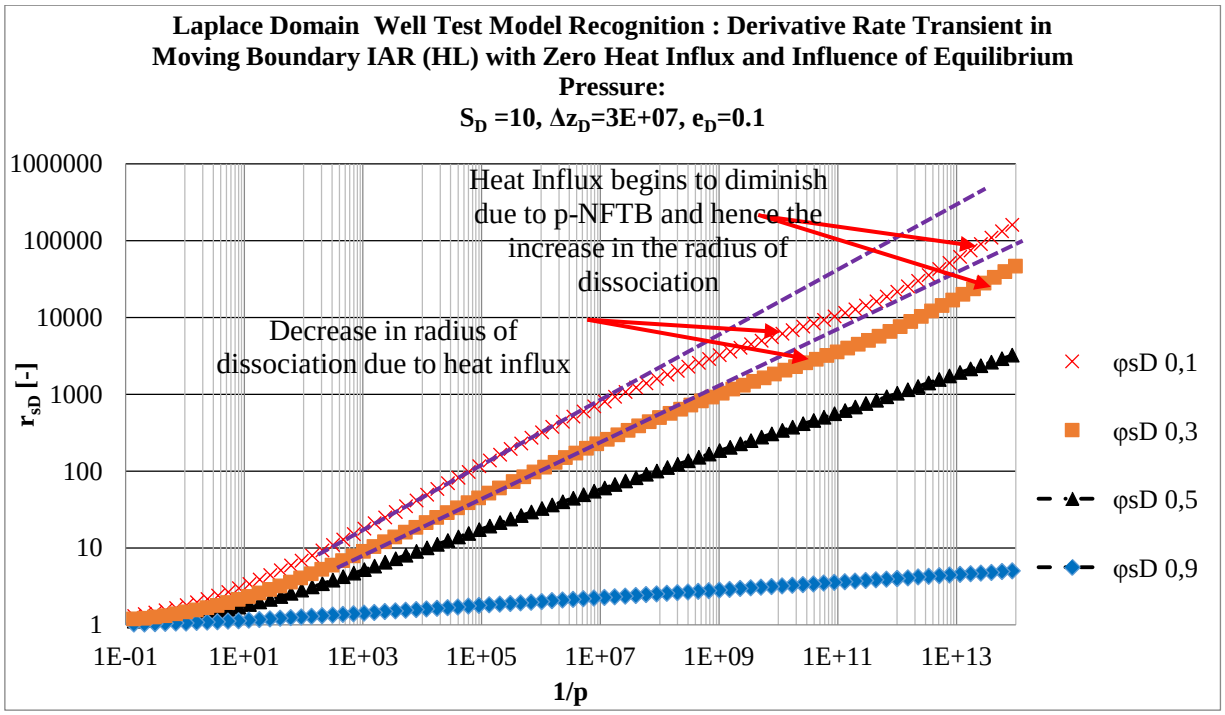

Figure A13- 12: Transient Dissociation Radius in Moving Boundary IAR (HL) and p-NFTB (CL)

Case 2: Constant Pressure Outer boundary

Solutions using the Boltzmann Transformation

Dissociated Zone

To develop a solution to the problem using similarity variables, the image well theory can be implemented; however, the solution can be very complex if multiple boundaries are used for the reservoir. Hence, we consider a reservoir with a single recharge boundary and the effects of this boundary on the dissociation. The solutions derived for the infinite acting system are therefore very different for this case due to the recharge boundary. The general solution is hence given thus for this case:

$$\varphi_D = AE_1\left(S_D\frac{{r_D}^2}{4t_{Dw}}\right) + BE_1\left(S_D\frac{{r_{sD}}^2}{4t_{Dw}}\right)$$

Boundary Conditions

$\varphi_D(r_D, t_{Dw}) = 1$ at r_D=1 and t_{Dw}>0 $v_D^2 = \frac{S_D}{4t_{Dw}}$

$\varphi_D(r_D, t_{Dw}) = \varphi_{sD}$ at r_{sD} and t_{Dw}>0 $v_D^2 = \frac{{r_{sD}}^2}{4t_{Dw}}$

Dimensionless Pseudo-Pressure

$$\varphi_D = \varphi_{sD}\frac{\left[E_1\left(S_D\frac{1}{4t_{Dw}}\right)-E_1\left(S_D\frac{{r_D}^2}{4t_{Dw}}\right)\right]}{\left[E_1\left(S_D\frac{1}{4t_{Dw}}\right)-E_1\left(S_D\frac{{r_{sD}}^2}{4t_{Dw}}\right)\right]} + \frac{\left[E_1\left(S_D\frac{{r_D}^2}{4t_{Dw}}\right)-E_1\left(S_D\frac{{r_{sD}}^2}{4t_{Dw}}\right)\right]}{\left[E_1\left(S_D\frac{1}{4t_{Dw}}\right)-E_1\left(S_D\frac{{r_{sD}}^2}{4t_{Dw}}\right)\right]} \quad \text{A13: 23}$$

Rate Transient

Dissociated Zone

$$\dot{m}_{tD} = (1-\varphi_{sD})\frac{2e^{-\left(\frac{{r_D}^2}{4t_{Dw}}S_D\right)}}{\left[E_1\left(S_D\frac{1}{4t_{Dw}}\right)-E_1\left(S_D\frac{{r_{sD}}^2}{4t_{Dw}}\right)\right]} \quad \text{A13: 24}$$

$P_{wf} \geq P_{eq}$

$$\varphi_D = \frac{\left[E_1\left(\frac{{r_D}^2}{4t_{Dw}}S_{Dk}\right)\right]-\left[E_1\left(\frac{(2l_D-r_D)^2}{4t_{Dw}}S_{Dk}\right)\right]}{\left[E_1\left(\frac{1}{4t_{Dw}}S_{Dk}\right)\right]-\left[E_1\left(\frac{(2l_D-1)^2}{4t_{Dw}}S_{Dk}\right)\right]} \quad \text{A13: 25}$$

$$\dot{m}_{tD} = 2\left\{\frac{\left[e^{-\left(\frac{{r_D}^2}{4t_{Dw}}S_D\right)}\right]+(2l_D-r_D)^{-1}r_D e^{-\frac{(2l_D-r_D)^2}{4t_{Dw}}S_D}}{\left[E_1\left(S_D\frac{1}{4t_{Dw}}\right)-E_1\left(S_D\frac{(2l_D-1)^2}{4t_{Dw}}\right)\right]}\right\} \quad \text{A13: 26}$$

Undissociated Zone

Like was done for the infinite acting well, we make efforts to predict the reservoir behavior for constant outer pressure boundary reservoirs.

Like the infinite acting reservoir, the following boundary conditions must hold at the crossover point:

$[\varphi_D]_{\text{dissociation front}} = \varphi_{sD}$

$[\dot{m}_{tD}]_{\text{front(dissociated zone)}} = [\dot{m}_{tD}]_{\text{front(undissociated zone)}}$

Dimensionless Pseudo-Pressure

Undissociated Zone

$$\varphi_D = \frac{B}{2}\left[E_1\left(\frac{{r_D}^2}{4t_{Dw}}S_{Dk}\right)\right] - \frac{B}{2}\left[E_1\left(\frac{(2l_D - r_D)^2}{4t_{Dw}}S_{Dk}\right)\right] \quad \text{A13: 27}$$

$$\varphi_D = \varphi_{sD}\frac{\left[E_1\left(\frac{{r_D}^2}{4t_{Dw}}S_{Dk}\right)\right] - \left[E_1\left(\frac{(2l_D - r_D)^2}{4t_{Dw}}S_{Dk}\right)\right]}{\left[E_1\left(-\frac{{r_{sD}}^2}{4t_{Dw}}S_{Dk}\right)\right] - \left[E_1\left(\frac{(2l_D - r_{sD})^2}{4t_{Dw}}S_{Dk}\right)\right]} \quad \text{A13: 28}$$

$$\dot{m}_{tD} = \frac{2\varphi_{sD}}{\left[E_1\left(\frac{{r_{sD}}^2}{4t_{Dw}}S_{Dk}\right)\right] - \left[E_1\left(\frac{(2l_D - r_{sD})^2}{4t_{Dw}}S_{Dk}\right)\right]}\left[e^{-\left(\frac{{r_D}^2}{4t_{Dw}}S_{Dk}\right)} + (2l_D - r_D)^{-1}r_D e^{-\frac{(2l_D - r_D)^2}{4t_{Dw}}S_{Dk}}\right] \quad \text{A13: 29}$$

By equating the mass rates at the crossover point, the criterion for the valid radius of dissociation is obtained.

Criterion for Valid Radius of Dissociation

The validity criterion is given below:

$$\dot{m}_{tD} = 2\varphi_{sD}\frac{\left[e^{-\left(\frac{{r_{sD}}^2}{4t_{Dw}}S_{Dk}\right)} + (2l_D - r_{sD})^{-1}r_{sD}e^{-\frac{(2l_D - r_{sD})^2}{4t_{Dw}}S_{Dk}}\right]}{\left[E_1\left(\frac{{r_{sD}}^2}{4t_{Dw}}S_{Dk}\right)\right] - \left[E_1\left(\frac{(2l_D - r_{sD})^2}{4t_{Dw}}S_{Dk}\right)\right]} = (1 - \varphi_{sD})\frac{2e^{-\left(\frac{{r_{sD}}^2}{4t_{Dw}}S_D\right)}}{\left[E_1\left(S_D\frac{1}{4t_{Dw}}\right) - E_1\left(S_D\frac{{r_{sD}}^2}{4t_{Dw}}\right)\right]} \quad \text{A13: 30}$$

Solutions with Laplace Transformation

Dimensionless Pseudo-Pressure

Dissociated Zone

$$\hat{\varphi}_D = c_1 I_o(r_D\sqrt{s}) + c_2 K_o(r_D\sqrt{s})$$

Boundary Conditions

r_{sD} $\qquad \hat{\varphi}_D = \frac{\varphi_{sD}}{p}$

r_D=1 $\qquad \hat{\varphi}_D = \frac{1}{p}$

Inserting c_1 and c_2 in the general equation yields:

$$\hat{\varphi}_D = \frac{[K_o(r_D\sqrt{s})I_o(r_{sD}\sqrt{s}) - K_o(r_{sD}\sqrt{s})I_o(r_D\sqrt{s})] - \varphi_{sD}[K_o(r_D\sqrt{s})I_o(\sqrt{s}) - K_o(\sqrt{s})I_o(r_D\sqrt{s})]}{p[I_o(r_{sD}\sqrt{s})K_o(\sqrt{s}) - I_o(\sqrt{s})K_o(r_{sD}\sqrt{s})]} \quad \text{A13: 31}$$

Rate Transient

Dissociated Zone

$$\hat{m}_{tD} = -r_D \frac{d\hat{\varphi}_D}{dr_D}$$

$$\hat{m}_{tD} = r_D \frac{\sqrt{s}}{p}\left\{\frac{[K_1(r_D\sqrt{s})I_o(r_{sD}\sqrt{s})+K_o(r_{sD}\sqrt{s})I_1(r_D\sqrt{s})]-\varphi_{sD}[K_1(r_D\sqrt{s})I_o(\sqrt{s})+K_o(\sqrt{s})I_1(r_D\sqrt{s})]}{[I_o(r_{sD}\sqrt{s})K_o(\sqrt{s})-I_o(\sqrt{s})K_o(r_{sD}\sqrt{s})]}\right\} \quad \text{A13: 32}$$

Undissociated Zone

$$\hat{\varphi}_D = c_1 I_o\left(r_D\sqrt{s_u}\right) + c_2 K_o\left(r_D\sqrt{s_u}\right)$$

For constant outer boundary pressure conditions, the above equation is:

$$c_1 = -c_2 \frac{K_o(r_{eD}\sqrt{s_u})}{I_o(r_{eD}\sqrt{s_u})} \quad \text{A13: 33}$$

$$\hat{\varphi}_D = c_2 \frac{K_o(r_D\sqrt{s_u})I_o(r_{eD}\sqrt{s_u})-K_o(r_{eD}\sqrt{s_u})I_o(r_D\sqrt{s_u})}{I_o(r_{eD}\sqrt{s_u})} \quad \text{A13: 34}$$

By imposing the boundary conditions at the dissociation front, the constant c_2 can be derived.

$$\frac{\varphi_{sD}}{p}\frac{I_o(r_{eD}\sqrt{s_u})}{K_o(r_{sD}\sqrt{s_u})I_o(r_{eD}\sqrt{s_u})-K_o(r_{eD}\sqrt{s_u})I_o(r_{sD}\sqrt{s_u})} = c_2 \quad \text{A13: 35}$$

The final equation is hence

$$\hat{\varphi}_D = \frac{\varphi_{sD}}{p}\frac{K_o(r_D\sqrt{s_u})I_o(r_{eD}\sqrt{s_u})-K_o(r_{eD}\sqrt{s_u})I_o(r_D\sqrt{s_u})}{K_o(r_{sD}\sqrt{s_u})I_o(r_{eD}\sqrt{s_u})-K_o(r_{eD}\sqrt{s_u})I_o(r_{sD}\sqrt{s_u})} \quad \text{A13: 36}$$

Considering the mass balance at the dissociation front, we obtain the criterion for the valid radius of dissociation:

$$\hat{m}_{tD} = \frac{\sqrt{s}}{p}\left\{\frac{[K_1(r_{sD}\sqrt{s})I_o(r_{sD}\sqrt{s})+K_o(r_{sD}\sqrt{s})I_1(r_{sD}\sqrt{s})]-\hat{\varphi}_{sD}[K_1(r_{sD}\sqrt{s})I_o(\sqrt{s})+K_o(\sqrt{s})I_1(r_{sD}\sqrt{s})]}{[I_o(r_{sD}\sqrt{s})K_o(\sqrt{s})-I_o(\sqrt{s})K_o(r_{sD}\sqrt{s})]}\right\} =$$
$$\frac{\varphi_{sD}}{p}\sqrt{s_u}\frac{K_1(r_{sD}\sqrt{s_u})I_o(r_{eD}\sqrt{s_u})+K_o(r_{eD}\sqrt{s_u})I_1(r_{sD}\sqrt{s_u})}{K_o(r_{sD}\sqrt{s_u})I_o(r_{eD}\sqrt{s_u})-K_o(r_{eD}\sqrt{s_u})I_o(r_{sD}\sqrt{s_u})} \quad \text{A13: 37}$$

Criterion for Valid Radius of Dissociation

The criterion for the dissociation radius is given by:

$$\varphi_{sD} = \sqrt{\frac{s}{s_u}}\frac{\{[K_1(r_{sD}\sqrt{s})I_o(r_{sD}\sqrt{s})+K_o(r_{sD}\sqrt{s})I_1(r_{sD}\sqrt{s})]-\hat{\varphi}_{sD}[K_1(r_{sD}\sqrt{s})I_o(\sqrt{s})+K_o(\sqrt{s})I_1(r_{sD}\sqrt{s})]\}}{[I_o(\sqrt{s})K_o(r_{sD}\sqrt{s})-I_o(r_{sD}\sqrt{s})K_o(\sqrt{s})]}\frac{[K_o(r_{sD}\sqrt{s_u})I_o(r_{eD}\sqrt{s_u})-K_o(r_{eD}\sqrt{s_u})I_o(r_{sD}\sqrt{s_u})]}{[K_1(r_{sD}\sqrt{s_u})I_o(r_{eD}\sqrt{s_u})+K_o(r_{eD}\sqrt{s_u})I_1(r_{sD}\sqrt{s_u})]} \quad \text{A13: 38}$$

Rate Transient Plots in Laplace Domain for CPOB Hydrate Layer with Moving Boundary
Rate Transient at Wellbore
$\hat{m}_{tD}p = \dot{m}_{tD} = \sqrt{s}\left\{\frac{[K_1(\sqrt{s})I_o(r_{sD}\sqrt{s}) + K_o(r_{sD}\sqrt{s})I_1(\sqrt{s})] - \varphi_{sD}[K_1(\sqrt{s})I_o(\sqrt{s}) + K_o(\sqrt{s})I_1(\sqrt{s})]}{[I_o(r_{sD}\sqrt{s})K_o(\sqrt{s}) - I_o(\sqrt{s})K_o(r_{sD}\sqrt{s})]}\right\}$
$p\hat{m}_{tD}$ Versus $\frac{1}{p}$

Pseudo-Pressure Profile for Reservoir

1. Dissociated Region

$$\hat{\varphi}_D p = \varphi_D = \frac{[K_o(r_D\sqrt{s})I_o(r_{sD}\sqrt{s}) - K_o(r_{sD}\sqrt{s})I_o(r_D\sqrt{s})] - \varphi_{sD}[K_o(r_D\sqrt{s})I_o(\sqrt{s}) - K_o(\sqrt{s})I_o(r_D\sqrt{s})]}{[I_o(r_{sD}\sqrt{s})K_o(\sqrt{s}) - I_o(\sqrt{s})K_o(r_{sD}\sqrt{s})]}$$

2.Undissociated Region

$$\hat{\varphi}_D p = \varphi_D = \varphi_{sD}\frac{K_o(r_D\sqrt{s_u})I_o(r_{eD}\sqrt{s_u}) - K_o(r_{eD}\sqrt{s_u})I_o(r_D\sqrt{s_u})}{K_o(r_{sD}\sqrt{s_u})I_o(r_{eD}\sqrt{s_u}) - K_o(r_{eD}\sqrt{s_u})I_o(r_{sD}\sqrt{s_u})}$$

Criterion for Valid Radius of Dissociation

$$\varphi_{sD} = \sqrt{\frac{s}{s_u}}\frac{\{[K_1(r_{sD}\sqrt{s})I_o(r_{sD}\sqrt{s}) + K_o(r_{sD}\sqrt{s})I_1(r_{sD}\sqrt{s})] - \hat{\varphi}_{sD}[K_1(r_{sD}\sqrt{s})I_o(\sqrt{s}) + K_o(\sqrt{s})I_1(r_{sD}\sqrt{s})]\}}{[I_o(\sqrt{s})K_o(r_{sD}\sqrt{s}) - I_o(r_{sD}\sqrt{s})K_o(\sqrt{s})]}\frac{[K_o(r_{sD}\sqrt{s_u})I_o(r_{eD}\sqrt{s_u}) - K_o(r_{eD}\sqrt{s_u})I_o(r_{sD}\sqrt{s_u})]}{[K_1(r_{sD}\sqrt{s_u})I_o(r_{eD}\sqrt{s_u}) + K_o(r_{eD}\sqrt{s_u})I_1(r_{sD}\sqrt{s_u})]}$$

Rate Transient Diagnostic Plot in Laplace Domain: Rate Derivative

$$\text{Der} = \frac{\Delta\left(\frac{1}{p\hat{m}_{tD}}\right)}{\Delta\left(\ln\frac{1}{p}\right)} \quad \text{Versus} \quad \frac{1}{p}$$

CPOB (HL) +IAR (CL)

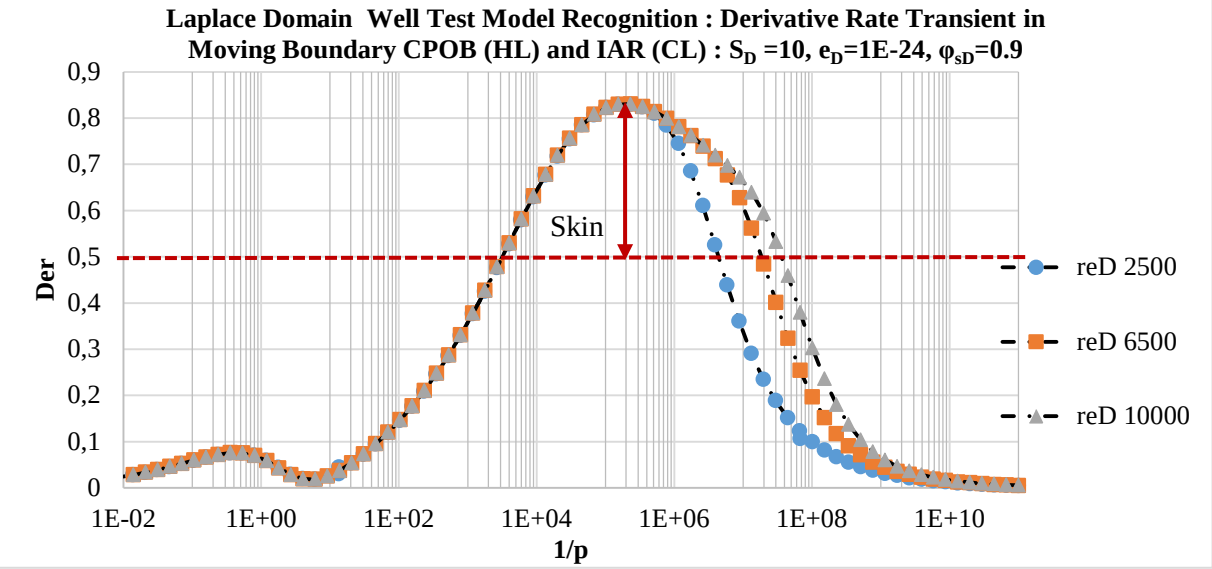

Figure A13- 13: Derivative Rate Transient in Moving Boundary CPOB (HL) and IAR (CL) with insignificant Heat Flux

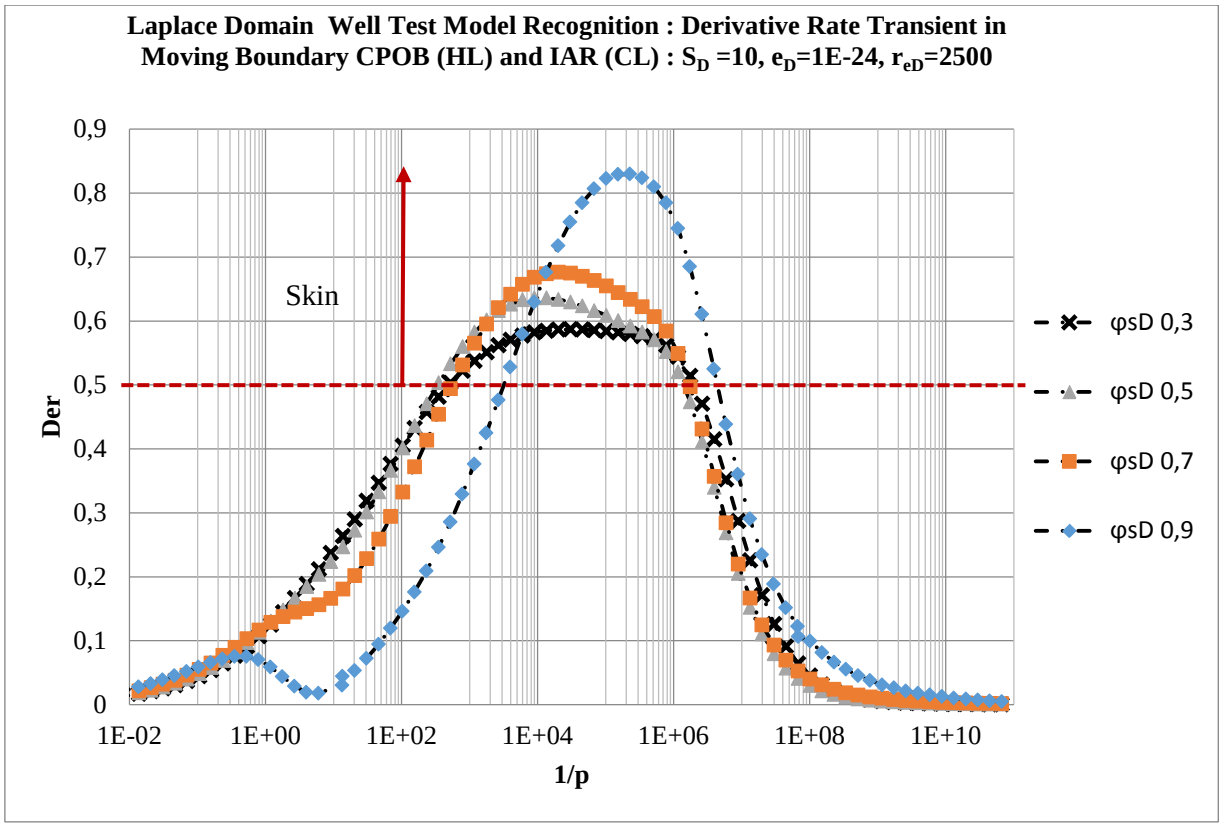

Figure A13- 14: Derivative Rate Transient in Moving Boundary CPOB (HL) and IAR (CL)

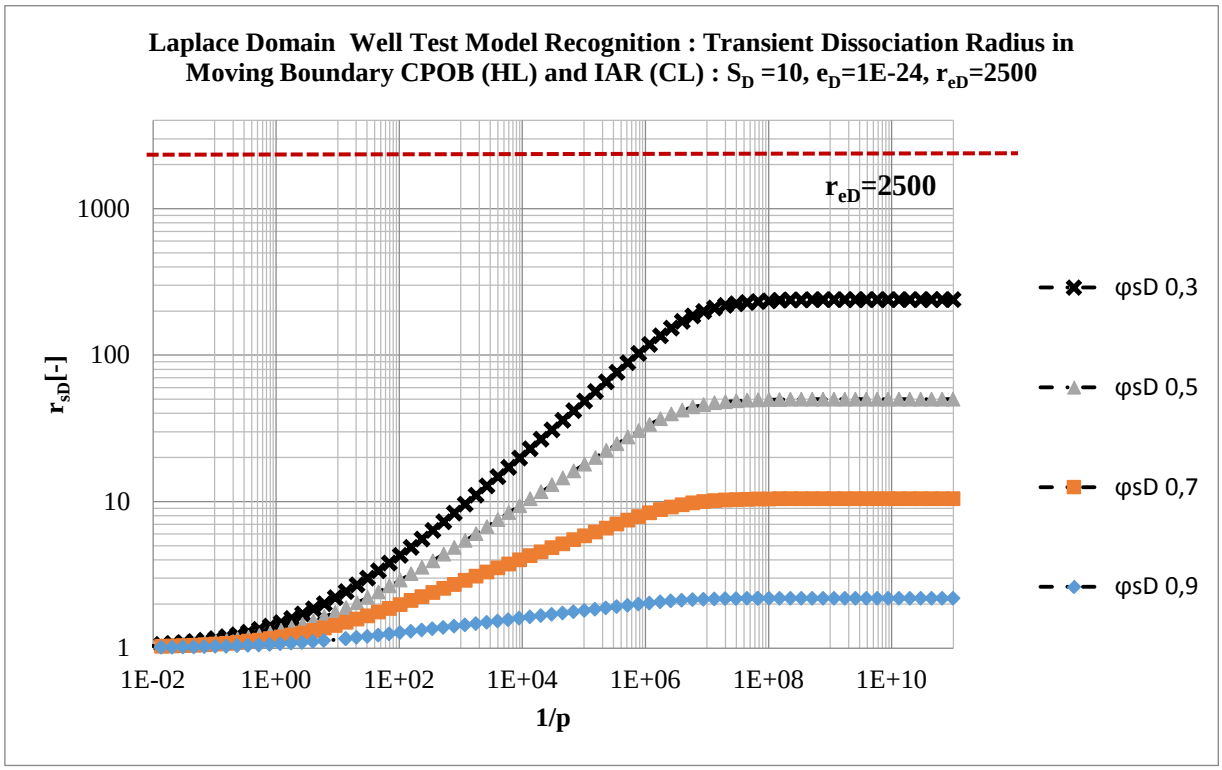

Figure A13- 15: Transient Dissociation Radius in Moving Boundary CPOB (HL) and IAR (CL)

Case 3: No-Flow Outer boundary

The no-flow boundary case is very complex due to the following reasons:

- In the early time of production, before the radius of dissociation reaches the boundary, the dissociated zone is characterized by a CPOB while the undissociated zone is a NFB. The reservoir response model can be generated for this case.
- During late time production, the radius of dissociation has reached the boundary and the entire reservoir now behaves with the NFB response. Deriving a general solution which encompasses both the early time and late time is very cumbersome especially when using the similarity solutions.

Dissociated zone

Dimensionless Pseudo-Pressure

$$\varphi_D = \varphi_{sD}\frac{\left[E_1\left(S_D\frac{1}{4t_{Dw}}\right)-E_1\left(S_D\frac{{r_D}^2}{4t_{Dw}}\right)\right]}{\left[E_1\left(S_D\frac{1}{4t_{Dw}}\right)-E_1\left(S_D\frac{{r_{sD}}^2}{4t_{Dw}}\right)\right]}+\frac{\left[E_1\left(S_D\frac{{r_D}^2}{4t_{Dw}}\right)-E_1\left(S_D\frac{{r_{sD}}^2}{4t_{Dw}}\right)\right]}{\left[E_1\left(S_D\frac{1}{4t_{Dw}}\right)-E_1\left(S_D\frac{{r_{sD}}^2}{4t_{Dw}}\right)\right]} \quad \text{A13: 39}$$

Rate Transient

$$\dot{m}_{tD} = (1-\varphi_{sD})\frac{2e^{-\left(\frac{{r_D}^2}{4t_{Dw}}S_D\right)}}{\left[E_1\left(S_D\frac{1}{4t_{Dw}}\right)-E_1\left(S_D\frac{{r_{sD}}^2}{4t_{Dw}}\right)\right]} \quad \text{A13: 40}$$

$P_{wf} \geq P_{eq}$

Producing above the equilibrium pressure needs to consider the effect of no-flow boundary as no dissociated zone will exist. Hence by applying the image well theory we get

$$\varphi_D(r_D,t_{Dw}) = \frac{\left[E_1\left(\frac{r_D^2}{4t_{Dw}}S_{Dk}\right)\right]+\left[E_1\left(\frac{(2l_D-r_D)^2}{4t_{Dw}}S_{Dk}\right)\right]}{\left[E_1\left(\frac{S_{Dk}}{4t_{Dw}}\right)\right]+\left[E_1\left(\frac{(2l_D-1)^2}{4t_{Dw}}S_{Dk}\right)\right]} \quad \text{A13: 41}$$

The model above is also valid if the reservoir pressure equals the equilibrium pressure prior to production (normally pressured gas hydrate). However, it should be emphasized that the reservoir will depict a different response if the reservoir pressure depletes below the equilibrium pressure when the well is still flowing.

$$\dot{m}_{tD}(r_D,t_{Dw}) = 2\frac{\left[e^{-\left(\frac{S_{Dk}}{4t_{Dw}}r_D\right)}-(2l_D-r_D)^{-1}r_D e^{-\frac{(2l_D-r_D)^2}{4t_{Dw}}S_{Dk}}\right]}{E_1\left(\frac{S_{Dk}}{4t_{Dw}}\right)+E_1\left(S_{Dk}\frac{(2l_D-1)^2}{4t_{Dw}}\right)} \quad \text{A13: 42}$$

Undissociated Zone

The impact of no-flow will first be felt in the undissociated zone hence the flow model is derived for no-flow boundary conditions.

Dimensionless Pseudo-Pressure

$$\varphi_D = \frac{B}{2}\left[E_1\left(\frac{r_D^2}{4t_{Dw}}S_{Dk}\right)+E_1\left(\frac{(2l_D-r_D)^2}{4t_{Dw}}S_{Dk}\right)\right] \quad \text{A13: 43}$$

The equation for the dimensionless pseudo-pressure in the un-dissociated zone is given thus:

$$\varphi_D = \varphi_{sD}\frac{\left[E_1\left(\frac{r_D^2}{4t_{Dw}}S_{Dk}\right)+E_1\left(\frac{(2l_D-r_D)^2}{4t_{Dw}}S_{Dk}\right)\right]}{\left\{E_1\left(S_{Dk}\frac{r_{sD}{}^2}{4t_{Dw}}\right)+E_1\left(S_{Dk}\frac{(2l_D-r_{sD})^2}{4t_{Dw}}\right)\right\}} \qquad \text{A13: 44}$$

$$\dot{m}_{tD} = 2\varphi_{sD}\frac{\left[e^{-\left(\frac{S_{Dk}}{4t_{Dw}}r_D^2\right)}-(2l_D-r_D)^{-1}r_D e^{-\frac{(2l_D-r_D)^2}{4t_{Dw}}S_{Dk}}\right]}{\left\{E_1\left(S_{Dk}\frac{r_{sD}{}^2}{4t_{Dw}}\right)+E_1\left(S_{Dk}\frac{(2l_D-r_{sD})^2}{4t_{Dw}}\right)\right\}} \qquad \text{A13: 45}$$

Using equating the mass rates at the crossover point the validity criterion for the radius of dissociation is derived

Criterion for Valid Radius of Dissociation

For the dimensionless pseudo-pressures at the cross over point to be the same, the following condition must be valid:

$$\dot{m}_{tD} = 2\varphi_{sD}\frac{\left[e^{-\left(\frac{S_{Dk}}{4t_{Dw}}r_{sD}^2\right)}-(2l_D-r_{sD})^{-1}r_{sD}e^{-\frac{(2l_D-r_{sD})^2}{4t_{Dw}}S_{Dk}}\right]}{\left\{E_1\left(S_{Dk}\frac{r_{sD}{}^2}{4t_{Dw}}\right)+E_1\left(S_{Dk}\frac{(2l_D-r_{sD})^2}{4t_{Dw}}\right)\right\}} = (1-\varphi_{sD})\frac{2e^{-\left(\frac{r_{sD}{}^2}{4t_{Dw}}S_D\right)}}{\left[E_1\left(S_{Dk}\frac{r_{sD}{}^2}{4t_{Dw}}\right)+E_1\left(S_{Dk}\frac{(2l_D-r_{sD})^2}{4t_{Dw}}\right)\right]} \qquad \text{A13: 46}$$

When the reservoir is fully dissociated and now acts similar to a normally pressured gas hydrate reservoir, i.e. the reservoir pressure has depleted below the equilibrium pressure, the dimensionless equilibrium pressure at the front is no longer constant but a function of time. By equating the dimensionless pseudo-pressure solution for the normally pressured NFB and over-pressured NFB reservoir, we get the following correction for the response:

$$\varphi_{sD} = \frac{2\left[E_1\left(S_D\frac{l_D{}^2}{4t_{Dw}}\right)\right]}{\left[E_1\left(S_D\frac{1}{4t_{Dw}}\right)+E_1\left(S_D\frac{(2l_D-1)^2}{4t_{Dw}}\right)\right]} \qquad \text{A13: 47}$$

Solutions with Laplace Transformation (Solutions in Laplace Domain)

$$\hat{\varphi}_D = c_1 I_o(r_D\sqrt{s}) + c_2 K_o(r_D\sqrt{s})$$

Dissociated Zone

The solutions given in Cases 1 and 2 earlier are also valid here for the dissociated zone.

Dimensionless Pseudo-Pressure

$$\hat{\varphi}_D = \frac{[K_o(r_D\sqrt{s})I_o(r_{sD}\sqrt{s})-K_o(r_{sD}\sqrt{s})I_o(r_D\sqrt{s})]-\varphi_{sD}[K_o(r_D\sqrt{s})I_o(\sqrt{s})-K_o(\sqrt{s})I_o(r_D\sqrt{s})]}{p[I_o(r_{sD}\sqrt{s})K_o(\sqrt{s})-I_o(\sqrt{s})K_o(r_{sD}\sqrt{s})]} \qquad \text{A13: 48}$$

Rate Transient

$$\hat{m}_{tD} = \frac{r_D\sqrt{s}}{p}\left\{\frac{[K_1(r_D\sqrt{s})I_o(r_{sD}\sqrt{s})+K_o(r_{sD}\sqrt{s})I_1(r_D\sqrt{s})]-\varphi_{sD}[K_1(r_D\sqrt{s})I_o(\sqrt{s})+K_o(\sqrt{s})I_1(r_D\sqrt{s})]}{[I_o(r_{sD}\sqrt{s})K_o(\sqrt{s})-I_o(\sqrt{s})K_o(r_{sD}\sqrt{s})]}\right\} \qquad \text{A13: 49}$$

Undissociated Zone

$$\widehat{\varphi}_D = c_1 I_o\left(r_D\sqrt{s_u}\right) + c_2 K_o\left(r_D\sqrt{s_u}\right)$$

Dimensionless Pseudo-Pressure

The general equation takes the form

$$\widehat{\varphi}_D = c_1 \frac{\left[K_1\left(r_{eD}\sqrt{s_u}\right)I_o\left(r_D\sqrt{s_u}\right)+I_1\left(r_{eD}\sqrt{s_u}\right)K_o\left(r_D\sqrt{s_u}\right)\right]}{K_1\left(r_{eD}\sqrt{s_u}\right)} \qquad \text{A13: 50}$$

$$\varphi_{sD}\frac{K_1\left(r_{eD}\sqrt{s_u}\right)}{p\left[K_1\left(r_{eD}\sqrt{s_u}\right)I_o\left(r_{sD}\sqrt{s_u}\right)+I_1\left(r_{eD}\sqrt{s_u}\right)K_o\left(r_{sD}\sqrt{s_u}\right)\right]} = c_1$$

$$\widehat{\varphi}_D = \varphi_{sD}\frac{\left[K_1\left(r_{eD}\sqrt{s_u}\right)I_o\left(r_D\sqrt{s_u}\right)+I_1\left(r_{eD}\sqrt{s_u}\right)K_o\left(r_D\sqrt{s_u}\right)\right]}{\left[K_1\left(r_{eD}\sqrt{s_u}\right)I_o\left(r_{sD}\sqrt{s_u}\right)+I_1\left(r_{eD}\sqrt{s_u}\right)K_o\left(r_{sD}\sqrt{s_u}\right)\right]}$$

The constant c_1 is hence derived using the inner boundary condition at the dissociation front

$$\widehat{m}_{tD} = -r_D\frac{d\widehat{\varphi}_D}{dr_D} = c_1 r_D\sqrt{s_u}\frac{\left[I_1\left(r_{eD}\sqrt{s_u}\right)K_1\left(r_D\sqrt{s_u}\right)-K_1\left(r_{eD}\sqrt{s_u}\right)I_1\left(r_D\sqrt{s_u}\right)\right]}{K_1\left(r_{eD}\sqrt{s_u}\right)} \qquad \text{A13: 51}$$

Dissociation front condition

$$\widehat{m}_{tD} = r_D\frac{\sqrt{s}}{p}\left\{\frac{\left[K_1\left(r_{sD}\sqrt{s}\right)I_o\left(r_{sD}\sqrt{s}\right)+K_o\left(r_{sD}\sqrt{s}\right)I_1\left(r_{sD}\sqrt{s}\right)\right]-\varphi_{sD}\left[K_1\left(r_{sD}\sqrt{s}\right)I_o\left(\sqrt{s}\right)+K_o\left(\sqrt{s}\right)I_1\left(r_{sD}\sqrt{s}\right)\right]}{\left[I_o\left(r_{sD}\sqrt{s}\right)K_o\left(\sqrt{s}\right)-I_o\left(\sqrt{s}\right)K_o\left(r_{sD}\sqrt{s}\right)\right]}\right\}$$

$$\widehat{m}_{tD} = \frac{\sqrt{s}}{p}\left\{\frac{\left[K_1\left(r_{sD}\sqrt{s}\right)I_o\left(r_{sD}\sqrt{s}\right)+K_o\left(r_{sD}\sqrt{s}\right)I_1\left(r_{sD}\sqrt{s}\right)\right]-\varphi_{sD}\left[K_1\left(r_{sD}\sqrt{s}\right)I_o\left(\sqrt{s}\right)+K_o\left(\sqrt{s}\right)I_1\left(r_{sD}\sqrt{s}\right)\right]}{\left[I_o\left(r_{sD}\sqrt{s}\right)K_o\left(\sqrt{s}\right)-I_o\left(\sqrt{s}\right)K_o\left(r_{sD}\sqrt{s}\right)\right]}\right\} =$$

$$\varphi_{sD}\frac{\sqrt{s_u}}{p}\frac{\left[I_1\left(r_{eD}\sqrt{s_u}\right)K_1\left(r_{sD}\sqrt{s_u}\right)-K_1\left(r_{eD}\sqrt{s_u}\right)I_1\left(r_{sD}\sqrt{s_u}\right)\right]}{\left[K_1\left(r_{eD}\sqrt{s_u}\right)I_o\left(r_{sD}\sqrt{s_u}\right)+I_1\left(r_{eD}\sqrt{s_u}\right)K_o\left(r_{sD}\sqrt{s_u}\right)\right]} \qquad \text{A13: 52}$$

Criterion for Valid Radius of Dissociation

$$\varphi_{sD} = \sqrt{\frac{s}{s_u}}A\frac{\left[K_1\left(r_{eD}\sqrt{s_u}\right)I_o\left(r_{sD}\sqrt{s_u}\right)+I_1\left(r_{eD}\sqrt{s_u}\right)K_o\left(r_{sD}\sqrt{s_u}\right)\right]}{\left[I_1\left(r_{eD}\sqrt{s_u}\right)K_1\left(r_{sD}\sqrt{s_u}\right)-K_1\left(r_{eD}\sqrt{s_u}\right)I_1\left(r_{sD}\sqrt{s_u}\right)\right]} \qquad \text{A13: 53}$$

Where,

$$A = \left\{\frac{\left[K_1\left(r_{sD}\sqrt{s}\right)I_o\left(r_{sD}\sqrt{s}\right)+K_o\left(r_{sD}\sqrt{s}\right)I_1\left(r_{sD}\sqrt{s}\right)\right]-\varphi_{sD}\left[K_1\left(r_{sD}\sqrt{s}\right)I_o\left(\sqrt{s}\right)+K_o\left(\sqrt{s}\right)I_1\left(r_{sD}\sqrt{s}\right)\right]}{\left[I_o\left(r_{sD}\sqrt{s}\right)K_o\left(\sqrt{s}\right)-I_o\left(\sqrt{s}\right)K_o\left(r_{sD}\sqrt{s}\right)\right]}\right\} \qquad \text{A13: 54}$$

When $r_{sD}=r_{eD,}$ the mass balance at the dissociation front reduces to

$$\left\{\frac{\left[K_1\left(r_{eD}\sqrt{s}\right)I_o\left(r_{eD}\sqrt{s}\right)+K_o\left(r_{eD}\sqrt{s}\right)I_1\left(r_{eD}\sqrt{s}\right)\right]}{\left[K_1\left(r_{eD}\sqrt{s}\right)I_o\left(\sqrt{s}\right)+K_o\left(\sqrt{s}\right)I_1\left(r_{eD}\sqrt{s}\right)\right]}\right\} = \varphi_{sD}$$

By inserting the function for the pseudo-pressure at the boundary, the rate transient equation takes the following form at the wellbore and boundary:

$$\widehat{m}_{tD}(r_D = 1, p) = \frac{\sqrt{s}}{p}\left[\frac{\left[I_1\left(r_{eD}\sqrt{s}\right)K_1\left(\sqrt{s}\right)-K_1\left(r_{eD}\sqrt{s}\right)I_1\left(\sqrt{s}\right)\right]}{K_o\left(\sqrt{s}\right)I_1\left(r_{eD}\sqrt{s}\right)+K_1\left(r_{eD}\sqrt{s}\right)I_o\left(\sqrt{s}\right)}\right]$$

$$\hat{m}_{tD}(r_{eD}=1,p)=0$$

This further validates the model

Rate Transient Plots in Laplace Domain for NFB Hydrate Layer with Moving Boundary

Rate Transient at Wellbore

$$\hat{m}_{tD}=\frac{\sqrt{s}}{p}\left\{\frac{\left[K_1(\sqrt{s})I_o(r_{sD}\sqrt{s})+K_o(r_{sD}\sqrt{s})I_1(\sqrt{s})\right]-\varphi_{sD}\left[K_1(\sqrt{s})I_o(\sqrt{s})+K_o(\sqrt{s})I_1(\sqrt{s})\right]}{\left[I_o(r_{sD}\sqrt{s})K_o(\sqrt{s})-I_o(\sqrt{s})K_o(r_{sD}\sqrt{s})\right]}\right\}$$

Plot

$\widehat{pm}_{tD}$ Versus $\frac{1}{p}$

Pseudo-Pressure Profile for Reservoir ($P_{wf}<P_{eq}$)

1. Dissociated Region

$$\hat{\varphi}_D=\frac{1}{p}\frac{\left[K_o(r_D\sqrt{s})I_o(r_{sD}\sqrt{s})-K_o(r_{sD}\sqrt{s})I_o(r_D\sqrt{s})\right]-\varphi_{sD}\left[K_o(r_D\sqrt{s})I_o(\sqrt{s})-K_o(\sqrt{s})I_o(r_D\sqrt{s})\right]}{\left[I_o(r_{sD}\sqrt{s})K_o(\sqrt{s})-I_o(\sqrt{s})K_o(r_{sD}\sqrt{s})\right]}$$

2.Undissociated Region

$$\hat{\varphi}_D=\frac{\varphi_{sD}}{p}\frac{\left[K_1(r_{eD}\sqrt{s_u})I_o(r_D\sqrt{s_u})+I_1(r_{eD}\sqrt{s_u})K_o(r_D\sqrt{s_u})\right]}{\left[K_1(r_{eD}\sqrt{s_u})I_o(r_{sD}\sqrt{s_u})+I_1(r_{eD}\sqrt{s_u})K_o(r_{sD}\sqrt{s_u})\right]}$$

For: $r_{sD}<r_{eD}$

$$\varphi_{sD}=\text{constant}$$

For: $r_{sD}=r_{eD}$

$$\hat{\varphi}_D p=\varphi_{sD}=\frac{\left[K_1(r_{eD}\sqrt{s})I_o(r_D\sqrt{s})+I_1(r_{eD}\sqrt{s})K_o(r_D\sqrt{s})\right]}{\left[K_1(r_{eD}\sqrt{s})I_o(\sqrt{s})+I_1(r_{eD}\sqrt{s})K_o(\sqrt{s})\right]}$$

Plot

$p\hat{\varphi}_D$ Versus r_D

Pseudo-Pressure Profile for Reservoir ($P_{wf}\geq P_{eq}$ during Production)

1. Un-dissociated Region (Reservoir depicts a conventional reservoir)

$$\hat{\varphi}_D=\frac{\left[K_1(r_{eD}\sqrt{s_u})I_o(r_D\sqrt{s_u})+I_1(r_{eD}\sqrt{s_u})K_o(r_D\sqrt{s_u})\right]}{p\left[K_1(r_{eD}\sqrt{s_u})I_o(r_{sD}\sqrt{s_u})+I_1(r_{eD}\sqrt{s_u})K_o(r_{sD}\sqrt{s_u})\right]}$$

Plot

$p\hat{\varphi}_D$ Versus r_D

Criterion for Valid Radius of Dissociation($P_{wf}<P_{eq}$ and $P_{avg}\geq P_{eq}$)

$$\varphi_{sD} = \sqrt{\frac{s}{s_u}}\left\{\frac{\left[K_1(r_{sD}\sqrt{s})I_o(r_{sD}\sqrt{s}) + K_o(r_{sD}\sqrt{s})I_1(r_{sD}\sqrt{s})\right] - \varphi_{sD}\left[K_1(r_{sD}\sqrt{s})I_o(\sqrt{s}) + K_o(\sqrt{s})I_1(r_{sD}\sqrt{s})\right]}{\left[I_o(r_{sD}\sqrt{s})K_o(\sqrt{s}) - I_o(\sqrt{s})K_o(r_{sD}\sqrt{s})\right]}\right\}\frac{\left[K_1(r_{eD}\sqrt{s_u})I_o(r_{sD}\sqrt{s_u}) + I_1(r_{eD}\sqrt{s_u})K_o(r_{sD}\sqrt{s_u})\right]}{\left[I_1(r_{eD}\sqrt{s_u})K_1(r_{sD}\sqrt{s_u}) - K_1(r_{eD}\sqrt{s_u})I_1(r_{sD}\sqrt{s_u})\right]}$$

Rate Transient Diagnostic Plot in Laplace Domain: Rate Derivative

$$\text{Der} = \frac{\Delta\left(\frac{1}{\widehat{pm}_{tD}}\right)}{\Delta\left(\ln\frac{1}{p}\right)} \quad \text{Versus} \quad \frac{1}{p}$$

Pseudo-Pressure Profile for Reservoir ($P_{avg}\leq P_{eq}$ at the beginning of Production)

1. Dissociated Region (Reservoir is now Normally Pressured at late production time)

$$\widehat{\varphi}_{D}p = \frac{\left[K_1(r_{eD}\sqrt{s})I_o(r_D\sqrt{s}) + I_1(r_{eD}\sqrt{s})K_o(r_D\sqrt{s})\right]}{\left[K_1(r_{eD}\sqrt{s})I_o(\sqrt{s}) + I_1(r_{eD}\sqrt{s})K_o(\sqrt{s})\right]}$$

$$p\widehat{m}_{tD} = \sqrt{s}\frac{\left[K_1(\sqrt{s})I_1(r_{eD}\sqrt{s})\right] - \left[K_1(r_{eD}\sqrt{s})I_1(\sqrt{s})\right]}{\left[K_1(r_{eD}\sqrt{s})I_o(\sqrt{s}) + K_o(\sqrt{s})I_1(r_{eD}\sqrt{s})\right]}$$

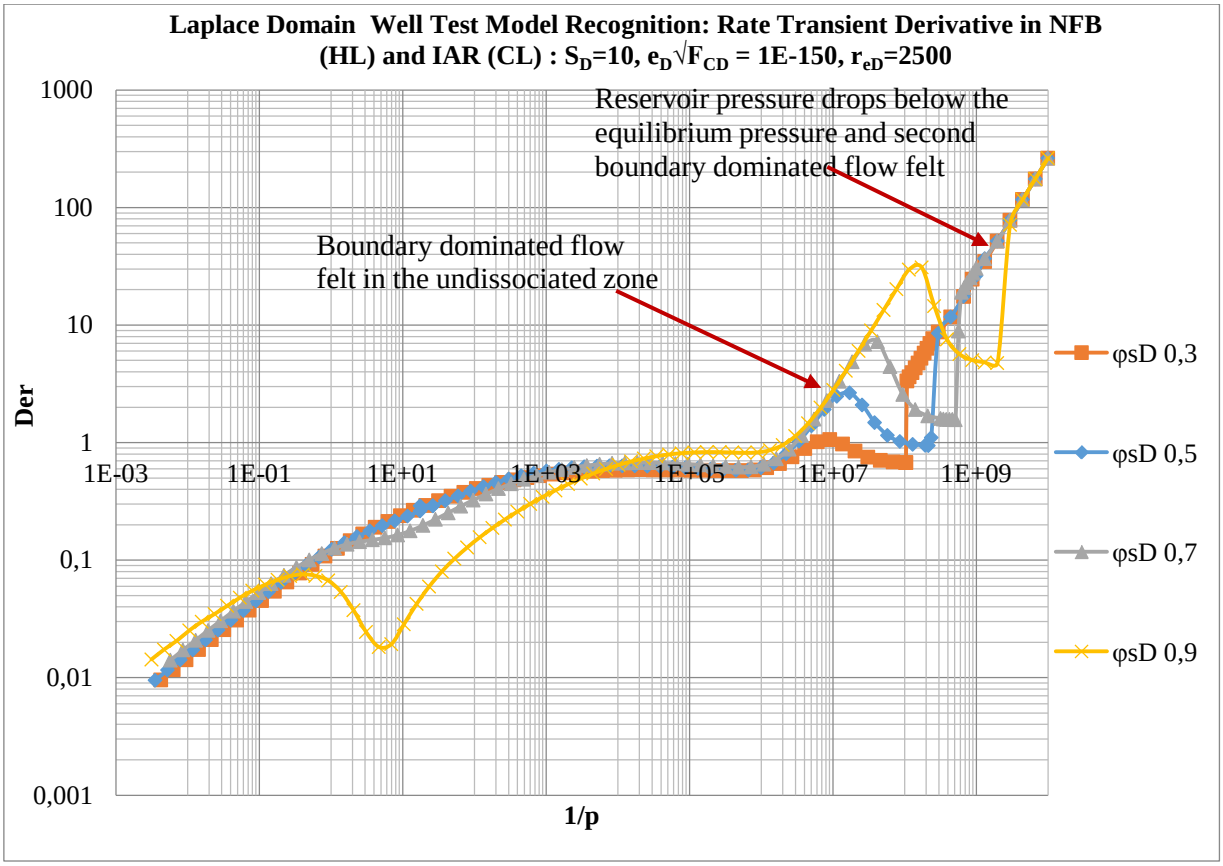

Figure A13- 16: Derivative Rate Transient in Moving Boundary NFB (HL) and IAR (CL)

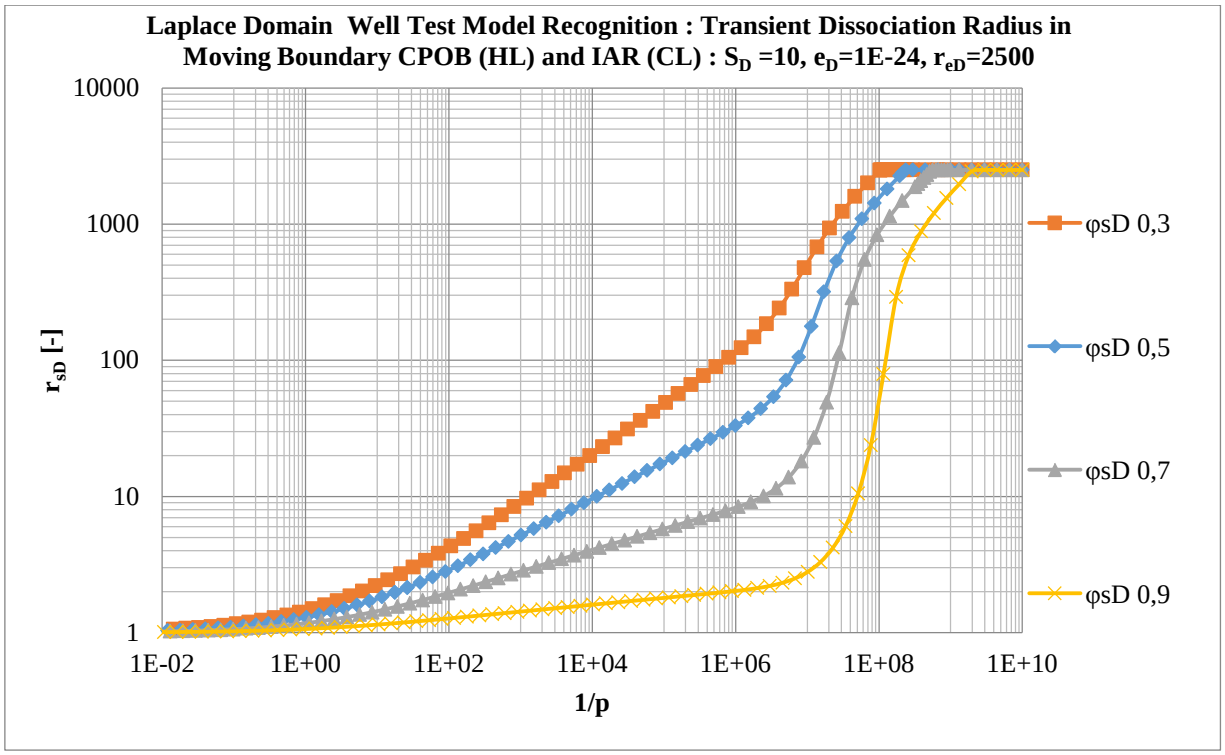

Figure A13- 17: Transient Dissociation Radius in Moving Boundary NFB (HL) and IAR (CL)

Appendix 14: Solutions to the Diffusivity Equation in Crossflow layer

Crossflow problems will be expected in Class 1 and 2 gas hydrate reservoirs if the boundary between the free fluid layer and the hydrate layer is permeable. Depending on the layer chosen for production, different crossflow regimes could be analyzed. Moreover, boundary conditions imposed on outer boundaries of the crossflow layer is very dependent on the layer of production.

Conventionally, for the hydrate reservoir to be considered for production, the layer above the hydrate layer should be impermeable (cap rock). For this reason, we consider no-flow at the outer boundary of the hydrate layer and just heat influx due to heat conduction from the cap rock is considered for the hydrate dissociation process. However, the effects of hydrate dissociation at the outer boundary of the hydrate layer could have significant influence of the reservoir response.

For cases where the production takes place in the free fluid layer, at the time pressure depression reaches the upper boundary of the hydrate layer, temperature depressions are also experienced due to the endothermic nature of hydrate dissociation. For this reason, dissociation as a result of heat flux from conduction will occur basically at the boundary and is controlled by the temperature depression at the boundary. When the hydrates dissociate at the boundary, the pressure at the dissociation front increases which implies, depending on the rate of hydrate dissociation, the pressure depression at the reservoir boundary could be supported by hydrate dissociation due to heat influx. The effect of pressure support at the boundary is a known phenomenon is usually described as the constant pressure outer boundary condition where pressure depression at the boundary is zero due to fluid influx. With a proper definition of the boundary conditions, this effect can be characterized with a rigorous model. However, other simplifications of the model can be made from the following assumptions:

- Constant Pressure Outer Boundary in Hydrate Layer: High hydrate dissociation at the outer boundary due to heat influx is very significant and contributes to pressure maintenance.
- No-flow Outer Boundary in Hydrate Layer: Insignificant hydrate dissociation at the outer boundary due to heat influx.

With these models, we can address the diffusivity equations for the crossflow layers. In the late phase of production, the effects of heat conduction could have become noticeable and hence an accelerated hydrate dissociation which also caused an increase in gas production.

Solution to the Diffusivity Equation in Crossflow Layer

Crossflow Layer is Hydrate Layer

$$\Delta x * \Delta y * \Delta(\rho_g * w_{g,T}) + \Delta x * \Delta y * \Delta(\rho_w * w_{w,T}) = \Delta x * \Delta y * \Delta z \frac{\Delta(S_g \emptyset \rho_g)}{\Delta t} + \Delta x * \Delta y * \Delta z \frac{\Delta(S_w \emptyset \rho_w)}{\Delta t} + \Delta x * \Delta y * \Delta z \frac{\Delta(S_h \emptyset \rho_h)}{\Delta t} \quad \text{A14: 1}$$

Crossflow Layer is Free Fluid Layer

$$\Delta x * \Delta y * \Delta(\rho_g * w_{g,T}) + \Delta x * \Delta y * \Delta(\rho_w * w_{w,T}) = \Delta x * \Delta y * \Delta z \frac{\Delta(S_g \emptyset \rho_g)}{\Delta t} + \Delta x * \Delta y * \Delta z \frac{\Delta(S_w \emptyset \rho_w)}{\Delta t} \quad \text{A14: 2}$$

After simplification and with consideration of the storativity ratios given in Appendix 11, both mass conservation equations take the general form:

$$\frac{\partial^2 \varphi_D}{\partial z_D^2} = [1-\omega]\left[\frac{\partial \varphi_D}{\partial t_{DwD}}\right]_{\text{layer 2}} \qquad \text{A14: 3}$$

Layer 2 simply denotes the crossflow layer while layer 1 represents the producing layer. It should however be noted that the compressibility terms in the diffusivity equation above are different for each crossflow layer considered.

Laplace Solution- Diffusivity Equation in Crossflow Layer

The leakage rate is a time function which makes its incorporation in the diffusivity equation of the producing layer and solving with similarity variables inapplicable. For this reason, Laplace transforms of the diffusivity equation of the crossflow layer is preferably used to derive the solution to the diffusivity equation of the producing layer. Hence, the diffusivity equation of the crossflow layer is given in Laplace domain and solved thus:

$$\left[\frac{\partial^2 \widehat{\varphi_D}}{\partial z_D^2}\right]_{\text{layer2}} = [1-\omega]p[\widehat{\varphi_D}]_{\text{layer 2}} \qquad \text{A14: 4}$$

Here, conventional techniques in solving the linear diffusivity equation in Laplace domain for finite reservoirs are used.

The general solution to the linear diffusivity equation in Laplace domain is given by:

$$\widehat{\varphi_D} = A\text{Cosh}\left(z_D\sqrt{p[1-\omega]}\right) + B\text{Sinh}\left(z_D\sqrt{p[1-\omega]}\right) \qquad \text{A14: 5}$$

Case 1: Constant Pressure Outer Boundary in Crossflow Layer

Boundary conditions

$z_D = \Delta z_D$ $\qquad\qquad$ $\widehat{\varphi_D} = 0$

$z_D = 1$ $\qquad\qquad$ $\widehat{\varphi_D} = [\widehat{\varphi_D}]_{layer1}$

With the above boundary conditions, the coefficients A and B are given thus:

$$A = -\frac{[\widehat{\varphi_D}]_{\text{layer1}}\text{Sinh}\left(\Delta z_D\sqrt{p[1-\omega]}\right)}{\left[\text{Sinh}\left(\sqrt{p[1-\omega]}\right)\text{Cosh}\left(\Delta z_D\sqrt{p[1-\omega]}\right) - \text{Sinh}\left(\Delta z_D\sqrt{p[1-\omega]}\right)\text{Cosh}\left(\sqrt{p[1-\omega]}\right)\right]} \qquad \text{A14: 6}$$

$$B = \frac{[\widehat{\varphi_D}]_{\text{layer1}}\text{Cosh}\left(\Delta z_D\sqrt{p[1-\omega]}\right)}{\left[\text{Sinh}\left(\sqrt{p[1-\omega]}\right)\text{Cosh}\left(\Delta z_D\sqrt{p[1-\omega]}\right) - \text{Sinh}\left(\Delta z_D\sqrt{p[1-\omega]}\right)\text{Cosh}\left(\sqrt{p[1-\omega]}\right)\right]} \qquad \text{A14: 7}$$

Final Equation in Laplace domain is given thus:

$$\widehat{\varphi_D} = [\widehat{\varphi_D}]_{\text{layer1}}\frac{\text{Sinh}\left(z_D\sqrt{p[1-\omega]}\right)\text{Cosh}\left(\Delta z_D\sqrt{p[1-\omega]}\right) - \text{Sinh}\left(\Delta z_D\sqrt{p[1-\omega]}\right)\text{Cosh}\left(z_D\sqrt{p[1-\omega]}\right)}{\left[\text{Sinh}\left(\sqrt{p[1-\omega]}\right)\text{Cosh}\left(\Delta z_D\sqrt{p[1-\omega]}\right) - \text{Sinh}\left(\Delta z_D\sqrt{p[1-\omega]}\right)\text{Cosh}\left(\sqrt{p[1-\omega]}\right)\right]} \qquad \text{A14: 8}$$

The above equation can further be simplified to:

$$\widehat{\varphi_D} = [\widehat{\varphi_D}]_{\text{layer1}}\frac{\text{Sinh}\left[\sqrt{p[1-\omega]}(z_D - \Delta z_D)\right]}{\text{Sinh}\left[\sqrt{p[1-\omega]}(1-\Delta z_D)\right]} \qquad \text{A14: 9}$$

The leakage rate function for the producing layer in Laplace domain is given thus:

$$\frac{d\widehat{\varphi_D}}{dz_D} = \left[\widehat{\varphi_D}\right]_{layer1}\sqrt{p[1-\omega]}\,\frac{Cosh\left[\sqrt{p[1-\omega]}(z_D-\Delta z_D)\right]}{Sinh\left[\sqrt{p[1-\omega]}(1-\Delta z_D)\right]} \quad \text{A14: 10}$$

At the crossflow point, the above differential takes the form:

$$\frac{d\widehat{\varphi_D}}{dz_D} = [\widehat{\varphi_D}]_{layer1}\sqrt{p[1-\omega]}\,\frac{Cosh\left[\sqrt{p[1-\omega]}(1-\Delta z_D)\right]}{Sinh\left[\sqrt{p[1-\omega]}(1-\Delta z_D)\right]} = [\widehat{\varphi_D}]_{layer1}\sqrt{p[1-\omega]}Coth\left[\sqrt{p[1-\omega]}(1-\Delta z_D)\right] \quad \text{A14: 11}$$

Case 2: No-Flow Outer Boundary in Crossflow Layer

Unlike the solutions depicted earlier with the Boltzmann transformation for the no-flow boundary condition, where the average reservoir pressure function is required for the outer boundary condition, here, this is not required.

Boundary conditions

$z_D=\Delta z_D$ $\qquad \frac{d\widehat{\varphi_D}}{dz_D} = 0$

$z_D=1$ $\qquad \widehat{\varphi_D} = [\widehat{\varphi_D}]_{layer1}$

After simplification we get the following for the coefficients A and B:

$$A = [\widehat{\varphi_D}]_{layer1}\,\frac{Cosh\left[\sqrt{p[1-\omega]}(\Delta z_D)\right]}{Cosh\left[\sqrt{p[1-\omega]}(1-\Delta z_D)\right]} \quad \text{A14: 12}$$

$$B = -[\widehat{\varphi_D}]_{layer1}\,\frac{Sinh\left[\sqrt{p[1-\omega]}(\Delta z_D)\right]}{Cosh\left[\sqrt{p[1-\omega]}(1-\Delta z_D)\right]} \quad \text{A14: 13}$$

The final equation in Laplace domain is hence:

$$\widehat{\varphi_D} = [\widehat{\varphi_D}]_{layer1}\,\frac{Cosh\left[\sqrt{p[1-\omega]}(z_D-\Delta z_D)\right]}{Cosh\left[\sqrt{p[1-\omega]}(1-\Delta z_D)\right]} \quad \text{A14: 14}$$

The leakage rate function in Laplace domain is given thus:

$$\frac{d\widehat{\varphi_D}}{dz_D} = [\widehat{\varphi_D}]_{layer1}\sqrt{p[1-\omega]}\,\frac{Sinh\left[\sqrt{p[1-\omega]}(z_D-\Delta z_D)\right]}{Cosh\left[\sqrt{p[1-\omega]}(1-\Delta z_D)\right]} \quad \text{A14: 15}$$

At the crossflow point, the above differential is:

$$\frac{d\widehat{\varphi_D}}{dz_D} = [\widehat{\varphi_D}]_{layer1}\sqrt{p[1-\omega]}\,\frac{Sinh\left[\sqrt{p[1-\omega]}(\Delta z_D-1)\right]}{Cosh\left[\sqrt{p[1-\omega]_i}(\Delta z_D-1)\right]} \quad \text{A14: 16}$$

$$\frac{d\widehat{\varphi_D}}{dz_D} = [\widehat{\varphi_D}]_{layer1}\sqrt{p[1-\omega]}\tanh\left[\sqrt{p[1-\omega]}(\Delta z_D-1)\right] \quad \text{A14: 17}$$

Case 3: No-Flow Outer Boundary in Hydrate Layer and Heat Flux at Outer Boundary

Here we consider the effects of heat flux at the outer boundary when pressure depletion reaches the outer boundary of the hydrate layer. First it is important to give major modifications of the heat leakage rate and hence the mass flux rate at the hydrate outer boundary.

$$\frac{\partial^2 T_{pD}}{\partial {z_D}^2} = F_{CDD}\frac{\partial T_{pD}}{\partial t_{DwD}} \qquad \text{A14: 18}$$

Where,

$$F_{CDD} = \frac{h^2}{4}\frac{(\rho c_p)_{eff}}{\lambda\left[\left(\frac{a_h+a_v}{a_h a_v}\right)\right]_i} \qquad \text{A14: 19}$$

The above representation of the dimensionless temperature conductivity is modified such that the same dimensionless times are used for the crossflow problem in all layers.

$$\frac{d\widehat{T_D}}{dz_D} = \widehat{\dot{Q}_{pD}} e_D \widehat{\varphi}_D = \left(\frac{d\widehat{\varphi_D}}{dz_D}\right)_{z_D=\Delta z_D} \qquad \text{A14: 20}$$

The leakage rate function for the producing layer in Laplace domain is given thus:

<u>Constant Temperature Outer Boundary (CTOB)</u>

$$\frac{d\widehat{T_D}}{dz_D} = \left\{\sqrt{pF_{CD}}\,\mathrm{Coth}\left[\sqrt{pF_{CDD}}\left(\Delta z_{D,2} - \Delta z_D\right)\right]\right\} e_D \widehat{\varphi}_D \qquad \text{A14: 21}$$

<u>Pseudo-No Flow Temperature Boundary (p-NFTB)</u>

$$\frac{d\widehat{T_D}}{dz_D} = \left\{\sqrt{pF_{CD}}\tanh\left[\sqrt{pF_{CDD}}\left(\Delta z_{D,2} - \Delta z_D\right)\right]\right\} e_D \widehat{\varphi}_D \qquad \text{A14: 22}$$

<u>Infinite Acting Temperature Outer Boundary</u>

$$\frac{d\widehat{T_D}}{dz_D} = \left[\sqrt{pF_{CDD}}\right] e_D \widehat{\varphi}_D \qquad \text{A14: 23}$$

<u>Hydrate Dissociation at Hydrate Layer-Caprock Interface When Producing from FFL</u>

Boundary conditions

$z_D = \Delta z_D$ $\qquad \left(\frac{d\widehat{\varphi_D}}{dz_D}\right)_{\Delta z_D} = \widehat{\dot{Q}_{pD}} e_D \widehat{\varphi}_D = \widehat{\dot{Q}_{pD}} e_D \left\{A\mathrm{Cosh}\left(\Delta z_D\sqrt{p[1-\omega]}\right) + B\mathrm{Sinh}\left(\Delta z_D\sqrt{p[1-\omega]}\right)\right\}$

$z_D = 1$ $\qquad \widehat{\varphi_D} = \left[\widehat{\varphi_D}\right]_{layer1}$

Notice that the heat flux at the boundary and hence hydrate dissociation have been defined as a function of the pseudo-pressure at the boundary and is still defined in terms of the coefficients A and B. With the above boundary conditions, the coefficients are given thus:

$$B = [\widehat{\varphi_D}]_{layer1}\frac{\left\{\left[\widehat{\dot{Q}_{pD}} e_D \mathrm{Cosh}\left(\Delta z_D\sqrt{p[1-\omega]}\right)\right] - \left[\sqrt{p[1-\omega]}\,\mathrm{Sinh}\left(\Delta z_D\sqrt{p[1-\omega]}\right)\right]\right\}}{\left[\left\{\widehat{\dot{Q}_{pD}} e_D \mathrm{Sinh}\left[(1-\Delta z_D)\sqrt{p[1-\omega]}\right]\right\} + \left\{\sqrt{p[1-\omega]}\,\mathrm{Cosh}\left[(1-\Delta z_D)\sqrt{p[1-\omega]}\right]\right\}\right]} \qquad \text{A14: 24}$$

$$A = [\widehat{\varphi_D}]_{layer1}\frac{\left\{\left[\sqrt{p[1-\omega]}\,\mathrm{Cosh}\left(\Delta z_D\sqrt{p[1-\omega]}\right)\right] - \left[\widehat{\dot{Q}_{pD}} e_D \mathrm{Sinh}\left(\Delta z_D\sqrt{p[1-\omega]}\right)\right]\right\}}{\left[\left\{\widehat{\dot{Q}_{pD}} e_D \mathrm{Sinh}\left[(1-\Delta z_D)\sqrt{p[1-\omega]}\right]\right\} + \left\{\sqrt{p[1-\omega]}\,\mathrm{Cosh}\left[(1-\Delta z_D)\sqrt{p[1-\omega]}\right]\right\}\right]} \qquad \text{A14: 25}$$

The solution to the dimensionless pseudo-pressure is hence given thus:

$$\widehat{\varphi_D} = \left[\widehat{\varphi_D}\right]_{layer1}\frac{\sqrt{p[1-\omega]}\,\mathrm{Cosh}\left(\left(z_D - \Delta z_D\right)\sqrt{p[1-\omega]}\right) + \widehat{\dot{Q}_{pD}} e_D \mathrm{Sinh}\left(\left(z_D - \Delta z_D\right)\sqrt{p[1-\omega]}\right)}{\sqrt{p[1-\omega]}\,\mathrm{Cosh}\left[\left(1-\Delta z_D\right)\sqrt{p[1-\omega]}\right] + \widehat{\dot{Q}_{pD}} e_D \mathrm{Sinh}\left[\left(1-\Delta z_D\right)\sqrt{p[1-\omega]}\right]} \qquad \text{A14: 26}$$

The mass flux due to crossflow from the hydrate layer is hence given thus:

$$\frac{d\widehat{\varphi_D}}{dz_D} = \left[\widehat{\varphi_D}\right]_{layer1} \frac{p[1-\omega]Sinh\left((z_D-\Delta z_D)\sqrt{p[1-\omega]}\right)+\widehat{Q_{pD}}e_D\sqrt{p[1-\omega]}Cosh\left((z_D-\Delta z_D)\sqrt{p[1-\omega]}\right)}{\sqrt{p[1-\omega]}Cosh\left[(1-\Delta z_D)\sqrt{p[1-\omega]}\right]+\widehat{Q_{pD}}e_D Sinh\left[(1-\Delta z_D)\sqrt{p[1-\omega]}\right]} \quad \text{A14: 27}$$

$$\left(\frac{d\widehat{\varphi_D}}{dz_D}\right)_{z_D=1} = \left[\widehat{\varphi_D}\right]_{layer1} \frac{p[1-\omega]Sinh\left[(1-\Delta z_D)\sqrt{p[1-\omega]}\right]+\widehat{Q_{pD}}e_D\sqrt{p[1-\omega]}Cosh\left((1-\Delta z_D)\sqrt{p[1-\omega]}\right)}{\sqrt{p[1-\omega]}Cosh\left[(1-\Delta z_D)\sqrt{p[1-\omega]}\right]+\widehat{Q_{pD}}e_D Sinh\left[(1-\Delta z_D)\sqrt{p[1-\omega]}\right]} \quad \text{A14: 28}$$

$$\left(\frac{d\widehat{\varphi_D}}{dz_D}\right)_{z_D=1} = [\widehat{\varphi_D}]_{layer1}\sqrt{p[1-\omega]}Coth\left[(1-\Delta z_D)\sqrt{p[1-\omega]}\right]\frac{\left\{\sqrt{p[1-\omega]}tanh\left[(1-\Delta z_D)\sqrt{p[1-\omega]}\right]+\widehat{Q_{pD}}e_D\right\}}{\left\{\sqrt{p[1-\omega]}Coth\left[(1-\Delta z_D)\sqrt{p[1-\omega]}\right]+\widehat{Q_{pD}}e_D\right\}} \quad \text{A14: 29}$$

Notice that if the heat influx is assumed to be negligible, the above equation simplifies to the NFB solution in Case 2 above and if the heat flux is very significant the equation above also simplifies to the solution in Case 1 above

Appendix 15: Diffusivity Problems in Class 1 and 2 Gas Hydrate Reservoirs (Crossflow)

Analogue the diffusivity equation derived in Appendix 1 and Appendix 5 we also derive the diffusivity equation for Classes 1 and 2 gas hydrate reservoirs.

Hydrate Layer is Producing Layer

Here, the mass influx from the free fluid layer and the hydrate mass dissociated from each heat source component has to be considered.

$$\frac{\partial^2\varphi}{\partial r_D^2}+\frac{1}{r_D}\frac{\partial}{\partial r_D}-\frac{\lambda}{h^2}\frac{\dot{Q}_D {r_w}^2}{h_d k\left[\rho_t\left(\frac{k_r}{\eta}\right)_t\right]}\left[\frac{dT_{eq}}{dp}\right](\varphi_i-\varphi)-\left[\frac{r_w^2}{\Delta z_2}\frac{k_{v2}}{k_{h1}}\frac{\partial\varphi}{\partial z}\right]_{layer\ 2}-\frac{c_p\Delta T}{h_d}\left[\frac{r_w^2}{\Delta z_2}\frac{k_{v2}}{k_{h1}}\frac{\partial\varphi}{\partial z}\right]_{layer\ 2}=\left[\frac{S_D}{a_{h,i}}\right]\frac{\partial\varphi}{\partial t} \quad \text{A15: 1}$$

$$\frac{\partial^2\varphi}{\partial r_D^2}+\frac{1}{r_D}\frac{\partial\varphi}{\partial r_D}-\gamma_D(\varphi_i-\varphi)-\left[\frac{r_w^2}{\Delta z_2}\frac{k_{v2}}{k_{h1}}\frac{\partial\varphi}{\partial z}\right]_{layer\ 2}-\frac{c_p\Delta T}{h_d}\left[\frac{r_w^2}{\Delta z_2}\frac{k_{v2}}{k_{h1}}\frac{\partial\varphi}{\partial z}\right]_{layer\ 2}=\left[\frac{1}{a_h}\frac{\partial\varphi}{\partial t}\right]_{PL} \quad \text{A15: 2}$$

$$\frac{\partial^2\varphi_D}{\partial r_D^2}+\frac{1}{r_D}\frac{\partial\varphi_D}{\partial r_D}-\gamma_D\varphi_D-\frac{r_w^2}{\Delta z_2\Delta z_1}\frac{k_{v2}}{k_{h1}}\left[\frac{\partial\varphi_D}{\partial z_D}\right]_{layer\ 2}-\frac{c_p\Delta T}{h_d}\left[\frac{r_w^2}{\Delta z_2\Delta z_1}\frac{k_{v2}}{k_{h1}}\frac{\partial\varphi_D}{\partial z_D}\right]_{layer\ 2}=\left[\frac{1}{a_h}\frac{\partial\varphi_D}{\partial t}\right]_{PL} \quad \text{A15: 3}$$

$$\frac{\partial^2\varphi_D}{\partial r_D^2}+\frac{1}{r_D}\frac{\partial\varphi_D}{\partial r_D}-\gamma_D\varphi_D-\delta_D\left[\frac{\partial\varphi_D}{\partial z_D}\right]_{layer\ 2}-\frac{c_p\Delta T}{h_d}\delta_D\left[\frac{\partial\varphi_D}{\partial z_D}\right]_{layer\ 2}=\omega\left[\frac{\partial\varphi_D}{\partial t_{DwD}}\right]_{layer\ 1} \quad \text{A15: 4}$$

$$\frac{\partial^2\varphi_D}{\partial r_D^2}+\frac{1}{r_D}\frac{\partial\varphi_D}{\partial r_D}-\gamma_D\varphi_D-\delta_D(1+\theta_D)\left[\frac{\partial\varphi_D}{\partial z_D}\right]_{layer\ 2}=\omega\left[\frac{\partial\varphi_D}{\partial t_{DwD}}\right]_{layer\ 1} \quad \text{A15: 5}$$

Where,

$$\delta_D=\frac{r_w^2}{\Delta z_2\Delta z_1}\frac{k_{v2}}{k_{h1}} \quad \text{A15: 6}$$

$$\theta_D=\frac{c_p\Delta T}{h_d} \quad \text{A15: 7}$$

$$t_{DwD}=\frac{t}{\left[\left(\frac{a_h+a_v}{a_h a_v}\right)\right]_i} \quad \text{A15: 8}$$

$$\frac{1}{a_h}=\frac{S_D}{a_{h,id}}=\frac{(\rho c_T)_{eff,id}}{\left[\rho_t k\left(\frac{k_r}{\eta}\right)_t\right]_{id}}{r_w}^2\left\{\frac{(\rho c_T)_{eff}}{(\rho c_T)_{eff,id}}\frac{\left[\rho_t k\left(\frac{k_r}{\eta}\right)_t\right]_{id}}{\left[\rho_t k\left(\frac{k_r}{\eta}\right)_t\right]}+\frac{c}{h_d(\rho c_T)_{eff,id}}\frac{\left[\rho_t k\left(\frac{k_r}{\eta}\right)_t\right]_{id}}{\left[\rho_t k\left(\frac{k_r}{\eta}\right)_t\right]}\right\} \quad \text{A15: 9}$$

$$(\rho c_T)_{eff}=\left(\rho_g c_{T,g}+\rho_w c_{T,w}\right) \quad \text{A15: 10}$$

$$c_{T,g}=S_g c_g+S_g c_F+S_H c_F\left(\frac{B_g E_g}{(B_g E_g+B_w E_w)}\right) \quad \text{A15: 11}$$

$$c_{T,w}=S_w c_w+S_w c_F+S_H c_F\left(\frac{E_w B_w}{(B_g E_g+B_w E_w)}\right) \quad \text{A15: 12}$$

$$c=\left[c_{p,g}S_g\rho_g\left(\frac{T(c_g+c_F)}{\left[\frac{dT_{eq}}{dp}\right]}+1\right)+c_{p,w}S_w\rho_w\left(\frac{T(c_w+c_F)}{\left[\frac{dT_{eq}}{dp}\right]}+1\right)+c_{p,H}S_H\rho_H\left(\frac{T(c_F)}{\left[\frac{dT_{eq}}{dp}\right]}+1\right)+c_{p,m}\frac{(1-\emptyset)}{\emptyset}\rho_m+S_H\rho_H\frac{dh_d}{dT_{eq}}\right]\left[\frac{dT_{eq}}{dp}\right] \quad \text{A15: 13}$$

$\gamma_D > 0$ and $\theta_D > 0$

Note that if the kinetic model is used, the diffusivity equation simply takes the form:

Kinetic Model

$$\frac{\partial^2\varphi}{\partial r_D^2}+\frac{1}{r_D}\frac{\partial\varphi}{\partial r_D}-\gamma_{Dk}\left(\varphi_i-\varphi\right)-\left[\frac{r_w^2}{\Delta z_2}\frac{k_{v2}}{k_{h1}}\frac{\partial\varphi}{\partial z}\right]_{\text{layer 2}}=\left[\frac{S_D k}{a_{h,i}}\frac{\partial\varphi}{\partial t}\right]_{PL} \quad \text{A15: 14}$$

$$\frac{\partial^2\varphi_D}{\partial r_D^2}+\frac{1}{r_D}\frac{\partial\varphi_D}{\partial r_D}-\gamma_{Dk}\varphi_D-\delta_D\left[\frac{\partial\varphi_D}{\partial z_D}\right]_{\text{layer 2}}=\omega\left[\frac{\partial\varphi_D}{\partial t_{DwD}}\right]_{\text{layer 1}} \quad \text{A15: 15}$$

Free Fluid Layer is Producing Layer

Here the mass leakage rate from the hydrate layer is quantified in one term as this is already reflected in the diffusivity equation of the crossflow layer (hydrate layer) incorporated in the diffusivity equation of the free fluid layer.

Hence:

$$\frac{\partial^2\varphi}{\partial r_D^2}+\frac{1}{r_D}\frac{\partial}{\partial r_D}-\left[\frac{r_w^2}{\Delta z_2}\frac{k_{v2}}{k_{h1}}\frac{\partial\varphi}{\partial z}\right]_{\text{layer 2}}=\left[\frac{S_{Dk}}{a_{h,i}}\right]\frac{\partial\varphi}{\partial t} \quad \text{A15: 16}$$

$$\frac{\partial^2\varphi_D}{\partial r_D^2}+\frac{1}{r_D}\frac{\partial\varphi_D}{\partial r_D}-\delta_D\left[\frac{\partial\varphi_D}{\partial z_D}\right]_{\text{layer 2}}=\omega\left[\frac{\partial\varphi_D}{\partial t_{DwD}}\right]_{\text{layer 1}} \quad \text{A15: 17}$$

Where,

$$\frac{1}{a_h}=\frac{S_{Dk}}{a_{h,id}}=\frac{(\rho c_T)_{eff,id}}{\left[\rho_t k\left(\frac{k_r}{\eta}\right)_t\right]_{id}}r_w{}^2\left\{\frac{(\rho c_T)_{eff}}{(\rho c_T)_{eff,id}}\frac{\left[\rho_t k\left(\frac{k_r}{\eta}\right)_t\right]_{id}}{\left[\rho_t k\left(\frac{k_r}{\eta}\right)_t\right]}\right\} \quad \text{A15: 18}$$

$$(\rho c_T)_{eff}=\rho_g c_{T,g}+\rho_w c_{T,w} \quad \text{A15: 19}$$

$$c_{T,g}=S_g c_g+S_g c_F \quad \text{A15: 20}$$

$$c_{T,w}=S_w c_w+S_w c_F \quad \text{A15: 21}$$

$$\delta_D=\frac{r_w^2}{\Delta z_2\Delta z_1}\frac{k_{v2}}{k_{h1}} \quad \text{A15: 22}$$

$$t_{DwD}=\frac{t}{\left[\left(\frac{a_h+a_v}{a_h a_v}\right)\right]_i} \quad \text{A15: 23}$$

$\gamma_D=0$ and $\theta_D=0$

Appendix 16: Solutions to the Diffusivity Equation when producing from the Free Fluid Layer

The diffusivity equation to the crossflow problem when producing from the free fluid layer is given by:

$$\frac{\partial^2\varphi_D}{\partial r_D^2}+\frac{1}{r_D}\frac{\partial\varphi_D}{\partial r_D}-\delta_D\left[\frac{\partial[\varphi_D]_{layer2}}{\partial z_D}\right]_{z_D=1}=\omega\frac{\partial\varphi_D}{\partial t_{DwD}} \qquad \text{A16: 1}$$

Using the Laplace transformation, the diffusivity equation above takes the form:

$$\frac{\partial^2\widehat{\varphi}_D}{\partial {r_D}^2}+\frac{1}{r_D}\frac{\partial\widehat{\varphi}_D}{\partial r_D}-\delta_D\left[\frac{\partial[\widehat{\varphi}_D]_{layer2}}{\partial z_D}\right]_{z_D=1}=\omega p\widehat{\varphi}_D \qquad \text{A16: 2}$$

From the solutions of the crossflow layer given in Appendix 14, we introduce use the general form of the solution for NFB with heat flux which has been shown to consider true NFB and CPOB all depending on the rate of heat flux hence hydrate dissociation at the boundary.

Mass Influx from Hydrate Layer

$$\left(\frac{\partial[\widehat{\varphi_D}]_{layer2}}{\partial z_D}\right)_{z_D=1}=[\widehat{\varphi_D}]_{layer1}\sqrt{p[1-\omega]}\,Coth\left[(1-\Delta z_D)\sqrt{p[1-\omega]}\right]\frac{\left\{\sqrt{p[1-\omega]}\tanh[(1-\Delta z_D)\sqrt{p[1-\omega]}]+\widehat{Q_{pD}}e_D\right\}}{\left\{\sqrt{p[1-\omega]}Coth[(1-\Delta z_D)\sqrt{p[1-\omega]}]+\widehat{Q_{pD}}e_D\right\}}$$

The general form of the above equations can be written thus:

$$\frac{d\widehat{\varphi_D}}{dz_D}=[\widehat{\varphi_D}]_{layer1}M_i \qquad \text{A16: 3}$$

Hence the diffusivity equation can be written thus:

$$\frac{\partial^2\widehat{\varphi}_D}{\partial {r_D}^2}+\frac{1}{r_D}\frac{\partial\widehat{\varphi}_D}{\partial r_D}-\delta_D M_i\widehat{\varphi_D}=\omega p\widehat{\varphi}_D \qquad \text{A16: 4}$$

$$\frac{\partial^2\widehat{\varphi}_D}{\partial {r_D}^2}+\frac{1}{r_D}\frac{\partial\widehat{\varphi}_D}{\partial r_D}-(\delta_D M_i+\omega p)\widehat{\varphi}_D=0 \qquad \text{A16: 5}$$

$$\frac{\partial^2\widehat{\varphi}_D}{\partial {r_D}^2}+\frac{1}{r_D}\frac{\partial\widehat{\varphi}_D}{\partial r_D}-\lambda_D^2\widehat{\varphi}_D=0 \qquad \text{A16: 6}$$

$${r_D}^2\frac{\partial^2\widehat{\varphi}_D}{\partial {r_D}^2}+r_D\frac{\partial\widehat{\varphi}_D}{\partial r_D}-{r_D}^2\lambda_D^2\widehat{\varphi}_D=0 \qquad \text{A16: 7}$$

As was done in Appendix 7, the above equation can be transformed into the modified Bessel equation given in the form:

$$\beta^2\widehat{\varphi}_D{}''+\beta^2\widehat{\varphi}_D{}'-(\beta^2+0)\widehat{\varphi}_D=0 \qquad \text{A16: 8}$$

The solution to modified Bessel equation is given thus:

General Solution in Laplace Domain

$$\widehat{\varphi}_D=c_1I_o(r_D\lambda_D)+c_2K_o(r_D\lambda_D) \qquad \text{A16: 9}$$

Where,

$$\lambda_D = \sqrt{(\delta_D M_i + \omega p)} \quad \text{A16: 10}$$

$$\hat{\varphi}_D{}' = \frac{\partial \hat{\varphi}_D}{\partial r_D} \quad \text{A16: 11}$$

$$\beta = r_D \lambda_D \quad \text{A16: 12}$$

Case 1: Constant Terminal Pressure Solutions

Case 1a: Infinite Acting Reservoir

For the infinite acting system, the coefficient c_1 equals zero and by using the inner boundary condition, the solutions in Laplace domain are given thus:

Inner Boundary

$$c_2 = \frac{1}{pK_o(\lambda_D)} \quad \text{A16: 13}$$

Dimensionless Pseudo-Pressure

$$\hat{\varphi}_D = \frac{K_o(r_D \lambda_D)}{pK_o(\lambda_D)} \quad \text{A16: 14}$$

Dimensionless Flow rate

$$\hat{m}_{tD} = -r_D \frac{d\hat{\varphi}_D}{dr_D} = \frac{r_D \lambda_D K_1(r_D \lambda_D)}{pK_o(\lambda_D)} \quad \text{A16: 15}$$

Rate Transient Plot in Laplace Domain

$\widehat{pm}_{tD}$ Versus $\frac{1}{p}$

$\hat{\varphi}_D p$ Versus r_D

$Der = \frac{\Delta\left(\frac{1}{\widehat{pm}_{tD}}\right)}{\Delta\left(\frac{1}{p}\right)}$ Versus $\frac{1}{p}$

Hydrate Layer Parameters		
ω	Δz_D	δ_D
1,00E-05	10	0,0001

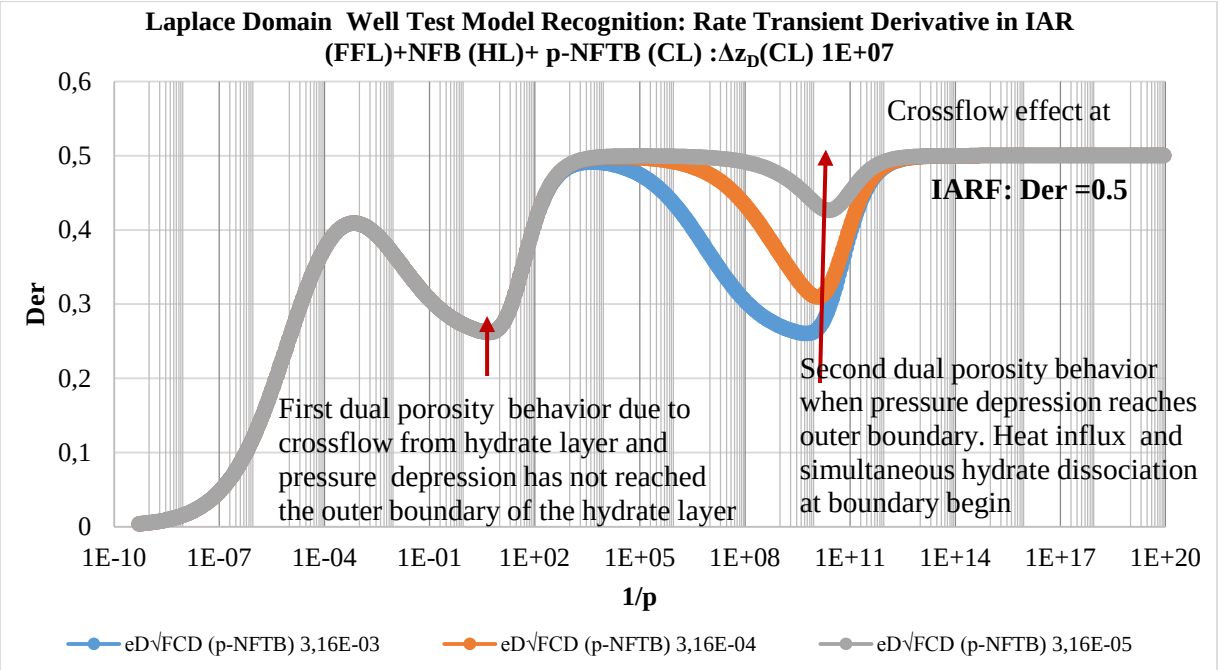

A16- 1: Derivative Rate Transient in Free Fluid Layer + NFB (HL) + p-NFTB (CL): Δz_D (CL) 1E+07

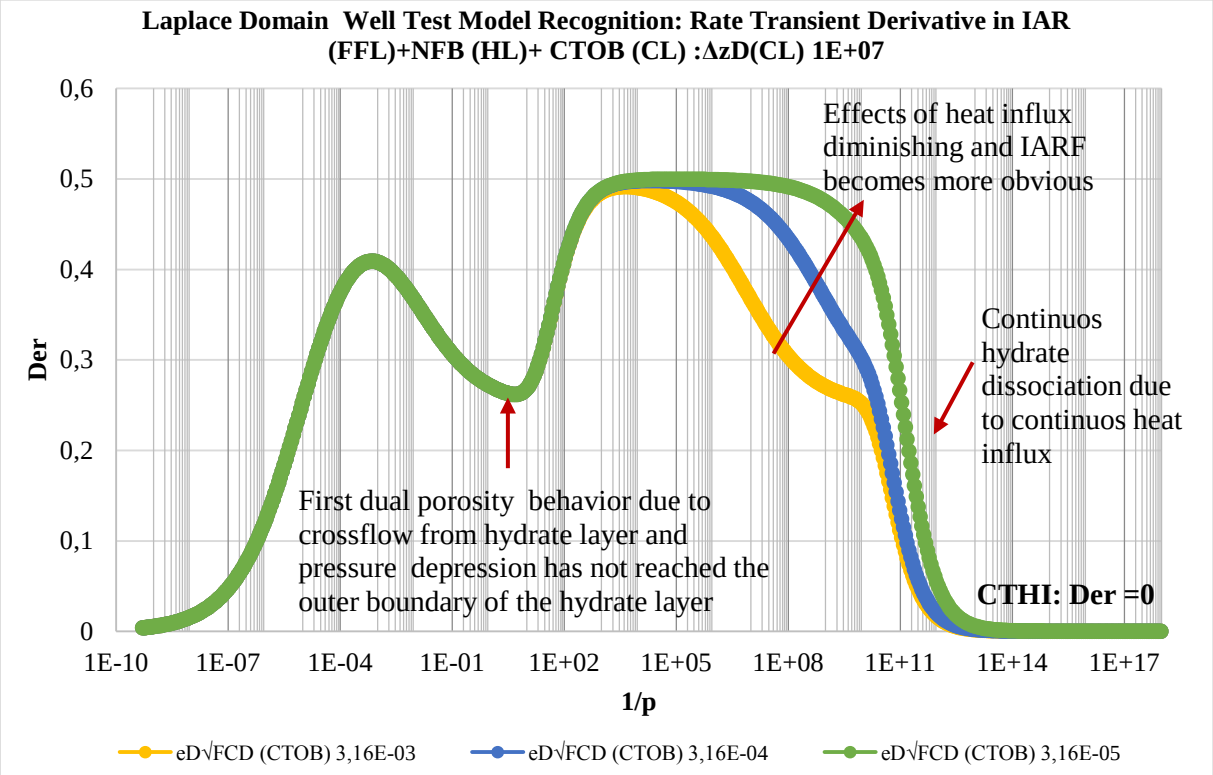

A16- 2: Derivative Rate Transient in Free Fluid Layer + NFB (HL) + CTOB (CL) :Δz_D(CL) 1E+07

Hydrate Layer Parameters		Confining Layer	
Δz_D	δ_D	Δz_D	$e_D\sqrt{F_{CD}}$
10	0,0001	1E+07	3.16E-03

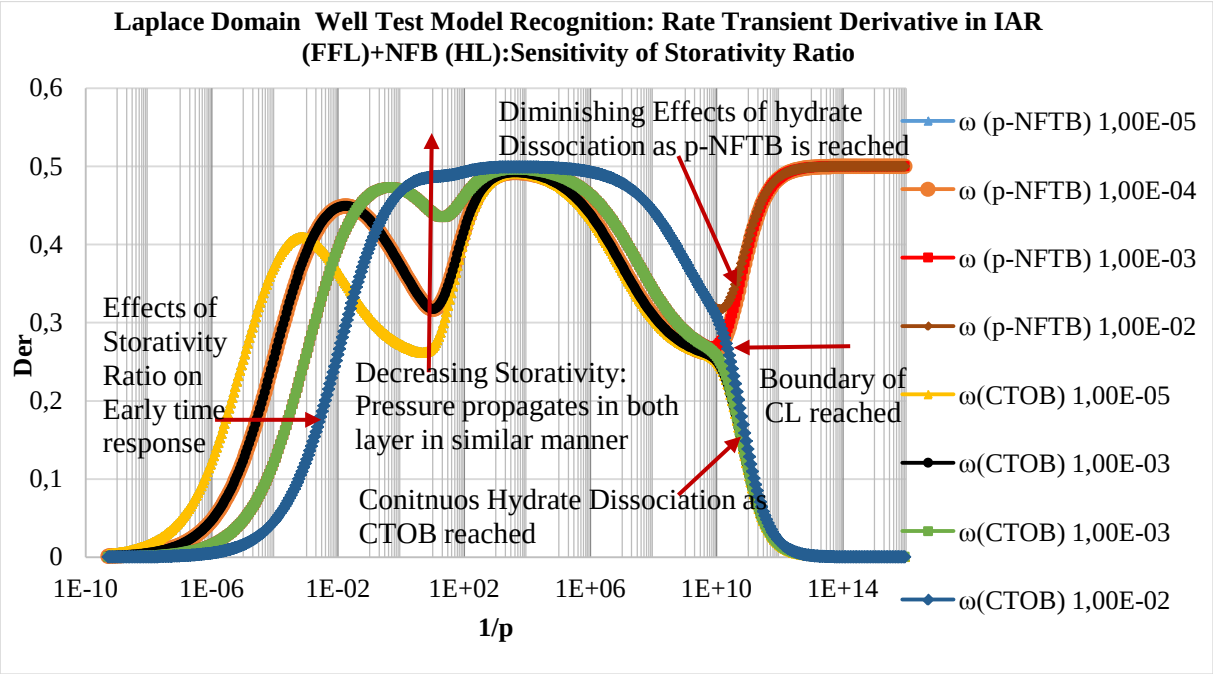

A16- 3: Derivative Rate Transient in Free Fluid Layer + NFB (HL) with Sensitivity of Storativity Ratio

Hydrate Layer Parameters		Confining Layer	
Δz_D	ω	Δz_D	$e_D\sqrt{F_{CD}}$
10	1E-05	1E+05	3.16E-03

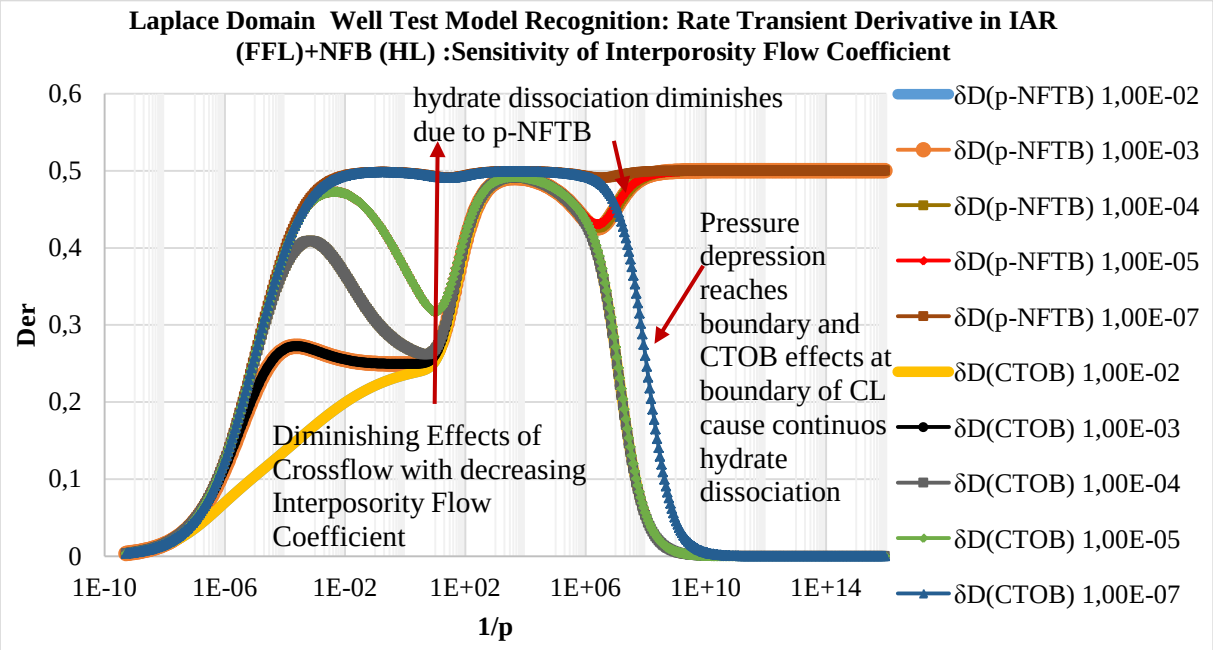

A16- 4: Derivative Rate Transient in Free Fluid Layer + NFB (HL) with Sensitivity of Interporosity Flow Coefficient

Hydrate Layer Parameters		Confining Layer	
δ_D	ω	Δz_D	$e_D\sqrt{F_{CD}}$
1E-02	1E-02	15	3.16E-03

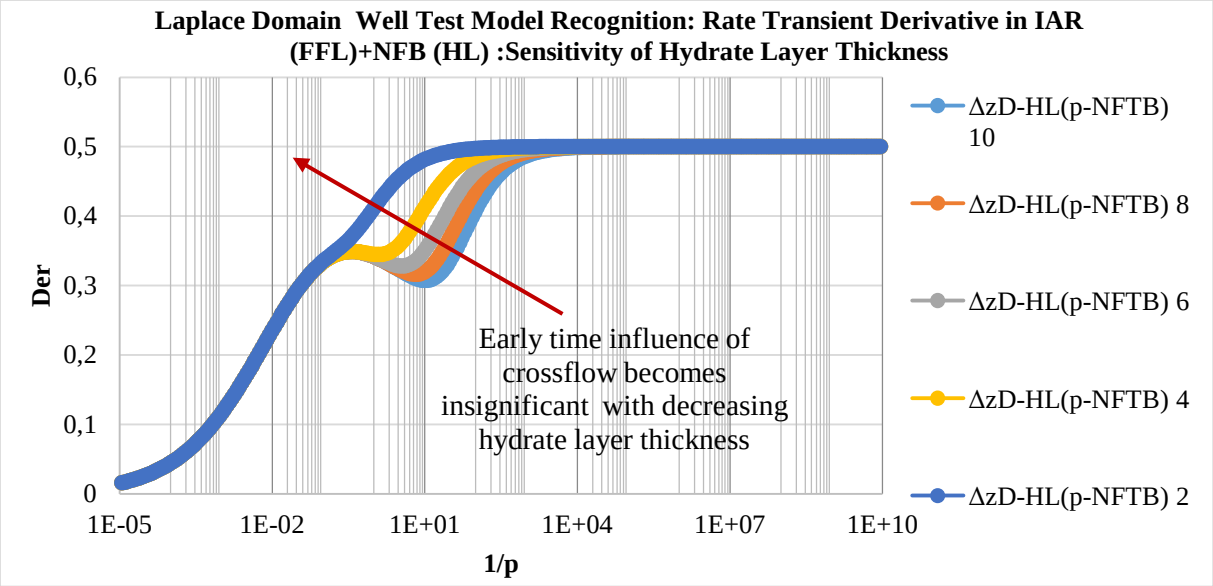

A16- 5: Derivative Rate Transient in Free Fluid Layer + NFB (HL) +p-NFTB (CL) with Sensitivity of Hydrate Layer Thickness

Solutions in Real-time Domain

Due to the time dependence of the leakage rate, Hantush [43] proposed approximate solutions for given time interval such that solutions to the diffusivity equation above could be easily derived; however for CPOB and NFB cases. The solutions are based on the approximations given in Appendix 12 for the hyperbolic functions. By applying the same methodology, asymptotic solutions analogue Hantush [43] are presented for specific time intervals according to the simplifications made for the leakage rate function.

Late Time Response for NFB in Hydrate Layer (No Heat Flux)

$$\lambda_D = \sqrt{p\omega\left(1+\frac{[1-\omega]}{\omega}\delta_D(\Delta z_D-1)\right)} = \sqrt{p\omega f_D} \qquad \text{A16: 16}$$

Dimensionless Pseudo-Pressure

$$\varphi_D = L^{-1}\left\{\frac{K_o\left[r_D\sqrt{p(\omega f_D)}\right]}{pK_o\left[\sqrt{p(\omega f_D)}\right]}\right\} = A\left(\frac{t_{DwD}}{\omega f_D}, r_D\right)$$

$$\varphi_D = A\left(\frac{t_{DwD}}{\omega f_D}, r_D\right) \qquad \text{A16: 17}$$

For $t_D = t_{DwD}/(f_D \omega r_D^2) > 500$

$$\varphi_D = \frac{Ei\left(\frac{r_D^2 f_D \omega}{4 t_{DwD}}\right)}{Ei\left(\frac{f_D \omega}{4 t_{DwD}}\right)} \quad \text{A16: 18}$$

Dimensionless Flow rate at Wellbore

$$\dot{m}_{tD} = G\left(\frac{t_{DwD}}{\omega f_D}\right) \quad \text{A16: 19}$$

Late Time Response for CPOB in Hydrate Layer

$$\lambda_D = \sqrt{p\omega\left(1 + \frac{[1-\omega]}{3\omega}\delta_D(\Delta z_D - 1)\right) + \frac{\delta_D}{(\Delta z_D - 1)}} = \sqrt{p\omega g_D + j_D} \quad \text{A16: 20}$$

Dimensionless Pseudo-Pressure

$$\varphi_D = Z\left(\frac{t_{DwD}}{\omega g_D}, r_D, \sqrt{j_D}\right) \quad \text{A16: 21}$$

Dimensionless Flow rate at Wellbore

$$\dot{m}_{tD} = G\left(\frac{t_{Dw}}{\omega g_D}, \sqrt{j_D}\right) \quad \text{A16: 22}$$

Case 1b: Constant Pressure Outer Boundary Reservoir

General Solution in Laplace Domain

$$\hat{\varphi}_D = c_1 I_o(r_D \lambda_D) + c_2 K_o(r_D \lambda_D)$$

Boundary conditions

r_{eD} $\quad \hat{\varphi}_D = 0$

r_D=1 $\quad \hat{\varphi}_D = \frac{1}{p}$

The coefficients are hence:

$$c_1 = -\frac{1}{p}\left[\frac{K_o(r_{eD}\lambda_D)}{(K_o(\lambda_D)I_o(r_{eD}\lambda_D)) - I_o(\lambda_D)K_o(r_{eD}\lambda_D)}\right] \quad \text{A16: 23}$$

$$c_2 = \frac{1}{p}\left[\frac{K_o(r_{eD}\lambda_D)I_o(r_{eD}\lambda_D)}{(K_o(\lambda_D)I_o(r_{eD}\lambda_D)) - I_o(\lambda_D)K_o(r_{eD}\lambda_D)}\right]\frac{1}{K_o(r_{eD}\lambda_D)} \quad \text{A16: 24}$$

Dimensionless Pseudo-Pressure

$$\hat{\varphi}_D = \frac{1}{p}\left[\frac{K_o(r_D\lambda_D)I_o(r_{eD}\lambda_D) - K_o(r_{eD}\lambda_D)I_o(r_D\lambda_D)}{I_o(r_{eD}\lambda_D)K_o(\lambda_D) - I_o(\lambda_D)K_o(r_{eD}\lambda_D)}\right] \quad \text{A16: 25}$$

Dimensionless Flow rate

$$\hat{m}_{tD} = -r_D\frac{d\hat{\varphi}_D}{dr_D} = -r_D\frac{1}{p}\left[\frac{1}{I_o(r_{eD}\lambda_D)K_o(\lambda_D) - I_o(\lambda_D)K_o(r_{eD}\lambda_D)}\right]\frac{d\left(K_o(r_D\lambda_D)I_o(r_{eD}\lambda_D) - K_o(r_{eD}\lambda_D)I_o(r_D\lambda_D)\right)}{dr_D} \quad \text{A16: 26}$$

$$\hat{m}_{tD} = \frac{r_D}{p}\lambda_D\left[\frac{K_1(r_D\lambda_D)I_o(r_{eD}\lambda_D) + K_o(r_{eD}\lambda_D)I_1(r_D\lambda_D)}{I_o(r_{eD}\lambda_D)K_o(\lambda_D) - I_o(\lambda_D)K_o(r_{eD}\lambda_D)}\right] \quad \text{A16: 27}$$

Rate Transient Plot in Laplace Domain

$\widehat{pm}_{tD}$ Versus $\frac{1}{p}$

$\widehat{\varphi}_D p$ Versus r_D

$Der = \frac{\Delta\left(\frac{1}{\widehat{pm}_{tD}}\right)}{\Delta\left(\frac{1}{p}\right)}$ Versus $\frac{1}{p}$

For large values of p i.e. early time production period where boundary dominated flow has not been reached, the reservoir is still acting infinite and from the characteristics of the modified Bessel´s functions given in Figure A7- 1, the solutions to the infinite acting reservoir are applicable.

Case 1c: No-Flow Outer Boundary Reservoir

Boundary Conditions

r_{eD} $\left(\frac{d\widehat{\varphi}_D}{dr_D}\right)_{r_{eD}} = 0$

r_D=1 $\widehat{\varphi}_D = \frac{1}{p}$

The coefficients are hence

$$c_1 = \frac{1}{p\lambda_D}\left[\frac{K_1(r_{eD}\lambda_D)}{I_o(\lambda_D)K_o(r_{eD}\lambda_D) - K_o(\lambda_D)I_1(r_{eD}\lambda_D)}\right] \quad \text{A16: 28}$$

$$c_2 = \frac{1}{p\lambda_D}\left[\frac{I_1(r_{eD}\lambda_D)}{I_o(\lambda_D)K_1(r_{eD}\lambda_D) - K_o(\lambda_D)I_1(r_{eD}\lambda_D)}\right] \quad \text{A16: 29}$$

Dimensionless Pseudo-Pressure

$$\widehat{\varphi}_D = \frac{1}{p\lambda_D}\left[\frac{K_1(r_{eD}\lambda_D)I_o(r_D\lambda_D) + I_1(r_{eD}\lambda_D)K_o(r_D\lambda_D)}{I_o(\lambda_D)K_1(r_{eD}\lambda_D) - K_o(\lambda_D)I_1(r_{eD}\lambda_D)}\right] \quad \text{A16: 30}$$

Dimensionless Flow rate

$$\widehat{m}_{tD} = -r_D\frac{d\widehat{\varphi}_D}{dr_D} = -r_D\frac{1}{p\lambda_D}\left[\frac{1}{I_o(\lambda_D)K_1(r_{eD}\lambda_D) - K_o(\lambda_D)I_1(r_{eD}\lambda_D)}\right]\frac{d\left(K_1(r_{eD}\lambda_D)I_o(r_D\lambda_D) + I_1(r_{eD}\lambda_D)K_o(r_D\lambda_D)\right)}{dr_D} \quad \text{A16: 31}$$

$$\widehat{m}_{tD} = \frac{r_D}{p}\left[\frac{K_1(r_{eD}\lambda_D)I_1(r_D\lambda_D) - I_1(r_{eD}\lambda_D)K_1(r_D\lambda_D)}{I_o(r_{eD}\lambda_D)K_o(\lambda_D) - I_o(\lambda_D)K_o(r_{eD}\lambda_D)}\right] \quad \text{A16: 32}$$

Rate Transient Plot in Laplace Domain

$\widehat{pm}_{tD}$ Versus $\frac{1}{p}$

$\widehat{\varphi}_D p$ Versus r_D

$Der = \frac{\Delta\left(\frac{1}{\widehat{pm}_{tD}}\right)}{\Delta\left(\frac{1}{p}\right)}$ Versus $\frac{1}{p}$

For large values of p i.e. early time production period where boundary dominated flow has not been reached, the reservoir is still acting infinite and from the characteristics of the modified Bessel´s functions given in Figure A7- 1, the solutions to the infinite acting reservoir are applicable.

Case 2: Constant Terminal Rate Solutions

Case 2a: Infinite Acting Reservoir

As shown earlier for the infinite acting reservoir, the coefficient c_1 equals zero and the pressure equation is of the form:

$$\hat{\varphi}_D = c_2 K_o(r_D \lambda_D)$$

The derivation of the coefficient c_2 for the constant terminal rate problem will depend on the definition of the inner boundary condition as finite wellbore radius and line source boundary conditions exist in deriving the solutions to the problem.

For finite wellbore radius solution	The line source solution
$\lim_{r_D \to 1}\left[r_D \frac{d\left(c_2 K_o(r_D\lambda_D)\right)}{dr_D}\right] = \frac{-1}{p}$	$\lim_{r_D \to 0}\left[r_D \frac{d\left(c_2 K_o(r_D\lambda_D)\right)}{dr_D}\right] = \frac{-1}{p}$
$\lim_{r_D \to 1}[r_D c_2 \lambda_D K_1(r_D\lambda_D)] = \frac{1}{p}$	$\lim_{r_D \to 0}[r_D c_2 \lambda_D K_1(r_D\lambda_D)] = \frac{1}{p}$
$c_2 = \frac{1}{p\lambda_D K_1(\lambda_D)}$	$c_2 = \frac{1}{p}$
Dimensionless Pseudo-Pressure	Dimensionless Pseudo-Pressure
$\hat{\varphi}_D = \frac{K_o(r_D\lambda_D)}{p\lambda_D K_1(\lambda_D)}$	$\hat{\varphi}_D = \frac{K_o(r_D\lambda_D)}{p}$

Pseudo-Pressure Transient Plot in Laplace Domain

$\hat{\varphi}_D p$ Versus $\frac{1}{p}$

Der $= \frac{\Delta(\hat{\varphi}_D p)}{\Delta\left(\frac{1}{p}\right)}$ Versus $\frac{1}{p}$

Hydrate Layer Parameters		Confining Layer	
Δz_D	ω	Δz_D	$e_D\sqrt{F_{CD}}$
10	1E-03	1E+07	3.16E-03

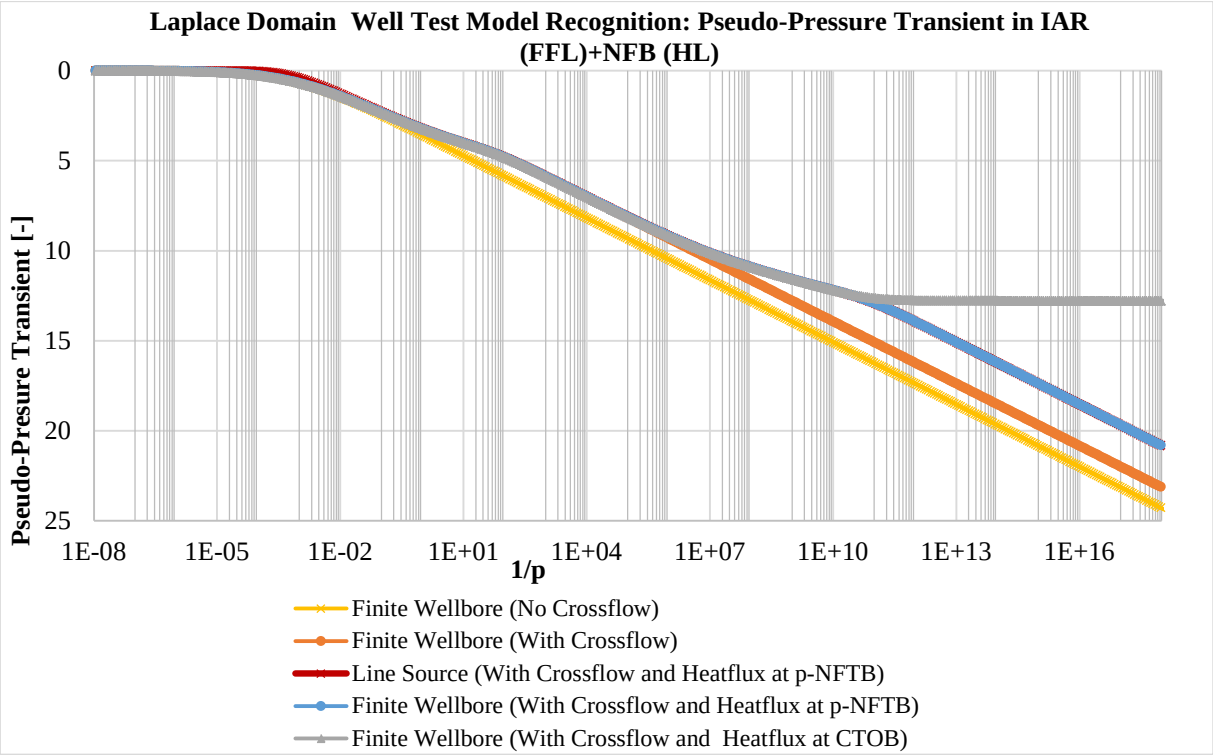

A16- 6: Pseudo-Pressure Transient in Infinite Acting Hydrate Layer + NFB (HL)

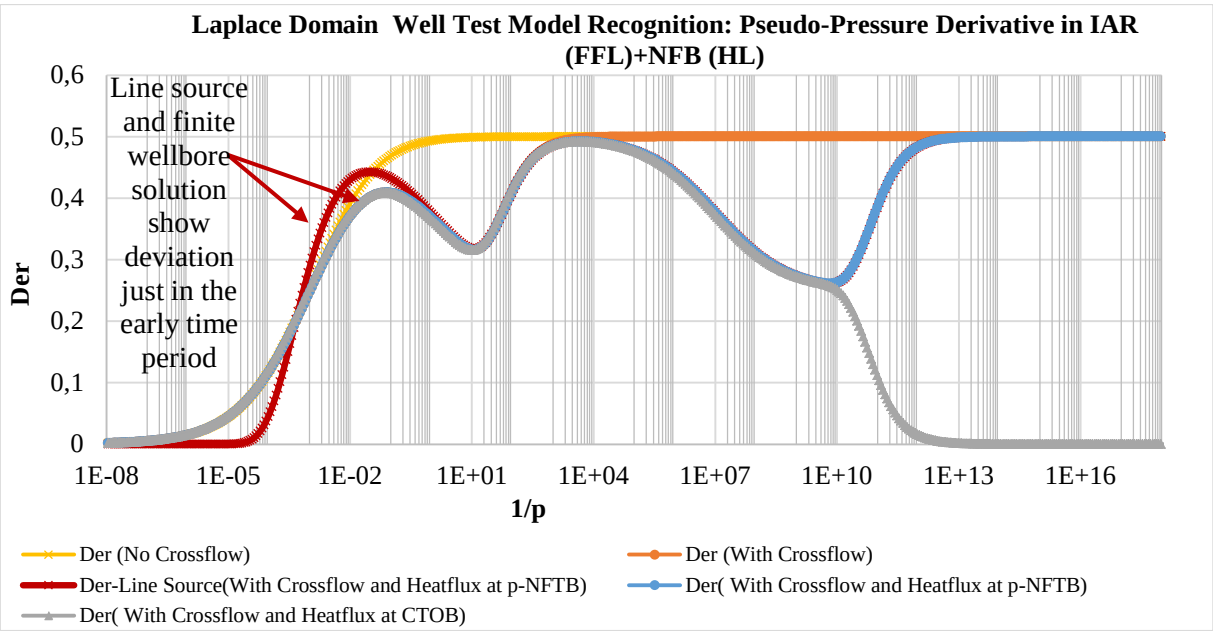

A16- 7: Pseudo-Pressure Derivative in Infinite Acting Hydrate Layer + NFB (HL)

Solutions in Real-Time Domain

Finite Well Radius Inner Boundary Solutions

$$\varphi_D\left(r_D, \frac{t_{Dw}}{f_D}, \sqrt{j_D}\right) = L^{-1}\left(\frac{K_o(r_D\lambda_D)}{p\lambda_D K_1(\lambda_D)}\right) \qquad \text{A16: 33}$$

The solution to the above inverse Laplace can be readily derived by proper application of numerical inverse Laplace techniques. However, using the line source solution, the solutions presented by [43] are easily applied. Once more the specific cases of CPOB and NFB are used.

The Line Source Inner Boundary Solutions

$$\varphi_D = L^{-1}\left(\frac{K_o(r_D\lambda_D)}{p}\right) \quad \text{A16: 34}$$

Early-Time Response for both NFB and CPOB in Hydrate Layer

$$\lambda_D = \sqrt{p\omega + \delta_D\sqrt{[1-\omega]}\sqrt{p}} = \sqrt{p\omega + \varepsilon_D\sqrt{p}} \quad \text{A16: 35}$$

$$\varphi_D = H\left(\frac{\omega r_D^2}{4t_{DwD}}, \frac{r_D\varepsilon_D}{4\sqrt{\omega}}\right) \quad \text{A16: 36}$$

Late Time Period for CPOB in Hydrate Layer

$$\lambda_D = \sqrt{p\omega\left(1 + \frac{[1-\omega]}{3\omega}\delta_D(\Delta z_D - 1)\right) + \frac{\delta_D}{(\Delta z_D - 1)}} = \sqrt{p\omega g_D + j_D} \quad \text{A16: 37}$$

$$\varphi_D = \frac{1}{2}W\left(\frac{r_D^2}{4t_{Dw}}g_D, r_D\sqrt{j_D}\right) \quad \text{A16: 38}$$

Late Time Period for NFB in Hydrate Layer

$$\lambda_D = \sqrt{p\omega\left(1 + \frac{[1-\omega]}{\omega}\delta_D(\Delta z_D - 1)\right)} = \sqrt{p\omega f_D} \quad \text{A16: 39}$$

$$\varphi_D = \frac{1}{2}E_1\left(\frac{\omega r_D^2}{4t_{DwD}}f_D\right) \quad \text{A16: 40}$$

Case 2b: Constant Pressure Outer Boundary Reservoir

Boundary Conditions

r_{eD} $\qquad \hat{\varphi}_D = 0$

r_D=1 $\qquad r_D\frac{d\hat{\varphi}_D}{dr_D} = -\frac{1}{p}$

The coefficients are:

$$c_1 = -\frac{1}{p\lambda_D}\left[\frac{K_o(r_{eD}\lambda_D)}{K_1(\lambda_D)I_o(r_{eD}\lambda_D)+I_1(\lambda_D)K_o(r_{eD}\lambda_D)}\right] \quad \text{A16: 41}$$

$$c_2 = \frac{1}{p\lambda_D}\left[\frac{I_o(r_{eD}\lambda_D)}{K_1(\lambda_D)I_o(r_{eD}\lambda_D)+I_1(\lambda_D)K_o(r_{eD}\lambda_D)}\right] \quad \text{A16: 42}$$

Dimensionless Pseudo-Pressure

$$\hat{\varphi}_D = \frac{1}{p\lambda_D}\left[\frac{K_o(r_D\lambda_D)I_o(r_{eD}\lambda_D)-K_o(r_{eD}\lambda_D)I_o(r_D\lambda_D)}{K_1(\lambda_D)I_o(r_{eD}\lambda_D)+I_1(\lambda_D)K_o(r_{eD}\lambda_D)}\right] \quad \text{A16: 43}$$

Pseudo-Pressure Transient Plot in Laplace Domain

$\hat{\varphi}_D p$ Versus $\frac{1}{p}$

$\text{Der} = \frac{\Delta(\hat{\varphi}_D p)}{\Delta\left(\frac{1}{p}\right)}$ Versus $\frac{1}{p}$

For large values of p i.e. early time production period where boundary dominated flow has not been reached, the reservoir is still acting infinite and from the characteristics of the modified Bessel´s functions given in Figure A7- 1, the solutions to the infinite acting reservoir are applicable.

Case 2c: No-Flow Outer Boundary in Producing Layer

Boundary Conditions

r_{eD} $\left(\frac{d\hat{\varphi}_D}{dr_D}\right)_{r_{eD}} = 0$

rD=1 $r_D \frac{d\hat{\varphi}_D}{dr_D} = -\frac{1}{p}$

The coefficients are hence:

$$c_1 = \frac{1}{p\lambda_D}\left[\frac{K_1(r_{eD}\lambda_D)}{K_1(\lambda_D)I_1(r_{eD}\lambda_D) - I_1(\lambda_D)K_1(r_{eD}\lambda_D)}\right] \quad \text{A16: 44}$$

$$c_2 = \frac{1}{p\lambda_D}\left[\frac{I_1(r_{eD}\lambda_D)}{K_1(\lambda_D)I_1(r_{eD}\lambda_D) - I_1(\lambda_D)K_1(r_{eD}\lambda_D)}\right] \quad \text{A16: 45}$$

Dimensionless Pseudo-Pressure

$$\hat{\varphi}_D = \frac{1}{p\lambda_D}\left[\frac{K_1(r_{eD}\lambda_D)I_o(r_D\lambda_D) + I_1(r_{eD}\lambda_D)K_o(r_D\lambda_D)}{K_1(\lambda_D)I_1(r_{eD}\lambda_D) - I_1(\lambda_D)K_1(r_{eD}\lambda_D)}\right] \quad \text{A16: 46}$$

Pseudo-Pressure Transient Plot in Laplace Domain

$\hat{\varphi}_D p$ Versus $\frac{1}{p}$

$\text{Der} = \frac{\Delta(\hat{\varphi}_D p)}{\Delta\left(\frac{1}{p}\right)}$ Versus $\frac{1}{p}$

For large values of p i.e. early time production period where boundary dominated flow has not been reached, the reservoir is still acting infinite and from the characteristics of the modified Bessel´s functions given in Figure A7- 1, the solutions to the infinite acting reservoir are applicable.

Appendix 17: Solutions to the Diffusivity Equation when producing from the Hydrate Layer

As derived earlier, the diffusivity equation when the hydrate is the producing layer is given by:

$$\frac{\partial^2\varphi_D}{\partial r_D^2}+\frac{1}{r_D}\frac{\partial\varphi_D}{\partial r_D}-\left[\frac{\partial T_{pD}}{\partial z_D}\right]_{Caprock,z_D=1}-\delta_D(1+\theta_D)\left[\frac{\partial[\varphi_D]_{layer2}}{\partial z_D}\right]_{z_D=1}=\omega\left[\frac{\partial\varphi_D}{\partial t_{DwD}}\right]_{layer\ 1} \quad \text{A17: 1}$$

The above equation is given in Laplace domain thus:

$$\frac{\partial^2\hat{\varphi}_D}{\partial r_D{}^2}+\frac{1}{r_D}\frac{\partial\hat{\varphi}_D}{\partial r_D}-\widehat{\dot{Q}_{pD}}e_D\hat{\varphi}_D-\delta_D(1+\theta_D)M_i\widehat{\varphi_D}=\omega p\hat{\varphi}_D \quad \text{A17: 2}$$

$$\frac{\partial^2\hat{\varphi}_D}{\partial r_D{}^2}+\frac{1}{r_D}\frac{\partial\hat{\varphi}_D}{\partial r_D}-\lambda_D^2\hat{\varphi}_D=0 \quad \text{A17: 3}$$

Where,

$$\lambda_D=\sqrt{\delta_D(1+\theta_D)M_i+\widehat{\dot{Q}_{pD}}e_D+\omega p} \quad \text{A17: 4}$$

It can be noticed that the complex variable λ_D above is very much different from the case whereby the reservoir is produced from the free fluid layer. It is important to investigate the influence of hydrate dissociation when producing from the hydrate layer such that representative reservoir response models and reservoir parameters for the hydrate layer can be derived.

The equation above can be transformed into the modified Bessel equation and the solution derived accordingly for which the general solution takes the form:

$$\hat{\varphi}_D=c_1I_o(r_D\lambda_D)+c_2K_o(r_D\lambda_D)$$

A number of combinations of solutions with different boundary conditions can be made to investigate the reservoir response but however needs care in deriving simplifications for the inverse Laplace transform. Since just CTOB and p-NFTB have been considered for the confining layer and CPOB and NFB for the free fluid layer, four different cases can be handled:

- CPOB (FFL) + p-NFTP (CL)
- CPOB (FFL) + CTOB (CL)
- NFB (FFL) + p-NFTP (CL)
- NFB (FFL) + CTOB (CL)

Case 1: Constant Terminal Pressure Solutions

Case 1a: Infinite Acting Reservoir

For the infinite acting system, the coefficient c1 equals zero and by using the inner boundary condition, the solutions in Laplace domain are given thus:

Inner Boundary

$$c_2 = \frac{1}{pK_o(\lambda_D)} \qquad \text{A17: 5}$$

Dimensionless Pseudo-Pressure

$$\hat{\varphi}_D = \frac{K_o(r_D\lambda_D)}{pK_o(\lambda_D)} \qquad \text{A17: 6}$$

Dimensionless Flow rate

$$\hat{m}_{tD} = -\frac{r_D\lambda_D K_1(r_D\lambda_D)}{pK_o(\lambda_D)} = \frac{r_D\lambda_D K_1(r_D\lambda_D)}{pK_o(\lambda_D)} \qquad \text{A17: 7}$$

Rate Transient Plot in Laplace Domain

$\widehat{pm}_{tD}$ Versus $\frac{1}{p}$

$\hat{\varphi}_D p$ Versus r_D

$Der = \frac{\Delta\left(\frac{1}{\widehat{pm}_{tD}}\right)}{\Delta\left(\frac{1}{p}\right)}$ Versus $\frac{1}{p}$

Free Fluid Layer Parameters			Confining Layer	
Δz_D	ω	δD	Δz_D	$e_D\sqrt{F_{CD}}$
1E+04	1E-04	1E-03	1E+04	3.16E-04

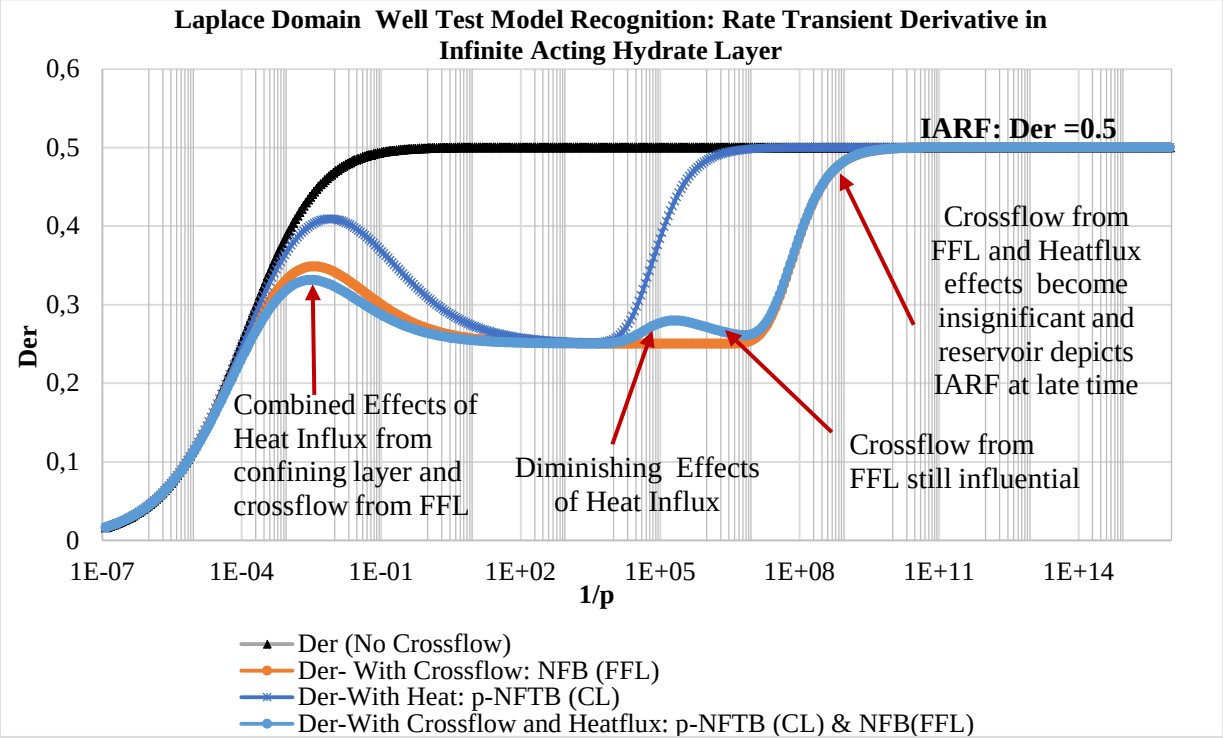

A17- 1: Derivative Rate Transient in Infinite Acting Hydrate Layer + NFB (HL) + p-NFTB (CL)

Free Fluid Layer Parameters			Confining Layer	
Δz_D	ω	δD	Δz_D	$e_D\sqrt{F_{CD}}$
1E+04	1E-04	1E-03	1E+04	3.16E-04

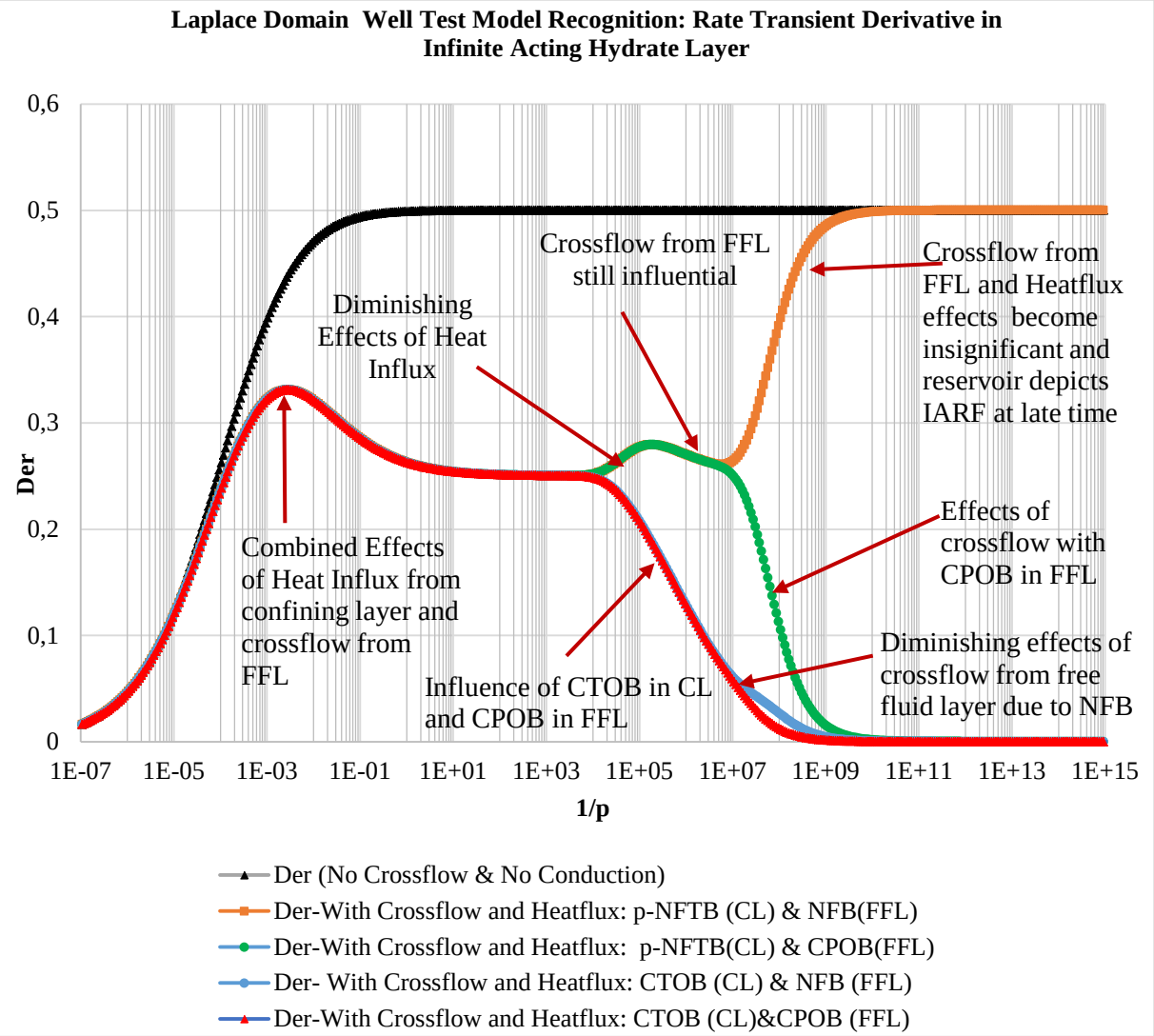

A17- 2: Derivative Rate Transient in Infinite Acting Hydrate Layer with different Boundary Conditions in the Confining Layers

Free Fluid Layer Parameters			Confining Layer	
Δz_D	ω	δD	Δz_D	$e_D\sqrt{F_{CD}}$
5	1E-04	1E-03	5	3.16E-04

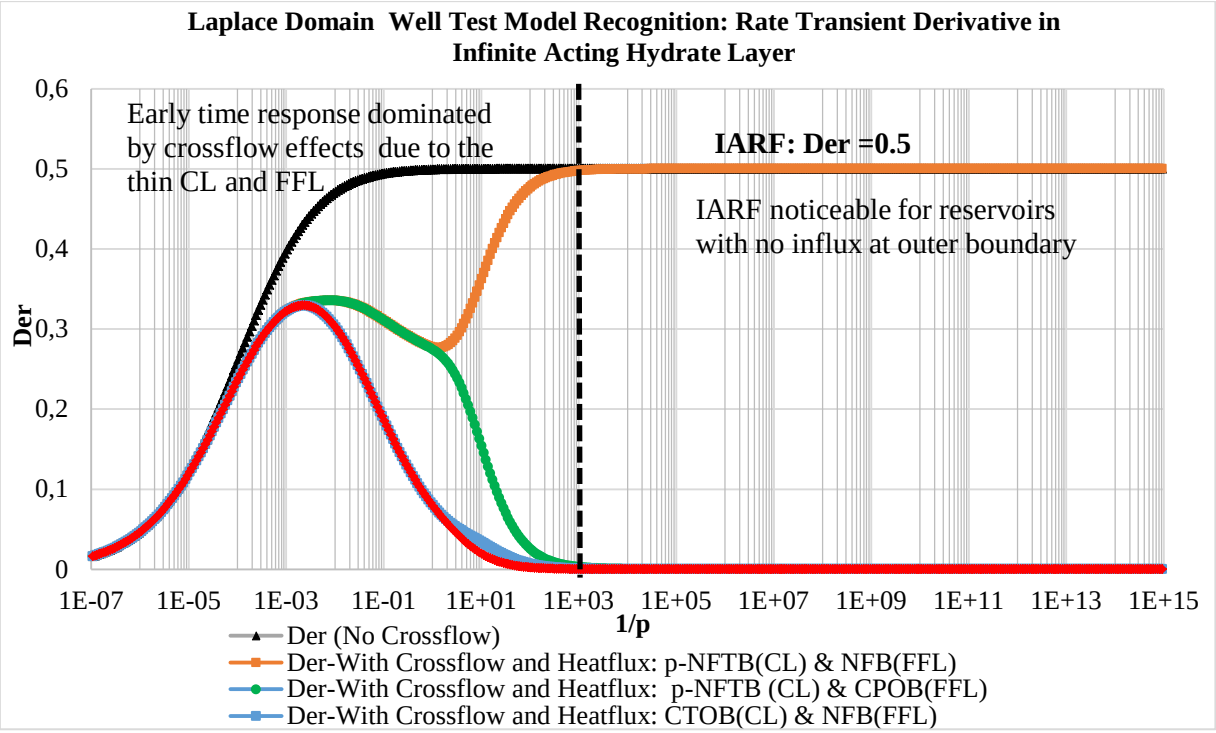

A17- 3: Derivative Rate Transient in Infinite Acting Hydrate Layer with different Boundary Conditions in the Confining Layers

Free Fluid Layer Parameters			Confining Layer	
Δz_D	ω	δ_D	Δz_D	$e_D\sqrt{F_{CD}}$
5	1E-04	1E-05	5	3.16E-07

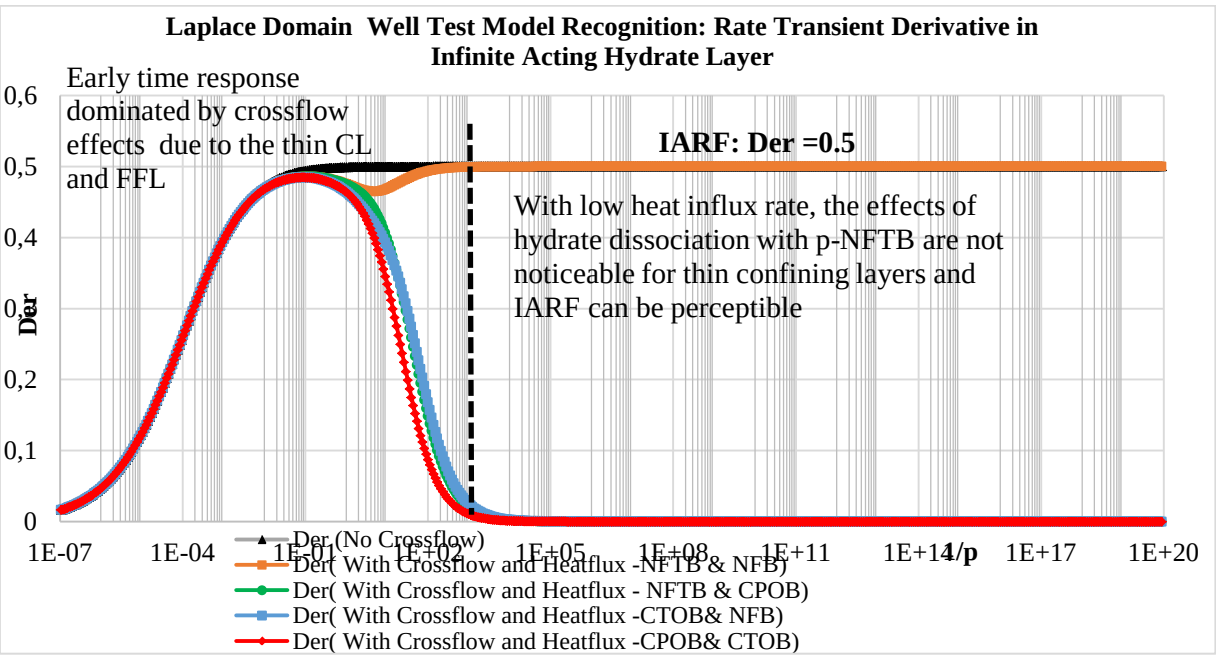

A17- 4: Derivative Rate Transient in Infinite Acting Hydrate Layer with different Boundary Conditions in the Thin Confining Layers

Solutions in Real-Time Domain

To obtain the solutions in real time domain, approximations of the leakage rates have to be made as also seen in Appendix 16.

Usually the effect of CTOB or CPOB overshadows the effects of NFB or p-NFTB all depending on the influx rate from both layers. We will however consider the following cases.

CPOB in Free Fluid Layer (FFL) and CTOB in Confining Layer (CL)

$$\lambda_D^2 = \left(p\omega + e_D\widehat{\dot{Q}_{pD}} + \frac{\delta_D(1+\theta_D)}{(\Delta z_{D,BL}-1)}\left[(\Delta z_{D,BL}-1)\sqrt{p[1-\omega]}\right]\mathrm{Coth}\left[\sqrt{p[1-\omega]}(\Delta z_{D,BL}-1)\right]\right) \quad \text{A17: 8}$$

As given in Appendix 7, the heat influx rate responsible for hydrate dissociation can be quantified and incorporated in the crossflow model.

$$\lambda_D^2 = \left(p\omega + \frac{(\Delta z_{D,TL}-1)}{(\Delta z_{D,TL}-1)}e_D\sqrt{pF_{CD}}\mathrm{Coth}\left[\sqrt{pF_{CD}}(\Delta z_{D,TL}-1)\right] + \frac{\delta_D(1+\theta_D)}{(\Delta z_{D,BL}-1)}\left[(\Delta z_{D,BL}-1)\sqrt{p[1-\omega]}\right]\mathrm{Coth}\left[\sqrt{p[1-\omega]}(\Delta z_{D,BL}-1)\right]\right) \quad \text{A17: 9}$$

NFB in Free Fluid Layer (FFL) and CTOB in Confining Layer (CL)

$$\lambda_D^2 = \left(p\omega + \frac{(\Delta z_{D,TL}-1)}{(\Delta z_{D,TL}-1)}e_D\sqrt{pF_{CD}}\mathrm{Coth}\left[\sqrt{pF_{CD}}(\Delta z_{D,TL}-1)\right] + \delta_D(1+\theta_D)\left[\sqrt{p[1-\omega]}\right]\tanh\left[\sqrt{p[1-\omega]}(\Delta z_{D,BL}-1)\right]\right) \quad \text{A17: 10}$$

Late Time Period for CPOB in FFL and CTOB in CL

$$\lambda_D = \sqrt{p\omega\left\{1 + \frac{1}{3\omega}\left[e_D F_{CD}(\Delta z_{D,TL}-1) + \delta_D(1+\theta_D)[1-\omega](\Delta z_{D,BL}-1)\right]\right\} + \left[\frac{\delta_D(1+\theta_D)}{(\Delta z_{D,BL}-1)} + \frac{e_D}{(\Delta z_{D,TL}-1)}\right]} = \sqrt{p\omega g_{D,2} + j_{D,2}} \quad \text{A17: 11}$$

Dimensionless Pseudo-Pressure

$$\varphi_D = Z\left(\frac{t_{DwD}}{\omega g_{D,2}}, r_D, \sqrt{j_{D,2}}\right) \quad \text{A17: 12}$$

Dimensionless Flowrate at Wellbore

$$\dot{m}_{tD} = G\left(\frac{t_{Dw}}{\omega g_{D,2}}, \sqrt{j_{D,2}}\right) \quad \text{A17: 13}$$

Late Time Period for NFB in FFL and CTOB in CL

$$\lambda_D = \sqrt{p\omega\left[1 + \frac{1}{3\omega}\left\{\left(e_D F_{CD}(\Delta z_{D,TL}-1) + 3\left[\delta_D(1+\theta_D)(1-\omega)(\Delta z_{D,BL}-1)\right]\right)\right\}\right] + \frac{e_D}{(\Delta z_{D,TL}-1)}} = \sqrt{p\omega f_{D,2} + Y_D} \quad \text{A17: 14}$$

Dimensionless Pseudo-Pressure

$$\varphi_D = Z\left(\frac{t_{DwD}}{\omega f_{D,2}}, r_D, \sqrt{Y_D}\right) \quad \text{A17: 15}$$

Dimensionless Flow rate at Wellbore

$$\dot{m}_{tD} = G\left(\frac{t_{DwD}}{\omega f_{D,2}}, \sqrt{Y_D}\right) \quad \text{A17: 16}$$

Case 1b: Constant Pressure Outer Boundary Reservoir

Boundary conditions

r_{eD} $\quad \hat{\varphi}_D = 0$

r_D=1 $\quad \hat{\varphi}_D = \frac{1}{p}$

The coefficients are hence:

$$c_1 = -\frac{1}{p}\left[\frac{K_o(r_{eD}\lambda_D)}{(K_o(\lambda_D)I_o(r_{eD}\lambda_D))-I_o(\lambda_D)K_o(r_{eD}\lambda_D)}\right] \quad \text{A17: 17}$$

$$c_2 = \frac{1}{p}\left[\frac{K_o(r_{eD}\lambda_D)I_o(r_{eD}\lambda_D)}{(K_o(\lambda_D)I_o(r_{eD}\lambda_D))-I_o(\lambda_D)K_o(r_{eD}\lambda_D)}\right]\frac{1}{K_o(r_{eD}\lambda_D)} \quad \text{A17: 18}$$

Dimensionless Pseudo-Pressure

$$\hat{\varphi}_D = \frac{1}{p}\left[\frac{K_o(r_D\lambda_D)I_o(r_{eD}\lambda_D)-K_o(r_{eD}\lambda_D)I_o(r_D\lambda_D)}{I_o(r_{eD}\lambda_D)K_o(\lambda_D)-I_o(\lambda_D)K_o(r_{eD}\lambda_D)}\right] \quad \text{A17: 19}$$

Dimensionless Flow rate

$$\hat{m}_{tD} = r_D\frac{\lambda_D}{p}\left[\frac{K_1(r_D\lambda_D)I_o(r_{eD}\lambda_D)+K_o(r_{eD}\lambda_D)I_1(r_D\lambda_D)}{I_o(\lambda_D)K_o(r_{eD}\lambda_D)-I_o(r_{eD}\lambda_D)K_o(\lambda_D)}\right] \quad \text{A17: 20}$$

$$\hat{m}_{tD} = \frac{\lambda_D}{p}\left[\frac{K_1(\lambda_D)I_o(r_{eD}\lambda_D)+K_o(r_{eD}\lambda_D)I_1(\lambda_D)}{I_o(\lambda_D)K_o(r_{eD}\lambda_D)-I_o(r_{eD}\lambda_D)K_o(\lambda_D)}\right] \quad \text{A17: 21}$$

Rate Transient Plot in Laplace Domain

$\widehat{pm}_{tD}$ Versus $\frac{1}{p}$

$\hat{\varphi}_D p$ Versus r_D

$\text{Der} = \frac{\Delta\left(\frac{1}{\widehat{pm}_{tD}}\right)}{\Delta\left(\frac{1}{p}\right)}$ Versus $\frac{1}{p}$

For large values of p i.e. early time production period where boundary dominated flow has not been reached, the reservoir is still acting infinite and from the characteristics of the modified Bessel´s functions given in Figure A7- 1, the solutions to the infinite acting reservoir are applicable.

Case 1c: No-Flow Outer Boundary in Producing Layer

r_{eD} $\quad \left(\frac{d\hat{\varphi}_D}{dr_D}\right)_{r_{eD}} = 0$

r_D=1 $\quad \hat{\varphi}_D = \frac{1}{p}$

The coefficients are hence:

$$c_1 = \frac{1}{p}\left[\frac{K_1(r_{eD}\lambda_D)}{I_o(\lambda_D)K_o(r_{eD}\lambda_D)-K_o(\lambda_D)I_1(r_{eD}\lambda_D)}\right] \quad \text{A17: 22}$$

$$c_2 = \frac{1}{p}\left[\frac{I_1(r_{eD}\lambda_D)}{I_o(\lambda_D)K_1(r_{eD}\lambda_D) - K_o(\lambda_D)I_1(r_{eD}\lambda_D)}\right] \quad \text{A17: 23}$$

Dimensionless Pseudo-Pressure

$$\hat{\varphi}_D = \frac{1}{p}\left[\frac{K_1(r_{eD}\lambda_D)I_o(r_D\lambda_D) + I_1(r_{eD}\lambda_D)K_o(r_D\lambda_D)}{I_o(\lambda_D)K_1(r_{eD}\lambda_D) - K_o(\lambda_D)I_1(r_{eD}\lambda_D)}\right] \quad \text{A17: 24}$$

Dimensionless Flow rate

$$\hat{m}_{tD} = -r_D\frac{d\hat{\varphi}_D}{dr_D} = -r_D\frac{1}{p}\left[\frac{1}{I_o(\lambda_D)K_1(r_{eD}\lambda_D) - K_o(\lambda_D)I_1(r_{eD}\lambda_D)}\right]\frac{d\left(K_1(r_{eD}\lambda_D)I_o(r_D\lambda_D) + I_1(r_{eD}\lambda_D)K_o(r_D\lambda_D)\right)}{dr_D} \quad \text{A17: 25}$$

$$\hat{m}_{tD} = \frac{1}{p}r_D\left[\frac{\lambda_D[K_1(r_{eD}\lambda_D)I_1(r_D\lambda_D) - I_1(r_{eD}\lambda_D)K_1(r_D\lambda_D)]}{I_o(\lambda_D)K_o(r_{eD}\lambda_D) - I_o(r_{eD}\lambda_D)K_o(\lambda_D)}\right] \quad \text{A17: 26}$$

$$\hat{m}_{tD} = \frac{1}{p}\left[\frac{\lambda_D[K_1(r_{eD}\lambda_D)I_1(\lambda_D) - I_1(r_{eD}\lambda_D)K_1(\lambda_D)]}{I_o(\lambda_D)K_o(r_{eD}\lambda_D) - I_o(r_{eD}\lambda_D)K_o(\lambda_D)}\right] \quad \text{A17: 27}$$

Rate Transient Plot in Laplace Domain

$p\hat{m}_{tD}$	Versus	$\frac{1}{p}$
$\hat{\varphi}_D p$	Versus	r_D
$Der = \frac{\Delta\left(\frac{1}{p\hat{m}_{tD}}\right)}{\Delta\left(\frac{1}{p}\right)}$	Versus	$\frac{1}{p}$

For large values of p i.e. early time production period where boundary dominated flow has not been reached, the reservoir is still acting infinite and from the characteristics of the modified Bessel´s functions given in Figure A7- 1, the solutions to the infinite acting reservoir are applicable.

Case 2: Constant Terminal Rate Solutions

Case 2a: Infinite Acting Reservoir

Inner Boundary Condition

$$c_2 = \frac{1}{p[\lambda_D K_1(\lambda_D)]} \quad \text{A17: 28}$$

Dimensionless Pseudo-Pressure

$$\hat{\varphi}_D = \frac{K_o(r_D\lambda_D)}{p[\lambda_D K_1(\lambda_D)]} \quad \text{A17: 29}$$

Dimensionless Pseudo-Pressure (Line Source)

$$\hat{\varphi}_D = \frac{K_o(r_D\lambda_D)}{p} \quad \text{A17: 30}$$

Pseudo-Pressure Transient Plot in Laplace Domain

$\hat{\varphi}_D p$	Versus	r_D
$\hat{\varphi}_D p$	Versus	$\frac{1}{p}$

$$\text{Der} = \frac{\Delta(\hat{\varphi}_D p)}{\Delta\left(\frac{1}{p}\right)} \qquad \text{Versus} \qquad \frac{1}{p}$$

The derivatives given in Case 1a for the rate transient solution are also representative for this case. Due to the uniqueness of each reservoir response, several reservoir response models could be generated.

Solutions in Real-Time Domain for Line Source Model

Early-Time Response for No-flow and Constant Pressure Outer Boundary in Crossflow Layer

$$\lambda_D = \sqrt{p\omega + \left(e_D\sqrt{F_{CD}} + \delta_D(1+\theta_D)\sqrt{[1-\omega]}\right)\sqrt{p}} = \sqrt{p\omega + \varepsilon_{D,2}\sqrt{p}} \qquad \text{A17: 31}$$

$$\varphi_D = H\left(\frac{\omega r_D^2}{4t_{DwD}}, \frac{r_D\varepsilon_{D,2}}{4\sqrt{\omega}}\right) \qquad \text{A17: 32}$$

Late Time Period for CPOB in FFL and CTOB in CL

$$\lambda_D = \sqrt{p\omega\left\{1 + \frac{1}{3\omega}\left[e_D F_{CD}\left(\Delta z_{D,TL} - 1\right) + \delta_D(1+\theta_D)[1-\omega]\left(\Delta z_{D,BL} - 1\right)\right]\right\} + \left[\frac{\delta_D(1+\theta_D)}{\left(\Delta z_{D,BL} - 1\right)} + \frac{e_D}{\left(\Delta z_{D,TL} - 1\right)}\right]} = \sqrt{p\omega g_{D,2} + j_{D,2}}$$

$$\varphi_D = \frac{1}{2}W\left(\frac{r_D^2}{4t_{DwD}}\omega g_{D,2}, r_D\sqrt{j_{D,2}}\right) \qquad \text{A17: 33}$$

Late Time Period NFB in FFL and CTOB in CL

$$\lambda_D = \sqrt{p\omega\left[1 + \frac{1}{3\omega}\left\{\left(e_D F_{CD}\left(\Delta z_{D,TL} - 1\right) + 3\left[\delta_D(1+\theta_D)(1-\omega)\left(\Delta z_{D,BL} - 1\right)\right]\right)\right\}\right] + \frac{e_D}{\left(\Delta z_{D,TL} - 1\right)}} = \sqrt{p\omega f_{D,2} + Y_D} \qquad \text{A17: 34}$$

$$\varphi_D = \frac{1}{2}W\left(\frac{r_D^2}{4t_{DwD}}\omega f_{D,2}, r_D\sqrt{Y_D}\right) \qquad \text{A17: 35}$$

Case 2b: Constant Outer Boundary Pressure in Producing Layer

Boundary Conditions

r_{eD} $\qquad\qquad$ $\hat{\varphi}_D = 0$

r_D=1 $\qquad\qquad$ $r_D\frac{d\hat{\varphi}_D}{dr_D} = -\frac{1}{p}$

The coefficients are hence:

$$c_1 = -\frac{K_o(r_{eD}\lambda_D)}{p\lambda_D[K_1(\lambda_D)I_o(r_{eD}\lambda_D) + K_o(r_{eD}\lambda_D)I_1(\lambda_D)]} \qquad \text{A17: 36}$$

$$c_2 = \frac{I_o(r_{eD}\lambda_D)}{p\lambda_D[K_1(\lambda_D)I_o(r_{eD}\lambda_D) + K_o(r_{eD}\lambda_D)I_1(\lambda_D)]} \qquad \text{A17: 37}$$

Dimensionless Pseudo-Pressure

$$\hat{\varphi}_D = \frac{K_o(r_D\lambda_D)I_o(r_{eD}\lambda_D) - K_o(r_{eD}\lambda_D)I_o(r_D\lambda_D)}{p\lambda_D[K_1(\lambda_D)I_o(r_{eD}\lambda_D) + K_o(r_{eD}\lambda_D)I_1(\lambda_D)]} \qquad \text{A17: 38}$$

Pseudo-Pressure Transient Plot in Laplace Domain

$\hat{\varphi}_D p$ $\qquad$ Versus $\qquad$ r_D

$\hat{\varphi}_D p$ Versus $\frac{1}{p}$

$\text{Der} = \frac{\Delta(\hat{\varphi}_D p)}{\Delta\left(\frac{1}{p}\right)}$ Versus $\frac{1}{p}$

For large values of p i.e. early time production period where boundary dominated flow has not been reached, the reservoir is still acting infinite and from the characteristics of the modified Bessel´s functions given in Figure A7- 1, the solutions to the infinite acting reservoir are applicable.

Case 2c: No-Flow Outer Boundary in Producing Layer

Boundary Conditions

r_{eD} $\left(\frac{d\hat{\varphi}_D}{dr_D}\right)_{r_{eD}} = 0$

r_D=1 $r_D \frac{d\hat{\varphi}_D}{dr_D} = -\frac{1}{p}$

The coefficients are hence

$$c_1 = \frac{K_1(r_{eD}\lambda_D)}{p\lambda_D\{[I_1(r_{eD}\lambda_D)K_1(\lambda_D)]-[K_1(r_{eD}\lambda_D)I_1(r_D\lambda_D)]\}} \quad \text{A17: 39}$$

$$c_2 = \frac{I_1(r_{eD}\lambda_D)}{p\lambda_D\{[I_1(r_{eD}\lambda_D)K_1(\lambda_D)]-[K_1(r_{eD}\lambda_D)I_1(r_D\lambda_D)]\}} \quad \text{A17: 40}$$

Dimensionless Pseudo-Pressure

$$\hat{\varphi}_D = \frac{K_1(r_{eD}\lambda_D)I_o(r_D\lambda_D)+I_1(r_{eD}\lambda_D)K_o(r_D\lambda_D)}{p\lambda_D\{[I_1(r_{eD}\lambda_D)K_1(\lambda_D)]-[K_1(r_{eD}\lambda_D)I_1(r_D\lambda_D)]\}} \quad \text{A17: 41}$$

Pressure Transient Plot in Laplace Domain

$\hat{\varphi}_D p$ Versus r_D

$\hat{\varphi}_D p$ Versus $\frac{1}{p}$

$\text{Der} = \frac{\Delta(\hat{\varphi}_D p)}{\Delta\left(\frac{1}{p}\right)}$ Versus $\frac{1}{p}$

For large values of p i.e. early time production period where boundary dominated flow has not been reached, the reservoir is still acting infinite and from the characteristics of the modified Bessel´s functions given in Figure A7- 1, the solutions to the infinite acting reservoir are applicable.

Appendix 18: Reservoir Response Functions

Hantush Functions [43]

Flowing Well Discharge Function for Leaky Aquifers

$$G(\mu,\beta)=\frac{\dot{m}_t(t)}{2\pi hk(\varphi_i-\varphi_{wf})}=\beta\frac{K_1(\beta)}{K_o(\beta)}+\frac{4}{\pi^2}\exp(-\mu\beta^2)\int_0^\infty \exp(-\mu x^2)\frac{x}{(x^2+\beta^2)[J_o^2(x)+Y_o^2(x)]}dx \quad \text{A18: 1}$$

Flowing Well Discharge Function for Non-Leaky Aquifers

$$G(\mu,0)=\frac{\dot{m}_t(t)}{2\pi hk(\varphi_i-\varphi_{wf})}=\frac{4}{\pi^2}\int_0^\infty \frac{\exp(-\mu x^2)}{[J_o^2(x)+Y_o^2(x)]}\frac{dx}{x} \quad \text{A18: 2}$$

Flowing Well Function for Non-Leaky Aquifers

$$A(\mu,\beta)=\frac{2\pi hk}{\dot{m}_t}[\varphi_i-\varphi(r,t)]=1-\frac{2}{\pi}\int_0^\infty \exp(-\mu x^2)\frac{[J_o(x)Y_o(\beta x)-Y_o(x)J_o(\beta x)]}{[J_o^2(x)+Y_o^2(x)]}\frac{dx}{x} \quad \text{A18: 3}$$

Flowing Well Function for Leaky Aquifers

$$Z(\mu,\beta,\tau)=\frac{2\pi hk}{\dot{m}_t}[\varphi_i-\varphi(r,t)]=\beta\frac{K_o(\tau\beta)}{K_o(\tau)}+\frac{2}{\pi}\exp(-\mu\tau^2)\int_0^\infty \frac{\exp(-\mu x^2)}{(x^2+\tau^2)}\frac{[J_o(\beta x)Y_o(x)-Y_o(\beta x)J_o(x)]}{[J_o^2(x)+Y_o^2(x)]}xdx \quad \text{A18: 4}$$

Well Function for Leaky Aquifers

$$W(\mu,\beta)=\frac{2\pi hk}{\dot{m}_t}\left[\varphi_i-\varphi(r,t)\right]=\int_\mu^\infty \frac{1}{x}\exp\left(-x-\frac{\beta^2}{4x}\right)dx \quad \text{A18: 5}$$

$$W(\mu,0)=E_1(\mu)=\frac{2\pi hk}{\dot{m}_t}\left[\varphi_i-\varphi(r,t)\right]=\int_\mu^\infty \frac{1}{x}\exp(-x)dx \quad \text{A18: 6}$$

Early Time Well Function for Leaky Aquifers

$$H(\mu,\beta)=\frac{2\pi hk}{\dot{m}_t}\left[\varphi_i-\varphi(r,t)\right]=\int_\mu^\infty \frac{exp(-x)}{x}\operatorname{erfc}\left(\frac{\beta\sqrt{\mu}}{\sqrt{x(x-\mu)}}\right)dx \quad \text{A18: 7}$$

Generalized Incomplete Gamma Function [88]

$$\Gamma(a,\mu;b)=\int_\mu^\infty \frac{1}{x^{1-a}}\exp\left(-x-\frac{b}{x}\right)dx \quad \text{A18: 8}$$

$$\frac{d\Gamma(a,\mu;b)}{dx}=-\frac{1}{x^{1-a}}\exp\left(-x-\frac{b}{x}\right) \quad \text{A18: 9}$$

$$\Gamma(0,\mu;b)=\int_\mu^\infty \frac{1}{x}\exp\left(-x-\frac{b}{x}\right)dx=W(\mu,\beta) \quad \text{A18: 10}$$

$$\Gamma(0,\mu;0)=\int_\mu^\infty \frac{1}{x}\exp(-x)dx=E_1(-\mu)=-Ei(-\mu) \quad \text{A18: 11}$$